

Aberration theory of electron mirrors with deflectors, and design of an aberration corrector with miniature electron mirrors

Dohi, H.

DOI

[10.4233/uuid:2912c7a2-e50d-458a-b7c6-41822b6590ef](https://doi.org/10.4233/uuid:2912c7a2-e50d-458a-b7c6-41822b6590ef)

Publication date

2025

Document Version

Final published version

Citation (APA)

Dohi, H. (2025). *Aberration theory of electron mirrors with deflectors, and design of an aberration corrector with miniature electron mirrors*. [Dissertation (TU Delft), Delft University of Technology].
<https://doi.org/10.4233/uuid:2912c7a2-e50d-458a-b7c6-41822b6590ef>

Important note

To cite this publication, please use the final published version (if applicable).
Please check the document version above.

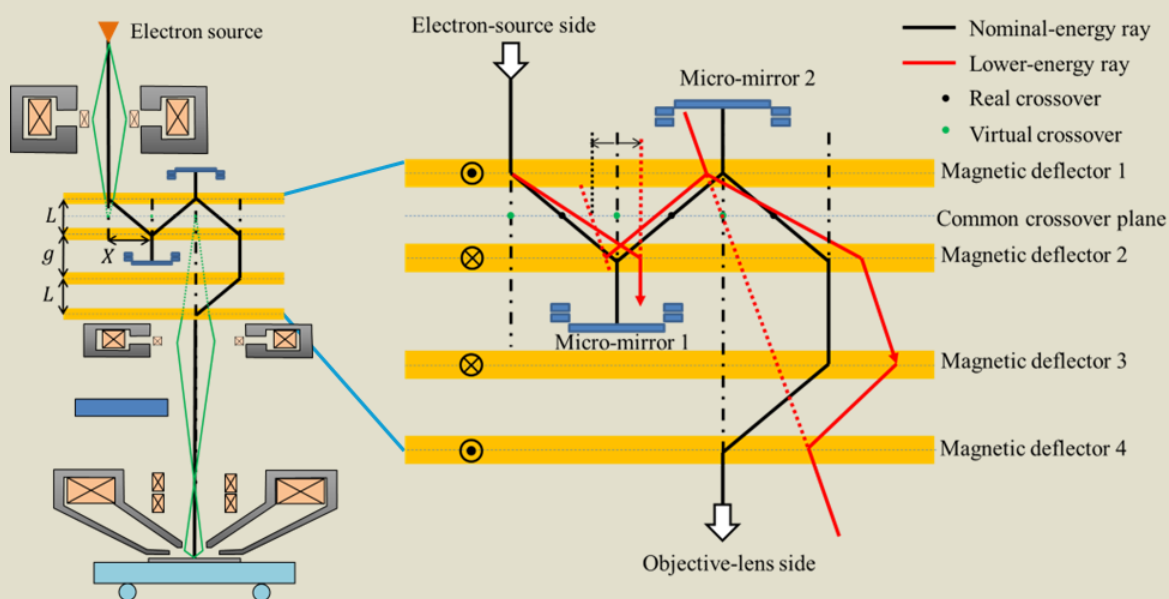
Copyright

Other than for strictly personal use, it is not permitted to download, forward or distribute the text or part of it, without the consent of the author(s) and/or copyright holder(s), unless the work is under an open content license such as Creative Commons.

Takedown policy

Please contact us and provide details if you believe this document breaches copyrights.
We will remove access to the work immediately and investigate your claim.

Aberration theory of electron mirrors with deflectors, and design of an aberration corrector with miniature electron mirrors



Hideto Dohi

**Aberration theory of electron mirrors with deflectors,
and
design of an aberration corrector
with miniature electron mirrors**

Dissertation

for the purpose of obtaining the degree of doctor

at Delft University of Technology

by the authority of the Rector Magnificus, Prof.dr.ir. T.H.J.J. van der Hagen,

chair of the Board for Doctorates to be defended publicly on

Wednesday 4 June 2025 at 10:00 o'clock

by

Hideto DOHI

Master of Science in Physics,

Osaka University, Japan

This dissertation has been approved by the

promotor: em.prof.dr.ir. P. Kruit

copromotor: dr. A. Mohammadi Gheidari

Composition of the doctoral committee:

Rector Magnificus, chairperson

Em.prof.dr.ir. P. Kruit, Delft University of Technology, promotor

Dr. A. Mohammadi Gheidari, Delft University of Technology, copromotor

Independent members:

Prof.dr. S.M. Witte, Delft University of Technology

Prof.dr. R.F. Mudde, Delft University of Technology

Prof.dr. M. Kuwahara, Nagoya University

Prof.dr. R. Nishi, Fukui University of Technology

Prof.dr.ir. J.P. Hoogenboom Delft University of Technology, reserve member



The work in this dissertation was conducted at the Charged Particle Optics group in the department of Imaging Physics, Faculty of Applied Sciences, Delft University of Technology.

Keywords: Scanning electron microscope, aberration correction, electron mirror, deflection aberration, time-dependent perturbation theory.

Printed by: Yamada Speed Printing Ltd.

Copyright © 2025 by H. Dohi

ISBN 978-94-6518-064-9

An electronic version of this dissertation is available at

<http://repository.tudelft.nl/>.

Contents

Summary	xi
Samenvatting	xv
Chapter 1	Introduction	1
1.1	The metrology method of semiconductor processes and a critical dimension scanning electron microscope (CD-SEM).....	1
1.2	Significance of a low voltage & high-resolution SEM.....	4
1.3	Decisive factors of a standard SEM resolution	5
1.4	Resolution improvement method.....	10
1.5	Aberration correction.....	12
1.6	Problem of aberration correctors and suggestion	16
1.7	About simulators for design.....	17
1.8	Scope of the dissertation	18
1.9	References	19
Chapter 2	Time-dependent perturbation for systems of Electron Mirrors and round electromagnetic fields	25
2.1	Introduction	25
2.2	Equation of motion and paraxial rays in the time-dependent formalism for electron mirrors	29
2.2.1	Reference electron	29
2.2.2	Equation of motion	30
2.2.3	Paraxial equation in lateral direction, longitudinal linear equation, and their fundamental solutions	34
2.2.4	General paraxial rays in lateral direction and general solutions of a linear longitudinal equation, which is called linear longitudinal path deviation.....	37
2.3	Path deviation in the time-dependent theory induced by perturbation.	41
2.3.1	Procedures of perturbation in the time-dependent theory.....	41
2.3.2	A method to transform lateral path-deviation defined at time into that defined at a plane perpendicular to the optic axis.....	45
2.3.3	Explicit form of perturbation functions of second- and third-rank	49

2.4	The second-rank lateral path deviation and the second-rank aberration coefficients and the chromatic aberrations.....	52
2.5	Second-order longitudinal path deviation, third-order geometrical lateral path deviation & third-order geometrical aberration coefficients.....	55
2.6	Analytic form and properties of a longitudinal path-deviation of first-rank.....	60
2.7	Proof of properties of third-order geometrical off-axis aberration coefficients of time-dependent theory: Coma-length and radius, anisotropic part of field curvature, and relation between field curvature and astigmatism	65
2.8	Transformation of the aberration coefficients, from time-dependent theory to standard electron optics, for a normal lens system.....	71
2.9	Aberration coefficients for variation of the voltages and the currents.....	75
2.10	Relations between the aberration coefficients for variation of the voltages and the currents and that of chromatic aberration	82
2.11	Aberration coefficients for an inclined incident beam	84
2.12	Conclusion	89
2.13	Appendix of chapter 2	91
2.13.1	Definitions of rank, order, and degree of aberrations	91
2.13.2	A linear second order ordinary differential equation and the variation method of a parameter for solving an inhomogeneous equation.....	91
2.13.3	Replacement of fundamental solutions of linear equations in the formal solution of perturbation	94
2.13.4	Third-order geometrical slope deviation and slope aberration	96
2.13.5	The paraxial trajectories and the path and the slope deviations and aberrations in the Cartesian coordinate system	100
2.14	References.....	103
Chapter 3	3rd-order relativistic aberration theory for the systems of round symmetric electromagnetic fields and deflectors.....	105
3.1	Introduction	105
3.2	Definitions of Deflection potentials	108
3.2.1	Definition of coordinates	108

3.2.2	Electrostatic potential of Deflectors	109
3.2.3	Scalar potential of magnetic deflectors and deflection coil currents	113
3.3	Electron optical eikonal, Euler-Lagrange equation in the Cartesian coordinate system, and trajectories.	114
3.3.1	The Electron optical eikonal of the system of lenses and deflectors.	114
3.3.2	The Euler-Lagrange equation.....	117
3.3.3	The paraxial trajectories in the Cartesian coordinate and those in the rotation coordinate.	118
3.3.4	The deflection trajectories.....	120
3.4	Perturbation theory of deflection.	121
3.4.1	Perturbation formalism	121
3.4.2	Geometrical deflection aberration coefficients for general type of deflectors	123
3.5	Geometrical aberration coefficients of the system, which is composed of a single electrostatic deflector and a single magnetic deflector.	130
3.5.1	Geometrical aberration coefficients	130
3.5.2	Conversion of deflection aberration coefficients.....	135
3.6	Geometrical aberration coefficients of the system, which is composed of two independent electrostatic deflectors.	137
3.7	Geometrical aberration coefficients of the system, which is composed of two independent magnetic deflectors.	139
3.8	Chromatic deflection aberration and aberrations of voltage and current variation of lenses.	142
3.8.1	Perturbation functions for chromatic deflection aberration and aberrations of voltage and current variation of lenses.....	142
3.8.2	Formal expressions of path-deviations.....	144
3.8.3	Explicit forms of path-deviations.....	147
3.8.4	Second-rank deflection aberration coefficients	150
3.8.5	Conversion of the aberration coefficients to those defined at the image plane and parameterized by the deflection beam shift.....	152
3.9	Conclusion.....	154
3.10	References.....	155

Chapter 4	3rd-order time-dependent aberration theory for systems of round symmetric electromagnetic fields and deflectors	157
4.1	Introduction	157
4.2	Field expansion and general equation of motion in time-dependent deflection theory.....	159
4.3	First order approximation of equation of motion and first-order solutions.....	161
4.4	First order approximation and solution of longitudinal equation of motion	163
4.5	Second-rank lateral path deviation and chromatic deflection aberration coefficients of time-dependent deflection theory	164
4.6	Second order geometrical longitudinal path deviation of time-dependent deflection theory.....	166
4.7	Third order geometrical lateral path deviation and geometrical aberration coefficients of time-dependent deflection theory	169
4.7.1	Expressions of third-order geometrical lateral path deviation	172
4.7.2	Expression of third-order geometrical aberration coefficients	184
4.8	Path deviation for variation of voltages and currents of rotationally symmetric electrodes and coils with deflection fields.....	185
4.9	Time-dependent deflection path deviation for the inclined incident beam	188
4.10	Conclusion	191
Chapter 5	Conceptual design for an aberration corrected scanning electron microscope using miniature electron mirrors	193
5.1	Outline.....	193
5.2	Configuration of corrector system	193
5.2.1	Concept of double mirrors	193
5.2.2	Concept of small-angle-deflection system with beam shift: S-corrector	194
5.2.3	Dispersion of S-corrector	197
5.2.4	Dispersion in a practical mirror of a S-corrector	201
5.2.5	Double micro-mirror corrector without beam shift: K-corrector	203
5.3	Electron optical systems with micro-mirror correctors	206
5.3.1	Presupposition and conditions	206
5.3.2	Optical system	207
5.3.3	Calculation of aberrations of electron mirrors.....	209

5.4	Estimates of other aberrations and FW50 of the corrected SEM.....	214
5.4.1	Deflector setup & Deflection aberration of the S-corrector.....	214
5.4.2	Combination aberrations of the dispersion by the deflection and aberrations of the mirrors and the objective lens.....	221
5.4.3	Combination aberrations between the double micro-mirrors	225
5.4.4	Combination aberration of mirrors with field curvature and astigmatism of deflectors	227
5.4.5	Estimates of beam spot size of the aberration corrected SEM by the post-deflection S-corrector.	229
5.5	Off-axis aberrations by misalignment of mirrors	234
5.6	Effects from misalignment of elements in the mirrors	236
5.7	Conclusion.....	237
5.8	References	238
Chapter 6	Conclusion	239
	Acknowledgements	243
	Curriculum Vitae.....	245
	List of Publications	247
	List of Patents	249

Summary

In the course of downscaling semiconductor devices, the density of integrated circuits had been increasing according to Moore's law until the late 2010s. Then the speed of downscaling decreased but recently continues again with the advent of extreme ultraviolet lithography (EUVL). The minimum half-pitch of a semiconductor device has already reached less than 20 nm and is predicted to reach sub-10 nm at the beginning of the 2030s. A critical-dimension scanning electron microscope (CD-SEM) is widely used for measuring the most important device pattern geometries, known as critical dimensions (CDs). When the geometries of patterns get smaller, the required CD measurement sensitivity becomes stricter to detect and quantify the tiny fluctuations of patterns in high-volume manufacturing processes.

Additionally, the radiation damage caused by the electron beam to patterns of materials recently introduced in the industry, such as EUV resist, is a serious issue. Since patterns shrink during irradiation, CD measurements become unstable, and their results deviate from the "true geometry." The lower the landing energy of electrons, the weaker the damage to the patterns. A low-voltage SEM (LV-SEM) provides a gentler metrology tool for patterns. However, both spherical and chromatic aberrations of the objective lens increase, and thus the beam spot size becomes larger when the landing energy is lower. Thus, aberration correction is necessary to improve the resolution of SEMs to reduce damage caused by low landing energy and to improve the sensitivity of CD measurements.

The resolution of SEMs is closely related to the spot size of the electron beam at the specimen surface. The decisive factors for the spot size are diffraction, source size, spherical aberration, and chromatic aberration in a conventional SEM. Scherzer's theorem shows that spherical and chromatic aberrations are inevitable in rotationally symmetric electron lenses.

Several correction methods have been proposed for both spherical and chromatic aberrations. A multipole corrector is the most typical method. To correct both aberrations, it requires quadrupole and octopole fields arranged in four stages along the longitudinal direction. Precise machining and assembly techniques are necessary to suppress parasitic aberrations. Four-stage dodecapole lenses are used to generate not only quadrupole and octopole fields but also dipole and hexapole fields to correct residual non-vanishing parasitic aberrations. Dozens of highly stable power supplies and their complex tuning are necessary to control aberrations.

The second typical corrector is an electron mirror, which reflects the incident electrons. A large-angle bending magnet, typically bending over angles greater than a few tens of degrees, is used to guide the incident electrons to the mirror and the reflected electrons to the objective lens. Such large-angle deflection causes significant deflection aberrations.

Special designs and precise machining and assembly have been implemented to suppress these aberrations, and multipole lenses have also been introduced to correct several of them.

The technology of micro-electro-mechanical systems (MEMS) has advanced considerably. For example, micro-fabrication technology for semiconductor devices is applied to make aperture arrays and electrostatic lens arrays. MEMS technology should, therefore, make it possible to realize miniature-scale mirrors as well. It will be possible to reduce the deflection angle of the electron beam further, sufficiently suppressing undesirable aberrations. This would drastically reduce not only manufacturing costs but also the size of the corrector unit.

The goal of this dissertation is to suggest a conceptual design of a low-voltage aberration-corrected scanning electron microscope using a novel miniature electron mirror corrector and small-angle deflectors to solve problems associated with conventional correctors and to suppress unwanted aberrations caused by the complexity of their structures. We did not have suitable simulators for calculating aberrations of mirrors and deflectors for the conceptual design. By referring to prior research, we decided to start by investigating perturbation theory for mirrors and deflectors to derive formulae for aberration coefficients and to create the necessary simulation program.

In chapter 2, we derive the aberration theory of electron mirrors. For the electron mirror, the incident electron must be reflected by the electrostatic field, and the slope of the trajectory, with respect to the optic axis, becomes divergent, causing the standard perturbation theory, which uses the coordinate of the optic axis as a parameter, to collapse. To avoid divergence, time was taken as a parameter. The reference electron, which travels along the optic axis with nominal energy, is introduced, and the trajectories and velocities of electrons are defined as the relative positions and velocities with respect to those of the reference electron. While the slope of electrons with respect to the optic axis diverges when electrons are reflected, the relative velocity never diverges. This feature allows for the construction of a well-defined perturbation theory for electron mirrors.

Integral aberration formulae for both on- and off-axis path deviation and aberration coefficients up to second rank and third order for the system of rotationally symmetric electrostatic and magnetic fields, which overlap with each other, are derived. The validity of the derived aberration coefficients was shown as follows: when the system is composed of round symmetric electrostatic and magnetic lenses, by changing the integration parameters of the aberration formulae from time to the coordinate of the optic axis and using partial integration, we prove that the derived coefficients of all second-rank and third-order on- and off-axis aberrations perfectly coincide with the formulae in standard electron optics theory. In addition, aberration formulae for variations in the voltages and currents of rotationally symmetric electrodes and coils are derived, showing electron displacement at the image plane when the

voltages or currents of electrodes and coils fluctuate. We establish a relationship between chromatic aberration coefficients and these aberrations.

In chapter 3, we derive the deflection aberration theory for standard lenses and deflectors. By applying perturbation theory to a system of round symmetric electrostatic and magnetic lenses and electrostatic and magnetic deflectors, relativistic deflection trajectory formulae and aberration coefficient formulae for deflection up to second rank and third order are derived for two independent deflectors in three types of configurations. The first is the combination of an electrostatic deflector and a magnetic deflector. The second and third are the configurations of two electrostatic deflectors and two magnetic deflectors, respectively. We also derive relationships between aberration coefficients parameterized by voltages and currents of deflectors and those parameterized by beam shifts caused by deflection at the image plane.

In chapter 4, we derive the deflection aberration theory for systems that include electron mirrors. A non-relativistic time-dependent deflection theory is developed based on the consideration of non-relativistic time-dependent aberration theory for round symmetric electrostatic and magnetic fields and on the deflection aberration theory of standard electron optics, where the parameter is the coordinate of the optic axis. The time-dependent deflection theory can analyze path deviations with small-angle deflectors. It is valid for systems composed of electrostatic and magnetic round symmetric fields and electrostatic and magnetic deflection fields, even when all field distributions overlap. Derived path deviation formulae and aberration coefficients, including those for electron mirrors and deflectors, are calculated up to second rank and third order.

In chapter 5, we propose a miniature aberration corrector consisting of double magnetic deflectors and double electrostatic mirrors, named the S-corrector. The optical properties of an SEM equipped with the proposed S-corrector with 50-mrad magnetic deflection are analyzed. The largest expected deflection aberration is first-rank dispersion. A post-deflection S-corrector, equipped with additional double magnetic deflectors beneath the S-corrector, was suggested as a configuration in which lateral dispersion vanishes at the final image plane of the SEM. Design examples of miniature mirrors and deflectors, as well as a possible configuration for an SEM with the post-deflection S-corrector, with a deflection angle of 50 mrad, are presented.

Numerical calculations of aberration properties for a miniature electron mirror and double deflectors are performed using the formulae derived in chapters 2 and 3. The estimation method for higher-rank combination aberrations up to fourth rank and fifth order was considered. When using the formulae derived in chapter 3 for deflection aberration, a focusing lens was necessary to calculate the deflection aberration to define an image plane where aberrations are determined. We calculate deflection aberration for a system composed of deflectors and dummy electrostatic lenses

and the off-axis aberration of the dummy lens. By properly subtracting off-axis aberrations from the corresponding deflection aberrations, the resulting aberration coefficients show contributions from the deflector itself.

We estimate the combination of aberrations between deflectors and mirrors, deflectors and the objective lens, and the first and second mirrors. The results of deflection aberrations and combination aberrations are, at their largest, 0.2 nm, which is negligible compared with target spot sizes of 1 nm for a landing voltage of 1000 V and 1.5 nm for a landing voltage of 100 V, except for fourth-rank chromatic spherical aberration and fifth-order spherical aberration. Numerical calculations based on wave optics are performed, accounting for all combination aberrations and residual deflection aberrations. The calculated spot sizes are 0.976 nm and 1.367 nm for landing voltages of 1000 V and 100 V, respectively. Thus we demonstrated the potential of an aberration-corrected LV-SEM.

Samenvatting

De dichtheid van geïntegreerde schakelingen is tot het einde van de jaren 2010 blijven toenemen, daarmee de wet van Moore volgende. Daarna is de snelheid van de verkleining afgenomen, maar deze gaat nu weer door dankzij de komst van extreem-ultraviolette lithografie (EUVL). De minimale half-pitch van een halfgeleiderstructuur is al minder dan 20 nm en wordt voorspeld om aan het begin van de jaren 2030 onder de 10 nm te komen. Een critical-dimension scanning-elektronenmicroscop (CD-SEM) wordt veel gebruikt voor het meten van de meest kritische afmetingen (“critical dimensions”) van patronen in halfgeleiderstructuren. Naarmate de afmetingen van patronen kleiner worden, worden de eisen aan de gevoeligheid van CD-metingen strenger om kleine fluctuaties van patronen in grootschalige productieprocessen te detecteren en kwantificeren.

Daarnaast vormt de stralingsschade aan patronen in recente halfgeleidermaterialen, zoals EUV-resist, veroorzaakt door de elektronenbundel, een serieus probleem. Omdat patronen krimpen tijdens bestraling, worden CD-metingen instabiel en wijken hun resultaten af van de “ware afmeting.” Hoe lager de landingsenergie van elektronen, hoe minder schade er aan de patronen wordt toegebracht. Een low-voltage SEM (LV-SEM) is een gedeeltelijke oplossing voor dit probleem. Echter, zowel sferische als chromatische aberraties van de objectieflens nemen toe, en de bundelspotgrootte wordt daarmee groter wanneer de landingsenergie lager is. Daarom is aberratiecorrectie noodzakelijk om de resolutie van SEM's te verbeteren, schade door lage landingsenergie te verminderen en de gevoeligheid van CD-metingen te vergroten.

De resolutie van SEM's is nauw verbonden met de spotgrootte van de elektronenbundel op het oppervlak van het specimen. De bepalende factoren voor de spotgrootte zijn diffractie, brongrootte, sferische aberratie en chromatische aberratie. Volgens de stelling van Scherzer zijn sferische en chromatische aberraties onvermijdelijk in rotatie symmetrische elektronenlenzen.

Er zijn verschillende correctiemethoden voorgesteld voor zowel sferische als chromatische aberraties. Een multipool-corrector is de meest gebruikelijke methode. Om beide aberraties te corrigeren, zijn quadrupool- en octopoolvelden nodig, gerangschikt in vier fasen langs de longitudinale richting. Precieze bewerking- en montagetechnieken zijn noodzakelijk om parasitaire aberraties te onderdrukken. Viertraps dodecapoollenzen worden gebruikt om niet alleen quadrupool- en octopoolvelden te genereren, maar ook dipool- en hexapoolvelden om resterende, niet-verdwijnde parasitaire aberraties te corrigeren. Tientallen stabiele voedingen en complexe afstellingen zijn nodig om aberraties te beheersen.

De tweede gebruikelijke corrector is een elektronenspiegel, die de invallende elektronen reflecteert. Groethoekige afbuigmagneten worden gebruikt om de invallende elektronen naar de spiegel en de gereflecteerde elektronen naar de objectieflens te leiden. Dergelijke groethoekige afbuiging veroorzaakt aanzienlijke afbuigingsaberraties. Speciale ontwerpen en precieze bewerking en montage zijn geïmplementeerd om deze aberraties te onderdrukken, en multipoollenzen zijn ook geïntroduceerd om enkele daarvan te corrigeren.

De reden voor die grote afbuighoeken, typisch groter dan enkele tientallen graden, is om voldoende ruimte te maken voor een standaardformaat elektronenspiegel. De technologie van micro-elektromechanische systemen (MEMS) is aanzienlijk gevorderd. Bijvoorbeeld, microfabricagetechnologie voor halfgeleiders wordt toegepast om diafragma's en elektrostatische lenselektrodes te maken. MEMS-technologie zou het mogelijk moeten maken om ook miniatuur spiegels te realiseren. Het zal daarmee mogelijk zijn om de afbuigingshoek van de elektronenbundel verder te verkleinen en ongewenste aberraties voldoende te onderdrukken. Dit zou niet alleen de productiekosten drastisch verlagen, maar ook de omvang van de correctoreenheid aanzienlijk verkleinen.

Het doel van dit proefschrift is om een conceptueel ontwerp te presenteren van een low-voltage aberratiegecorrigeerde scanning-elektronenmicroscop (LV-SEM) met gebruik van een nieuwe miniatuur-elektronenspiegelcorrector en kleine-hoek deflectoren. Dit ontwerp moet de problemen van conventionele correctoren oplossen en ongewenste aberraties door de complexe structuren onderdrukken. Aangezien er geen geschikte simulators beschikbaar waren voor het berekenen van aberraties van spiegels en afbuigers, werd besloten om, op basis van eerdere onderzoeken, de verstoringstheorie voor spiegels en afbuigers te bestuderen. Dit leidde tot de afleiding van formules voor aberratiecoëfficiënten en de ontwikkeling van een noodzakelijk simulatieprogramma.

In hoofdstuk 2 wordt de aberratietheorie van elektronenspiegels afgeleid. Voor de elektronenspiegel moet het invallende elektron worden gereflecteerd door het elektrostatische veld. De helling van de elektronenbaan ten opzichte van de optische as divergeert, waardoor de standaard verstoringstheorie, die gebruik maakt van de z-coördinaat van de optische as als parameter, niet meer werkt. Om divergentie te vermijden, wordt tijd als parameter genomen. Een referentie-elektron, dat langs de optische as reist met nominale energie, wordt geïntroduceerd. De banen en snelheden van elektronen worden gedefinieerd als relatieve posities en snelheden ten opzichte van die van het referentie-elektron. Terwijl de helling van elektronen ten opzichte van de optische as divergeert tijdens reflectie, is er geen divergentie in de relatieve snelheid. Deze eigenschap maakt het mogelijk om een goed gedefinieerde verstoringstheorie voor elektronenspiegels op te bouwen.

Integrale aberratieformules voor zowel axiale als niet-axiale baanafwijkingen en aberratiecoëfficiënten tot de tweede rang en derde orde worden afgeleid voor systemen van rotatiesymmetrische elektrostatische en magnetische velden,

die elkaar kunnen overlappen. De geldigheid van de afgeleide aberratiecoëfficiënten wordt aangetoond. Wanneer het systeem bestaat uit rond-symmetrische elektrostatische en magnetische lenzen, wordt bewezen dat de afgeleide coëfficiënten van alle aberraties van de tweede rang en derde orde perfect overeenkomen met formules uit de standaard elektronenoptische theorie.

In hoofdstuk 3 wordt de afbuigingsaberratietheorie voor standaardlenzen en afbuigers afgeleid. Door verstoringstheorie toe te passen op een systeem van rond-symmetrische elektrostatische en magnetische lenzen en afbuigers, worden relativistische afbuigingsbaanvergelijkingen en aberratiecoëfficiënten voor afbuiging tot de tweede rang en derde orde afgeleid. De formules voor de volgende specifieke configuraties worden ook gegeven: een combinatie van een elektrostatische en een magnetische afbuiger, twee elektrostatische afbuigers, en twee magnetische afbuigers.

In hoofdstuk 4 wordt de afbuigingsaberratietheorie ontwikkeld voor systemen met elektronenspiegels. Een niet-relativistische tijdsafhankelijke afbuigingstheorie wordt geïntroduceerd. Deze kan baanafwijkingen analyseren met kleine-hoekafbuigers en is toepasbaar op systemen van overlappende elektrostatische en magnetische velden en afbuigingsvelden. Afgeleide baanafwijkingen en aberratiecoëfficiënten voor elektronenspiegels en afbuigers worden berekend tot de tweede rang en derde orde.

In hoofdstuk 5 wordt een miniatuur-aberratiecorrector voorgesteld, bestaande uit dubbele magnetische afbuigers en dubbele elektrostatische spiegels, genaamd de S-corrector. De optische eigenschappen van een SEM met de voorgestelde S-corrector en een magnetische afbuiging van 50 mrad worden geanalyseerd. Een aanvullende configuratie met een post-afbuiging S-corrector wordt voorgesteld, waarbij laterale dispersie verdwijnt op het uiteindelijke beeldvlak van de SEM. Ontwerpvoorbeelden van miniatuur spiegels en afbuigers en een mogelijke configuratie van een SEM met de S-corrector worden gepresenteerd.

Numerieke berekeningen van aberratie-eigenschappen voor een miniatuur-elektronenspiegel en dubbele afbuigers worden uitgevoerd met de formules uit hoofdstukken 2 en 3. De geschatte combinatie-aberraties tussen afbuigers en spiegels bleken in de meeste gevallen verwaarloosbaar (0,2 nm) in vergelijking met de doelspotgrootte (1 nm bij 1000 V landingsspanning en 1,5 nm bij 100 V). Golfoptische berekeningen, inclusief alle combinatie-aberraties en overblijvende afbuigingsaberraties, resulteerden in spotgroottes van respectievelijk 0,976 nm en 1,367 nm. Hiermee is de haalbaarheid van een aberratie-gecorrigeerde LV-SEM aangetoond.

Chapter 1 Introduction

This chapter states the background and the motivation of this dissertation. The metrology methods of semiconductor patterns and dedicated scanning electron microscopes (SEMs), called critical-dimension SEMs, are reviewed. Next, the significance of low-voltage and high-resolution SEMs for recent semiconductor metrology is introduced. Decisive factors, including aberrations, and improvement methods for SEM resolution are explained briefly. Then, we discuss the history and features of known aberration correction methods and their problems. At the end of this chapter, we present the motivation and basic idea of a novel aberration corrector, which is composed of a miniature electron mirror, and state the scope of this dissertation.

1.1 The metrology method of semiconductor processes and a critical dimension scanning electron microscope (CD-SEM)

By downscaling semiconductor devices, the integration density of integrated circuits had been getting higher and higher according to Moore's rule until the late 2010s. Recently, the downscaling speed has decreased but has continued with the advent of extreme ultraviolet lithography (EUVL), whose wavelength is 13.5 nm. The minimum half-pitch of a semiconductor device has already reached less than 20 nm [1.1]. The half-pitch of DRAM will reach below 10 nm at the beginning of the 2030s [1.1]. Important geometries of semiconductor devices are called critical dimensions (CDs). Typical CDs include the line width of line and space patterns and the diameter of contact holes. In the development phase of devices, transmission electron microscopes (TEMs), which have 0.1 nm order resolution, are often used for measuring CDs and for checking fabricated structures. However, since silicon wafers must be destroyed to prepare TEM specimens, TEM measurements take too much time to measure CDs in high-volume manufacturing. Even for sampling measurements, since manufacturers must stop processing during measurements, it reduces the production volume of a certain period, and it increases cost and decreases profit. Therefore, "in-line" measurements, which are incorporated into the fabrication process, are significant.

Optical critical dimension (OCD), critical-dimension small-angle X-ray scattering (CD-SAXS), and critical-dimension scanning electron microscopy (CD-SEM) are used as significant in-line CD measurement methods. OCD and CD-SAXS are based on similar methods. OCD, which is also known as scatterometry, measures the spectrum of reflected diffraction light by repetition patterns. CD-SAXS measures the distribution of scattered diffraction X-ray intensity for an incident angle of X-ray. Users must prepare simulations of spectra and distributions by adjusting

geometries of a pattern model, such as line width, pattern pitch, pattern height, and angles of pattern edges, in advance. CD values are determined by comparing measured data with simulation data. The determined CD values are dependent on a simulated data library, and they are mean values of the illuminated area by light or X-ray. OCD measurement is much faster than other CD measurement methods, but it does not give CDs of local patterns. CD-SAXS provides much higher resolution due to the short wavelength of X-rays, and it offers information about internal structures of 3D patterns because X-rays penetrate wafers, but it still gives the mean CDs. In addition, since the incident angle of X-rays changes for a single measurement, CD-SAXS measurement is slower than other methods.

CD-SEM measurement is not based on simulation but directly on SEM images. Fig. 1.1 shows a schematic of an electron optical column of a typical CD-SEM. Primary electrons (PEs) are emitted from an electron source and accelerated by an electron gun. At least two condenser lenses form crossovers of the electron beam to tune both the probe current and aperture half-angle, and the objective lens focuses the beam and creates a small spot on the wafer. The beam is scanned on semiconductor patterns by scanning deflectors. Primary electrons penetrate patterns and are scattered several times. As a result, secondary electrons (SEs) emerge from the scattered area. SEs are detected by a detector and are converted into an electric signal, whose intensity is proportional to the number of detected SEs. The electric signals are converted to gradation values to make an SEM image.

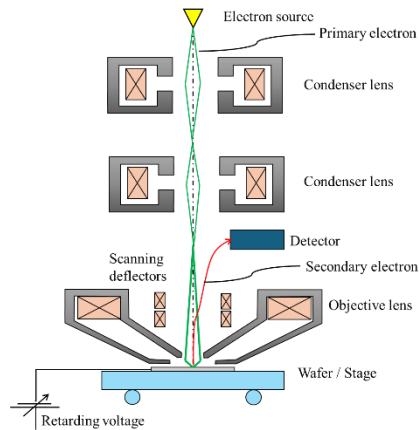


Fig. 1.1 Schematic of an electron optical column of a typical CD-SEM

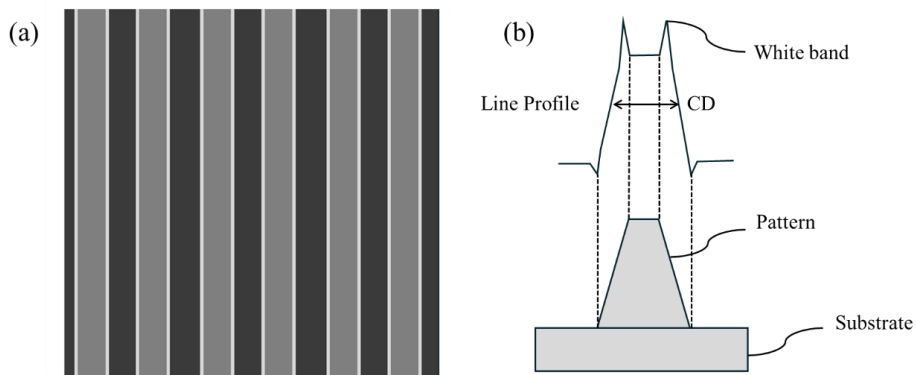


Fig. 1.2 Schematic of CD-measurement by a CD-SEM

(a): A SEM image of a line and space (LS) pattern. (b): A line profile of a LS image and schematic of a pattern structure.

A schematic of CD-measurement by a CD-SEM is shown in Fig. 1.2. Fig. 1.2 (a) shows a schematic of an SEM image of a typical line and space pattern. Fig. 1.2 (b) shows a schematic of the profile of gradation values of the SEM image, which is called a line profile, for a single line, and a schematic of the structure of the pattern. The penetration depth of the PEs, that is the interaction volume of PEs inside the specimen, and the yield of SEs are dependent on the materials of the specimen and the irradiation energy of PEs. However, when the PEs illuminate an edge of a pattern, the surface area of the specimen that faces the interaction volume of the PEs is larger than when the PEs illuminate a flat area of the specimen. As a result, when PEs illuminate the edge, SEs escape much more easily from the specimen and the signal intensity gets strong. This is called the edge effect, and it makes the edge region much brighter than other regions in an SEM image, see Fig. 1.2 (a). It results in strong peaks in the line profile around the edges, which are called white bands; see Fig. 1.2 (b). Due to the white bands, we can determine the position of the edges in SEM images easily. The definition of CD from an SEM image is dependent on the selection by users. A typical method is as follows. Detect the left and right edges of a line as the local maximum points of the corresponding region of the line profile. Detect the local minimum points on the left and right sides of the maxima. Search for the left side point that has a 50 % gradation. Repeat the search for the right side. Measure the distance between the half points of the left and right sides, as a CD value. However, there is no reason why the actual positions of the top and bottom edges of the patterns match with the maxima and the minima in the line profile. The CD-SEM is calibrated to certify the accuracy of CDs, using a standard calibration specimen of a line and space, whose line width and pitch are already

known. The CD-SEM measures CDs in real space and can give local CDs, that is, it can measure even an isolated pattern, in contrast to the fact that the OCD and the CD-SAXS measure only average CDs of repeating patterns in the illuminated area, comparing diffraction spectra or scattering distributions with the simulation data library. Due to these properties, the CD-SEM is used for obtaining tuning data for OCD measurement, for measuring local CD uniformity (LCDU) of the photoresist patterns in an area where lithography exposes by the same shot, and for measuring the line edge roughness of patterns. CD-SEMs measure CDs from SEM images automatically, including automatic identification of a region of interest to within a few 10 nm of precision, automatic alignment of the beam axis, and autofocus as preparation.

Recently, the most significant requirement for CD-SEMs is the improvement of measurement precision of CDs. So far, in general, the usual process margin is 10 % of the design value of the CD. The necessary precision of CD-SEM measurement has been said to be less than 10 % of the process margin, meaning smaller than 1 % of the design CD. If the minimum CD reaches 5 nm, the required precision of CD measurement by CD-SEMs is only 0.05 nm [1.2]. This measurement precision does not mean only the repeatability of measurements, which is the measurement error when a single CD-SEM measures the same pattern repeatedly, but also includes a tool-to-tool matching error, which is the difference among measured CDs of the same patterns by different CD-SEM machines.

1.2 Significance of a low voltage & high-resolution SEM

The most significant specification of the CD-SEMs is the precision of the CD-measurement, since users regard the CD-SEM as a measuring instrument. However, the CD-SEM is a special kind of scanning electron microscope. How do we think about a spec of a resolution for the CD-SEM? When the geometries of patterns get smaller, necessary CD-measurement sensitivity gets stricter, that is, even tinier changes of smaller patterns must be measured. In general, high sensitivity of the CD-measurement contradicts the high precision, since when geometries of measured patterns get smaller, requirement of the measurement precision gets stricter. However, even if the measurement precision is high, low CD-measurement sensitivity is insufficient for managing production yields of semiconductor devices. At least, sufficient high CD-measurement sensitivity is necessary. Therefore, resolution of the CD-SEM must be improved for measuring CDs of the sub-10 nm scale.

However, irradiation damage to the patterns of recent semiconductor materials, such as EUV resist, by the electron beam, is a serious issue. Since patterns are shrinking during the irradiation, CD-measurement gets unstable. Irradiation damage depends on the acceleration voltage of the beam on the sample surface. To reduce the damage of EUV resist,

the significance of low energy irradiation of the beam is reported [1.3]-[1.7]. In addition, the low landing energy of the beam is suitable not only for reducing irradiation damage, but also for obtaining rich surface information. Film thickness of EUV resist gets around 30-nm scales or less for 32 nm pitch process of line and space pattern, because of the depth of focus (DOF) of the EUV lithography [1.6]. In the near future, a high NA (numerical aperture) EUV lithography will be applied to manufacturing. For 16 nm pitch process, the desirable film thickness of the photoresist is 15 nm [1.6]. The electron beam penetrates the photoresist material and SEs are emitted from a certain area. On the other hand, emission areas of SEs depend on the landing energy of the PEs, since higher-energy PEs penetrates the sample deeper and interacts with materials strongly. For example, radii of emission area of SEs, whose intensity decays to 5% compared with the maximum, are about 16 nm for PEs of 800 eV, 6 nm for those of 300 eV, and 4 nm for those of 100 eV [1.3]. When pattern pitch becomes 16 nm, that is pattern geometries of the EUV resist are 8 nm linewidth, 8 nm space distance, and around 15 nm film thickness or less. If PE energy is set to be around 1000 eV, an interaction region is comparable to both the film thickness and the pattern pitch. It means that landing PEs reaches to an underlayer of patterns and to adjacent lines, even if the spot size of the PEs is sufficiently small. SEM images include the information of signal SEs, which are emitted from the underlayer and the adjacent lines. Then, the underlayer and the adjacent lines affect the measured CD of the target line. To suppress and avoid it, it is necessary that PEs of low landing energy, such as 100 eV, are used as a probe of the CD-SEMs. However, there is the trade-off between the low landing energy and the small spot size of the PEs, which is explained in next section.

1.3 Decisive factors of a standard SEM resolution

The limit of the spot size of the PEs is determined by diffraction, the source size, and the aberrations.

Diffraction

First, we explain the diffraction. The diffraction is the spatial distribution according to wave optics. An electron has the duality of wave and particle, that is the probability of existence follows the Schrödinger equation of quantum mechanics. Since the wavelength of the electron wave is much smaller than the typical length scale of changes in the electro-magnetic field in a usual SEM, we can apply the so-called eikonal approximation to the Schrödinger equation. The solution of the Schrödinger equation is then given by the integral form similar to the Fresnel-Kirchhoff integral of the theory of wave optics of light [1.8]. As a result, the same diffraction phenomena as for light occurs for electrons by using a beam limitation aperture. Diffraction is inevitable, and it limits the minimum beam spot size, when we can ignore the source-size and the aberrations. Usually, circular apertures are used in many SEMs, and the distribution in the image plane, which is special X-Y plane, where the beam is focused, is known as:

$$S(r_i) = 2\pi I_p \left(\frac{\alpha_i}{\lambda_i}\right)^2 \text{sinc}^2\left(\frac{\alpha_i}{\lambda_i} r_i\right), \quad (1.1)$$

where r_i is the distance from the origin, I_p is a total probe current, α_i is absolute value of the aperture half angle of the beam in the image plane, λ_i is the de Broglie wavelength of electrons in the image plane, and

$$\text{sinc}\left(\frac{\alpha_i}{\lambda_i} r_i\right) = 2 \left(\frac{J_1\left(2\pi \frac{\alpha_i}{\lambda_i} r_i\right)}{2\pi \frac{\alpha_i}{\lambda_i} r_i} \right), \quad (1.2)$$

where $J_n(x)$ is n -th order Bessel function of the first kind. J_1 has several zero points, where the value of the function gets zero. The first zero point of Eq. (1.1) is given by

$$r_{\text{zero}} = 0.609835 \cdots \times \frac{\lambda_i}{\alpha_i}. \quad (1.3)$$

According to the conventional criterion, called Rayleigh criterion of the optics of light, the diffraction limited spot, which is obtained by ignoring the source-size and the aberrations, has spatial “resolution” of r_{zero} . The diameter of the spot is conventionally considered as the same size as r_{zero} , that means the radius of the spot is a half of r_{zero} . In addition, the probe current inside of the radius r_i is given by

$$I_F(r_i) = I_p \left[1 - J_0^2\left(2\pi \frac{\alpha_i}{\lambda_i} r_i\right) - J_1^2\left(2\pi \frac{\alpha_i}{\lambda_i} r_i\right) \right]. \quad (1.4)$$

The ratio of probe current to the total probe current inside of the half of the first zero radius, $r_{\text{zero}}/2$, is about 58.84 %.

Source-size

We consider the effect of the electron source-size on the beam spot size. When a large current beam is used as a probe of CD-SEMs, the amount of the signal electrons in a unit time increase, it reduces the acquisition time of SEM images and improves throughput of measurements. That is why we want to use an electron source, which provides large emission current. But to make the beam spot smaller, we want to use a small source and small deviation of kinetic energy of emitted electrons, since source-size, which is demagnified by the electron optical system, contributes to the spot size. The source-size formula for a given probe current is determined by

$$d_I = \frac{2}{\pi \alpha_i} \sqrt{\frac{I_p}{B_r \Phi_i}}, \quad (1.5)$$

where Φ_i is the landing energy of PEs, and B_r is called reduced brightness, whose unit is given by $\text{A}/\text{m}^2 \cdot \text{sr} \cdot \text{V}$. It is the probe current, which is emitted from a unit area of the (virtual) source surface, and is measured in a unit solid angle, and is normalized by the acceleration voltage. The reduced brightness depends on the properties of the material and emission temperature of the sources. An energy spread of emitted electrons also mainly depends on the temperature of the sources, such as $\Delta E \propto k_B T$, where k_B is the Boltzmann constant and T is the absolute temperature. The energy spread contributes to the spot size via the chromatic aberration of the electron optical system.

In addition, not only material properties, but also the effects caused by coulomb interactions contribute to the virtual source size and the energy spread. In general, when emission current gets large, coulomb interactions among emitted electrons gets significant. The Coulomb interaction effects, called the Boersch effect and the trajectory displacement effect, generates lateral and longitudinal displacement of electrons by collisions among electrons, and repulsion due to negative charges. It also enlarges the energy spread of the PEs.

Aberrations

Aberrations are trajectory displacement caused by electric and magnetic field distribution itself. In usual SEMs, which are composed of rotationally symmetric electric and magnetic fields, the most significant aberrations are the spherical aberration and the axial chromatic aberration. In rotationally symmetric fields, the Coulomb force by the electrostatic field, and the Lorentz force by the magnetic field, to the electrons, depend on the lateral position of electron trajectories. Their dependence is series expansion of the lateral distance of electrons from the optic axis, of odd-order, and the forces directs in the radial direction:

$$F_r = F_1 r + F_3 r^3 + F_5 r^5 + \dots \quad (1.6)$$

As is well-known, the first-order component F_1 causes the lens effect. When only the geometrical trajectories of the electrons are considered, all electrons, which start at the axial object point, intersect with the optic axis at the so-called axial image point. By focusing the PEs on the sample surface, an infinitesimal spot is formed by the first-order force. However, higher order force, such as third order force, makes deviation of the electron trajectories, whose dependence is nonlinear on the lateral electron position from the optic axis. By the third-order force component, which is the second strongest component, causes the third-order spherical aberration to the PEs in the sample surface.

One of the other significant aberrations for normal SEMs is the axial chromatic aberration. Energy of PEs spreads because of thermal fluctuation of the electron source. The lens effect is determined by momentum transfer to PEs. Electrons of higher/lower energy receive relatively smaller/larger momentum transfer, compared with the momentum transfer of the mean energy electrons, since their initial speed is different from that of the mean energy electron. As a result, even if the first-order force of electromagnetic fields is adjusted to make a focus of mean energy electrons on the sample, electrons of higher and lower energy are not perfectly focused on the sample. It makes the trajectory deviation, which is called the axial chromatic aberration. Other aberrations of a standard SEM are called parasitic aberrations, which stem from incompleteness of the electron optical system. The causes are, for example, machining error of polepieces or electrodes, assembly error of lenses, and misalignment between the PEs and lenses. The resulting

primary parasitic aberrations are the chromatic dispersion, the axial coma, and the axial astigmatism. Usually, these parasitic aberrations are not considered when we calculate the minimum spot size of the electron optical system, because parasitic aberrations are corrected by tuning alignment of lenses and adjusting a stigmator.

Spot size definition

Usually, the factors of the resolution of the standard SEM are diffraction, the demagnified source-size, the spherical aberration, and the axial chromatic aberration. However, the contributions of these factors to the spot-size are complicated, because of wave optical properties of electrons. By the wave optics of electrons, the distribution of the beam spot is given by the convolution of the electron source intensity distribution \hat{S}_E , which is mapped into the sample surface by an electron optical system, and the generalized point spread function of the electron beam PSE_{EX} :

$$I(x, y) = \hat{S}_E * PSE_{EX}, \quad (1.7)$$

where the generalized point spread function (PSF) is given as follows[1.9]:

$$PSE_{EX}(x, y) = \int_{-\infty}^{\infty} |FT[G(v_x, v_y; E)]|^2 P(E) dE. \quad (1.8)$$

It is the integral with respect to the energy of PEs. $P(E)$ means an energy distribution of PEs. Usually, Gaussian distribution is used as a form of $P(E)$. For the other factor of the integrand, $FT[G]$ means a two-dimensional Fourier transformation of G^1 :

$$FT[G(v_x, v_y)] = \iint_{-\infty}^{\infty} G(v_x, v_y) \exp[2\pi i(xv_x + yv_y)] dv_x dv_y, \quad (1.9)$$

where spatial frequencies v_x and v_y are related to the electron's illumination angle ω at the sample via

$$v_x = \frac{\omega_x}{\lambda_i}, \quad v_y = \frac{\omega_y}{\lambda_i}, \quad (1.10)$$

and λ_i is wavelength of electrons. The generalized pupil function is given as follows:

$$G(v_x, v_y; E) = g_a(v_x, v_y) \exp\left[-\frac{2\pi i}{\lambda_i} W(v_x, v_y; E)\right], \quad (1.11)$$

where g_a is the pupil function, which represents a shape of a diaphragm. W is called a wave aberration. Even if the wave aberration is given, we must calculate the Fourier transformation of the generalized pupil function and perform integral with respect to energy of PEs to obtain the generalized PSF and calculate convolution of the generalized PSF and the source intensity distribution. Eq. (1.7) only gives a beam intensity distribution. There are two typical criteria for the beam spot size. One is called 59 % diameter d_{59} . It is the diameter of the two-dimensional beam intensity distribution, which includes 59 % of the whole beam current inside of that diameter [1.9]. It is interpreted as an extension of the Rayleigh criterion, because without aberration, with infinitesimally small source, and using round

¹ In this thesis, we define the Fourier transformation by Eq. (1.9). The sign factor of the argument of the exponential function is positive, such as $\exp[2\pi i(xv_x + yv_y)]$. For the inverse Fourier transformation, the sign factor is negative, such as $\exp[-2\pi i(xv_x + yv_y)]$.

symmetric aperture, the beam intensity distribution must be same as Eq. (1.1). Haider et al. calculated a beam intensity distribution based on the wave optical simulation using Eqs. (1.7) to (1.11) and extracted d_{59} for given aberrations. However, because of the simulation time, the wave optical calculation is not so useful especially when we seek suitable parameters of a design of an electron optical system, such as lens geometries and position of the beam crossovers. In addition, because of the Fourier transformation, the contribution of each aberration to the spot size is unclear. Instead of the wave optical calculation, Barth and Kruit suggested a useful approximation formula of the beam spot size. They also introduced a different criterion of the beam spot size, which is called FW50 [1.10]. FW50 is considered as the spot diameter, inside of which includes 50 % of the whole current of the PEs. They gave a much simpler formula for FW50, which reproduces the result of 50 % current diameter of the spot, which is calculated by wave optical calculation. This formula is called the root power sum (RPS) [1.10]. The RPS ignores parasitic aberrations, and its factors are the diffraction, the source size, the spherical aberration, and the axial chromatic aberration. The RPS formula of FW50 is given as follows [1.10]:

$$d_{FW50} = \left[\left(d_I^{1.3} + \left\{ (d_A^4 + d_S^4)^{\frac{1}{4}} \right\}^{1.3} \right)^{\frac{1}{1.3}} + d_C^2 \right]^{\frac{1}{2}}, \quad (1.12)$$

where d_I is the estimate of the source size given by Eq. (1.5), which corresponds to the full width of half maximum (FWHM) of the distribution, and the estimate of the diffraction is given by

$$d_A = 0.54 \frac{\lambda_i}{\alpha_i}, \quad (1.13)$$

the estimate of the spherical aberration is

$$d_S = 0.18 C_{Si} \alpha_i^3, \quad (1.14)$$

and that of the axial chromatic aberration is

$$d_C = 0.6 C_{Ci} \alpha_i \frac{\Delta\Phi}{\Phi_i}, \quad (1.15)$$

C_{Si} is the spherical aberration coefficient, C_{Ci} is the axial chromatic aberration coefficient, and $\Delta\Phi$ is the FWHM of the potential distribution of PEs.

The FW50 formula in Eq. (1.12) gives a good approximation of the spot diameter, inside of which includes 50 % of the whole current of PEs, calculated by the wave optical calculation using Eqs. (1.7) to (1.11). In this thesis, for simplicity, we use Eq. (1.12) as a beam spot size, basically.

In a practical system of an SEM, the beam spot size is not the sole decisive factor of quality of SEM images. There are many factors, such as SE yield from sample, statistical error of PE and SE emission, quantum noise of detector system, electrical noise of circuits and image vibration. However, when we consider a conceptual design of the electron

optical system, problems by these factors are assumed to be solved, because we would like to concentrate on a performance of the electron optical system about the resolution.

According to the decisive factors of the FW50, the control parameter of each factor is aperture half angle α_i . As long as probe current is fixed, if α_i gets larger, the diffraction and the source-size get smaller. However, the spherical aberration and the axial chromatic aberration get larger. Optimal aperture half angle, which gives minimum FW50 value, exists.

1.4 Resolution improvement method

To make a beam spot size smaller, by Eq. (1.12), we should think about the methods to reduce value of each decisive factor. We assume that probe current and irradiation voltage are determined, that is, I_p and the wavelength are fixed. Under this condition, fundamental methods to improve beam spot size are considered as follows:

1. Deform diffraction distribution by annular illumination.
2. Use brighter electron source for smaller source-size.
3. Reduce energy spread of PEs to make the axial chromatic aberration smaller.
4. Cs and Cc reduction by improving the objective lens design.
5. Aberration correction.

Here, we give brief explanation for each

For the first one: Diffraction, spread of the beam spot by the diffraction is inevitable. In a transmission electron microscope (TEM), a special shape of aperture is used for improving transfer limit of information, which is restricted by the diffraction, for example using a ring-shaped aperture for an annular illumination. However, it does not improve SEM resolution. The center part of the ring-shaped aperture is shut by a material. Open part is ring-shaped, see Fig. 1.3 (a). The narrower open ring is, the narrower the main peak of the diffraction distribution is, but the larger side-lobes are, and the smaller the probe current is, see Fig. 1.3 (b). In practice, irradiation damage and charging of the center part by PEs are inevitable problems, because the aperture is irradiated by much more PEs to obtain sufficient probe current. Despite the main peak of the diffraction distribution getting narrower by the annular illumination, side-lobes get stronger. Since the main peak of the beam spot gets narrower, the SEM resolution seems to be improved, apparently. However, since the diameter, which includes 50 % or 60 % of the total current gets larger according to the

shading rate of the ring-shaped aperture, see Fig. 1.3 (c), the SEM resolution rather worse than that of a normal circular aperture.

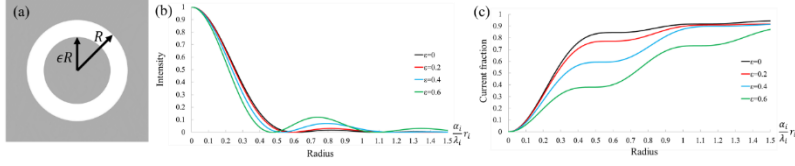


Fig. 1.3 The ring-shape aperture, diffraction distribution, and current fraction of the beam spot by the annular illumination. (a) The schematic of the shape of the ring aperture. ϵ means a rate of a radius of the shading part. (b) The Intensity distribution of the beam spot for different values of ϵ . (c) The current fraction about the total current inside the designated radius for different values of ϵ .

For the second one: Electron source, according to Eq. (1.5), when the electron source, whose reduced brightness B_r is larger, is used, the source-size gets smaller for the given value of the probe current. Usually, Schottky emitters are used for many CD-SEMs. Cold field-emission (CFE) sources are not only brighter, but also have smaller energy spread of emitted electrons, than the Schottky source. However, it is difficult to obtain sufficiently stable probe current from CFE sources. Electron emission rate of CFE sources depends on their surface state and quality of vacuum, since it needs to keep work function of the sources. Very small outgas changes the surface state and the emission current decays easily. CFE sources have been applied to recent inline defect review and inspection SEMs for semiconductor process [1.11]. However, since fluctuation of the probe current is impeditive to stable CD-measurements, CFE sources have not been used for recent CD-SEMs yet.

For the third one: Energy spread, there are two ways to reduce energy spread of PEs. One is to use CFE electron source, since energy spread of CFE source is about half of that of Schottky emitters. The problem is unstable emission of CFE sources. The other way is to use a monochromator. Monochromators remove electrons, whose energy is deviated from the nominal energy, from PEs, as follows. It gives lateral displacement to electron trajectories, which is proportional to energy deviation of PEs. A very narrow slit or small aperture is placed in a convergent plane of PEs. Electrons of deviated energy stop at the slit, and electrons very close to the nominal energy can go through it. Several types of monochromators are proposed [1.12], and some of them are installed into multipurpose SEMs. However, since the monochromator removes electrons, it reduces the probe current so much. Since CD-SEMs often use the lowest probe current possible to CD-measurement, such as several tens of picoamperes, to make beam spot smaller, the monochromator is not suitable for CD-SEMs.

For the fourth one: Lens design improvement, so far, it is a conventional way to improve SEMs resolution. In SEMs, a lens of the most significant aberrations is an objective lens. In history of CD-SEMs, breakthroughs in lens design have been achieved by the shortening of the working distance, which is a distance between the specimen and the pole piece of the objective lens, and the introduction of a decelerating electric field to the sample [1.13]. The spherical aberration and the axial chromatic aberration are roughly proportional to the cube and to the square of the focal length of the objective lens, respectively.

Using the decelerating electric field, the acceleration voltage of the electric gun can be increased without changing the irradiation voltage of PEs to the sample. Then, the speed of PEs traveling inside of the magnetic field of the objective lens gets higher, and it reduces the axial chromatic aberration. In addition, since decelerating field acts in z -direction, mainly, an irradiation angle at the sample, gets larger. When the same designated irradiation angle is set, lateral displacement of the trajectories of PEs from the optic axis, inside the magnetic field of the objective lens, gets smaller, compared with that without the decelerating field. Since the axial spherical aberration is proportional to the cube of the lateral displacement of the lens axis, the decelerating field reduces the spherical aberration, as well.

These fundamental improvement methods of the objective lens have been investigated for a long time. Recently, it almost reaches limitation, because of a saturation of the ferromagnetic material of the objective lens and outstanding voltage.

For the final one: Aberration correction, it is discussed in the next section.

1.5 Aberration correction

Since aberrations of the optical system restrict the beam spot size, aberration correction is a very important but is a very old problem. Originally, Scherzer gave so-called Scherzer's theorem [1.14], in 1936. It was expanded to relativistic cases by Prekšzas and Rose [1.15]. Scherzer's theorem tells that round symmetric electron lenses always have nonzero spherical and chromatic aberrations, based on the following assumptions.

1. Electric and magnetic fields are static.
2. The system has no on-axis electrodes.
3. Potentials, fields, and their derivatives are smooth and continuous.
4. All elements are rotationally symmetric.
5. Electrons are never reflected.

Accordingly, Scherzer showed aberration correction to be theoretically possible by violating at least one of the above assumptions, and he proposed one concrete structure of corrector using octopole-type lenses to correct the spherical aberration [1.16][1.17]. Since then, many types of aberration correctors have been proposed and constructed.

Here, we introduce several aberration correction methods for SEMs which violate each assumption. For violating the first assumption, the method is introducing time-dependent fields. In general, it is difficult to apply time-dependent fields in high-resolution electron microscopes, since much stable high-frequency power sources are required, and electromagnetic fields must be precisely controlled. Recently, negative spherical aberration lenses, caused by so-called ponderomotive forces, are proposed by Uesugi et al. [1.18]-[1.20]. In these proposals, high intensity optical laser beam collides with an electron beam. Electron beam receives force, which is proportional to the laser power. They showed that ponderomotive force generated negative third-order spherical aberration under suitable setting of the optical system and a laser of Bessel beam or Laguerre-Gaussian beam, theoretically. Since electromagnetic waves are time-dependent oscillating electric field and magnetic field, which are perpendicular to each other, ponderomotive lens are classified into the aberration correction method using time-dependent electromagnetic fields.

For violating the second assumption, correctors with on-axis electrodes have been proposed [1.21]-[1.24]. It is theoretically shown that an electrostatic lens, which includes an on-axis electrode, contributes to negative spherical aberration. However, since on-axis electrode shut a part of electron beam around the optic axis, it also acts as a kind of a ring shape aperture. Because of not only damage, charging, and contamination by irradiation, but also large side-lobe of the beam spot by the diffraction of the ring shape aperture, which was explained in section 1.4, on-axis electrode has not achieved the resolution improvement, yet.

For violating the third assumption, foil lenses with discontinuous electric fields have also been proposed [1.25][1.26]. However, they were not successful because of heating, charging, and contamination by PEs at the foils.

The methods for violating the fourth assumption are the most famous. They are called multipole-type aberration correctors, which generate non-rotationally symmetric electromagnetic fields, called multipole fields. After many years of development, they were finally successfully applied in the 1990s [1.27]-[1.31]. Nowadays, correctors using a hexapole doublet for correcting the spherical aberration are commercially available and widely used in transmission electron microscopes (TEMs) and scanning transmission electron microscopes (STEMs). In addition, wire-type magnetic hexapole correctors, which are composed of specific configuration of current wires, are proposed [1.32]-[1.36].

Other types of multipole correctors have also been proposed. One of them, a non-dispersive Wien filter, has been proposed but not demonstrated [1.37]. Pure electrostatic chromatic aberration correctors have been proposed by

Weißbäcker and Rose [1.38][1.39] and by Henstra *et al.*, [1.40]-[1.43]. These correctors consist of electrostatic quadrupoles and round einzel lenses. The former type consists of one quadrupole and three superimposed units of quadrupoles and einzel lenses. The latter type consists of four quadrupoles and five superimposed units. The latter type was further improved by Baranova *et al.* [1.44][1.45].

Especially for LV-SEMs, it is necessary to correct both spherical and chromatic aberrations. Both spherical and chromatic aberrations of an SEM have been corrected by using a quadrupole-octopole corrector [1.27][1.28]. However, practical correctors consist of complicated dodecapole electromagnetic elements to generate not only quadrupole and octopole fields but also dipole and hexapole fields to correct lower order parasitic aberrations of the corrector unit itself. Reducing these parasitic aberrations requires quite precise machining and assembly, but they never vanish. Moreover, methods of tuning electromagnetic fields are complicated. That is, various aberrations must be measured, analyzed, and fed back to appropriately adjust the settings of voltages and currents of the corrector [1.46][1.47]. As commercial products, CD-SEMs for measuring photomask have been sold by Holon co., Ltd. [1.48], whose Cs/Cc correctors were developed by CEOS GmbH [1.49]. Since photomask is composed of insulator materials, to suppress charge-up of the specimen, it is difficult to use strong decelerating voltage and very low-voltage observation. Photomask CD-SEMs cannot realize high resolution compared with high resolution CD-SEMs. Then, Cs/Cc corrector improves the resolution for the irradiation voltage to the specimen around 1.5 keV [1.49].

The last possibility of an aberration corrector is an electron mirror. Theoretical studies of aberration correction by electron mirrors and experimental verification were done [1.50]-[1.56]. Mirror correctors are mainly used for low-energy electron microscopes (LEEMs) [1.57]-[1.62]. They are expected to be much simpler than multipoles, and their main parasitic aberration is astigmatism because they consist of rotationally symmetric electrodes just like normal electrostatic lenses. Standard stigmators are sufficient to correct it.

The problem with installing an electron mirror in an electron microscope is that it must be installed with bending magnets, so-called beam separators, to separate the beam reflected by the mirror from the incident beam [1.55]-[1.62]. One of the possible configurations of an SEM with a normal-scale mirror corrector and a bending magnet is shown in Fig. 1.4. Since the electron mirror is produced by machining, its size is similar to that of a condenser lens or an objective lens. The beam path must therefore be bent at a large angle, in the example shown in Fig. 1.4, 90 degrees. In general, this deflection generates much larger energy dispersion and second-order geometrical aberrations than the spherical and chromatic aberrations of the objective lens. To eliminate these aberrations, the beam separator has to be specially designed on the basis of the theory of curved-axis optics [1.63]. An example is the system that was designed and built for the SMART project [1.62][1.64][1.65]. However, to compensate unexpected aberrations due to

imperfection of machining and assembly of the separator, multipole elements for generating quadrupole and hexapole fields were still necessary [1.66]-[1.68]. A LV-SEM with a mirror corrector using a beam separator (which was designed based on the same concept as the SMART project) was also developed [1.69]. It was reported that sub-nanometer resolution was achieved at 100 eV [1.69][1.70].

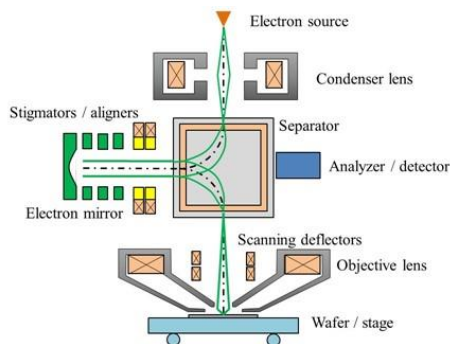


Fig. 1.4. Schematic of a possible SEM configuration with a normal-scale mirror corrector. It is depicted by referring to the references [1.62]-[1.66]. An electron beam emitted from an electron source is focused on the entrance of a beam separator by a condenser lens. The beam is bent 90° by the separator and directed to an electron mirror. The mirror reflects the beam straight back while adding aberrations that are used for correcting those of an objective lens. The separator then deflects the reflected beam again by 90° to the objective lens. The aberration-corrected beam forms a small spot on the sample and is scanned over the sample by the scanning deflectors. Stigmators and aligners compensate for the astigmatism and misalignments of the beam. The secondary electrons from the sample are deflected toward the opposite side of the mirror, where they are detected by an analyzer and a detector.

Rempfer *et al.*, proposed and built a system with a beam separation deflector that deflected the beam only over an angle of 20-30 degrees [1.55][1.56]. To reduce the deflection aberrations further, deflection occurs only in image planes. Part of the optics is now built around the inclined beam. The electron source and the sample are next to each other. The latter design decision necessitates a fairly large separation distance between the mirror's entrance and exit beam. For a system in which the sample is a 300 mm semiconductor wafer, as is our design goal, this is not very practical. We will take the principle of a small angle beam separation deflector but implement it in a different manner: by adding a second mirror, the beam emerges from the corrector in the same direction as it entered. This allows the electron source, condenser system, the objective lens, and sample stage to remain unchanged. The corrector then fits in an extension of the electron optical column, just like a multipole corrector.

1.6 Problem of aberration correctors and suggestion

In section 1.5, we discussed already-known aberration correction methods. The methods, which have proven track records, are a multipole-type corrector and a mirror corrector. Typical problems of both types are summarized as cost, size, and difficulty of fine-tuning. Of course, precise machining of the corrector and stable power supply of multi-channels increase manufacturing cost, and the price of the aberration-corrected CD-SEM, drastically. In addition, the size of the correctors causes problems. Whether the Cs/Cc corrector is multipole-type or mirror-type, when the corrector is installed, the size of CD-SEM column gets larger and longer. Cs/Cc corrector is effective to correct aberrations of low-voltage SEM. The range of Irradiation voltage of CD-SEM is from a few 100 eV to around 10 keV. Cs/Cc corrector cannot be used for voltages larger than a few keV. Even if the aberration corrector is turned off, a balance of the electron optical conditions, such as positions of crossover, the probe current, the aperture angle, is not kept because of the wasted space. As a result, when the corrector is turned off, the resolution of CD-SEM gets worse than that of the normal CD-SEM, especially for high irradiation voltage range. The final problem is tuning of correctors. A multipole-type corrector generates parasitic aberrations due to manufacturing tolerances. It is necessary to tune strengths of many multipole fields to correct not only the spherical and the chromatic aberrations, but also parasitic aberrations, which are generated by the excitation of the primary fields to correct the spherical and the chromatic aberrations. To correct parasitic aberrations, which are mainly lower-order errors, such as the second-order axial aberrations, the astigmatism, the defocus, and the misalignments of the corrector and the objective lens, specific fields to counter the errors are excited and tuned, but they generate additional parasitic aberrations, as well. Then, complicated fine tuning of many kinds of multipole fields, as if patching over a patch, is necessary. A mirror-type corrector has a similar problem of tuning a beam separator. A beam separator causes large parasitic aberrations according to the incident angle and the position of the beam to the separator and those to the mirror. To adjust it, precise tuning and high stability of the beam is required, since if the trajectory of the beam fluctuated before reaching the beam separator, it needs to readjust the separator. The causes of difficulty of tuning the correctors are their high sensitivities of parasitic aberrations to the incident beam trajectory error and manufacturing error, due to complicated structure of multiples and large bending angle of the separator. We think that these problems stem from the large size and complicated structure of the correctors, mainly. However, even if small multipole corrector can be fabricated, it might make sensitivities of parasitic aberrations higher, because bore size of poles rules sensitivities, and it shall not be a solution. On the contrary, in a mirror-type corrector, the significant undesirable aberrations are caused by large bending angle such as larger than a few-10 degrees, because it is necessary to install a standard-size electron mirror. Recently, micro-electro-mechanical systems (MEMS) have advanced considerably. For example, micro-fabrication

technology for semiconductor devices is applied to make aperture arrays and electrostatic lens arrays for multi-beam SEMs [1.71]-[1.73], multi-beam lithography [1.74]-[1.76], and multi-electron sources [1.77][1.78]. MEMS should therefore make it possible to realize miniature-scale mirrors as well. As a result, it will be possible to reduce the deflection of the electron beam even further to suppress the undesirable aberrations sufficiently small. It shall reduce not only manufacturing costs but also the size of the corrector unit drastically.

1.7 About simulators for design

To suggest a conceptual design of novel correctors, we should calculate aberration properties numerically to predict performance of aberration correction, that is the beam spot size after correction. In general, ray tracing calculation is often used for investigating a beam property. It is a method to calculate their trajectories under given electric and magnetic fields, and initial conditions of the electrons, by solving equation of motion of electrons, numerically. Accuracy of the trajectories depends on fineness of mesh points and accuracy of calculated electric and magnetic fields. The electron speed gets quite low around the reflection point inside the mirror fields and the electron finally stops and is reflected. For such very low-speed electrons, the calculation errors of fields have a significant impact on the accuracy of the trajectory. In addition, to find aberration correction conditions by changing mirror electrode voltages, and deflector excitations, the field strength at mesh points must be re-calculated. Even when we make a focus with mirror at a specific position, iterative calculations of field strength and trajectories are necessary. Although ray tracing has the advantage of being able to calculate trajectories in an arbitrary system, the burden of calculation is heavy, and it is not suitable for iterative calculation such as for searching correction conditions.

Dedicated simulators for calculating aberration coefficients are desirable. For the system of standard lenses and deflectors, several simulators using aberration integral formulae based on perturbation theory are commercially available, for example see the reference [1.81]. For mirror aberration calculation, a software based on differential algebra method is commercially available [1.81]. However, TU Delft does not have licenses. Prior research shows ideas and methods to derive aberration integral formulae for electrostatic mirrors, and for the system composed of standard lenses and deflectors. We have started by investigating perturbation theory and deriving aberration integral formulae and have created a simulator for calculating aberration coefficients for the mirrors and the deflectors to design a miniature mirror corrector.

1.8 Scope of the dissertation

This dissertation is organized into 6 chapters as follows. From Chapter 2 to Chapter 4, the aberration theory of electron optical systems with electron mirrors and small-angle deflectors are discussed. This can be used for conceptual design of the novel corrector system discussed in Chapter 5, and the conclusion of the dissertation is given in Chapter 6.

Chapter 2 discusses aberration theory of electron mirrors, in which the main parameter is not the coordinate of the optic axis, but the time. This theory avoids divergence of the slope of the electron trajectory at the reflection by the mirrors and gives theoretically correct formulae of aberrations, which can be calculated numerically. This theory is called a time-dependent perturbation theory. It was originally studied by Preikszas and Rose [1.68]. The original works discussed on- and off-axis aberrations of pure electrostatic mirror. Rose gave the paraxial properties of systems in which electrostatic mirrors and round symmetric magnetic fields are superimposed. In chapter 2 we extend this to both on- and off-axis aberration formulae for such systems in which electrostatic mirrors and round symmetric magnetic fields are superimposed. The detailed review of basic theory, derivation of aberration formulae including expanded part and theoretical validation are discussed.

Chapter 3 describes aberration theory of electron optical systems which are composed of round symmetric electrostatic and magnetic lenses, and small-angle electrostatic and magnetic deflectors. Such theories were studied by several groups from 1970s to 1990s. Since the works are old and difficult to trace, the author derived the aberration formulae of small-angle deflection system. This theory gives a method for calculating small-angle deflector aberrations.

Chapter 4 discusses a time-dependent aberration theory of systems which are composed of electrostatic mirror, round symmetric magnetic fields, and small-angle electrostatic and magnetic deflectors. This theory gives aberrations even when all fields are superimposed.

Chapter 5 discusses the principles and conceptual designs of novel aberration corrector systems which are composed of miniature electron mirrors and small-angle deflectors. Numerical calculation of electron optical properties is given. Expectations and issues are described.

1.9 References

- [1.1] [INTERNATIONAL ROADMAP FOR DEVICES AND SYSTEMS™ \(IRDS\) 2023 UPDATE METROLOGY](#), (accessed August 13, 2024).
- [1.2] Z. Wang, K. Sakai, Y. Ebizaka, S. Masumi, M. Makoto, High-accuracy, high-speed, and smart metrology in the EUV era, Proc. SPIE 11325 (2020) 113251Q-1.
- [1.3] Zh.H. Cheng, H. Dohi, S. Hayashi, K. Hirose, H. Kazumi, Application of aberration corrected low voltage SEM for metrology and inspection, Proc. SPIE 10959 (2019) 1095922-1.
- [1.4] M.T. Postek, et al., Ultra-low landing energy scanning electron microscopy for nanoengineering applications and metrology, Proc. SPIE 11467 (2020) 114670Q-1.
- [1.5] G.F. Lorusso, The Unavoidable Renaissance of Electron Metrology in the Age of High NA EUV, Proc. SPIE 11611 (2021) 1161127-1.
- [1.6] G.F. Lorusso, et al., Metrology of Thin Resist for High NA EUVL, Proc. SPIE 12053 (2022) 120530O-1.
- [1.7] M. Zidan, et al., Low-Voltage Aberration-Corrected SEM Metrology of Thin Resist for High-NA EUVL, Proc. SPIE 12053 (2022) 120530P-1.
- [1.8] P. Hawkes, E. Kasper, Principle of Electron Optics, vol. III, Wave optics, Academic Press.
- [1.9] M. Haider, S. Uhlemann, J. Zach, Upper limits for the residual aberrations of a high-resolution aberration-corrected STEM, Ultramicroscopy 81 (2000) pp. 163-175.
- [1.10] J. E. Barth, P. Kruit, Addition of different contributions to the charged particle probe size, Optik 101(3) (1996) pp. 101-109.
- [1.11] [Applied Materials Breakthrough in Electron Beam Imaging Technology Accelerates Development of the World's Most Advanced Computer Chips | Applied Materials](#), (accessed August 13, 2024).
- [1.12] P.W. Hawkes, The correction of electron lens aberrations, Ultramicroscopy 156 (2015) A1-64.
- [1.13] Y. Ose, M. Ezumi, H. Todokoro, Improved CD-SEM optics with retarding and boosting electric fields, Proc. SPIE 3677 (1999) 930-939.
- [1.14] O. Scherzer, Über einige Fehler von Elektronenlinsen, Z. Physik 101 (1936) pp.593-603.
- [1.15] D. Preikszas, H. Rose, Procedures for minimizing the aberration of electromagnetic compound lenses, Optik 100 (1995) pp.179-187.
- [1.16] O. Scherzer, Sphärische und chromatische Korrektur von Elektronen-Linsen, Optik 2 (1947) pp.114-132.
- [1.17] H. Rose, Historical aspects of aberration correction, J. Electron Microsc. 58 (2009) pp.77-85.
- [1.18] Y. Uesugi, Y. Kozawa, S. Sato, Electron Round Lenses with Negative Spherical Aberration by a Tightly Focused Cylindrically Polarized Light Beam, Phys. Rev. Applied 16 (2021) L011002.

- [1.19] Y. Uesugi, Y. Kozawa, S. Sato, Properties of electron lenses produced by ponderomotive potential with Bessel and Laguerre-Gaussian beams, *J. Opt.* 24, (2022) 054013.
- [1.20] Y. Uesugi, The properties of ponderomotive lenses, *Adv. Imaging Electron Phys.* 228 (2023) pp.1-41.
- [1.21] A. Takaoka, R. Nishi, H. Ito, Low-aberration optics for large-angle beam with unit core lenses, *Optik* 126 (2015) pp.1666-1671.
- [1.22] A. Khurshed, W.K. Ang, On-Axis Electrode Aberration Correctors for Scanning Electron/Ion Microscopes, *Microsc. Microanal.* 4 Suppl. 21 (2015) pp. 106-111.
- [1.23] T. Kawasaki, et al., Development of a new electrostatic Cs-corrector consisted of annular and circular electrodes.
- [1.24] T. Kodama, T. Kawasaki, T. Ikuta, Properties of electrostatic correcting systems with annular apertures, *Microscopy* 68(6) (2019) pp.457-466.
- [1.25] R.H. van Aken, C.W. Hagen, J.E. Barth, P. Kruit, Low-energy foil aberration corrector, *Ultramicroscopy* 93 (2002) pp.312-330.
- [1.26] R. Shiloh, et al., Spherical aberration correction in a scanning transmission electron microscope using a sculpted thin film, *Ultramicroscopy* 189 (2018) pp.46-53.
- [1.27] J. Zach, M. Haider, Correction of spherical and chromatic aberration in a low voltage SEM, *Optik* 93 (1995) pp.112-118.
- [1.28] J. Zach, M. Haider, Aberration correction in a low voltage SEM by a multipole corrector, *Nucl. Instrum. Meth. A* 363 (1995) pp.316-325.
- [1.29] M. Haider, G. Braunshausen, E. Schwan, Correction of the spherical aberration of a 200 kV TEM by means of a Hexapole-corrector, *Optik* 99 (1995) pp.167-179.
- [1.30] M. Haider, H. Rose, S. Uhlemann, B. Kabius, K. Urban, Towards 0.1 nm resolution with the first spherically corrected transmission electron microscope, *J. Electron. Microsc.* 47 (1998) pp.395-405.
- [1.31] O.L. Krivanek, N. Dellby, A.R. Lupini, Towards sub-Å electron beams, *Ultramicroscopy* 78 (1999) pp.1-11.
- [1.32] S. Hoque, H. Ito, R. Nishi, E. Munro, Spherical aberration correction with threefold symmetric line currents, *Ultramicroscopy* 161 (2016) pp.74-82.
- [1.33] S. Hoque, H. Ito, A. Takaoka, R. Nishi, Axial geometrical aberration correction up to 5th order with N-SYLC, *Ultramicroscopy* 182 (2017) pp.68-80.
- [1.34] S. Hoque, H. Ito, R. Nishi, Spherical aberration correction with an in-lens N-fold symmetric line currents model, *Ultramicroscopy* 187 (2018) pp.135-143.
- [1.35] T. Nakano, Y. Yamazawa, Analysis of multipole fields for a practical wire lens of an aberration corrector, *J. Vac. Sci. Technol.* B37 (2019) 012901.

- [1.36] T. Nakano, Y. Yamazawa, Correcting an Aberration with a Wire Corrector for SEM, *Microsc. Microanal.* 25(S2) (2019) pp.846-847.
- [1.37] H. Rose, Inhomogeneous Wien filter as a corrector compensating for the chromatic and spherical aberration of low-voltage electron microscopes, *Optik* 84 (1990) pp.91-107.
- [1.38] C. Weißbäcker, H. Rose, Electrostatic correction of the chromatic and of the spherical aberration of charged \cdot particle lenses, *J. Electron. Microsc.* 50 (2001) pp.383-390.
- [1.39] C. Weißbäcker, H. Rose, Electrostatic correction of the chromatic and of the spherical aberration of charged \cdot particle lenses (Part II), *J. Electron. Microsc.* 51 (2002) pp.45-51.
- [1.40] A. Henstra, M.P.C.M. Krijn, *Proc. 12th Eur. Cong. Electron. Microsc.* vol. III (2000) I.155-I.156.
- [1.41] D.J. Maas, S. Henstra, M.P.C.M. Krijn, S.A.M. Mentink, Electrostatic correction in LV-SEM, *Microsc. Microanal.* 6 Suppl. 2 (2000) pp.746-747.
- [1.42] D.J. Maas, S. Henstra, M. Krijn, S. Mentink, Electrostatic correction in low-voltage SEM, *Proc. SPIE* vol.4510 (2001) pp.205-217.
- [1.43] D.J. Maas, S. Mentink, S. Henstra, Electrostatic Aberration Correction in Low-Voltage SEM, *Microsc. Microanal.* 9 Suppl. 3 (2003) pp.24-25.
- [1.44] L.A. Baranova, F.H. Read, D. Cubric, Computer simulation of an electrostatic aberration corrector for a low-voltage scanning electron microscope, *Proc. 8th Seminar on Recent Trends in Charged Particle Optics and Surface Physics Instrumentation*, (2002) pp.74.
- [1.45] L.A. Baranova, F.H. Read, D. Cubric, Computational simulation of an electrostatic aberration corrector for a low-voltage scanning electron microscope, *Nucl. Instrum. Meth. A* 519 (2004) pp.42-47.
- [1.46] S. Uno, K. Honda, N. Nakamura, M. Matsuya, J. Zach, Aberration correction and its automatic control in scanning electron microscopes, *Optik* 116 (2005) pp.438-448.
- [1.47] K. Hirose, T. Nakano, T. Kawasaki, Automatic aberration-correction system for scanning electron microscopy, *Microelectron. Eng.* 88 (2011) pp.2559-2562.
- [1.48] [Photomask CD-SEM | Products | Holon Co., Ltd. \(holon-ltd.co.jp\)](#), (accessed August 13, 2024).
- [1.49] [CEOS_SEMCOR_whitepaper_012.dvi \(ceos-gmbh.de\)](#), (accessed August 13, 2024).
- [1.50] E.G. Ramberg, Aberration Correction with Electron Mirrors, *J. Appl. Phys.* 20 (1949) pp.183-186.
- [1.51] G.F. Rempfer, A theoretical study of the hyperbolic electron mirror as a correcting element for spherical and chromatic aberration in electron optics, *J. Appl. Phys.* 67 (1990) pp.6027-6040.

- [1.52] Z. Shao, X. Wu, Properties of a four - electrode adjustable electron mirror as an aberration corrector, *Rev. Sci. Instrum.* 61 (1990) pp.1230-1235.
- [1.53] J.P.S. Fitzgerald, R.C. Word. R. Könenkamp, Simultaneous and independent adaptive correction of spherical and chromatic aberration using an electron mirror and lens combination, *Ultramicroscopy* 115 (2012) pp.35-40.
- [1.54] J. Straton, Analytic solution for a quartic electron mirror, *Ultramicroscopy* 148 (2015) pp.168-179.
- [1.55] G.F. Rempfer, M.S. Mauck, Correction of chromatic aberration with an electron mirror, *Optik* 92 (1992) pp.3-8.
- [1.56] G.F. Rempfer, D.M. Desloge, W.P. Skoczylas, O.H. Griffith, Simultaneous Correction of Spherical and Chromatic Aberrations with an Electron Mirror: An Electron Optical Achromat, *Microsc.Microanal.* 3 (1997) pp.14-27.
- [1.57] R.M. Tromp, J.B. Hannon, A.W. Ellis, W. Wan, A. Berghaus, O. Schaff, A new aberration-corrected, energy-filtered LEEM/PEEM instrument. I. Principles and design, *Ultramicroscopy* 110 (2010) pp.852-861.
- [1.58] R.M. Tromp, J.B. Hannon, W. Wan, A. Berghaus, O. Schaff, A new aberration-corrected, energy-filtered LEEM/PEEM instrument II. Operation and results, *Ultramicroscopy* 127 (2013) pp.25-39.
- [1.59] M. Mankos, D. Adler, L. Veneklasen, E. Munro, Electron optics for low energy electron microscopy, *Physics Procedia* 1 (2008) pp.485-504
- [1.60] M. Mankos, K. Shadman, A.T. N'Diaye, A.K. Schmid, H.H.J. Persson, R.W. Davis, Progress toward an aberration-corrected low energy electron microscope for DNA sequencing and surface analysis, *J. Vac. Sci. Technol. B* 30 (2012) 06F402.
- [1.61] M. Mankos, K. Shadman, A monochromatic, aberration-corrected, dual-beam low energy electron microscope, *Ultramicroscopy* 130 (2013) pp.13-28.
- [1.62] R. Fink, M.R. Weiss, E. Umbach, D. Preikszas, H. Rose, R. Spehr, P. Hartel, W. Engel, R. Defenhardt, R. Wichtendahl, H. Kühlenbeck, W. Erlebach, K. Ihmann, R. Schlögl, H.-J. Freund, A.M. Bradshaw, G. Lilienkamp, Th. Schmidt, E. Bauer, SMART: a planned ultrahigh-resolution spectromicroscope for BESSY II, *J. Electron. Spectrosc. Relat. Phenom.* 84 (1997) pp.231-250.
- [1.63] H. Rose, Aberration correction of homogeneous magnetic deflection system, *Optik* 51 (1978) pp.15-38.
- [1.64] H. Müller, D. Preikszas, H. Rose, *J. Electron. Microsc.* 48 (1999) pp.191-204.
- [1.65] Y.K. Wu, D.S. Robin, E. Forest, R. Schlueter, S. Anders, J. Feng, H. Padmore, D.H. Wei, Design and analysis of beam separator magnets for third generation aberration compensated PEEMs, *Nucl. Instrum. Meth. A* 519 (2004) pp.230-241.
- [1.66] P. Hartel, D. Preikszas, R. Spehr, H. Müller, H. Rose, Mirror corrector for low-voltage electron microscopes, in: P.W. Hawkes (Eds.), *Adv. Imaging. Electron. Phys.* 120 (2003) pp.42-133.
- [1.67] P. Schmid, J. Feng, H. Padmore, D. Robin, H. Rose, R. Schlueter, W. Wan, Correction and alignment strategies for the beam separator of the photoemission electron microscope 3 (PEEM3), *Rev. Sci. Instrum.* 76 (2005) 023302.

- [1.68] H. Rose, Geometrical Charged Particle Optics, second ed., Springer, Berlin, Heidelberg, 2013.
- [1.69] M. Steigerwald, presentation at NIST Frontiers 2013 Gaithersburg MD (2013).
- [1.70] B. Bunday, A.F. Bello. E. Solecky, A. Valid, 7/5 nm Logic Manufacturing Capabilities and Requirements of Metrology, Proc. SPIE 10585 (2018) 105850I-1.
- [1.71] A. Mohammadi-Gheidari, C.W. Hagen, P. Kruit, Multibeam scanning electron microscope: Experimental results, J. Vac. Sci. Technol. B 28 (2010) C6G5-G10.
- [1.72] T. Ichimura Y. Ren, P. Kruit, A large current scanning electron microscope with MEMS-based multi-beam optics, Microelectron. Eng. 113 (2014) pp.109-113.
- [1.73] T. Doi, M. Yamazaki, T. Ichimura, Y. Ren, P. Kruit, A high-current scanning electron microscope with multi-beam optics, Microelectron. Eng. 159 (2015) pp.132-138.
- [1.74] P. Kruit, The role of MEMS in maskless lithography, Microelectron. Eng. 84 (2007) pp.1027-1032.
- [1.75] L.P. Muray, et al., Advances in arrayed microcolumn lithography, J. Vac. Sci. Technol. B 18 (2000) pp.3099-3104.
- [1.76] C.S. Silver, J.P. Spallas, L.P. Muray, Multiple beam sub-80-nm lithography with miniature electron beam column arrays, J. Vac. Sci. Technol. B 25 (2007) pp.2258-2265.
- [1.77] P.N. Minh T. Ono, N. Sato, H. Miura, M. Esashi, Microelectron field emitter array with focus lenses for multielectron beam lithography based on silicon on insulator wafer, J. Vac. Sci. Technol. B 22 (2004) pp.1273-1276.
- [1.78] M.J. van Bruggen, B. van Someren, P. Kruit, Development of a multi-electron-beam source for sub-10 nm electron beam induced deposition, J. Vac. Sci. Technol. B23 (2005) pp.2833-2839.
- [1.79] H.W. Mook, P. Kruit, Optics and design of the fringe field monochromator for a Schottky field emission gun, Nucl. Instrum. Meth. A427 (1999) pp.109-120.
- [1.80] H.W. Mook, P. Kruit, Construction and characterization of the fringe field monochromator for a field emission gun, Ultramicroscopy 81 (2000) pp.129-139.
- [1.81] [Munro's Electron Beam Software | Munro's Electron Beam Software](#) (accessed November 6, 2024)

Chapter 2 Time-dependent perturbation for systems of Electron Mirrors and round electromagnetic fields

The content of this chapter was published in "Time-dependent perturbation theory for electron mirrors, Advances in Imaging and Electron Physics" vol. 234, Chapter 2, (2025) pp. 97-278.

2.1 Introduction

Recently, electron optical systems using electron mirrors have been developed, such as aberration-correctors for scanning electron microscopes (SEMs) and low energy electron microscopes (LEEMs). In the conventional theory of geometrical electron optics, electrons are assumed to be confined in the vicinity of the optic axis of the electron optical system and the slopes of their trajectories relative to the optic axis are also assumed to be sufficiently small. When the coordinate z is chosen as the optic axis, the above conditions are given as follows:

$$\begin{aligned} x(z) &\ll R, & y(z) &\ll R, \\ x' = \frac{dx}{dz} &\ll 1, & y' = \frac{dy}{dz} &\ll 1, \end{aligned} \tag{2.1}$$

where x and y are lateral electron trajectories in the Cartesian coordinate system, which are defined as functions of the coordinate of the optic axis z , x' and y' are their slopes, and R is a typical scale of the electron lenses such as the radius of the central hole of a pole piece or an aperture of an electrode.

Aberrations of the electron optical system are calculated by considering small perturbation of trajectories and their slopes. The higher the order of the aberrations is, the less significant it is in the optical system. It is sufficient to stop the calculation of aberrations at the orders that gives a precise approximation of the optical system. However, if the slope of the trajectories is large ($x' \gg 1$) or even divergent, the conventional perturbation collapses because such a large slope contributes more significantly to higher order aberrations than to lower order aberrations. Such situations occur in systems with electron mirrors or electron guns. In electron mirrors, the incident electrons are reflected and return. The slope of the trajectory is divergent and large at and around the reflection point. In the electron gun, the angle of the trajectory relative to the optic axis can be almost 90-degree at the emission surface because the kinetic energy of electrons is almost zero.

To avoid the difficulty caused by the large slope, it is useful to change the independent variable from the coordinate of the optic axis z to time t . Then, the coordinate z becomes the longitudinal trajectory of the electron. Instead of the lateral slopes of trajectories x' and y' , the lateral velocities $v_x = dx/dt$ and $v_y = dy/dt$ are considered for the perturbation. Around the reflection point and the emission surface, the kinetic energy of electrons is very low: less

than 1 eV, compared with that in a field-free region, where electrons are accelerated to higher than a few keV. Thus, using lateral velocity for the perturbation provides a more accurate approximation of the optical system because even in regions where the slope of trajectories becomes large, lateral velocity is sufficiently smaller than the total velocity in the field-free region.

Early studies of the perturbation theory regarding time as an independent parameter for mirrors were advanced by Kel'man *et. al.*, [1.82],[1.83] and by other authors [1.84]-[1.87]. Rose and Preikszas developed an appropriate formulation for electrostatic mirrors, called time-dependent perturbation formalism, and derived formulae for axial aberration coefficients (the spherical aberration and the axial chromatic aberration) for electrostatic mirrors [1.88]. They extended the theory to combined electromagnetic mirrors and derived formulae for axial aberration coefficients [1.89]. Preikszas derived sophisticated forms for the off-axis aberration of non-relativistic electrostatic mirrors in case where the field ray is restricted to intersect the optic axis, when the reference electron, which travels along the optic axis, is reflected. This means that for probe forming systems like SEMs, and in the case of the mirror of unit magnification, the central trajectory of the incident beam to the mirror is completely symmetric with respect to the optic axis of the mirror [1.90]. In this situation, it is implicitly assumed that the central trajectory is inclined to the optic axis in the object plane by an appropriate angle. Rose also applied the time-dependent perturbation formalism to cathode lenses for deriving paraxial properties and aberration coefficients of an electrostatic electron gun [1.91].

We are interested in using a mirror system as a Cc and Cs aberration corrector for probe forming. In the ideal situation, the central trajectory of the beam perfectly traces the optic axis. But of course, there can be misalignment: the object point may be located at an off-axis position in an arbitrary direction. Preikszas derived off-axis aberration coefficients for the electrostatic mirror, which can be directly used for the situation where the central trajectory of the incident beam is perfectly symmetric with respect to the optic axis of the mirror [1.90]. However, these coefficients are not directly applicable for estimating the significance of misalignment of the mirror for an arbitrary incident beam. Since off-axis aberration coefficients derived by Preikszas are not directly related to the incident angle at the object plane, it is not easy to consider the relation and they are not easy to use for the realistic design of the optical system because we need to consider the lateral beam position and angle relative to the optic axis not at the reflection plane, but at the conjugate planes.

Often, a mirror is part of a fully electrostatic system, however, in order to reduce the aberrations of a cathode lens, it is helpful to add a magnetic lens, whose field overlaps with the electrostatic field of the mirror/cathode. Similarly, it is valuable to know the third order aberration formulae of the electromagnetic mirror. Therefore, we will derive both

the on- and off-axis aberration coefficients for situations involving overlapping round symmetric magnetic and electrostatic fields, for which only on-axis aberration coefficients were derived by Rose and Preikszas [1.89].

Here, we derive both on- and off-axis aberration coefficients of the mirror composed of round symmetric electrostatic fields and magnetic fields, which are overlapping each other, in the case where the incident field ray is parallel to the optic axis in the object plane, similar to the condition for standard electron optics. We also provide the method to construct the off-axis aberration coefficients of an arbitrary incident beam, which originates at an arbitrary lateral position and has an arbitrary incident angle in the object plane, from the coefficients derived here. Having these coefficients will allow us to derive requirements for the alignment of the beam into the aberration corrector and for the alignment of the different mirrors with respect to each other.

In addition, when the beam is misaligned, fluctuations of the voltages on the electrodes will have a different effect compared to when the beam is perfectly aligned. We want to know these effects and will derive them from the off-axis aberration coefficients.

In this study, the calculation method for aberration properties of combined electromagnetic mirrors based on the time-dependent perturbation formalism is derived. Relativistic effects are not considered in this study because they are negligible in the region where electrons are slow.

First, in section 2.2, the calculation method based on the time-dependent perturbation formalism shall be explained, the equations of motion shall be derived and applied to the first-order trajectory tracing. In section 2.3, the effects of higher order on the trajectories shall be derived using a perturbation approach. In section 2.4, the results of section 2.3 will be used to find the chromatic aberrations, both defocus and the chromatic magnification error. In section 2.5, the core result of the article is derived: the perturbed trajectory, found in section 2.3, is split into all the complex third order aberrations that come with a combined electrostatic and magnetic field. In section 2.6, analytic forms of the fundamental solutions of the linear longitudinal equation are derived, which will be used after section 2.7. In section 2.7, we prove three features of third order geometrical aberration coefficients derived in section 2.5. These features are found in standard electron optics theory of systems with round symmetric electrostatic and magnetic fields. Section 2.8 then checks the results by simplifying the aberration expressions to find the known expressions for aberration coefficients of lenses without reflection. Section 2.9 uses the theory to find the effects of changes in the voltages of the electrodes and changes in the coil current generating magnetic field strength, while section 2.10 compares those results to the chromatic aberration coefficients. In Section 2.11, the formulae to calculate off-axis aberration coefficients for the arbitrary inclined incident beam up to the third order, which are given by suitable combinations of the aberration coefficients, derived in section 2.4 and 2.5. Also, the transformation of aberration coefficients defined

at the image plane from those defined in the object plane is given. Section 2.12 gives a summary and a conclusion of this article. In the appendices, section 2.13 of this article, we provide fundamental mathematical preparation and additional results, which stem from the result of section 2.5. In section 2.13.1, definitions of rank, degree, and order, which are used to classify aberrations, are explained. In section 2.13.2, the mathematical properties of second-order linear ordinal differential equations and the parameter variation method for solving an inhomogeneous equation are introduced. In section 2.13.3, we discuss the replacement of linear solutions used in formal solutions of the perturbation method. In section 2.13.4, we discuss the expression for the third-order geometrical path deviation in the rotation coordinate system. In section 2.13.5, the fundamental trajectories of the paraxial equation, the path deviation and the aberration, the slope deviation and the slope aberration in the Cartesian coordinate system are considered. The expressions are related to those defined in the rotation coordinate system.

Before jumping into the math, some of the parameters will be defined here and the symbols summarized for later reference:

t : time,

τ : the reduced time,

(x, y, z) : the Cartesian coordinate of the optical system, where z axis is set to the optic axis, and (x, y) is the lateral coordinate. The coordinate system is defined as right-handed system,

\mathbf{r} : 3-dimensional position vector in the Cartesian coordinate system,

\mathbf{E}, \mathbf{B} : static electric field vector and static magnetic field vector in Cartesian coordinate system,

e : elementary charge,

m_e : electron rest mass,

\mathbf{v} : 3-dimendional velocity vector of electron,

Φ_c : the column potential, the value of the electron potential in the field-free region,

ζ : the coordinate of the reference electron,

h : the relative position of the electron in z direction compared to the reference electron,

w : the complex lateral coordinate in Cartesian coordinate system, given by $w = x + iy$,

u : the complex lateral coordinate in rotation coordinate system, given by $w = e^{i\chi}u$,

χ : the rotation angle of rotation coordinate system,

E_w, B_w : the complex expression of lateral field strengths

$\Delta\Phi$: the potential deviation corresponding to the energy deviation of the electron,

λ_o : the complex initial normalized slope

f' : the differentiation of the function f with respect to the coordinate of the optic axis ζ

\dot{f} : the differentiation of the function f with respect to the reduced time τ

The aberration coefficients, defined in the objective plane, are written as follows:

the axial chromatic aberration C_{Co} ,

the off axis chromatic aberration, isotropic part C_{Mo} , anisotropic part C_{Ro} , these two coefficients are known as chromatic distortion or chromatic magnification error,

the spherical aberration C_{So} ,

the complex expression of off-axis third order geometrical aberration coefficients:

the coma radius $K_{Ro} = C_{Ko} - iC_{ko}$, the coma length $K_{Lo} = 2\bar{K}_{Ro}$, where bar means complex conjugate, the field curvature C_{Fo} , the astigmatism $A_o = C_{Ao} + iC_{ao}$, the distortion $D_o = C_{Do} + iC_{do}$,

the aberration of vibration in the j -th electrode voltage, axial C_{E1o}^j , the isotropic part of off-axial C_{E2o}^j , the anisotropic part of off-axial C_{E3o}^j ,

the aberration of vibration in the ℓ -th coil current axial C_{B1o}^ℓ , the isotropic part of off-axial C_{B2o}^ℓ , the anisotropic part of off-axial C_{B3o}^ℓ ,

2.2 Equation of motion and paraxial rays in the time-dependent formalism for electron mirrors

This section gives mainly a detailed review of the time-dependent perturbation formalism for electron mirrors based on reference [1.88] and [1.91], but the equations were re-derived and explained in a bit more detail than in the original texts.

2.2.1 Reference electron

The coordinates of the electron trajectory are defined as a function of time t as

$$x = x(t), \quad y = y(t), \quad z = \zeta(t) + h(t). \quad (2.2)$$

The positive direction of the longitudinal coordinate z is defined as the incident direction of electrons to the electron mirror. Thus, after reflection, the electrons go back in the negative direction of z . The coordinate of the optic axis z is divided into two parts. One is $\zeta(t)$, which is a trajectory of a reference electron. The reference electron travels along the optic axis of the mirror. Its coordinate is given by

$$x = 0, \quad y = 0, \quad z = \zeta(t). \quad (2.3)$$

The other part, $h(t)$ is the longitudinal path deviation of a general electron from the path of the reference electron measured at the same time. The trajectories of the general electron and of the reference electron are illustrated in Fig. 2.1, which is illustrated by referring to Fig. 1 of reference [1.89].

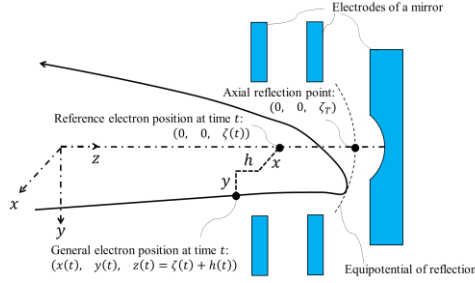


Fig. 2.1. Trajectories of the general electron and of the reference electron measured at the same time. Coordinate $(x(t), y(t), z(t))$ means position of the general electron. $h(t)$ is the longitudinal path deviation of the general electron measured from the position of the corresponding reference electron $\zeta(t)$. ζ_T is the reflection point on the optic axis for the reference electron of nominal energy E_n .

2.2.2 Equation of motion

According to the convention of the theory of geometrical electron optics, the electrostatic gauge of the system is determined to be zero at the cathode surface of the electron gun: $\varphi_{\text{cathode}} = 0$. In the case of an electron mirror, the electrostatic potential $\varphi(x, y, z)$ vanishes at the axial reflection point ζ_T for the reference electron of nominal energy E_n , where Fig. 2.1 shows, that is,

$$\varphi(x = 0, y = 0, z = \zeta_T) = \Phi(z = \zeta_T) = 0, \quad (2.4)$$

where $\Phi(z)$ is the axial potential of the electron, because of the conservation rule of total non-relativistic energy,

$$E_{\text{total}} = \frac{1}{2} m_e v^2 - e\varphi(x, y, z) = \delta E, \quad (2.5)$$

where m_e, v, e , are electron rest mass, electron velocity vector, and elementary charge, respectively and δE is the energy deviation from the nominal energy. To simplify the formulae, instead of time t , it is advantageous to use a new parameter called reduced time τ as independent variable of various functions, which is defined by

$$d\tau = v_c dt = \frac{p_c}{m_e} dt = \sqrt{\frac{2e\Phi_c}{m_e}} dt, \quad (2.6)$$

where $d\tau$ corresponds to the length, which free electrons with velocity v_c travel during time dt , and p_c is the non-relativistic kinetic momentum of the velocity v_c , and Φ_c is the column potential. The column potential Φ_c is the value of the electron potential in the field-free region, where acceleration in the electron gun has finished, that is, the column

potential ϕ_c is equal to the nominal acceleration voltage of the electron optical system under the conventional gauge condition. Throughout this article, the differentiation of arbitrary function f with respect to the position of the reference electron ζ is expressed by a prime as $f' = df/d\zeta$ and the differentiation with respect to the reduced time τ is expressed by a dot as $\dot{f} = df/d\tau$. The second order differentiations are denoted by double prime and double dot. The n -th differentiation with respect to ζ is denoted by $f^{[n]}$. To obtain appropriate forms of the time-dependent theory, the derivation is started from the non-relativistic Lorentz's equation of motion for the electrons:

$$m_e \frac{d^2 \mathbf{r}}{dt^2} = -e(\mathbf{E} + \mathbf{v} \times \mathbf{B}), \quad (2.7)$$

where \mathbf{E} and \mathbf{B} are an electrostatic field vector and a magnetic flux density vector, respectively. By the convention of electromagnetism, electrostatic field and stationary magnetic field is given by $\mathbf{E} = -\nabla\phi$, $\mathbf{B} = -\nabla\psi$, where ψ is the magnetic scalar potential of the system.

Considering Eq. (2.6), Lorentz's equation is transformed into

$$\ddot{\mathbf{r}} = -\frac{\mathbf{E}}{2\phi_c} - \frac{\eta}{\sqrt{\phi_c}} \dot{\mathbf{r}} \times \mathbf{B}, \quad (2.8)$$

where

$$\eta := \sqrt{\frac{e}{2m_e}}, \quad (2.9)$$

and three-dimensional trajectory \mathbf{r} is a function of the reduced time τ .

Introducing complex expressions for the lateral coordinate for the lateral trajectory and field strengths

$$w = x + iy, \quad E_w = E_x + iE_y, \quad B_w = B_x + iB_y. \quad (2.10)$$

Using Eq. (2.10), the three-dimensional equation of motion Eq. (2.8) is decomposed into two complex equations,

$$\ddot{w} = -\frac{E_w}{2\phi_c} - \frac{i\eta}{\sqrt{\phi_c}} (B_w \dot{z} - B_z \dot{w}), \quad (2.11)$$

$$\ddot{z} = \ddot{\zeta} + \ddot{h} = -\frac{E_z}{2\phi_c} - \frac{\eta}{\sqrt{\phi_c}} \text{Im}(B_w \dot{w}). \quad (2.12)$$

Since in the time-dependent theory, an electron trajectory is parametrized by time, the z coordinate of the electron is considered as a component of the trajectory. The equation of motion of the reference electron, which travels along the optic axis and whose energy is the same as the nominal electron energy, is given as follows:

$$\ddot{\zeta} = -\frac{1}{2\phi_c} E_z(w=0, \quad h=0, \quad \zeta) = \frac{\Phi'(\zeta)}{2\phi_c}, \quad (2.13)$$

where it is obtained by setting $w=0$, $h=0$, $\delta E=0$ in Eq. (2.12). Using Eqs. (2.5) and (2.6) in the case of $w=0$, $h=0$, $\delta E=0$, energy conservation of the reference electron is expressed as

$$\dot{\zeta}^2 = \frac{\Phi(\zeta)}{\phi_c}. \quad (2.14)$$

Due to the definition of the direction of incident and reflected electrons, reduced “velocity” of the reference electron is given as

$$\dot{\zeta}(\tau) = \pm \sqrt{\frac{\Phi(\zeta(\tau))}{\Phi_c}} \begin{cases} + & \text{for } \tau < \tau_T \\ - & \text{for } \tau > \tau_T \end{cases} \quad (2.15)$$

where τ_T is the reduced time at the axial reflection point for the reference electron ζ_T . $\Phi(\zeta(\tau))$ means that the axial potential distribution is a function of reference electron position ζ , which is given by a solution of Eq. (2.13). However, the reference electron position is a function of the reduced time. That means the axial potential distribution is an implicit function of the reduced time. Note that all functions of ζ have the same implicit dependence on τ . Hereafter, such an implicit dependence on the reduced time is not explicitly expressed unless it is necessary.

The axial reflection point is defined as the point where the axial potential vanishes:

$$\Phi(\zeta_T) = 0, \quad (2.16)$$

and the axial reflection reduced time is defined as

$$\zeta_T = \zeta(\tau_T). \quad (2.17)$$

Because the reduced velocity of the reference electron is antisymmetric about the reflection time and it is zero at the reflection time, as a function of the reduced time, the reference electron trajectory is symmetric about the reflection time:

$$\dot{\zeta}(2\tau_T - \tau) = -\dot{\zeta}(\tau), \quad (2.18)$$

$$\zeta(2\tau_T - \tau) = \zeta(\tau), \quad (2.19)$$

where $\tau < \tau_T$.

It is easier to construct a theory by transforming the coordinate system from the Cartesian coordinate system into a rotation coordinate system, which is viewed by an observer rotating around the optic axis of the rotation angle,

$$\chi(\tau) = \int_{\tau_o}^{\tau} \frac{\eta B}{2\sqrt{\Phi_c}} d\tau, \quad (2.20)$$

where τ_o is initial reduced time of the electron trajectory, and B is the rotationally symmetric magnetic flux density, that is, $B = B(\zeta(\tau)) = B_z(w = 0, \zeta)$.

The lateral complex trajectory u in the rotation coordinate system is given by

$$w = e^{i\chi(\tau)} u(\tau). \quad (2.21)$$

To construct theory, we need concrete expressions of electric and magnetic field strengths. They are given by

$$\begin{aligned} E_w &= E_x + iE_y = -2 \frac{\partial \varphi}{\partial \bar{w}}, & E_z &= -\frac{\partial \varphi}{\partial h}, \\ B_w &= B_x + iB_y = -2 \frac{\partial \psi}{\partial \bar{w}}, & B_z &= -\frac{\partial \psi}{\partial h}, \end{aligned} \quad (2.22)$$

Where φ is electrostatic potential and ψ is magnetic scalar potential. Power series expansions of the rotationally symmetric potentials are given by

$$\begin{aligned}\varphi(w, \bar{w}, \zeta, h) &= \sum_{n=0}^{\infty} \frac{(-1)^n}{(n!)^2} \left(\frac{w\bar{w}}{4}\right)^n \phi^{[2n]}(z = \zeta + h) \\ &= \sum_{n=0}^{\infty} \sum_{m=0}^{\infty} \frac{(-1)^n}{m! (n!)^2} \left(\frac{w\bar{w}}{4}\right)^n h^m \phi^{[2n+m]}(\zeta),\end{aligned}\quad (2.23)$$

$$\psi(w, \bar{w}, \zeta, h) = \sum_{n=0}^{\infty} \sum_{m=0}^{\infty} \frac{(-1)^n}{m! (n!)^2} \left(\frac{w\bar{w}}{4}\right)^n h^m \psi^{[2n+m]}(\zeta), \quad (2.24)$$

where Ψ is the axial magnetic scalar potential and $\Psi' = -B$.

Then, the power series expansions of the field strengths are given by

$$E_w = \sum_{n=0}^{\infty} \sum_{m=0}^{\infty} \frac{(-1)^n}{2(n+1)! n! m!} \left(\frac{w\bar{w}}{4}\right)^n w h^m \phi^{[2n+m+2]}(\zeta), \quad (2.25)$$

$$E_z = \sum_{n=0}^{\infty} \sum_{m=0}^{\infty} \frac{(-1)^{n+1}}{(n!)^2 m!} \left(\frac{w\bar{w}}{4}\right)^n h^m \phi^{[2n+m+1]}(\zeta), \quad (2.26)$$

$$B_w = \sum_{n=0}^{\infty} \sum_{m=0}^{\infty} \frac{(-1)^{n+1}}{2(n+1)! n! m!} \left(\frac{w\bar{w}}{4}\right)^n w h^m B^{[2n+m+1]}(\zeta), \quad (2.27)$$

$$B_z = \sum_{n=0}^{\infty} \sum_{m=0}^{\infty} \frac{(-1)^n}{(n!)^2 m!} \left(\frac{w\bar{w}}{4}\right)^n h^m B^{[2n+m]}(\zeta). \quad (2.28)$$

To obtain the formulae for the third order aberrations, the power series expansion of fields up to the third order terms are sufficient. The explicit expansions up to terms of the third order product of the lateral rotation coordinate u and the longitudinal path deviation h are given here.

$$E_w = e^{i\chi} \left(\frac{1}{2} \Phi'' u + \frac{1}{2} \Phi^{[3]} u h - \frac{1}{16} \Phi^{[4]} u^2 \bar{u} + \frac{1}{4} \Phi^{[4]} u h^2 \right) + \dots, \quad (2.29)$$

$$E_z = - \left(\Phi' + \Phi'' h - \frac{1}{4} \Phi^{[3]} u \bar{u} + \frac{1}{2} \Phi^{[3]} h^2 - \frac{1}{4} \Phi^{[4]} u \bar{u} h + \frac{1}{6} \Phi^{[4]} h^3 \right) + \dots, \quad (2.30)$$

$$B_w = -e^{i\chi} \left(\frac{1}{2} B' u + \frac{1}{2} B'' u h - \frac{1}{16} B^{[3]} u^2 \bar{u} + \frac{1}{4} B^{[3]} u h^2 \right) + \dots, \quad (2.31)$$

$$B_z = B + B' h - \frac{1}{4} B'' u \bar{u} + \frac{1}{2} B'' h^2 - \frac{1}{4} B^{[3]} u \bar{u} h + \frac{1}{6} B^{[3]} h^3 + \dots. \quad (2.32)$$

Using Eqs. (2.13), and (2.29) - (2.32), Lorentz's equation of motion Eq. (2.11) is transformed into

$$\ddot{u} + \frac{N}{4\Phi_C} u = P_u, \quad (2.33)$$

where

$$N = \Phi'' + \eta^2 B^2, \quad (2.34)$$

$$\begin{aligned}P_u &= \frac{i\eta}{\sqrt{\Phi_C}} \left[-\frac{1}{2} B' \zeta u - B_w e^{-i\chi} (\zeta + h) + (B_z - B) \dot{u} \right] \\ &\quad - \frac{\eta^2 B}{2\Phi_C} (B_z - B) u - \frac{E_w}{2\Phi_C} e^{-i\chi} + \frac{\Phi''}{4\Phi_C} u,\end{aligned}\quad (2.35)$$

and P_u is the lateral perturbation function. In the time-dependent theory, we have to know about longitudinal trajectory parametrized by time. Since Eq. (2.13) gives equation of the reference electron trajectory, equation of the longitudinal path deviation, which is relative position of the electron viewed from the reference electron at the same time, is given by subtracting Eq. (2.13) from Eq. (2.12). The equation of longitudinal path deviation is given by

$$\ddot{h} - \frac{\Phi''}{2\Phi_c} h = P_h, \quad (2.36)$$

where the right-hand side is the longitudinal perturbation function:

$$P_h = \frac{1}{\sqrt{\Phi_c}} \text{Im}(\eta \bar{B}_w e^{ix} \dot{u}) + \frac{\eta^2 B}{2\Phi_c} \text{Re}(\bar{B}_w e^{ix} u) - \frac{1}{2\Phi_c} (\Phi' + \Phi'' h + E_z). \quad (2.37)$$

These equations are the trajectory equations in the time-dependent formalism. In the form of Eqs. (2.33) and (2.36), terms in left hand side of the equations have only linear terms of u and h , whereas perturbation functions in right hand side have no linear terms of u and h . So, we are now at the point where the general equation is derived in order to get to the final goal of this section, we still need to introduce paraxial equation and study the properties of fundamental solutions.

2.2.3 Paraxial equation in lateral direction, longitudinal linear equation, and their fundamental solutions

In the time-dependent theory, the three-dimensional electron positions are given as a function of time. To apply perturbation theory, the magnitude of the electron position must be kept small. In lateral direction, if the electron position must be confined around the optic axis, it is satisfied, which is the same as in standard electron optics. On the other hand, the value of the z -coordinate of the electron cannot be suppressed. As explained in section 2.2.1, we introduced a reference electron, which travels along the optic axis with nominal electron energy. The electron trajectory at a certain time is defined as the relative three-dimensional position viewed from the reference electron at the same time. Since the reference electron position is located on the optic axis and has no lateral position, the relative lateral position of other electrons is the same as its actual lateral position. However, the relative position in the z -direction, which is called longitudinal path deviation, must be sufficiently small to treat it as a perturbation. In rotation coordinate system, the equation of motion of the lateral trajectory is derived as Eq. (2.34). The equation for the longitudinal path deviation, which gives the relative position in z -direction viewed from the reference electron, is derived as Eq. (2.36).

In this section, a detailed review of the paraxial equations in lateral direction, the linearly approximated equation of the longitudinal path deviation, and their fundamental solutions are explained. The homogeneous equations of lateral trajectory and longitudinal path deviation in the time-dependent formalism are obtained by neglecting perturbation functions in Eqs. (2.33) and (2.36). It is called paraxial approximation because of analogy of standard electron optics. As explained later, a solution of linearly approximated equation of longitudinal path deviation cannot be called “paraxial” solution. That is the reason why it is called the longitudinal linear equation here.

The lateral paraxial equation is

$$\ddot{u} + \frac{N}{4\Phi_c} u = 0, \quad (2.38)$$

and the longitudinal linear equation is

$$\ddot{h} - \frac{\Phi''}{2\Phi_c} h = 0. \quad (2.39)$$

Because of analogy to standard electron optics, these equations are called paraxial equations because they are second order linear ordinary differential equations.

First, we give a review of so-called lateral fundamental rays and their properties. They are two independent solutions of Eq. (2.36), on which the following initial conditions at τ_o are imposed. We call a solution of the lateral paraxial equation a fundamental “ray”, since it matches with the concept of a fundamental ray in standard electron optics.

$$\begin{aligned} u_{\alpha o} = u_{\alpha}(\tau_o) = 0, & \quad \dot{u}_{\alpha o} = 1, \\ u_{\gamma o} = 1, & \quad \dot{u}_{\gamma o} = 0, \end{aligned} \quad (2.40)$$

where $u_{\alpha}(\tau)$ and $u_{\gamma}(\tau)$ are named the axial ray and the field ray, respectively. The axial ray starts from the optic axis at the object plane of unit reduced velocity in lateral direction. Reduced velocity is considered as a ratio of the velocity over non-relativistic velocity of column potential given in Eq. (2.6). A field ray starts at the point of a lateral displacement of unit distance at the object plane with zero lateral reduced velocity, that means the field ray starts parallel to the optic axis. The Wronskian of two fundamental rays is given by

$$W[u_{\gamma}, u_{\alpha}] = u_{\gamma}\dot{u}_{\alpha} - \dot{u}_{\gamma}u_{\alpha}. \quad (2.41)$$

Because of differentiation of Eq. (2.41) with respect to the reduced time,

$$\dot{W}[u_{\gamma}, u_{\alpha}] = u_{\gamma}\ddot{u}_{\alpha} - \ddot{u}_{\gamma}u_{\alpha} = -\frac{N}{4\Phi_c}(u_{\gamma}u_{\alpha} - u_{\gamma}\dot{u}_{\alpha}) = 0. \quad (2.42)$$

The Wronskian is an invariant whose value is the same whenever the reduced time is,

$$W[u_{\gamma}, u_{\alpha}] = u_{\gamma}\dot{u}_{\alpha} - \dot{u}_{\gamma}u_{\alpha} = u_{\gamma o}\dot{u}_{\alpha o} - \dot{u}_{\gamma o}u_{\alpha o} = 1. \quad (2.43)$$

Other useful combinations of fundamental solutions of Eq. (2.38) are introduced here. They are called a symmetric ray u_{σ} and an antisymmetric ray u_{ν} . The symmetry is defined with respect to the reflection time of the reference

electron. Since corresponding reduced time to reflection time is expressed by τ_T , the boundary conditions of those rays are given by

$$\begin{aligned} u_{vT} &= u_v(\tau_T) = 0, & \dot{u}_{vT} &= -1, \\ u_{\sigma T} &= 1, & \dot{u}_{\sigma T} &= 0. \end{aligned} \quad (2.44)$$

The Wronskian $W[u_v, u_\sigma]$ is also an invariant, whose value is 1. These rays are constructed by linear combinations of the axial and the field rays as follows,

$$u_v = u_{\alpha T} u_\gamma - u_{\gamma T} u_\alpha, \quad (2.45)$$

$$u_\sigma = \dot{u}_{\alpha T} u_\gamma - \dot{u}_{\gamma T} u_\alpha. \quad (2.46)$$

Here we give the longitudinal fundamental solutions of Eq. (2.39). A longitudinal path deviation from the reference electron position is only introduced in the time-dependent theory. Since standard electron optics does not have such a concept, solutions of a longitudinal linear equation cannot be visualized like “rays” in lateral direction. Mathematical expressions are similar to those of lateral fundamental rays, however, to avoid confusion, we call them not “longitudinal fundamental rays” but “longitudinal fundamental solutions”. Because of analogy to Eq. (2.40), the imposed initial conditions for the two fundamental solutions h_α , and h_γ are

$$\begin{aligned} h_{\alpha 0} &= 0, & \dot{h}_{\alpha 0} &= 1, \\ h_{\gamma 0} &= 1, & \dot{h}_{\gamma 0} &= 0. \end{aligned} \quad (2.47)$$

The Wronskian of h_α , and h_γ is given by

$$W[h_\gamma, h_\alpha] = h_\gamma \dot{h}_\alpha - \dot{h}_\gamma h_\alpha = 1. \quad (2.48)$$

Longitudinal fundamental solutions have analytic forms. These analytic forms do not appear in aberration theory of time-dependent theory explicitly. In numerical calculation, there are two ways to obtain fundamental solutions. One is calculating analytic forms numerically. The other is solving Eq. (2.39) under initial condition of Eq. (2.47) directly. The second way is much easier since analytic forms are very complicated. It is worth to give a review and to discuss their properties because the analytic forms and the properties are used to prove that aberration coefficients in the time-dependent theory reproduce the aberration coefficients in standard electron optics in the case of a system of electron lenses without mirrors. A detailed review about analytic forms of the longitudinal fundamental solutions is given in section 2.6.

2.2.4 General paraxial rays in lateral direction and general solutions of a linear longitudinal equation, which is called linear longitudinal path deviation.

We now have the two fundamental solutions of paraxial trajectories in both lateral direction and longitudinal direction. But for a full aberration theory, we need a solution for the general paraxial ray. The general “paraxial” ray is obtained in this section as a linear combination of u_α and u_γ for the lateral ray, and that of h_α and h_γ for the longitudinal path deviation. In the rotation coordinate, the position and the reduced velocity of the general electron trajectory at the initial time is given by $(u_o, z_o = \zeta_o + h_o)$ and by $(\dot{u}_o, \dot{z}_o = \dot{\zeta}_o + \dot{h}_o)$, respectively. Because these rays are defined to satisfy the boundary conditions at the initial reduced time τ_o , that means, Eqs. (2.40) and (2.47), the general lateral ray and its reduced velocity are given by

$$u_p(\tau) = \dot{u}_o u_\alpha(\tau) + u_o u_\gamma(\tau), \quad (2.49)$$

$$\dot{u}_p(\tau) = \dot{u}_o \dot{u}_\alpha(\tau) + u_o \dot{u}_\gamma(\tau), \quad (2.50)$$

where u_o and \dot{u}_o are the lateral position and the lateral reduced velocity of the electron at the initial time. The suffix p means a general solution of the paraxial equation. These u_o and \dot{u}_o are called geometrical parameters in this article. For the longitudinal path deviation, a general solution of the homogeneous longitudinal equation of trajectory is given by

$$h_p(\tau) = \dot{h}_o h_\alpha(\tau) + h_o h_\gamma(\tau), \quad (2.51)$$

where h_o and \dot{h}_o are the deviations of longitudinal position and longitudinal reduced velocity from those of the reference electron at the initial time. This solution cannot be called a paraxial solution. The reason is explained next. To analyze the optical properties of electron mirrors, it is not so advantageous to assume electron beam spread in z -direction at the initial time. So, initial longitudinal deviation is chosen to be zero:

$$h_o = 0. \quad (2.52)$$

It means that all electrons start to travel from the same z -plane at the initial time. This plane is considered as the object plane of standard electron optics theory. The position of the object plane is given by the position of the reference electron at the initial time:

$$\zeta_o = \zeta(\tau_o). \quad (2.53)$$

On the other hand, an initial relative reduced velocity in longitudinal direction, \dot{h}_o , is not freely given because of energy conservation rule. The total energy conservation Eq. (2.5) is transformed into

$$\dot{w}\dot{w} + (\dot{\zeta} + \dot{h})^2 - \frac{\varphi}{\Phi_c} = \dot{\zeta}_o^2 \kappa_o, \quad (2.54)$$

where κ_o is the chromatic parameter, which is given as a ratio of energy deviation and nominal energy of electrons at the initial time:

$$\kappa_o = \frac{\delta E}{e\Phi_o}. \quad (2.55)$$

In rotation coordinate, w and \dot{w} are expressed by

$$w = e^{i\chi}u, \quad (2.56)$$

$$\dot{w} = e^{i\chi}(\dot{u} + i\dot{\chi}u). \quad (2.57)$$

Using these equations, total energy conservation rule is transformed into

$$\dot{u}\dot{u} + \dot{\chi}^2 u\bar{u} + i\dot{\chi}(u\dot{\bar{u}} - \dot{u}\bar{u}) + (\dot{\chi} + \dot{h})^2 - \frac{\varphi}{\Phi_c} = \dot{\zeta}_o^2 \kappa_o. \quad (2.58)$$

We want to know the expression for \dot{h}_o . Since Eq. (2.58) is an invariant, taking account of Eqs. (2.20), (2.23), and (2.52), \dot{h}_o is given as a function of the geometrical parameters u_o and \dot{u}_o and the chromatic parameter κ_o by

$$\begin{aligned} \dot{h}_o = \dot{\zeta}_o \left[\left(1 - \frac{1}{\dot{\zeta}_o^2} \left(\dot{u}_o \dot{\bar{u}}_o + \frac{\eta^2 B_o^2}{4\Phi_c} u_o \bar{u}_o + i \frac{\eta B_o}{2\sqrt{\Phi_c}} (u_o \dot{\bar{u}}_o - \dot{u}_o \bar{u}_o) \right) + \kappa_o \right. \right. \\ \left. \left. + \sum_{n=1}^{\infty} \frac{(-1)^n}{(n!)^2} \left(\frac{u_o \bar{u}_o}{4} \right)^n \frac{\Phi_o^{[2n]}}{\dot{\zeta}_o^2 \Phi_c} \right)^{\frac{1}{2}} - 1 \right]. \end{aligned} \quad (2.59)$$

To make the discussion clear, we introduce the concept of rank, order and degree. Detailed definitions are given in Appendix 2.13.1. The “order” is the number of geometrical parameters u_o and \dot{u}_o in an exponent of a term. The “degree” is the number of chromatic parameters in an exponent of a term. The “rank” of a term is defined as the sum of “order” and “degree”.

Since geometrical and chromatic parameters have the first-rank, \dot{h}_o is decomposed into terms of rank- r :

$$\dot{h}_o = \sum_{r=1} \dot{h}_o^{(r)}, \quad (2.60)$$

where concrete expressions of the first-rank and the second-rank are, respectively,

$$\dot{h}_o^{(1)} = \frac{1}{2} \dot{\zeta}_o \kappa_o, \quad (2.61)$$

$$\dot{h}_o^{(2)} = -\frac{1}{2\dot{\zeta}_o} \dot{u}_o \dot{\bar{u}}_o - \frac{N_o}{8\dot{\zeta}_o \Phi_c} u_o \bar{u}_o - \frac{i\eta B_o}{4\dot{\zeta}_o \sqrt{\Phi_c}} (u_o \dot{\bar{u}}_o - \dot{u}_o \bar{u}_o) - \frac{1}{8} \dot{\zeta}_o \kappa_o^2. \quad (2.62)$$

The initial relative reduced velocity in longitudinal direction of the first-rank depends only on the chromatic parameter. Eq. (2.61) shows the trivial fact that if an electron has different energy by δE , compared with nominal energy, and even if that electron travels along the optic axis, the initial velocity in z-direction of that electron is different from that of nominal energy electron at the initial time. Eq. (2.62) means that even if a nominal energy electron is considered,

when it starts from an off-axis lateral point and/or has velocity in lateral direction in the object plane, the initial reduced velocity of that electron in z-direction differs from that of the reference electron. But the dependence of relative reduced velocity in z-direction on geometrical parameters is not linear but quadratic. These considerations show that an initial reduced velocity in z-direction never depends on geometrical parameters of the first-order. A general solution of linear longitudinal equation Eq. (2.51) is also decomposed into a power series of rank:

$$h_p = h_p^{(1)} + \sum_{r=2} h_p^{(r)} = \dot{h}_o^{(1)} h_\alpha + \sum_{r=2} \dot{h}_o^{(r)} h_\alpha. \quad (2.63)$$

Since h_p is the solution of the homogeneous equation, $h_p^{(1)}$ means the longitudinal path deviation of the first-rank:

$$h^{(1)} = h_p^{(1)} = \dot{h}_o^{(1)} h_\alpha = \frac{1}{2} \dot{\zeta}_o \kappa_o h_\alpha. \quad (2.64)$$

Since the first-rank longitudinal path deviation depends on only the chromatic parameter, it never depends on geometrical parameters of the first-order. This is the reason why it is not called a paraxial solution because the paraxial solution depends on geometrical parameters of the first-order due to analogy of standard electron optics. On the other hand, solutions of longitudinal linear equation have contributions of all rank, that is $h_p^{(r)}$. Not only perturbation but also a solution of longitudinal linear equation, which has corresponding rank, must contribute to path deviations of higher rank.

Here, we return to a general lateral paraxial ray and discuss paraxial optical properties. Since a ray of Eq. (2.49) is the first-order, that is, the 0-th degree, the first-order, and the first-rank, precisely, we can write it as

$$u^{(1)} = u_p(\tau) = \dot{u}_o u_\alpha(\tau) + u_o u_\gamma(\tau). \quad (2.65)$$

By analogy to standard electron optics, the time τ_i , when the axial ray converges, is defined by

$$u_{\alpha i} = u_\alpha(\tau_i) = 0, \quad (2.66)$$

where $\tau_i > \tau_o$. Since the first-rank longitudinal path deviation vanishes for the electrons of nominal energy, as long as the paraxial lateral rays (the first-order geometrical rays), the z-coordinate of the rays at a certain reduced time is the same as that of reference electron at the same reduced time. Then, the z-coordinate ζ_i where the axial ray converges is given by

$$\zeta_i = \zeta(\tau_i). \quad (2.67)$$

It means that the position of the Gaussian image plane of the optical system. For the convenience, τ_i is named the reduced convergent time. By analogy to standard electron optics, linear magnification and focal length in the time-dependent perturbation theory are also defined as follows. The linear magnification M is defined by the value of the field ray at the reduced convergent time:

$$M = u_\gamma(\tau_i). \quad (2.68)$$

The angular magnification M_α is the ratio of the slope of the axial ray at the image plane and that at the object plane. To derive it, it is advantageous to use a relation that a differentiation of an arbitrary function g with respect to a reduced time is given by a product of reduced velocity of a reference electron, $\dot{\zeta}$, and a differentiation of g with respect to optic axis coordinate:

$$\dot{g} = \frac{d\zeta}{d\tau} \frac{dg}{d\zeta} = \dot{\zeta} g' \quad (2.69)$$

Using Eqs. (2.40) and (2.69), the angular magnification is given by

$$M_\alpha = \frac{u'_{\alpha i}}{u'_{\alpha o}} = \frac{\dot{\zeta}_o}{\dot{\zeta}_i} \dot{u}_{\alpha i}. \quad (2.70)$$

Evaluating the Wronskian Eq. (2.43) at the convergent time, we get

$$\dot{u}_{\alpha i} = \frac{1}{M}, \quad (2.71)$$

The angular magnification is

$$M_\alpha = \frac{\dot{\zeta}_o}{\dot{\zeta}_i} \frac{1}{M}. \quad (2.72)$$

The value of the slope of the field ray at the convergent time gives the real focal length of the image-side f_i by

$$u'_{\gamma i} = \frac{1}{\dot{\zeta}_i} \dot{u}_{\gamma i} =: -\frac{1}{f_i}. \quad (2.73)$$

In fact, the discussion of this chapter and derived trajectories are also valid for the standard lens system. There are two differences between the mirror theory and the standard lens theory. The first difference is the sign of the reduced velocity of the reference electron at the convergent time. In the standard lens system, since reflection never occurs, the reference electron always travels in the same direction and its reduced velocity is always positive. In the system of an electron mirror, reflection reverses the direction of motion of the reference electron. The reduced velocity of the reference electron after reflection has an opposite sign to that of an incident reference electron. Taking into account Eq. (2.14), the reduced velocity of the reference electron at the convergent time is given by

$$\dot{\zeta}_i = \pm \sqrt{\frac{\Phi_i}{\Phi_c}} \begin{cases} + \text{ for the standard lens system,} \\ - \text{ for the electron mirror system.} \end{cases} \quad (2.74)$$

The angular magnification, Eq. (2.72), is also transformed into

$$M_\alpha = \pm \sqrt{\frac{\Phi_i}{\Phi_o}} \frac{1}{M} \begin{cases} + \text{ for the standard lens system,} \\ - \text{ for the electron mirror system.} \end{cases} \quad (2.75)$$

The other difference is the initial condition of the lateral paraxial ray. To discriminate the lateral rays in standard lens theory from those in the mirror theory, which is discussed here, to the former rays are added the symbol of tilde such as $\tilde{u}_A(z)$. The standard theory's rays are function of z -coordinate, and their initial condition is given by

$$\begin{aligned}\tilde{u}_{\alpha o} &= \tilde{u}_{\alpha}(z_o) = 0, & \tilde{u}'_{\alpha o} &= 1, \\ \tilde{u}_{\gamma o} &= 1, & \tilde{u}'_{\gamma o} &= 0,\end{aligned}\tag{2.76}$$

\tilde{u}_{α} and \tilde{u}_{γ} are proportional to u_{α} and u_{γ} , respectively. Since the first-rank longitudinal path deviation does not include the geometrical contribution of the first-order, the variable of $\tilde{u}_A(z)$ is equivalent to the reference electron trajectory ζ . Comparing Eq. (2.40) with Eq. (2.76), it is easy to guess that

$$\begin{aligned}\tilde{u}_{\alpha}(\zeta(\tau)) &= \dot{\zeta}_o u_{\alpha}(\tau), & \tilde{u}'_{\alpha} &= \frac{\dot{\zeta}_o}{\zeta} \dot{u}_{\alpha}, \\ \tilde{u}_{\gamma} &= u_{\gamma}, & \tilde{u}'_{\gamma} &= \frac{1}{\zeta} \dot{u}_{\gamma}.\end{aligned}\tag{2.77}$$

Lagrange's relation of standard electron optics is given by

$$\tilde{u}_{\gamma} \tilde{u}'_{\alpha} - \tilde{u}'_{\gamma} \tilde{u}_{\alpha} = \frac{\dot{\zeta}_o}{\zeta} = \sqrt{\frac{\Phi(\zeta)}{\Phi_o}}.\tag{2.78}$$

Eqs. (2.77) and (2.78) are used for the proof discussed in section 2.7.

Now we are at the point where the general paraxial ray, the first order optical properties, and the relation with the paraxial rays in the standard formalism, where the optic axis coordinate is taken as the parameter of the trajectory, are introduced. In the next section, we will explain perturbation theory.

2.3 Path deviation in the time-dependent theory induced by perturbation.

2.3.1 Procedures of perturbation in the time-dependent theory

Here, we continue the review of the time dependent perturbation theory. We consider perturbation to obtain the perturbative form of the solution of the general equation, considering the perturbative terms in the R.H.S. of Eqs. (2.33) and (2.36). The general lateral and longitudinal paths are given by the solutions of Eqs. (2.38) and (2.39), respectively, and can be decomposed into terms of different rank:

$$\begin{aligned}u(\tau) &= u^{(1)} + \Delta u, \\ h(\tau) &= h^{(1)} + \Delta h,\end{aligned}\tag{2.79}$$

where

$$\Delta u(\tau) = \sum_{r=2} u^{(r)}, \quad \Delta h(\tau) = \sum_{r=2} h^{(r)}.\tag{2.80}$$

Since geometrical and chromatic parameters are much smaller than 1, path deviations of higher rank are less significant than those of lower rank. Formally, Eqs. (2.33) and (2.36) are solved by the parameter variation method explained in Appendix 2.13.2. Using Eqs. (2.43) and (2.48), formal solutions of the lateral and longitudinal paths are given by²

² Here, to obtain formal particular solutions of the inhomogeneous equations Eqs. (2.33) and (2.36), u_{α}, u_{γ} and h_{α}, h_{γ} are selected as fundamental solutions of the homogeneous equations Eq. (2.38) and (2.39). Even if other combinations of solutions, for example, u_{σ}, u_{ν} and h_{σ}, h_{ν} , are selected as fundamental solutions, formal particular

$$u(\tau) = u_p(\tau) - u_\gamma(\tau) \int_{\tau_0}^{\tau} P_u(\tau) u_\alpha(\tau) d\tau + u_\alpha(\tau) \int_{\tau_0}^{\tau} P_u(\tau) u_\gamma(\tau) d\tau, \quad (2.81)$$

$$h(\tau) = h_p(\tau) - h_\gamma(\tau) \int_{\tau_0}^{\tau} P_h(\tau) h_\alpha(\tau) d\tau + h_\alpha(\tau) \int_{\tau_0}^{\tau} P_h(\tau) h_\gamma(\tau) d\tau. \quad (2.82)$$

However, perturbation functions P_u , and P_h included inside the integrands are complicated functions of not only the reduced time τ , but also are functions of unknown lateral and longitudinal paths and their reduced velocities³, which we would like to know exactly, as the L.H.S of equations. Because these are integral equations, it is impossible to solve them in general. Using rank decomposition of Eqs. (2.63) and (2.80), if perturbation functions P_u , and P_h are decomposed into a power series according to rank, the lateral and longitudinal path-deviations Eqs. (2.81) and (2.82) are also decomposed into a series according to rank as follows:

$$u^{(r)}(\tau) = -u_\gamma(\tau) \int_{\tau_0}^{\tau} P_u^{(r)}(\tau) u_\alpha(\tau) d\tau + u_\alpha(\tau) \int_{\tau_0}^{\tau} P_u^{(r)}(\tau) u_\gamma(\tau) d\tau, \quad (2.83)$$

$$h^{(r)}(\tau) = h_p^{(r)}(\tau) - h_\gamma(\tau) \int_{\tau_0}^{\tau} P_h^{(r)}(\tau) h_\alpha(\tau) d\tau + h_\alpha(\tau) \int_{\tau_0}^{\tau} P_h^{(r)}(\tau) h_\gamma(\tau) d\tau, \quad (2.84)$$

where $P_u^{(r)}$ and $P_h^{(r)}$ are perturbation functions of rank- r . If a proper approximation represents $P_u^{(r)}$ and $P_h^{(r)}$ by a combination of known functions, we can calculate Eqs. (2.83) and (2.84), and they give proper correction to path deviations.

The method to obtain an appropriate approximation of $P_u^{(r)}$ and $P_h^{(r)}$ is called perturbation. The concept of perturbation in electron optics has been explained in many literatures, for instance, references [1.90] and [1.91]. However, in many references, they give too much weight to the derivation of general perturbation formulae in mathematics. In addition, after derivation of general formulae, they explain the concrete calculation of the third order geometrical aberration coefficients of a round symmetric system in the standard electron optics theory. Since it provides less information, especially for beginners, to understand the whole procedure of perturbation, systematically, we provide a detailed procedure of perturbation and its meaning, which is not clearly explained in many references. This helps us to understand the derivations of path-deviations explained in section 2.3 and 2.5. Since perturbation functions are also decomposed into a power series according to the exponent of the product of the lateral trajectories, the longitudinal path deviations, and their reduced velocities, i.e., $u, \dot{u}, \ddot{u}, \dot{h}, \ddot{h}$. For the lateral perturbation function,

$$P_u = \sum_{\ell=2}^{\infty} P_{u,\ell}, \quad (2.85)$$

solutions are given by the simple replacement of fundamental solutions inside the integrands, and the resulting particular solutions are equivalent to those before replacement. See Appendix 2.13.3 for details.

³ Accurately, these should not be called functions but functionals, which are functions whose variables are not parameters but are functions, such as $g(f(x), k(x))$. But unless it is confusing, we call them functions.

where

$$P_{u,\ell} = \sum_{\ell_1, \ell_2, \dots, \ell_6 \geq 0} F_{\ell_1 \ell_2 \ell_3 \ell_4 \ell_5 \ell_6}(\tau) u^{\ell_1} \bar{u}^{\ell_2} \dot{u}^{\ell_3} \dot{\bar{u}}^{\ell_4} h^{\ell_5} \dot{h}^{\ell_6}, \quad (2.86)$$

$$\ell = \ell_1 + \ell_2 + \ell_3 + \ell_4 + \ell_5 + \ell_6. \quad (2.87)$$

$P_{u,\ell}$ means a polynomial of products of $u, \bar{u}, \dot{u}, \dot{\bar{u}}, h, \dot{h}$ and the sum of their exponent is ℓ . This expression of a power series is also applicable to the longitudinal perturbation function, whose polynomial is expressed by $P_{h,\ell}$. Rank of $P_{u,\ell}$ and $P_{h,\ell}$ are unknown at this stage, since it depends on the rank of the trajectories of the terms. The subscript ℓ of $P_{u,\ell}$ and $P_{h,\ell}$ shows that the exponent of the polynomial is ℓ .

A procedure so-called perturbation gives an approximate solution as follows.

Step 1, Solving linear equations. Solve the reference electron trajectory equation Eq. (2.13) and the lateral and longitudinal linear equations Eqs. (2.38) and (2.39) to obtain the lateral fundamental rays and the longitudinal fundamental solutions of linear equations. Then, the general paraxial ray Eq. (2.65) and a general longitudinal path deviation of the first-rank Eq. (2.64) are constructed.

Step 2, Approximation of perturbation function up to the lowest exponent ℓ_{min} . Expand perturbation functions as power series of trajectories such as Eq. (2.85) and neglect all terms higher than ℓ_{min} . Note that, as mentioned in section 2.4, for a rotationally symmetric system, $\ell_{min} = 2$.

Step 3, Approximation of trajectories by linear solutions.

At this point, the most precise approximation of trajectories are linear solutions. Replace all lateral trajectory u , and longitudinal path deviation h , their reduced velocities \dot{u}, \dot{h} , and complex conjugates of lateral trajectory and velocity $\bar{u}, \dot{\bar{u}}$, which are included in the lowest exponent terms of the perturbation function obtained in step 3, with corresponding linear solutions of $u^{(1)}, h^{(1)}, \dot{u}^{(1)}, \dot{h}^{(1)}, \bar{u}^{(1)}, \dot{\bar{u}}^{(1)}$. Since all substituted solutions are those of the first-rank, the lowest exponent as terms of rank- ℓ_{min} . We write these terms as

$$\begin{aligned} P_u^{(\ell_{min})} &= P_{u,\ell_{min}}[u^{(1)}, \dot{u}^{(1)}, \bar{u}^{(1)}, \dot{\bar{u}}^{(1)}, h^{(1)}, \dot{h}^{(1)}; \tau], \\ P_h^{(\ell_{min})} &= P_{h,\ell_{min}}[u^{(1)}, \dot{u}^{(1)}, \bar{u}^{(1)}, \dot{\bar{u}}^{(1)}, h^{(1)}, \dot{h}^{(1)}; \tau], \end{aligned} \quad (2.88)$$

where the superscript (ℓ_{min}) shows the rank of the polynomial is ℓ_{min} .

Step 4, Sorting terms by geometrical and chromatic parameters.

Substitute Eqs. (2.64) and (2.65), and their reduced velocities into the solution of the first-rank appeared in the perturbation terms as a result of step 3. Sort these terms by geometrical parameters u_o, \dot{u}_o and the chromatic parameter κ_o . Applying this approximation to Eqs. (2.83) and (2.84), the resulting formulae become path deviation of the lowest rank, which include no unknown trajectories and can be calculated. These give the primary correction to the solutions

of the linear equations Eqs. (2.38) and (2.39). These are path deviations of rank- ℓ_{min} . The lateral path deviation is $u^{(\ell_{min})}$, and the longitudinal path deviation is $h^{(\ell_{min})}$.

Procedures from step 1 to 4 are primary perturbation. In the standard theory of electron optics, whose basic parameter is the optic axis coordinate, for a rotationally symmetric electron lens system, the lowest rank path deviations are rank 2, which is the first order and first degree, proportional to terms such as $u'_o \kappa_o$ which correspond to chromatic aberrations. The lowest rank path deviations that depend on geometrical parameters are the third-rank, that is, third-order in geometrical parameters and with no dependence on the chromatic parameter. Since the second-rank path deviation does not contribute to the third-order geometrical aberrations, in the standard electron optics theory, both procedures to derive the lowest tank chromatic aberration and the lowest order geometrical aberrations of a normal lens system are regarded as primary perturbation, respectively. As we discuss in detail later, in the time-dependent theory, the lowest primary perturbation of a system of round symmetric electrostatic and magnetic fields is of the second-rank for both for lateral and longitudinal path deviations. Similar to standard electron optics, second-rank lateral path deviations are of first-order in geometrical parameters and first-degree for chromatic parameter, and these never contribute to third-order geometrical aberrations. However, for the second-rank longitudinal path deviations $h^{(2)}$, several terms depend on only geometrical parameters, proportional to such as $\dot{u}_o \ddot{u}_o$. Those terms, called the second-order geometrical longitudinal path deviations, contribute to the third-order geometrical path deviations in the lateral direction. A detailed derivation is given later. In the time-dependent theory, secondary perturbation is necessary to obtain the third-order geometrical aberrations. The procedure of secondary perturbation is explained as follows.

Step 5, Calculation of terms of lateral perturbation functions of up to those of the second lowest exponent ℓ_{next} , that is, $P_{u, \ell_{next}}$. Note that, as mentioned in section 2.4, for a rotationally symmetric system, $\ell_{next} = 3$.

Step 6, Approximation of trajectories

At this point, the most precise approximation of trajectories in the lateral and longitudinal directions are formally given by

$$\begin{aligned} u &\approx u^{(1)} + u^{(\ell_{min})}, \\ h &\approx h^{(1)} + h^{(\ell_{min})}, \end{aligned} \quad (2.89)$$

respectively, where $u^{(\ell_{min})}$, and $h^{(\ell_{min})}$ are calculated in step 4. In this step, we aim to obtain path-deviations of rank- ℓ_{next} . Since $P_{u, \ell_{next}}$ includes only terms, whose exponent is ℓ_{next} , contribution to the perturbation function of rank- ℓ_{next} is obtained by substituting $u^{(1)}, h^{(1)}, \dot{u}^{(1)}, \dot{h}^{(1)}, \ddot{u}^{(1)}, \ddot{h}^{(1)}$ into the trajectories of $P_{u, \ell_{next}}$. However the contribution of rank- ℓ_{next} also stems from $P_{u, \ell_{min}}$. At this stage, the most precise known approximation of trajectories is given by

Eq. (2.89). To obtain the contribution to $P_u^{(\ell_{next})}$, Eq. (2.89) should be substituted into $P_{u,\ell_{min}}$, and only terms of rank ℓ_{next} , are collected. This operation gives perturbation terms of rank- ℓ_{next} as follows:

$$P_u^{(\ell_{next})} = P_{u,\ell_{next}}[u^{(1)}, \dot{u}^{(1)}, \bar{u}^{(1)}, \dot{\bar{u}}^{(1)}, h^{(1)}, \dot{h}^{(1)}; \tau] + D^{\ell_{min}} P_{u,\ell_{min}}[u^{(1)}, \dot{u}^{(1)}, \bar{u}^{(1)}, \dot{\bar{u}}^{(1)}, h^{(1)}, \dot{h}^{(1)}; \tau], \quad (2.90)$$

where

$$D^{\ell_{min}} = u^{(\ell_{min})} \frac{\partial}{\partial u^{(1)}} + \bar{u}^{(\ell_{min})} \frac{\partial}{\partial \bar{u}^{(1)}} + \dot{u}^{(\ell_{min})} \frac{\partial}{\partial \dot{u}^{(1)}} + \dot{\bar{u}}^{(\ell_{min})} \frac{\partial}{\partial \dot{\bar{u}}^{(1)}} + h^{(\ell_{min})} \frac{\partial}{\partial h^{(1)}} + \dot{h}^{(\ell_{min})} \frac{\partial}{\partial \dot{h}^{(1)}}. \quad (2.91)$$

Step 7 Sorting terms by geometrical and chromatic parameters.

In this step, the actual operation is the same as that in step 4. The actual expression of the rank- ℓ_{min} and the first-rank trajectories are substituted into Eq. (2.90) and terms are sorted according to dependence on the geometrical and chromatic parameters. As mentioned in section 2.5, to obtain only the third-order geometrical aberration, the terms, that include the chromatic parameters, can be neglected. The resulting expression is substituted into Eq. (2.83), and then the formulae of the third-order geometrical lateral path-deviation is obtained. Note that, if we want to derive the lateral path-deviation of a further higher rank, as preparation, the longitudinal path-deviation of rank- ℓ_{next} is necessary can be calculated by the same method as this step using the longitudinal perturbation function and Eq. (2.84). So, now we are at the point where a procedure of the primary and secondary perturbation of the time-dependent theory is obtained. However, to reach the final goal of this section, further investigation is needed into a method to compensate for difference between the lateral path deviation in the time-dependent theory and that at the image plane.

2.3.2 A method to transform lateral path-deviation defined at time into that defined at a plane perpendicular to the optic axis.

In the standard theory of electron optics, the lateral path deviation at the Gaussian image plane is considered an aberration. Usually, aberration is classified according to its rank and dependence on geometrical parameters, and on the chromatic parameter. We would like to know the aberrations of mirrors in the same sense. However, in the time-dependent theory, since the lateral path deviation is a function of a reduced time, evaluating the lateral path deviation at the convergent time, when an axial ray is focused at the image plane, is not identical to the aberration. In general, when we evaluate the lateral path deviation of an electron at a reduced time τ , since the longitudinal path deviation has a nonzero value, the perturbed electron positions in the z-direction at the reduced time τ are different from one another, according to their dependence on geometrical and chromatic parameters.

Here, to understand the aberration, which indicates lateral electron positions at the image plane, we give a review of a method to compensate for these differences in the z -direction, which was suggested by Preikszas and Rose [1.88][1.89] and further considered by Rose [1.91]. Although they gave this transformation for a system, which consists of both rotationally symmetric electrostatic fields and magnetic fields, we think that their formulae are insufficient in the case that field strength of a rotationally symmetric magnetic field exists at the plane, where path-deviation is transformed. Usually, even if we design electron mirrors which consist of both electrostatic and magnetic field, i.e., the conjugate planes, that is the objective plane and the image plane, are set in a field-free region. As a result, aberration coefficients, which are derived based on their transformation, are valid. However, nowadays, a specimen of a high-resolution SEM is usually located inside the magnetic field of the objective lens to reduce its spherical and chromatic aberration. Such a lens is known as a magnetic immersion lens. In addition, to reduce aberrations in a low-voltage SEM, a retarding electrostatic voltage is imposed on the specimen and a boosting voltage is imposed on the region of the objective lens, which generates a strong electrostatic field around the specimen surface. In a recent SEM, the final image plane is not located in field free region. To analyze an entire system of lenses and mirrors, it is better to consider a more general transformation including the case where an image plane is located inside the magnetic field of a lens. One of the motivations is completion of the time-dependent theory. The author has investigated the modification, which is necessary for a magnetic immersion lens field. In this section, we introduce a modified transformation of the lateral path-deviation.

First, to understand the concept of transformation, we consider electron trajectories in the Cartesian coordinate system. Since the longitudinal path deviation is expressed as a function of the geometrical parameters of the electron, which are the lateral position and reduced velocity at the initial time: w_o , \bar{w}_o , the chromatic parameter κ_o , and the reduced time, explicitly, the longitudinal position is given by

$$z(\tau) = \zeta(\tau) + h(w_o, \bar{w}_o, \dot{w}_o, \dot{\bar{w}}_o, \kappa_o; \zeta(\tau)). \quad (2.92)$$

Since in Eq. (2.92), the reduced time appears, implicitly, only through the reference electron trajectory ζ , the z -coordinate can be regarded as a function of ζ .

According to Rose [1.91], we can use the Lagrange inversion theorem, which gives an inverse function as a power series expansion.

Assuming that z is a function of ζ :

$$z = f(\zeta), \quad (2.93)$$

and the function f is analytic at $z = a$ and has a nonzero first-order derivative, $f'(a) \neq 0$. The inverse function of f is given by

$$\zeta = g(z) = a + \sum_{m=0}^{\infty} \frac{1}{(m+1)!} g_m [z - f(a)]^{m+1}, \quad (2.94)$$

where

$$g_m = \lim_{\zeta \rightarrow a} \left[\frac{d^m}{d\zeta^m} \left(\frac{\zeta - a}{f(\zeta) - f(a)} \right)^{m+1} \right]. \quad (2.95)$$

In our case, z is given by

$$z = f(\zeta) = \zeta + h(\zeta). \quad (2.96)$$

To use Eq. (2.94), we regard a as z , then, by Eq. (2.96), $f(z)$ is given as

$$f(z) = z + h(z). \quad (2.97)$$

Using Eqs. (2.96) and (2.97), we get

$$z - f(z) = f(\zeta) - f(z) = -h(z), \quad (2.98)$$

and

$$\zeta - z = -h(\zeta). \quad (2.99)$$

Then, Eq. (2.95) is transformed as follows:

$$g_m = \lim_{\zeta \rightarrow z} \left[\frac{d^m}{d\zeta^m} \left(\frac{\zeta - z}{f(\zeta) - f(z)} \right)^{m+1} \right] = \frac{1}{h^{m+1}(z)} \frac{d^m}{d\zeta^m} h^{m+1}(\zeta) \Big|_{\zeta=z}. \quad (2.100)$$

Using Eqs. (2.98) and (2.100), Inversion theorem, Eq. (2.94) gives

$$\zeta(z) = z + \sum_{m=0}^{\infty} \frac{(-1)^{m+1}}{(m+1)!} \frac{d^m}{d\zeta^m} h^{m+1}(\zeta) \Big|_{\zeta=z}. \quad (2.101)$$

An explicit expansion of Eq. (2.101), up to cubic order of h , is

$$\zeta(z) = z - h(z) + h(z)h'(z) - \frac{1}{2}h^2(z)h''(z) - h(z)h'^2(z) + \dots \quad (2.102)$$

z in the R.H.S. of Eq. (2.101) means the position of a plane, where we evaluate lateral path-deviation. $\zeta(z)$ means the corresponding reference electron position, when the lateral path-deviation of an electron, whose longitudinal path deviation is given by $h(z)$, is evaluated at an arbitrary plane z .

Here, we can discuss the transformation of lateral path-deviation defined in time into that evaluated at a plane. We consider the trajectory of the lateral direction in a Cartesian coordinate system first. We express the lateral trajectory, which is evaluated at a plane z with a “hat”, such as $\hat{w}(z)$, to distinguish it from the lateral trajectory defined in time, which is written as $w(\tau)$. In time-dependent theory, a reference electron position ζ has correspondence to a reduced time τ . The dependence of w on τ is replaced by that on ζ , formally, such as $w(\zeta(\tau))$. Since a reference electron position ζ is given as a function of the evaluation plane of lateral trajectory z by Eq. (2.101), and taking into account Taylor expansion around $\zeta = z$, we obtain

$$\begin{aligned} \hat{w}(z) &= w(\zeta(z)) \\ &= w(z) - w'(z)h(z) + w'(z)h(z)h'(z) + \frac{1}{2}w''(z)h^2(z) + \dots \end{aligned} \quad (2.103)$$

Although this dependence is not one-to-one for electron mirrors, since a reference electron passes through the same position along the optic axis before and after reflection, as long as we concentrate on path deviation after reflection, Eq. (2.103) provides an appropriate transformation of lateral path deviation defined in time to that evaluated at a plane. It is also valid around the image plane, where we want to evaluate lateral path deviation.

We have obtained a formal transformation of lateral path deviation from that defined in time to that evaluated at a plane. To advance the analysis, a rank-expansion of this transformation is necessary. Since both lateral and longitudinal path deviation w and h are composed of terms of various ranks $r \geq 1$, the transformation of Eq. (2.103) is also decomposed into transformations of different ranks. Up to the third-rank, transformations are given as follows:

$$\hat{w}^{(1)}(z) = w^{(1)}(z), \quad (2.104)$$

$$\hat{w}^{(2)}(z) = w^{(2)}(z) - w'^{(1)}(z)h^{(1)}(z), \quad (2.105)$$

$$\begin{aligned} \hat{w}^{(3)}(z) = & w^{(3)}(z) - w'^{(1)}(z)h^{(2)}(z) - w'^{(2)}(z)h^{(1)}(z) \\ & + w'^{(1)}(z)h^{(1)}(z)h'^{(1)}(z) + \frac{1}{2}w''^{(1)}(z)h^{(1)^2}(z). \end{aligned} \quad (2.106)$$

Since Eq. (2.103) includes derivatives of lateral and longitudinal path deviations with respect to ζ , these terms are divergent at the reflection point. According to Eq. (2.69), such divergence stems from that of $1/\zeta$, because path deviations w , h , and their derivatives with respect to the reduced time are convergent. Especially, we are particularly interested in the lateral rays of mirrors around the image plane. In practical optical systems, the image plane is usually designed to be far from the reflection point, so Eq. (2.103) and the resulting Eqs. (2.104) to (2.106) are not divergent around the image plane.

We have discussed the transformation in a Cartesian coordinate system in Eqs. (2.104) to (2.106). The coordinate system is then moved to a rotation coordinate system to obtain the transformation in that system. According to Eq. (2.21), the first-order and second-order derivatives of the lateral trajectory in the Cartesian coordinate w with respect to ζ are expressed in terms of those in the rotation coordinate u as follows:

$$w' = e^{i\chi}(u' + i\chi'u) = e^{i\chi}\left(u' + i\frac{\eta B}{2\zeta\sqrt{\Phi_c}}u\right), \quad (2.107)$$

and

$$w'' = e^{i\chi}(u'' - \chi'^2u + i\chi''u + 2i\chi'u'). \quad (2.108)$$

Employing Eqs. (2.107) and (2.108) to Eqs. (2.104) to (2.106), the transformation of lateral path deviations, which are defined in the time-dependent theory, and which are the first, second, and third-rank, in the rotation coordinate system into those evaluated at a plane, is as follows:

$$\hat{u}^{(1)}(z) = u^{(1)}(z), \quad (2.109)$$

$$\hat{u}^{(2)} = u^{(2)} - u'^{(1)}h^{(1)} - i\frac{\chi}{\zeta}u^{(1)}h^{(1)}, \quad (2.110)$$

and

$$\begin{aligned}
\hat{u}^{(3)}(z) = & u^{(3)} - u^{(1)}h^{(2)} - i\frac{\dot{\chi}}{\zeta}u^{(1)}h^{(2)} - u^{(2)}h^{(1)} - i\frac{\dot{\chi}}{\zeta}u^{(2)}h^{(1)} + u^{(1)}h^{(1)}h^{(1)} \\
& + i\frac{\dot{\chi}}{\zeta}u^{(1)}h^{(1)}h^{(1)} + \frac{1}{2}u''^{(1)}h^{(1)^2} - \frac{\dot{\chi}^2}{2\zeta^2}u^{(1)}h^{(1)^2} \\
& + i\frac{\dot{\chi}}{2\zeta^2}u^{(1)}h^{(1)^2} + i\frac{\dot{\chi}}{\zeta}u^{(1)}h^{(1)^2},
\end{aligned} \tag{2.111}$$

where $\dot{\chi}$ is given by the integrand of Eq. (2.20), and ζ is given by Eq. (2.15). The reduced time derivative of the rotation angle χ , which corresponds to a reduced angular velocity, is given by

$$\dot{\chi} = \frac{\eta B}{2\sqrt{\Phi_c}} \tag{2.112}$$

which are proportional to the rotationally symmetric magnetic field on the optic axis. As long as the plane, where the lateral trajectory is evaluated using Eqs. (2.109) to (2.111), is located in a field-free region, where both $\Phi' = 0$, and $B = 0$, the reduced angular velocity is $\dot{\chi} = 0$, and $\ddot{\chi} = 0$. As a result, if $B = 0$ at a certain plane z , Eqs. (2.110) and (2.111) simplify significantly:

$$\hat{u}^{(2)} = u^{(2)} - u^{(1)}h^{(1)}, \tag{2.113}$$

$$\hat{u}^{(3)}(z) = u^{(3)} - u^{(1)}h^{(2)} - u^{(2)}h^{(1)} + u^{(1)}h^{(1)}h^{(1)} + \frac{1}{2}u''^{(1)}h^{(1)^2}. \tag{2.114}$$

Rose and Preikszas derived transformations up to the third-rank, in the rotation coordinate, for a field-free region, Eqs. (2.113) and (2.114), only. However, in a more general case where the image plane is located inside a rotationally symmetric magnetic field, Eqs. (2.110) and (2.111) derived here give the proper transformation.

Now, we review transformation formulae of lateral path deviation from those defined in the time-dependent theory to that evaluated at a plane perpendicular to the optic axis. These transformation formulae are valid for mirrors when we consider them either before or after reflection and the evaluation plane is located far from the reflection plane. We have modified the original theory, which was only valid when the evaluation plane was located in a field-free region. The formulae derived in this review are valid in cases where the image plane is located inside a rotationally symmetric magnetic field. However, to derive path deviations concretely, we still need to calculate the concrete form of the perturbation functions.

2.3.3 Explicit form of perturbation functions of second- and third-rank

Here, we review the explicit form of the lateral perturbation function up to cubic contributions to the path deviations.

Based on the procedure explained in section 2.3.1.

Employing Eqs. (2.25) to (2.28) and (2.35) to (2.37), we obtain the general form of perturbation functions as follows:

$$P_u = \frac{i\eta B'}{2\sqrt{\Phi_c}} u\dot{h} + \sum_{n+m \geq 1}^{\infty} \frac{(-1)^n}{(n!)^2 m!} \left(\frac{u\bar{u}}{4}\right)^n h^m B^{[2n+m]} \left(-\frac{\eta^2 B}{2\Phi_c} u + \frac{i\eta}{\sqrt{\Phi_c}} \dot{u} \right) - \sum_{n+m \geq 1}^{\infty} \frac{(-1)^n}{2(n+1)! n! m!} \left(\frac{u\bar{u}}{4}\right)^n u h^m \left(\frac{\Phi^{[2n+m+2]}}{2\Phi_c} + \frac{i\eta}{\sqrt{\Phi_c}} (\dot{\zeta} + \dot{h}) B^{[2n+m+1]} \right), \quad (2.115)$$

and

$$P_h = \sum_{n=0}^{\infty} \sum_{m=0}^{\infty} \frac{(-1)^{n+1}}{2(n+1)! n! m!} \left(\frac{u\bar{u}}{4}\right)^n h^m B^{[2n+m+1]} \left[\frac{\eta^2 B}{2\Phi_c} u\bar{u} + \frac{i\eta}{2\sqrt{\Phi_c}} (u\dot{\bar{u}} - \bar{u}\dot{u}) \right] + \sum_{n=1}^{\infty} \sum_{m=0}^{\infty} \frac{(-1)^n}{(n!)^2 m!} \left(\frac{u\bar{u}}{4}\right)^n h^m \frac{\Phi^{[2n+m+1]}}{2\Phi_c} + \sum_{m=0}^{\infty} \frac{1}{(m+2)!} h^{m+2} \frac{\Phi^{[m+3]}}{2\Phi_c}, \quad (2.116)$$

where equivalent formulae of these two equations, with different notation, were already given in reference [1.89].

Explicit expansions of Eqs. (2.115) and (2.116), up to cubic terms of path deviations and their reduced time derivatives, are given as follows:

$$P_u = \frac{i\eta}{\sqrt{\Phi_c}} \left[\frac{1}{2} \dot{\zeta} B'' u h - \frac{1}{16} \dot{\zeta} B^{[3]} u^2 \bar{u} + \frac{1}{4} \dot{\zeta} B^{[3]} u h^2 + \frac{1}{2} B' u \dot{h} + \frac{1}{2} B'' u h \dot{h} + B' \dot{u} h - \frac{1}{4} B'' u \bar{u} \dot{u} + \frac{1}{2} B'' \dot{u} h^2 \right] - \frac{1}{4\Phi_c} (\Phi^{[3]} + 2\eta^2 B B') u h + \frac{1}{32\Phi_c} (\Phi^{[4]} + 4\eta^2 B B'') u^2 \bar{u} - \frac{1}{8\Phi_c} (\Phi^{[4]} + 2\eta^2 B B'') u h^2 + \dots, \quad (2.117)$$

where

$$\begin{aligned} L_1 &= \Phi^{[3]} + 2\eta^2 B B', \\ L_2 &= \Phi^{[4]} + 4\eta^2 B B'. \end{aligned} \quad (2.118)$$

These explicit expressions up to cubic terms were not shown in reference [1.89], and the explicit expressions for only pure electrostatic mirror system were given in reference [1.88] and [1.91], which corresponds to the case where B and its differentiation with respect to the optic axis coordinate vanish. To make the calculation simpler, we can find that several terms form a total derivative with respect to the reduced time:

$$P_u = \frac{i\eta}{\sqrt{\Phi_c}} \left[\frac{1}{2} \frac{d}{d\tau} (B' u h) + \frac{1}{2} B' \dot{u} h + \frac{1}{4} \frac{d}{d\tau} (B'' u h^2) + \frac{1}{4} B'' \dot{u} h^2 - \frac{1}{16} \dot{\zeta} B^{[3]} u^2 \bar{u} - \frac{1}{4} B'' u \bar{u} \dot{u} \right] - \frac{L_1}{4\Phi_c} u h + \frac{L_2}{32\Phi_c} u^2 \bar{u} - \frac{1}{8\Phi_c} (\Phi^{[4]} + 2\eta^2 B B'') u h^2 + \dots. \quad (2.119)$$

Since the reduced time-variable integration will be done using perturbation functions during the procedure of perturbation, total derivative terms are calculated by partial integration and simplify the formulae. An explicit calculation is given in the next section.

For the longitudinal perturbation function, it is sufficient to calculate the explicit expansion up to quadratic terms, since the second rank longitudinal path deviation contributes to the lateral aberration of mirrors up to the third order.

It is given as follows:

$$P_h = -\frac{i\eta B'}{4\sqrt{\Phi_C}}(u\dot{\bar{u}} - \bar{u}\dot{u}) - \frac{L_1}{8\Phi_C}u\bar{u} + \frac{\Phi^{[3]}}{4\Phi_C}h^2 + \dots \quad (2.120)$$

Now we have derived explicit expressions of perturbation functions, which correspond to the results indicated in step 2 and step 5 of the perturbation procedure given in section 2.3.1. For step 3 of the perturbation procedure, general linear solutions of the lateral and longitudinal directions are substituted into $u, \bar{u}, \dot{u}, \dot{\bar{u}}, h, \dot{h}$ of the quadratic term of Eqs. (2.119) and (2.120). The lateral perturbation function of the second rank is given by

$$P_u^{(2)} = \frac{i\eta}{\sqrt{\Phi_C}} \left[\frac{1}{2} \frac{d}{d\tau} (B'u^{(1)}h^{(1)}) + \frac{1}{2} B'\dot{u}^{(1)}h^{(1)} \right] - \frac{L_1}{4\Phi_C} u^{(1)}h^{(1)}, \quad (2.121)$$

and the longitudinal perturbation function of the second rank is given by

$$P_h^{(2)} = -\frac{i\eta B'}{4\sqrt{\Phi_C}}(u^{(1)}\dot{\bar{u}}^{(1)} - \bar{u}^{(1)}\dot{u}^{(1)}) - \frac{L_1}{8\Phi_C}u^{(1)}\bar{u}^{(1)} + \frac{\Phi^{[3]}}{4\Phi_C}h^{(1)2}. \quad (2.122)$$

To calculate the lateral perturbation function of the third rank, according to step 6 of a procedure of the perturbation, we must substitute linear solutions into the cubic terms of the lateral perturbation function. In addition, not only linear solutions but also second-rank perturbative path deviations of the lateral and longitudinal directions, which result from the primary perturbation calculated concretely in the next section, are substituted into the quadratic terms of lateral function to generate third rank terms. The resulting third rank lateral perturbation function is given by

$$\begin{aligned} P_u^{(3)} = & \frac{i\eta}{\sqrt{\Phi_C}} \left[\frac{1}{2} \frac{d}{d\tau} (B'u^{(2)}h^{(1)} + B'u^{(1)}h^{(2)}) + \frac{1}{2} B'(\dot{u}^{(2)}h^{(1)} + \dot{u}^{(1)}h^{(2)}) \right. \\ & + \frac{1}{4} \frac{d}{d\tau} (B''u^{(1)}h^{(1)2}) + \frac{1}{4} B''\dot{u}^{(1)}h^{(1)2} - \frac{1}{16} \zeta B^{[3]}u^{(1)2}\bar{u}^{(1)} \\ & \left. - \frac{1}{4} B''u^{(1)}\bar{u}^{(1)}\dot{u}^{(1)} \right] - \frac{L_1}{4\Phi_C} (u^{(2)}h^{(1)} + u^{(1)}h^{(2)}) \\ & + \frac{L_2}{32\Phi_C} u^{(1)2}\bar{u}^{(1)} - \frac{1}{8\Phi_C} (\Phi^{[4]} + 2\eta^2 BB'')u^{(1)}h^{(1)2}. \end{aligned} \quad (2.123)$$

Eqs. (2.122) and (2.123) are still too complicated, because we are only interested in the third order geometrical path deviation in the lateral direction. Terms including the chromatic parameter in Eqs. (2.122) and (2.123) can be neglected. Since the first rank longitudinal path deviation $h^{(1)}$ depends on the chromatic parameter according to Eq. (2.64), the second order geometrical longitudinal perturbation function is given by

$$\begin{aligned} P_{h_{\text{geo}}}^{(2)} = & -\frac{i\eta B'}{4\sqrt{\Phi_C}}(u^{(1)}\dot{\bar{u}}^{(1)} - \bar{u}^{(1)}\dot{u}^{(1)}) - \frac{L_1}{8\Phi_C}u^{(1)}\bar{u}^{(1)} + \dots \\ & = -\frac{i\eta B'}{4\sqrt{\Phi_C}}(u_o\dot{\bar{u}}_o - \dot{u}_o\bar{u}_o) - \frac{L_1}{8\Phi_C}u^{(1)}\bar{u}^{(1)}, \end{aligned} \quad (2.124)$$

where the relation

$$u^{(1)}\dot{\bar{u}}^{(1)} - \bar{u}^{(1)}\dot{u}^{(1)} = u_o\dot{\bar{u}}_o - \dot{u}_o\bar{u}_o = \text{const}, \quad (2.125)$$

is used in the second line. Due to the second order geometrical longitudinal perturbation function, the primary perturbation gives the second order geometrical longitudinal path deviation $h_{\text{geo}}^{(2)}$, which contributes to third order geometrical perturbation function in the lateral direction:

$$P_u^{(3)}{}_{\text{geo.}} = \frac{i\eta}{\sqrt{\Phi_C}} \left[\frac{1}{2} \frac{d}{d\tau} (B' u^{(1)} h_{\text{geo}}^{(2)}) + \frac{1}{2} B' \dot{u}^{(1)} h_{\text{geo}}^{(2)} - \frac{1}{16} \zeta B^{[3]} u^{(1)^2} \ddot{u}^{(1)} - \frac{1}{4} B'' u^{(1)} \ddot{u}^{(1)} \dot{u}^{(1)} \right] - \frac{L_1}{4\Phi_C} u^{(1)} h_{\text{geo}}^{(2)} + \frac{L_2}{32\Phi_C} u^{(1)^2} \ddot{u}^{(1)} \quad (2.126)$$

We are at the point where explicit formulae for the perturbation function of the second rank and third order geometrical path deviations are derived. The calculation of path deviations is given in the next section 2.4.

2.4 The second-rank lateral path deviation and the second-rank aberration coefficients and the chromatic aberrations

Here, concrete formulae for the second-rank lateral path deviation and the second-rank aberration coefficients are derived. We mention the earlier research of aberration formulae by Rose and Preiksas again. Off-axis aberration coefficients and lateral path deviations for the system composed of only electrostatic mirrors were derived by Preiksas [1.90]. On-axis aberrations, such as Cs and Cc, in the case of a magnetic field overlapping with the electrostatic field, were derived by Rose and Preiksas [1.89]. These results are only valid when the image plane is located inside a field-free region.

In this section, the review of the method as done in sections 2.2 and 2.3, finished and formulae including new results are derived, specifically off-axis aberration coefficients in cases where there is a magnetic field overlapping with the electrostatic field. These derived results are also valid when the object plane is located inside a magnetic field. Of course, the method of derivation is still based on reference [1.88][1.89] and [1.91], reviewed in section 2.3.1 and 2.3.2. In this section, we derive formulae for aberrations and path deviations of the second-rank. The third-order geometrical aberrations will be derived in section 2.5. In the previous section 2.3.3, we derived the lateral perturbation functions of second-rank in Eq. (2.121). According to step 4 of the perturbation procedure, using Eq. (2.121), Eq. (2.83) is applied to calculate the lateral path deviation of second-rank:

$$u^{(2)} = -u_\gamma \int_{\tau_0}^{\tau} \left(-\frac{L_1}{4\Phi_C} u^{(1)} h^{(1)} + \frac{i\eta}{2\sqrt{\Phi_C}} \left[\frac{d}{d\tau} (B' u^{(1)} h^{(1)}) + B' \dot{u}^{(1)} h^{(1)} \right] \right) u_\alpha d\tau + u_\alpha \int_{\tau_0}^{\tau} \left(-\frac{L_1}{4\Phi_C} u^{(1)} h^{(1)} + \frac{i\eta}{2\sqrt{\Phi_C}} \left[\frac{d}{d\tau} (B' u^{(1)} h^{(1)}) + B' \dot{u}^{(1)} h^{(1)} \right] \right) u_\gamma d\tau. \quad (2.127)$$

The integrand includes differentiation with respect to the reduced velocity. Since trajectories u and h , their reduced velocities and the magnetic field B are smooth and have no singularities with respect to the reduced time, the contribution from these differentiations to the path deviations can be simplified by partial integration as follows:

$$\begin{aligned}
u^{(2)} &= u_\gamma \int_{\tau_o}^{\tau} \frac{L_1}{4\Phi_C} u^{(1)} h^{(1)} u_\alpha d\tau - u_\alpha \int_{\tau_o}^{\tau} \frac{L_1}{4\Phi_C} u^{(1)} h^{(1)} u_\gamma d\tau \\
&+ \frac{i\eta}{2\sqrt{\Phi_C}} \left(-u_\gamma \int_{\tau_o}^{\tau} B' \dot{u}^{(1)} h^{(1)} u_\alpha d\tau + u_\alpha \int_{\tau_o}^{\tau} B' \dot{u}^{(1)} h^{(1)} u_\gamma d\tau + u_\gamma \int_{\tau_o}^{\tau} B' u^{(1)} h^{(1)} \dot{u}_\alpha d\tau \right. \\
&\quad \left. - u_\alpha \int_{\tau_o}^{\tau} B' u^{(1)} h^{(1)} \dot{u}_\gamma d\tau - B'_o u_o h_o^{(1)} u_\alpha \right) \\
&= u_\gamma \int_{\tau_o}^{\tau} \frac{L_1}{4\Phi_C} u^{(1)} h^{(1)} u_\alpha d\tau - u_\alpha \int_{\tau_o}^{\tau} \frac{L_1}{4\Phi_C} u^{(1)} h^{(1)} u_\gamma d\tau \\
&+ \frac{i\eta}{2\sqrt{\Phi_C}} \left(u^{(1)} \int_{\tau_o}^{\tau} B' h^{(1)} d\tau - B'_o u_o h_o^{(1)} u_\alpha \right),
\end{aligned} \tag{2.128}$$

where, we used

$$\begin{aligned}
\dot{u}^{(1)} u_\gamma - u^{(1)} \dot{u}_\gamma &= \dot{u}_o, \\
\dot{u}^{(1)} u_\alpha - u^{(1)} \dot{u}_\alpha &= -u_o,
\end{aligned} \tag{2.129}$$

which are obtained by using Eqs. (2.40) and (2.41).

By Eqs. (2.52) and (2.61), the initial value of the first-rank longitudinal path deviation and its derivative are given by

$$h_o^{(1)} = 0, \quad \dot{h}_o^{(1)} = \frac{1}{2} \dot{\zeta}_o \kappa_o. \tag{2.130}$$

Using Eqs. (2.49) to (2.51), the second-rank path deviation in Eq. (2.128) is transformed as follows:

$$u^{(2)} = (u_{\alpha\kappa}^{(R)} + i u_{\alpha\kappa}^{(I)}) \dot{u}_o \kappa_o + (u_{\gamma\kappa}^{(R)} + i u_{\gamma\kappa}^{(I)}) u_o \kappa_o, \tag{2.131}$$

where

$$u_{\alpha\kappa}^{(R)} = u_\gamma \int_{\tau_o}^{\tau} \frac{\dot{\zeta}_o}{8\Phi_C} L_1 u_\alpha^2 h_\alpha d\tau - u_\alpha \int_{\tau_o}^{\tau} \frac{\dot{\zeta}_o}{8\Phi_C} L_1 u_\alpha u_\gamma h_\alpha d\tau, \tag{2.132}$$

$$u_{\alpha\kappa}^{(I)} = u_\alpha \int_{\tau_o}^{\tau} \frac{\dot{\zeta}_o \eta B'}{4\sqrt{\Phi_C}} h_\alpha d\tau, \tag{2.133}$$

$$u_{\gamma\kappa}^{(R)} = u_\gamma \int_{\tau_o}^{\tau} \frac{\dot{\zeta}_o}{8\Phi_C} L_1 u_\alpha u_\gamma h_\alpha d\tau - u_\alpha \int_{\tau_o}^{\tau} \frac{\dot{\zeta}_o}{8\Phi_C} L_1 u_\gamma^2 h_\alpha d\tau, \tag{2.134}$$

$$u_{\gamma\kappa}^{(I)} = u_\gamma \int_{\tau_o}^{\tau} \frac{\dot{\zeta}_o \eta B'}{4\sqrt{\Phi_C}} h_\alpha d\tau. \tag{2.135}$$

The differentiation of the second-rank lateral path deviation with respect to the reduced time is given by

$$\dot{u}^{(2)} = (\dot{u}_{\alpha\kappa}^{(R)} + i \dot{u}_{\alpha\kappa}^{(I)}) \dot{u}_o \kappa_o + (\dot{u}_{\gamma\kappa}^{(R)} + i \dot{u}_{\gamma\kappa}^{(I)}) u_o \kappa_o, \tag{2.136}$$

where

$$\dot{u}_{\alpha\kappa}^{(R)} = \dot{u}_\gamma \int_{\tau_o}^{\tau} \frac{\dot{\zeta}_o}{8\Phi_C} L_1 u_\alpha^2 h_\alpha d\tau - \dot{u}_\alpha \int_{\tau_o}^{\tau} \frac{\dot{\zeta}_o}{8\Phi_C} L_1 u_\alpha u_\gamma h_\alpha d\tau, \tag{2.137}$$

$$\dot{u}_{\alpha\kappa}^{(I)} = \dot{u}_\alpha \int_{\tau_o}^{\tau} \frac{\dot{\zeta}_o \eta B'}{4\sqrt{\Phi_C}} h_\alpha d\tau + \frac{\dot{\zeta}_o \eta B'}{4\sqrt{\Phi_C}} h_\alpha u_\alpha, \tag{2.138}$$

$$\dot{u}_{\gamma\kappa}^{(R)} = \dot{u}_\gamma \int_{\tau_o}^{\tau} \frac{\dot{\zeta}_o}{8\Phi_C} L_1 u_\alpha u_\gamma h_\alpha d\tau - \dot{u}_\alpha \int_{\tau_o}^{\tau} \frac{\dot{\zeta}_o}{8\Phi_C} L_1 u_\gamma^2 h_\alpha d\tau, \tag{2.139}$$

$$\dot{u}_{\gamma\kappa}^{(I)} = \dot{u}_\gamma \int_{\tau_o}^{\tau} \frac{\dot{\zeta}_o \eta B'}{4\sqrt{\Phi_C}} h_\alpha d\tau + \frac{\dot{\zeta}_o \eta B'}{4\sqrt{\Phi_C}} h_\alpha u_\gamma. \tag{2.140}$$

We have derived the second-rank lateral path deviation as defined in time-dependent theory. As explained in section 2.3.2, we must transform it to the path deviation evaluated in a plane perpendicular to the optic axis. For the second-

rank, that transformation is given by Eq. (2.110). The second-rank lateral path deviation at an arbitrary plane is given by

$$\hat{u}^{(2)}(z) = \left(\hat{u}_{\alpha\kappa}^{(R)}(z) + i\hat{u}_{\alpha\kappa}^{(I)}(z) \right) \dot{u}_o \kappa_o + \left(\hat{u}_{\gamma\kappa}^{(R)}(z) + i\hat{u}_{\gamma\kappa}^{(I)}(z) \right) u_o \kappa_o, \quad (2.141)$$

where

$$\hat{u}_{\alpha\kappa}^{(R)}(z) = \left[u_{\alpha\kappa}^{(R)}(\tau) - \frac{\dot{\zeta}_o}{2\dot{\zeta}(\tau)} \dot{u}_\alpha(\tau) h_\alpha(\tau) \right]_{\zeta(\tau)=z}, \quad (2.142)$$

$$\hat{u}_{\alpha\kappa}^{(I)} = u_{\alpha\kappa}^{(I)} - \frac{\dot{\zeta}_o}{\dot{\zeta}} \frac{\eta B}{4\sqrt{\Phi_c}} u_\alpha h_\alpha, \quad (2.143)$$

$$\hat{u}_{\gamma\kappa}^{(R)} = u_{\gamma\kappa}^{(R)} - \frac{\dot{\zeta}_o}{2\dot{\zeta}} \dot{u}_\gamma h_\alpha, \quad (2.144)$$

$$\hat{u}_{\gamma\kappa}^{(I)} = u_{\gamma\kappa}^{(I)} - \frac{\dot{\zeta}_o}{\dot{\zeta}} \frac{\eta B}{4\sqrt{\Phi_c}} u_\gamma h_\alpha. \quad (2.145)$$

The argument of the right-hand-side of these formulae is the reduced time τ when the reference electron reaches the given plane z . This τ is given by $\zeta(\tau) = z$.

As mentioned before, these formulae are valid when z is far from the reflection plane. Since $\dot{u}_o = \dot{\zeta}_o u'_o$, as long as the object plane is far from the reflection plane, Eq. (2.141) is transformed as follows:

$$\hat{u}^{(2)}(z) = \dot{\zeta}_o \left(\hat{u}_{\alpha\kappa}^{(R)}(z) + i\hat{u}_{\alpha\kappa}^{(I)}(z) \right) u'_o \kappa_o + \left(\hat{u}_{\gamma\kappa}^{(R)}(z) + i\hat{u}_{\gamma\kappa}^{(I)}(z) \right) u_o \kappa_o. \quad (2.146)$$

We derived the actual path deviations of second rank, which are defined by u_o and u'_o , and κ_o , similar to standard electron optics. The value of Eq. (2.146) at the image plane gives the second-rank aberration of the mirror system. Considering the analogy to the standard electron optics, the second-rank aberration, defined at the object plane, is given by

$$\Delta u_o^{(2)} = \frac{\hat{u}^{(2)}(z_i)}{M} = C_{co} u'_o \kappa_o + (C_{mo} + iC_{ro}) u_o \kappa_o, \quad (2.147)$$

where C_{co} , C_{mo} , and C_{ro} are the axial chromatic aberration coefficient, the chromatic magnification coefficient, and the chromatic rotation coefficient, respectively.

Using the equations $u_{\alpha i} = 0$, $u_{\gamma i} = M$, and $\dot{u}_{\alpha i} = \frac{1}{M}$, these coefficients are given by

$$C_{co} = \int_{\tau_o}^{\tau_i} \frac{\dot{\zeta}_o^2}{8\Phi_c} L_1 u_\alpha^2 h_\alpha d\tau - \frac{\dot{\zeta}_o^2}{2\dot{\zeta}_i} \dot{u}_{\alpha i}^2 h_{\alpha i}, \quad (2.148)$$

$$C_{mo} = \int_{\tau_o}^{\tau_i} \frac{\dot{\zeta}_o}{8\Phi_c} L_1 u_\alpha u_\gamma h_\alpha d\tau - \frac{\dot{\zeta}_o}{2\dot{\zeta}_i} \dot{u}_{\alpha i} \dot{u}_{\gamma i} h_{\alpha i}, \quad (2.149)$$

$$C_{ro} = \int_{\tau_o}^{\tau_i} \frac{\dot{\zeta}_o \eta B'}{4\sqrt{\Phi_c}} h_\alpha d\tau - \frac{\dot{\zeta}_o}{\dot{\zeta}_i} \frac{\eta B_i}{4\sqrt{\Phi_c}} h_{\alpha i}, \quad (2.150)$$

and the coefficient of $u'_o \kappa_o$ has no imaginary part because Eq. (2.143) vanishes at the image plane. We derived second-rank chromatic aberration coefficients as defined at the object plane. In addition, we can obtain second-rank slope

deviations by using Eq. (2.146). By Eq. (2.38), the second order differentiation of the lateral paraxial solutions with respect to the reduced time is transformed as follows:

$$\ddot{u}_A = -\frac{N}{4\Phi_C} u_A, \quad (2.151)$$

where the subscript A takes either α or γ . The second-rank slope deviation is given by

$$\hat{u}'^{(2)}(z) = \dot{\zeta}_o \left(\hat{u}'_{\alpha\kappa}^{(R)}(z) + i\hat{u}'_{\alpha\kappa}^{(I)}(z) \right) u'_o \kappa_o + \left(\hat{u}'_{\gamma\kappa}^{(R)}(z) + i\hat{u}'_{\gamma\kappa}^{(I)}(z) \right) u_o \kappa_o, \quad (2.152)$$

where

$$\hat{u}_{\alpha\kappa}^{(R)} = \frac{1}{\dot{\zeta}} \dot{u}_{\alpha\kappa}^{(R)} + \frac{\dot{\zeta}_o \Phi'}{4\dot{\zeta}^2 \Phi_C} \dot{u}_\alpha h_\alpha - \frac{\dot{\zeta}_o N}{8\dot{\zeta}^2 \Phi_C} u_\alpha h_\alpha - \frac{\dot{\zeta}_o}{2\dot{\zeta}^2} \dot{u}_\alpha \dot{h}_\alpha, \quad (2.153)$$

$$\hat{u}_{\alpha\kappa}^{(I)} = \frac{1}{\dot{\zeta}} \dot{u}_{\alpha\kappa}^{(I)} - \frac{\dot{\zeta}_o}{\dot{\zeta}^2} \frac{\eta B}{4\sqrt{\Phi_C}} (\dot{u}_\alpha h_\alpha + u_\alpha \dot{h}_\alpha) - \frac{\dot{\zeta}_o}{\dot{\zeta}} \frac{\eta B'}{4\sqrt{\Phi_C}} u_\alpha h_\alpha + \frac{\dot{\zeta}_o}{\dot{\zeta}^3} \frac{\Phi' \eta B}{8\Phi_C^{3/2}} u_\alpha h_\alpha, \quad (2.154)$$

$$\hat{u}_{\gamma\kappa}^{(R)} = \frac{1}{\dot{\zeta}} \dot{u}_{\gamma\kappa}^{(R)} + \frac{\dot{\zeta}_o \Phi'}{4\dot{\zeta}^2 \Phi_C} \dot{u}_\gamma h_\alpha - \frac{\dot{\zeta}_o N}{8\dot{\zeta}^2 \Phi_C} u_\gamma h_\alpha - \frac{\dot{\zeta}_o}{2\dot{\zeta}^2} \dot{u}_\gamma \dot{h}_\alpha, \quad (2.155)$$

$$\hat{u}_{\gamma\kappa}^{(I)} = \frac{1}{\dot{\zeta}} \dot{u}_{\gamma\kappa}^{(I)} - \frac{\dot{\zeta}_o}{\dot{\zeta}^2} \frac{\eta B}{4\sqrt{\Phi_C}} (\dot{u}_\gamma h_\alpha + u_\gamma \dot{h}_\alpha) - \frac{\dot{\zeta}_o}{\dot{\zeta}} \frac{\eta B'}{4\sqrt{\Phi_C}} u_\gamma h_\alpha + \frac{\dot{\zeta}_o}{\dot{\zeta}^3} \frac{\Phi' \eta B}{8\Phi_C^{3/2}} u_\gamma h_\alpha. \quad (2.156)$$

Here, we are the point where the second-rank path deviation, the chromatic aberration coefficients as defined at the object plane, and the second-rank slope deviation have been derived. The next section discusses concrete forms of the third order geometrical aberrations.

2.5 Second-order longitudinal path deviation, third-order geometrical lateral path deviation & third-order geometrical aberration coefficients

Here we discuss the third-order geometrical aberrations in the time-dependent formalism. These formulae apply to the case of a magnetic field overlapping with the electrostatic field, including both on- and off-axis aberrations, and are still valid when the image plane is located inside a magnetic field. As we mentioned, an earlier study derived on- and off-axis third-order geometrical aberration coefficients only for electrostatic mirrors [1.90], and on-axis aberration, such as spherical aberration, in the case of a magnetic field overlapping with the electrostatic field [1.89], which are only valid when the image plane is located inside a field-free region.

Since the third-order geometrical lateral perturbation function Eq. (2.126), includes the second-order longitudinal path deviation $h_{\text{geo.}}^{(2)}$, according to step 4 and 7, first, the second-order longitudinal path deviation should be calculated. By Eqs. (2.62) and (2.84), the second-order geometrical longitudinal path deviation is given by

$$\begin{aligned} h_{\text{geo.}}^{(2)}(\tau) &= h_p^{(2)}(\tau) - h_\gamma(\tau) \int_{\tau_o}^{\tau} P_h^{(2)}(\tau) h_\alpha(\tau) d\tau \\ &+ h_\alpha(\tau) \int_{\tau_o}^{\tau} P_h^{(2)}(\tau) h_\gamma(\tau) d\tau, \end{aligned} \quad (2.157)$$

where

$$h_p^{(2)}{}_{\text{geo.}} = \left[-\frac{1}{2\dot{\zeta}_o} \dot{u}_o \ddot{u}_o - \frac{N_o}{8\dot{\zeta}_o \Phi_C} u_o \bar{u}_o - \frac{i\eta B_o}{4\dot{\zeta}_o \sqrt{\Phi_C}} (u_o \ddot{u}_o - \dot{u}_o \bar{u}_o) \right] h_\alpha. \quad (2.158)$$

Using Eq. (2.124), the parameter expansion of the second-order geometrical longitudinal path deviation is given by

$$h_{\text{geo.}}^{(2)}(\tau) = h_{\alpha\bar{\alpha}}(\tau) \dot{u}_o \ddot{u}_o + h_{\alpha\gamma}^{(R)}(\tau) (u_o \ddot{u}_o + \bar{u}_o \dot{u}_o) + i h_{\alpha\gamma}^{(I)}(\tau) (u_o \ddot{u}_o - \bar{u}_o \dot{u}_o) + h_{\gamma\bar{\gamma}}(\tau) u_o \bar{u}_o, \quad (2.159)$$

where

$$h_{\alpha\bar{\alpha}}(\tau) = -\frac{1}{2\dot{\zeta}_o} h_\alpha + h_\gamma \int_{\tau_o}^\tau \frac{L_1}{8\Phi_C} u_\alpha^2 h_\alpha d\tau - h_\alpha \int_{\tau_o}^\tau \frac{L_1}{8\Phi_C} u_\alpha^2 h_\gamma d\tau, \quad (2.160)$$

$$h_{\alpha\gamma}^{(R)}(\tau) = h_\gamma \int_{\tau_o}^\tau \frac{L_1}{8\Phi_C} u_\alpha u_\gamma h_\alpha d\tau - h_\alpha \int_{\tau_o}^\tau \frac{L_1}{8\Phi_C} u_\alpha u_\gamma h_\gamma d\tau, \quad (2.161)$$

$$h_{\alpha\gamma}^{(I)}(\tau) = -\frac{\eta B_o}{4\dot{\zeta}_o \sqrt{\Phi_C}} h_\alpha + h_\gamma \int_{\tau_o}^\tau \frac{\eta B'}{4\sqrt{\Phi_C}} h_\alpha d\tau - h_\alpha \int_{\tau_o}^\tau \frac{\eta B'}{4\sqrt{\Phi_C}} h_\gamma d\tau, \quad (2.162)$$

$$h_{\gamma\bar{\gamma}}(\tau) = -\frac{N_o}{8\dot{\zeta}_o \Phi_C} h_\alpha + h_\gamma \int_{\tau_o}^\tau \frac{L_1}{8\Phi_C} u_\gamma^2 h_\alpha d\tau - h_\alpha \int_{\tau_o}^\tau \frac{L_1}{8\Phi_C} u_\gamma^2 h_\gamma d\tau. \quad (2.163)$$

Now we have derived the second-order geometrical longitudinal path deviations. Using these formulae, the third-order geometrical aberrations can be derived. Using Eqs. (2.83), (2.126), and (2.159), and sorting by order of u_o , and \dot{u}_o , the third order geometrical path deviation can be derived. However, it is advantageous to simplify part of them in advance. Part of the third-order geometrical perturbation function includes terms for differentiation with respect to the reduced time. This differentiation produces many complicated terms. Since a corresponding part of the lateral path deviation has reduced time integration, where integrand is composed of a product of the lateral paraxial ray, u_α or u_γ , and derivative terms, this derivative can be removed by partial integration as follows:

$$\begin{aligned} I_u^{(3)} &= -u_\gamma \int_{\tau_o}^\tau \frac{i\eta}{\sqrt{\Phi_C}} \left[\frac{1}{2} \frac{d}{d\tau} (B' u^{(1)} h^{(2)}) + \frac{1}{2} B' \dot{u}^{(1)} h^{(2)} - \frac{1}{16} \frac{d}{d\tau} (B'') u^{(1)2} \bar{u}^{(1)} \right. \\ &\quad \left. - \frac{1}{4} B'' u^{(1)} \bar{u}^{(1)} \dot{u}^{(1)} \right] u_\alpha d\tau \\ &+ u_\alpha \int_{\tau_o}^\tau \frac{i\eta}{\sqrt{\Phi_C}} \left[\frac{1}{2} \frac{d}{d\tau} (B' u^{(1)} h^{(2)}) + \frac{1}{2} B' \dot{u}^{(1)} h^{(2)} - \frac{1}{16} \frac{d}{d\tau} (B'') u^{(1)2} \bar{u}^{(1)} \right. \\ &\quad \left. - \frac{1}{4} B'' u^{(1)} \bar{u}^{(1)} \dot{u}^{(1)} \right] u_\gamma d\tau \\ &= \frac{i\eta}{2\sqrt{\Phi_C}} \left[u_\gamma \int_{\tau_o}^\tau B' h^{(2)} (u^{(1)} \dot{u}_\alpha - \dot{u}^{(1)} u_\alpha) d\tau - u_\alpha \int_{\tau_o}^\tau B' h^{(2)} (u^{(1)} \dot{u}_\gamma - \dot{u}^{(1)} u_\gamma) d\tau \right] \\ &+ \frac{i\eta}{16\sqrt{\Phi_C}} \left[u_\gamma \int_{\tau_o}^\tau B'' \left(2u^{(1)} \bar{u}^{(1)} \dot{u}^{(1)} u_\alpha - u^{(1)2} \dot{\bar{u}}^{(1)} u_\alpha - u^{(1)2} \bar{u}^{(1)} \dot{u}_\alpha \right) d\tau \right. \\ &\quad \left. - u_\alpha \int_{\tau_o}^\tau B'' \left(2u^{(1)} \bar{u}^{(1)} \dot{u}^{(1)} u_\gamma - u^{(1)2} \dot{\bar{u}}^{(1)} u_\gamma - u^{(1)2} \bar{u}^{(1)} \dot{u}_\gamma \right) d\tau \right] + \frac{i\eta B_o''}{16\sqrt{\Phi_C}} u_o^2 \bar{u}_o u_\alpha. \end{aligned} \quad (2.164)$$

To simplify the formula further, the terms in the last line are transformed as follows:

$$\begin{aligned} 2u^{(1)} \bar{u}^{(1)} \dot{u}^{(1)} u_A - u^{(1)2} \dot{\bar{u}}^{(1)} u_A - u^{(1)2} \bar{u}^{(1)} \dot{u}_A \\ = -(u^{(1)} \dot{\bar{u}}^{(1)} - \bar{u}^{(1)} \dot{u}^{(1)}) u^{(1)} u_A + (\dot{u}^{(1)} u_A - u^{(1)} \dot{u}_A) u^{(1)} \bar{u}^{(1)}. \end{aligned} \quad (2.165)$$

As a result, this integration is transformed into

$$\begin{aligned}
I_u^{(3)} = & \frac{i\eta}{2\sqrt{\Phi_C}} u^{(1)} \int_{\tau_o}^{\tau} B' h^{(2)} d\tau + \frac{i\eta B_o''}{16\sqrt{\Phi_C}} u_o^2 \bar{u}_o u_\alpha \\
& - \frac{i\eta}{16\sqrt{\Phi_C}} u_\gamma \int_{\tau_o}^{\tau} B'' [(u_o \dot{\bar{u}}_o - \bar{u}_o \dot{u}_o) u^{(1)} u_\alpha + u_o u^{(1)} \bar{u}^{(1)}] d\tau \\
& + \frac{i\eta}{16\sqrt{\Phi_C}} u_\alpha \int_{\tau_o}^{\tau} B'' [(u_o \dot{\bar{u}}_o - \bar{u}_o \dot{u}_o) u^{(1)} u_\gamma - \dot{u}_o u^{(1)} \bar{u}^{(1)}] d\tau.
\end{aligned} \tag{2.166}$$

Using Eq. (2.164), the third-order path deviation is given by

$$\begin{aligned}
u^{(3)}_{\text{geo.}}(\tau) = & \frac{1}{32\Phi_C} u_\gamma \int_{\tau_o}^{\tau} (8L_1 u^{(1)} h^{(2)}_{\text{geo.}} - L_2 u^{(1)2} \bar{u}^{(1)}) u_\alpha d\tau \\
& - \frac{1}{32\Phi_C} u_\alpha \int_{\tau_o}^{\tau} (8L_1 u^{(1)} h^{(2)}_{\text{geo.}} - L_2 u^{(1)2} \bar{u}^{(1)}) u_\gamma d\tau \\
& + \frac{i\eta}{16\sqrt{\Phi_C}} u^{(1)} \int_{\tau_o}^{\tau} (8B' h^{(2)}_{\text{geo.}} - B'' u^{(1)} \bar{u}^{(1)}) d\tau + \frac{i\eta B_o''}{16\sqrt{\Phi_C}} u_o^2 \bar{u}_o u_\alpha \\
& - \frac{i\eta}{16\sqrt{\Phi_C}} (u_o \dot{\bar{u}}_o - \bar{u}_o \dot{u}_o) \left[u_\gamma \int_{\tau_o}^{\tau} B'' u^{(1)} u_\alpha d\tau - u_\alpha \int_{\tau_o}^{\tau} B'' u^{(1)} u_\gamma d\tau \right],
\end{aligned} \tag{2.167}$$

and the lateral path deviation at an arbitrary plane is given by

$$\hat{u}^{(3)}_{\text{geo.}}(z) = u^{(3)}_{\text{geo.}} - \frac{1}{\zeta} \hat{u}^{(1)} h^{(2)}_{\text{geo.}} - i \frac{\dot{\zeta}}{\zeta} u^{(1)} h^{(2)}_{\text{geo.}}. \tag{2.168}$$

Expanding terms by geometrical parameters, the third-order geometrical lateral path deviation, evaluated at a plane,

is sorted as follows:

$$\begin{aligned}
\hat{u}^{(3)}_{\text{geo.}}(z) = & (\hat{u}^{(R)}_{\alpha\alpha\bar{\alpha}} + i\hat{u}^{(I)}_{\alpha\alpha\bar{\alpha}}) \dot{u}_o^2 \bar{u}_o + (\hat{u}^{(R)}_{\alpha\bar{\alpha}\gamma} + i\hat{u}^{(I)}_{\alpha\bar{\alpha}\gamma}) u_o \dot{u}_o \bar{u}_o \\
& + (\hat{u}^{(R)}_{\alpha\alpha\bar{\gamma}} + i\hat{u}^{(I)}_{\alpha\alpha\bar{\gamma}}) u_o \dot{u}_o^2 + (\hat{u}^{(R)}_{\alpha\gamma\bar{\gamma}} + i\hat{u}^{(I)}_{\alpha\gamma\bar{\gamma}}) u_o \bar{u}_o \dot{u}_o \\
& + (\hat{u}^{(R)}_{\bar{\alpha}\gamma\gamma} + i\hat{u}^{(I)}_{\bar{\alpha}\gamma\gamma}) u_o^2 \dot{u}_o + (\hat{u}^{(R)}_{\gamma\gamma\bar{\gamma}} + i\hat{u}^{(I)}_{\gamma\gamma\bar{\gamma}}) u_o^2 \bar{u}_o.
\end{aligned} \tag{2.169}$$

where the lateral path deviation of the shape of the spherical aberration:

$$\begin{aligned}
\hat{u}^{(R)}_{\alpha\alpha\bar{\alpha}} = & u_\gamma \int_{\tau_o}^{\tau} \frac{1}{32\Phi_C} (8L_1 u_\alpha^2 h_{\alpha\bar{\alpha}} - L_2 u_\alpha^4) d\tau \\
& - u_\alpha \int_{\tau_o}^{\tau} \frac{1}{32\Phi_C} (8L_1 u_\alpha u_\gamma h_{\alpha\bar{\alpha}} - L_2 u_\alpha^3 u_\gamma) d\tau - \frac{1}{\zeta} \dot{u}_\alpha h_{\alpha\bar{\alpha}},
\end{aligned} \tag{2.170}$$

$$\hat{u}^{(I)}_{\alpha\alpha\bar{\alpha}} = u_\alpha \int_{\tau_o}^{\tau} \frac{\eta}{16\sqrt{\Phi_C}} (8B' h_{\alpha\bar{\alpha}} - B'' u_\alpha^2) d\tau - \frac{\eta B}{2\zeta\sqrt{\Phi_C}} u_\alpha h_{\alpha\bar{\alpha}}, \tag{2.171}$$

that of the shape of the coma-length:

$$\begin{aligned}
\hat{u}^{(R)}_{\alpha\bar{\alpha}\gamma} = & u_\gamma \int_{\tau_o}^{\tau} \frac{1}{32\Phi_C} [8L_1 (u_\alpha^2 h_{\alpha\gamma}^{(R)} + u_\alpha u_\gamma h_{\alpha\bar{\alpha}}) - 2L_2 u_\alpha^3 u_\gamma] d\tau \\
& - u_\alpha \int_{\tau_o}^{\tau} \frac{1}{32\Phi_C} [8L_1 (u_\alpha u_\gamma h_{\alpha\gamma}^{(R)} + u_\gamma^2 h_{\alpha\bar{\alpha}}) - 2L_2 u_\alpha^2 u_\gamma^2] d\tau \\
& - u_\alpha \int_{\tau_o}^{\tau} \frac{\eta B'}{2\sqrt{\Phi_C}} h_{\alpha\gamma}^{(I)} d\tau - \frac{1}{\zeta} (\dot{u}_\alpha h_{\alpha\gamma}^{(R)} + \dot{u}_\gamma h_{\alpha\bar{\alpha}}) + \frac{\eta B}{2\zeta\sqrt{\Phi_C}} u_\alpha h_{\alpha\gamma}^{(I)},
\end{aligned} \tag{2.172}$$

$$\begin{aligned}
\hat{u}^{(I)}_{\alpha\bar{\alpha}\gamma} = & u_\gamma \int_{\tau_o}^{\tau} \left[\frac{L_1}{4\Phi_C} u_\alpha^2 h_{\alpha\gamma}^{(I)} + \frac{\eta}{8\sqrt{\Phi_C}} (4B' h_{\alpha\bar{\alpha}} - B'' u_\alpha^2) \right] d\tau \\
& - u_\alpha \int_{\tau_o}^{\tau} \left(\frac{L_1}{4\Phi_C} u_\alpha u_\gamma h_{\alpha\gamma}^{(I)} - \frac{\eta B'}{2\sqrt{\Phi_C}} h_{\alpha\gamma}^{(R)} \right) d\tau - \frac{1}{\zeta} \dot{u}_\alpha h_{\alpha\gamma}^{(I)} - \frac{\eta B}{2\zeta\sqrt{\Phi_C}} u_\gamma h_{\alpha\bar{\alpha}},
\end{aligned} \tag{2.173}$$

that of the shape of the coma-radius:

$$\begin{aligned}\hat{u}_{\alpha\alpha\gamma}^{(R)} &= u_\gamma \int_{\tau_o}^{\tau} \frac{1}{32\Phi_C} (8L_1 u_\alpha^2 h_{\alpha\gamma}^{(R)} - L_2 u_\alpha^2 u_\gamma) d\tau \\ &\quad - u_\alpha \int_{\tau_o}^{\tau} \left[\frac{1}{32\Phi_C} (8L_1 u_\alpha u_\gamma h_{\alpha\gamma}^{(R)} - L_2 u_\alpha^2 u_\gamma^2) - \frac{\eta B'}{2\sqrt{\Phi_C}} h_{\alpha\gamma}^{(I)} \right] d\tau - \frac{1}{\zeta} \dot{u}_\alpha h_{\alpha\gamma}^{(R)} - \frac{\eta B}{2\zeta\sqrt{\Phi_C}} u_\alpha h_{\alpha\gamma}^{(I)},\end{aligned}\quad (2.174)$$

$$\begin{aligned}\hat{u}_{\alpha\alpha\gamma}^{(I)} &= -u_\gamma \int_{\tau_o}^{\tau} \left(\frac{L_1}{4\Phi_C} u_\alpha^2 h_{\alpha\gamma}^{(I)} - \frac{\eta B''}{16\sqrt{\Phi_C}} u_\alpha^2 \right) d\tau - \frac{\eta B}{2\zeta\sqrt{\Phi_C}} u_\alpha h_{\alpha\gamma}^{(R)} \\ &\quad + u_\alpha \int_{\tau_o}^{\tau} \left[\frac{L_1}{4\Phi_C} u_\alpha u_\gamma h_{\alpha\gamma}^{(I)} + \frac{\eta}{8\sqrt{\Phi_C}} (4B' h_{\alpha\gamma}^{(R)} - B'' u_\alpha u_\gamma) \right] d\tau + \frac{1}{\zeta} \dot{u}_\alpha h_{\alpha\gamma}^{(I)},\end{aligned}\quad (2.175)$$

that of the shape of the field-curvature:

$$\begin{aligned}\hat{u}_{\alpha\gamma\gamma}^{(R)} &= u_\gamma \int_{\tau_o}^{\tau} \frac{1}{32\Phi_C} [8L_1 (u_\alpha^2 h_{\gamma\bar{\gamma}} + u_\alpha u_\gamma h_{\alpha\gamma}^{(R)}) - 2L_2 u_\alpha^2 u_\gamma^2] d\tau \\ &\quad - u_\alpha \int_{\tau_o}^{\tau} \frac{1}{32\Phi_C} [8L_1 (u_\alpha u_\gamma h_{\gamma\bar{\gamma}} + u_\gamma^2 h_{\alpha\gamma}^{(R)}) - 2L_2 u_\alpha u_\gamma^3] d\tau \\ &\quad + u_\gamma \int_{\tau_o}^{\tau} \frac{\eta B'}{2\sqrt{\Phi_C}} h_{\alpha\gamma}^{(I)} d\tau - \frac{1}{\zeta} (\dot{u}_\alpha h_{\gamma\bar{\gamma}} + \dot{u}_\gamma h_{\alpha\gamma}^{(R)}) - \frac{\eta B}{2\zeta\sqrt{\Phi_C}} u_\gamma h_{\alpha\gamma}^{(I)},\end{aligned}\quad (2.176)$$

$$\begin{aligned}\hat{u}_{\alpha\gamma\gamma}^{(I)} &= -u_\gamma \int_{\tau_o}^{\tau} \left(\frac{L_1}{4\Phi_C} u_\alpha u_\gamma h_{\alpha\gamma}^{(I)} - \frac{\eta B'}{2\sqrt{\Phi_C}} h_{\alpha\gamma}^{(R)} \right) d\tau \\ &\quad + u_\alpha \int_{\tau_o}^{\tau} \left[\frac{L_1}{4\Phi_C} u_\gamma^2 h_{\alpha\gamma}^{(I)} - \frac{\eta}{8\sqrt{\Phi_C}} (4B' h_{\gamma\bar{\gamma}} - B'' u_\gamma^2) \right] d\tau + \frac{1}{\zeta} \dot{u}_\gamma h_{\alpha\gamma}^{(I)} - \frac{\eta B}{2\zeta\sqrt{\Phi_C}} (u_\alpha h_{\gamma\bar{\gamma}} + u_\gamma h_{\alpha\gamma}^{(R)}),\end{aligned}\quad (2.177)$$

that of the shape of the astigmatism:

$$\begin{aligned}\hat{u}_{\alpha\gamma\gamma}^{(R)} &= u_\gamma \int_{\tau_o}^{\tau} \frac{1}{32\Phi_C} (8L_1 u_\alpha u_\gamma h_{\alpha\gamma}^{(R)} - L_2 u_\alpha^2 u_\gamma^2) d\tau \\ &\quad - u_\gamma \int_{\tau_o}^{\tau} \frac{\eta B'}{2\sqrt{\Phi_C}} h_{\alpha\gamma}^{(I)} d\tau - u_\alpha \int_{\tau_o}^{\tau} \frac{1}{32\Phi_C} (8L_1 u_\gamma^2 h_{\alpha\gamma}^{(R)} - L_2 u_\alpha u_\gamma^3) d\tau - \frac{1}{\zeta} \dot{u}_\gamma h_{\alpha\gamma}^{(R)} + \frac{\eta B}{2\zeta\sqrt{\Phi_C}} u_\gamma h_{\alpha\gamma}^{(I)},\end{aligned}\quad (2.178)$$

$$\begin{aligned}\hat{u}_{\alpha\gamma\gamma}^{(I)} &= u_\gamma \int_{\tau_o}^{\tau} \frac{L_1}{4\Phi_C} u_\alpha u_\gamma h_{\alpha\gamma}^{(I)} d\tau + u_\gamma \int_{\tau_o}^{\tau} \frac{\eta}{8\sqrt{\Phi_C}} (4B' h_{\alpha\gamma}^{(R)} - B'' u_\alpha u_\gamma) d\tau \\ &\quad - u_\alpha \int_{\tau_o}^{\tau} \frac{L_1}{4\Phi_C} u_\gamma^2 h_{\alpha\gamma}^{(I)} d\tau + u_\alpha \int_{\tau_o}^{\tau} \frac{\eta B''}{16\sqrt{\Phi_C}} u_\gamma^2 d\tau - \frac{1}{\zeta} \dot{u}_\gamma h_{\alpha\gamma}^{(I)} - \frac{\eta B}{2\zeta\sqrt{\Phi_C}} u_\gamma h_{\alpha\gamma}^{(R)},\end{aligned}\quad (2.179)$$

and that of the shape of the distortion:

$$\begin{aligned}\hat{u}_{\gamma\gamma\bar{\gamma}}^{(R)} &= u_\gamma \int_{\tau_o}^{\tau} \frac{1}{32\Phi_C} (8L_1 u_\alpha u_\gamma h_{\gamma\bar{\gamma}} - L_2 u_\alpha u_\gamma^3) d\tau \\ &\quad - u_\alpha \int_{\tau_o}^{\tau} \frac{1}{32\Phi_C} (8L_1 u_\gamma^2 h_{\gamma\bar{\gamma}} - L_2 u_\gamma^4) d\tau - \frac{1}{\zeta} \dot{u}_\gamma h_{\gamma\bar{\gamma}},\end{aligned}\quad (2.180)$$

$$\hat{u}_{\gamma\gamma\bar{\gamma}}^{(I)} = u_\gamma \int_{\tau_o}^{\tau} \frac{\eta}{16\sqrt{\Phi_C}} (8B' h_{\gamma\bar{\gamma}} - B'' u_\gamma^2) d\tau - \frac{\eta B}{2\zeta\sqrt{\Phi_C}} u_\gamma h_{\gamma\bar{\gamma}} + \frac{\eta B_o''}{16\sqrt{\Phi_C}} u_\alpha. \quad (2.181)$$

The third-order geometrical aberration defined at the object plane is given by

$$\begin{aligned}\Delta u_o^{(3)}{}_{\text{geo.}} &= \frac{\hat{u}^{(3)}{}_{\text{geo.}}(z_i)}{M} \\ &= C_{S_o} u_o'^2 \bar{u}_o' + (C_{KLo} + iC_{kLo}) u_o u_o' \bar{u}_o' + (C_{KR_o} + iC_{kR_o}) \bar{u}_o u_o'^2 \\ &\quad + (C_{Fo} + iC_{f_o}) u_o \bar{u}_o u_o' + (C_{Ao} + iC_{a_o}) \bar{u}_o u_o'^2 + (C_{Do} + iC_{d_o}) u_o^2 \bar{u}_o,\end{aligned}\quad (2.182)$$

where the spherical aberration coefficient:

$$C_{S_o} = \int_{\tau_o}^{\tau_i} \frac{\zeta_o^3}{32\Phi_C} (8L_1 u_\alpha^2 h_{\alpha\bar{\alpha}} - L_2 u_\alpha^4) d\tau - \frac{\zeta_o^3}{\zeta_i} \dot{u}_\alpha^2 h_{\alpha\bar{\alpha}i}, \quad (2.183)$$

the real part of the coma-length coefficient:

$$C_{KLo} = \int_{\tau_o}^{\tau_i} \frac{\zeta_o^2}{32\Phi_C} [8L_1 (u_\alpha^2 h_{\alpha\gamma}^{(R)} + u_\alpha u_\gamma h_{\alpha\bar{\alpha}}) - 2L_2 u_\alpha^3 u_\gamma] d\tau - \frac{\zeta_o^2}{\zeta_i} (\dot{u}_{\alpha i}^2 h_{\alpha\gamma i}^{(R)} + \dot{u}_{\alpha i} \dot{u}_{\gamma i} h_{\alpha\bar{\alpha}i}), \quad (2.184)$$

the imaginary part of the coma-length coefficient:

$$C_{kLo} = \int_{\tau_o}^{\tau_i} \left[\frac{\xi_o^2 L_1}{4\Phi_C} u_a^2 h_{a\gamma}^{(I)} + \frac{\xi_o^2 \eta}{8\sqrt{\Phi_C}} (4B' h_{a\bar{a}} - B'' u_a^2) \right] d\tau - \frac{\xi_o^2}{\xi_i} \dot{u}_{ai}^2 h_{a\gamma i}^{(I)} - \frac{\xi_o^2 \eta B_i}{2\xi_i \sqrt{\Phi_C}} h_{a\bar{a}i} \quad (2.185)$$

the real part of the coma-radius coefficient:

$$C_{KR0} = \int_{\tau_o}^{\tau_i} \frac{\xi_o^2}{32\Phi_C} (8L_1 u_a^2 h_{a\gamma}^{(R)} - L_2 u_a^3 u_\gamma) d\tau - \frac{\xi_o^2}{\xi_i} \dot{u}_{ai}^2 h_{a\gamma i}^{(R)}, \quad (2.186)$$

the imaginary part of the coma-radius coefficient:

$$C_{kRo} = - \int_{\tau_o}^{\tau_i} \left(\frac{\xi_o^2 L_1}{4\Phi_C} u_a^2 h_{a\gamma}^{(I)} - \frac{\xi_o^2 \eta B''}{16\sqrt{\Phi_C}} u_a^2 \right) d\tau + \frac{\xi_o^2}{\xi_i} \dot{u}_{ai}^2 h_{a\gamma i}^{(I)}, \quad (2.187)$$

the real part of the field-curvature coefficient:

$$C_{Fo} = \int_{\tau_o}^{\tau_i} \frac{\xi_o}{32\Phi_C} \left[8L_1 (u_a^2 h_{\gamma\bar{\gamma}} + u_a u_\gamma h_{a\gamma}^{(R)}) - 2L_2 u_a^2 u_\gamma^2 \right] d\tau \\ + \int_{\tau_o}^{\tau_i} \frac{\xi_o \eta B'}{2\sqrt{\Phi_C}} h_{a\gamma}^{(I)} d\tau - \frac{\xi_o}{\xi_i} (\dot{u}_{ai} h_{\gamma\bar{\gamma}i} + \dot{u}_{ai} \dot{u}_{\gamma i} h_{a\gamma i}^{(R)}) - \frac{\xi_o \eta B_i}{2\xi_i \sqrt{\Phi_C}} h_{a\gamma i}^{(I)}, \quad (2.188)$$

the imaginary part of the field-curvature:

$$C_{fo} = - \int_{\tau_o}^{\tau_i} \left(\frac{\xi_o L_1}{4\Phi_C} u_a u_\gamma h_{a\gamma}^{(I)} - \frac{\xi_o \eta B'}{2\sqrt{\Phi_C}} h_{a\gamma}^{(R)} \right) d\tau + \frac{\xi_o}{\xi_i} \dot{u}_{ai} \dot{u}_{\gamma i} h_{a\gamma i}^{(I)} - \frac{\xi_o \eta B_i}{2\xi_i \sqrt{\Phi_C}} h_{a\gamma i}^{(R)}, \quad (2.189)$$

the real part of the astigmatism coefficient:

$$C_{Ao} = \int_{\tau_o}^{\tau_i} \left[\frac{\xi_o}{32\Phi_C} (8L_1 u_a u_\gamma h_{a\gamma}^{(R)} - L_2 u_a^2 u_\gamma^2) - \frac{\xi_o \eta B'}{2\sqrt{\Phi_C}} h_{a\gamma}^{(I)} \right] d\tau - \frac{\xi_o}{\xi_i} \dot{u}_{ai} \dot{u}_{\gamma i} h_{a\gamma i}^{(R)} + \frac{\xi_o \eta B_i}{2\xi_i \sqrt{\Phi_C}} h_{a\gamma i}^{(I)}, \quad (2.190)$$

the imaginary part of the astigmatism coefficient:

$$C_{ao} = \int_{\tau_o}^{\tau_i} \left[\frac{\xi_o}{4\Phi_C} L_1 u_a u_\gamma h_{a\gamma}^{(I)} + \frac{\xi_o \eta}{8\sqrt{\Phi_C}} (4B' h_{a\gamma}^{(R)} - B'' u_a u_\gamma) \right] d\tau \\ - \frac{\xi_o}{\xi_i} \dot{u}_{ai} \dot{u}_{\gamma i} h_{a\gamma i}^{(I)} - \frac{\xi_o \eta B_i}{2\xi_i \sqrt{\Phi_C}} h_{a\gamma i}^{(R)}, \quad (2.191)$$

the real part of the distortion coefficient:

$$C_{Do} = \int_{\tau_o}^{\tau_i} \frac{1}{32\Phi_C} (8L_1 u_a u_\gamma h_{\gamma\bar{\gamma}} - L_2 u_a u_\gamma^3) d\tau - \frac{1}{\xi_i} \dot{u}_{ai} \dot{u}_{\gamma i} h_{\gamma\bar{\gamma}i}, \quad (2.192)$$

the imaginary part of the distortion coefficient:

$$C_{do} = \int_{\tau_o}^{\tau_i} \frac{\eta}{16\sqrt{\Phi_C}} (8B' h_{\gamma\bar{\gamma}} - B'' u_\gamma^2) d\tau - \frac{\eta B_i}{2\xi_i \sqrt{\Phi_C}} h_{\gamma\bar{\gamma}i}, \quad (2.193)$$

and the imaginary part of the spherical aberration coefficient vanishes, as we expected.

Finally, we are at the point where third-order geometrical aberration coefficients in time-dependent theory are derived.

However, Eq. (2.189) apparently indicates the imaginary part of the field-curvature, which does not appear in the standard electron optics. In addition, in standard theory of electron optics, we have a relation between the coma-length coefficient and the coma-radius coefficient as follows:

$$C_{KLo} = 2C_{KR0}, \\ C_{kLo} = -2C_{kRo}. \quad (2.194)$$

and the subtraction $C_{Fo} - 2C_{Ao}$, which is called the Petzval coefficient, does not depend on any lateral rays but on the electromagnetic field. Since only round symmetric fields are considered, these features are expected to be valid for

time-dependent theory, by analogy to the standard electron optics. To verify these features, we need to investigate the analytic form and properties of linear solutions of longitudinal path deviation in advance. We will return to a review of the properties of linear solutions of longitudinal path deviations in the next section 2.6.

2.6 Analytic form and properties of a longitudinal path-deviation of first-rank

In this section, we return to a review of the fundamental solutions of the linear longitudinal path equation in Eq. (2.39), based on reference [1.91]. We give a detailed review about analytic form of the fundamental solutions of linear longitudinal equation and their properties, which will later be used to prove several features of aberration coefficients of time-dependent theory. These results give the regular aberrations of lenses without a mirror, as given in section 2.7 and 2.8.

Using Eq (2.13), the linear longitudinal trajectory equation Eq. (2.39), is transformed into

$$\frac{\ddot{h}}{h} = \frac{\Phi''}{2\Phi_C} = \frac{1}{\zeta} \frac{d}{d\tau} \frac{\Phi'}{2\Phi_C} = \frac{\ddot{\zeta}}{\zeta}. \quad (2.195)$$

Then, one of the fundamental solutions is given by

$$h_A = \zeta. \quad (2.196)$$

Employing the method of variation of parameter to solve the ordinal differential equation, the other independent solution is assumed to be a product of the known solution h_A and a new unknown function of reduced time $C(\tau)$:

$$h_B = C(\tau)h_A. \quad (2.197)$$

By substituting Eq.(2.197) into Eq. (2.39), the equation with respect to $C(\tau)$ is obtained as follows:

$$\frac{\ddot{C}}{C} = -2 \frac{\ddot{\zeta}}{\zeta}, \quad (2.198)$$

Then, the solution of $C(\tau)$ is

$$\dot{C} = \frac{1}{\zeta^2}, \quad (2.199)$$

$$C = \int_{\tau_{\text{ini}}}^{\tau} \frac{d\tau}{\zeta^2}, \quad (2.200)$$

$$h_B = \zeta \int_{\tau_{\text{ini}}}^{\tau} \frac{d\tau}{\zeta^2} \quad (2.201)$$

where τ_{ini} is an arbitrary integration lower limit. It is convenient to consider a symmetric and an antisymmetric solution, h_σ and h_v with respect to the reflection time of the reference electron. The boundary conditions are assumed as follows,

$$\begin{aligned} h_{vT} &= 0, & \dot{h}_{vT} &= a, \\ h_{\sigma T} &= -\frac{1}{a}, & \dot{h}_{\sigma T} &= 0, \end{aligned} \quad (2.202)$$

where a is constant determined later, which meets the condition of the Wronskian $W[h_v, h_\sigma] = 1$. Because the reduced velocity of the reference electron $\dot{\zeta}$ is antisymmetric about the reflection time, the antisymmetric solution h_v is proportional to h_A :

$$h_v = C_1 h_A = C_1 \dot{\zeta}. \quad (2.203)$$

where C_1 is a constant. To determine the constant a in Eq. (2.202), the reduced time derivative of h_v is considered as,

$$\dot{h}_v = C_1 \ddot{\zeta}. \quad (2.204)$$

Because of Eq. (2.202), we get

$$\dot{h}_{vT} = C_1 \ddot{\zeta}_T = a. \quad (2.205)$$

For simplicity, C_1 is chosen to be 1 then, the constant a and antisymmetric solution h_v are determined as follows:

$$a = \ddot{\zeta}_T = \frac{\Phi'_T}{2\Phi_C}, \quad (2.206)$$

$$h_v = \dot{\zeta}. \quad (2.207)$$

With this consideration, h_σ is assumed that

$$h_\sigma = C_2 h_B = C_2 \dot{\zeta} \int_{\tau_\sigma}^{\tau} \frac{d\tau}{\dot{\zeta}^2} = C_2 h_v \int_{\tau_\sigma}^{\tau} \frac{d\tau}{h_v^2}, \quad (2.208)$$

where C_2 and τ_σ are to be determined. A differentiation of Eq. (2.208) with respect to reduced time is

$$\dot{h}_\sigma = C_2 \left(\dot{\zeta} \int_{\tau_\sigma}^{\tau} \frac{d\tau}{\dot{\zeta}^2} + \frac{1}{\dot{\zeta}} \right), \quad (2.209)$$

and because of the Wronskian $W[h_v, h_\sigma] = 1$, C_2 is determined as

$$C_2 = 1. \quad (2.210)$$

Since h_σ is symmetric about τ_{turn} , the condition of the lower limit of the integration $\tau_\sigma = \dot{h}_{\sigma T} = 0$. Then, by changing the integration variable from the reduced time to the position of the reference electron,

$$\dot{h}_\sigma = \dot{\zeta} \int_{\tau_\sigma}^{\tau} \frac{d\tau}{\dot{\zeta}^2} + \frac{1}{\dot{\zeta}} = \dot{\zeta} \int_{\zeta_\sigma}^{\zeta} \frac{d\zeta}{\dot{\zeta}^3} + \frac{1}{\dot{\zeta}}, \quad (2.211)$$

where ζ_σ is the axial position determined by $\zeta_\sigma = \zeta(\tau_\sigma)$. Since $\dot{\zeta}_T = 0$, the right-hand side of Eq. (2.64) diverges at the reflection time. Thus, ζ_σ is determined to avoid this divergence as follows. Firstly, for the first term of Eq. (2.211), the limit of $\dot{\zeta}$ approaching $\dot{\zeta}_T$ from $\dot{\zeta} < \dot{\zeta}_T$ is considered.

$$\lim_{\dot{\zeta} \rightarrow \dot{\zeta}_T - 0} \dot{\zeta} \int_{\zeta_\sigma}^{\zeta} \frac{d\zeta}{\dot{\zeta}^3} = \lim_{\dot{\zeta} \rightarrow \dot{\zeta}_T - 0} \dot{\zeta} \Phi_C^{3/2} \int_{\zeta_\sigma}^{\zeta} \frac{\Phi'}{\Phi' \Phi^{3/2}} d\zeta, \quad (2.212)$$

where $\Phi' \neq 0$ in the range of $\zeta_\sigma < \zeta < \zeta_T$. Using the integral,

$$\int_{\zeta_\sigma}^{\zeta} \frac{\Phi'}{\Phi^{3/2}} d\zeta = -2 \left(\frac{1}{\sqrt{\Phi}} - \frac{1}{\sqrt{\Phi_\sigma}} \right), \quad (2.213)$$

then, the following partial integration is obtained:

$$\lim_{\dot{\zeta} \rightarrow \dot{\zeta}_T} \dot{\zeta} \int_{\zeta_\sigma}^{\zeta} \frac{d\zeta}{\dot{\zeta}^3} = - \lim_{\dot{\zeta} \rightarrow \dot{\zeta}_T} \left(\frac{1}{\dot{\zeta}} - \int_{\zeta_\sigma}^{\zeta} \frac{\Phi''}{\Phi'^2 \sqrt{\Phi}} \Phi'_T \sqrt{\Phi_C} d\zeta \right) + \frac{\Phi'_T}{\Phi'_\sigma} \sqrt{\frac{\Phi_C}{\Phi_\sigma}}. \quad (2.214)$$

Thus, $\dot{h}_{\sigma T}$ is transformed into

$$\dot{h}_{\sigma T} = \frac{\Phi'_T}{\Phi'_\sigma} \sqrt{\frac{\Phi_C}{\Phi_\sigma}} \left(1 - \Phi'_\sigma \sqrt{\Phi_\sigma} \int_{\zeta_\sigma}^{\zeta_T} \frac{\Phi''}{\Phi'^2 \sqrt{\Phi}} d\zeta \right). \quad (2.215)$$

Since the boundary condition of the symmetric longitudinal ray at the axial reflection point is $\dot{h}_{\sigma T} = 0$, this requires the condition that

$$\Phi'_\sigma \sqrt{\Phi_\sigma} \int_{\zeta_\sigma}^{\zeta_T} \frac{\Phi''}{\Phi'^2 \sqrt{\Phi}} d\zeta = 1, \quad (2.216)$$

where $\zeta_\sigma < \zeta < \zeta_T$. Eq. (2.116) determines the start of the integration ζ_σ . The necessary condition for taking the limit of Eq. (2.112); $\Phi' \neq 0$ where $\zeta_\sigma < \zeta < \zeta_T$, restricts the solution ζ_σ . This condition means that the axial potential distribution Φ does not have any local maxima or minima in the interval of integration $\zeta_\sigma < \zeta < \zeta_T$. In general, since electron mirrors consist of multi-electrodes with different voltages, the axial potential distribution has several local maxima and minima. Since the axial potential of electrons are non-negative, except for the diode mirror, the closest extreme to the reflection point is a local maximum ζ_{\max} . ζ_σ must be located somewhere between the closest local maximum ζ_{\max} and the reflection point ζ_T . In the case of diode mirrors, which consist of two round electrodes and where the potential of either electrode is the same as the column potential Φ_C , ζ_{\max} can be regarded as infinity, that is, $\zeta_{\max} = -\infty$. Examples of the axial potential distributions for a general mirror and a diode mirror are shown in Fig. 2.2.

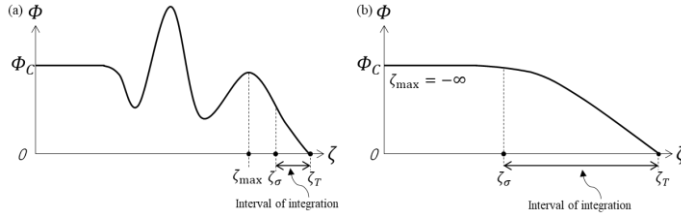


Fig. 2.2 The axial potential distribution of the electron: (a) a general electron mirror, (b) a diode mirror. Since general electron mirrors are composed of multi-electrodes with different voltages, there are several local maxima and minima. However, since the axial potential is non-negative, the closest extreme is the local maximum ζ_{\max} . The lower bound of the integral in Eq. (2.211), ζ_σ is located between ζ_{\max} and the reflection point ζ_T . On the other hand, in the case of diode mirrors, the voltage of the electrode located on the electron-source side is the same as the column potential Φ_C . This Φ_C is the maximum value of the potential and there are no extremes. In this case, ζ_{\max} can be regarded as infinity, that is, $\zeta_{\max} = -\infty$.

Here, we write the analytic forms of the symmetric and antisymmetric solutions of the homogeneous longitudinal equation and their boundary values, again:

$$h_v = \dot{\zeta}, \quad (2.217)$$

$$\dot{h}_v = \ddot{\zeta} = \frac{\Phi'}{2\Phi_c}, \quad (2.218)$$

$$h_\sigma = \dot{\zeta} \int_{\tau_o}^{\tau} \frac{d\tau}{\dot{\zeta}^2} = h_v \int_{\tau_o}^{\tau} \frac{d\tau}{h_v^2}, \quad (2.219)$$

$$\dot{h}_\sigma = \ddot{\zeta} \int_{\tau_o}^{\tau} \frac{d\tau}{\dot{\zeta}^2} + \frac{1}{\dot{\zeta}}, \quad (2.220)$$

$$\begin{aligned} h_{vT} &= 0, & \dot{h}_{vT} &= \ddot{\zeta}_T = \frac{\Phi'_T}{2\Phi_c}, \\ h_{\sigma T} &= -\frac{2\Phi_c}{\Phi'_T}, & \dot{h}_{\sigma T} &= 0. \end{aligned} \quad (2.221)$$

We are at the point, where the analytic forms of fundamental solutions of Eq. (2.39) have been obtained, but they are symmetric and anti-symmetric solutions with respect to the reflection time. In the integrand of the derived aberration integral formulae in section 2.5, fundamental solutions of linear longitudinal trajectory equation for h_α and h_γ , whose boundary condition is designated at the object plane by Eq. (2.47), appear. We need the analytic form of them. Although earlier studies did not show the analytic expressions of h_α and h_γ , they are obtained as a suitable combination of h_σ and h_v as follows. Because $\int_{\tau_o}^{\tau} f d\tau = \int_{\tau_o}^{\tau} f d\tau + \int_{\tau_o}^{\tau_o} f d\tau$, h_σ in Eq. (2.219) is transformed as

$$h_\sigma = h_D + C_\sigma h_v, \quad (2.222)$$

where

$$h_D = \dot{\zeta} \int_{\tau_o}^{\tau} \frac{d\tau}{\dot{\zeta}^2}, \quad (2.223)$$

and

$$C_\sigma = -\int_{\tau_o}^{\tau_o} \frac{d\tau}{\dot{\zeta}^2} = -\int_{\zeta_o}^{\zeta_\sigma} \left(\frac{\Phi_c}{\Phi}\right)^{\frac{3}{2}} d\zeta, \quad (2.224)$$

but

$$\zeta_o = \zeta(\tau_o). \quad (2.225)$$

Since ζ_σ is the position of the local maximum of the axial potential distribution before the reflection point, the integrand of Eq. (2.224) has no singularity in the interval of the integral and C_σ is a convergent constant. Considering that lower boundary of the integral of h_D is τ_o but that of h_σ is τ_σ , to construct other pair of fundamental solutions h_α, h_γ , whose boundary conditions are given at the start time τ_o by Eq. (2.47), when a reference electron starts to travel from the object plane, it is more natural to consider a linear combination of h_v and h_D , instead of h_σ . h_α and h_γ are assumed as follows.

$$\begin{aligned} h_\alpha &= Ah_v + Bh_D, \\ h_\gamma &= Ch_v + Dh_D. \end{aligned} \quad (2.226)$$

Since $h_{D0} = h_D(\tau_o) = 0$ and $\dot{h}_{D0} = 1/\dot{\zeta}_o$, the boundary conditions, Eq. (2.47), provide conditions as follows:

$$\begin{aligned} h_{\alpha o} &= A\dot{\zeta}_o = 0, & \dot{h}_{\alpha o} &= A\ddot{\zeta}_o + \frac{B}{\dot{\zeta}_o} = 1, \\ h_{\gamma o} &= C\dot{\zeta}_o = 1, & \dot{h}_{\gamma o} &= C\ddot{\zeta}_o + \frac{D}{\dot{\zeta}_o} = 0. \end{aligned} \quad (2.227)$$

Then, the coefficients in Eq. (2.226) are determined:

$$\begin{aligned} A &= 0, & B &= \dot{\zeta}_o, \\ C &= \frac{1}{\dot{\zeta}_o}, & D &= -\ddot{\zeta}_o. \end{aligned} \quad (2.228)$$

Analytic forms of h_α and h_γ are obtained as follows:

$$h_\alpha = \dot{\zeta}_o h_D = \dot{\zeta}_o (h_\sigma - C_\sigma h_v) = \dot{\zeta}_o \dot{\zeta} \int_{\tau_o}^{\tau} \frac{d\tau}{\dot{\zeta}^2}, \quad (2.229)$$

$$\begin{aligned} h_\gamma &= \frac{1}{\dot{\zeta}_o} h_v - \dot{\zeta}_o h_D = \left(\frac{1}{\dot{\zeta}_o} + \dot{\zeta}_o C_\sigma \right) h_v - \dot{\zeta}_o h_\sigma \\ &= \frac{\dot{\zeta}}{\dot{\zeta}_o} - \frac{\ddot{\zeta}_o}{\dot{\zeta}_o} h_\alpha = \frac{\dot{\zeta}}{\dot{\zeta}_o} - \dot{\zeta}_o \dot{\zeta} \int_{\tau_o}^{\tau} \frac{d\tau}{\dot{\zeta}^2}. \end{aligned} \quad (2.230)$$

Analytic forms of their differentiation, with respect to reduced time, are given by

$$\dot{h}_\alpha = \dot{\zeta}_o \left(\dot{\zeta} \int_{\tau_o}^{\tau} \frac{d\tau}{\dot{\zeta}^2} + \frac{1}{\dot{\zeta}} \right), \quad (2.231)$$

$$\dot{h}_\gamma = \frac{\dot{\zeta}}{\dot{\zeta}_o} - \frac{\ddot{\zeta}_o}{\dot{\zeta}_o} \dot{h}_\alpha = \frac{\dot{\zeta}}{\dot{\zeta}_o} - \dot{\zeta}_o \left(\dot{\zeta} \int_{\tau_o}^{\tau} \frac{d\tau}{\dot{\zeta}^2} + \frac{1}{\dot{\zeta}} \right). \quad (2.232)$$

These analytic forms provide Wronskian Eq. (2.48), directly,

$$W[h_\gamma, h_\alpha] = h_\gamma \dot{h}_\alpha - \dot{h}_\gamma h_\alpha = \frac{\dot{\zeta}}{\dot{\zeta}_o} \dot{h}_\alpha - \frac{\dot{\zeta}}{\dot{\zeta}_o} h_\alpha = 1 \quad (2.233)$$

We are at the point, where the analytic forms of fundamental solutions h_α and h_γ of the linear longitudinal path equation have been derived, which will be used to prove several properties of aberration coefficients of mirrors.

At the end of this section, we provide representation of h_σ and h_v as linear combinations of h_α and h_γ . By Eqs. (2.229) to (2.232), we obtain representation of h_σ and h_v by

$$\begin{pmatrix} h_\gamma \\ h_\alpha \end{pmatrix} = \begin{pmatrix} -\dot{\zeta}_o & \frac{1}{\dot{\zeta}_o} + \dot{\zeta}_o C_\sigma \\ \dot{\zeta}_o & -\dot{\zeta}_o C_\sigma \end{pmatrix} \begin{pmatrix} h_\sigma \\ h_v \end{pmatrix}. \quad (2.234)$$

In Eq. (2.221), the values of h_α , h_γ , and their reduced time differentiations, at the convergent time τ_T , are given by

$$\begin{aligned} h_{\gamma T} &= \frac{2\Phi'_o}{\Phi'_T}, & h_{\alpha T} &= -2 \frac{\sqrt{\Phi_o \Phi_C}}{\Phi'_T}, \\ \dot{h}_{\gamma T} &= \left(\frac{1}{\dot{\zeta}_o} + \dot{\zeta}_o C_\sigma \right) \frac{\Phi'_T}{2\Phi_C}, & \dot{h}_{\alpha T} &= -\dot{\zeta}_o C_\sigma \frac{\Phi'_T}{2\Phi_C}. \end{aligned} \quad (2.235)$$

The coefficients in Eq. (2.234) are expressed by the values in Eq. (2.235):

$$h_v = \frac{\Phi'_T}{2\Phi_C} (h_{\gamma T} h_\alpha - h_{\alpha T} h_\gamma), \quad (2.236)$$

$$h_\sigma = \frac{2\Phi_C}{\Phi'_T} (\dot{h}_{\gamma T} h_\alpha - \dot{h}_{\alpha T} h_\gamma). \quad (2.237)$$

In this section, we have reviewed the analytic forms of fundamental solutions of the linear longitudinal path equations, which are symmetric and antisymmetric about the reflection time, and derived forms of fundamental solutions whose boundary conditions are defined at the initial time. These forms are used to prove several properties of aberration coefficients of the time-dependent theory later.

2.7 Proof of properties of third-order geometrical off-axis aberration coefficients of time-dependent theory: Coma-length and radius, anisotropic part of field curvature, and relation between field curvature and astigmatism

In this section, we prove several properties of the third-order geometrical off-axis aberration coefficients of the time-dependent theory. As mentioned towards the end of section 2.5, we expect that off-axis aberration coefficients of the time-dependent theory have the same properties as those of standard electron optics in a normal lens system. The expected properties are three. First, the anisotropic part of the field curvature coefficient vanishes. Second, the coma-length coefficient is related to the coma-radius coefficient by Eq. (2.194). Third, the isotropic part of the astigmatism relates to the field curvature through the so-called Petzval curvature. We give proof and derivation here.

To verify these properties, it is advantageous to consider several specific integrations for the appropriate transformation of aberration coefficient formulae. The first one is the following double integral:

$$J[g_1, g_2](\tau) = \int_{\tau_0}^{\tau} \left[g_1(\tau) h_{\gamma}(\tau) \left(\int_{\tau_0}^{\tau} g_2(\xi) h_{\alpha}(\xi) d\xi \right) + g_2(\tau) h_{\alpha}(\tau) \left(\int_{\tau_0}^{\tau} g_1(\xi) h_{\gamma}(\xi) d\xi \right) \right] d\tau, \quad (2.238)$$

where g_1 and g_2 are non-singular functions with respect to reduced time. Using these and the analytic form of h_{γ} from

Eq. (2.230), we obtain an integration I_1 as follows:

$$\begin{aligned} I_1[g_1, g_2] &= J[g_1, g_2] - J[g_2, g_1] \\ &= \int_{\tau_0}^{\tau} h_{\gamma} \left[g_1 \left(\int_{\tau_0}^{\tau} g_2 h_{\alpha} d\xi \right) - g_2 \left(\int_{\tau_0}^{\tau} g_1 h_{\alpha} d\xi \right) \right] d\tau - \int_{\tau_0}^{\tau} h_{\alpha} \left[g_1 \left(\int_{\tau_0}^{\tau} g_2 h_{\gamma} d\xi \right) - g_2 \left(\int_{\tau_0}^{\tau} g_1 h_{\gamma} d\xi \right) \right] d\tau \\ &= \int_{\tau_0}^{\tau} \frac{\dot{\zeta}}{\zeta} \left[g_1 \left(\int_{\tau_0}^{\tau} g_2 h_{\alpha} d\xi \right) - g_2 \left(\int_{\tau_0}^{\tau} g_1 h_{\alpha} d\xi \right) \right] d\tau - \int_{\tau_0}^{\tau} h_{\alpha} \left[g_1 \left(\int_{\tau_0}^{\tau} \frac{\dot{\zeta}}{\zeta} g_2 d\xi \right) - g_2 \left(\int_{\tau_0}^{\tau} \frac{\dot{\zeta}}{\zeta} g_1 d\xi \right) \right] d\tau. \end{aligned} \quad (2.239)$$

In the case where the functions g_1 and g_2 have the forms as follows:

$$\begin{aligned} g_1(\tau) &= G'_1(\tau) = \frac{1}{\zeta} \dot{G}_1(\tau), \\ g_2(\tau) &= G'_2(\tau) f(\tau) = \frac{1}{\zeta} \dot{G}_2(\tau) f(\tau), \end{aligned} \quad (2.240)$$

by partial integration with respect to reduced time, Eq. (2.239) can be transformed into

$$\begin{aligned} I_1[G'_1, G'_2 f](\tau) &= \frac{1}{\zeta_0} \int_{\tau_0}^{\tau} \left[\dot{G}_1 \left(\int_{\tau_0}^{\tau} G'_2 f h_{\alpha} d\xi \right) - \dot{G}_2 f \left(\int_{\tau_0}^{\tau} G'_1 h_{\alpha} d\xi \right) \right] d\tau \\ &\quad - \frac{1}{\zeta_0} \int_{\tau_0}^{\tau} h_{\alpha} \left[G'_1 \left(\int_{\tau_0}^{\tau} \dot{G}_2 f d\xi \right) - G'_2 f \left(\int_{\tau_0}^{\tau} \dot{G}_1 d\xi \right) \right] d\tau. \\ &= \frac{1}{\zeta_0} \left[(G_1 - G_{10}) \left(\int_{\tau_0}^{\tau} G'_2 f h_{\alpha} d\xi \right) - (G_2 f - G_{20} f_0) \left(\int_{\tau_0}^{\tau} G'_1 h_{\alpha} d\xi \right) \right] \\ &\quad + \frac{1}{\zeta_0} \int_{\tau_0}^{\tau} G'_1 h_{\alpha} \left(\int_{\tau_0}^{\tau} G_2 f d\xi \right) d\tau + \frac{1}{\zeta_0} \int_{\tau_0}^{\tau} G_2 f \left(\int_{\tau_0}^{\tau} G'_1 h_{\alpha} d\xi \right) d\tau. \end{aligned} \quad (2.241)$$

To apply this integral to the proof, we consider

$$G_2 = N, \quad G'_2 = L_1, \quad f = u_A u_B, \quad (2.242)$$

where the subscripts A and B take either α or γ . Using Eq. (2.38), we obtain

$$G_2 \dot{f} = N \frac{d}{d\tau} (u_A u_B) = N(u_A \dot{u}_B + u_B \dot{u}_A) = -4\Phi_C(\dot{u}_A \dot{u}_B + \dot{u}_A \dot{u}_B) - 4\Phi_C \frac{d}{d\tau} (\dot{u}_A \dot{u}_B). \quad (2.243)$$

Using Eq. (2.243), we obtain

$$\begin{aligned} & \int_{\tau_0}^{\tau} G_1' h_{\alpha} \left(\int_{\tau_0}^{\tau} G_2 \dot{f} d\xi \right) d\tau + \int_{\tau_0}^{\tau} G_2 \dot{f} \left(\int_{\tau_0}^{\tau} G_1' h_{\alpha} d\xi \right) d\tau \\ &= -4\Phi_C \int_{\tau_0}^{\tau} G_1' h_{\alpha} (\dot{u}_A \dot{u}_B - \dot{u}_{A0} \dot{u}_{B0}) d\tau - 4\Phi_C \int_{\tau_0}^{\tau} \frac{d}{d\tau} (\dot{u}_A \dot{u}_B) \left(\int_{\tau_0}^{\tau} G_1' h_{\alpha} d\xi \right) d\tau \\ &= -4\Phi_C (\dot{u}_A \dot{u}_B - \dot{u}_{A0} \dot{u}_{B0}) \int_{\tau_0}^{\tau} G_1' h_{\alpha} d\tau. \end{aligned} \quad (2.244)$$

By Eq. (2.244), the integral of Eq. (2.241) for Eq. (2.242), is transformed into

$$\begin{aligned} I_1[G_1', L_1 u_A u_B](\tau) &= \frac{1}{\zeta_0} \left\{ G_1 \int_{\tau_0}^{\tau} L_1 u_A u_B h_{\alpha} d\tau - \int_{\tau_0}^{\tau} G_1 L_1 u_A u_B h_{\alpha} d\tau \right\} \\ &- \frac{1}{\zeta_0} \left[N u_A u_B \left(\int_{\tau_0}^{\tau} G_1' h_{\alpha} d\tau \right) - \int_{\tau_0}^{\tau} N \left\{ \frac{d}{d\tau} (u_A u_B) \right\} \left\{ \int_{\tau_0}^{\tau} G_1' h_{\alpha} d\xi \right\} d\tau - \int_{\tau_0}^{\tau} G_1' N u_A u_B h_{\alpha} d\xi \right] \\ &- \frac{1}{\zeta_0} \left[\int_{\tau_0}^{\tau} G_1' (N u_A u_B - N_0 u_{A0} u_{B0}) h_{\alpha} d\tau - \int_{\tau_0}^{\tau} G_1' h_{\alpha} \left(\int_{\tau_0}^{\tau} N \left\{ \frac{d}{d\tau} (u_A u_B) \right\} d\xi \right) d\tau \right] \\ &+ \frac{1}{\zeta_0} \left[\int_{\tau_0}^{\tau} (G_1 - G_{10}) L_1 u_A u_B h_{\alpha} d\tau \right] \\ &= \frac{1}{\zeta_0} \left[(G_1 - G_{10}) \int_{\tau_0}^{\tau} L_1 u_A u_B h_{\alpha} d\tau - (N u_A u_B - N_0 u_{A0} u_{B0}) \int_{\tau_0}^{\tau} G_1' h_{\alpha} d\tau \right. \\ &\quad \left. - 4\Phi_C (\dot{u}_A \dot{u}_B - \dot{u}_{A0} \dot{u}_{B0}) \int_{\tau_0}^{\tau} G_1' h_{\alpha} d\tau \right]. \end{aligned} \quad (2.245)$$

The second useful integral is

$$\begin{aligned} I_2[u_A, u_B, u_C, u_D](\tau) &= \int_{\tau_0}^{\tau} L_1 u_A u_B h_{\gamma} \left\{ \int_{\tau_0}^{\tau} L_1 u_C u_D h_{\alpha} d\xi \right\} d\tau \\ &- \int_{\tau_0}^{\tau} L_1 u_A u_B h_{\alpha} \left\{ \int_{\tau_0}^{\tau} L_1 u_C u_D h_{\gamma} d\xi \right\} d\tau, \end{aligned} \quad (2.246)$$

where the subscripts A, B, C , and D take either α or γ . This integral is transformed as follows. Using the analytic forms of h_{γ} Eq. (2.230) and Eq. (2.243), we get

$$\begin{aligned} & I_2[u_A, u_B, u_C, u_D](\tau) \\ &= \frac{1}{\zeta_0} \left[\int_{\tau_0}^{\tau} N u_A u_B \left\{ \int_{\tau_0}^{\tau} L_1 u_C u_D h_{\alpha} d\xi \right\} d\tau - \int_{\tau_0}^{\tau} L_1 u_A u_B h_{\alpha} \left\{ \int_{\tau_0}^{\tau} N u_C u_D d\xi \right\} d\tau \right] \\ &= \frac{1}{\zeta_0} \left[N u_A u_B \left\{ \int_{\tau_0}^{\tau} L_1 u_C u_D h_{\alpha} d\xi \right\} - \int_{\tau_0}^{\tau} N \left\{ \frac{d}{d\tau} (u_A u_B) \right\} \left\{ \int_{\tau_0}^{\tau} L_1 u_C u_D h_{\alpha} d\xi \right\} d\tau \right. \\ &\quad \left. - \int_{\tau_0}^{\tau} N L_1 u_A u_B u_C u_D h_{\alpha} d\tau - \int_{\tau_0}^{\tau} L_1 u_A u_B h_{\alpha} (N u_C u_D - N_0 u_{C0} u_{D0}) d\tau \right. \\ &\quad \left. + \int_{\tau_0}^{\tau} L_1 u_A u_B h_{\alpha} \left\{ \int_{\tau_0}^{\tau} N \left\{ \frac{d}{d\xi} (u_C u_D) \right\} d\xi \right\} d\tau \right] \\ &= \frac{1}{\zeta_0} \left[N u_A u_B \int_{\tau_0}^{\tau} L_1 u_C u_D h_{\alpha} d\tau + 4\Phi_C \int_{\tau_0}^{\tau} \left\{ \frac{d}{d\tau} (\dot{u}_A \dot{u}_B) \right\} \left\{ \int_{\tau_0}^{\tau} L_1 u_C u_D h_{\alpha} d\xi \right\} d\tau \right. \\ &\quad \left. - \int_{\tau_0}^{\tau} N L_1 u_A u_B u_C u_D h_{\alpha} d\tau - \int_{\tau_0}^{\tau} L_1 u_A u_B h_{\alpha} (N u_C u_D - N_0 u_{C0} u_{D0}) d\tau \right. \\ &\quad \left. - 4\Phi_C \int_{\tau_0}^{\tau} L_1 u_A u_B h_{\alpha} \left\{ \int_{\tau_0}^{\tau} \left\{ \frac{d}{d\xi} (\dot{u}_C \dot{u}_D) \right\} d\xi \right\} d\tau \right] \\ &= \frac{1}{\zeta_0} \left[N u_A u_B \int_{\tau_0}^{\tau} L_1 u_C u_D h_{\alpha} d\tau + 4\Phi_C \left(\dot{u}_A \dot{u}_B \int_{\tau_0}^{\tau} L_1 u_C u_D h_{\alpha} d\tau - \int_{\tau_0}^{\tau} L_1 \dot{u}_A \dot{u}_B u_C u_D h_{\alpha} d\tau \right) \right. \\ &\quad \left. - 2 \int_{\tau_0}^{\tau} N L_1 u_A u_B u_C u_D h_{\alpha} d\tau + N_0 u_{C0} u_{D0} \int_{\tau_0}^{\tau} L_1 u_A u_B h_{\alpha} d\tau \right. \\ &\quad \left. - 4\Phi_C \int_{\tau_0}^{\tau} L_1 u_A u_B (\dot{u}_C \dot{u}_D - \dot{u}_{C0} \dot{u}_{D0}) h_{\alpha} d\tau \right]. \end{aligned} \quad (2.247)$$

The third useful integral is

$$I_3[f'_1, f_2] = h_\gamma \int_{\tau_0}^{\tau} f'_1 f_2 h_\alpha d\tau - h_\alpha \int_{\tau_0}^{\tau} f'_1 f_2 h_\gamma d\tau. \quad (2.248)$$

Using Eq. (2.230), we get

$$\begin{aligned} I_3[f'_1, f_2] &= \frac{\dot{\zeta}}{\zeta_0} \int_{\tau_0}^{\tau} f'_1 f_2 h_\alpha d\tau - h_\alpha \int_{\tau_0}^{\tau} \frac{1}{\zeta_0} \dot{f}_1 f_2 d\tau \\ &= \frac{\dot{\zeta}}{\zeta_0} \int_{\tau_0}^{\tau} f'_1 f_2 h_\alpha d\tau - \frac{1}{\zeta_0} h_\alpha (f_1 f_2 - f_{10} f_{20}) + h_\alpha \int_{\tau_0}^{\tau} \frac{1}{\zeta_0} f_1 \dot{f}_2 d\tau, \end{aligned} \quad (2.249)$$

where f_1 and f_2 are smooth and non-singular functions with respect to reduced time. Suppose $f'_1 = N' = L_1$, and

$f_2 = u_A u_B$, where the subscripts A and B take either α or γ , we get

$$\begin{aligned} I_3[L_1, u_A u_B] &= h_\gamma \int_{\tau_0}^{\tau} L_1 u_A u_B h_\alpha d\tau - h_\alpha \int_{\tau_0}^{\tau} L_1 u_A u_B h_\gamma d\tau \\ &= \frac{\dot{\zeta}}{\zeta_0} \int_{\tau_0}^{\tau} L_1 u_A u_B h_\alpha d\tau - \frac{1}{\zeta_0} h_\alpha (N u_A u_B - N_0 u_{A0} u_{B0}) - \frac{4}{\zeta_0} \Phi_C (\dot{u}_A \dot{u}_B - \dot{u}_{A0} \dot{u}_{B0}) h_\alpha. \end{aligned} \quad (2.250)$$

Here, we consider the transformation of the second-order geometrical longitudinal path deviations given by Eqs.

(2.160) to (2.163), taking into account Eqs. (2.249) and (2.250), as follows:

$$h_{\alpha\bar{\alpha}}(\tau) = -\frac{1}{2\zeta_0} h_\alpha + \frac{1}{8\Phi_C} I_3[L_1, u_\alpha^2] = -\frac{1}{2\zeta_0} \dot{u}_\alpha^2 h_\alpha + \frac{1}{8\zeta_0 \Phi_C} \left(\dot{\zeta} \int_{\tau_0}^{\tau} L_1 u_\alpha^2 h_\alpha d\tau - N u_\alpha^2 h_\alpha \right), \quad (2.251)$$

$$h_{\alpha\gamma}^{(R)}(\tau) = \frac{1}{8\Phi_C} I_3[L_1, u_\alpha u_\gamma] = -\frac{1}{2\zeta_0} \dot{u}_\alpha \dot{u}_\gamma h_\alpha + \frac{1}{8\zeta_0 \Phi_C} \left(\dot{\zeta} \int_{\tau_0}^{\tau} L_1 u_\alpha u_\gamma h_\alpha d\tau - N u_\alpha u_\gamma h_\alpha \right), \quad (2.252)$$

$$h_{\alpha\gamma}^{(I)}(\tau) = -\frac{\eta B_0}{4\zeta_0 \sqrt{\Phi_C}} h_\alpha + \frac{\eta}{4\sqrt{\Phi_C}} I_3[B', 1] = \frac{\eta}{4\zeta_0 \sqrt{\Phi_C}} \left(\dot{\zeta} \int_{\tau_0}^{\tau} B' h_\alpha d\tau - B h_\alpha \right), \quad (2.253)$$

$$h_{\gamma\bar{\gamma}}(\tau) = -\frac{N_0}{8\zeta_0 \Phi_C} h_\alpha + \frac{1}{8\Phi_C} I_3[L_1, u_\gamma^2] = -\frac{1}{2\zeta_0} \dot{u}_\gamma^2 h_\alpha + \frac{1}{8\zeta_0 \Phi_C} \left(\dot{\zeta} \int_{\tau_0}^{\tau} L_1 u_\gamma^2 h_\alpha d\tau - N u_\gamma^2 h_\alpha \right). \quad (2.254)$$

Then, the values of the second-order longitudinal path deviations at the reduced convergent time τ_i are given by

$$h_{\alpha\bar{\alpha}i} = -\frac{1}{2\zeta_0} \dot{u}_{\alpha i}^2 h_{\alpha i} + \frac{\dot{\zeta}_i}{8\zeta_0 \Phi_C} \int_{\tau_0}^{\tau_i} L_1 u_\alpha^2 h_\alpha d\tau, \quad (2.255)$$

$$h_{\alpha\gamma i}^{(R)} = -\frac{1}{2\zeta_0} \dot{u}_{\alpha i} \dot{u}_{\gamma i} h_{\alpha i} + \frac{\dot{\zeta}_i}{8\zeta_0 \Phi_C} \int_{\tau_0}^{\tau_i} L_1 u_\alpha u_\gamma h_\alpha d\tau, \quad (2.256)$$

$$h_{\alpha\gamma i}^{(I)} = \frac{\dot{\zeta}_i \eta}{4\zeta_0 \sqrt{\Phi_C}} \int_{\tau_0}^{\tau_i} B' h_\alpha d\tau - \frac{\eta B_i}{4\zeta_0 \sqrt{\Phi_C}} h_{\alpha i}, \quad (2.257)$$

$$h_{\gamma\bar{\gamma}i} = -\frac{1}{2\zeta_0} \dot{u}_{\gamma i}^2 h_{\alpha i} - \frac{N_i}{8\zeta_0 \Phi_C} u_{\gamma i}^2 h_{\alpha i} + \frac{\dot{\zeta}_i}{8\zeta_0 \Phi_C} \int_{\tau_0}^{\tau_i} L_1 u_\gamma^2 h_\alpha d\tau. \quad (2.258)$$

Comparing these with Eqs. (2.148) to (2.150), the chromatic aberration coefficients are related to the second-order longitudinal path deviation at the reduced convergent time via

$$C_{Co} = \frac{\dot{\zeta}_0^3}{\dot{\zeta}_i} h_{\alpha\bar{\alpha}i}, \quad C_{Mo} = \frac{\dot{\zeta}_0^2}{\dot{\zeta}_i} h_{\alpha\gamma i}^{(R)}, \quad C_{Ro} = \frac{\dot{\zeta}_0^2}{\dot{\zeta}_i} h_{\alpha\gamma i}^{(I)}. \quad (2.259)$$

Finally, we have finished the preparation for the proof. Using Eqs. (2.161) and (2.162) as the formulae for the longitudinal path deviations and Eqs. (2.255) to (2.258) for those at the reduced convergent time, then, we can use Eqs. (2.245), (2.249), and (2.250) to prove that the anisotropic part of the field curvature coefficient vanishes, $C_{fo} =$

0. Applying Eqs. (2.161) and (2.162) along with Eqs. (2.256) and (2.257) to Eq. (2.189), the imaginary part of the field-curvature coefficient is transformed into

$$\begin{aligned}
C_{fo} &= - \int_{\tau_o}^{\tau_i} \left(\frac{\zeta_o L_1}{4\Phi_C} u_\alpha u_\gamma h_{\alpha\gamma}^{(I)} - \frac{\zeta_o \eta B'}{2\sqrt{\Phi_C}} h_{\alpha\gamma}^{(R)} \right) d\tau + \frac{\zeta_o}{\zeta_i} \dot{u}_{ai} \dot{u}_{\gamma i} h_{\alpha\gamma i}^{(I)} - \frac{\zeta_o \eta B_i}{2\zeta_i \sqrt{\Phi_C}} h_{\alpha\gamma i}^{(R)} \\
&= \frac{\zeta_o \eta}{16\Phi_C^{3/2}} I_1[B', L_1 u_\alpha u_\gamma](\tau_i) + \int_{\tau_o}^{\tau_i} \frac{\zeta_o \eta B_o}{16\Phi_C^{3/2}} L_1 u_\alpha u_\gamma h_\alpha d\tau \\
&\quad + \frac{\eta}{4\sqrt{\Phi_C}} \dot{u}_{ai} \dot{u}_{\gamma i} \int_{\tau_o}^{\tau_i} B' h_\alpha d\tau - \frac{\eta B_i}{4\zeta_i \sqrt{\Phi_C}} \dot{u}_{ai} \dot{u}_{\gamma i} h_{ai} + \frac{\eta B_i}{4\zeta_i \sqrt{\Phi_C}} \dot{u}_{ai} \dot{u}_{\gamma i} h_{ai} - \frac{\eta B_i}{16\Phi_C^{3/2}} \int_{\tau_o}^{\tau_i} L_1 u_\alpha u_\gamma h_\alpha d\tau \\
&= \frac{\zeta_o \eta}{16\Phi_C^{3/2}} I_1[B', L_1 u_\alpha u_\gamma](\tau_i) - \left(\frac{\eta}{16\Phi_C^{3/2}} (B_i - B_o) \int_{\tau_o}^{\tau_i} L_1 u_\alpha u_\gamma h_\alpha d\tau - \frac{\eta}{4\sqrt{\Phi_C}} \dot{u}_{ai} \dot{u}_{\gamma i} \int_{\tau_o}^{\tau_i} B' h_\alpha d\tau \right),
\end{aligned} \tag{2.260}$$

where Eq. (2.239) is used for this transformation. Employing Eq. (2.245) and using that $u_{ai} = 0$, $u_{ao} = 0$, and $\dot{u}_{\gamma o} = 0$, we get

$$\frac{\zeta_o \eta}{16\Phi_C^{3/2}} I_1[B', L_1 u_\alpha u_\gamma](\tau_i) = \frac{\eta}{16\Phi_C^{3/2}} \left[(B_i - B_o) \int_{\tau_o}^{\tau_i} L_1 u_\alpha u_\gamma h_\alpha d\tau - 4\Phi_C \dot{u}_{ai} \dot{u}_{\gamma i} \int_{\tau_o}^{\tau_i} B' h_\alpha d\tau \right] \tag{2.261}$$

Substituting it into Eq. (2.260), the anisotropic part of the field curvature coefficient vanishes:

$$C_{fo} = 0. \tag{2.262}$$

A proof of the relations between the coma-length and the coma-radius, which is expected in Eq. (2.194), is given as follows. Using Eqs. (2.160) to (2.162), (2.184), (2.186), and (2.246), for the real part, we get

$$\begin{aligned}
C_{KLo} - 2C_{KRo} &= \zeta_o^2 \int_{\tau_o}^{\tau_i} \frac{L_1}{4\Phi_C} (-u_\alpha^2 h_{\alpha\gamma}^{(R)} + u_\alpha u_\gamma h_{\alpha\bar{\gamma}}) d\tau + \frac{\zeta_o^2}{\zeta_i} (\dot{u}_{ai}^2 h_{\alpha\gamma i}^{(R)} - \dot{u}_{ai} \dot{u}_{\gamma i} h_{\alpha\bar{\gamma} i}) \\
&= \frac{\zeta_o^2}{32\Phi_C^2} (-I_2[u_\alpha, u_\alpha, u_\alpha, u_\gamma](\tau_i) + I_2[u_\alpha, u_\gamma, u_\alpha, u_\alpha](\tau_i)) \\
&\quad - \frac{\zeta_o}{8\Phi_C} \int_{\tau_o}^{\tau_i} L_1 u_\alpha u_\gamma h_\alpha d\tau + \frac{\zeta_o^2}{\zeta_i} (\dot{u}_{ai}^2 h_{\alpha\gamma i}^{(R)} - \dot{u}_{ai} \dot{u}_{\gamma i} h_{\alpha\bar{\gamma} i}).
\end{aligned} \tag{2.263}$$

Using Eq. (2.247) and $u_{ai} = 0$, $u_{ao} = 0$, $\dot{u}_{ao} = 1$, and $\dot{u}_{\gamma o} = 0$, we get

$$\begin{aligned}
&\frac{\zeta_o^2}{32\Phi_C^2} (-I_2[u_\alpha, u_\alpha, u_\alpha, u_\gamma](\tau_i) + I_2[u_\alpha, u_\gamma, u_\alpha, u_\alpha](\tau_i)) \\
&= -\frac{\zeta_o}{32\Phi_C^2} \left[4\Phi_C \left(\dot{u}_{ai}^2 \int_{\tau_o}^{\tau_i} L_1 u_\alpha u_\gamma h_\alpha d\tau - \int_{\tau_o}^{\tau_i} L_1 \dot{u}_{ai}^2 u_\alpha u_\gamma h_\alpha d\tau \right), \right. \\
&\quad \left. -2 \int_{\tau_o}^{\tau_i} N L_1 u_\alpha^3 u_\gamma h_\alpha d\tau - 4\Phi_C \int_{\tau_o}^{\tau_i} L_1 u_\alpha^2 \dot{u}_{ai} u_\gamma h_\alpha d\tau \right] \\
&\quad + \frac{\zeta_o}{32\Phi_C^2} \left[4\Phi_C \left(\dot{u}_{ai} \dot{u}_{\gamma i} \int_{\tau_o}^{\tau_i} L_1 u_\alpha^2 h_\alpha d\tau - \int_{\tau_o}^{\tau_i} L_1 \dot{u}_{ai} \dot{u}_{\gamma i} u_\alpha^2 h_\alpha d\tau \right), \right. \\
&\quad \left. -2 \int_{\tau_o}^{\tau_i} N L_1 u_\alpha^3 u_\gamma h_\alpha d\tau - 4\Phi_C \int_{\tau_o}^{\tau_i} L_1 u_\alpha u_\gamma \dot{u}_{ai}^2 h_\alpha d\tau + 4\Phi_C \int_{\tau_o}^{\tau_i} L_1 u_\alpha u_\gamma h_\alpha d\tau \right] \\
&= -\frac{\zeta_o}{8\Phi_C} \left[\dot{u}_{ai}^2 \int_{\tau_o}^{\tau_i} L_1 u_\alpha u_\gamma h_\alpha d\tau - \dot{u}_{ai} \dot{u}_{\gamma i} \int_{\tau_o}^{\tau_i} L_1 u_\alpha^2 h_\alpha d\tau \right] + \frac{\zeta_o}{8\Phi_C} \int_{\tau_o}^{\tau_i} L_1 u_\alpha u_\gamma h_\alpha d\tau.
\end{aligned} \tag{2.264}$$

And, using Eqs. (2.255) and (2.256), we get

$$\begin{aligned}
&\frac{\zeta_o^2}{\zeta_i} (\dot{u}_{ai}^2 h_{\alpha\gamma i}^{(R)} - \dot{u}_{ai} \dot{u}_{\gamma i} h_{\alpha\bar{\gamma} i}) \\
&= -\frac{\zeta_o}{2\zeta_i} \dot{u}_{ai}^3 \dot{u}_{\gamma i} h_{ai} + \frac{\zeta_o}{8\Phi_C} \dot{u}_{ai}^2 \int_{\tau_o}^{\tau_i} L_1 u_\alpha u_\gamma h_\alpha d\tau + \frac{\zeta_o}{2\zeta_i} \dot{u}_{ai}^3 \dot{u}_{\gamma i} h_{ai} - \frac{\zeta_o}{8\Phi_C} \dot{u}_{ai} \dot{u}_{\gamma i} \int_{\tau_o}^{\tau_i} L_1 u_\alpha^2 h_\alpha d\tau \\
&= \frac{\zeta_o}{8\Phi_C} \left[\dot{u}_{ai}^2 \int_{\tau_o}^{\tau_i} L_1 u_\alpha u_\gamma h_\alpha d\tau - \dot{u}_{ai} \dot{u}_{\gamma i} \int_{\tau_o}^{\tau_i} L_1 u_\alpha^2 h_\alpha d\tau \right].
\end{aligned} \tag{2.265}$$

Employing Eqs. (2.264) and (2.265) to Eq. (2.263), we conclude that

$$C_{KLo} = 2C_{KR0}. \quad (2.266)$$

For the imaginary part, using Eqs. (2.160) to (2.162), (2.185), (2.187), and (2.241), we get

$$\begin{aligned} C_{kLo} + 2C_{kRo} &= \dot{\zeta}_o^2 \int_{\tau_o}^{\tau_i} \left(-\frac{L_1}{4\Phi_C} u_a^2 h_{a\gamma}^{(l)} + \frac{\eta B'}{2\sqrt{\Phi_C}} h_{a\bar{a}} \right) d\tau + \frac{\dot{\zeta}_o^2}{\dot{\zeta}_i} \dot{u}_{ai}^2 h_{a\gamma i}^{(l)} - \frac{\dot{\zeta}_o^2 \eta B_i}{2\dot{\zeta}_i \sqrt{\Phi_C}} h_{a\bar{a}i} \\ &= \frac{\dot{\zeta}_o^2 \eta}{16\Phi_C^{3/2}} I_1[B', L_1 u_a^2](\tau_i) - \frac{\dot{\zeta}_o \eta}{4\sqrt{\Phi_C}} \int_{\tau_o}^{\tau_i} B' h_a d\tau + \frac{\dot{\zeta}_o \eta B_o}{16\Phi_C^{3/2}} \int_{\tau_o}^{\tau_i} L_1 u_a^2 h_a d\tau \\ &\quad + \frac{\dot{\zeta}_o^2}{\dot{\zeta}_i} \dot{u}_{ai}^2 h_{a\gamma i}^{(l)} - \frac{\dot{\zeta}_o^2 \eta B_i}{2\dot{\zeta}_i \sqrt{\Phi_C}} h_{a\bar{a}i}. \end{aligned} \quad (2.267)$$

Using Eqs. (2.245), (2.255), and (2.257), and $u_{ai} = 0$, $u_{ao} = 0$, and $\dot{u}_{ao} = 1$, we get

$$\begin{aligned} &\frac{\dot{\zeta}_o^2 \eta}{16\Phi_C^{3/2}} I_1[B', L_1 u_a^2](\tau_i) \\ &= \frac{\dot{\zeta}_o \eta}{16\Phi_C^{3/2}} \left[(B_i - B_o) \int_{\tau_o}^{\tau_i} L_1 u_a^2 h_a d\tau - 4\Phi_C (\dot{u}_{ai}^2 - 1) \int_{\tau_o}^{\tau_i} B' h_a d\tau \right], \end{aligned} \quad (2.268)$$

and

$$\begin{aligned} &\frac{\dot{\zeta}_o^2}{\dot{\zeta}_i} \dot{u}_{ai}^2 h_{a\gamma i}^{(l)} - \frac{\dot{\zeta}_o^2 \eta B_i}{2\dot{\zeta}_i \sqrt{\Phi_C}} h_{a\bar{a}i} = \frac{\dot{\zeta}_o \eta}{4\sqrt{\Phi_C}} \dot{u}_{ai}^2 \int_{\tau_o}^{\tau_i} B' h_a d\tau - \frac{\dot{\zeta}_o \eta B_i}{4\dot{\zeta}_i \sqrt{\Phi_C}} h_{ai} \\ &\quad + \frac{\dot{\zeta}_o \eta B_i}{4\dot{\zeta}_i \sqrt{\Phi_C}} \dot{u}_{ai}^2 h_{ai} - \frac{\dot{\zeta}_o \eta B_i}{16\Phi_C^{3/2}} \int_{\tau_o}^{\tau_i} L_1 u_a^2 h_a d\tau. \end{aligned} \quad (2.269)$$

Employing Eqs. (2.268) and (2.269) to (2.267), we conclude that

$$C_{kLo} = -2C_{kRo}. \quad (2.270)$$

Using Eqs. (2.260), (2.266), and (2.270), the third-order geometrical aberration in the object plane, Eq. (2.182), becomes the following formula, which has the same structure as that of standard electron optics,

$$\begin{aligned} \Delta u_o^{(3)}{}_{\text{geo.}} &= C_{So} u_o'^2 \bar{u}_o' + 2(C_{Ko} + iC_{ko}) u_o u_o' \bar{u}_o' + (C_{Ko} - iC_{ko}) \bar{u}_o u_o'^2 \\ &\quad + C_{Fo} u_o \bar{u}_o u_o' + (C_{Ao} + iC_{ao}) \bar{u}_o u_o'^2 + (C_{Do} + iC_{do}) u_o^2 \bar{u}_o, \end{aligned} \quad (2.271)$$

where

$$C_{Ko} = C_{KR0} = \int_{\tau_o}^{\tau_i} \frac{\dot{\zeta}_o^2}{32\Phi_C} (8L_1 u_a^2 h_{a\gamma}^{(R)} - L_2 u_a^3 u_\gamma) d\tau - \frac{\dot{\zeta}_o^2}{\dot{\zeta}_i} \dot{u}_{ai}^2 h_{a\gamma i}^{(R)}, \quad (2.272)$$

$$C_{ko} = -C_{kRo} = \int_{\tau_o}^{\tau_i} \left(\frac{\dot{\zeta}_o^2 L_1}{4\Phi_C} u_a^2 h_{a\gamma}^{(l)} - \frac{\dot{\zeta}_o^2 \eta B''}{16\sqrt{\Phi_C}} u_a^2 \right) d\tau - \frac{\dot{\zeta}_o^2}{\dot{\zeta}_i} \dot{u}_{ai}^2 h_{a\gamma i}^{(l)}. \quad (2.273)$$

At the end of this section, we discuss the so-called Petzval coefficient, which describes the relation between field curvature coefficient and real part of astigmatism coefficient.

The Petzval coefficient is given by

$$C_P = C_{Fo} - 2C_{Ao}. \quad (2.274)$$

In the standard electron optics, the Petzval coefficient is given as in an integral form similar to aberration coefficients, but it does not include any lateral trajectories in its integrand. This means the Petzval coefficient is determined only by field-strength and distributions. Specifically, if the lens field is sufficiently thin and both the object and the image

planes are located inside field-free regions, the Petzval coefficient does not depend on the position of the object and image planes. In the time-dependent theory, we expect the same features. The Petzval coefficient is defined by

$$C_P = C_{Fo} - 2C_{Ao}. \quad (2.275)$$

In the time-dependent theory, using Eqs. (2.188) and (2.189), we find that:

$$\begin{aligned} C_P = & \int_{\tau_o}^{\tau_i} \frac{\dot{\zeta}_o}{4\Phi_C} L_1(u_\alpha^2 h_{\gamma\bar{\gamma}} - u_\alpha u_\gamma h_{\alpha\gamma}^{(R)}) d\tau + \frac{3\dot{\zeta}_o\eta}{2\sqrt{\Phi_C}} \int_{\tau_o}^{\tau_i} B' h_{\alpha\gamma}^{(I)} d\tau \\ & + \frac{\dot{\zeta}_i}{\dot{\zeta}_i} (-\dot{u}_{ai}^2 h_{\gamma\bar{\gamma}i} + \dot{u}_{ai} \dot{u}_{\gamma i} h_{\alpha\gamma i}^{(R)}) - \frac{3\dot{\zeta}_o\eta B_i}{2\dot{\zeta}_i\sqrt{\Phi_C}} h_{\alpha\gamma i}^{(I)}. \end{aligned} \quad (2.276)$$

Let us calculate this part by part. Using Eqs. (2.161), (2.163), and (2.246), the first term of the R.H.S is transformed into

$$\begin{aligned} & \int_{\tau_o}^{\tau_i} \frac{\dot{\zeta}_o}{4\Phi_C} L_1(u_\alpha^2 h_{\gamma\bar{\gamma}} - u_\alpha u_\gamma h_{\alpha\gamma}^{(R)}) d\tau \\ & = \frac{\dot{\zeta}_o}{32\Phi_C^2} \{I_2[u_\alpha, u_\alpha, u_\gamma, u_\gamma](\tau_i) - I_2[u_\alpha, u_\gamma, u_\alpha, u_\gamma](\tau_i)\} - \frac{N_o}{32\Phi_C^2} \int_{\tau_o}^{\tau_i} L_1 u_\alpha^2 h_\alpha d\tau \end{aligned} \quad (2.277)$$

Using Eq. (2.247), and considering boundary values of lateral fundamental trajectories, $u_{ai} = 0, u_{ao} = 0, \dot{u}_{ao} = 1, u_{\gamma o} = 1, \dot{u}_{\gamma o} = 0$, we get

$$\begin{aligned} & \frac{\dot{\zeta}_o}{32\Phi_C^2} \{I_2[u_\alpha, u_\alpha, u_\gamma, u_\gamma](\tau_i) - I_2[u_\alpha, u_\gamma, u_\alpha, u_\gamma](\tau_i)\} - \frac{N_o}{32\Phi_C^2} \int_{\tau_o}^{\tau_i} L_1 u_\alpha^2 h_\alpha d\tau \\ & = \frac{1}{8\Phi_C} \left(\dot{u}_{ai}^2 \int_{\tau_o}^{\tau_i} L_1 u_\gamma^2 h_\alpha d\tau - \int_{\tau_o}^{\tau_i} L_1 \dot{u}_\alpha^2 u_\gamma^2 h_\alpha d\tau \right) \\ & - \frac{1}{8\Phi_C} \left(\dot{u}_{ai} \dot{u}_{\gamma i} \int_{\tau_o}^{\tau_i} L_1 u_\alpha u_\gamma h_\alpha d\tau - \int_{\tau_o}^{\tau_i} L_1 u_\alpha u_\gamma \dot{u}_\alpha \dot{u}_\gamma h_\alpha d\tau \right) + \frac{N_o}{32\Phi_C^2} \int_{\tau_o}^{\tau_i} L_1 u_\alpha^2 h_\alpha d\tau \\ & - \frac{1}{8\Phi_C} \int_{\tau_o}^{\tau_i} L_1 (u_\alpha^2 \dot{u}_\gamma^2 - u_\alpha u_\gamma \dot{u}_\alpha \dot{u}_\gamma) h_\alpha d\tau - \frac{N_o}{32\Phi_C^2} \int_{\tau_o}^{\tau_i} L_1 u_\alpha^2 h_\alpha d\tau \\ & = \frac{1}{8\Phi_C} \left(\dot{u}_{ai}^2 \int_{\tau_o}^{\tau_i} L_1 u_\gamma^2 h_\alpha d\tau - \dot{u}_{ai} \dot{u}_{\gamma i} \int_{\tau_o}^{\tau_i} L_1 u_\alpha u_\gamma h_\alpha d\tau \right) - \frac{1}{8\Phi_C} \int_{\tau_o}^{\tau_i} L_1 (u_\gamma \dot{u}_\alpha - \dot{u}_\gamma u_\alpha)^2 h_\alpha d\tau \\ & = \frac{1}{8\Phi_C} \left(\dot{u}_{ai}^2 \int_{\tau_o}^{\tau_i} L_1 u_\gamma^2 h_\alpha d\tau - \dot{u}_{ai} \dot{u}_{\gamma i} \int_{\tau_o}^{\tau_i} L_1 u_\alpha u_\gamma h_\alpha d\tau \right) - \frac{1}{8\Phi_C} \int_{\tau_o}^{\tau_i} L_1 h_\alpha d\tau. \end{aligned} \quad (2.278)$$

Using Eqs. (2.162), the second term of Eq. (2.276) is

$$\begin{aligned} & \frac{3\dot{\zeta}_o\eta}{2\sqrt{\Phi_C}} \int_{\tau_o}^{\tau_i} B' h_{\alpha\gamma}^{(I)} d\tau = \frac{3\eta}{8\Phi_C} \int_{\tau_o}^{\tau_i} \left(\dot{B} \int_{\tau_o}^{\tau} B' h_\alpha d\xi - B B' h_\alpha \right) d\tau \\ & = \frac{3\eta^2 B_i}{8\Phi_C} \int_{\tau_o}^{\tau_i} B' h_\alpha d\tau - \frac{3\eta^2}{4\Phi_C} \int_{\tau_o}^{\tau_i} B B' h_\alpha d\tau. \end{aligned} \quad (2.279)$$

Using Eqs. (2.256) to (2.258), the third and fourth terms of Eq. (2.276) are:

$$\begin{aligned} & \frac{\dot{\zeta}_o}{\dot{\zeta}_i} \left(-\dot{u}_{ai}^2 h_{\gamma\bar{\gamma}i} + \dot{u}_{ai} \dot{u}_{\gamma i} h_{\alpha\gamma i}^{(R)} \right) - \frac{3\dot{\zeta}_o\eta B_i}{2\dot{\zeta}_i\sqrt{\Phi_C}} h_{\alpha\gamma i}^{(I)} \\ & = \frac{1}{2\dot{\zeta}_i} \dot{u}_{ai}^2 \dot{u}_{\gamma i}^2 h_{ai} + \frac{N_i}{8\dot{\zeta}_i\Phi_C} \dot{u}_{ai}^2 \dot{u}_{\gamma i}^2 h_{ai} - \frac{1}{8\Phi_C} \dot{u}_{ai}^2 \int_{\tau_o}^{\tau_i} L_1 u_\gamma^2 h_\alpha d\tau \\ & - \frac{1}{2\dot{\zeta}_i} \dot{u}_{ai}^2 \dot{u}_{\gamma i}^2 h_{ai} + \frac{1}{8\Phi_C} \dot{u}_{ai} \dot{u}_{\gamma i} \int_{\tau_o}^{\tau_i} L_1 u_\alpha u_\gamma h_\alpha d\tau - \frac{3\eta^2 B_i}{8\Phi_C} \int_{\tau_o}^{\tau_i} B' h_\alpha d\tau + \frac{3\eta^2 B_i^2}{8\dot{\zeta}_i\Phi_C} h_{ai} \\ & = \frac{N_i}{8\dot{\zeta}_i\Phi_C} \dot{u}_{ai}^2 \dot{u}_{\gamma i}^2 h_{ai} + \frac{3\eta^2 B_i^2}{8\dot{\zeta}_i\Phi_C} h_{ai} - \frac{1}{8\Phi_C} \dot{u}_{ai}^2 \int_{\tau_o}^{\tau_i} L_1 u_\gamma^2 h_\alpha d\tau \\ & + \frac{1}{8\Phi_C} \dot{u}_{ai} \dot{u}_{\gamma i} \int_{\tau_o}^{\tau_i} L_1 u_\alpha u_\gamma h_\alpha d\tau - \frac{3\eta^2 B_i}{8\Phi_C} \int_{\tau_o}^{\tau_i} B' h_\alpha d\tau. \end{aligned} \quad (2.280)$$

Taking into account Eqs. (2.277) to (2.279), the Petzval coefficient, Eq. (2.276), is

$$C_p = -\frac{1}{8\Phi_c} \int_{\tau_0}^{\tau_i} (L_1 + 6\eta^2 BB') h_\alpha d\tau + \frac{N_i + 3\eta^2 B_i^2}{8\dot{\zeta}_i \Phi_c} h_{\alpha i}, \quad (2.281)$$

where $u_{yi}\dot{u}_\alpha = 1$ is used. Eq. (2.281) shows that the integral form of the Petzval coefficient does not include lateral fundamental rays. By Eq. (2.229), the analytic form of h_α is given by an integral form of a function of $\dot{\zeta}$, that is, a function of an axial potential Φ . This means that C_p depends only on the potential and the magnetic field of the mirror system, as we expected.

We are at the point where three properties of aberration coefficients of time-dependent theory, which are expected according to an analogy to standard electron optics, are verified. The verified properties are as follows. First, the anisotropic part of the field curvature coefficient vanishes. Second, the relation between the coma-length and the coma-radius coefficients are given by Eqs. (2.266) and (2.270). Third, the relation between the isotropic part of the field curvature coefficient and that of the astigmatism coefficient is given by the so-called Petzval coefficient, see Eqs. (2.274) and (2.281), and it is independent of the lateral fundamental rays.

2.8 Transformation of the aberration coefficients, from time-dependent theory to standard electron optics, for a normal lens system.

Since the time-dependent theory is not limited to systems of electron mirrors, the derived formulae of aberration coefficients must be valid for normal lens systems as well. Because the axial potential of the electron never vanishes in normal lens system, the parameter of the integration can be converted from reduced time to the coordinate of the optic axis. In this case, partial integration with respect to the coordinate of the optic axis is valid because the integrand has no singularities. In this way, aberration coefficients in the time-dependent theory, whose integral parameter is reduced time, must be transformed into aberration coefficients in the standard electron optics theory, whose integral parameter is the coordinate of the optic axis.

Rose and Preikszas provided a transformation of the spherical aberration coefficient and the axial chromatic aberration coefficient only for systems composed of pure-electrostatic round fields. They also verified that the results of transformation perfectly match the mathematical formulae of those coefficients in the standard electron optics [1.88]. In this section, we investigate the transformation of derived aberration coefficients in the time-dependent theory, in the case of a magnetic field overlapping with the electrostatic field, and we show that those formulae match those in the standard electron optics theory.

First, the on- and off-axis chromatic aberration coefficients in the time-dependent theory, Eqs. (2.148) to (2.150), are considered. Because in systems of standard lenses, the reduced velocity of the reference electron is always positive, $\dot{\zeta} > 0$, the integration variable τ can be transformed into ζ through the relation

$$d\tau = \frac{1}{\dot{\zeta}} d\zeta. \quad (2.282)$$

To obtain the transformation of aberration coefficients, the following integration is convenient. Using Eqs. (2.229) and (2.248), and $L_1 = N'$, considering partial integration with respect to ζ , it is obtained as follows:

$$\begin{aligned} I_4[u_A, u_B] &= \int_{\tau_o}^{\tau_i} L_1 u_A u_B h_a d\tau \\ &= \dot{\zeta}_o (N_i u_{Ai} u_{Bi} + 4\Phi_C \dot{u}_{Ai} \dot{u}_{Bi}) \int_{\zeta_o}^{\zeta_i} \frac{1}{\dot{\zeta}^3} d\zeta - \dot{\zeta}_o \int_{\zeta_o}^{\zeta_i} \frac{1}{\dot{\zeta}^3} (N u_A u_B + 4\Phi_C \dot{u}_A \dot{u}_B) d\zeta, \end{aligned} \quad (2.283)$$

where the subscripts A and B , take either α or γ . Note that, the boundary values of the lateral fundamental rays, Eqs. (2.40) and (2.66), and the Wronskian Eqs. (2.43) and (2.48) are often used in the transformation below. Taking into account that the fundamental rays, $\tilde{u}_\alpha, \tilde{u}_\gamma$, of the standard electron optics is related to those of the time-dependent theory through Eq. (2.76), the chromatic aberration coefficients are transformed as follows:

The axial chromatic aberration coefficient, Eq. (2.148), is transformed into

$$\begin{aligned} C_{Co} &= \frac{\dot{\zeta}_o^2}{8\Phi_C} I_4[u_\alpha, u_\alpha] - \frac{\dot{\zeta}_o^2}{2\dot{\zeta}_i} \dot{u}_{\alpha i}^2 h_{\alpha i} = -\frac{\dot{\zeta}_o^3}{2} \int_{\tau_o}^{\tau_i} \frac{\dot{u}_\alpha^2}{\dot{\zeta}^3} d\zeta - \frac{\dot{\zeta}_o^3}{8\Phi_C} \int_{\tau_o}^{\tau_i} \frac{N u_\alpha^2}{\dot{\zeta}^3} d\zeta \\ &= -\frac{\dot{\zeta}_o}{2} \int_{\tau_o}^{\tau_i} \frac{\tilde{u}_\alpha'^2}{\dot{\zeta}} d\zeta - \frac{\dot{\zeta}_o}{8\Phi_C} \int_{\tau_o}^{\tau_i} \frac{N \tilde{u}_\alpha^2}{\dot{\zeta}^3} d\zeta = -\sqrt{\Phi_o} \int_{\zeta_o}^{\zeta_i} \left(\frac{1}{2\sqrt{\Phi}} \tilde{u}_\alpha'^2 + \frac{\Phi'' + \eta^2 B^2}{\Phi^{3/2}} \tilde{u}_\alpha^2 \right) d\zeta. \end{aligned} \quad (2.284)$$

The isotropic part of the off-axis chromatic aberration coefficient, Eq. (2.149), is transformed into

$$\begin{aligned} C_{Mo} &= \frac{\dot{\zeta}_o}{8\Phi_C} I_4[u_\alpha, u_\gamma] - \frac{\dot{\zeta}_o}{2\dot{\zeta}_i} \dot{u}_{\alpha i} \dot{u}_{\gamma i} h_{\alpha i} = -\frac{\dot{\zeta}_o^2}{2} \int_{\tau_o}^{\tau_i} \frac{\dot{u}_\alpha \dot{u}_\gamma}{\dot{\zeta}^2} d\tau - \frac{\dot{\zeta}_o^2}{8\Phi_C} \int_{\tau_o}^{\tau_i} \frac{N u_\alpha u_\gamma}{\dot{\zeta}^2} d\tau \\ &= \frac{\dot{\zeta}_o}{2} \int_{\tau_o}^{\tau_i} \frac{\tilde{u}_\alpha' \tilde{u}_\gamma'}{\dot{\zeta}} d\zeta - \frac{\dot{\zeta}_o}{8\Phi_C} \int_{\tau_o}^{\tau_i} \frac{N \tilde{u}_\alpha \tilde{u}_\gamma}{\dot{\zeta}^3} d\zeta = -\sqrt{\Phi_o} \int_{\zeta_o}^{\zeta_i} \left(\frac{1}{2\sqrt{\Phi}} \tilde{u}_\alpha' \tilde{u}_\gamma' + \frac{\Phi'' + \eta^2 B^2}{\Phi^{3/2}} \tilde{u}_\alpha \tilde{u}_\gamma \right) d\zeta. \end{aligned} \quad (2.285)$$

The anisotropic part of the off-axis chromatic aberration coefficient, Eq. (2.150), is transformed into

$$C_{Ro} = -\frac{\dot{\zeta}_o^2}{4\sqrt{\Phi_C}} \int_{\tau_o}^{\tau_i} \frac{\eta B}{\dot{\zeta}^2} d\tau = -\Phi_o \int_{\zeta_o}^{\zeta_i} \frac{\eta B}{\Phi^{3/2}} d\zeta. \quad (2.286)$$

These formulae match the non-relativistic chromatic aberration coefficients in standard electron optics theory.

Second, to obtain the transformation of the geometrical aberration coefficients, it is convenient to consider the second-order longitudinal path deviation and several useful integrals in advance. Employing Eqs. (2.229) and (2.282) through Eqs. (2.251) to (2.254), the second-order geometrical longitudinal path deviations for the standard lens system are given as follows. For the real component of path deviations, using Eq. (2.243), we get

$$\begin{aligned}
h_{AB}^{(R)}(\zeta) &= -\frac{1}{2\zeta_o} \dot{u}_A \dot{u}_B h_\alpha + \frac{1}{8\zeta_o \Phi_C} \left(\zeta \int_{\tau_o}^{\tau} L_1 u_A u_B h_\alpha d\tau - N u_A u_B h_\alpha \right) \\
&= -\frac{1}{2\zeta_o} \dot{u}_A \dot{u}_B h_\alpha - \frac{1}{8\Phi_C} \zeta \int_{\tau_o}^{\tau} N \frac{d}{d\tau} (u_A u_B) \left(\int_{\tau_o}^{\tau} \frac{d\tau}{\zeta^2} \right) d\tau - \frac{1}{8\Phi_C} \zeta \int_{\tau_o}^{\tau} \frac{N u_A u_B}{\zeta^2} d\tau \\
&= -\frac{1}{2\zeta_o} \dot{u}_A \dot{u}_B h_\alpha + \frac{1}{2} \zeta \int_{\tau_o}^{\tau} \frac{d}{d\tau} (\dot{u}_A \dot{u}_B) \left(\int_{\tau_o}^{\tau} \frac{d\tau}{\zeta^2} \right) d\tau - \frac{1}{8\Phi_C} \zeta \int_{\tau_o}^{\tau} \frac{N u_A u_B}{\zeta^2} d\tau \\
&= -\frac{\zeta}{8\Phi_C} \int_{\zeta_o}^{\zeta} \frac{1}{\zeta^3} (N u_A u_B + 4\Phi_C \zeta^2 u'_A u'_B) d\zeta,
\end{aligned} \tag{2.287}$$

where the subscripts A and B take α or γ . $h_{\alpha\gamma}^{(I)}$ for the standard lens system is given by

$$h_{\alpha\gamma}^{(I)}(\zeta) = -\frac{\zeta \eta}{4\sqrt{\Phi_C}} \int_{\zeta_o}^{\zeta} \frac{B}{\zeta^3} d\zeta. \tag{2.288}$$

In addition, we consider the finite integration as follows. Using Eqs. (2.229), (2.243), and (2.287),

$$\begin{aligned}
I_5[u_A u_B u_C u_D] &= \int_{\tau_o}^{\tau_i} L_1 u_A u_B h_{CD}^{(R)} d\tau = \int_{\zeta_o}^{\zeta_i} \frac{1}{\zeta} L_1 u_A u_B h_{CD}^{(R)} d\zeta \\
&= -\frac{1}{8\Phi_C} \int_{\zeta_o}^{\zeta_i} N' u_A u_B \left(\int_{\zeta_o}^{\zeta} \frac{1}{\zeta^3} (N u_C u_D + 4\Phi_C \zeta^2 u'_C u'_D) d\zeta \right) d\zeta \\
&= -\frac{1}{8\Phi_C} N_i u_{Ai} u_{Bi} \int_{\zeta_o}^{\zeta_i} \frac{1}{\zeta^3} (N u_C u_D + 4\Phi_C \zeta^2 u'_C u'_D) d\zeta \\
&\quad + \frac{1}{8\Phi_C} \int_{\zeta_o}^{\zeta_i} N (u_A u_B)' \left(\int_{\zeta_o}^{\zeta} \frac{1}{\zeta^3} (N u_C u_D + 4\Phi_C \zeta^2 u'_C u'_D) d\zeta \right) d\zeta \\
&\quad + \frac{1}{8\Phi_C} \int_{\zeta_o}^{\zeta_i} \frac{1}{\zeta^3} N u_A u_B (N u_C u_D + 4\Phi_C \zeta^2 u'_C u'_D) d\zeta,
\end{aligned} \tag{2.289}$$

Where the subscripts A, B, C , and D take either α or γ .

By Eq. (2.243), we get

$$N(u_A u_B)' = \frac{N}{\zeta} \frac{d}{d\tau} (u_A u_B) = -4\Phi_C (\zeta^2 u'_A u'_B)'. \tag{2.290}$$

Using Eq. (2.290), Eq. (2.289) is transformed as follows:

$$\begin{aligned}
I_5[u_A u_B u_C u_D] &= \int_{\tau_o}^{\tau_i} L_1 u_A u_B h_{CD}^{(R)} d\tau \\
&= \frac{1}{2} \int_{\zeta_o}^{\zeta_i} \frac{1}{\zeta} N (u'_A u'_B u_C u_D + u_A u_B u'_C u'_D) d\zeta \\
&\quad + \frac{1}{8\Phi_C} \int_{\zeta_o}^{\zeta_i} \frac{1}{\zeta^3} N^2 u_A u_B u_C u_D d\zeta + 2\Phi_C \int_{\zeta_o}^{\zeta_i} \zeta u'_A u'_B u'_C u'_D d\zeta \\
&\quad + \frac{1}{\zeta_i} (N_i u_{Ai} u_{Bi} + 4\Phi_C \zeta_i^2 u'_{Ai} u'_{Bi}) h_{CDi}^{(R)}.
\end{aligned} \tag{2.291}$$

In addition, we consider three finite integrations as follows:

$$\begin{aligned}
I_6[u_A u_B] &= \int_{\tau_o}^{\tau_i} L_1 u_A u_B h_{\alpha\gamma}^{(I)} d\tau \\
&= \frac{1}{4\sqrt{\Phi_C}} \int_{\zeta_o}^{\zeta_i} \left(\frac{N\eta B}{\zeta^3} u_A u_B + 4\Phi_C \frac{\eta B}{\zeta} u'_A u'_B \right) d\zeta + \frac{1}{\zeta_i} (N_i u_{Ai} u_{Bi} + 4\Phi_C \zeta_i^2 u'_{Ai} u'_{Bi}) h_{\alpha\gamma i}^{(I)},
\end{aligned} \tag{2.292}$$

$$I_{7AB} = \int_{\tau_o}^{\tau_i} \eta B' h_{AB}^{(R)} d\tau = \frac{\eta B_i}{\zeta_i} h_{ABi}^{(R)} + \frac{1}{8\Phi_C} \int_{\zeta_o}^{\zeta_i} \frac{\eta B}{\zeta^3} (N u_A u_B + 4\Phi_C \zeta^2 u'_A u'_B) d\zeta, \tag{2.293}$$

$$I_8 = \int_{\tau_o}^{\tau_i} \eta B' h_{\alpha\gamma}^{(I)} d\tau = \frac{\eta B_i}{\zeta_i} h_{\alpha\gamma i}^{(I)} + \frac{1}{4\sqrt{\Phi_C}} \int_{\zeta_o}^{\zeta_i} \frac{\eta^2 B^2}{\zeta^3} d\zeta, \tag{2.294}$$

where the subscripts A and B take either α or γ . We have finally finished the preparation for obtaining the transformation of the third-order geometrical aberration coefficients in the time-dependent theory to those in the standard electron optics.

The third-order geometrical aberration coefficient formulae in the time-dependent theory are given as follows: the spherical aberration is Eq. (2.183). The isotropic and anisotropic parts of the coma coefficient are Eqs. (2.272) and (2.273), respectively. The field curvature is Eq. (2.188). The isotropic and the anisotropic parts of the astigmatism are Eqs. (2.190) and (2.191), respectively. The isotropic and the anisotropic parts of the distortion are Eqs. (2.192) and (2.193), respectively. For the spherical aberration, using Eq. (2.291), and performing the partial integration, the spherical aberration coefficient is transformed as follows:

$$\begin{aligned}
C_{So} &= \int_{\tau_o}^{\tau_i} \frac{\xi_o^3}{32\Phi_C} (8L_1 u_\alpha^2 h_{\alpha\alpha} - L_2 u_\alpha^4) d\tau - \frac{\xi_o^3}{\xi_i} \dot{u}_{\alpha i}^2 h_{\alpha\alpha i} \\
&= \frac{\xi_o^3}{4\Phi_C} I_5 [u_\alpha u_\alpha u_\alpha] - \int_{\xi_o}^{\xi_i} \frac{\xi_o^3}{32\Phi_C} \frac{1}{\xi} L_2 u_\alpha^4 d\xi - \xi_o^3 \xi_i u_{\alpha i}'^2 h_{\alpha\alpha i} \\
&= \frac{\xi_o^3}{32\Phi_C} \int_{\xi_o}^{\xi_i} \left[\left(\frac{1}{\xi^3 \Phi_C} N^2 + \frac{1}{\xi} L_2 \right) u_\alpha^4 + \frac{4}{\xi} N u_\alpha^2 u_\alpha'^2 + 16\Phi_C \xi u_\alpha'^4 \right] d\xi \\
&= \frac{1}{32\sqrt{\Phi_o}} \int_{\xi_o}^{\xi_i} \sqrt{\Phi} \left[\left(\frac{N^2}{\Phi^2} - \frac{L_2}{\Phi} \right) \tilde{u}_\alpha^4 + 4 \frac{N}{\Phi} \tilde{u}_\alpha^2 \tilde{u}_\alpha'^2 + 16\tilde{u}_\alpha'^4 \right] d\xi \\
&= \frac{1}{32\sqrt{\Phi_o}} \int_{\xi_o}^{\xi_i} \sqrt{\Phi} \left[\left(\frac{\Phi''^2 + \eta^4 B^4 + 2\Phi''\eta^2 B^2}{\Phi^2} - \frac{\Phi^{[4]} + 4\eta^2 B B''}{\Phi} \right) \tilde{u}_\alpha^4 + 4 \frac{\Phi'' + \eta^2 B^2}{\Phi} \tilde{u}_\alpha^2 \tilde{u}_\alpha'^2 \right. \\
&\quad \left. + 16\tilde{u}_\alpha'^4 \right] d\xi.
\end{aligned} \tag{2.295}$$

This form agrees with the formula of the non-relativistic spherical aberration coefficient in the standard theory.

Similarly, the other coefficients are transformed as follows.

The isotropic part of the coma coefficient:

$$\begin{aligned}
C_{Ko} &= \frac{\xi_o^2}{4\Phi_C} I_5 [u_\alpha u_\alpha u_\gamma] - \frac{\xi_o^2}{32\Phi_C} \int_{\xi_o}^{\xi_i} \frac{1}{\xi} L_2 u_\alpha^3 u_\gamma d\xi - \xi_o^2 \xi_i u_{\alpha i}'^2 h_{\alpha\gamma i}^{(R)} \\
&= \frac{1}{32\sqrt{\Phi_o}} \int_{\xi_o}^{\xi_i} \sqrt{\Phi} \left[\left(\frac{N^2}{\Phi^2} - \frac{L_2}{\Phi} \right) \tilde{u}_\alpha^3 \tilde{u}_\gamma + 4 \frac{N}{\Phi} \tilde{u}_\alpha \tilde{u}_\alpha' (\tilde{u}_\alpha \tilde{u}_\gamma)' + 16\tilde{u}_\alpha'^3 \tilde{u}_\gamma' \right] d\xi.
\end{aligned} \tag{2.296}$$

The anisotropic part of the coma coefficient:

$$\begin{aligned}
C_{ko} &= \frac{\xi_o^2}{4\Phi_C} I_6 [u_\alpha u_\alpha] - \frac{\xi_o^2}{16\sqrt{\Phi_C}} \int_{\xi_o}^{\xi_i} \frac{\eta B''}{\xi} u_\alpha^2 d\xi - \xi_o^2 \xi_i u_{\alpha i}'^2 h_{\alpha\gamma i}^{(I)} \\
&= \frac{1}{16\sqrt{\Phi_o}} \int_{\xi_o}^{\xi_i} \left[\left(\frac{N\eta B}{\Phi^{3/2}} - \frac{\eta B''}{\sqrt{\Phi}} \right) \tilde{u}_\alpha^2 + 4 \frac{\eta B}{\sqrt{\Phi}} \tilde{u}_\alpha'^2 \right] d\xi.
\end{aligned} \tag{2.297}$$

The field-curvature coefficient:

$$\begin{aligned}
C_{Fo} &= \frac{\xi_o}{4\Phi_C} (I_5 [u_\alpha u_\alpha u_\gamma u_\gamma] + I_5 [u_\alpha u_\gamma u_\alpha u_\gamma]) - \frac{\xi_o}{16\Phi_C} \int_{\xi_o}^{\xi_i} \frac{1}{\xi} L_2 u_\alpha^2 u_\gamma'^2 d\xi + \frac{\xi_o}{2\sqrt{\Phi_C}} I_8 \\
&\quad - \xi_o^2 \xi_i (u_{\alpha i}'^2 h_{\gamma\gamma i} + u_{\alpha i}' u_{\gamma i}' h_{\alpha\gamma i}^{(R)}) - \frac{\xi_o \eta B_i}{2\xi_i \sqrt{\Phi_C}} h_{\alpha\gamma i}^{(I)} \\
&= \frac{1}{16\sqrt{\Phi_o}} \int_{\xi_o}^{\xi_i} \sqrt{\Phi} \left[\left(\frac{N^2}{\Phi^2} - \frac{L_2}{\Phi} \right) \tilde{u}_\alpha^2 \tilde{u}_\gamma'^2 + 2 \frac{N}{\Phi} (\tilde{u}_\alpha' \tilde{u}_\gamma + \tilde{u}_\alpha \tilde{u}_\gamma')^2 + 16\tilde{u}_\alpha'^2 \tilde{u}_\gamma'^2 + 2\Phi_o \frac{\eta^2 B^2}{\Phi^2} \right] d\xi.
\end{aligned} \tag{2.298}$$

The isotropic part of the astigmatism coefficient:

$$\begin{aligned}
C_{Ao} &= \frac{\dot{\zeta}_o}{4\Phi_C} I_5 [u_\alpha u_\gamma u_\alpha u_\gamma] - \frac{\dot{\zeta}_o}{32\Phi_C} \int_{\zeta_o}^{\zeta_i} \frac{1}{\zeta} L_2 u_\alpha^2 u_\gamma^2 d\zeta - \frac{\dot{\zeta}_o}{2\sqrt{\Phi_C}} I_8 \\
&\quad - \dot{\zeta}_o^2 \dot{\zeta}_i u_{\alpha i} u'_{\gamma i} h_{\alpha\gamma i}^{(R)} + \frac{\dot{\zeta}_o \eta B_i}{2\dot{\zeta}_i \sqrt{\Phi_C}} h_{\alpha\gamma i}^{(I)} \\
&= \frac{1}{32\sqrt{\Phi_o}} \int_{\zeta_o}^{\zeta_i} \sqrt{\Phi} \left[\left(\frac{N^2}{\Phi^2} - \frac{L_2}{\Phi} \right) \tilde{u}_\alpha^2 \tilde{u}_\gamma^2 + 8 \frac{N}{\Phi} \tilde{u}_\alpha \tilde{u}_\gamma \tilde{u}'_\alpha \tilde{u}'_\gamma + 16 \tilde{u}'_\alpha \tilde{u}'_\gamma - 4\Phi_o \frac{\eta^2 B^2}{\Phi^2} \right] d\zeta.
\end{aligned} \tag{2.299}$$

The anisotropic part of the astigmatism coefficient:

$$\begin{aligned}
C_{ao} &= \frac{\dot{\zeta}_o}{4\Phi_C} I_6 [u_\alpha u_\gamma] + \frac{\dot{\zeta}_o}{2\sqrt{\Phi_C}} I_{7\alpha\gamma} - \frac{\dot{\zeta}_o}{8\sqrt{\Phi_C}} \int_{\zeta_o}^{\zeta_i} \frac{\eta B''}{\zeta} u_\alpha u_\gamma d\zeta - \dot{\zeta}_o^2 \dot{\zeta}_i u'_{\alpha i} u'_{\gamma i} h_{\alpha\gamma i}^{(I)} - \frac{\dot{\zeta}_o \eta B_i}{2\dot{\zeta}_i \sqrt{\Phi_C}} h_{\alpha\gamma i}^{(R)} \\
&= \frac{1}{8} \int_{\zeta_o}^{\zeta_i} \left[\left(\frac{N\eta B}{\Phi^{3/2}} - \frac{\eta B''}{\sqrt{\Phi}} \right) \tilde{u}_\alpha \tilde{u}_\gamma + 4 \frac{\eta B}{\sqrt{\Phi}} \tilde{u}'_\alpha \tilde{u}'_\gamma \right] d\zeta.
\end{aligned} \tag{2.300}$$

The isotropic part of the distortion coefficient:

$$\begin{aligned}
C_{Do} &= \frac{1}{4\Phi_C} I_5 [u_\alpha u_\gamma u_\alpha u_\gamma] - \frac{1}{32\Phi_C} \int_{\zeta_o}^{\zeta_i} \frac{1}{\zeta} L_2 u_\alpha u_\gamma^3 d\zeta - \dot{\zeta}_o^2 \dot{\zeta}_i u'_{\alpha i} u'_{\gamma i} h_{\gamma\gamma i} \\
&= \frac{1}{32\sqrt{\Phi_o}} \int_{\zeta_o}^{\zeta_i} \sqrt{\Phi} \left[\left(\frac{N^2}{\Phi^2} - \frac{L_2}{\Phi} \right) \tilde{u}_\alpha \tilde{u}_\gamma^3 + 4 \frac{N}{\Phi} \tilde{u}_\gamma \tilde{u}'_\gamma (\tilde{u}_\alpha \tilde{u}_\gamma)' + 16 \tilde{u}'_\alpha \tilde{u}_\gamma^3 \right] d\zeta.
\end{aligned} \tag{2.301}$$

The anisotropic part of the distortion coefficient:

$$\begin{aligned}
C_{do} &= \frac{1}{2\sqrt{\Phi_C}} I_{7\gamma\gamma} - \frac{1}{16\sqrt{\Phi_C}} \int_{\zeta_o}^{\zeta_i} \frac{\eta B''}{\zeta} u_\gamma^2 d\zeta - \frac{\eta B_i}{2\dot{\zeta}_i \sqrt{\Phi_C}} h_{\gamma\gamma i} \\
&= \frac{1}{16} \int_{\zeta_o}^{\zeta_i} \left[\left(\frac{N\eta B}{\Phi^{3/2}} - \frac{\eta B''}{\sqrt{\Phi}} \right) \tilde{u}_\gamma^2 + 4 \frac{\eta B}{\sqrt{\Phi}} \tilde{u}'_\gamma^2 \right] d\zeta.
\end{aligned} \tag{2.302}$$

In addition, the Petzval coefficient, Eq. (2.281), is transformed into

$$\begin{aligned}
C_p &= -\frac{\dot{\zeta}_o}{8\Phi_C} \int_{\tau_o}^{\tau_i} \left[\left\{ \frac{d}{d\tau} (N + 3\eta^2 B^2) \right\} \int_{\tau_o}^{\tau} \frac{d\xi}{\xi^2} d\tau + \frac{\dot{\zeta}_o}{8\Phi_C} (N_i + 3\eta^2 B_i^2) \int_{\tau_o}^{\tau_i} \frac{d\tau}{\xi^2} \right. \\
&= \frac{\dot{\zeta}_o}{8\Phi_C} \int_{\tau_o}^{\tau_i} \frac{N + 3\eta^2 B^2}{\xi^2} d\tau = \frac{\dot{\zeta}_o}{8\Phi_C} \int_{\zeta_o}^{\zeta_i} \frac{N + 3\eta^2 B^2}{\xi^3} d\zeta = \sqrt{\Phi_o} \int_{\zeta_o}^{\zeta_i} \frac{\Phi'' + 4\eta^2 B^2}{8\Phi^{3/2}} d\zeta.
\end{aligned} \tag{2.303}$$

For Eqs. (2.295) to (2.303), these forms of coefficients match those in the standard electron optics completely. It is concluded that the derived aberration coefficients in the time-dependent theory agree with those in the standard electron optics theory for a normal lens system, which is in the case of a magnetic field overlapping with the electrostatic field and even in the case where both the object and the image planes are located inside both magnetic and electrostatic fields. The consideration, given in this section, supports the validity of the aberration coefficients formulae in the time-dependent theory for a mirror system.

2.9 Aberration coefficients for variation of the voltages and the currents

In general, the system of electromagnetic mirrors has several voltage sources and current sources. When we consider tiny variations of the voltages and currents and treat these as perturbations, tiny changes in the electron trajectory must arise and those changes at the image plane are expected to have similar formulae to the on- and off-axis chromatic aberrations. We call them aberrations for variation of the voltages and the currents of electrodes and coils. These aberration coefficients are useful, when we consider the specific design of the electron optical system, since the on-

axis type aberration indicates the defocus, and the off-axis type aberration indicates a beam shift due to changes of voltages and currents. For example, these aberrations tell us the magnitude of a beam blur and that of image vibration due to instability of power supplies. These coefficients are also used to calculate focus sensitivity and the beam axis condition, under which image shift does not happen when voltages or currents are changed intentionally. In this section, we derive these coefficients.

First, let us imagine N round symmetric electrodes. They are connected to voltage sources, which supply different voltages to each electrode. An electron optics column is composed of metal vacuum chambers, and it is connected to ground, usually. The voltage of the j -th electrode is expressed by V_j , where $j = 1, \dots, N$. Since an electron column is also regarded as an electrode, whose voltage is grounded, we consider this as the 0-th electrode of zero voltage. Note that if the k -th electrode is grounded, we also have $V_k = 0$. However, since the zero of the electron potential is the electron source and the column potential is Φ_c , the potential of the j -th electrode is $V_j + \Phi_c$. When only the j -th electrode has unit voltage and all the other electrodes have zero voltages, the axial potential distribution is given by $f_j(z)$. For example, Fig. 2.3 (a) shows a schematic of electrodes for $N = 4$, where Electrode 0, which corresponds to an electron optical column, is connected to ground. Fig. 2.3 (b) shows the normalized axial potential distributions f_j of the j -th electrode. In this figure, we also consider the axial distribution of f_0 , which is given when 0-th electrode is connected to unit voltage and all the other electrodes are set to be zero voltage.

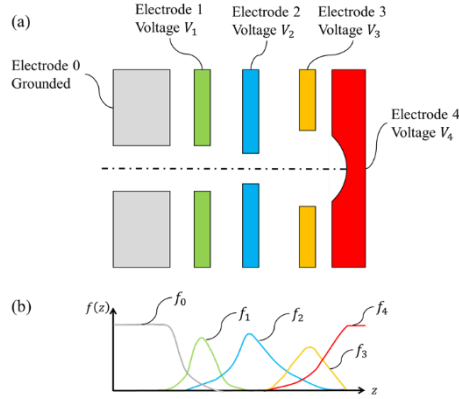


Fig. 2.3 (a) A schematic of the cross-section of the electrodes for an electron mirror for $N = 4$. Electrode 0 is connected to ground. The voltage V_j is imposed on the j -th electrode, for $j = 1, 2, 3, 4$, respectively. (b) Normalized axial potential distributions f_j of the j -th electrode. In this figure, we also consider the axial distribution of f_0 , which is given when the 0-th electrode is connected to unit voltage and all the other electrodes are set to be zero voltage.

Then, the axial potential distribution of electrons of the system is expressed as follows:

$$\Phi(z) = \Phi_c f_0(z) + \sum_{j=1}^N (V_j + \Phi_c) f_j(z). \quad (2.304)$$

If all electrodes have unit voltage, the axial potential distribution must be a constant distribution of unit voltage, that is,

$$f_0(z) + \sum_{j=1}^N f_j(z) = 1. \quad (2.305)$$

The axial potential distribution is transformed into

$$\Phi(z) = \Phi_c + \sum_{j=1}^N \Phi_j(z), \quad (2.306)$$

where Φ_j is contribution of the j -th electrode to the axial potential:

$$\Phi_j(z) = V_j f_j(z). \quad (2.307)$$

Second, the axial magnetic field distribution of the system is considered. The system has L round coils connected to different current sources and a round symmetric yoke for magnetic lenses, where the current of the ℓ -th coil is I_ℓ . For example, Fig. 2.4 shows a schematic of magnetic lenses and coils for $L = 3$.

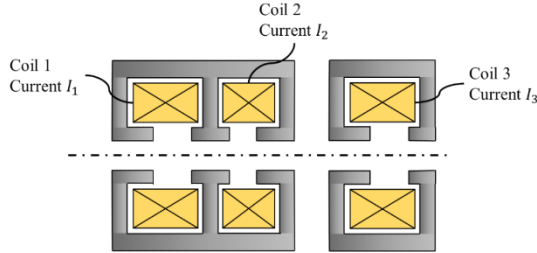


Fig. 2.4 A schematic of cross-section of magnetic round lenses and coils for $L = 3$. Current of the ℓ -th coil is I_ℓ , for $\ell = 1, 2, 3$, respectively.

If the ℓ -th coil has unit current and all the other currents are zero, the normalized axial magnetic field distribution of the ℓ -th coil $d_\ell(z)$ is obtained. Then, the axial magnetic field distribution of the system is given by

$$B(z) = \sum_{\ell=1}^L B_\ell(z), \quad (2.308)$$

where B_ℓ is the magnetic field generated by the ℓ -th coil:

$$B_\ell(z) = I_\ell d_\ell(z). \quad (2.309)$$

It is considered that the variation of the voltage of the j -th electrode and the current of the ℓ -th coil by ΔV_j and ΔI_ℓ , respectively. The variation of the potential and the magnetic field is given by

$$\Delta \Phi_j(z) = \frac{\Delta V_j}{V_j} \Phi_j(z) = \kappa_{V_j} \Phi_j(z), \quad (2.310)$$

$$\Delta B_\ell(z) = \frac{\Delta I_\ell}{I_\ell} B_\ell(z) = \kappa_{I_\ell} B_\ell(z), \quad (2.311)$$

where κ_{V_j} , κ_{I_ℓ} are parameters of the variation of the voltage and the current, respectively.

The variation of the voltage ΔV_j and the current ΔI_ℓ give the variation of the electrostatic potential and the magnetic scalar potential as follows:

$$\Delta \varphi = \sum_{j=1}^N \kappa_{V_j} \sum_{n=0}^{\infty} \sum_{m=0}^{\infty} \frac{(-1)^n}{m! (n!)^2} \left(\frac{w\bar{w}}{4} \right)^n h^m \Phi_j^{[2n+m]}(\zeta), \quad (2.312)$$

$$\Delta \psi = \sum_{\ell=1}^L \kappa_{I_\ell} \sum_{n=0}^{\infty} \sum_{m=0}^{\infty} \frac{(-1)^n}{m! (n!)^2} \left(\frac{w\bar{w}}{4} \right)^n h^m \Psi_\ell^{[2n+m]}(\zeta), \quad (2.313)$$

where

$$\Psi_\ell(z) = - \int^z B_\ell(\zeta) d\zeta. \quad (2.314)$$

The variation of the field strengths is given as follows:

$$\begin{aligned} \Delta E_w &= -2 \frac{\partial \Delta \varphi}{\partial \bar{w}}, & \Delta E_z &= -\frac{\partial \Delta \varphi}{\partial h}, \\ \Delta B_w &= -2 \frac{\partial \Delta \psi}{\partial \bar{w}}, & \Delta B_z &= -\frac{\partial \Delta \psi}{\partial h}. \end{aligned} \quad (2.315)$$

Considering the variation of fields, the complex equations of trajectory, Eqs. (2.11) and (2.12) are modified as follows:

$$\ddot{w} = -\frac{E_w}{2\Phi_c} - \frac{i\eta}{\sqrt{\Phi_c}} (B_w \dot{z} - B_z \dot{w}) - \frac{\Delta E_w}{2\Phi_c} - \frac{i\eta}{\sqrt{\Phi_c}} (\Delta B_w \dot{z} - \Delta B_z \dot{w}), \quad (2.316)$$

$$\ddot{z} = \ddot{\zeta} + \ddot{h} = -\frac{E_z}{2\Phi_c} - \frac{\eta}{\sqrt{\Phi_c}} \text{Im}(B_w \dot{w}) - \frac{\Delta E_z}{2\Phi_c} - \frac{\eta}{\sqrt{\Phi_c}} \text{Im}(\Delta B_w \dot{w}). \quad (2.317)$$

When the ratio κ_{V_j} and κ_{I_ℓ} are regarded as the parameters that represent the rank of the trajectory, since the trajectory of the reference electron does not depend on the variation of fields, Eq. (2.13) does not change and the linear equation of longitudinal path deviation, Eq. (2.39), changes into

$$\ddot{h} - \frac{\Phi''}{2\Phi_c} h = \sum_{j=1}^N \kappa_{V_j} \frac{\Phi'_j}{2\Phi_c}. \quad (2.318)$$

Since the right-hand-side of Eq. (2.318) does not depend on the longitudinal path deviation, h , the particular solution h_{V_j} is given by the variation of the parameter using the linear solutions h_α and h_γ , strictly:

$$h^{(1)}(\tau) = \frac{1}{2} \dot{\zeta}_o \kappa_o h_\alpha(\tau) + \sum_{j=1}^N \kappa_{V_j} h_{V_j}(\tau), \quad (2.319)$$

where

$$h_{V_j} = h_\alpha \int_{\tau_o}^{\tau} \frac{\Phi_j'}{2\Phi_C} h_\gamma d\tau - h_\gamma \int_{\tau_o}^{\tau} \frac{\Phi_j'}{2\Phi_C} h_\alpha d\tau. \quad (2.320)$$

Since we only consider the aberration caused by the variation of fields, the energy deviation of primary electrons is ignored: $\kappa_o = 0$.

Using the analytic forms of h_α and h_γ , that is Eqs. (2.229) and (2.230), h_{V_j} is transformed into

$$h_{V_j} = \frac{\Phi_j - \Phi_{j0}}{2\zeta_o \Phi_C} h_\alpha - \zeta \int_{\tau_o}^{\tau} \frac{\Phi_j'}{2\zeta_o \Phi_C} h_\alpha d\tau. \quad (2.321)$$

At the initial reduced time, h_{V_j} and its reduced time derivative satisfy that

$$h_{V_j}(\tau_o) = 0, \quad \dot{h}_{V_j}(\tau_o) = 0. \quad (2.322)$$

We regard the ratio of the variation of the voltage of the j -th electrode and the current of the ℓ -th coil κ_{V_j} and κ_{I_ℓ} as chromatic parameters. The primary perturbation function of the lateral trajectory equation Eq. (2.316) is the second-rank and the lateral trajectory equation becomes

$$\ddot{u} + \frac{N}{4\Phi_C} u = P_{u,\text{var}}^{(2)}. \quad (2.323)$$

where

$$P_{u,\text{var}}^{(2)} = \sum_{j=1}^N \kappa_{V_j} \left[-\frac{L_1}{4\Phi_C} u^{(1)} h_{V_j} - \frac{\Phi_j''}{4\Phi_C} u^{(1)} + \frac{i\eta}{2\sqrt{\Phi_C}} \left\{ \frac{d}{d\tau} (B' u^{(1)} h_{V_j}) + B' \dot{u}^{(1)} h_{V_j} \right\} \right] \\ + \sum_{\ell=1}^L \kappa_{I_\ell} \left[\frac{\eta^2 B B_\ell}{2\Phi_C} + \frac{i\eta}{2\sqrt{\Phi_C}} \left\{ B_\ell \dot{u}^{(1)} + \frac{d}{d\tau} (B_\ell u^{(1)}) \right\} \right]. \quad (2.324)$$

Using Eqs. (2.83), (2.110), and (2.319), the lateral path deviation of the second-rank caused by the variation of fields is given by

$$\hat{u}^{(2)}(z) = \sum_{j=1}^N \left[\left(\hat{u}_{\alpha E_j}^{(R)} + i \hat{u}_{\alpha E_j}^{(I)} \right) u'_o + \left(\hat{u}_{\gamma E_j}^{(R)} + i \hat{u}_{\gamma E_j}^{(I)} \right) u_o \right] \kappa_{V_j} \\ + \sum_{\ell=1}^L \left[\left(\hat{u}_{\alpha B_\ell}^{(R)} + i \hat{u}_{\alpha B_\ell}^{(I)} \right) u'_o + \left(\hat{u}_{\gamma B_\ell}^{(R)} + i \hat{u}_{\gamma B_\ell}^{(I)} \right) u_o \right] \kappa_{I_\ell}, \quad (2.325)$$

where, the isotropic part of the on-axis type path deviation for the j -th electrode voltage vibration:

$$\hat{u}_{\alpha E_j}^{(R)} = u_\gamma \int_{\tau_o}^{\tau} \frac{\dot{\zeta}_o}{4\Phi_C} (L_1 h_{V_j} + \Phi_j'') u_\alpha^2 d\tau - u_\alpha \int_{\tau_o}^{\tau} \frac{\dot{\zeta}_o}{4\Phi_C} (L_1 h_{V_j} + \Phi_j'') u_\alpha u_\gamma d\tau - \frac{\dot{\zeta}_o}{\zeta} \dot{u}_\alpha h_{V_j}, \quad (2.326)$$

the isotropic part of the off-axis type path deviation for the j -th electrode voltage vibration:

$$\hat{u}_{\gamma E_j}^{(R)} = u_\gamma \int_{\tau_o}^{\tau} \frac{1}{4\Phi_C} (L_1 h_{V_j} + \Phi_j'') u_\alpha u_\gamma d\tau - u_\alpha \int_{\tau_o}^{\tau} \frac{1}{4\Phi_C} (L_1 h_{V_j} + \Phi_j'') u_\gamma^2 d\tau - \frac{1}{\zeta} \dot{u}_\gamma h_{V_j}, \quad (2.327)$$

the anisotropic part of the on-axis type path deviation for the j -th electrode voltage vibration:

$$\hat{u}_{\alpha E_j}^{(I)} = u_\alpha \int_{\tau_o}^{\tau} \frac{\dot{\zeta}_o \eta B'}{2\sqrt{\Phi_C}} h_{V_j} d\tau + \frac{\dot{\zeta}_o \eta B'}{2\sqrt{\Phi_C}} u_\alpha^2 h_{V_j} - \frac{\dot{\zeta}_o \eta B}{2\zeta \sqrt{\Phi_C}} u_\alpha h_{V_j}, \quad (2.328)$$

the anisotropic part of the off-axis type path deviation for the j -th electrode voltage vibration:

$$\hat{u}_{\gamma E_j}^{(I)} = u_\gamma \int_{\tau_o}^{\tau} \frac{\eta B'}{2\sqrt{\Phi_C}} h_{V_j} d\tau + \frac{\eta B'}{2\sqrt{\Phi_C}} u_\alpha u_\gamma h_{V_j} - \frac{\eta B}{2\zeta \sqrt{\Phi_C}} u_\gamma h_{V_j}, \quad (2.329)$$

the isotropic part of the on-axis type path deviation for the ℓ -th coil current vibration:

$$\hat{u}_{\alpha B_\ell}^{(R)} = u_\gamma \int_{\tau_o}^{\tau} \frac{\dot{\zeta}_o \eta^2 B B_\ell}{2\Phi_C} u_\alpha^2 d\tau - u_\alpha \int_{\tau_o}^{\tau} \frac{\dot{\zeta}_o \eta^2 B B_\ell}{2\Phi_C} u_\alpha u_\gamma d\tau, \quad (2.330)$$

the isotropic part of the off-axis type path deviation for the ℓ -th coil current vibration:

$$\hat{u}_{\gamma B_\ell}^{(R)} = u_\gamma \int_{\tau_o}^{\tau} \frac{\eta^2 B B_\ell}{2\Phi_C} u_\alpha u_\gamma d\tau - u_\alpha \int_{\tau_o}^{\tau} \frac{\eta^2 B B_\ell}{2\Phi_C} u_\gamma^2 d\tau, \quad (2.331)$$

the anisotropic part of the on-axis type path deviation for the ℓ -th coil current vibration:

$$\hat{u}_{\alpha B_\ell}^{(I)} = u_\alpha \int_{\tau_o}^{\tau} \frac{\dot{\zeta}_o \eta B_\ell}{2\sqrt{\Phi_C}} d\tau + \frac{\dot{\zeta}_o \eta B_\ell}{2\sqrt{\Phi_C}} u_\alpha^2, \quad (2.332)$$

the anisotropic part of the off-axis type path deviation for the ℓ -th coil current vibration:

$$\hat{u}_{\gamma B_\ell}^{(I)} = u_\gamma \int_{\tau_o}^{\tau} \frac{\eta B_\ell}{2\sqrt{\Phi_C}} d\tau + \frac{\eta B_\ell}{2\sqrt{\Phi_C}} u_\alpha u_\gamma. \quad (2.333)$$

The second-rank aberration caused by the variation of the voltages and the currents, which is defined in the object plane, is given by

$$\Delta u_o^{(2)} = \sum_{j=1}^N [C_{E10}^j u_o' + (C_{E20}^j + iC_{E30}^j) u_o] \kappa_{V_j} + \sum_{\ell=1}^L [C_{B10}^\ell u_o' + (C_{B20}^\ell + iC_{B30}^\ell) u_o] \kappa_{I_\ell}, \quad (2.334)$$

where, the on-axis type aberration coefficient of the vibration of the j -th electrode voltage:

$$C_{E10}^j = \dot{\zeta}_o \int_{\tau_o}^{\tau_i} \frac{1}{4\Phi_C} (L_1 h_{V_j} + \Phi_j'') u_\alpha^2 d\tau - \frac{\dot{\zeta}_o}{\xi} \dot{u}_{\alpha i}^2 h_{V_j i}, \quad (2.335)$$

the isotropic part of the off-axis type aberration coefficient of the vibration of the j -th electrode voltage:

$$C_{E20}^j = \int_{\tau_o}^{\tau_i} \frac{1}{4\Phi_C} (L_1 h_{V_j} + \Phi_j'') u_\alpha u_\gamma d\tau - \frac{\dot{\zeta}_o}{\xi} \dot{u}_{\alpha i} \dot{u}_{\gamma i} h_{V_j i}, \quad (2.336)$$

the anisotropic part of the off-axis type aberration coefficient of the vibration of the j -th electrode voltage:

$$C_{E30}^j = \int_{\tau_o}^{\tau_i} \frac{\eta B'}{2\sqrt{\Phi_C}} h_{V_j} d\tau - \frac{\eta B_i}{2\dot{\zeta}_i \sqrt{\Phi_C}} h_{V_j i}, \quad (2.337)$$

the on-axis type aberration coefficient of the vibration of the ℓ -th coil current:

$$C_{B10}^\ell = \dot{\zeta}_o \int_{\tau_o}^{\tau_i} \frac{\eta^2 B B_\ell}{2\Phi_C} u_\alpha^2 d\tau, \quad (2.338)$$

the isotropic part of the off-axis type aberration coefficient of the vibration of the ℓ -th coil current:

$$C_{B20}^\ell = \int_{\tau_o}^{\tau_i} \frac{\eta^2 B B_\ell}{2\Phi_C} u_\alpha u_\gamma d\tau, \quad (2.339)$$

the anisotropic part of the off-axis type aberration coefficient of the vibration of the ℓ -th coil current:

$$C_{B30}^\ell = \int_{\tau_o}^{\tau_i} \frac{\eta B_\ell}{2\sqrt{\Phi_C}} d\tau. \quad (2.340)$$

We are at the point, where we now have formulae for aberration coefficients due to variation of electrode voltages and coil currents of round symmetric electrostatic and magnetic fields. We discuss one application of the on-axis type coefficient here. To consider a simple situation, we assume that a central electron of an incident beam passes through along the optic axis. The incident beam is composed of a lot of electrons, whose initial lateral position is zero, but

whose initial complex angle ω_o , at the object plane is arbitrary within the limitation, which is called an aperture half-angle α_o . That is

$$\omega_o = x'_o + iy'_o, \quad (2.341)$$

where ω_o is an incident angle measured in the rotation coordinate, and it must satisfy that

$$0 \leq |\omega_o| \leq \alpha_o. \quad (2.342)$$

The defocus Δz is defined as the distance along the optic axis between the designated image plane and the actual crossover position of the lateral axial ray. If Δz is positive, it means the actual crossover position shifts to the positive direction of the optic axis from the designated image plane. In the rotation coordinate system, the lateral landing position of an electron with the defocus is given by

$$\Delta u_i = -\Delta z_{DF} \omega_i, \quad (2.343)$$

where the “paraxial” landing angle of an electron is given by

$$\omega_i = M_\alpha \omega_o. \quad (2.344)$$

In this case, we can regard the initial slope of the electron u'_o as ω_o and the initial lateral position is zero, that is $u_o = 0$. Taking into account Eqs. (2.334) and (2.344), the second-rank aberration due to variation of electrode voltages and coil currents is given by

$$\Delta u_i = M \Delta u_o^{(2)} = \left[\sum_{j=1}^N \frac{M}{M_\alpha} C_{E1o}^j \kappa_{V_j} + \sum_{\ell=1}^L \frac{M}{M_\alpha} C_{B1o}^\ell \kappa_{I_\ell} \right] \omega_i. \quad (2.345)$$

Comparing Eq. (2.345) with Eq. (2.343), the linearly dependent component of the defocus on the variation of the voltages and the currents is given by

$$\Delta z_{DF} = \sum_{j=1}^N \Delta z_{DF}^{V_j} + \sum_{\ell=1}^L \Delta z_{DF}^{I_\ell}, \quad (2.346)$$

where the linear defocus component of the j -th electrode voltage variation and that of the ℓ -th coil current variation are

$$\begin{aligned} \Delta z_{DF}^{V_j} &= -\frac{M}{M_\alpha} \frac{C_{E1o}^j}{V_j} \Delta V_j = S_{DF}^{V_j} \Delta V_j, \\ \Delta z_{DF}^{I_\ell} &= -\frac{M}{M_\alpha} \frac{C_{B1o}^\ell}{I_\ell} \Delta I_\ell = S_{DF}^{I_\ell} \Delta I_\ell, \end{aligned} \quad (2.347)$$

respectively. $S_{DF}^{V_j}$ is the linear focus sensitivity of the j -th electrode voltage. $S_{DF}^{I_\ell}$ is the linear focus sensitivity of the ℓ -th coil current.

We are at the point, where the formulae of the second-rank lateral path deviation and the aberration coefficients caused by the variation of the electrode voltages and the coil currents are derived in the time-dependent theory. Using the on-axis type aberration coefficients, the formulae of the focus sensitivities, which are linearly dependent on the variation of an electrode voltage or a coil current, are derived.

2.10 Relations between the aberration coefficients for variation of the voltages and the currents and that of chromatic aberration

In the previous section, we have derived the aberration coefficients for the variation of electrode voltages and coil currents. When the voltages and the currents are slightly and intentionally changed, the electron optical focal length of an electron mirror changes slightly and causes path deviations. When we consider incident electrons, which have non-zero energy deviation from nominal energy, the focal length of mirror fields for these electrons is different according to their energy. Due to these two considerations about the focal length of the mirror, we can expect that there is a relation between chromatic aberration coefficients and aberration coefficients for the variation of the electrode voltages and the coil currents. In this section, we derive this relation. We assume that the ratio of the variation of the voltages is the same value κ_V , that is:

$$\kappa_{V_1} = \kappa_{V_2} = \dots = \kappa_{V_l} = \dots = \kappa_{V_N} = \kappa_V. \quad (2.348)$$

And the ratio of the variation of the currents are assumed to be the same value κ_I :

$$\kappa_{I_1} = \kappa_{I_2} = \dots = \kappa_{I_\ell} = \dots = \kappa_{I_L} = \kappa_I. \quad (2.349)$$

Then, if all voltages and currents change according to Eqs. (2.348) and (2.349), simultaneously, the variation of the axial potential and the axial magnetic field is given as follows:

$$\Delta\Phi(z) = \sum_{j=1}^N \kappa_{V_j} \Phi_j = \kappa_V (\Phi(z) - \Phi_C), \quad (2.350)$$

$$\Delta B(z) = \sum_{\ell=1}^L \kappa_{I_\ell} B_\ell = \kappa_I B(z). \quad (2.351)$$

Considering Eqs. (2.229) and (2.321), and performing partial integration, the longitudinal path deviation of the first-rank due to variation of the electrode voltage is transformed to

$$h_V = \sum_{j=1}^N h_{V_j} = \frac{\Phi - \Phi_o}{2\dot{\zeta}_o \Phi_C} h_\alpha - \frac{\dot{\zeta}}{\dot{\zeta}_o} \int_{\tau_o}^{\tau} \dot{\zeta} h_\alpha d\tau = \frac{1}{2} \dot{\zeta} (\tau - \tau_o) - \frac{\dot{\zeta}_o}{2} h_\alpha. \quad (2.352)$$

In this case, the aberration coefficients for the variation of the voltages and the currents are obtained by replacing h_{V_j} , Φ_j'' , and B_ℓ of Eqs. (2.335) to (2.340) with h_V , Φ'' , and B , respectively:

$$C_{E1o} = \sum_{j=1}^N C_{E1o}^j = \dot{\zeta}_o \int_{\tau_o}^{\tau_i} \frac{1}{4\Phi_C} (L_1 h_V + \Phi'') u_\alpha^2 d\tau - \frac{\dot{\zeta}_o}{\dot{\zeta}} \dot{u}_{\alpha i}^2 h_{Vi}, \quad (2.353)$$

$$C_{E2o} = \sum_{j=1}^N C_{E2o}^j = \int_{\tau_o}^{\tau_i} \frac{1}{4\Phi_C} (L_1 h_V + \Phi'') u_\alpha u_\gamma d\tau - \frac{\dot{\zeta}_o}{\dot{\zeta}} \dot{u}_{\alpha i} \dot{u}_{\gamma i} h_{Vi}, \quad (2.354)$$

$$C_{E3o} = \sum_{j=1}^N C_{E3o}^j = \int_{\tau_o}^{\tau_i} \frac{\eta B'}{2\sqrt{\Phi_C}} h_V d\tau - \frac{\eta B_i}{2\dot{\zeta}_i \sqrt{\Phi_C}} h_{Vi}, \quad (2.355)$$

$$C_{B1o} = \sum_{\ell=1}^L C_{B1o}^{\ell} = \dot{\zeta}_o \int_{\tau_o}^{\tau_i} \frac{\eta^2 B^2}{2\Phi_C} u_{\alpha}^2 d\tau, \quad (2.356)$$

$$C_{B2o} = \sum_{\ell=1}^L C_{B2o}^{\ell} = \int_{\tau_o}^{\tau_i} \frac{\eta^2 B^2}{2\Phi_C} u_{\alpha} u_{\gamma} d\tau, \quad (2.357)$$

$$C_{B3o} = \sum_{\ell=1}^L C_{B3o}^{\ell} = \int_{\tau_o}^{\tau_i} \frac{\eta B}{2\sqrt{\Phi_C}} d\tau. \quad (2.358)$$

To compare the coefficients for the variation of the voltages and the currents in Eqs. (2.353) to (2.358) with those of the chromatic aberrations in Eqs. (2.148) to (2.150), we consider the following integral:

$$\begin{aligned} I_{VS1}[u_A, u_B] &= \int_{\tau_o}^{\tau_i} \frac{1}{4\Phi_C} (L_1 h_V + N) u_A u_B d\tau - \frac{1}{\dot{\zeta}_i} \dot{u}_{Ai} \dot{u}_{Bi} h_{Vi} \\ &= \int_{\tau_o}^{\tau_i} \frac{N}{8\Phi_C} (\tau - \tau_o) u_A u_B d\tau - \frac{\dot{\zeta}_o}{8\Phi_C} \int_{\tau_o}^{\tau_i} L_1 u_A u_B h_{\alpha} d\tau + \frac{\dot{\zeta}_o}{2\dot{\zeta}_i} \dot{u}_{Ai} \dot{u}_{Bi} h_{\alpha i} \\ &\quad + \int_{\tau_o}^{\tau_i} \frac{N}{4\Phi_C} u_A u_B d\tau - \frac{1}{2} (\tau_i - \tau_o) \dot{u}_{Ai} \dot{u}_{Bi} + \frac{\dot{\zeta}_o}{2\dot{\zeta}_i} \dot{u}_{Ai} \dot{u}_{Bi} h_{\alpha i} \\ &= \frac{N_i}{8\Phi_C} (\tau_i - \tau_o) u_{Ai} u_{Bi} - \int_{\tau_o}^{\tau_i} \frac{N}{8\Phi_C} (\tau - \tau_o) \left(\frac{d}{d\tau} (u_A u_B) \right) d\tau \\ &\quad + \int_{\tau_o}^{\tau_i} \frac{N}{8\Phi_C} u_A u_B d\tau - \frac{\dot{\zeta}_o}{8\Phi_C} \int_{\tau_o}^{\tau_i} L_1 u_A u_B h_{\alpha} d\tau - \frac{1}{2} (\tau_i - \tau_o) \dot{u}_{Ai} \dot{u}_{Bi} \\ &= \frac{N_i}{8\Phi_C} (\tau_i - \tau_o) u_{Ai} u_{Bi} + \int_{\tau_o}^{\tau_i} \frac{1}{2} (\tau - \tau_o) \left(\frac{d}{d\tau} (\dot{u}_A \dot{u}_B) \right) d\tau + \frac{\dot{\zeta}_o}{2\dot{\zeta}_i} \dot{u}_{Ai} \dot{u}_{Bi} h_{\alpha i} \\ &\quad + \int_{\tau_o}^{\tau_i} \frac{N}{8\Phi_C} u_A u_B d\tau - \frac{\dot{\zeta}_o}{8\Phi_C} \int_{\tau_o}^{\tau_i} L_1 u_A u_B h_{\alpha} d\tau - \frac{1}{2} (\tau_i - \tau_o) \dot{u}_{Ai} \dot{u}_{Bi} \\ &= \frac{N_i}{8\Phi_C} (\tau_i - \tau_o) u_{Ai} u_{Bi} - \frac{1}{4} \int_{\tau_o}^{\tau_i} \left\{ \frac{d^2}{d\tau^2} (u_A u_B) \right\} d\tau - \frac{\dot{\zeta}_o}{8\Phi_C} \int_{\tau_o}^{\tau_i} L_1 u_A u_B h_{\alpha} d\tau - \frac{\dot{\zeta}_o}{2\dot{\zeta}_i} \dot{u}_{Ai} \dot{u}_{Bi} h_{\alpha i} \\ &= \frac{N_i}{8\Phi_C} (\tau_i - \tau_o) u_{Ai} u_{Bi} - \frac{1}{4} (u_{Ai} \dot{u}_{Bi} + u_{Ai} \dot{u}_{Bi} - u_{Ao} \dot{u}_{Bo} - \dot{u}_{Ao} u_{Bo}) \\ &\quad - \frac{\dot{\zeta}_o}{8\Phi_C} \int_{\tau_o}^{\tau_i} L_1 u_A u_B h_{\alpha} d\tau + \frac{\dot{\zeta}_o}{2\dot{\zeta}_i} \dot{u}_{Ai} \dot{u}_{Bi} h_{\alpha i}, \end{aligned} \quad (2.359)$$

where the subscripts of the first-rank lateral path deviation, A and B , take either α or γ , and

$$\begin{aligned} I_{VS2} &= \int_{\tau_o}^{\tau_i} \left(\frac{\eta B'}{2\sqrt{\Phi_C}} h_V + \frac{\eta B}{4\sqrt{\Phi_C}} \right) d\tau - \frac{\eta B_i}{2\dot{\zeta}_i \sqrt{\Phi_C}} h_{Vi} \\ &= \frac{\eta}{4\sqrt{\Phi_C}} \int_{\tau_o}^{\tau_i} (\dot{B} (\tau - \tau_o) - \dot{\zeta}_o B' h_{\alpha} + B) d\tau - \frac{\eta B_i}{4\sqrt{\Phi_C}} (\tau_i - \tau_o) - \frac{\dot{\zeta}_o}{\dot{\zeta}_i} \frac{\eta B_i}{4\sqrt{\Phi_C}} h_{\alpha i} \\ &= - \left(\int_{\tau_o}^{\tau_i} \frac{\dot{\zeta}_o \eta B'}{4\sqrt{\Phi_C}} h_{\alpha} d\tau - \frac{\dot{\zeta}_o}{\dot{\zeta}_i} \frac{\eta B_i}{4\sqrt{\Phi_C}} h_{\alpha i} \right). \end{aligned} \quad (2.360)$$

Then, when we consider the following summations between the coefficients for the variation of the voltages and those of the currents, the relations are obtained as follows:

$$C_{E1o} + \frac{1}{2} C_{B1o} = \dot{\zeta}_o I_{VS1}[u_{\alpha}, u_{\alpha}] = -C_{Co}, \quad (2.361)$$

$$C_{E2o} + \frac{1}{2} C_{B2o} = I_{VS1}[u_{\alpha}, u_{\gamma}] = -C_{Mo}, \quad (2.362)$$

$$C_{E3o} + \frac{1}{2} C_{B3o} = I_{VS2} = -C_{Ro}. \quad (2.363)$$

These relations tell us that we can derive the chromatic aberration coefficients of the mirrors by measuring the coefficients for the variation of the voltages and the currents.

2.11 Aberration coefficients for an inclined incident beam

The derived formulae of the second-rank chromatic aberration, Eq. (2.147), those of the third-order geometrical aberration, Eq. (2.182), and those of the variation of voltages and currents, Eq. (2.334), express the lateral deviation of the single electron position at the image plane from the paraxial image point, but they are converted to the object plane, where the initial condition is that the incident electron starts at the off-axis lateral point u_o at the object plane with the slope u'_o with respect to the optic axis in the rotation coordinate. Since $u' = \frac{1}{\zeta} \dot{u}$, as long as $|u'_o| \ll 1$, $|\dot{u}_o| \ll 1$, $|u_i^{(1)}| \ll 1$, and $|\dot{u}_i^{(1)}| \ll 1$, that is, the axial potential does not take very small value around both the object plane and the image plane, the following discussion is valid. To analyze the aberration of the beam, we consider two characteristic paraxial trajectories in the rotation coordinate system. Fig. 2.5 shows the schematic of paraxial trajectory of a central electron of the beam and that of inclined with respect to the central trajectory at the object plane. The green dot trajectory is that of a central electron of the beam, which starts at the lateral point u_o in the complex rotation coordinate at the object plane ζ_o . The red trajectory means a general electron trajectory, which starts at the same lateral point u_o at the object plane, and whose complex slope is s_o with respect to the central trajectory of the beam at the object plane, where $|s_o| \leq \alpha_o$, and α_o corresponds to the aperture half-angle at the object plane. Fig. 2.5 (a) shows the case that the whole incident beam is parallel to the optic axis. The central electron trajectory is parallel to the optic axis at the object plane, that is, the incident angle of the central trajectory with respect to the optic axis is zero: $\gamma_o = 0$. In this case, the incident complex angle of the general trajectory s_o is not only with respect to the central trajectory at the object plane, but also with respect to the optic axis, then, $u'_o = s_o$. Fig. 2.5 (b) shows the case that the whole incident beam is inclined with respect to the optic axis. The central electron has non-zero incident angle γ_o with respect to the optic axis at the object plane. The incident angle of the general electron with respect to the optic axis at the object plane is $u'_o = \gamma_o + s_o$.

In the rotation coordinate system, the initial lateral reduced complex velocity is given by

$$\dot{u}_o = \zeta_o u'_o = \zeta_o (\gamma_o + s_o). \quad (2.364)$$

In many cases, the trajectory of the central electron, which minimizes specific off-axis aberrations, is of interest. To analyze it, it is advantageous to assume that γ_o is composed of two parts. One is the incident angle proportional to the initial lateral point, in the rotation coordinate system, and the other part is independent of the initial lateral point:

$$\gamma_o = t_o + \lambda_o u_o = t_o + (\lambda_{Ro} + i\lambda_{Io})u_o, \quad (2.365)$$

where t_o is a complex initial slope independent of u_o and λ_o is a complex normalized initial slope.

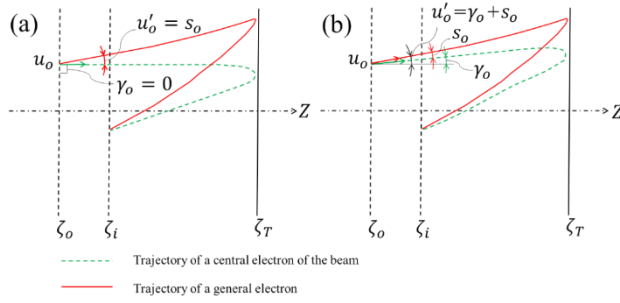


Fig. 2.5 Schematic of the paraxial trajectory of a central electron of the beam and that of an inclined electron with respect to the central trajectory at the object plane, in the rotation coordinate system. The green dot trajectory is that of a central electron of the beam. The red trajectory represents a general electron trajectory, whose initial complex slope is s_o with respect to the central trajectory of the beam at the object plane. (a) shows the case that the whole incident beam is parallel to the optic axis. (b) shows the case where the whole incident beam is inclined with respect to the optic axis.

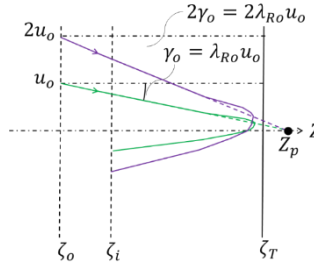


Fig. 2.6 Schematic of the central electron trajectory in the cross-section of the direction of u_o , in the rotation coordinate system, in the case where the independent initial slope vanishes, and the normalized initial slope is real. Two trajectories, where the initial lateral positions are u_o and $2u_o$, respectively, are displayed. Asymptotes of incident trajectories are shown with dashed lines. They intersect with the optic axis at Z_p , which is a virtual pivot of the beam.

Fig. 2.6 shows a schematic of the central electron trajectory in the cross-section of the direction of u_o , in the rotation coordinate system, in the case that $t_o = 0$ and the normalized initial slope is real. Two trajectories, where the initial lateral positions are u_o and $2u_o$, respectively, are displayed. Asymptotes of incident trajectories are shown with dashed lines. They intersect with the optic axis at Z_p , which is a virtual pivot of the beam. The position of Z_p is given by

$$Z_p = \zeta_o - \frac{1}{\lambda_{Ro}}. \quad (2.366)$$

However, in general, when the normalized initial slope is complex, a virtual pivot cannot be defined.

Using Eq. (2.49), (2.364), and (2.365), the general lateral paraxial trajectory is given by

$$u^{(1)} = \dot{u}_o u_\alpha + u_o u_\gamma = \dot{\zeta}_o s_o u_\alpha + \dot{\zeta}_o t_o u_\alpha + u_o (u_\gamma + \dot{\zeta}_o \lambda_o u_\alpha). \quad (2.367)$$

Employing Eq. (2.21), the lateral paraxial trajectory in the Cartesian coordinate system and its reduced velocity are given by

$$w^{(1)} = e^{i\chi} [\dot{\zeta}_o s_o u_\alpha + \dot{\zeta}_o t_o u_\alpha + u_o (u_\gamma + \dot{\zeta}_o \lambda_o u_\alpha)], \quad (2.368)$$

and

$$\begin{aligned} \dot{w}^{(1)} = e^{i\chi} & [\dot{\zeta}_o s_o (\dot{u}_\alpha + i\dot{\chi} u_\alpha) + \dot{\zeta}_o t_o (\dot{u}_\alpha + i\dot{\chi} u_\alpha) \\ & + u_o \{ (\dot{u}_\gamma + \dot{\zeta}_o \lambda_{Ro} \dot{u}_\alpha - \dot{\zeta}_o \lambda_{Io} \dot{\chi} u_\alpha) + i(\dot{\chi} u_\gamma + \dot{\zeta}_o \lambda_{Ro} \dot{\chi} u_\alpha + \dot{\zeta}_o \lambda_{Io} \dot{u}_\alpha) \}]. \end{aligned} \quad (2.369)$$

Then, in the Cartesian coordinate system, the lateral off-axis point and the slope of the paraxial trajectory at the object plane and at the image plane are expressed by the initial position and slope in the rotation coordinate system as follows:

$$w_o = u_o, \quad (2.370)$$

$$w'_o = \frac{1}{\dot{\zeta}_o} \dot{w}_o = s_o + t_o + \left[\lambda_{Ro} + i \left(\lambda_{Io} + \frac{\eta B_o}{2\sqrt{\Phi_o}} \right) \right] u_o, \quad (2.371)$$

$$w_i^{(1)} = e^{i\chi_i} M u_o = e^{i\chi_i} u_i^{(1)}, \quad (2.372)$$

$$\begin{aligned} w_i'^{(1)} = \frac{1}{\dot{\zeta}_i} \dot{w}_i^{(1)} &= e^{i\chi_i} \left[M_\alpha (s_o + t_o) + \left\{ \left(-\frac{1}{f_i} + \lambda_{Ro} M_\alpha \right) + i \left(\frac{\dot{\chi}_i}{\dot{\zeta}_i} M + \lambda_{Io} M_\alpha \right) \right\} u_o \right] \\ &= e^{i\chi_i} \left[s_i^{(1)} + t_i^{(1)} + \left(-\frac{1}{M f_i} + i \frac{\dot{\chi}_i}{\dot{\zeta}_i} + \lambda_i \right) u_i^{(1)} \right], \end{aligned} \quad (2.373)$$

where

$$s_i^{(1)} = M_\alpha s_o, \quad t_i^{(1)} = M_\alpha t_o, \quad \lambda_i = \frac{M_\alpha}{M} \lambda_o. \quad (2.374)$$

Eqs. (2.370) and (2.371) indicate that when the object plane is immersed in the magnetic round lens field, for the off-axis paraxial trajectory, the initial slope in the Cartesian coordinate is different from that in the rotation coordinate, because of the Lorentz force, which causes Larmor rotation, despite the fact that both coordinates match with each other.

We consider the expression of the third-order geometrical aberration parametrized by s_o , t_o , and u_o . We consider Eqs. (2.182), (2.364) and (2.365), and it is convenient to express the aberration coefficients by the following complex aberration coefficients:

$$\begin{aligned} K_{Lo} &= 2C_{Ko} + 2iC_{ko}, \\ K_{Ro} &= C_{Ko} - iC_{ko}, \\ A_o &= C_{Ao} + iC_{ao}, \\ D_o &= C_{Do} + iC_{do}, \end{aligned} \quad (2.375)$$

where the complex coefficients for the spherical aberration coefficient and the field curvature coefficient are not introduced, since it has been proved that they are real, in section 2.7. Since s_o is the complex initial slope of a general electron, which is a component of the beam, with respect to the central electron of the beam, and for the outermost

electron, $|s_o|$ corresponds to the aperture half angle at the object plane, the aberration can be classified by the exponent of terms involving s_o , and its complex conjugate:

$$\begin{aligned}
\Delta u_o^{(3)} \text{ geo.} &= \tilde{C}_{S_o} s_o^2 \bar{s}_o \\
&+ \tilde{K}_{L_o} u_o s_o \bar{s}_o + 2C_{S_o} t_o s_o \bar{s}_o \\
&+ \tilde{K}_{R_o} \bar{u}_o s_o^2 + C_{S_o} \bar{t}_o s_o^2 \\
&+ \tilde{C}_{F_o} u_o \bar{u}_o s_o + 2C_{S_o} t_o \bar{t}_o s_o + \tilde{K}_{L_o} u_o \bar{t}_o s_o + 2\tilde{K}_{R_o} \bar{u}_o t_o s_o \\
&+ \tilde{A}_o u_o^2 \bar{s}_o + C_{S_o} t_o^2 \bar{s}_o + \tilde{K}_{L_o} u_o t_o \bar{s}_o \\
&+ \tilde{D}_o u_o^2 \bar{u}_o + C_{S_o} t_o^2 \bar{t}_o + \tilde{C}_{F_o} u_o \bar{u}_o t_o \\
&+ \tilde{A}_o u_o^2 \bar{t}_o + \tilde{K}_{L_o} u_o t_o \bar{t}_o + \tilde{K}_{R_o} \bar{u}_o t_o^2.
\end{aligned} \tag{2.376}$$

The first line of the right-hand side corresponds to the spherical aberration. The second line is the coma-length. The third line is the coma-radius. The fourth line is the field-curvature. The fifth line is the astigmatism. The sixth and the seventh lines are the distortion. The aberration coefficients in Eq. (2.376), on which a tilde is put such as \tilde{C} , are expressed by the coefficients without a tilde as follows:

$$\tilde{C}_{S_o} = C_{S_o}, \tag{2.377}$$

$$\tilde{K}_{L_o} = K_{L_o} + 2\lambda_o C_{S_o} = 2(C_{K_o} + \lambda_{R_o} C_{S_o}) + 2i(C_{k_o} + \lambda_{l_o} C_{S_o}), \tag{2.378}$$

$$\tilde{K}_{R_o} = K_{R_o} + \bar{\lambda}_o C_{S_o} = C_{K_o} + \lambda_{R_o} C_{S_o} - i(C_{k_o} + \lambda_{l_o} C_{S_o}), \tag{2.379}$$

$$\begin{aligned}
\tilde{C}_{F_o} &= C_{F_o} + \bar{\lambda}_o K_{L_o} + 2\lambda_o K_{R_o} + 2\lambda_o \bar{\lambda}_o C_{S_o} \\
&= C_{F_o} + 4\lambda_{R_o} C_{K_o} + 4\lambda_{l_o} C_{k_o} + 2(\lambda_{R_o}^2 + \lambda_{l_o}^2) C_{S_o},
\end{aligned} \tag{2.380}$$

$$\begin{aligned}
\tilde{A}_o &= A_o + \lambda_o K_{L_o} + \lambda_o^2 C_{S_o} \\
&= C_{A_o} + 2\lambda_{R_o} C_{K_o} - 2\lambda_{l_o} C_{k_o} + (\lambda_{R_o}^2 - \lambda_{l_o}^2) C_{S_o} + i(C_{a_o} + 2\lambda_{R_o} C_{k_o} + 2\lambda_{l_o} C_{K_o} + 2\lambda_{R_o} \lambda_{l_o} C_{S_o}),
\end{aligned} \tag{2.381}$$

$$\begin{aligned}
\tilde{D}_o &= D_o + \lambda_o C_{F_o} + \bar{\lambda}_o A_o + \lambda_o \bar{\lambda}_o K_{L_o} + \lambda_o^2 K_{R_o} + \lambda_o^2 \bar{\lambda}_o C_{S_o} \\
&= C_{D_o} + \lambda_{R_o} (C_{F_o} + C_{A_o}) + \lambda_{l_o} C_{a_o} + (3\lambda_{R_o}^2 + \lambda_{l_o}^2) C_{K_o} + 2\lambda_{R_o} \lambda_{l_o} C_{k_o} + \lambda_{R_o} (\lambda_{R_o}^2 + \lambda_{l_o}^2) C_{S_o} \\
&\quad + i[C_{d_o} + \lambda_{R_o} C_{a_o} + \lambda_{l_o} (C_{F_o} - C_{A_o}) + (\lambda_{R_o}^2 + 3\lambda_{l_o}^2) C_{k_o} + 2\lambda_{R_o} \lambda_{l_o} C_{K_o} + \lambda_{l_o} (\lambda_{R_o}^2 + \lambda_{l_o}^2) C_{S_o}].
\end{aligned} \tag{2.382}$$

Similarly, the second-rank aberration for the chromatic aberration in Eq. (2.147) and that for the variation of the fields in Eq. (2.334) can be expressed by the parameters s_o , t_o , and u_o as follows:

$$\begin{aligned}
\Delta u_o^{(2)} &= [\tilde{C}_{C_o} s_o + (\tilde{C}_{M_o} + i\tilde{C}_{R_o}) u_o + \tilde{C}_{C_o} t_o] \kappa_o \\
&+ \sum_{j=1}^N [\tilde{C}_{E_{1o}}^j s_o + (\tilde{C}_{E_{2o}}^j + i\tilde{C}_{E_{3o}}^j) u_o + \tilde{C}_{E_{1o}}^j t_o] \kappa_{v_j} \\
&+ \sum_{\ell=1}^L [\tilde{C}_{B_{1o}}^\ell s_o + (\tilde{C}_{B_{2o}}^\ell + i\tilde{C}_{B_{3o}}^\ell) u_o + \tilde{C}_{B_{1o}}^\ell t_o] \kappa_{l_\ell},
\end{aligned} \tag{2.383}$$

where

$$\begin{aligned}
\tilde{C}_{C_o} &= C_{C_o}, \\
\tilde{C}_{M_o} &= C_{M_o} + \lambda_{R_o} C_{C_o}, \\
\tilde{C}_{R_o} &= C_{R_o} + \lambda_{l_o} C_{C_o},
\end{aligned} \tag{2.384}$$

$$\begin{aligned}
\tilde{C}_{E_{1o}}^j &= C_{E_{1o}}^j, \\
\tilde{C}_{E_{2o}}^j &= C_{E_{2o}}^j + \lambda_{R_o} C_{E_{1o}}^j, \\
\tilde{C}_{E_{3o}}^j &= C_{E_{3o}}^j + \lambda_{l_o} C_{E_{1o}}^j,
\end{aligned} \tag{2.385}$$

$$\begin{aligned}
\tilde{C}_{B_{1o}}^\ell &= C_{B_{1o}}^\ell, \\
\tilde{C}_{B_{2o}}^\ell &= C_{B_{2o}}^\ell + \lambda_{R_o} C_{B_{1o}}^\ell, \\
\tilde{C}_{B_{3o}}^\ell &= C_{B_{3o}}^\ell + \lambda_{l_o} C_{B_{1o}}^\ell.
\end{aligned} \tag{2.386}$$

In this chapter, the aberrations defined at the object plane are discussed. In practice, we are interested in the aberration at the image plane. The relation between the aberration defined at the image plane and that at the object plane is given by

$$\Delta u_i^{(r)}(\omega_i^{(1)}, t_i^{(1)}, u_i^{(1)}; \lambda_i) = M \Delta u_o^{(r)}(\omega_o, t_o, u_o; \lambda_o), \quad (2.387)$$

where the aberration at the image plane is parametrized by paraxial parameters defined at the image plane. Thus, for the image aberrations, corresponding equations to Eqs. (2.376) to (2.386) have the completely same forms under the following replacement:

$$\begin{aligned} \Delta u_o^{(2)} &\rightarrow \Delta u_i^{(2)}, \quad \Delta u_o^{(3)}_{\text{geo.}} \rightarrow \Delta u_i^{(3)}_{\text{geo.}}, \\ s_o &\rightarrow s_i^{(1)}, \quad t_o \rightarrow t_i^{(1)}, \quad u_o \rightarrow u_i^{(1)}, \\ \lambda_o &\rightarrow \lambda_i, \quad \kappa_o \rightarrow \kappa_i = \frac{\Delta\Phi}{\Phi_i}, \\ \tilde{C}_{S_o} &\rightarrow \tilde{C}_{S_i}, \quad \tilde{K}_{L_o} \rightarrow \tilde{K}_{L_i}, \quad \tilde{K}_{R_o} \rightarrow \tilde{K}_{R_i}, \\ \tilde{C}_{F_o} &\rightarrow \tilde{C}_{F_i}, \quad \tilde{A}_o \rightarrow \tilde{A}_i, \quad \tilde{D}_o \rightarrow \tilde{D}_i, \\ \tilde{C}_{C_o} &\rightarrow \tilde{C}_{C_i}, \quad \tilde{C}_{M_o} \rightarrow \tilde{C}_{M_i}, \quad \tilde{C}_{R_o} \rightarrow \tilde{C}_{R_i}, \\ \tilde{C}_{E1o}^j &\rightarrow \tilde{C}_{E1i}^j, \quad \tilde{C}_{E2o}^j \rightarrow \tilde{C}_{E2i}^j, \quad \tilde{C}_{E3o}^j \rightarrow \tilde{C}_{E3i}^j, \\ \tilde{C}_{B1o}^\ell &\rightarrow \tilde{C}_{B1i}^\ell, \quad \tilde{C}_{B2o}^\ell \rightarrow \tilde{C}_{B2i}^\ell, \quad \tilde{C}_{B3o}^\ell \rightarrow \tilde{C}_{B3i}^\ell, \end{aligned} \quad (2.388)$$

where coefficients without a tilde, such as C_{X_o} , are replaced by C_{X_i} , similarly. The aberration coefficients, whose subscript is i , are defined in the image plane and are given using coefficients defined in the object plane as follows:

$$\begin{aligned} \tilde{C}_{S_i} &= \frac{M}{M_\alpha^3} \tilde{C}_{S_o}, \quad \tilde{K}_{L_i} = \frac{1}{M_\alpha^2} \tilde{K}_{L_o}, \quad \tilde{K}_{R_i} = \frac{1}{M_\alpha^2} \tilde{K}_{R_o}, \\ \tilde{C}_{F_i} &= \frac{1}{MM_\alpha} \tilde{C}_{F_o}, \quad \tilde{A}_i = \frac{1}{MM_\alpha} \tilde{A}_o, \quad \tilde{D}_i = \frac{1}{M^2} \tilde{D}_o, \end{aligned} \quad (2.389)$$

$$\tilde{C}_{C_i} = \frac{1}{MM_\alpha^3} \tilde{C}_{C_o}, \quad \tilde{C}_{M_i} = \frac{1}{M^2 M_\alpha^2} \tilde{C}_{M_o}, \quad \tilde{C}_{R_i} = \frac{1}{M^2 M_\alpha^2} \tilde{C}_{R_o}, \quad (2.390)$$

$$\begin{aligned} \tilde{C}_{E1i}^j &= \frac{M}{M_\alpha} \tilde{C}_{E1o}^j, \quad \tilde{C}_{E2o}^j = \tilde{C}_{E2i}^j, \quad \tilde{C}_{E3o}^j = \tilde{C}_{E3i}^j, \\ \tilde{C}_{B1o}^\ell &= \frac{M}{M_\alpha} \tilde{C}_{B1i}^\ell, \quad \tilde{C}_{B2o}^\ell = \tilde{C}_{B2i}^\ell, \quad \tilde{C}_{B3o}^\ell = \tilde{C}_{B3i}^\ell. \end{aligned} \quad (2.391)$$

We are at the point, where the aberration coefficients for an inclined incident beam are constructed from those for an incident beam parallel to the optic axis.

2.12 Conclusion

We used time-dependent perturbation theory for calculating the properties of rotationally symmetric electrostatic and magnetic fields and investigated the electron optics theory for electron mirrors. This theory is valid for the case where both round symmetric magnetic fields and electrostatic fields are combined and overlapping.

1. We obtained the following results: A detailed review of the paraxial approximation of the lateral and the longitudinal trajectories is given. First-order optical properties of the paraxial trajectories are formulated. However, we are mainly interested in the lateral position of each electron in a same z value, that is, in a same XY plane. In time-dependent theory, since the trajectory is parametrized by time, the longitudinal position of each electron at the same time generally differs from one another. This relative longitudinal position difference causes the difference of lateral position for the electron, in the concerned XY plane, from that at an evaluated time. This lateral position difference is roughly estimated by the product of the longitudinal position difference and the lateral velocity at the evaluated time. The lateral position difference can also be expanded as a power series of the geometrical and chromatic parameters. However, the lateral position difference includes only terms higher than the second-rank. If we focus on the first-order trajectories, the z -position of the lateral trajectories coincides with that of the reference electron trajectory.
2. The concrete forms of the chromatic second-rank path deviation and the third-order geometrical path deviations in the time-dependent theory are derived. When the path deviation is considered, the lateral position is a function of the reduced time and is not identical to the lateral path deviation evaluated as a function of position, because the longitudinal path deviation has a nonzero value. This means that the perturbed electron positions in the z -direction at the reduced time τ are different from one another, according to their dependence on geometrical and chromatic parameters. To derive aberration formulae, the transformation from path deviation, parameterized by reduced time, to that, evaluated at a position, is derived. The Lagrange inversion theorem gives us a systematic way of the series expansion of the lateral position difference. Taking this into account, that expansion can compensate for the lateral position difference of the concerned rank. As a result, the formulae of the path deviation for the electron mirrors estimated in the arbitrary plane are derived.
3. Since the aberration is defined as a path deviation value at the image plane, the aberration coefficient formulae are derived in time-dependent theory. Appropriate transformation of the formulae using partial integration of the reduced time shows that these formulae satisfy the same properties as the aberration coefficients in the standard

electron optics theory: The relation between the coma-length and the coma-radius $K_{Lo} = 2\bar{K}_{Ro}$, and the anisotropic part of the field curvature coefficient vanishes. The formulae for the aberration coefficients are derived in forms as general as possible. The derived concrete formulae of the aberration coefficients do not assume that the optical system includes electron mirrors. If no reflection happens, the derived coefficients must coincide with the aberration coefficients formulae in the standard electron optics. Changing the integration parameters from the reduced time to the coordinate of the optic axis, and using partial integration, we can prove that the derived coefficients of all second-rank, and the third-order, on-, and off-axis aberrations, which are parametrized by reduced time, perfectly coincide with the aberration coefficient formulae in the standard electron optics theory. This shows the validity of the derived formulae of the aberration coefficients.

4. We consider the tiny difference in the trajectory caused by the fluctuation of electric and magnetic fields, as a kind of path deviation. We name that kind of aberration the aberration coefficients for variation of the voltages and the currents. The second-rank aberration coefficients, of which the aberration is linearly dependent on the variation of one of the voltages or the currents, are derived. The relationship between these coefficients and the chromatic aberration coefficients is derived.
5. We consider the aberration specifically for probe-forming systems. In earlier work, the derived off-axis aberration coefficients were only applied in situations where the incident beam was parallel to the optic axis in the object plane. We investigated the method for constructing the off-axis aberration coefficients for arbitrary tilted incident beams by a suitable combination of the off-axis coefficients. The result shows the residual aberrations after the beam is aligned according to a specific way, for example, the off-axis chromatic aberration under coma-free axis alignment.

2.13 Appendix of chapter 2

2.13.1 Definitions of rank, order, and degree of aberrations

In general, aberrations are expressed by polynomials of geometric parameters, such as lateral positions and reduced velocities in the object plane, and a chromatic parameter, which is the ratio of energy spread and nominal energy of electrons: $\Delta E/E$. They are classified according to the exponents of those parameters. Complicated combination aberrations of the geometric and chromatic parameters are generated in an optical system with deflection because aberrations that depend on energy spread such as dispersion are significant. Terminology to segregate contributions of the geometric parameters from those of the chromatic parameter is introduced according to reference [1.91] as follows.

Geometrical aberrations are defined as aberrations that depend on only geometric parameters. The “order” of the aberration is the sum of the exponents of the geometric parameters. If an aberration includes the chromatic parameter, its “degree” is its exponent. “Rank” is defined as the sum of the order and degree: rank = order + degree. For example, all geometric aberrations have no “degree” and their rank equals the “order”. Since axial chromatic aberration has a bi-linear form composed of an aperture half-angle and the chromatic parameter, it is the first-order, the first-degree, and the second-rank aberration. Since the absolute values of the geometric parameters u_o, \dot{u}_o and the chromatic parameter κ_o are much smaller than 1, the higher the rank of path-deviations is, the less significant their contribution. The magnitude of aberrations is measured by their rank.

2.13.2 A linear second order ordinary differential equation and the variation method of a parameter for solving an inhomogeneous equation.

Here is a brief review of a linear ordinary differential equation and the variation method of a parameter given. We assume that a function x , whose variable is τ , satisfies a homogeneous linear second order ordinary differential equation:

$$L[x] = \ddot{x} + p(\tau)\dot{x} + q(\tau)x = 0, \quad (2.392)$$

where p and q are functions of τ . In general, this equation has two independent solutions x_1 and x_2 , that is, $L[x_1] = 0$, and $L[x_2] = 0$. Then, a general solution of Eq. (2.392) is given by a linear combination of independent solutions:

$$x(\tau) = C_1 x_1(\tau) + C_2 x_2(\tau), \quad (2.393)$$

where C_1 and C_2 are arbitrary constants. The Wronskian is defined as

$$W[x_1, x_2] = x_1 \dot{x}_2 - \dot{x}_1 x_2. \quad (2.394)$$

Using Eq. (2.392), the derivative gives the first order differential equation:

$$\frac{d}{d\tau} W[x_1, x_2] = x_1 \ddot{x}_2 - \ddot{x}_1 x_2 = -p(\tau) W[x_1, x_2]. \quad (2.395)$$

The solution is as follows:

$$W[x_1, x_2] = C \exp \left[- \int^{\tau} p(\xi) d\xi \right], \quad (2.396)$$

where C is an arbitrary constant. If the Wronskian vanishes but neither x_1 nor x_2 is zero, x_2 must be proportional to x_1 and it is not an independent solution. If the coefficient function of \dot{x} vanishes: $p = 0$, the wronskian is conserved. Even if p does not vanish, the original differential equation can always be transformed to the form without the coefficient function of \dot{x} . A new function y is introduced by

$$y(\tau) = a(\tau)x(\tau), \quad (2.397)$$

where a is a non-vanishing function. The function y satisfies the homogeneous linear second order ordinary differential equation:

$$\tilde{L}[y] = \ddot{y} + \left(p + \frac{2\dot{a}}{a} \right) \dot{y} + \left(q + p \frac{\dot{a}}{a} + \frac{\ddot{a}}{a} \right) y = 0. \quad (2.398)$$

When the function a is chosen to satisfy that

$$p = -\frac{2\dot{a}}{a}, \quad (2.399)$$

that is,

$$a(\tau) = C \exp \left[-\frac{1}{2} \int^{\tau} p(\xi) d\xi \right], \quad (2.400)$$

then, y satisfies the equation:

$$\tilde{L}[y] = \ddot{y} + \left(q - \frac{1}{4} p^2 - \frac{1}{2} \dot{p} \right) y = 0, \quad (2.401)$$

and the Wronskian for y is a constant. When one of the independent solutions x_1 is known, the other independent solution x_2 is given using x_1 . We assume that

$$x_2 = b(\tau)x_1, \quad (2.402)$$

where b is a function of τ . Because of $L[x_1] = L[x_2] = 0$, the differential equation for b is given by

$$\ddot{b} = - \left[p + 2 \frac{\dot{x}_1}{x_1} \right] \dot{b} \quad (2.403)$$

and the solution is given by

$$\dot{b} = \frac{C}{x_1^2} \exp \left[- \int^{\tau} p(\xi) d\xi \right], \quad (2.404)$$

where C is an integration constant. Then, the other solution is given by

$$x_2(\tau) = C x_1(\tau) \int^{\tau} \frac{\exp \left[- \int^{\xi} p(v) dv \right]}{x_1^2(\xi)} d\xi = x_1 \int^{\tau} \frac{W}{x_1^2} d\xi, \quad (2.405)$$

where C is an integration constant. This method is called variation method of constant or parameter. Then, we consider an inhomogeneous equation:

$$L[x] = \ddot{x} + p(\tau)\dot{x} + q(\tau)x = r(\tau), \quad (2.406)$$

where $r(\tau)$ does not include x or \dot{x} . If a particular solution x_s , which satisfies Eq. (2.406), is found, the general solution is given by

$$x(\tau) = C_1 x_1(\tau) + C_2 x_2(\tau) + x_s(\tau), \quad (2.407)$$

where x_1 , and x_2 are independent solutions of the homogeneous equation Eq. (2.392) and C_1 , and C_2 are arbitrary constants.

The particular solution x_s is expressed by x_1 , and x_2 using the variation method of constant. The particular solution is assumed to take the form:

$$x_s(\tau) = A_1(\tau)x_1(\tau) + A_2(\tau)x_2(\tau), \quad (2.408)$$

where A_1 , and A_2 are functions of τ . To determine A_1 , and A_2 , we consider

$$L[x_s] = \ddot{A}_1 x_1 + \dot{A}_1 (p x_1 + 2\dot{x}_1) + \ddot{A}_2 x_2 + \dot{A}_2 (p x_2 + 2\dot{x}_2) = r(\tau). \quad (2.409)$$

It is transformed into

$$\frac{d}{d\tau}(\dot{A}_1 x_1 + \dot{A}_2 x_2) + p(\dot{A}_1 x_1 + \dot{A}_2 x_2) + \dot{A}_1 \dot{x}_1 + \dot{A}_2 \dot{x}_2 = r(\tau). \quad (2.410)$$

Since we have two degrees of freedom A_1 , and A_2 , without loss of generality, the solution is restricted to a form that satisfies:

$$F = \dot{A}_1 x_1 + \dot{A}_2 x_2 = 0, \quad (2.411)$$

for all ranges of τ . We obtain $\dot{F} = 0$ and Eq. (2.410) becomes a very simple form:

$$\dot{A}_1 \dot{x}_1 + \dot{A}_2 \dot{x}_2 = r(\tau). \quad (2.412)$$

Thus, combined equation of Eqs. (2.411) and (2.412) should be solved. It is expressed in a matrix form as follows:

$$D \begin{pmatrix} \dot{A}_1 \\ \dot{A}_2 \end{pmatrix} = \begin{pmatrix} 0 \\ r \end{pmatrix}, \quad (2.413)$$

where

$$D = \begin{pmatrix} \dot{x}_1 & \dot{x}_2 \\ \dot{x}_1 & \dot{x}_2 \end{pmatrix}. \quad (2.414)$$

Since the determinant of D is the wronskian, the inverse matrix of D is

$$D^{-1} = \frac{1}{W[x_1 \ x_2]} \begin{pmatrix} \dot{x}_2 & -x_2 \\ -\dot{x}_1 & x_1 \end{pmatrix}. \quad (2.415)$$

Thus, we get

$$\begin{pmatrix} \dot{A}_1 \\ \dot{A}_2 \end{pmatrix} = D^{-1} \begin{pmatrix} 0 \\ r \end{pmatrix} = \frac{r(\tau)}{W[x_1 \ x_2]} \begin{pmatrix} -x_2(\tau) \\ x_1(\tau) \end{pmatrix}, \quad (2.416)$$

and performing integration, A_1 , and A_2 are determined:

$$\begin{pmatrix} A_1 \\ A_2 \end{pmatrix} = \begin{pmatrix} -\int_{\tau_A}^{\tau} \frac{r(\xi)x_2(\xi)}{W[x_1 \quad x_2]} d\xi \\ \int_{\tau_B}^{\tau} \frac{r(\xi)x_1(\xi)}{W[x_1 \quad x_2]} d\xi \end{pmatrix}, \quad (2.417)$$

where τ_A and τ_B are lower boundaries of integrals, which are given by initial conditions.

Therefore, the particular solution is given by

$$x_s(\tau) = -x_1(\tau) \int_{\tau_A}^{\tau} \frac{r(\xi)x_2(\xi)}{W[x_1 \quad x_2]} d\xi + x_2(\tau) \int_{\tau_B}^{\tau} \frac{r(\xi)x_1(\xi)}{W[x_1 \quad x_2]} d\xi. \quad (2.418)$$

Its derivative is given by

$$\dot{x}_s(\tau) = -\dot{x}_1(\tau) \int_{\tau_A}^{\tau} \frac{r(\xi)x_2(\xi)}{W[x_1 \quad x_2]} d\xi + \dot{x}_2(\tau) \int_{\tau_B}^{\tau} \frac{r(\xi)x_1(\xi)}{W[x_1 \quad x_2]} d\xi. \quad (2.419)$$

The particular solution x_s is designated by the choice of the lower boundaries of integrals τ_A and τ_B . When we choose

$\tau_A = \tau_B = \tau_{\text{int}}$ in Eqs. (2.418) and (2.419), the appropriate initial condition of x_s is

$$x_s(\tau_{\text{int}}) = 0, \quad \dot{x}_s(\tau_{\text{int}}) = 0. \quad (2.420)$$

Then, the initial second order derivative is

$$\ddot{x}_s(\tau_{\text{int}}) = r(\tau_{\text{int}}). \quad (2.421)$$

2.13.3 Replacement of fundamental solutions of linear equations in the formal solution of perturbation

Using the parameter variation method to solve inhomogeneous second order ordinary differential equations, explained in Appendix 2.13.2, formal solutions of perturbation are given by Eqs. (2.81) and (2.82). In these formulae, the solutions $u_\alpha, u_\gamma, h_\alpha, h_\gamma$ are used as the fundamental solutions instead of x_1 and x_2 in Appendix 2.13.2. However, we can take other solutions of the linear equations as fundamental solutions. Actually, in references [1.88], to derive on-axis aberration coefficients, symmetric and antisymmetric solutions h_σ, h_p , with respect to the reflection time, are used as fundamental solutions for the linear longitudinal equation. In the time-dependent theory, the full-equations for the lateral and longitudinal trajectories are given by

$$\ddot{u} + \frac{N}{4\Phi_c} u = P_u, \quad \ddot{h} - \frac{\Phi''}{2\Phi_c} h = P_h. \quad (2.422)$$

In general, we assume that general solutions of the homogeneous equations, which are obtained by setting $P_u = 0$, and

$P_h = 0$ in Eq. (2.422), are

$$\begin{aligned} u^{(1)}(\tau) &= u_A u_1(\tau) + u_B u_2(\tau), \\ h^{(1)}(\tau) &= h_A h_1(\tau) + h_B h_2(\tau), \end{aligned} \quad (2.423)$$

where u_A, u_B, h_A, h_B are appropriately given parameters and u_1, u_2, h_1, h_2 are the fundamental solutions. Since the homogeneous equations are linear differential equations, a pair of fundamental solutions is expressed by a proper linear combination of another pair of fundamental solution, to which we set $u_\alpha, u_\gamma, h_\alpha, h_\gamma$:

$$\begin{pmatrix} u_1 \\ u_2 \end{pmatrix} = \begin{pmatrix} C_1 & C_2 \\ C_3 & C_4 \end{pmatrix} \begin{pmatrix} u_\gamma \\ u_\alpha \end{pmatrix} = C \begin{pmatrix} u_\gamma \\ u_\alpha \end{pmatrix}, \\ \begin{pmatrix} h_1 \\ h_2 \end{pmatrix} = \begin{pmatrix} D_1 & D_2 \\ D_3 & D_4 \end{pmatrix} \begin{pmatrix} h_\gamma \\ h_\alpha \end{pmatrix} = D \begin{pmatrix} h_\gamma \\ h_\alpha \end{pmatrix}. \quad (2.424)$$

Using Eqs. (2.43) and (2.48), The Wronskians are expressed by

$$\begin{aligned} W[u_1, u_2] &= C_1 C_4 - C_2 C_3 = \det C, \\ W[h_1, h_2] &= D_1 D_4 - D_2 D_3 = \det D. \end{aligned} \quad (2.425)$$

By Eqs. (2.418), (2.422), (2.423), and (2.425), the formal solutions of a particular solution of Eq. (2.418) are given and transformed as follows:

$$\begin{aligned} u_s(\tau) &= -u_1(\tau) \int_{\tau_A}^{\tau} P_u u_2 d\xi + u_2(\tau) \int_{\tau_B}^{\tau} P_u u_1 d\xi \\ &= -u_\gamma \int_{\tau_A}^{\tau} P_u u_\alpha d\xi + u_\alpha \int_{\tau_A}^{\tau} P_u u_\gamma d\xi + \frac{C_3 u_\gamma + C_4 u_\alpha}{\det C} \int_{\tau_B}^{\tau_A} P_u (C_1 u_\gamma + C_2 u_\alpha) d\xi, \end{aligned} \quad (2.426)$$

and

$$h_s(\tau) = -h_\gamma \int_{\tau_A}^{\tau} P_h h_\alpha d\xi + h_\alpha \int_{\tau_A}^{\tau} P_h h_\gamma d\xi + \frac{C_3 h_\gamma + C_4 h_\alpha}{\det C} \int_{\tau_B}^{\tau_A} P_u (C_1 h_\gamma + C_2 h_\alpha) d\xi. \quad (2.427)$$

If we take $\tau_A = \tau_B = \tau_o$, we obtain the formal solutions for the aberration in the lateral direction at the convergent time, and the longitudinal path-deviation of arbitrary reduced time are given by

$$u_s(\tau_i) = -u_1(\tau_i) \int_{\tau_o}^{\tau_i} P_u u_2 d\xi + u_2(\tau_i) \int_{\tau_o}^{\tau_i} P_u u_1 d\xi = -M \int_{\tau_o}^{\tau_i} P_u u_\alpha d\xi, \quad (2.428)$$

and

$$h_s(\tau) = -h_1 \int_{\tau_o}^{\tau} P_h h_2 d\xi + h_2 \int_{\tau_o}^{\tau} P_h h_1 d\xi = -h_\gamma \int_{\tau_o}^{\tau} P_h h_\alpha d\xi + h_\alpha \int_{\tau_o}^{\tau} P_h h_\gamma d\xi. \quad (2.429)$$

No matter which pair of fundamental solutions we choose, the form of the formal solution remains the same, if we take $\tau_A = \tau_B = \tau_o$. Note that the result of perturbation depends on the choice of approximation of trajectories, which consist of P_u and P_h . The procedure of approximation is explained in section 2.3.1.

2.13.4 Third-order geometrical slope deviation and slope aberration

The general form of the third-order slope deviation in the rotation coordinate is given by

$$\begin{aligned} \Delta u_{geo}^{(3)'} &= (S_{aa\bar{a}}^{(R)} + iS_{aa\bar{a}}^{(I)})u_o'^2\bar{u}_o' \\ &+ (S_{a\bar{a}\gamma}^{(R)} + iS_{a\bar{a}\gamma}^{(I)})u_o u_o' \bar{u}_o' + (S_{aa\bar{\gamma}}^{(R)} + iS_{aa\bar{\gamma}}^{(I)})\bar{u}_o u_o'^2 \\ &+ (S_{a\gamma\bar{\gamma}}^{(R)} + iS_{a\gamma\bar{\gamma}}^{(I)})u_o \bar{u}_o u_o' + (S_{\bar{a}\gamma\gamma}^{(R)} + iS_{\bar{a}\gamma\gamma}^{(I)})u_o'^2 \bar{u}_o' \\ &+ (S_{\gamma\gamma\bar{\gamma}}^{(R)} + iS_{\gamma\gamma\bar{\gamma}}^{(I)})u_o'^2 \bar{u}_o'. \end{aligned} \quad (2.430)$$

The concrete expressions of each slope deviation in the rotation coordinate are obtained by differentiation of the path deviations, which are listed in Eqs. (2.171) to (2.180), with respect to the optic axis coordinate. The slope deviation of the spherical aberration type is:

$$\begin{aligned} \delta_{aaa}^{(R)} &= \dot{\zeta}_o^3 \dot{u}_{aaa}^{(R)'} = \frac{\dot{\zeta}_o^3}{\zeta} \dot{u}_{aaa}^{(R)} = \frac{\dot{\zeta}_o^3}{\zeta} \dot{u}_\gamma \int_{\tau_o}^{\tau} \frac{1}{32\Phi_C} (8L_1 u_a^2 h_{a\bar{a}} - L_2 u_a^4) d\tau \\ &- \frac{\dot{\zeta}_o^3}{\zeta} \dot{u}_a \int_{\tau_o}^{\tau} \frac{1}{32\Phi_C} (8L_1 u_a u_\gamma h_{a\bar{a}} - L_2 u_a^3 u_\gamma) d\tau + \frac{\dot{\zeta}_o^3}{\zeta} \frac{\Phi'}{2\Phi} \dot{u}_a h_{a\bar{a}} - \frac{\dot{\zeta}_o^3}{\zeta^2} \dot{u}_a h_{a\bar{a}} - \frac{\dot{\zeta}_o^3}{\zeta^2} \dot{u}_a h_{a\bar{a}}, \end{aligned} \quad (2.431)$$

and

$$\begin{aligned} \delta_{aaa}^{(I)} &= \frac{\dot{\zeta}_o^3}{\zeta} \dot{u}_a \int_{\tau_o}^{\tau} \frac{\eta}{16\sqrt{\Phi_C}} (8B' h_{a\bar{a}} - B'' u_a^2) d\tau - \frac{\eta B''}{16\zeta\sqrt{\Phi_C}} u_a^3 \\ &+ \frac{\dot{\zeta}_o^3 \eta B}{2\sqrt{\Phi_C}} \left(\frac{1}{\zeta} \frac{\Phi'}{2\Phi} u_a h_{a\bar{a}} - \frac{1}{\zeta^2} \dot{u}_a h_{a\bar{a}} - \frac{1}{\zeta^2} u_a \dot{h}_{a\bar{a}} \right). \end{aligned} \quad (2.432)$$

That of the coma-length type is:

$$\begin{aligned} S_{a\bar{a}\gamma}^{(R)} &= \frac{\dot{\zeta}_o^2}{\zeta} \dot{u}_\gamma \int_{\tau_o}^{\tau} \frac{1}{32\Phi_C} [8L_1 (u_a^2 h_{a\gamma}^{(R)} + u_a u_\gamma h_{a\bar{a}}) - 2L_2 u_a^3 u_\gamma] d\tau \\ &- \frac{\dot{\zeta}_o^2}{\zeta} \dot{u}_a \int_{\tau_o}^{\tau} \frac{1}{32\Phi_C} [8L_1 (u_a u_\gamma h_{a\gamma}^{(R)} + u_\gamma^2 h_{a\bar{a}}) - 2L_2 u_a^2 u_\gamma^2] d\tau \\ &+ \frac{\dot{\zeta}_o^2}{\zeta} \left(\frac{\zeta}{\zeta^2} (\dot{u}_a h_{a\gamma}^{(R)} + \dot{u}_\gamma h_{a\bar{a}}) - \frac{1}{\zeta} (\dot{u}_a h_{a\gamma}^{(R)} + \dot{u}_a h_{a\gamma}^{(R)} + \dot{u}_\gamma h_{a\bar{a}} + \dot{u}_\gamma h_{a\bar{a}}) \right) \\ &- \frac{\dot{\zeta}_o^2}{\zeta} \dot{u}_a \int_{\tau_o}^{\tau} \frac{\eta B'}{2\sqrt{\Phi_C}} h_{a\gamma}^{(I)} d\tau + \frac{\dot{\zeta}_o^2}{\zeta} \frac{\eta B}{2\sqrt{\Phi_C}} \left(-\frac{\zeta}{\zeta^2} u_a h_{a\gamma}^{(I)} + \frac{1}{\zeta} \dot{u}_a h_{a\gamma}^{(I)} + \frac{1}{\zeta} u_a \dot{h}_{a\gamma}^{(I)} \right), \end{aligned} \quad (2.433)$$

$$\begin{aligned} S_{a\bar{a}\gamma}^{(R)} &= \frac{\dot{\zeta}_o^2}{\zeta} \dot{u}_\gamma \int_{\tau_o}^{\tau} \frac{1}{32\Phi_C} [8L_1 (u_a^2 h_{a\gamma}^{(R)} + u_a u_\gamma h_{a\bar{a}}) - 2L_2 u_a^3 u_\gamma] d\tau \\ &- \frac{\dot{\zeta}_o^2}{\zeta} \dot{u}_a \int_{\tau_o}^{\tau} \frac{1}{32\Phi_C} [8L_1 (u_a u_\gamma h_{a\gamma}^{(R)} + u_\gamma^2 h_{a\bar{a}}) - 2L_2 u_a^2 u_\gamma^2] d\tau \\ &+ \frac{\dot{\zeta}_o^2}{\zeta} \left(\frac{\zeta}{\zeta^2} (\dot{u}_a h_{a\gamma}^{(R)} + \dot{u}_\gamma h_{a\bar{a}}) - \frac{1}{\zeta} (\dot{u}_a h_{a\gamma}^{(R)} + \dot{u}_a h_{a\gamma}^{(R)} + \dot{u}_\gamma h_{a\bar{a}} + \dot{u}_\gamma h_{a\bar{a}}) \right) \\ &- \frac{\dot{\zeta}_o^2}{\zeta} \dot{u}_a \int_{\tau_o}^{\tau} \frac{\eta B'}{2\sqrt{\Phi_C}} h_{a\gamma}^{(I)} d\tau + \frac{\dot{\zeta}_o^2}{\zeta} \frac{\eta B}{2\sqrt{\Phi_C}} \left(-\frac{\zeta}{\zeta^2} u_a h_{a\gamma}^{(I)} + \frac{1}{\zeta} \dot{u}_a h_{a\gamma}^{(I)} + \frac{1}{\zeta} u_a \dot{h}_{a\gamma}^{(I)} \right). \end{aligned} \quad (2.434)$$

That of the coma-radius type is:

$$\begin{aligned} S_{a\bar{a}\gamma}^{(R)} &= \frac{\dot{\zeta}_o^2}{\zeta} \dot{u}_\gamma \int_{\tau_o}^{\tau} \frac{1}{32\Phi_C} (8L_1 u_a^2 h_{a\gamma}^{(R)} - L_2 u_a^3 u_\gamma) d\tau \\ &- \frac{\dot{\zeta}_o^2}{\zeta} \dot{u}_a \int_{\tau_o}^{\tau} \left[\frac{1}{32\Phi_C} (8L_1 u_a u_\gamma h_{a\gamma}^{(R)} - L_2 u_a^2 u_\gamma^2) - \frac{\eta B'}{2\sqrt{\Phi_C}} h_{a\gamma}^{(I)} \right] d\tau \\ &+ \frac{\dot{\zeta}_o^2}{\zeta} \left(\frac{\zeta}{\zeta^2} \dot{u}_a h_{a\gamma}^{(R)} - \frac{1}{\zeta} \dot{u}_a h_{a\gamma}^{(R)} - \frac{1}{\zeta} \dot{u}_a h_{a\gamma}^{(R)} \right) - \frac{\dot{\zeta}_o^2}{\zeta} \frac{\eta B}{2\sqrt{\Phi_C}} \left(-\frac{\zeta}{\zeta^2} u_a h_{a\gamma}^{(I)} + \frac{1}{\zeta} \dot{u}_a h_{a\gamma}^{(I)} + \frac{1}{\zeta} u_a \dot{h}_{a\gamma}^{(I)} \right), \end{aligned} \quad (2.435)$$

$$\begin{aligned}
S_{\alpha\gamma}^{(I)} = & -\frac{\dot{\zeta}_o^2}{\zeta} \dot{u}_\gamma \int_{\tau_o}^{\tau} \left(\frac{L_1}{4\Phi_C} u_\alpha^2 h_{\alpha\gamma}^{(I)} - \frac{\eta B''}{16\sqrt{\Phi_C}} u_\alpha^2 \right) d\tau \\
& + \frac{\dot{\zeta}_o^2}{\zeta} \dot{u}_\alpha \int_{\tau_o}^{\tau} \left[\frac{L_1}{4\Phi_C} u_\alpha u_\gamma h_{\alpha\gamma}^{(I)} + \frac{\eta}{8\sqrt{\Phi_C}} (4B' h_{\alpha\gamma}^{(R)} - B'' u_\alpha u_\gamma) \right] d\tau \\
& + \frac{\dot{\zeta}_o^2}{\zeta} \left(-\frac{\dot{\zeta}}{\zeta} \dot{u}_\alpha h_{\alpha\gamma}^{(I)} + \frac{1}{\zeta} \dot{u}_\alpha h_{\alpha\gamma}^{(I)} + \frac{1}{\zeta} \dot{u}_\alpha h_{\alpha\gamma}^{(I)} \right) - \frac{\dot{\zeta}_o^2}{\zeta} \frac{\eta B}{2\sqrt{\Phi_C}} \left(-\frac{\dot{\zeta}}{\zeta^2} u_\alpha h_{\alpha\gamma}^{(R)} + \frac{1}{\zeta} \dot{u}_\alpha h_{\alpha\gamma}^{(R)} + \frac{1}{\zeta} u_\alpha \dot{h}_{\alpha\gamma}^{(R)} \right).
\end{aligned} \tag{2.436}$$

That of the field-curvature type is:

$$\begin{aligned}
S_{\alpha\gamma\bar{\gamma}}^{(R)} = & \frac{\dot{\zeta}_o}{\zeta} \dot{u}_\gamma \int_{\tau_o}^{\tau} \frac{1}{32\Phi_C} [8L_1 (u_\alpha^2 h_{\gamma\bar{\gamma}} + u_\alpha u_\gamma h_{\alpha\gamma}^{(R)}) - 2L_2 u_\alpha^2 u_\gamma^2] d\tau \\
& + \frac{\dot{\zeta}_o}{\zeta} \dot{u}_\gamma \int_{\tau_o}^{\tau} \frac{\eta B'}{2\sqrt{\Phi_C}} h_{\alpha\gamma}^{(I)} d\tau + \frac{\dot{\zeta}_o}{\zeta} \frac{\eta B'}{2\sqrt{\Phi_C}} u_\gamma h_{\alpha\gamma}^{(I)} \\
& - \frac{\dot{\zeta}_o}{\zeta} \dot{u}_\alpha \int_{\tau_o}^{\tau} \frac{1}{32\Phi_C} [8L_1 (u_\alpha u_\gamma h_{\gamma\bar{\gamma}} + u_\gamma^2 h_{\alpha\gamma}^{(R)}) - 2L_2 u_\alpha u_\gamma^3] d\tau \\
& - \frac{\dot{\zeta}_o}{\zeta} \left(-\frac{\dot{\zeta}}{\zeta^2} (\dot{u}_\alpha h_{\gamma\bar{\gamma}} + \dot{u}_\gamma h_{\alpha\gamma}^{(R)}) + \frac{1}{\zeta} (\dot{u}_\alpha h_{\gamma\bar{\gamma}} + \dot{u}_\gamma h_{\alpha\gamma}^{(R)}) + \frac{1}{\zeta} (\dot{u}_\alpha h_{\gamma\bar{\gamma}} + \dot{u}_\gamma h_{\alpha\gamma}^{(R)}) \right) \\
& - \frac{\dot{\zeta}_o}{\zeta} \frac{\eta B}{2\sqrt{\Phi_C}} \left(-\frac{\dot{\zeta}}{\zeta^2} u_\gamma h_{\alpha\gamma}^{(I)} + \frac{1}{\zeta} \dot{u}_\gamma h_{\alpha\gamma}^{(I)} + \frac{1}{\zeta} u_\gamma \dot{h}_{\alpha\gamma}^{(I)} \right),
\end{aligned} \tag{2.437}$$

$$\begin{aligned}
S_{\alpha\gamma\bar{\gamma}}^{(I)} = & -\frac{\dot{\zeta}_o}{\zeta} \dot{u}_\gamma \int_{\tau_o}^{\tau} \left(\frac{L_1}{4\Phi_C} u_\alpha u_\gamma h_{\alpha\gamma}^{(I)} - \frac{\eta B'}{2\sqrt{\Phi_C}} h_{\alpha\gamma}^{(R)} \right) d\tau \\
& + \frac{\dot{\zeta}_o}{\zeta} \dot{u}_\alpha \int_{\tau_o}^{\tau} \left[\frac{L_1}{4\Phi_C} u_\gamma^2 h_{\alpha\gamma}^{(I)} - \frac{\eta}{8\sqrt{\Phi_C}} (4B' h_{\gamma\bar{\gamma}} - B'' u_\gamma^2) \right] d\tau \\
& + \frac{\dot{\zeta}_o}{\zeta} \frac{\eta B''}{8\sqrt{\Phi_C}} u_\alpha u_\gamma^2 + \frac{\dot{\zeta}_o}{\zeta} \frac{\eta B'}{\sqrt{\Phi_C}} u_\alpha h_{\gamma\bar{\gamma}} + \frac{\dot{\zeta}_o}{\zeta} \left(-\frac{\dot{\zeta}}{\zeta^2} \dot{u}_\gamma h_{\alpha\gamma}^{(I)} + \frac{1}{\zeta} \dot{u}_\gamma h_{\alpha\gamma}^{(I)} + \frac{1}{\zeta} \dot{u}_\gamma h_{\alpha\gamma}^{(I)} \right) \\
& - \frac{\dot{\zeta}_o}{\zeta} \frac{\eta B}{2\sqrt{\Phi_C}} \left(-\frac{\dot{\zeta}}{\zeta^2} (u_\alpha h_{\gamma\bar{\gamma}} + u_\gamma h_{\alpha\gamma}^{(R)}) + \frac{1}{\zeta} (\dot{u}_\alpha h_{\gamma\bar{\gamma}} + \dot{u}_\gamma h_{\alpha\gamma}^{(R)}) + \frac{1}{\zeta} (u_\alpha \dot{h}_{\gamma\bar{\gamma}} + u_\gamma \dot{h}_{\alpha\gamma}^{(R)}) \right).
\end{aligned} \tag{2.438}$$

That of the astigmatism type is:

$$\begin{aligned}
S_{\alpha\gamma\bar{\gamma}}^{(R)} = & \frac{\dot{\zeta}_o}{\zeta} \dot{u}_\gamma \int_{\tau_o}^{\tau} \frac{1}{32\Phi_C} (8L_1 u_\alpha u_\gamma h_{\alpha\gamma}^{(R)} - L_2 u_\alpha^2 u_\gamma^2) d\tau \\
& - \frac{\dot{\zeta}_o}{\zeta} \dot{u}_\gamma \int_{\tau_o}^{\tau} \frac{\eta B'}{2\sqrt{\Phi_C}} h_{\alpha\gamma}^{(I)} d\tau - \frac{\dot{\zeta}_o}{\zeta} \dot{u}_\alpha \int_{\tau_o}^{\tau} \frac{1}{32\Phi_C} (8L_1 u_\gamma^2 h_{\alpha\gamma}^{(R)} - L_2 u_\alpha u_\gamma^3) d\tau \\
& - \frac{\dot{\zeta}_o}{\zeta} \left(-\frac{\dot{\zeta}}{\zeta^2} \dot{u}_\gamma h_{\alpha\gamma}^{(R)} + \frac{1}{\zeta} \dot{u}_\gamma h_{\alpha\gamma}^{(R)} + \frac{1}{\zeta} \dot{u}_\gamma h_{\alpha\gamma}^{(R)} \right) + \frac{\dot{\zeta}_o}{\zeta} \frac{\eta B}{2\sqrt{\Phi_C}} \left(-\frac{\dot{\zeta}}{\zeta^2} u_\gamma h_{\alpha\gamma}^{(I)} + \frac{1}{\zeta} \dot{u}_\gamma h_{\alpha\gamma}^{(I)} + \frac{1}{\zeta} u_\gamma \dot{h}_{\alpha\gamma}^{(I)} \right),
\end{aligned} \tag{2.439}$$

$$\begin{aligned}
S_{\alpha\gamma\bar{\gamma}}^{(I)} = & \frac{\dot{\zeta}_o}{\zeta} \dot{u}_\gamma \int_{\tau_o}^{\tau} \frac{L_1}{4\Phi_C} u_\alpha u_\gamma h_{\alpha\gamma}^{(I)} d\tau - \frac{\dot{\zeta}_o}{\zeta} \dot{u}_\alpha \int_{\tau_o}^{\tau} \frac{L_1}{4\Phi_C} u_\gamma^2 h_{\alpha\gamma}^{(I)} d\tau \\
& + \frac{\dot{\zeta}_o}{\zeta} \dot{u}_\gamma \int_{\tau_o}^{\tau} \frac{\eta}{8\sqrt{\Phi_C}} (4B' h_{\alpha\gamma}^{(R)} - B'' u_\alpha u_\gamma) d\tau + \frac{\dot{\zeta}_o}{\zeta} \dot{u}_\alpha \int_{\tau_o}^{\tau} \frac{\eta B''}{16\sqrt{\Phi_C}} u_\gamma^2 d\tau \\
& - \frac{\dot{\zeta}_o}{\zeta} \left(-\frac{\dot{\zeta}}{\zeta^2} \dot{u}_\gamma h_{\alpha\gamma}^{(I)} + \frac{1}{\zeta} \dot{u}_\gamma h_{\alpha\gamma}^{(I)} + \frac{1}{\zeta} \dot{u}_\gamma h_{\alpha\gamma}^{(I)} \right) - \frac{\dot{\zeta}_o}{\zeta} \frac{\eta B}{2\sqrt{\Phi_C}} \left(-\frac{\dot{\zeta}}{\zeta^2} u_\gamma h_{\alpha\gamma}^{(R)} + \frac{1}{\zeta} \dot{u}_\gamma h_{\alpha\gamma}^{(R)} + \frac{1}{\zeta} u_\gamma \dot{h}_{\alpha\gamma}^{(R)} \right).
\end{aligned} \tag{2.440}$$

That of the distortion type is:

$$\begin{aligned}
S_{\gamma\bar{\gamma}}^{(R)} = & \frac{1}{\zeta} \dot{u}_\gamma \int_{\tau_o}^{\tau} \frac{1}{32\Phi_C} (8L_1 u_\alpha u_\gamma h_{\gamma\bar{\gamma}} - L_2 u_\alpha u_\gamma^3) d\tau - \frac{1}{\zeta} \dot{u}_\alpha \int_{\tau_o}^{\tau} \frac{1}{32\Phi_C} (8L_1 u_\gamma^2 h_{\gamma\bar{\gamma}} - L_2 u_\gamma^4) d\tau \\
& + \frac{1}{\zeta} \left(\frac{\dot{\zeta}}{\zeta^2} \dot{u}_\gamma h_{\gamma\bar{\gamma}} - \frac{1}{\zeta} \dot{u}_\gamma h_{\gamma\bar{\gamma}} - \frac{1}{\zeta} \dot{u}_\gamma h_{\gamma\bar{\gamma}} \right),
\end{aligned} \tag{2.441}$$

$$\begin{aligned}
S_{\gamma\bar{\gamma}}^{(I)} = & \frac{1}{\zeta} \dot{u}_\gamma \int_{\tau_o}^{\tau} \frac{\eta}{16\sqrt{\Phi_C}} (8B' h_{\gamma\bar{\gamma}} - B'' u_\gamma^2) d\tau - \frac{1}{\zeta} \frac{\eta B''}{16\sqrt{\Phi_C}} u_\gamma^3 \\
& + \frac{1}{\zeta} \frac{\eta B}{2\sqrt{\Phi_C}} \left(\frac{\dot{\zeta}}{\zeta^2} u_\gamma h_{\gamma\bar{\gamma}} - \frac{1}{\zeta} \dot{u}_\gamma h_{\gamma\bar{\gamma}} - \frac{1}{\zeta} u_\gamma \dot{h}_{\gamma\bar{\gamma}} \right) + \frac{1}{\zeta} \frac{\eta B_o''}{16\sqrt{\Phi_C}} \dot{u}_\alpha.
\end{aligned} \tag{2.442}$$

The slope aberration coefficients in the rotation coordinate are given by the value of the slope deviations at the image plane. The total geometrical slope aberration of the third order is given by

$$\begin{aligned} \Delta u_{geoi}^{(3)'} &= (S_{aa\bar{a}i}^{(R)} + iS_{aa\bar{a}i}^{(I)})u_o'^2\bar{u}_o' \\ &+ (S_{a\bar{a}yi}^{(R)} + iS_{a\bar{a}yi}^{(I)})u_o u_o' \bar{u}_o' + (S_{a\bar{a}yi}^{(R)} + iS_{a\bar{a}yi}^{(I)})\bar{u}_o u_o'^2 \\ &+ (S_{a\gamma\bar{y}i}^{(R)} + iS_{a\gamma\bar{y}i}^{(I)})u_o \bar{u}_o u_o' + (S_{a\gamma\bar{y}i}^{(R)} + iS_{a\gamma\bar{y}i}^{(I)})u_o^2 \bar{u}_o' \\ &+ (S_{\gamma\gamma\bar{y}i}^{(R)} + iS_{\gamma\gamma\bar{y}i}^{(I)})u_o^2 \bar{u}_o. \end{aligned} \quad (2.443)$$

The slope aberration coefficients are given as follows. Note that, several terms, which appears as integration forms in the slope aberration coefficients, relate to geometrical aberration coefficients, which are defined in the object plane.

The slope aberration coefficient of the spherical aberration type is

$$\begin{aligned} S_{aa\bar{a}i}^{(R)} &= \frac{1}{\xi_i} \dot{u}_{yi} \left(C_{So} + \frac{\xi_o^3}{\xi_i} \dot{u}_{ai}^2 h_{a\bar{a}i} \right) \\ &- \frac{\dot{\xi}_o}{\xi_i} \dot{u}_{ai} \left(C_{KRo} + \frac{\xi_o^2}{\xi_i} \dot{u}_{ai}^2 h_{a\gamma i}^{(R)} \right) + \frac{\xi_o^3}{\xi_i} \frac{\Phi_i'}{2\Phi_i} \dot{u}_{ai} h_{a\bar{a}i} - \frac{\dot{\xi}_o^3}{\xi_i^2} \dot{u}_{ai} h_{a\bar{a}i}, \end{aligned} \quad (2.444)$$

$$S_{aa\bar{a}i}^{(I)} = \frac{\dot{\xi}_o^3}{\xi_i} \dot{u}_{ai} \int_{\tau_o}^{\tau_i} \frac{\eta}{16\sqrt{\Phi_C}} (8B' h_{a\bar{a}} - B'' u_a^2) d\tau - \frac{\dot{\xi}_o^3}{\xi_i^2} \frac{\eta B_i}{2\sqrt{\Phi_C}} \dot{u}_{ai} h_{a\bar{a}i} \quad (2.445)$$

That of the coma-length type is

$$\begin{aligned} S_{a\bar{a}\gamma i}^{(R)} &= \frac{1}{\xi_i} \dot{u}_{yi} \left(C_{KLo} + \frac{\xi_o^2}{\xi_i} \left(\dot{u}_{ai}^2 h_{a\gamma i}^{(R)} + \dot{u}_{ai} \dot{u}_{yi} h_{a\bar{a}i} \right) \right) \\ &- \frac{\dot{\xi}_o^2}{\xi_i} \dot{u}_{ai} \int_{\tau_o}^{\tau_i} \frac{1}{32\Phi_C} \left[8L_1 \left(u_a u_{\gamma} h_{a\gamma}^{(R)} + u_{\gamma}^2 h_{a\bar{a}} \right) - 2L_2 u_a^2 u_{\gamma}^2 \right] d\tau - \frac{\dot{\xi}_o^2}{\xi_i} \dot{u}_{ai} \int_{\tau_o}^{\tau_i} \frac{\eta B'}{2\sqrt{\Phi_C}} h_{a\gamma}^{(I)} d\tau \end{aligned} \quad (2.446)$$

$$\begin{aligned} &+ \frac{\dot{\xi}_o^2}{\xi_i} \left(\frac{\dot{\xi}_i}{\xi_i^2} \left(\dot{u}_{ai} h_{a\gamma i}^{(R)} + \dot{u}_{yi} h_{a\bar{a}i} \right) - \frac{1}{\xi_i} \left(\dot{u}_{ai} \dot{h}_{a\gamma i}^{(R)} - \frac{N_i}{4\Phi_C} M h_{a\bar{a}i} + \dot{u}_{yi} \dot{h}_{a\bar{a}i} \right) \right) + \frac{\dot{\xi}_o^2}{\xi_i^2} \frac{\eta B_i}{2\sqrt{\Phi_C}} \dot{u}_{ai} h_{a\gamma i}^{(I)}, \\ S_{a\bar{a}\gamma i}^{(I)} &= \frac{\dot{\xi}_o^2}{\xi_i} \dot{u}_{yi} \int_{\tau_o}^{\tau_i} \left[\frac{L_1}{4\Phi_C} u_a^2 h_{a\gamma}^{(I)} + \frac{\eta}{8\sqrt{\Phi_C}} (4B' h_{a\bar{a}} - B'' u_a^2) \right] d\tau \\ &- \frac{\dot{\xi}_o^2}{\xi_i} \dot{u}_{ai} \int_{\tau_o}^{\tau_i} \left(\frac{L_1}{4\Phi_C} u_a u_{\gamma} h_{a\gamma}^{(I)} - \frac{\eta B'}{2\sqrt{\Phi_C}} h_{a\gamma}^{(R)} \right) d\tau + \frac{\dot{\xi}_o^2}{\xi_i} \left(\frac{\dot{\xi}_i}{\xi_i^2} \dot{u}_{ai} h_{a\gamma i}^{(I)} - \frac{1}{\xi_i} \dot{u}_{ai} \dot{h}_{a\gamma i}^{(I)} \right) \\ &- \frac{\dot{\xi}_o^2}{\xi_i} \frac{\eta B_i}{2\sqrt{\Phi_C}} \left(-\frac{\dot{\xi}_i}{\xi_i^2} u_{yi} h_{a\bar{a}i} + \frac{1}{\xi_i} \dot{u}_{ai} h_{a\gamma i}^{(R)} + \frac{1}{\xi_i} \dot{u}_{yi} h_{a\bar{a}i} + \frac{1}{\xi_i} u_{yi} \dot{h}_{a\bar{a}i} \right). \end{aligned} \quad (2.447)$$

That of the coma-radius type is

$$\begin{aligned} S_{a\bar{a}\gamma i}^{(R)} &= \frac{1}{\xi_i} \dot{u}_{yi} \left(C_{KRo} + \frac{\xi_o^2}{\xi_i} \dot{u}_{ai}^2 h_{a\gamma i}^{(R)} \right) \\ &- \frac{\dot{\xi}_o}{\xi_i} \dot{u}_{ai} \left(C_{Ao} + \frac{\dot{\xi}_o}{\xi_i} \dot{u}_{ai} \dot{u}_{yi} h_{a\gamma i}^{(R)} \right) + \frac{\dot{\xi}_o^2}{\xi_i} \left(\frac{\dot{\xi}_i}{\xi_i^2} \dot{u}_{ai} h_{a\gamma i}^{(R)} - \frac{1}{\xi_i} \dot{u}_{ai} \dot{h}_{a\gamma i}^{(R)} \right) \end{aligned} \quad (2.448)$$

$$\begin{aligned} S_{a\bar{a}\gamma i}^{(I)} &= \frac{1}{\xi_i} \dot{u}_{yi} \left(C_{KRo} - \frac{\dot{\xi}_o^2}{\xi_i} \dot{u}_{ai}^2 h_{a\gamma i}^{(I)} \right) \\ &+ \frac{\dot{\xi}_o}{\xi_i} \dot{u}_{ai} \left(C_{ao} + \frac{\dot{\xi}_o}{\xi_i} \dot{u}_{ai} \dot{u}_{yi} h_{a\gamma i}^{(I)} \right) + \frac{\dot{\xi}_o^2}{\xi_i} \left(-\frac{\dot{\xi}_i}{\xi_i} \dot{u}_{ai} h_{a\gamma i}^{(I)} + \frac{1}{\xi_i} \dot{u}_{ai} \dot{h}_{a\gamma i}^{(I)} \right). \end{aligned} \quad (2.449)$$

That of the field-curvature type is

$$\begin{aligned}
S_{\alpha\gamma\bar{\gamma}i}^{(R)} &= \frac{1}{\zeta_i} \dot{u}_{\gamma i} \left(C_{Fo} + \frac{\zeta_o}{\zeta_i} \left(\dot{u}_{ai}^2 h_{\gamma\bar{\gamma}i} + \dot{u}_{ai} \dot{u}_{\gamma i} h_{\alpha\gamma i}^{(R)} \right) \right) \\
&- \frac{\zeta_o}{\zeta_i} \dot{u}_{ai} \int_{\tau_o}^{\tau_i} \frac{1}{32\Phi_C} \left[8L_1 \left(u_{\alpha} u_{\gamma} h_{\gamma\bar{\gamma}} + u_{\gamma}^2 h_{\alpha\gamma}^{(R)} \right) - 2L_2 u_{\alpha} u_{\gamma}^3 \right] d\tau \\
&- \frac{\zeta_o}{\zeta_i} \left(-\frac{\zeta_i}{\zeta_i^2} \left(\dot{u}_{ai} h_{\gamma\bar{\gamma}i} + \dot{u}_{\gamma i} h_{\alpha\gamma i}^{(R)} \right) - \frac{N_i}{4\zeta_i \Phi_C} M h_{\alpha\gamma i}^{(R)} + \frac{1}{\zeta_i} \left(\dot{u}_{ai} \dot{h}_{\gamma\bar{\gamma}i} + \dot{u}_{\gamma i} \dot{h}_{\alpha\gamma i}^{(R)} \right) \right)
\end{aligned} \tag{2.450}$$

$$\begin{aligned}
&+ \frac{\zeta_o}{\zeta_i} \frac{\eta B_i'}{2\sqrt{\Phi_C}} M h_{\alpha\gamma i}^{(I)} - \frac{\zeta_o}{\zeta_i} \frac{\eta B_i}{2\sqrt{\Phi_C}} \left(-\frac{\zeta_i}{\zeta_i^2} M h_{\alpha\gamma i}^{(I)} + \frac{1}{\zeta_i} M \dot{h}_{\alpha\gamma i}^{(I)} \right), \\
S_{\alpha\gamma\bar{\gamma}i}^{(I)} &= -\frac{\zeta_o}{\zeta_i} \dot{u}_{\gamma i} \int_{\tau_o}^{\tau_i} \left(\frac{L_1}{4\Phi_C} u_{\alpha} u_{\gamma} h_{\alpha\gamma}^{(I)} - \frac{\eta B'}{2\sqrt{\Phi_C}} h_{\alpha\gamma}^{(R)} \right) d\tau \\
&+ \frac{\zeta_o}{\zeta_i} \dot{u}_{ai} \int_{\tau_o}^{\tau_i} \left[\frac{L_1}{4\Phi_C} u_{\gamma}^2 h_{\alpha\gamma} - \frac{\eta}{8\sqrt{\Phi_C}} (4B' h_{\gamma\bar{\gamma}} - B'' u_{\gamma}^2) \right] d\tau \\
&+ \frac{\zeta_o}{\zeta_i} \left(-\frac{\zeta_i}{\zeta_i^2} \dot{u}_{\gamma i} h_{\alpha\gamma i}^{(I)} - \frac{N_i}{4\zeta_i \Phi_C} M h_{\alpha\gamma}^{(I)} + \frac{1}{\zeta_i} \dot{u}_{\gamma i} \dot{h}_{\alpha\gamma i}^{(I)} \right) \\
&- \frac{\zeta_o}{\zeta_i} \frac{\eta B_i}{2\sqrt{\Phi_C}} \left(-\frac{\zeta_i}{\zeta_i^2} M h_{\alpha\gamma i}^{(R)} + \frac{1}{\zeta_i} \left(\dot{u}_{ai} h_{\gamma\bar{\gamma}i} + \dot{u}_{\gamma i} h_{\alpha\gamma i}^{(R)} \right) + \frac{1}{\zeta_i} M \dot{h}_{\alpha\gamma i}^{(R)} \right).
\end{aligned} \tag{2.451}$$

That of the astigmatism type is

$$\begin{aligned}
S_{\alpha\gamma\bar{\gamma}i}^{(R)} &= \frac{1}{\zeta_i} \dot{u}_{\gamma i} \left(C_{Ao} + \frac{\zeta_o}{\zeta_i} \dot{u}_{ai} \dot{u}_{\gamma i} h_{\alpha\gamma i}^{(R)} - \frac{\zeta_o \eta B_i}{2\zeta_i \sqrt{\Phi_C}} h_{\alpha\gamma i}^{(I)} \right) \\
&- \frac{\zeta_o}{\zeta_i} \dot{u}_{ai} \int_{\tau_o}^{\tau_i} \frac{1}{32\Phi_C} \left(8L_1 u_{\gamma}^2 h_{\alpha\gamma}^{(R)} - L_2 u_{\alpha} u_{\gamma}^3 \right) d\tau \\
&- \frac{\zeta_o}{\zeta_i} \left(-\frac{\zeta_i}{\zeta_i^2} \dot{u}_{\gamma i} h_{\alpha\gamma i}^{(R)} - \frac{N_i}{4\zeta_i \Phi_C} M h_{\alpha\gamma i}^{(R)} + \frac{1}{\zeta_i} \dot{u}_{\gamma i} \dot{h}_{\alpha\gamma i}^{(R)} \right) \\
&+ \frac{\zeta_o}{\zeta_i} \frac{\eta B}{2\sqrt{\Phi_C}} \left(-\frac{\zeta_i}{\zeta_i^2} M h_{\alpha\gamma i}^{(I)} + \frac{1}{\zeta_i} \dot{u}_{\gamma i} h_{\alpha\gamma i}^{(I)} + \frac{1}{\zeta_i} M \dot{h}_{\alpha\gamma i}^{(I)} \right),
\end{aligned} \tag{2.452}$$

$$\begin{aligned}
S_{\alpha\gamma\bar{\gamma}i}^{(I)} &= \frac{1}{\zeta_i} \dot{u}_{\gamma i} \left(C_{ao} + \frac{\zeta_o}{\zeta_i} \dot{u}_{ai} \dot{u}_{\gamma i} h_{\alpha\gamma i}^{(I)} \right) - \frac{\zeta_o}{\zeta_i} \dot{u}_{ai} \int_{\tau_o}^{\tau_i} \left(\frac{L_1}{4\Phi_C} u_{\gamma}^2 h_{\alpha\gamma} - \frac{\eta B''}{16\sqrt{\Phi_C}} u_{\gamma}^2 \right) d\tau \\
&- \frac{\zeta_o}{\zeta_i} \left(-\frac{\zeta_i}{\zeta_i^2} \dot{u}_{\gamma i} h_{\alpha\gamma i}^{(I)} - \frac{N_i}{4\zeta_i \Phi_C} M h_{\alpha\gamma}^{(I)} + \frac{1}{\zeta_i} \dot{u}_{\gamma i} \dot{h}_{\alpha\gamma i}^{(I)} \right) - \frac{\zeta_o}{\zeta_i} \frac{\eta B_i}{2\sqrt{\Phi_C}} \left(-\frac{\zeta_i}{\zeta_i^2} M h_{\alpha\gamma i}^{(R)} + \frac{1}{\zeta_i} M \dot{h}_{\alpha\gamma i}^{(R)} \right).
\end{aligned} \tag{2.453}$$

That of the distortion type is

$$\begin{aligned}
S_{\gamma\bar{\gamma}i}^{(R)} &= \frac{1}{\zeta_i} \dot{u}_{\gamma i} \left(C_{Do} + \frac{1}{\zeta_i} \dot{u}_{ai} \dot{u}_{\gamma i} h_{\gamma\bar{\gamma}i} \right) - \frac{1}{\zeta_i} \dot{u}_{ai} \int_{\tau_o}^{\tau_i} \frac{1}{32\Phi_C} (8L_1 u_{\gamma}^2 h_{\gamma\bar{\gamma}} - L_2 u_{\gamma}^4) d\tau \\
&+ \frac{1}{\zeta_i} \left(\frac{\zeta_i}{\zeta_i^2} \dot{u}_{\gamma i} h_{\gamma\bar{\gamma}i} + \frac{N_i}{4\zeta_i \Phi_C} M h_{\gamma\bar{\gamma}i} - \frac{1}{\zeta_i} \dot{u}_{\gamma i} \dot{h}_{\gamma\bar{\gamma}i} \right),
\end{aligned} \tag{2.454}$$

$$\begin{aligned}
S_{\gamma\bar{\gamma}i}^{(I)} &= \frac{1}{\zeta_i} \dot{u}_{\gamma i} C_{do} - \frac{1}{\zeta_i} \frac{\eta B_i''}{16\sqrt{\Phi_C}} u_{\gamma i}^3 + \frac{1}{\zeta_i} \frac{\eta B_i}{2\sqrt{\Phi_C}} \left(\frac{\zeta_i}{\zeta_i^2} u_{\gamma i} h_{\gamma\bar{\gamma}i} - \frac{1}{\zeta_i} u_{\gamma i} \dot{h}_{\gamma\bar{\gamma}i} \right) + \frac{1}{\zeta_i} \frac{\eta B_o''}{16\sqrt{\Phi_C}} \dot{u}_{ai}.
\end{aligned} \tag{2.455}$$

2.13.5 The paraxial trajectories and the path and the slope deviations and aberrations in the Cartesian coordinate system

Here, the relationship between the expressions of trajectories and slope in the Cartesian coordinate system and those in the rotation coordinate system is discussed. Once that relation is given, it shall be sufficient to calculate only the rotation coordinate system. The basic relationship of the trajectories between the coordinate systems is

$$w = e^{ix}u, \quad \dot{w} = e^{ix}(\dot{u} + i\dot{x}u). \quad (2.456)$$

These equations shall be valid not only for the paraxial trajectories, but also for the path and the slope deviations and aberrations of the same type. By Eq. (2.456), the initial lateral position and the initial lateral reduced velocity in the Cartesian coordinate are related to those in the rotation coordinate as follows:

$$w_o = u_o, \quad \dot{w}_o = \dot{u}_o + i\dot{x}_o u_o. \quad (2.457)$$

The difference appears in the initial reduced velocity of the electron, which starts at an off-axis point, if the rotationally symmetric magnetic field overlaps with the object plane, because the Lorentz force gives the velocity in the azimuthal direction to the electron, which passes through the off-axis position. Similar to the case in the rotation coordinate system, the paraxial trajectory in the Cartesian coordinate system is also given by

$$w^{(1)} = w_o w_\gamma + \dot{w}_o w_\alpha, \quad \dot{w}^{(1)} = w_o \dot{w}_\gamma + \dot{w}_o \dot{w}_\alpha, \quad (2.458)$$

where the initial conditions of the fundamental rays are given by

$$\begin{aligned} w_{\gamma o} &= 1, & \dot{w}_{\gamma o} &= 0, \\ w_{\alpha o} &= 0, & \dot{w}_{\alpha o} &= 1. \end{aligned} \quad (2.459)$$

Taking into account Eqs. (2.456) and (2.458), the fundamental rays in the Cartesian coordinate system are related to those in the rotation coordinate system as follows:

$$\begin{aligned} w_\gamma &= e^{ix}(u_\gamma - i\dot{x}_o u_\alpha), & w_\alpha &= e^{ix}u_\alpha, \\ \dot{w}_\gamma &= e^{ix}(\dot{u}_\gamma + \dot{x}_o \dot{x}u_\alpha + i(\dot{x}u_\gamma - \dot{x}_o \dot{u}_\alpha)), & \dot{w}_\alpha &= e^{ix}(\dot{u}_\alpha + i\dot{x}u_\alpha). \end{aligned} \quad (2.460)$$

The values of the fundamental rays in the image plane are

$$\begin{aligned} w_{\gamma i} &= e^{ix_i}M, & w_{\alpha i} &= 0, \\ \dot{w}_{\gamma i} &= e^{ix_i}\left(\dot{u}_{\gamma i} + i\left(\dot{x}_i M - \frac{1}{M}\dot{x}_o\right)\right), & \dot{w}_{\alpha i} &= \frac{1}{M}e^{ix_i}. \end{aligned} \quad (2.461)$$

In the Cartesian coordinate system, the position and the reduced velocity of the paraxial trajectories in the image plane are

$$\begin{aligned} w_i^{(1)} &= e^{ix_i}Mw_o, \\ \dot{w}_i^{(1)} &= e^{ix_i}\left[\left\{\dot{u}_{\gamma i} + i\left(\dot{x}_i M - \frac{1}{M}\dot{x}_o\right)\right\}w_o + \frac{1}{M}\dot{w}_o\right] \\ &= \left\{\frac{\dot{u}_{\gamma i}}{M} + i\left(\dot{x}_i - \frac{1}{M^2}\dot{x}_o\right)\right\}w_i^{(1)} + v_{wi}. \end{aligned} \quad (2.462)$$

where v_{wi} is the lateral reduced velocity for the axial trajectory component in the image plane. Through v_{wi} , the complex slope value for the axial trajectory component in the image plane is related to that in the object plane as follows:

$$\hat{s}_i = \frac{1}{\hat{z}_i} v_{wi} = \frac{1}{\hat{z}_i} \frac{1}{M} e^{i\chi_i} \dot{w}_o = e^{i\chi_i} M_\alpha w_o. \quad (2.463)$$

Note that the hat of s shows that the slope is defined in the Cartesian coordinate system. We consider the path deviation in the Cartesian coordinate system as follows:

$$\begin{aligned} \Delta w_{geo}^{(3)} &= \hat{w}_{aa\bar{a}} \dot{w}_o^2 \bar{w}_o + \hat{w}_{a\bar{a}\gamma} w_o \dot{w}_o \bar{w}_o + \hat{w}_{a\bar{a}\bar{\gamma}} \bar{w}_o \dot{w}_o^2 \\ &+ \hat{w}_{a\gamma\bar{\gamma}} w_o \bar{w}_o \dot{w}_o + \hat{w}_{\bar{a}\gamma\gamma} w_o^2 \dot{w}_o + \hat{w}_{\gamma\bar{\gamma}\bar{\gamma}} w_o^2 \bar{w}_o. \end{aligned} \quad (2.464)$$

The path deviation in the rotation coordinate system is

$$\begin{aligned} \Delta u_{geo}^{(3)} &= (\hat{u}_{aa\bar{a}}^{(R)} + i\hat{u}_{aa\bar{a}}^{(I)}) \dot{u}_o^2 \bar{u}_o + (\hat{u}_{a\bar{a}\gamma}^{(R)} + i\hat{u}_{a\bar{a}\gamma}^{(I)}) u_o \dot{u}_o \bar{u}_o + (\hat{u}_{a\bar{a}\bar{\gamma}}^{(R)} + i\hat{u}_{a\bar{a}\bar{\gamma}}^{(I)}) \bar{u}_o \dot{u}_o^2 \\ &+ (\hat{u}_{a\gamma\bar{\gamma}}^{(R)} + i\hat{u}_{a\gamma\bar{\gamma}}^{(I)}) u_o \bar{u}_o \dot{u}_o + (\hat{u}_{\bar{a}\gamma\gamma}^{(R)} + i\hat{u}_{\bar{a}\gamma\gamma}^{(I)}) u_o^2 \bar{u}_o + (\hat{u}_{\gamma\bar{\gamma}\bar{\gamma}}^{(R)} + i\hat{u}_{\gamma\bar{\gamma}\bar{\gamma}}^{(I)}) u_o^2 \bar{u}_o. \end{aligned} \quad (2.465)$$

Taking into account Eqs. (2.458) to (2.464), the coefficient in Eq. (2.465) are given by

$$\begin{aligned} \hat{w}_{aa\bar{a}} &= e^{i\chi} \left(\hat{u}_{aa\bar{a}}^{(R)} + i\hat{u}_{aa\bar{a}}^{(I)} \right), \\ \hat{w}_{a\bar{a}\gamma} &= e^{i\chi} \left[\hat{u}_{a\bar{a}\gamma}^{(R)} + 2\dot{\chi}_o \hat{u}_{aa\bar{a}}^{(I)} + i \left(\hat{u}_{a\bar{a}\gamma}^{(I)} - 2\dot{\chi}_o \hat{u}_{aa\bar{a}}^{(R)} \right) \right], \\ \hat{w}_{a\bar{a}\bar{\gamma}} &= e^{i\chi} \left[\hat{u}_{a\bar{a}\bar{\gamma}}^{(R)} - \dot{\chi}_o \hat{u}_{aa\bar{a}}^{(I)} + i \left(\hat{u}_{a\bar{a}\bar{\gamma}}^{(I)} + \dot{\chi}_o \hat{u}_{aa\bar{a}}^{(R)} \right) \right], \\ \hat{w}_{a\gamma\bar{\gamma}} &= e^{i\chi} \left[\hat{u}_{a\gamma\bar{\gamma}}^{(R)} + 2\dot{\chi}_o \hat{u}_{a\bar{a}\bar{\gamma}}^{(I)} - \dot{\chi}_o \hat{u}_{a\bar{a}\gamma}^{(R)} + 2\dot{\chi}_o^2 \hat{u}_{aa\bar{a}}^{(R)} \right. \\ &\quad \left. + i \left(\hat{u}_{a\gamma\bar{\gamma}}^{(I)} - 2\dot{\chi}_o \hat{u}_{a\bar{a}\bar{\gamma}}^{(R)} + \dot{\chi}_o \hat{u}_{a\bar{a}\gamma}^{(R)} + 2\dot{\chi}_o^2 \hat{u}_{aa\bar{a}}^{(I)} \right) \right], \\ \hat{w}_{\bar{a}\gamma\gamma} &= e^{i\chi} \left[\hat{u}_{\bar{a}\gamma\gamma}^{(R)} + \dot{\chi}_o \hat{u}_{a\bar{a}\gamma}^{(I)} - \dot{\chi}_o^2 \hat{u}_{aa\bar{a}}^{(R)} + i \left(\hat{u}_{\bar{a}\gamma\gamma}^{(I)} - \dot{\chi}_o \hat{u}_{a\bar{a}\gamma}^{(R)} - \dot{\chi}_o^2 \hat{u}_{aa\bar{a}}^{(I)} \right) \right], \\ \hat{w}_{\gamma\bar{\gamma}\bar{\gamma}} &= e^{i\chi} \left[\hat{u}_{\gamma\bar{\gamma}\bar{\gamma}}^{(R)} + \dot{\chi}_o \left(\hat{u}_{a\gamma\bar{\gamma}}^{(I)} - \hat{u}_{\bar{a}\gamma\gamma}^{(I)} \right) + \dot{\chi}_o^2 \left(\hat{u}_{a\bar{a}\gamma}^{(R)} - \hat{u}_{a\bar{a}\bar{\gamma}}^{(R)} \right) + \dot{\chi}_o^3 \hat{u}_{aa\bar{a}}^{(I)} \right. \\ &\quad \left. + i \left\{ \hat{u}_{\gamma\bar{\gamma}\bar{\gamma}}^{(I)} - \dot{\chi}_o \left(\hat{u}_{a\gamma\bar{\gamma}}^{(R)} - \hat{u}_{\bar{a}\gamma\gamma}^{(R)} \right) + \dot{\chi}_o^2 \left(\hat{u}_{a\bar{a}\gamma}^{(I)} - \hat{u}_{a\bar{a}\bar{\gamma}}^{(I)} \right) - \dot{\chi}_o^3 \hat{u}_{aa\bar{a}}^{(R)} \right\} \right]. \end{aligned} \quad (2.466)$$

Note that, if the object plane is located inside the magnetic-field free space, then, $\dot{\chi}_o = 0$ and Eq. (2.466) become much simpler.

The aberration in the Cartesian coordinate system is also defined as the value of the path deviation at the image plane. Here, we introduce the aberration coefficients of the Cartesian coordinate system defined in the image plane, which are parameterized by the position and the slope in the image plane for the Cartesian coordinate system, as follows:

$$\Delta w_{geot}^{(3)} = \hat{C}_{Si} \hat{s}_i^2 \bar{s}_i + \hat{K}_{Li} w_i^{(1)} \hat{s}_i \bar{s}_i + \hat{R}_{Li} \bar{w}_i^{(1)} \hat{s}_i^2 + \hat{C}_{Fi} w_i^{(1)} \bar{w}_i^{(1)} \hat{s}_i + \hat{A}_i w_i^{(1)2} \bar{s}_i + \hat{D}_i w_i^{(1)2} \bar{w}_i^{(1)}. \quad (2.467)$$

where coefficients with the hat are defined in the Cartesian coordinate system.

The coefficients in Eq. (2.467) relate to the aberration coefficients in the rotation coordinate system as follows:

$$\begin{aligned} \hat{C}_{Si} &= C_{Si}, \quad \hat{R}_{Li} = K_{Li} - i \frac{2}{\dot{\chi}_o} \dot{\chi}_o C_{Si}, \quad \hat{R}_{Li} = R_{Li} + i \frac{1}{\dot{\chi}_o} \dot{\chi}_o C_{Si}, \\ \hat{C}_{Fi} &= C_{Fi} - \frac{4}{\dot{\chi}_o} \dot{\chi}_o C_{Ki} + \frac{2}{\dot{\chi}_o^2} \dot{\chi}_o^2 C_{Si}, \quad \hat{A}_i = A_i - i \frac{1}{\dot{\chi}_o} \dot{\chi}_o K_{Li} - \frac{1}{\dot{\chi}_o^2} \dot{\chi}_o^2 C_{Si}, \\ \hat{D}_i &= D_i - \frac{1}{\dot{\chi}_o} \dot{\chi}_o C_{Ai} + \frac{1}{\dot{\chi}_o^2} \dot{\chi}_o^2 C_{Ki} + i \left\{ -\frac{1}{\dot{\chi}_o} \dot{\chi}_o (C_{Fi} - C_{Ai}) + \frac{3}{\dot{\chi}_o^2} \dot{\chi}_o^2 C_{Ki} - \frac{1}{\dot{\chi}_o^3} \dot{\chi}_o^3 C_{Si} \right\}, \end{aligned} \quad (2.468)$$

If the object plane is located inside the magnetic field-free space, the aberration coefficients define in the image plane for the Cartesian coordinate system are exactly the same as those for the rotation coordinate system. We consider the

slope deviation and the slope aberration in the Cartesian coordinate system. Because of Eq. (2.456), the geometrical third-order deviation of the lateral reduced velocity and the slope deviation are given by

$$\Delta \dot{w}_{geo}^{(3)} = e^{i\chi} \left(\Delta \dot{u}_{geo}^{(3)} + i\dot{\chi} \Delta u_{geo}^{(3)} \right), \quad \Delta w_{geo}^{(3)'} = \frac{1}{\dot{\chi}} e^{i\chi} \left(\Delta \dot{u}_{geo}^{(3)} + i\dot{\chi} \Delta u_{geo}^{(3)} \right). \quad (2.469)$$

Then, using slope deviations and path deviations in the rotation coordinate system, the total third-order geometrical slope deviation in the Cartesian coordinate system is expressed as follows:

$$\begin{aligned} \Delta w_{geo}^{(3)'} &= e^{i\chi} \left(S_{aa\bar{a}}^{(R)} + iS_{aa\bar{a}}^{(I)} + i\frac{\dot{\chi}}{\dot{\chi}} \dot{\chi}_o^3 (\hat{u}_{aa\bar{a}}^{(R)} + i\hat{u}_{aa\bar{a}}^{(I)}) \right) u_o'^2 \bar{u}_o' \\ &+ e^{i\chi} \left(S_{a\bar{a}y}^{(R)} + iS_{a\bar{a}y}^{(I)} + i\frac{\dot{\chi}}{\dot{\chi}} \dot{\chi}_o^2 (\hat{u}_{a\bar{a}y}^{(R)} + i\hat{u}_{a\bar{a}y}^{(I)}) \right) u_o u_o' \bar{u}_o' + e^{i\chi} \left(S_{a\bar{a}y}^{(R)} + iS_{a\bar{a}y}^{(I)} + i\frac{\dot{\chi}}{\dot{\chi}} \dot{\chi}_o^2 (\hat{u}_{a\bar{a}y}^{(R)} + i\hat{u}_{a\bar{a}y}^{(I)}) \right) \bar{u}_o u_o'^2 \\ &+ e^{i\chi} \left(S_{a\bar{y}y}^{(R)} + iS_{a\bar{y}y}^{(I)} + i\frac{\dot{\chi}}{\dot{\chi}} \dot{\chi}_o (\hat{u}_{a\bar{y}y}^{(R)} + i\hat{u}_{a\bar{y}y}^{(I)}) \right) u_o \bar{u}_o u_o' + e^{i\chi} \left(S_{a\bar{y}y}^{(R)} + iS_{a\bar{y}y}^{(I)} + i\frac{\dot{\chi}}{\dot{\chi}} \dot{\chi}_o (\hat{u}_{a\bar{y}y}^{(R)} + i\hat{u}_{a\bar{y}y}^{(I)}) \right) u_o'^2 \bar{u}_o' \\ &+ e^{i\chi} \left(S_{y\bar{y}y}^{(R)} + iS_{y\bar{y}y}^{(I)} + i\frac{\dot{\chi}}{\dot{\chi}} \dot{\chi}_o (\hat{u}_{y\bar{y}y}^{(R)} + i\hat{u}_{y\bar{y}y}^{(I)}) \right) u_o'^2 \bar{u}_o'. \end{aligned} \quad (2.470)$$

The slope aberration is obtained by evaluating Eq. (2.470) in the image plane, as follows:

$$\begin{aligned} \Delta w_{geoi}^{(3)'} &= e^{i\chi_i} \left[S_{aa\bar{a}i}^{(R)} + i \left(S_{aa\bar{a}i}^{(I)} + \frac{\dot{\chi}_i}{\dot{\chi}_i} MC_{so} \right) \right] u_o'^2 \bar{u}_o' \\ &+ e^{i\chi_i} \left[\left(S_{a\bar{a}yi}^{(R)} - 2\frac{\dot{\chi}_i}{\dot{\chi}_i} MC_{ko} \right) + i \left(S_{a\bar{a}yi}^{(I)} + 2\frac{\dot{\chi}_i}{\dot{\chi}_i} MC_{ko} \right) \right] u_o u_o' \bar{u}_o' \\ &+ e^{i\chi_i} \left[\left(S_{a\bar{a}yi}^{(R)} + \frac{\dot{\chi}_i}{\dot{\chi}_i} MC_{ko} \right) + i \left(S_{a\bar{a}yi}^{(I)} + \frac{\dot{\chi}_i}{\dot{\chi}_i} MC_{ko} \right) \right] \bar{u}_o u_o'^2 + e^{i\chi_i} \left[S_{a\bar{y}yi}^{(R)} + i \left(S_{a\bar{y}yi}^{(I)} + \frac{\dot{\chi}_i}{\dot{\chi}_i} MC_{ro} \right) \right] u_o \bar{u}_o u_o' \\ &+ e^{i\chi_i} \left[\left(S_{a\bar{y}yi}^{(R)} - \frac{\dot{\chi}_i}{\dot{\chi}_i} MC_{ao} \right) + i \left(S_{a\bar{y}yi}^{(I)} + \frac{\dot{\chi}_i}{\dot{\chi}_i} MC_{ao} \right) \right] u_o'^2 \bar{u}_o' \\ &+ e^{i\chi_i} \left[\left(S_{y\bar{y}yi}^{(R)} - \frac{\dot{\chi}_i}{\dot{\chi}_i} MC_{do} \right) + i \left(S_{y\bar{y}yi}^{(I)} + \frac{\dot{\chi}_i}{\dot{\chi}_i} MC_{do} \right) \right] u_o'^2 \bar{u}_o'. \end{aligned} \quad (2.471)$$

Note that, despite these slope deviations and slope aberrations being estimated in the Cartesian coordinate system, for simplicity, the geometrical parameters in Eqs. (2.470) and (2.471) are still the lateral initial position and the lateral initial slope at the object plane for the rotation coordinate system. If the object plane is located inside the magnetic field-free space, u_o and u_o' in Eqs. (2.470) and (2.471) can be replaced by w_o and w_o' , respectively. Otherwise, appropriate transformation is necessary to change the parameters. This transformation can be derived by the same procedure used when the path deviation and the aberration in the Cartesian coordinate system were discussed.

In addition, if the object plane is located inside the magnetic field-free space, we give the slope aberration expression parametrized by the axial slope and the lateral position of the paraxial order in the image plane:

$$\begin{aligned} \Delta w_{geoi}^{(3)'} &= \left[\frac{1}{M_\alpha^3} S_{aa\bar{a}i}^{(R)} + i \left(\frac{1}{M_\alpha^3} S_{aa\bar{a}i}^{(I)} + \frac{\dot{\chi}_i}{\dot{\chi}_i} C_{si} \right) \right] \hat{s}_i^2 \bar{s}_i \\ &+ \left[\left(\frac{1}{MM_\alpha^2} S_{a\bar{a}yi}^{(R)} - 2\frac{\dot{\chi}_i}{\dot{\chi}_i} C_{ki} \right) + i \left(\frac{1}{MM_\alpha^2} S_{a\bar{a}yi}^{(I)} + 2\frac{\dot{\chi}_i}{\dot{\chi}_i} C_{ki} \right) \right] w_i^{(1)} \hat{s}_i \bar{s}_i \\ &+ \left[\left(\frac{1}{MM_\alpha^2} S_{a\bar{a}yi}^{(R)} + \frac{\dot{\chi}_i}{\dot{\chi}_i} C_{ki} \right) + i \left(\frac{1}{MM_\alpha^2} S_{a\bar{a}yi}^{(I)} + \frac{\dot{\chi}_i}{\dot{\chi}_i} C_{ki} \right) \right] \bar{w}_i^{(1)} \hat{s}_i^2 \\ &+ \left[\frac{1}{M^2 M_\alpha} S_{a\bar{y}yi}^{(R)} + i \left(\frac{1}{M^2 M_\alpha} S_{a\bar{y}yi}^{(I)} + \frac{\dot{\chi}_i}{\dot{\chi}_i} C_{fi} \right) \right] w_i^{(1)} \bar{w}_i^{(1)} \hat{s}_i \\ &+ \left[\left(\frac{1}{M^2 M_\alpha} S_{a\bar{y}yi}^{(R)} - \frac{\dot{\chi}_i}{\dot{\chi}_i} C_{ai} \right) + i \left(\frac{1}{M^2 M_\alpha} S_{a\bar{y}yi}^{(I)} + \frac{\dot{\chi}_i}{\dot{\chi}_i} C_{ai} \right) \right] w_i^{(1)2} \bar{s}_i \\ &+ \left[\left(\frac{1}{M^3} S_{y\bar{y}yi}^{(R)} - \frac{\dot{\chi}_i}{\dot{\chi}_i} C_{di} \right) + i \left(\frac{1}{M^3} S_{y\bar{y}yi}^{(I)} + \frac{\dot{\chi}_i}{\dot{\chi}_i} C_{di} \right) \right] w_i^{(1)2} \bar{w}_i^{(1)}. \end{aligned} \quad (2.472)$$

2.14 References

- [1.82] V.M. Kel'man, L.M. Sekunova, E.M. Yakushev, Theory of axisymmetric electron mirrors. I. Trajectory equations. *Sov. Phys. Tech. Phys.* **18**, (1973) 1142-1146.
- [1.83] V.M. Kel'man, L.M. Sekunova, E.M. Yakushev, Theory of axisymmetric electron mirrors. II. Electron-optical properties. *Sov. Phys. Tech. Phys.* **18**, (1973) 1147-1152.
- [1.84] T.D. Daumenov, A.A. Sapargaliev, E.M. Yakushev, A new method for deriving the characteristic function of charged particles in electron-optical systems with a straight optical axis, *Sov. Phys. Tech. Phys.* **23**, (1978) 1400-1404.
- [1.85] S.B. Bimurzaev, E.M. Yakushev, Methods of parameterization of exact electron trajectory equations, *Proc. SPIE* **5398**, (2004) 51-58.
- [1.86] E.M. Yakushev, L.M. Sekunova, Theory of electron mirrors and cathode lenses, *Adv. Electron. Electron Phys.* **68**, (1986) 337-419.
- [1.87] E.M. Yakushev, Theory and Computation of Electron Mirrors: The Central Particle Method, *Adv. Imaging. Electron Phys.* **178**, (2013) 147-247.
- [1.88] H. Rose, D. Preikszas, Time-dependent perturbation formalism for calculating the aberrations of systems with large ray gradients, *Nucl. Instrum. Meth. A* **363**, (1995) 301-315. doi: [https://doi.org/10.1016/0168-9002\(95\)00065-8](https://doi.org/10.1016/0168-9002(95)00065-8).
- [1.89] D. Preikszas, H. Rose, Correction properties of electron mirrors, *J. Electron. Microsc.* **1** (1997) 1-9. doi:
- [1.90] P. Hawkes, E. Kasper, Principles of Electron Optics, second ed., Vol. 1, Basic Geometrical Optics, Academic Press, London, 2017, Chap. 18 pp. 281-295 and Chap. 28 pp. 471-484.
- [1.91] H. Rose, Geometrical Charged Particle Optics, second ed., Springer, Berlin, Heidelberg, 2013. doi: <https://doi.org/10.1007/978-3-540-85916-1>.

Chapter 3 3rd-order relativistic aberration theory for the systems of round symmetric electromagnetic fields and deflectors

3.1 Introduction

Since electron mirrors reflect the incident electron beam along the optic axis without any deflection effects on electrons, the only possible electron optical system is as follows: an electron gun and an electron mirror face each other, and their central axes coincide with the common optic axis. This system is useless as a scientific apparatus because an emitted electron beam from the gun travels to the mirror, is reflected by the electron mirror, and returns to the electron gun. To utilize an electron mirror as an electron optical element, the trajectories of incident electrons to the mirror must be separated from those of reflected electrons. In previous research on systems of electron mirrors, e.g., references [3.1]-[3.3], bending magnets, called beam separators, are used because a magnetic dipole field deflects an incident beam and a reflected beam in directions opposite to each other. However, due to the size of normal electron mirrors, the size of a bending magnet becomes large, such as a square of a few hundred millimeters, and the resulting bent angle of electrons reaches 90 degrees or more. Such a large angle deflection causes significant aberrations. Special designs of beam separators and beam alignment methods inside a beam separator are investigated to suppress large deflection aberrations [3.4]-[3.7]. For that purpose, a very complicated aberration theory of a curved optic axis was constructed.

It regards a central electron trajectory of a beam, whose path is bent and curved by a magnet, as an optic axis. Fields are expanded around this curved optic axis, and lateral rays, and even aberrations are defined with respect to the curved axis. As long as a ray and its slope are measured as distance and relative slope from the curved axis, they remain small values, and the perturbation method can be used for aberration calculation. However, the theory of the curved optic axis is not easy to understand and use.

The goal of this thesis is to provide a conceptual design of an aberration-corrected SEM system using a miniature electron mirror. A small angle deflection, such as a few degrees, can guide an electron beam towards the mirror as long as the mirror size is sufficiently small. For small angle deflection, even if we use a straight optic axis, the lateral position and slope of deflected rays with respect to the optic axis remain small and we can expect that the perturbation method will provide a good approximation, as long as the beam deflection angle by deflectors is less than around 5 degrees. From the late 1970s to the early 1990s, the aberration theory of a system of focusing lenses and deflectors with respect to a straight optic axis, which was called deflection aberration theory, was investigated for the purpose of

analyzing an electron beam lithography system [3.8]-[3.17]. In previous research, even relativistic corrected fifth-order deflection aberration theory was derived. However, these articles are old and difficult to trace in their calculation, since details of derivations were not shown, and the used notation was unfamiliar. It is easier for the author to re-derive deflection aberration formulae than to check existing formulae.

Since deflection aberration theory is parametrized by not time, but by a coordinate of the optic axis, it cannot treat reflection by electron mirrors, and it is not directly applied to a mirror system with deflectors. However, when deflection fields and mirror fields do not overlap with each other, the contribution to aberrations from the deflection field part can be calculated by the deflection aberration theory. In addition, once we understand deflection aberration theory, we can introduce deflection fields into a time-dependent theory, which is discussed in Chapter 2, and can construct a time-dependent deflection aberration theory, which is used for analyzing a system including all focusing-lens fields, deflection fields, and mirror fields. This will be discussed in Chapter 4.

In this chapter, we provide a detailed review and re-derivation of the deflection theory of third-order geometrical aberration and second-rank aberrations based on references [3.8]-[3.10]. Since these references provide non-relativistic deflection theory for a system including focusing lenses and deflection fields, we re-derive the theory, taking into account relativistic correction. Throughout this chapter, we provide formulae, explanations, and interpretation of the theory compared with the original references [3.8]-[3.10]. In standard electron optics theory of focusing round symmetric lenses, we move to a rotation coordinate system to simplify the theory, since it cancels rotation by round symmetric magnetic fields. In Chapter 2, we also moved to a rotation coordinate system to construct an aberration theory of round symmetric mirror fields. However, since deflection fields are not rotationally symmetric, when viewed from a rotation coordinate, deflection fields rotate in the opposite direction to the direction of rotation of electrons by round symmetric magnetic fields. Since rotations never vanish in a rotation coordinate and there is no advantage to use it, deflection aberration theory is discussed in a Cartesian coordinate system.

In section 3.2, definitions of the coordinate system and deflection potentials, and the series expansion of both electrostatic and magnetic deflection potentials, which are parametrized by voltage and current of deflectors, are reviewed.

In section 3.3, the series expansion of the electron optical Lagrangian, also known as an eikonal, including deflection fields, is re-derived. The paraxial trajectory equation is introduced and the first-order deflection effect on electron trajectories, which is called the deflection trajectory, is re-derived.

From section 0, we consider systems including two independent deflectors and deflection aberration of a point beam, where contribution from an off-axis point in the object plane is ignored. In Section 3.4, third-order geometrical

aberration formulae of integral forms are re-derived. Since concrete expressions of formulae of deflection aberration coefficients are different for types of deflectors, i.e., deflectors being electrostatic or magnetic and differing for combinations of two deflectors' type, aberration formulae expressions here are given as general forms, which can be applied to both types and any combinations of deflectors.

From section 3.5, we discuss concrete expressions of the third-order geometrical aberration for the specific two deflectors' type. Fig. 3.1 shows a schematic of an example of an electron optical system where the considered theory of deflection aberrations discussed in this chapter can be applied. As an example, the two deflectors in Fig. 3.1 are a magnetic deflector and an electrostatic deflector. Additionally, we also discuss the cases where two deflectors are both electrostatic or both magnetic deflectors.

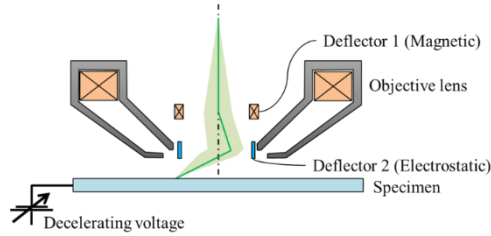


Fig. 3.1 Schematic of an example of an electron optical system where the considered theory of deflection aberrations can be applied. The system includes not only the magnetic objective lens, and the decelerating voltage imposed on the specimen, but also a magnetic deflector and an electrostatic deflector. The objective lens and the decelerating voltage generate rotationally symmetric magnetic and electrostatic fields, which focus the incident beam on the specimen, respectively. The magnetic deflector and the electrostatic deflector generate magnetic and electrostatic deflection fields, respectively. The deflection aberration theory discussed in this chapter allows the distributions of these fields along the optic axis to overlap with one another. In this system, fields generated by the objective lens, the decelerating voltage, and the electrostatic deflector overlap with one another.

In section 3.5, we provide concrete expressions of third-order geometrical deflection aberration coefficient formulae in the case where one deflector is an electrostatic deflector, and the other is a magnetic deflector. In addition, the transformation of deflection aberration coefficients from those defined in the object plane to those defined in the image plane is given. We provide relations of deflection aberration coefficients between those parametrized by voltage and currents of deflectors, and those parametrized by first-order beam shifts by deflection in the image plane.

In section 3.6, we provide concrete expressions of third-order geometrical deflection aberration coefficient formulae in the case where both deflectors are electrostatic ones. However, we only discuss cross-deflection aberration

coefficients, whose parameters include voltages of both deflectors, since deflection aberration formulae, whose parameters are given by a single deflector, are already given in section 3.6. Transformations of deflection aberration coefficients are also discussed.

In section 3.7, we provide concrete expressions of third-order geometrical cross-deflection aberration coefficient formulae in the case where both deflectors are magnetic ones. Transformations of deflection aberration coefficients are also discussed.

In section 3.8, chromatic deflection aberration coefficients and aberration coefficients of voltage and current variation of lenses are given. In particular, the latter aberration coefficients are derived by the author. In section 3.9, a conclusion of this chapter is given.

3.2 Definitions of Deflection potentials

In this section, we review the definitions of the coordinate system and the deflection potentials, which express the deflection force on incident electrons, based on references [3.8]-[3.10].

3.2.1 Definition of coordinates

Here the definitions of the Cartesian coordinate system used in this chapter are explained. Fig. 3.2 shows the Cartesian coordinate system. The optic axis coincides with the z -axis. The direction of the z -axis is the same as that from the objective plane towards the image plane. The X, Y -axes are set according to the right-handed system. The azimuth angle is measured from the $+X$ direction and increases in a clockwise direction, as viewed from the objective plane side towards the image plane side, as shown in Fig. 3.2 (b).

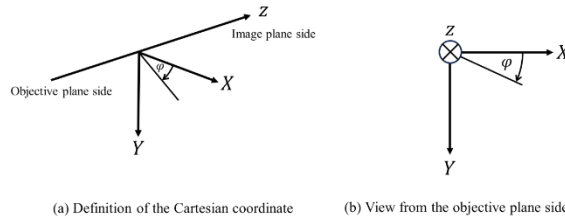


Fig. 3.2 Definition of the Cartesian coordinate system. The optic axis coincides with the z -axis. The direction of the z -axis is the same as that from the objective plane towards the image plane. The X, Y -axes are set according to the right-handed system. The azimuth angle is measured from the $+X$ direction and increases in a clockwise direction, as viewed from the objective plane side towards the image plane side.

3.2.2 Electrostatic potential of Deflectors

Here we introduce definitions of the electrostatic potential and fields, and the voltage configuration of electrodes. In the optical system of the straight optic axis, a multipole expansion of the electrostatic potential is given by

$$\phi(w, \bar{w}, z) = \sum_{n=0}^{\infty} \sum_{\ell=0}^{\infty} \frac{(-1)^\ell n!}{4^\ell \ell! (n + \ell)!} (w\bar{w})^\ell \text{Re}[\phi_n^{[2\ell]}(z)\bar{w}^n], \quad (3.1)$$

in the Cartesian coordinate system [3.18], where w is the complex lateral coordinate: $w = X + iY$. $\phi_n = \phi_{nc} + i\phi_{ns}$ is the z -distribution of the electrostatic multipole component of $2n$ -pole, and the component with subscript c is the normal component and that with subscript s the skew component.

Since on the electrostatic potential of the electrostatic deflector, the restriction

$$\phi(w, \bar{w}, z) = -\phi(-w, -\bar{w}, z). \quad (3.2)$$

is imposed, all even order terms of multipole expansion of the electrostatic potential vanish. The expansion of the electrostatic deflection potential up to third order is given as follows:

$$\phi_{DEF} = \text{Re} \left[\phi_1 \bar{w} + \phi_3 \bar{w}^3 - \frac{1}{8} \phi_1'' w \bar{w}^2 + \dots \right], \quad (3.3)$$

where the dipole component and hexapole component are given by

$$\begin{aligned} \phi_1 &= \phi_{1c} + i\phi_{1s}, \\ \phi_3 &= \phi_{3c} + i\phi_{3s}. \end{aligned} \quad (3.4)$$

The subscript c such as ϕ_{1c} shows that it is a normal component of electrostatic multipole. The subscript s means a skew component. The lateral component of electrostatic field is given by

$$\begin{aligned} E_w &= E_X + iE_Y = -2 \frac{\partial \phi}{\partial \bar{w}} \\ &= - \left[\phi_1 + 3\phi_3 \bar{w}^2 - \frac{1}{4} \phi_1'' w \bar{w} - \frac{1}{8} \bar{\phi}_1'' w^2 + \dots \right]. \end{aligned} \quad (3.5)$$

The lateral component of the electrostatic Coulomb force is

$$F_w = -eE_w = e \left[\phi_1 + 3\phi_3 \bar{w}^2 - \frac{1}{4} \phi_1'' w \bar{w} - \frac{1}{8} \bar{\phi}_1'' w^2 + \dots \right]. \quad (3.6)$$

In the X-Y plane, uniform components of the lateral force are given by the electrostatic dipole field as follows:

$$\begin{aligned} F_X &\approx e\phi_{1c}, \\ F_Y &\approx e\phi_{1s}. \end{aligned} \quad (3.7)$$

The normal component of the electrostatic dipole component deflects the primary electrons in the X-direction, and skew component deflects in the Y-direction in the Cartesian coordinate system.

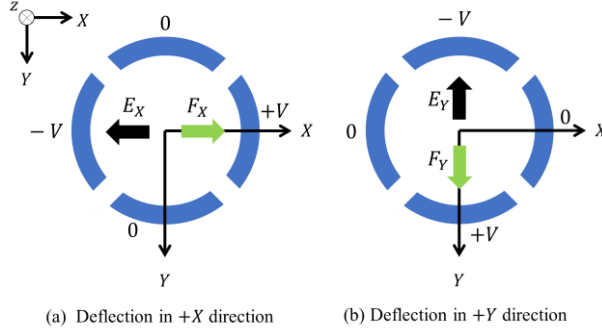


Fig. 3.3 Schematic of configuration example of Electrostatic deflectors. One of the simplest forms of electrostatic deflectors, which can deflect electrons in an arbitrary direction, and the corresponding voltage settings are shown. (a): Voltage setting for deflection in the $+X$ direction. (b): Voltage setting for deflection in the $+Y$ direction. E_X, E_Y indicate the direction of the electric field. F_X and F_Y indicate the direction of the Coulomb force on electrons passing through the deflectors.

Fig. 3.3 shows a typical configuration of an electrostatic deflector, which consists of four electrodes. The same electrodes of cylindrical surface shape are located by 90-degree pitch in a circular direction. One of the simplest forms of electrostatic deflectors, which can deflect electrons in an arbitrary direction, and the corresponding voltage settings are shown. (a): Voltage setting for deflection in the $+X$ direction. (b): Voltage setting for deflection in the $+Y$ direction. E_X and E_Y indicate the direction of the electric field. F_X and F_Y indicate the direction of the Coulomb force on electrons passing through the deflectors. Thus, dipole and hexapole distributions, along the optic axis, of a voltage setting of 1 V, are the same both for normal and skew components. Then, electrostatic dipole components are given by

$$\begin{aligned}\Phi_{1c}(z) &= V_X f_1(z), \\ \Phi_{1s}(z) &= V_Y f_1(z),\end{aligned}\tag{3.8}$$

where f_1 is the distribution of the electrostatic dipole component. V_X and V_Y are the voltages of X-deflection and Y-deflection, respectively. According to the lateral Coulomb force shown in Fig. 3.3, the definition of the sign of the voltage of X-deflection is determined such that a positive sign of V_X , $V_X > 0$, indicates that the primary electrons are deflected in the positive direction of the X coordinate, $F_X > 0$, and it is the same for Y-deflection. Then, the complex deflection voltage is defined as

$$V = V_X + iV_Y.\tag{3.9}$$

The dipole component is given by

$$\Phi_1(z) = V f_1(z). \quad (3.10)$$

To consider the relation between the electrostatic hexapole component and the voltage setting of the deflector, it is advantageous to simplify the electrostatic potential by ignoring the fringing terms, that is, the z-derivative in the electrostatic deflection potential of Eq. (3.3) is neglected. The deflection potential is

$$\phi_{DEF} = \Phi_{1c} r \cos \varphi + \Phi_{1s} r \sin \varphi + \Phi_{3c} r^3 \cos 3\varphi + \Phi_{3s} r^3 \sin 3\varphi + \dots, \quad (3.11)$$

where the deflection potential expansion is expressed in the cylindrical coordinate (r, φ, z) . According to Fig. 3.3 (a), the voltage setting of a positive voltage for the electrode in the 0-degree direction in the X-Y plane, and a negative voltage for the electrode in the 180-degree direction, and ground for the 90- and 270-degree directions, provides deflection of primary electrons in the positive X-direction. Thus, the signs of the deflection potential in the 4-directions, are positive for 0-degree, negative for 90-degree, and 0 potential value for 90- and 270-degrees. For positive X-deflection and positive Y-deflection, the relations between the sign of electrode voltage settings and values of the deflection potential and directions are given in Table 3.1. In Table 3.2, values of sine and cosine in the 4-directions, 0, 90, 180, and 270-degrees, are given. The ignored fringing terms in Eq. (3.11) are re-considered concretely to derive the third-order geometrical deflection aberrations after section 3.4.2.

Table 3.1 Sign of electrode voltage settings and values of deflection potential for positive X and positive Y directions

Direction (deg.)	Deflection for +X		Deflection for +Y	
	Electrode voltage	ϕ_{DEF}	Electrode voltage	ϕ_{DEF}
0	Positive	Positive	Ground	0
90	Ground	0	Positive	Positive
180	Negative	Negative	Ground	0
270	Ground	0	Negative	Negative

Table 3.2 Values of sine and cosine in 4-directions

Direction (deg.)	$\cos \varphi$	$\cos 3\varphi$	$\sin \varphi$	$\sin 3\varphi$
0	+1	+1	0	0
90	0	0	1	-1
180	-1	-1	0	0
270	0	0	-1	+1

According to Table 3.1 and Table 3.2, in the 4-directions, 0, 90, 180, and 270-degrees, the signs of $\cos \varphi$ and of $\cos 3\varphi$ coincide with those of ϕ_{DEF} for X-deflection. However, for Y-deflection, the signs of ϕ_{DEF} in the 4-directions coincide with those of $\sin \varphi$, but are opposite to those of $\sin 3\varphi$. Thus, with the given voltage setting of the electrodes, the sign of the normal electrostatic dipole component has the same sign as the normal electrostatic hexapole

component. However, the sign of the skew electrostatic hexapole component is opposite to that of the skew electrostatic hexapole component.

Normal and skew potential components of the hexapole are given by

$$\begin{aligned}\Phi_{3c}(z) &= V_X f_3(z), \\ \Phi_{3s}(z) &= -V_Y f_3(z).\end{aligned}\tag{3.12}$$

where V_X and V_Y are deflection voltages and f_3 is the hexapole distribution for a unit deflection voltage. The complex expression of the hexapole potential component is given by

$$\Phi_3(z) = \bar{V} f_3(z),\tag{3.13}$$

where \bar{V} is the complex conjugate of the deflection voltage. The electrostatic dipole potential component is proportional to the complex deflection voltage, but hexapole component is proportional to complex conjugate of the deflection voltage.

Next, we consider the case where the deflector is rotated about the optic axis by an azimuth angle φ_f . If the physical system is rotated by φ_f , the coordinate system is considered to be rotated by $-\varphi_f$. We can get the electrostatic potential expression of the rotated deflector by shifting φ to $\varphi - \varphi_f$ in Eq. (3.11).

$$\begin{aligned}\phi_{DEF} &= \Phi_{1c} r \cos(\varphi - \varphi_f) + \Phi_{1s} r \sin(\varphi - \varphi_f) \\ &+ \Phi_{3c} r^3 \cos 3(\varphi - \varphi_f) + \Phi_{3s} r^3 \sin 3(\varphi - \varphi_f) \\ &= \text{Re}[\Phi_1 r e^{-i(\varphi - \varphi_f)} + \Phi_3 r^3 e^{-3i(\varphi - \varphi_f)}] \\ &= \text{Re}[\Phi_1 e^{i\varphi_f} \bar{w} + \Phi_3 e^{3i\varphi_f} \bar{w}^3].\end{aligned}\tag{3.14}$$

Comparing (3.14) with (3.11), the dipole and hexapole electrostatic component of rotated deflectors are expressed by the following replacement:

$$\begin{aligned}\Phi_1 &\rightarrow \Phi_1 e^{i\varphi_f}, \\ \Phi_3 &\rightarrow \Phi_3 e^{3i\varphi_f}.\end{aligned}\tag{3.15}$$

If we define the rotated dipole and hexapole distribution for a unit voltage as

$$\begin{aligned}F_1(z) &= e^{i\varphi_f} f_1(z), \\ F_3(z) &= e^{3i\varphi_f} f_3(z).\end{aligned}\tag{3.16}$$

Thus, the replacement of Eq. (3.15) is

$$\begin{aligned}\Phi_1(z) e^{i\varphi_f} &= V F_1(z), \\ \Phi_3(z) e^{3i\varphi_f} &= \bar{V} F_3(z).\end{aligned}\tag{3.17}$$

The electrostatic deflection potential of rotated deflector up to the third order is given by

$$\phi_{DEF} = \text{Re} \left[F_1 V \bar{w} + F_3 \bar{V} \bar{w}^3 - \frac{1}{8} F_1'' V w \bar{w}^2 + \dots \right].\tag{3.18}$$

3.2.3 Scalar potential of magnetic deflectors and deflection coil currents

Here we introduce the definition of the scalar potential of magnetic deflectors and deflection coil currents. This discussion is basically the same as in section 3.2.2. The series expansion of the magnetic scalar potential of magnetic deflectors up to the third order is given by

$$\Psi_{DEF} = \text{Re} \left[\Psi_1 \bar{w} + \Psi_3 \bar{w}^3 - \frac{1}{8} \Psi_1'' w \bar{w}^2 + \dots \right]. \quad (3.19)$$

The lateral magnetic field is given by

$$B_w = -2 \frac{\partial \Psi_{DEF}}{\partial \bar{w}} = - \left[\Psi_1 + 3 \Psi_3 \bar{w}^2 - \frac{1}{4} \Psi_1'' w \bar{w} - \frac{1}{8} \bar{\Psi}_1'' w^2 + \dots \right]. \quad (3.20)$$

The Lorentz force is given by

$$\begin{aligned} F_w &= -iev_z B_w + ie v_z B_x w', \\ F_z &= -ev_z \text{Im}(\bar{w}' B_w). \end{aligned} \quad (3.21)$$

The significant Lorentz force is given by $F_w \approx -iev_z B_w$:

$$F_w \approx ie v_z \left(\Psi_1 + 3 \Psi_3 \bar{w}^2 - \frac{1}{4} \Psi_1'' w \bar{w} - \frac{1}{8} \bar{\Psi}_1'' w^2 + \dots \right). \quad (3.22)$$

We write the complex expression of Ψ_1 and Ψ_3 by

$$\begin{aligned} \Psi_1 &= \Psi_{1c} + i \Psi_{1s}, \\ \Psi_3 &= \Psi_{3c} + i \Psi_{3s}. \end{aligned} \quad (3.23)$$

First, we assume a uniform magnetic dipole component. The lateral Lorentz force of the significant component is given by

$$F_w \approx ie v_z \Psi_1 = ev_z (-\Psi_{1s} + i \Psi_{1c}). \quad (3.24)$$

Comparing with (3.6), the role of the multipole components with the subscript c and s is inverted. That is the reason why the magnetic multipole component with the subscript s is called the normal component, and that with the subscript c is called the skew component. If we set the current I_x as deflection for the X-direction and I_y as deflection for the Y-direction, we write

$$\begin{aligned} \Psi_{1c} &= I_y d_1, \\ \Psi_{1s} &= -I_x d_1, \end{aligned} \quad (3.25)$$

where d_1 is the z-distribution of the magnetic dipole component for a unit current. The complex scalar potential of magnetic dipole component is given by

$$\Psi_1 = -i I d_1, \quad (3.26)$$

where complex deflection current is given by

$$I = I_x + i I_y. \quad (3.27)$$

Note that, the normal component of the magnetic field is given by the sine component and the skew component is given by the cosine component.

By the same consideration discussed in section 3.2.2, the sign of the hexapole component of the cosine part for the dipole is the same as that for the hexapole, and the sign of the sine part is opposite. If we write the hexapole z -distribution for a unit current as d_3 , the hexapole scalar potential components are given by

$$\begin{aligned}\psi_{3c} &= I_Y d_1, \\ \psi_{3s} &= I_X d_1,\end{aligned}\tag{3.28}$$

and its complex expression is

$$\psi_3 = i\bar{I}d_3.\tag{3.29}$$

Next, we consider the rotation of the magnetic deflector by the azimuth angle φ_d . We repeat the same discussion as for the electrostatic potential. The rotated dipole and hexapole distributions for a unit current are written as

$$\begin{aligned}D_1(z) &= e^{i\varphi_d} d_1(z), \\ D_3(z) &= e^{3i\varphi_d} d_3(z).\end{aligned}\tag{3.30}$$

Thus, the magnetic scalar potential of the rotated deflector is given via the replacement of dipole and hexapoles:

$$\psi_1 \rightarrow -iID_1, \quad \psi_3 \rightarrow i\bar{I}D_3,\tag{3.31}$$

in Eq. (3.19) and

$$\psi_{DEF} = \text{Im} \left[ID_1\bar{w} - \bar{I}D_3\bar{w}^3 - \frac{1}{8}ID_1''w\bar{w}^2 + \dots \right],\tag{3.32}$$

where the relation, $\text{Re}(if) = -\text{Im}(f)$, was used.

3.3 Electron optical eikonal, Euler-Lagrange equation in the Cartesian coordinate system, and trajectories.

Here we consider the electron optical system of round symmetric electrostatic and magnetic fields, composed of electrostatic dipole and hexapole, and magnetic dipole and hexapole. The discussion given hereafter is based on reference [3.10], which discusses aberration formulae for a system composed of round symmetric electrostatic and magnetic fields and deflection fields, whose spatial distributions superimpose one another. However, the discussion of reference [3.10] is limited to the nonrelativistic case. Hereafter, all formulae are re-derived with relativistic correction.

3.3.1 The Electron optical eikonal of the system of lenses and deflectors.

The expansion of the electrostatic potential up to third order is given by

$$\begin{aligned}\phi(w, \bar{w}, z) &= \Phi - \frac{1}{4}\Phi''w\bar{w} + \frac{1}{64}\Phi^{[4]}w^2\bar{w}^2 + \frac{1}{2}(VF_1\bar{w} + \bar{V}\bar{F}_1w) \\ &\quad - \frac{1}{16}w\bar{w}(VF_1''\bar{w} + \bar{V}\bar{F}_1''w) + \frac{1}{2}(\bar{V}F_3\bar{w}^3 + V\bar{F}_3w^3) + \dots,\end{aligned}\tag{3.33}$$

where $\Phi = \Phi(z)$ is the axial potential of the primary electron.

The electron optical eikonal is divided into an electrostatic part and a magnetic part:

$$\mu = \mu_E + \mu_B. \quad (3.34)$$

The electrostatic part is

$$\mu_E = \sqrt{\frac{(\phi^* + \Delta\phi^*)}{\phi_o^*}} (1 + w'\bar{w}'), \quad (3.35)$$

where ϕ^* means the relativistically corrected acceleration potential:

$$\phi^* = \phi(1 + \epsilon\phi), \quad (3.36)$$

and

$$\epsilon = \frac{1}{2mc^2}, \quad (3.37)$$

and m is the rest mass of electrons, c is the speed of light in the vacuum, and $\Delta\phi$ is the energy deviation of primary electrons from the nominal energy, and ϕ_o is the value of the axial potential in the object plane. If the relativistic acceleration potential is differentiated by the optic axis coordinate,

$$\phi^{*'} = \phi'(1 + 2\epsilon\phi) = \gamma\phi', \quad (3.38)$$

where γ is the so-called gamma factor of special relativity, which is given by

$$\gamma(w, \bar{w}, z) = 1 + 2\epsilon\phi(w, \bar{w}, z). \quad (3.39)$$

Hereafter, the axial value of the gamma factor is expressed with the subscript 0:

$$\gamma_0(z) = 1 + 2\epsilon\phi(z). \quad (3.40)$$

Several convenient relations are given as follows:

$$\gamma_0^2 = 1 + 4\epsilon\phi + 4\epsilon^2\phi^2 = 1 + 4\epsilon\phi^*, \quad (3.41)$$

and

$$\gamma_0'\phi^* = 2\epsilon\phi^*\phi' = \frac{1}{2}(\gamma_0^2 - 1)\phi'. \quad (3.42)$$

The expansion of the electrostatic eikonal is given as follows:

$$\begin{aligned} \mu_E = & \sqrt{\frac{\phi^*}{\phi_o^*}} \left[1 + \frac{\gamma_0\Delta\phi}{2\phi^*} - \frac{\gamma_0^2\Delta\phi^2}{8\phi^{*2}} - \frac{\gamma_0\phi''}{8\phi^*} w\bar{w} + \frac{1}{2}w'\bar{w}' + \frac{\gamma_0}{4\phi^*}(VF_1\bar{w} + \bar{V}\bar{F}_1w) \right. \\ & + \Delta\phi \left\{ \frac{\gamma_0}{4\phi^*}w'\bar{w}' + \frac{1}{16\phi^{*2}}\phi''w\bar{w} - \frac{1}{8\phi^{*2}}(VF_1\bar{w} + \bar{V}\bar{F}_1w) \right\} \\ & + \frac{1}{128} \left(\frac{\gamma_0\phi^{[4]}}{\phi^*} - \frac{\phi''^2}{\phi^{*2}} \right) w^2\bar{w}^2 - \frac{\gamma_0\phi''}{16\phi^*} w\bar{w}w'\bar{w}' - \frac{1}{8}w'^2\bar{w}'^2 \\ & - \frac{\gamma_0}{32\phi^*} w\bar{w}(VF_1''\bar{w} + \bar{V}\bar{F}_1''w) + \frac{\phi''}{32\phi^{*2}} w\bar{w}(VF_1\bar{w} + \bar{V}\bar{F}_1w) \\ & + \frac{\gamma_0}{8\phi^*} w'\bar{w}'(VF_1\bar{w} + \bar{V}\bar{F}_1w) - \frac{1}{32\phi^{*2}} (V^2F_1^2\bar{w}^2 + \bar{V}^2F_1^2w^2 + 2V\bar{V}F_1\bar{F}_1w\bar{w}) \\ & \left. + \frac{\gamma_0}{4\phi^*} (\bar{V}F_3\bar{w}^3 + VF_3w^3) \right] + \dots. \end{aligned} \quad (3.43)$$

Next, we consider the magnetic part of the eikonal, which is given by

$$\mu_B = -\frac{\eta}{\sqrt{\Phi_o^*}} \{A_z + \text{Re}(A_w \bar{w}')\}. \quad (3.44)$$

The Expansion of the vector potential including magnetic deflection potential in the Coulomb gauge is given by

$$\begin{aligned} A_w &= -\frac{i}{2} \left(-Bw + \frac{1}{8} B'' w^2 \bar{w} \right) + \frac{1}{4} \bar{I} \bar{D}_1' w^2, \\ A_z &= -\frac{1}{2} \left(I D_1 \bar{w} + \bar{I} \bar{D}_1 w - \frac{1}{8} I D_1' w \bar{w}^2 - \frac{1}{8} \bar{I} \bar{D}_1' w^2 \bar{w} - \bar{I} \bar{D}_3 w^3 - I \bar{D}_3 \bar{w}^3 \right), \end{aligned} \quad (3.45)$$

where

$$\eta = \sqrt{\frac{e}{2m}}. \quad (3.46)$$

The concrete expansion of the magnetic eikonal up to the third order is given as follows:

$$\begin{aligned} \mu_B &= \sqrt{\frac{\Phi^*}{\Phi_o^*}} \left[-\frac{i\eta}{4\sqrt{\Phi^*}} B(w\bar{w}' - \bar{w}w') + \frac{i\eta}{32\sqrt{\Phi^*}} B'' w\bar{w}(w\bar{w}' - \bar{w}w') + \frac{\eta}{2\sqrt{\Phi^*}} (I D_1 \bar{w} + \bar{I} \bar{D}_1 w) \right. \\ &\quad \left. - \frac{\eta}{16\sqrt{\Phi^*}} w\bar{w}(I D_1' \bar{w} + \bar{I} \bar{D}_1' w) - \frac{\eta}{8\sqrt{\Phi^*}} (I D_1' \bar{w}^2 w' + \bar{I} \bar{D}_1' w^2 \bar{w}') - \frac{\eta}{2\sqrt{\Phi^*}} (I D_3 \bar{w}^3 + I \bar{D}_3 w^3) \right]. \end{aligned} \quad (3.47)$$

The eikonal is classified according to the order as

$$\mu = \mu^{(0)} + \mu_{\kappa 1}^{(0)} + \mu_{\kappa 2}^{(0)} + \mu_G^{(2)} + \Delta\mu, \quad (3.48)$$

where

$$\mu^{(0)} = \sqrt{\frac{\Phi^*}{\Phi_o^*}}, \mu_{\kappa 1}^{(0)} = \sqrt{\frac{\Phi^*}{\Phi_o^*}} \frac{\gamma_0 \Delta\Phi}{2\Phi^*}, \mu_{\kappa 2}^{(0)} = -\sqrt{\frac{\Phi^*}{\Phi_o^*}} \frac{\gamma_0^2 \Delta\Phi^2}{8\Phi^{*2}}, \quad (3.49)$$

where subscript $\kappa 1$ and $\kappa 2$ indicate the degree of energy deviation, that is, κd indicates that the terms depend on $\Delta\Phi^d$.

The number indicated in the superscript is the order of the geometrical parameters, and subscript G of $\mu_G^{(2)}$ means the terms only depend on geometrical parameters. The extra term $\Delta\mu$ is considered as the perturbation term.

The paraxial order term is expressed as

$$\begin{aligned} \mu_G^{(2)} &= \sqrt{\frac{\Phi^*}{\Phi_o^*}} \left[-\frac{\gamma_0 \Phi''}{8\Phi^*} w\bar{w} + \frac{1}{2} w' \bar{w}' - \frac{i\eta}{4\sqrt{\Phi^*}} B(w\bar{w}' - \bar{w}w') \right. \\ &\quad \left. + \frac{\gamma_0}{4\Phi^*} (V F_1 \bar{w} + \bar{V} \bar{F}_1 w) + \frac{\eta}{2\sqrt{\Phi^*}} (I D_1 \bar{w} + \bar{I} \bar{D}_1 w) \right], \end{aligned} \quad (3.50)$$

where for the focusing and deflection system, the geometrical parameter is not only w_o and w_o' , but also deflection voltage and deflection current, V and I . The residual term is expressed by

$$\Delta\mu = \mu_{\kappa 1}^{(2)} + \mu_G^{(4)} + \dots. \quad (3.51)$$

In this chapter, the lateral complex position in the object plane in the Cartesian coordinate system: w_o , the slope in the object plane: w_o' , and the complex voltage and current of the deflectors: V and I , are regarded as the geometrical parameters, which parametrize the electron trajectories. Since it only includes $\Delta\Phi$ and does not depend on any geometrical parameters, it does not contribute to the electron trajectory.

The lowest term, which affects the electron trajectories, is $\mu_{\kappa 1}^{(2)}$:

$$\mu_{\kappa 1}^{(2)} = \frac{\Delta\Phi}{\Phi_o^*} \sqrt{\frac{\Phi^*}{\Phi_o^*}} \left[\frac{\gamma_0}{4\Phi^*} w' \bar{w}' + \frac{1}{16\Phi^{*2}} w \bar{w} - \frac{1}{8\Phi^{*2}} (V F_1 \bar{w} + \bar{V} \bar{F}_1 w) \right]. \quad (3.52)$$

Since it depends on the first-degree of energy deviation, and the second order of geometrical parameters, it contributes to the chromatic path deviation of the third rank.

The lowest pure term depending on only geometrical parameters, which contributes to the third-order geometrical path deviations, is given as follows:

$$\begin{aligned} \mu_G^{(4)} = & \sqrt{\frac{\Phi^*}{\Phi_o^*}} \left[\frac{1}{128} \left(\frac{\gamma_0 \Phi^{[4]}}{\Phi^*} - \frac{\Phi'^2}{\Phi^{*2}} \right) w^2 \bar{w}^2 - \frac{\gamma_0 \Phi''}{16\Phi^*} w \bar{w} w' \bar{w}' - \frac{1}{8} w'^2 \bar{w}'^2 \right. \\ & + \frac{i\eta}{32\sqrt{\Phi^*}} B'' w \bar{w} (w \bar{w}' - \bar{w} w') - \frac{\gamma_0}{32\Phi^*} w \bar{w} (V F_1' \bar{w} + \bar{V} \bar{F}_1' w) + \frac{\Phi''}{32\Phi^{*2}} w \bar{w} (V F_1 \bar{w} + \bar{V} \bar{F}_1 w) \\ & + \frac{\gamma_0}{8\Phi^*} w' \bar{w}' (V F_1 \bar{w} + \bar{V} \bar{F}_1 w) - \frac{1}{32\Phi^{*2}} (V^2 F_1^2 \bar{w}^2 + \bar{V}^2 \bar{F}_1^2 w^2 + 2V \bar{V} F_1 \bar{F}_1 w \bar{w}) \\ & - \frac{\eta}{16\sqrt{\Phi^*}} w \bar{w} (I D_1' \bar{w} + \bar{I} \bar{D}_1' w) - \frac{\eta}{8\sqrt{\Phi^*}} (I D_1' \bar{w}^2 w' + \bar{I} \bar{D}_1' w^2 \bar{w}') \\ & \left. + \frac{\gamma_0}{4\Phi^*} (V F_3 \bar{w}^3 + V \bar{F}_3 w^3) - \frac{\eta}{2\sqrt{\Phi^*}} (I D_3 \bar{w}^3 + \bar{I} \bar{D}_3 w^3) \right]. \end{aligned} \quad (3.53)$$

Since we concentrate on up to the third order geometrical aberration of the system, it is sufficient to consider these terms.

3.3.2 The Euler-Lagrange equation

Here we introduce the forms of the Euler-Lagrange equation of the given eikonal, μ , which gives electron trajectories:

$$\frac{d}{dz} \frac{\partial \mu}{\partial \bar{w}'} - \frac{\partial \mu}{\partial \bar{w}} = 0 \quad (3.54)$$

Since $\mu^{(0)}$, $\mu_{\kappa 1}^{(0)}$, and $\mu_{\kappa 2}^{(0)}$ do not include w, \bar{w}, w' , and \bar{w}' , the Euler-Lagrange equation has the form:

$$\frac{d}{dz} \frac{\partial \mu_G^{(2)}}{\partial \bar{w}'} - \frac{\partial \mu_G^{(2)}}{\partial \bar{w}} = - \left[\frac{d}{dz} \frac{\partial \Delta \mu}{\partial \bar{w}'} - \frac{\partial \Delta \mu}{\partial \bar{w}} \right]. \quad (3.55)$$

Employing Eq. (3.50), the equation of trajectory becomes as follows:

$$w'' + \left(\frac{\gamma_0 \Phi'}{2\Phi^*} - \frac{i\eta B}{\sqrt{\Phi^*}} \right) w' + \left(\frac{\gamma_0 \Phi''}{4\Phi^*} - \frac{i\eta B'}{2\sqrt{\Phi^*}} \right) w = P_{DEF} + P_{ptb}. \quad (3.56)$$

where

$$P_{DEF} = \frac{\gamma_0 F_1}{2\Phi^*} V + \frac{\eta D_1}{\sqrt{\Phi^*}} I, \quad (3.57)$$

and

$$P_{ptb} [w, w', V, I, \Delta\Phi] = -2 \sqrt{\frac{\Phi_o^*}{\Phi^*}} \left[\frac{d}{dz} \frac{\partial \Delta \mu}{\partial \bar{w}'} - \frac{\partial \Delta \mu}{\partial \bar{w}} \right]. \quad (3.58)$$

Eq. (3.57) is the deflection term of the trajectory equation. Eq. (3.58) is the perturbation terms, which is a function of the electron trajectory, w , its slope, w' , the voltage of the electrostatic deflector, V , the current of the magnetic deflector, I , the complex conjugate of these parameters, and the energy deviation of electrons $\Delta\Phi$.

3.3.3 The paraxial trajectories in the Cartesian coordinate and those in the rotation coordinate.

When the R.H.S. of (3.56) is approximated to zero, it gives the paraxial equation of the lens system:

$$w'' + \left(\frac{\gamma_0 \Phi'}{2\Phi^*} - \frac{i\eta B}{\sqrt{\Phi^*}} \right) w' + \left(\frac{\gamma_0 \Phi''}{4\Phi^*} - \frac{i\eta B'}{2\sqrt{\Phi^*}} \right) w = 0. \quad (3.59)$$

The general solution of this equation is given as follows:

$$w^{(1)} = w'_o w_\alpha(z) + w_o w_\gamma(z), \quad (3.60)$$

where w_o , and w'_o are the lateral position and slope in the object plane in the Cartesian coordinate. w_α is the axial ray, and w_γ is the field ray. These are fundamental rays in the Cartesian coordinate, and are given by the initial conditions:

$$\begin{aligned} w_{\alpha o} &= 0, & w'_{\alpha o} &= 1, \\ w_{\gamma o} &= 1, & w'_{\gamma o} &= 0. \end{aligned} \quad (3.61)$$

The following coordinate transformation from the Cartesian coordinate into the rotation coordinate is given by

$$w(z) = e^{i\chi(z)} u(z), \quad (3.62)$$

where u is the lateral trajectory in the rotation coordinate, and the rotation angle and its slope is given by

$$\chi(z) = \int_{z_o}^z \frac{\eta B(\zeta)}{2\sqrt{\Phi^*(\zeta)}} d\zeta, \quad \chi' = \frac{\eta B}{2\sqrt{\Phi^*}}. \quad (3.63)$$

Employing this transformation, the paraxial equation, in the rotation coordinate, is obtained as follows:

$$u'' + \frac{\gamma_0 \Phi'}{2\Phi^*} u' + \frac{\gamma_0 \Phi'' + \eta^2 B^2}{4\Phi^*} u = 0. \quad (3.64)$$

The fundamental rays are given by the initial conditions:

$$\begin{aligned} u_{\alpha o} &= 0, & u'_{\alpha o} &= 1, \\ u_{\gamma o} &= 1, & u'_{\gamma o} &= 0. \end{aligned} \quad (3.65)$$

The general solution in the rotation coordinate is given by

$$u^{(1)} = u_o u_\gamma + u'_o u_\alpha \quad (3.66)$$

where u_o , and u'_o are the lateral position and slope in the object plane in the rotation coordinate. The position of the image plane z_i is defined by

$$u_\alpha(z_i) = 0. \quad (3.67)$$

The magnification and the angular magnification, and the rotation angle in the image plane are given by

$$M = u_\gamma(z_i), \quad M_\alpha = u'_\alpha(z_i), \quad \chi_i = \int_{z_o}^{z_i} \frac{\eta B}{2\sqrt{\Phi^*}} dz, \quad (3.68)$$

respectively. The relations of the paraxial trajectories between the Cartesian coordinate and the rotation coordinate are given as follows. Using Eq. (3.61) and (3.65), the relations of the lateral initial position and slope are given by

$$\begin{aligned} w_o &= u_o, \\ w'_o &= u'_o + i\chi'_o u_o = u'_o + i \frac{\eta B_o}{2\sqrt{\Phi_o^*}} u_o. \end{aligned} \quad (3.69)$$

The lateral initial position in the Cartesian coordinate is the same as that in the rotation coordinate. If the object plane is immersed into the axial magnetic field and the initial lateral position is a not zero, the initial lateral slope in the

Cartesian coordinate is different from that in the rotation coordinate. Even if the electron starts in parallel to the optic axis at non-zero off-axis point in the object plane in the Cartesian coordinate system, in the rotation coordinate system, the initial lateral slope in the object plane, is non-zero and its direction is perpendicular to the direction of the initial off-axis point.

In addition, the relationship of the fundamental rays, between the Cartesian coordinate and the rotation coordinate, is given by

$$\begin{aligned} w_\gamma &= e^{i\chi}(u_\gamma - i\chi'_o u_\alpha), \\ w_\alpha &= e^{i\chi} u_\alpha, \\ w'_\gamma &= e^{i\chi} \left(u'_\gamma + \chi' \chi'_o u_\alpha + i(\chi' u_\gamma - \chi'_o u'_\alpha) \right), \\ w'_\alpha &= e^{i\chi} (u'_\alpha + i\chi' u_\alpha). \end{aligned} \quad (3.70)$$

The values of the fundamental rays of the Cartesian coordinate, in the object plane, are given by

$$\begin{aligned} w_{\gamma i} &= e^{i\chi_i} M, \\ w_{\alpha i} &= 0, \\ w'_{\gamma i} &= e^{i\chi_i} (u'_{\gamma i} + i\chi'_i M), \\ w'_{\alpha i} &= e^{i\chi_i} M_\alpha. \end{aligned} \quad (3.71)$$

Thus, the general trajectory and its slope, in the image plane, are given by

$$\begin{aligned} w_i^{(1)} &= e^{i\chi_i} M, \\ w_i^{(1)'} &= e^{i\chi_i} (w_o(u'_{\gamma i} + i\chi'_i M) + w'_o M_\alpha) = w_i^{(1)} \left(\frac{u'_{\gamma i}}{M} + i\chi'_i \right) + s_i, \end{aligned} \quad (3.72)$$

where the paraxial landing slope for the axial ray in the image plane is

$$s_i = e^{i\chi_i} M_\alpha w'_o. \quad (3.73)$$

The paraxial invariant in the rotation coordinate is given as follows:

$$\sqrt{\Phi^*} (u_\gamma u'_\alpha - u'_\gamma u_\alpha) = \sqrt{\Phi_o^*} = \text{const.} \quad (3.74)$$

From this relation, the Helmholtz relation is given by

$$M M_\alpha = \sqrt{\frac{\Phi_o^*}{\Phi_i^*}}. \quad (3.75)$$

Using Eq. (3.70), in the Cartesian coordinate system, we get

$$w_\gamma w'_\alpha - w'_\gamma w_\alpha = e^{2i\chi} (u_\gamma u'_\alpha - u'_\gamma u_\alpha) = e^{2i\chi} \sqrt{\frac{\Phi_o^*}{\Phi^*}}. \quad (3.76)$$

Taking into account the complex conjugate of Eq. (3.70), we get

$$w_\gamma \bar{w}_\alpha - \bar{w}_\gamma w_\alpha = -2i\chi'_o w_\alpha \bar{w}_\alpha, \quad (3.77)$$

and

$$w_\gamma \bar{w}'_\alpha - \bar{w}'_\gamma w_\alpha = u_\gamma u'_\alpha - u'_\gamma u_\alpha - 2i\chi'_o w_\alpha \bar{w}'_\alpha = \sqrt{\frac{\Phi_o^*}{\Phi^*}} - 2i\chi'_o w_\alpha \bar{w}'_\alpha. \quad (3.78)$$

3.3.4 The deflection trajectories

Here the expressions of the deflection trajectories are discussed. The deflection trajectories are given under consideration of deflectors, which are the first-order of the deflection parameter, that is V and I . We have to consider (3.57) in Eq. (3.56). Then, we can obtain the special solution by the parameter variation method in the Cartesian coordinate system. Using a similar discussion in the appendix of Chapter 2, we can get the following conclusions. The general trajectory equation in the Cartesian coordinate is

$$w'' + \left(\frac{\gamma_0 \Phi'}{2\Phi^*} - \frac{i\eta B}{\sqrt{\Phi^*}} \right) w' + \left(\frac{\gamma_0 \Phi''}{4\Phi^*} - \frac{i\eta B'}{2\sqrt{\Phi^*}} \right) w = P, \quad (3.79)$$

where P is a function of $w, w', V, I, \Delta\Phi$. The formal solution of Eq. (3.79), w_s , is given by the parameter variation method as follows:

$$w_s = -w_\gamma \int_{z_0}^z \sqrt{\frac{\Phi^*}{\Phi_0^*}} P \bar{w}_\alpha dz + w_\alpha \int_{z_0}^z \sqrt{\frac{\Phi^*}{\Phi_0^*}} P (\bar{w}_\gamma - 2i\chi'_0 \bar{w}_\alpha) dz, \quad (3.80)$$

and its slope is given by

$$w'_s = -w'_\gamma \int_{z_0}^z \sqrt{\frac{\Phi^*}{\Phi_0^*}} P \bar{w}_\alpha dz + w'_\alpha \int_{z_0}^z \sqrt{\frac{\Phi^*}{\Phi_0^*}} P (\bar{w}_\gamma - 2i\chi'_0 \bar{w}_\alpha) dz. \quad (3.81)$$

These special solutions satisfy the condition that the trajectory coincides with the paraxial solution, in the object plane.

That is,

$$w_s(z_0) = 0, \quad w'_s(z_0) = 0. \quad (3.82)$$

When Eq. (3.57) is substituted into Eq. (3.80), the shape of the trajectory must be written as the following form, which depends on both the complex voltage and the complex current of the deflectors:

$$\begin{aligned} w_{DEF} &= Vw_e + Iw_m, \\ w'_{DEF} &= Vw'_e + Iw'_m, \end{aligned} \quad (3.83)$$

where w_e is called the electrostatic deflection trajectory, and w_m is called the magnetic deflection trajectory. Since in Eq. (3.57), the terms are independent from the trajectory and its slope, the parameter variation method gives a rigorous solution without approximation such as perturbation. The formal expressions are given as follows:

$$w_e = -w_\gamma \int_{z_0}^z \sqrt{\frac{\Phi^*}{\Phi_0^*}} \frac{\gamma_0 F_1}{2\Phi^*} \bar{w}_\alpha dz + w_\alpha \int_{z_0}^z \sqrt{\frac{\Phi^*}{\Phi_0^*}} \frac{\gamma_0 F_1}{2\Phi^*} (\bar{w}_\gamma - 2i\chi'_0 \bar{w}_\alpha) dz, \quad (3.84)$$

$$w_m = -w_\gamma \int_{z_0}^z \sqrt{\frac{\Phi^*}{\Phi_0^*}} \frac{\eta D_1}{\sqrt{\Phi^*}} \bar{w}_\alpha dz + w_\alpha \int_{z_0}^z \sqrt{\frac{\Phi^*}{\Phi_0^*}} \frac{\eta D_1}{\sqrt{\Phi^*}} (\bar{w}_\gamma - 2i\chi'_0 \bar{w}_\alpha) dz, \quad (3.85)$$

Their slopes are given by

$$w'_e = -w'_\gamma \int_{z_0}^z \sqrt{\frac{\Phi^*}{\Phi_0^*}} \frac{\gamma_0 F_1}{2\Phi^*} \bar{w}_\alpha dz + w'_\alpha \int_{z_0}^z \sqrt{\frac{\Phi^*}{\Phi_0^*}} \frac{\gamma_0 F_1}{2\Phi^*} (\bar{w}_\gamma - 2i\chi'_0 \bar{w}_\alpha) dz, \quad (3.86)$$

$$w'_m = -w'_\gamma \int_{z_0}^z \sqrt{\frac{\Phi^*}{\Phi_o^*}} \frac{\eta D_1}{\sqrt{\Phi^*}} \bar{w}_\alpha dz + w'_\alpha \int_{z_0}^z \sqrt{\frac{\Phi^*}{\Phi_o^*}} \frac{\eta D_1}{\sqrt{\Phi^*}} (\bar{w}_\gamma - 2i\chi'_o \bar{w}_\alpha) dz. \quad (3.87)$$

The values of deflection trajectories in the image plane are expressed as

$$\begin{aligned} w_{ei} &= -M \int_{z_0}^{z_i} \sqrt{\frac{\Phi^*}{\Phi_o^*}} \frac{\gamma_0 F_1}{2\Phi^*} \bar{w}_\alpha dz, \\ w_{mi} &= -M \int_{z_0}^{z_i} \sqrt{\frac{\Phi^*}{\Phi_o^*}} \frac{\eta D_1}{\sqrt{\Phi^*}} \bar{w}_\alpha dz, \end{aligned} \quad (3.88)$$

where these are complex deflection sensitivities for the unit voltage and the unit current.

The values of deflection slope in the image plane, which are called the deflection slope sensitivity, are given by

$$\begin{aligned} w'_{ei} &= -w'_{\gamma i} \int_{z_0}^{z_i} \sqrt{\frac{\Phi^*}{\Phi_o^*}} \frac{\gamma_0 F_1}{2\Phi^*} \bar{w}_\alpha dz + M_\alpha \int_{z_0}^{z_i} \sqrt{\frac{\Phi^*}{\Phi_o^*}} \frac{\gamma_0 F_1}{2\Phi^*} (\bar{w}_\gamma - 2i\chi'_o \bar{w}_\alpha) dz, \\ w'_{mi} &= -w'_{\gamma i} \int_{z_0}^{z_i} \sqrt{\frac{\Phi^*}{\Phi_o^*}} \frac{\eta D_1}{\sqrt{\Phi^*}} \bar{w}_\alpha dz + M_\alpha \int_{z_0}^{z_i} \sqrt{\frac{\Phi^*}{\Phi_o^*}} \frac{\eta D_1}{\sqrt{\Phi^*}} (\bar{w}_\gamma - 2i\chi'_o \bar{w}_\alpha) dz. \end{aligned} \quad (3.89)$$

Thus, the general form of the first-order geometrical electron trajectory is given as

$$w^{(1)} = w_o w_\gamma + w'_o w_\alpha + V w_e + I w_m. \quad (3.90)$$

3.4 Perturbation theory of deflection.

3.4.1 Perturbation formalism

Using Eq. (3.58) in Eq. (3.80), we can get the formal expression of the path-deviation. However, Eq. (3.58) includes the term of total derivative by z . Since straightforward differentiation is complicated, a partial integral is performed before the concrete expansion is substituted into the eikonal:

$$\begin{aligned} \int_{z_0}^z \sqrt{\frac{\Phi^*}{\Phi_o^*}} P_{\text{pth}} \bar{w}_A dz &= -2 \int_{z_0}^z \left(\frac{d}{dz} \frac{\partial \Delta \mu}{\partial \bar{w}'} - \frac{\partial \Delta \mu}{\partial \bar{w}} \right) \bar{w}_A dz \\ &= 2 \int_{z_0}^z \left(\frac{\partial \Delta \mu}{\partial \bar{w}'} \bar{w}'_A + \frac{\partial \Delta \mu}{\partial \bar{w}} \bar{w}_A \right) dz - 2 \left[\frac{\partial \Delta \mu}{\partial \bar{w}'} \bar{w}_A \right]_{z_0}^z, \end{aligned} \quad (3.91)$$

where subscript A takes either α or γ . Using Eq. (3.91), the formal expression of path deviation is given by

$$\begin{aligned} w_{\text{pth.}} &= -w_\gamma \int_{z_0}^z \sqrt{\frac{\Phi^*}{\Phi_o^*}} P_{\text{pth}} \bar{w}_\alpha dz + w_\alpha \int_{z_0}^z \sqrt{\frac{\Phi^*}{\Phi_o^*}} P_{\text{pth}} (\bar{w}_\gamma - 2i\chi'_o \bar{w}_\alpha) dz \\ &= 2 \frac{\partial \Delta \mu}{\partial \bar{w}'} \Big|_{z=z_0} w_\alpha - 2(w_\gamma + 2i\chi'_o w_\alpha) \int_{z_0}^z \left(\frac{\partial \Delta \mu}{\partial \bar{w}'} \bar{w}'_\alpha + \frac{\partial \Delta \mu}{\partial \bar{w}} \bar{w}_\alpha \right) dz \\ &\quad + 2w_\alpha \int_{z_0}^z \left(\frac{\partial \Delta \mu}{\partial \bar{w}'} \bar{w}'_\gamma + \frac{\partial \Delta \mu}{\partial \bar{w}} \bar{w}_\gamma \right) dz, \end{aligned} \quad (3.92)$$

where $w_{\alpha o} = 0$, $w_{\gamma o} = 1$, and Eq. (3.77) are employed.

The formal expression of the slope deviation is given by differentiation of Eq. (3.92) as follows:

$$\begin{aligned}
w'_{\text{ptb.}} = & 2 \frac{\partial \Delta \mu}{\partial \bar{w}'} \Big|_{z=z_0} w'_{\alpha} - 2 \sqrt{\frac{\Phi_o^*}{\Phi^*}} \frac{\partial \Delta \mu}{\partial \bar{w}'} - 2(w'_\gamma + 2i\chi'_o w'_\alpha) \int_{z_0}^z \left(\frac{\partial \Delta \mu}{\partial \bar{w}'} \bar{w}'_\alpha + \frac{\partial \Delta \mu}{\partial \bar{w}} \bar{w}_\alpha \right) dz \\
& + 2w'_\alpha \int_{z_0}^z \left(\frac{\partial \Delta \mu}{\partial \bar{w}'} \bar{w}'_\gamma + \frac{\partial \Delta \mu}{\partial \bar{w}} \bar{w}_\gamma \right) dz,
\end{aligned} \tag{3.93}$$

where Eq. (3.77) and (3.78) are employed.

The formal expression of the aberration is defined as the value of the path-deviation in the image plane as follows:

$$\begin{aligned}
w_{\text{ptb.}}(z_i) = & -2w_{\gamma i} \int_{z_0}^{z_i} \left(\frac{\partial \Delta \mu}{\partial \bar{w}'} \bar{w}'_\alpha + \frac{\partial \Delta \mu}{\partial \bar{w}} \bar{w}_\alpha \right) dz \\
= & -2w_{\gamma i} \int_{z_0}^{z_i} F[w, \bar{w}, w', \bar{w}'] dz
\end{aligned} \tag{3.94}$$

The slope aberration is expressed as

$$\begin{aligned}
w'_{\text{ptb.}}(z_i) = & 2 \frac{\partial \Delta \mu}{\partial \bar{w}'} \Big|_{z=z_0} w'_{\alpha i} - 2 \sqrt{\frac{\Phi_o^*}{\Phi_i^*}} \frac{\partial \Delta \mu}{\partial \bar{w}'} \Big|_{z=z_i} \\
& - 2(w'_{\gamma i} + 2i\chi'_o w'_{\alpha i}) \int_{z_0}^{z_i} \left(\frac{\partial \Delta \mu}{\partial \bar{w}'} \bar{w}'_\alpha + \frac{\partial \Delta \mu}{\partial \bar{w}} \bar{w}_\alpha \right) dz + 2w'_{\alpha i} \int_{z_0}^{z_i} \left(\frac{\partial \Delta \mu}{\partial \bar{w}'} \bar{w}'_\gamma + \frac{\partial \Delta \mu}{\partial \bar{w}} \bar{w}_\gamma \right) dz.
\end{aligned} \tag{3.95}$$

However, the perturbation terms of the eikonal depend on the trajectory and its slope, which are to be solved. In this sense, these equations are inconsistent. An appropriate approximated solution is obtained by the method called perturbation.

The perturbation terms and integrands of Eq. (3.94) are classified by the order and the degree as follows:

$$\begin{aligned}
\Delta \mu = & \sum_{n=4} \Delta \mu_G^{(n)} + \sum_{d=1} \sum_{n=2} \Delta \mu_{\kappa d}^{(n)}, \\
F = & \sum_{k=3} F_G^{(k)} + \sum_{d=1} \sum_{k=1} F_{\kappa d}^{(k)}.
\end{aligned} \tag{3.96}$$

The lowest order geometrical perturbation term is $\Delta \mu_G^{(4)}$, and the chromatic perturbation term of the lowest degree is $\Delta \mu_{\kappa 1}^{(2)}$. These give the lowest order geometrical aberration, and the lowest rank chromatic aberration, respectively. In the case of third-order geometrical aberration, the integrand of Eq. (3.94) is calculated for $\Delta \mu_G^{(4)}$. We define it as $F_G^{(3)}$, since differentiation by \bar{w} , and \bar{w}' reduces the order from 4 to 3.

However, the first-order geometrical trajectory Eq. (3.90) and its slope are the only known solutions. It is regarded as the most precise approximation of the actual electron trajectory at this step. Then, the trajectory and the slope inside of the calculated integrand of Eq. (3.94) are replaced by the first-order solutions:

$$F_G^{(3)}[w, \bar{w}, w', \bar{w}'] \rightarrow F_G^{(3)}[w^{(1)}, \bar{w}^{(1)}, w^{(1)'}, \bar{w}^{(1)'}]. \tag{3.97}$$

The formal expression of the lowest order geometrical aberration is given by

$$w_G^{(3)}(z_i) = w_{\gamma i} \int_{z_0}^{z_i} F_G^{(3)}[w^{(1)}, \bar{w}^{(1)}, w^{(1)'}, \bar{w}^{(1)'}] dz, \tag{3.98}$$

where

$$F_G^{(3)}[w, \bar{w}, w', \bar{w}'] = -2 \left(\frac{\partial \Delta \mu_G^{(4)}}{\partial \bar{w}'} \bar{w}'_\alpha + \frac{\partial \Delta \mu_G^{(4)}}{\partial \bar{w}} \bar{w}_\alpha \right). \tag{3.99}$$

The explained procedure, to derive the lowest order aberration of Eq. (3.98), is called primary perturbation. This procedure is applicable to the second-rank chromatic aberration when $\Delta\mu_{\kappa 1}^{(2)}$ is considered as the perturbation term in Eq. (3.94), instead of $\Delta\mu_G^{(4)}$.

3.4.2 Geometrical deflection aberration coefficients for general type of deflectors

The specific series expansion of Eq. (3.99) is given by

$$\begin{aligned}
 F_G^{(3)}[w, \bar{w}, w', \bar{w}'] = & \sqrt{\frac{\Phi^*}{\Phi_0^*}} \left[-\frac{1}{32} \left(\frac{\gamma_0 \Phi^{[4]}}{\Phi^*} - \frac{\Phi'^2}{\Phi^{*2}} \right) w^2 \bar{w} \bar{w}_\alpha + \frac{\gamma_0 \Phi''}{8\Phi^*} w w' \bar{w}' \bar{w}_\alpha \right. \\
 & - \frac{i\eta}{16\sqrt{\Phi^*}} B'' (w^2 \bar{w}' \bar{w}_\alpha - 2w \bar{w} w' \bar{w}_\alpha) + \frac{\gamma_0 \Phi''}{8\Phi^*} w \bar{w} w' \bar{w}_\alpha' + \frac{1}{2} w'^2 \bar{w}' \bar{w}_\alpha' \\
 & - \frac{i\eta}{16\sqrt{\Phi^*}} B'' w^2 \bar{w} \bar{w}_\alpha' + \frac{\gamma_0}{16\Phi^*} (2VF_1'' w \bar{w} \bar{w}_\alpha + \bar{V} F_1'' w^2 \bar{w}_\alpha) \\
 & - \frac{\Phi''}{16\Phi^{*2}} (2VF_1 w \bar{w} \bar{w}_\alpha + \bar{V} F_1 w^2 \bar{w}_\alpha) - \frac{\gamma_0}{4\Phi^*} VF_1 w' \bar{w}' \bar{w}_\alpha \\
 & + \frac{1}{8\Phi^{*2}} (V^2 F_1^2 \bar{w} \bar{w}_\alpha + V \bar{V} F_1 F_1 w \bar{w}_\alpha) - \frac{\gamma_0}{4\Phi^*} w' (VF_1 \bar{w} \bar{w}_\alpha' + \bar{V} F_1 w \bar{w}_\alpha') \\
 & + \frac{\eta}{8\sqrt{\Phi^*}} (2ID_1' w \bar{w} \bar{w}_\alpha + \bar{I} \bar{D}_1' w^2 \bar{w}_\alpha) + \frac{\eta}{2\sqrt{\Phi^*}} ID_1' \bar{w} w' \bar{w}_\alpha + \frac{\eta}{4\sqrt{\Phi^*}} \bar{I} \bar{D}_1' w^2 \bar{w}_\alpha' \\
 & \left. - \frac{3\gamma_0}{2\Phi^*} F_3 \bar{w}^2 \bar{w}_\alpha + \frac{3\eta}{\sqrt{\Phi^*}} \bar{I} D_3 \bar{w}^2 \bar{w}_\alpha \right]. \tag{3.100}
 \end{aligned}$$

According to the procedure, Eq. (3.90) should be substituted into Eq. (3.100). However, we are interested in the aberration theory for a probe-forming system of SEMs with deflectors. The off-axis aberration, whose parameter includes lateral position in the objective plane, w_o , is not considered, since the source size is not significant. When we analyze the aberration property of the alignment of the lenses using deflectors for an arbitrary lateral position and an initial angle of the incident electron beam in the object plane, the off-axis aberration coefficients are necessary. In Chapter 4, we derive the off-axis deflection aberration coefficients for the system that includes a mirror.

We would like to consider both magnetic and electrostatic deflectors of several types. In accordance with the terminology used by Munro et al. [3.10], we call a voltage of an electrostatic deflector and a current of a magnetic deflector a signal of a deflector. The first-order trajectory, which is used in Eq. (3.100), is restricted to

$$\begin{aligned}
 w^{(1)} &= w_o' w_\alpha + S_A w_A + S_B w_B, \\
 w^{(1)'} &= w_o' w_\alpha' + S_A w_A' + S_B w_B', \tag{3.101}
 \end{aligned}$$

where S_A, S_B are either one of a complex signal of the deflectors, and w_A, w_B are corresponding deflection trajectory of first order. That is, if a corresponding deflector is an electrostatic deflector, the signal S_A and deflection trajectory w_A , should be the complex voltage, V_A and electrostatic deflection trajectory w_{eA} . In the case of a magnetic deflector, the signal S_A and deflection trajectory w_A , should be the complex current, I_A and magnetic deflection trajectory w_{mA} . The subscript A, B are independent No of deflectors. We consider three cases. The first case is one electrostatic

deflector and one magnetic deflector, whose signals and deflection trajectories are V, I, w_e , and w_m ⁴. The second case is two independent electrostatic deflectors, whose voltages and deflection trajectories are V_A, V_B, w_{eA} , and w_{eB} . The third case is two independent magnetic deflectors, whose currents and deflection trajectories are I_A, I_B, w_{mA} , and w_{mB} .

In Eq. (3.100), fourth-order differentiation of the axial potential $\Phi^{[4]}$, is included. Numerical error worsens with numerical differentiation. Using an integral in Eq. (3.98), partial integral is done for reducing the order of differentiation of potential and magnetic field of lenses. Of course, differentiation of potential vanishes by repeating partial integral. Instead, differentiation order of the first order trajectories increases. From Eq. (3.59), since the second order differentiation of the first order trajectory is given by

$$w^{(1)''} = -\left(\frac{\gamma_0 \Phi'}{2\Phi^*} - \frac{i\eta B}{\sqrt{\Phi^*}}\right) w^{(1)'} - \left(\frac{\gamma_0 \Phi''}{4\Phi^*} - \frac{i\eta B'}{2\sqrt{\Phi^*}}\right) w^{(1)} + \frac{\gamma_0 F_1}{2\Phi^*} V + \frac{\eta D_1}{\sqrt{\Phi^*}} I, \quad (3.102)$$

the numerical accuracy of the second order differentiation of the trajectory is determined by that of Φ'' and B' . By partial integral, it is possible to reduce the differential order of the axial potential to second order, since appeared maximum order of the differentiation of the first order trajectory is second order. Then, the numerical accuracy of the integrand of corresponding term is ruled by that of the second order differentiation of the axial potential. In the same meaning, the order of the differentiation of the axial magnetic field of lenses, B , can reduced to the first order. The differentiation order of deflection fields F_1 and D_1 can vanish since emerging differentiation order of the first order trajectory is just second order. The second order differentiation of fundamental rays and the deflection rays are given as follows:

$$\begin{aligned} w''_\alpha &= -\left(\frac{\gamma_0 \Phi'}{2\Phi^*} - \frac{i\eta B}{\sqrt{\Phi^*}}\right) w'_\alpha - \left(\frac{\gamma_0 \Phi''}{4\Phi^*} - \frac{i\eta B'}{2\sqrt{\Phi^*}}\right) w_\alpha, \\ w''_\gamma &= -\left(\frac{\gamma_0 \Phi'}{2\Phi^*} - \frac{i\eta B}{\sqrt{\Phi^*}}\right) w'_\gamma - \left(\frac{\gamma_0 \Phi''}{4\Phi^*} - \frac{i\eta B'}{2\sqrt{\Phi^*}}\right) w_\gamma, \\ w''_e &= -\left(\frac{\gamma_0 \Phi'}{2\Phi^*} - \frac{i\eta B}{\sqrt{\Phi^*}}\right) w'_e - \left(\frac{\gamma_0 \Phi''}{4\Phi^*} - \frac{i\eta B'}{2\sqrt{\Phi^*}}\right) w_e + \frac{\gamma_0 F_1}{2\Phi^*}, \\ w''_m &= -\left(\frac{\gamma_0 \Phi'}{2\Phi^*} - \frac{i\eta B}{\sqrt{\Phi^*}}\right) w'_m - \left(\frac{\gamma_0 \Phi''}{4\Phi^*} - \frac{i\eta B'}{2\sqrt{\Phi^*}}\right) w_m + \frac{\eta D_1}{\sqrt{\Phi^*}} \end{aligned} \quad (3.103)$$

We consider several integrals. The following integral is considered:

$$\int_{z_0}^z \sqrt{\frac{\Phi^*}{\Phi_0^*}} \frac{\gamma_0 \Phi^{[4]}}{\Phi^*} w_A w_B w_C w_D dz, \quad (3.104)$$

where w_A, w_B, w_C, w_D , take an arbitral either one the first order trajectory, its slope, and their complex conjugates, $w^{(1)}, \bar{w}^{(1)}, w^{(1)'}, \bar{w}^{(1)'}$. We consider partial integral for this integral. Since if we set w_A, w_B, w_C, w_D to proper

⁴ When we regard the electrostatic and magnetic fields of a Wien filter as the deflectors, by imposing the appropriate relationship on the voltage and the current of the electrostatic and magnetic deflectors, we can approximately calculate the aberrations of the Wien filter.

combination of $w^{(1)}, \bar{w}^{(1)}, w^{(1)'}, \bar{w}^{(1)'}$, if we calculate partial integral, twice, it simplifies the partial integral of the terms in Eq. (3.100). So, Eq. (3.104) is transformed as follows:

$$\begin{aligned} \int_{z_0}^z \sqrt{\frac{\Phi^*}{\Phi_o^*}} \frac{\gamma_0 \Phi^{[4]}}{\Phi^*} w_A w_B w_C w_D dz &= \left[\sqrt{\frac{\Phi^*}{\Phi_o^*}} \frac{\gamma_0 \Phi^{[3]}}{\Phi^*} w_A w_B w_C w_D \right]_{z_0}^z \\ &- \left[\sqrt{\frac{\Phi^*}{\Phi_o^*}} \left(-\frac{\Phi'' \Phi'}{2\Phi^{*2}} w_A w_B w_C w_D + \frac{\gamma_0 \Phi''}{\Phi^*} (w_A w_B w_C w_D)' \right) \right]_{z_0}^z \\ &+ \int_{z_0}^z \sqrt{\frac{\Phi^*}{\Phi_o^*}} \left[\left(-\frac{\Phi''^2}{2\Phi^{*2}} + \frac{3\gamma_0 \Phi'' \Phi'^2}{4\Phi^{*3}} \right) w_A w_B w_C w_D - \frac{\Phi' \Phi''}{\Phi^{*2}} (w_A w_B w_C w_D)' \right. \\ &\quad \left. + \frac{\gamma_0 \Phi''}{\Phi^*} (w_A w_B w_C w_D)'' \right] dz. \end{aligned} \quad (3.105)$$

Other four terms, of which partial integral should be done, are

$$\int_{z_0}^z \sqrt{\frac{\Phi^*}{\Phi_o^*}} \frac{\eta B''}{\sqrt{\Phi^*}} w_A w_B w_C w_D dz = \left[\sqrt{\frac{\Phi^*}{\Phi_o^*}} \frac{\eta B'}{\sqrt{\Phi^*}} w_A w_B w_C w_D \right]_{z_0}^z - \int_{z_0}^z \sqrt{\frac{\Phi^*}{\Phi_o^*}} \frac{\eta B'}{\sqrt{\Phi^*}} (w_A w_B w_C w_D)' dz, \quad (3.106)$$

$$\begin{aligned} \int_{z_0}^z \sqrt{\frac{\Phi^*}{\Phi_o^*}} \frac{\gamma_0}{\Phi^*} F_1'' w_A w_B w_C dz &= \left[\sqrt{\frac{\Phi^*}{\Phi_o^*}} \frac{\gamma_0 F_1'}{\Phi^*} w_A w_B w_C \right]_{z_0}^z \\ &- \left[\sqrt{\frac{\Phi^*}{\Phi_o^*}} \left[-\frac{\Phi' F_1}{2\Phi^{*2}} w_A w_B w_C + \frac{\gamma_0 F_1}{\Phi^*} (w_A w_B w_C)' \right] \right]_{z_0}^z \\ &+ \int_{z_0}^z \sqrt{\frac{\Phi^*}{\Phi_o^*}} \left[\left(\frac{3\gamma_0 \Phi'^2}{4\Phi^{*3}} - \frac{\Phi''}{2\Phi^{*2}} \right) F_1 w_A w_B w_C - \frac{F_1 \Phi'}{\Phi^{*2}} (w_A w_B w_C)' + \frac{\gamma_0 F_1}{\Phi^*} (w_A w_B w_C)'' \right] dz, \end{aligned} \quad (3.107)$$

$$\begin{aligned} \int_{z_0}^z \sqrt{\frac{\Phi^*}{\Phi_o^*}} \frac{\eta}{\sqrt{\Phi^*}} D_1' w_A w_B w_C dz &= \left[\sqrt{\frac{\Phi^*}{\Phi_o^*}} \frac{\eta D_1'}{\sqrt{\Phi^*}} w_A w_B w_C \right]_{z_0}^z \\ &- \left[\sqrt{\frac{\Phi^*}{\Phi_o^*}} \frac{\eta D_1}{\sqrt{\Phi^*}} (w_A w_B w_C)' \right]_{z_0}^z + \int_{z_0}^z \sqrt{\frac{\Phi^*}{\Phi_o^*}} \frac{\eta D_1}{\sqrt{\Phi^*}} (w_A w_B w_C)'' dz, \end{aligned} \quad (3.108)$$

and

$$\begin{aligned} \int_{z_0}^z \sqrt{\frac{\Phi^*}{\Phi_o^*}} \frac{\eta}{\sqrt{\Phi^*}} D_1' w_A w_B w_C dz &= \left[\sqrt{\frac{\Phi^*}{\Phi_o^*}} \frac{\eta D_1}{\sqrt{\Phi^*}} w_A w_B w_C \right]_{z_0}^z - \int_{z_0}^z \sqrt{\frac{\Phi^*}{\Phi_o^*}} \frac{\eta D_1}{\sqrt{\Phi^*}} (w_A w_B w_C)' dz. \end{aligned} \quad (3.109)$$

Employing Eq. (3.105) to (3.109), Eq. (3.98) is transformed into the form as

$$w_G^{(3)}(z_i) = -2w_{\gamma i} \int_{z_0}^{z_i} \left[\frac{\partial \mu_G^{(4)}}{\partial \bar{w}'} \bar{w}'_\alpha + \frac{\partial \mu_G^{(4)}}{\partial \bar{w}} \bar{w}_\alpha \right] dz = w_{\gamma i} \left[\int_{z_0}^{z_i} A dz + B \right]. \quad (3.110)$$

The integrand of R.H.S. of Eq. (3.110) has the form:

$$A = \frac{1}{32} \sqrt{\frac{\Phi^*}{\Phi_o^*}} [A_L + A_{EDEF} + A_{BDEF}], \quad (3.111)$$

where A_L is lens-terms:

$$A_L = A_1 w^{(1)2} \bar{w}^{(1)} + A_2 w^{(1)2} \bar{w}'^{(1)} + A_3 w^{(1)} \bar{w}^{(1)} w'^{(1)} + A_4 w^{(1)} w''^{(1)} \bar{w}^{(1)} + A_5 w^{(1)2} \bar{w}''^{(1)} + A_6 w'^{(1)2} \bar{w}^{(1)} + A_7 w'^{(1)2} \bar{w}'^{(1)}, \quad (3.112)$$

A_{EDEF} is electrostatic deflection-terms:

$$A_{EDEF} = 2E_1 VF_1 w^{(1)} \bar{w}^{(1)} + E_2 VF_1 (w'^{(1)} \bar{w}^{(1)} + w^{(1)} \bar{w}'^{(1)}) + E_3 VF_1 (w''^{(1)} \bar{w}^{(1)} + w^{(1)} \bar{w}''^{(1)}) + E_4 VF_1 w^{(1)} \bar{w}'^{(1)} + E_1 \bar{V} \bar{F}_1 w^{(1)2} + E_2 \bar{V} \bar{F}_1 w^{(1)} w'^{(1)} + E_3 \bar{V} \bar{F}_1 (w^{(1)} w''^{(1)} + w'^{(1)2}) + E_5 (V^2 F_1^2 \bar{w}^{(1)} + V \bar{V} F_1 \bar{F}_1 w^{(1)}) + E_6 F_3 \bar{w}^{(1)2}, \quad (3.113)$$

A_{BDEF} is magnetic deflection-terms:

$$A_{BDEF} = G_1 ID_1 (w^{(1)} \bar{w}''^{(1)} - w''^{(1)} \bar{w}^{(1)}) + 2G_2 ID_1 \bar{w}'_\alpha w^{(1)} \bar{w}^{(1)} + G_3 ID_1 \bar{w}'_\alpha w^{(1)} \bar{w}'^{(1)} + G_1 \bar{ID}_1 (w'^{(1)2} + w^{(1)} w^{(1)''}) - G_2 \bar{ID}_1 w^{(1)2} + G_4 \bar{ID}_3 \bar{w}^{(1)2}, \quad (3.114)$$

where

$$\begin{aligned} A_1 &= \left(\frac{3\Phi''^2}{2\Phi^{*2}} - \frac{3\gamma_0 \Phi'' \Phi'^2}{4\Phi^{*3}} \right) \bar{w}_\alpha + \frac{\Phi' \Phi''}{\Phi^{*2}} \bar{w}'_\alpha - \left(\frac{\gamma_0 \Phi''}{\Phi^*} - i \frac{2\eta B'}{\sqrt{\Phi^*}} \right) \bar{w}''_\alpha, \\ A_2 &= \frac{\Phi' \Phi''}{\Phi^{*2}} \bar{w}_\alpha - 2 \left(\frac{\gamma_0 \Phi''}{\Phi^*} - i \frac{2\eta B'}{\sqrt{\Phi^*}} \right) \bar{w}'_\alpha, \quad A_3 = 2 \frac{\Phi' \Phi''}{\Phi^{*2}} \bar{w}_\alpha, \\ A_4 &= -2 \left(\frac{\gamma_0 \Phi''}{\Phi^*} + i \frac{2\eta B'}{\sqrt{\Phi^*}} \right) \bar{w}_\alpha, \quad A_5 = - \left(\frac{\gamma_0 \Phi''}{\Phi^*} - i \frac{2\eta B'}{\sqrt{\Phi^*}} \right) \bar{w}_\alpha, \\ A_6 &= -2 \left(\frac{\gamma_0 \Phi''}{\Phi^*} + i \frac{2\eta B'}{\sqrt{\Phi^*}} \right) \bar{w}_\alpha, \quad A_7 = 16, \\ E_1 &= \frac{3}{2} \left(\frac{\gamma_0 \Phi'^2}{\Phi^{*3}} - 2 \frac{\Phi''}{\Phi^{*2}} \right) \bar{w}_\alpha - 2 \frac{\Phi'}{\Phi^{*2}} \bar{w}'_\alpha + 2 \frac{\gamma_0}{\Phi^*} \bar{w}''_\alpha, \\ E_2 &= -4 \frac{\Phi'}{\Phi^{*2}} \bar{w}_\alpha, \quad E_3 = 4 \frac{\gamma_0}{\Phi^*} \bar{w}_\alpha, \\ E_4 &= 8 \frac{\gamma_0}{\Phi^*} \bar{w}'_\alpha, \quad E_5 = \frac{4}{\Phi^{*2}} \bar{w}_\alpha, \quad E_6 = -\frac{48\gamma_0}{\Phi^*} \bar{w}_\alpha, \\ G_1 &= \frac{8\eta}{\sqrt{\Phi^*}} \bar{w}_\alpha, \quad G_2 = \frac{4\eta}{\sqrt{\Phi^*}} \bar{w}''_\alpha, \quad G_3 = \frac{16\eta}{\sqrt{\Phi^*}} \bar{w}'_\alpha, \quad G_4 = \frac{96\eta}{\sqrt{\Phi^*}} \bar{w}_\alpha. \end{aligned} \quad (3.115)$$

And the terms outside of the integral are given by

$$\begin{aligned} B &= \frac{1}{32} \sqrt{\frac{\Phi_i^*}{\Phi_o^*}} \left(\frac{\gamma_{0i} \Phi_i'}{\Phi_i^*} - 2 \frac{\eta B_i'}{\sqrt{\Phi_i^*}} \right) w_i^{(1)2} \bar{w}_i^{(1)} \bar{w}_{ai}' - \frac{1}{8} V \sqrt{\frac{\Phi_i^*}{\Phi_o^*}} \frac{\gamma_{0i} F_{1i}}{\Phi_i^*} w_i^{(1)} \bar{w}_i^{(1)} \bar{w}_{ai}' \\ &- \frac{1}{16} \bar{V} \sqrt{\frac{\Phi_i^*}{\Phi_o^*}} \frac{\gamma_{0i} \bar{F}_{1i}}{\Phi_i^*} w_i^{(1)2} \bar{w}_{ai}' - I \sqrt{\frac{\Phi_i^*}{\Phi_o^*}} \frac{\eta D_{1i}}{4\sqrt{\Phi_i^*}} w_i^{(1)} \bar{w}_i^{(1)} \bar{w}_{ai}' + \bar{I} \sqrt{\frac{\Phi^*}{\Phi_o^*}} \frac{\eta \bar{D}_{1i}}{8\sqrt{\Phi_i^*}} w_i^{(1)2} \bar{w}_{ai}', \end{aligned} \quad (3.116)$$

where the terms related to off-axis aberration, are neglected, and we used $w_{ai} = 0$.

To derive the aberration of an arbitrary combination of two independent deflectors, later, we write VF_1 and ID_1 , included in Eq. (3.115) and (3.116), as follows:

$$VF_1 = S_C^V F_1^C + S_D^V F_1^D, \quad ID_1 = S_E^I D_1^E + S_F^I D_1^F, \quad (3.117)$$

where S_C^V means the complex voltage of the electrostatic deflector of No. C. S_E^I means the complex current of the magnetic deflector of No. E, etc.

To transform Eq. (3.111) into the form of third-order geometrical aberration, we consider the concrete expansion of Eq. (3.112) to (3.114) using the form of Eq. (3.101) and (3.117). By direct calculation, we get:

$$\begin{aligned}
A_L = & (A_1 w_\alpha^2 \bar{w}_\alpha + A_2 w_\alpha^2 \bar{w}'_\alpha + A_3 w_\alpha \bar{w}_\alpha w'_\alpha + A_4 w_\alpha \bar{w}_\alpha w''_\alpha + A_5 w_\alpha^2 \bar{w}''_\alpha + A_6 w_\alpha'^2 \bar{w}_\alpha \\
& + A_7 w_\alpha'^2 \bar{w}'_\alpha) w_o'^2 \bar{w}_o' \\
& + (2A_1 w_\alpha \bar{w}_\alpha w_A + 2A_2 w_\alpha \bar{w}'_\alpha w_A + A_3 \bar{w}_\alpha (w_A w'_\alpha + w'_A w_\alpha) + A_4 \bar{w}_\alpha (w_A w''_\alpha + w''_A w_\alpha) \\
& + 2A_5 w_\alpha \bar{w}''_\alpha w_A + 2A_6 w'_\alpha w'_B \bar{w}_\alpha + 2A_7 w'_\alpha \bar{w}'_\alpha w'_A) w'_o \bar{w}'_o S_A \\
& + (A_1 w_\alpha^2 \bar{w}_A + A_2 w_\alpha^2 \bar{w}'_A + A_3 w_\alpha \bar{w}_A w'_\alpha + A_4 w_\alpha \bar{w}_A w''_\alpha + A_5 w_\alpha^2 \bar{w}''_A + A_6 w_\alpha'^2 \bar{w}_A \\
& + A_7 w_\alpha'^2 \bar{w}'_A) w_o'^2 \bar{S}_A \\
& + (2A_1 w_\alpha \bar{w}_\alpha w_B + 2A_2 w_\alpha \bar{w}'_\alpha w_B + A_3 \bar{w}_\alpha (w_B w'_\alpha + w_\alpha w'_B) + A_4 \bar{w}_\alpha (w_B w''_\alpha + w_\alpha w'_B) \\
& + 2A_5 w_\alpha \bar{w}''_\alpha w_B + 2A_6 w'_\alpha w'_B \bar{w}_\alpha + 2A_7 w'_\alpha \bar{w}'_\alpha w'_B) w'_o \bar{w}'_o S_B \\
& + (A_1 w_\alpha^2 \bar{w}_B + A_2 w_\alpha^2 \bar{w}'_B + A_3 w_\alpha \bar{w}_B w'_\alpha + A_4 w_\alpha \bar{w}_B w''_\alpha + A_5 w_\alpha^2 \bar{w}''_B + A_6 w_\alpha'^2 \bar{w}_B \\
& + A_7 w_\alpha'^2 \bar{w}'_B) w_o'^2 \bar{S}_B \\
& + (2A_1 w_\alpha w_A \bar{w}_A + 2A_2 w_\alpha w_A \bar{w}'_A + A_3 \bar{w}_A (w_A w'_\alpha + A_3 w_\alpha w'_A) \\
& + A_4 \bar{w}_A (w_A w''_\alpha + A_3 w_\alpha w''_A) + 2A_5 w_\alpha w_A \bar{w}''_A + 2A_6 w'_\alpha w'_A \bar{w}_A \\
& + 2A_7 w'_\alpha w'_A \bar{w}'_A) w'_o S_A \bar{S}_A \\
& + (2A_1 w_\alpha w_B \bar{w}_B + 2A_2 w_\alpha w_B \bar{w}'_B + A_3 \bar{w}_B (w_B w'_\alpha + w_\alpha w'_B) \\
& + A_4 \bar{w}_B (w_B w''_\alpha + w_\alpha w'_B) + 2A_5 w_\alpha w_B \bar{w}''_B + 2A_6 w'_\alpha w'_B \bar{w}_B \\
& + 2A_7 w'_\alpha w'_B \bar{w}'_B) w'_o S_B \bar{S}_B \\
& + (2A_1 w_\alpha w_A \bar{w}_B + 2A_2 w_\alpha w_A \bar{w}'_B + A_3 \bar{w}_B (w_A w'_\alpha + w_\alpha w'_A) + A_4 \bar{w}_B (w_A w''_\alpha + w_\alpha w'_A) \\
& + 2A_5 w_\alpha w_A \bar{w}''_B + 2A_6 w'_\alpha w'_A \bar{w}_B + 2A_7 w'_\alpha w'_A \bar{w}'_B) w'_o S_A \bar{S}_B \\
& + (2A_1 w_\alpha \bar{w}_A w_B + 2A_2 w_\alpha \bar{w}'_A w_B + A_3 \bar{w}_A (w_B w'_\alpha + w_\alpha w'_B) + A_4 \bar{w}_A (w_B w''_\alpha + w_\alpha w'_B) \\
& + 2A_5 w_\alpha \bar{w}_B \bar{w}'_A + 2A_6 w'_\alpha w'_B \bar{w}_A + 2A_7 w'_\alpha w'_B \bar{w}'_A) w'_o \bar{S}_A S_B \\
& + (A_1 \bar{w}_\alpha w_A^2 + A_2 \bar{w}'_\alpha w_A^2 + A_3 \bar{w}_\alpha w_A w'_A + A_4 \bar{w}_\alpha w_A w''_A + A_5 \bar{w}''_\alpha w_A^2 + A_6 w_A'^2 \bar{w}_\alpha \\
& + A_7 w_A'^2 \bar{w}'_\alpha) \bar{w}_o S_A^2 \\
& + (A_1 \bar{w}_\alpha w_B^2 + A_2 \bar{w}'_\alpha w_B^2 + A_3 \bar{w}_\alpha w_B w'_B + A_4 \bar{w}_\alpha w_B w''_B + A_5 \bar{w}''_\alpha w_B^2 + A_6 w_B'^2 \bar{w}_\alpha \\
& + A_7 w_B'^2 \bar{w}'_\alpha) \bar{w}_o S_B^2 \\
& + (2A_1 \bar{w}_\alpha w_A w_B + 2A_2 \bar{w}'_\alpha w_A w_B + A_3 \bar{w}_\alpha (w_A w'_B + w_B w'_A) + A_4 \bar{w}_\alpha (w_A w''_B + w_B w'_A) \\
& + 2A_5 \bar{w}''_\alpha w_A w_B + 2A_6 \bar{w}'_\alpha w'_A w'_B + 2A_7 w'_A w'_B \bar{w}'_A) \bar{w}'_o S_A S_B \\
& + (A_1 w_A^2 \bar{w}_B + A_2 w_A^2 \bar{w}'_B + A_3 w_A \bar{w}_A w'_A + A_4 w_A \bar{w}_A w''_A + A_5 w_A^2 \bar{w}''_A + A_6 w_A'^2 \bar{w}_A \\
& + A_7 w_A'^2 \bar{w}'_A) S_A^2 \bar{S}_A \\
& + (A_1 w_B^2 \bar{w}_B + A_2 w_B^2 \bar{w}'_B + A_3 w_B \bar{w}_B w'_B + A_4 w_B \bar{w}_B w''_B + A_5 w_B^2 \bar{w}''_B + A_6 w_B'^2 \bar{w}_B \\
& + A_7 w_B'^2 \bar{w}'_B) S_B^2 \bar{S}_B \\
& + (A_1 w_A^2 \bar{w}_B + A_2 w_A^2 \bar{w}'_B + A_3 w_A \bar{w}_B w'_A + A_4 w_A \bar{w}_B w''_A + A_5 w_A^2 \bar{w}''_B + A_6 w_A'^2 \bar{w}_B \\
& + A_7 w_A'^2 \bar{w}'_B) S_A^2 \bar{S}_B \\
& + (2A_1 w_A \bar{w}_A w_B + 2A_2 w_A \bar{w}'_A w_B + A_3 \bar{w}_A (w_B w'_A + w_A w'_B) + A_4 \bar{w}_A (w_B w''_A + w_A w'_B) \\
& + 2A_5 w_A \bar{w}''_A w_B + A_6 w'_A w'_B \bar{w}_A + A_7 w'_A w'_B \bar{w}'_A) S_A \bar{S}_A S_B \\
& + (2A_1 w_A w_B \bar{w}_B + 2A_2 w_A w_B \bar{w}'_B + A_3 \bar{w}_B (w_B w'_A + w_A w'_B) + A_4 \bar{w}_B (w_B w''_A + w_A w'_B) \\
& + 2A_5 w_A w_B \bar{w}''_B + A_6 w'_A w'_B \bar{w}_B + A_7 w'_A w'_B \bar{w}'_B) S_A S_B \bar{S}_B \\
& + (A_1 w_B^2 \bar{w}_A + A_2 w_B^2 \bar{w}'_A + A_3 \bar{w}_A w_B w'_B + A_4 \bar{w}_A w_B w''_B + A_5 w_B^2 \bar{w}''_A + A_6 w_B'^2 \bar{w}_A \\
& + A_7 w_B'^2 \bar{w}'_A) S_B^2 \bar{S}_A,
\end{aligned} \tag{3.118}$$

and

$$\begin{aligned}
A_{\text{DEF}} = & (2E_1 F_1^C w_\alpha \bar{w}_\alpha + E_2 F_1^C (w'_\alpha \bar{w}_\alpha + w_\alpha \bar{w}'_\alpha) + E_3 F_1^C (w''_\alpha \bar{w}_\alpha + w_\alpha \bar{w}''_\alpha) \\
& + E_4 F_1^C w_\alpha \bar{w}'_\alpha) S_C^V w'_0 \bar{w}'_0 \\
& + (2E_1 F_1^D w_\alpha \bar{w}_\alpha + E_2 F_1^D (w'_\alpha \bar{w}_\alpha + w_\alpha \bar{w}'_\alpha) + E_3 F_1^D (w''_\alpha \bar{w}_\alpha + w_\alpha \bar{w}''_\alpha) + E_4 F_1^D w_\alpha \bar{w}'_\alpha) S_D^V w'_0 \bar{w}'_0 \\
& + (E_1 \bar{F}_1^C w_\alpha^2 + E_2 \bar{F}_1^C w_\alpha w'_\alpha + E_3 \bar{F}_1^C (w_\alpha w''_\alpha + w'_\alpha{}^2)) \bar{S}_C^V w_0'^2 \\
& + (E_1 \bar{F}_1^D w_\alpha^2 + E_2 \bar{F}_1^D w_\alpha w'_\alpha + E_3 \bar{F}_1^D (w_\alpha w''_\alpha + w'_\alpha{}^2)) \bar{S}_B^V w_0'^2 \\
& + (2E_1 F_1^C w_\alpha \bar{w}_\alpha + E_2 F_1^C (w'_\alpha \bar{w}_\alpha + w_\alpha \bar{w}'_\alpha) + E_3 F_1^C (w''_\alpha \bar{w}_\alpha + w_\alpha \bar{w}''_\alpha) + E_4 F_1^C w_\alpha \bar{w}'_\alpha) w'_0 S_C^V \bar{S}_A \\
& + (2E_1 \bar{F}_1^C w_\alpha w_\alpha + E_2 \bar{F}_1^C (w_\alpha w'_\alpha + w'_\alpha w_\alpha) + E_3 \bar{F}_1^C (w_\alpha w''_\alpha + w''_\alpha w_\alpha + 2w'_\alpha w'_\alpha)) w'_0 \bar{S}_C^V S_A \\
& + (2E_1 F_1^C w_\alpha \bar{w}_\alpha + E_2 F_1^C (w'_\alpha \bar{w}_\alpha + w_\alpha \bar{w}'_\alpha) + E_3 F_1^C (w''_\alpha \bar{w}_\alpha + w_\alpha \bar{w}''_\alpha) + E_4 F_1^C w_\alpha \bar{w}'_\alpha) w'_0 S_C^V \bar{S}_B \\
& + (2E_1 F_1^C w_\alpha \bar{w}_B + E_2 F_1^C (w'_\alpha \bar{w}_B + w_\alpha \bar{w}'_B) + E_3 F_1^C (w''_\alpha \bar{w}_B + w_\alpha \bar{w}''_B) + E_4 F_1^C w_\alpha \bar{w}'_B) w'_0 S_C^V \bar{S}_B \\
& + (2E_1 F_1^D w_\alpha \bar{w}_\alpha + E_2 F_1^D (w'_\alpha \bar{w}_\alpha + w_\alpha \bar{w}'_\alpha) + E_3 F_1^D (w''_\alpha \bar{w}_\alpha + w_\alpha \bar{w}''_\alpha) + E_4 F_1^D w_\alpha \bar{w}'_\alpha) w'_0 S_D^V \bar{S}_A \\
& + (2E_1 \bar{F}_1^D w_\alpha w_\alpha + E_2 \bar{F}_1^D (w_\alpha w'_\alpha + w'_\alpha w_\alpha) + E_3 \bar{F}_1^D (w_\alpha w''_\alpha + w''_\alpha w_\alpha + 2w'_\alpha w'_\alpha)) w'_0 \bar{S}_D^V S_A \\
& + (2E_1 F_1^D w_\alpha \bar{w}_\alpha + E_2 F_1^D (w'_\alpha \bar{w}_\alpha + w_\alpha \bar{w}'_\alpha) + E_3 F_1^D (w''_\alpha \bar{w}_\alpha + w_\alpha \bar{w}''_\alpha) + E_4 F_1^D w_\alpha \bar{w}'_\alpha) w'_0 S_D^V \bar{S}_B \\
& + (2E_1 F_1^D w_\alpha \bar{w}_B + E_2 F_1^D (w'_\alpha \bar{w}_B + w_\alpha \bar{w}'_B) + E_3 F_1^D (w''_\alpha \bar{w}_B + w_\alpha \bar{w}''_B) + E_4 F_1^D w_\alpha \bar{w}'_B) w'_0 S_D^V \bar{S}_B \\
& + (2E_1 \bar{F}_1^D w_\alpha w_B + E_2 \bar{F}_1^D (w_\alpha w'_B + w'_\alpha w_B) + E_3 \bar{F}_1^D (w_\alpha w''_B + w''_\alpha w_B + 2w'_\alpha w'_B)) w'_0 \bar{S}_D^V S_B \\
& + (2E_1 F_1^D \bar{w}_\alpha w_B + E_2 F_1^D (w'_\alpha \bar{w}_B + w_B \bar{w}'_\alpha) + E_3 F_1^D (w''_\alpha \bar{w}_B + w_B \bar{w}''_\alpha) + E_4 F_1^D w_B \bar{w}'_\alpha) w'_0 S_D^V \bar{S}_B \\
& + (2E_1 F_1^C w_A \bar{w}_A + E_2 F_1^C (w'_A \bar{w}_A + w_A \bar{w}'_A) + E_3 F_1^C (w''_A \bar{w}_A + w_A \bar{w}''_A + 2w'_A w'_A) \\
& + E_4 F_1^C w_A \bar{w}'_A) S_C^V S_A S_A \\
& + (E_1 \bar{F}_1^C w_A^2 + E_2 \bar{F}_1^C w_A w'_A + E_3 \bar{F}_1^C (w_A w''_A + w'_A{}^2)) \bar{S}_C^V S_A^2 \\
& + (2E_1 F_1^C w_A \bar{w}_B + E_2 F_1^C (w'_A \bar{w}_B + w_B \bar{w}'_A) + E_3 F_1^C (w''_A \bar{w}_B + w_B \bar{w}''_A + 2w'_A w'_B) \\
& + E_4 F_1^C w_A \bar{w}'_B) S_C^V S_B \bar{S}_B \\
& + (E_1 \bar{F}_1^C w_B^2 + E_2 \bar{F}_1^C w_B w'_B + E_3 \bar{F}_1^C (w_B w''_B + w'_B{}^2)) \bar{S}_C^V S_B^2 \\
& + (2E_1 F_1^D w_A \bar{w}_A + E_2 F_1^D (w'_A \bar{w}_A + w_A \bar{w}'_A) + E_3 F_1^D (w''_A \bar{w}_A + w_A \bar{w}''_A + 2w'_A w'_A) \\
& + E_4 F_1^D w_A \bar{w}'_A) S_D^V S_A S_A \\
& + (E_1 F_1^D w_A^2 + E_2 F_1^D w_A w'_A + E_3 F_1^D (w_A w''_A + w'_A{}^2)) S_D^V S_A^2 \\
& + (2E_1 F_1^D w_B \bar{w}_B + E_2 F_1^D (w'_B \bar{w}_B + w_B \bar{w}'_B) + E_3 F_1^D (w''_B \bar{w}_B + w_B \bar{w}''_B + 2w'_B w'_B) \\
& + E_4 F_1^D w_B \bar{w}'_B) S_D^V S_B \bar{S}_B \\
& + (E_1 \bar{F}_1^D w_B^2 + E_2 \bar{F}_1^D w_B w'_B + E_3 \bar{F}_1^D (w_B w''_B + w'_B{}^2)) \bar{S}_D^V S_B^2 \\
& + (2E_1 F_1^C w_A \bar{w}_B + E_2 F_1^C (w'_A \bar{w}_B + w_A \bar{w}'_B) + E_3 F_1^C (w''_A \bar{w}_B + w_A \bar{w}''_B + 2w'_A w'_B) \\
& + E_4 F_1^C w_A \bar{w}'_B) S_A \bar{S}_B S_C^V \\
& + (2E_1 F_1^C \bar{w}_A w_B + E_2 F_1^C (w_B \bar{w}'_A + w'_B w_A) + E_3 F_1^C (w''_B \bar{w}_A + w_B \bar{w}''_A + 2w'_B w'_A) \\
& + E_4 F_1^C w_B \bar{w}'_A) S_A S_B S_C^V \\
& + (2E_1 \bar{F}_1^C w_A w_B + E_2 \bar{F}_1^C (w_A w'_B + w_B w'_A) + E_3 \bar{F}_1^C (w_A w''_B + w_B w''_A + 2w'_A w'_B)) S_A S_B \bar{S}_C^V \\
& + (2E_1 F_1^D w_A \bar{w}_B + E_2 F_1^D (w'_A \bar{w}_B + w'_B w_A) + E_3 F_1^D (w''_A \bar{w}_B + w_A \bar{w}''_B + 2w'_A w'_B) \\
& + E_4 F_1^D w_A \bar{w}'_B) S_A \bar{S}_B S_D^V \\
& + (2E_1 F_1^D \bar{w}_A w_B + E_2 F_1^D (w_B \bar{w}'_A + w'_B w_A) + E_3 F_1^D (w''_B \bar{w}_A + w_B \bar{w}''_A + 2w'_B w'_A) \\
& + E_4 F_1^D w_B \bar{w}'_A) S_A S_B \bar{S}_D^V \\
& + (2E_1 \bar{F}_1^D w_A w_B + E_2 \bar{F}_1^D (w_A w'_B + w_B w'_A) + E_3 \bar{F}_1^D (w_A w''_B + w_B w''_A + 2w'_A w'_B)) S_A S_B S_D^V \\
& + E_5 F_1^C \bar{F}_1^C w_\alpha S_C^V S_C^V w'_0 + E_5 F_1^C \bar{F}_1^C w_\alpha S_C^V \bar{S}_C^V S_A + E_5 F_1^C \bar{F}_1^C w_\alpha S_C^V S_C^V S_B \\
& + E_5 F_1^D \bar{F}_1^D w_\alpha S_D^V S_D^V w'_0 + E_5 F_1^D \bar{F}_1^D w_\alpha S_D^V \bar{S}_D^V S_A + E_5 F_1^D \bar{F}_1^D w_\alpha S_D^V S_D^V S_B \\
& + E_5 F_1^C \bar{F}_1^D w_\alpha S_C^V S_D^V w'_0 + E_5 F_1^C \bar{F}_1^D w_\alpha S_C^V \bar{S}_D^V S_A + E_5 F_1^C \bar{F}_1^D w_\alpha S_C^V S_D^V S_B \\
& + E_5 F_1^D \bar{F}_1^C w_\alpha S_D^V S_C^V w'_0 + E_5 F_1^D \bar{F}_1^C w_\alpha S_D^V \bar{S}_C^V S_A + E_5 F_1^D \bar{F}_1^C w_\alpha S_D^V S_C^V S_B \\
& + E_5 F_1^C \bar{w}_\alpha S_C^{V^2} w'_0 + E_5 F_1^C \bar{w}_\alpha S_C^{V^2} \bar{S}_A + E_5 F_1^C \bar{w}_\alpha S_C^{V^2} \bar{S}_B \\
& + E_5 F_1^D \bar{w}_\alpha S_D^{V^2} w'_0 + E_5 F_1^D \bar{w}_\alpha S_D^{V^2} \bar{S}_A + E_5 F_1^D \bar{w}_\alpha S_D^{V^2} \bar{S}_B \\
& + E_5 F_1^C \bar{F}_1^D w_\alpha S_C^V S_D^V w'_0 + E_5 F_1^C \bar{F}_1^D w_\alpha S_C^V S_D^V S_A + E_5 F_1^C \bar{F}_1^D w_\alpha S_C^V S_D^V S_B \\
& + E_5 F_1^D \bar{F}_1^C w_\alpha S_D^V S_C^V w'_0 + E_5 F_1^D \bar{F}_1^C w_\alpha S_D^V S_C^V S_A + E_5 F_1^D \bar{F}_1^C w_\alpha S_D^V S_C^V S_B \\
& + E_5 F_1^C \bar{w}_\alpha S_C^V S_A w'_0 + E_5 F_1^C \bar{w}_\alpha S_C^V S_C^V S_B w'_0 + E_5 F_1^C \bar{w}_\alpha S_C^V S_C^V S_A S_B \\
& + E_5 F_1^D \bar{w}_\alpha S_D^V S_A w'_0 + E_5 F_1^D \bar{w}_\alpha S_D^V S_D^V S_B w'_0 + E_5 F_1^D \bar{w}_\alpha S_D^V S_D^V S_A S_B \\
& + E_5 F_1^C \bar{w}_\alpha S_C^V S_B S_A w'_0 + E_5 F_1^C \bar{w}_\alpha S_C^V S_D^V S$$

and

$$\begin{aligned}
A_{BDEF} = & (G_1 D_1^E (w_\alpha \bar{w}_\alpha'' - w_\alpha'' \bar{w}_\alpha) + G_2 D_1^E w_\alpha \bar{w}_\alpha + G_3 D_1^E w_\alpha \bar{w}_\alpha') S_E^I w_0' \bar{w}_0' \\
& + (G_1 \bar{D}_1^E (w_\alpha'^2 + w_\alpha w_\alpha'') - G_2 w_\alpha'^2) S_E^I w_0'^2 \\
& + (G_1 D_1^F (w_\alpha \bar{w}_\alpha'' - w_\alpha'' \bar{w}_\alpha) + G_2 D_1^F w_\alpha \bar{w}_\alpha + G_3 D_1^F w_\alpha \bar{w}_\alpha') S_F^I w_0' \bar{w}_0' \\
& + (G_1 \bar{D}_1^F (w_\alpha'^2 + w_\alpha w_\alpha'') - G_2 w_\alpha'^2) S_F^I w_0'^2 \\
& + (G_1 D_1^E (w_\alpha \bar{w}_\alpha'' - w_\alpha'' \bar{w}_\alpha) + G_2 D_1^E w_\alpha \bar{w}_\alpha + G_3 D_1^E w_\alpha \bar{w}_\alpha') w_0' S_E^I \bar{S}_A \\
& + (G_1 \bar{D}_1^E (2w_\alpha' w_\alpha' + w_\alpha'' w_\alpha + w_\alpha w_\alpha'') - 2G_2 \bar{D}_1^E w_\alpha w_\alpha') S_E^I S_A w_0' \\
& + (G_1 D_1^E (w_\alpha \bar{w}_\alpha'' - w_\alpha'' \bar{w}_\alpha) + G_2 D_1^E w_\alpha \bar{w}_\alpha + G_3 D_1^E w_\alpha \bar{w}_\alpha') w_0' S_E^I \bar{S}_B \\
& + (G_1 \bar{D}_1^E (2w_\alpha' w_\alpha' + w_\alpha'' w_\alpha + w_\alpha w_\alpha'') - 2G_2 \bar{D}_1^E w_\alpha w_\alpha') S_E^I S_B w_0' \\
& + (G_1 D_1^F (w_\alpha \bar{w}_\alpha'' - w_\alpha'' \bar{w}_\alpha) + G_2 D_1^F w_\alpha \bar{w}_\alpha + G_3 D_1^F w_\alpha \bar{w}_\alpha') w_0' S_F^I \bar{S}_A \\
& + (G_1 \bar{D}_1^F (2w_\alpha' w_\alpha' + w_\alpha'' w_\alpha + w_\alpha w_\alpha'') - 2G_2 \bar{D}_1^F w_\alpha w_\alpha') S_F^I S_A w_0' \\
& + (G_1 D_1^F (w_\alpha \bar{w}_\alpha'' - w_\alpha'' \bar{w}_\alpha) + G_2 D_1^F w_\alpha \bar{w}_\alpha + G_3 D_1^F w_\alpha \bar{w}_\alpha') w_0' S_F^I \bar{S}_B \\
& + (G_1 \bar{D}_1^F (2w_\alpha' w_\alpha' + w_\alpha'' w_\alpha + w_\alpha w_\alpha'') - 2G_2 \bar{D}_1^F w_\alpha w_\alpha') S_F^I S_B w_0' \\
& + (G_1 D_1^E (w_\alpha \bar{w}_\alpha'' - w_\alpha'' \bar{w}_\alpha) + G_2 D_1^E w_\alpha \bar{w}_\alpha + G_3 D_1^E w_\alpha \bar{w}_\alpha') w_0' S_E^I \bar{S}_A \\
& + (G_1 \bar{D}_1^E (2w_\alpha' w_\alpha' + w_\alpha'' w_\alpha + w_\alpha w_\alpha'') - 2G_2 \bar{D}_1^E w_\alpha w_\alpha') S_E^I S_A w_0' \\
& + (G_1 D_1^E (w_\alpha \bar{w}_\alpha'' - w_\alpha'' \bar{w}_\alpha) + G_2 D_1^E w_\alpha \bar{w}_\alpha + G_3 D_1^E w_\alpha \bar{w}_\alpha') w_0' S_E^I \bar{S}_B \\
& + (G_1 \bar{D}_1^E (2w_\alpha' w_\alpha' + w_\alpha'' w_\alpha + w_\alpha w_\alpha'') - 2G_2 \bar{D}_1^E w_\alpha w_\alpha') S_E^I S_B w_0' \\
& + (G_1 D_1^F (w_\alpha \bar{w}_\alpha'' - w_\alpha'' \bar{w}_\alpha) + G_2 D_1^F w_\alpha \bar{w}_\alpha + G_3 D_1^F w_\alpha \bar{w}_\alpha') w_0' S_F^I \bar{S}_A \\
& + (G_1 \bar{D}_1^F (2w_\alpha' w_\alpha' + w_\alpha'' w_\alpha + w_\alpha w_\alpha'') - 2G_2 \bar{D}_1^F w_\alpha w_\alpha') S_F^I S_A w_0' \\
& + (G_1 D_1^F (w_\alpha \bar{w}_\alpha'' - w_\alpha'' \bar{w}_\alpha) + G_2 D_1^F w_\alpha \bar{w}_\alpha + G_3 D_1^F w_\alpha \bar{w}_\alpha') w_0' S_F^I \bar{S}_B \\
& + (G_1 \bar{D}_1^F (2w_\alpha' w_\alpha' + w_\alpha'' w_\alpha + w_\alpha w_\alpha'') - 2G_2 \bar{D}_1^F w_\alpha w_\alpha') S_F^I S_B w_0' \\
& + (G_1 \bar{D}_1^E (w_B'^2 + w_B w_B'') - G_2 \bar{D}_1^E w_B^2) S_E^I S_B^2 \\
& + (G_1 D_1^E (w_B \bar{w}_B'' - w_B'' \bar{w}_B) + G_2 D_1^E w_B \bar{w}_B + G_3 D_1^E w_B \bar{w}_B') S_E^I S_B \bar{S}_B \\
& + (G_1 \bar{D}_1^E (w_B'^2 + w_B w_B'') - G_2 \bar{D}_1^E w_B^2) S_E^I \bar{S}_B^2 \\
& + (G_1 D_1^E (w_B \bar{w}_B'' - w_B'' \bar{w}_B) + G_2 D_1^E w_B \bar{w}_B + G_3 D_1^E w_B \bar{w}_B') S_A S_B S_E^I \\
& + (G_1 \bar{D}_1^E (2w_A' w_B' + w_A'' w_B + w_A w_B'') - 2G_2 \bar{D}_1^E w_A w_B) S_A S_B S_E^I \\
& + (G_1 D_1^F (w_A \bar{w}_A'' - w_A'' \bar{w}_A) + G_2 D_1^F w_A \bar{w}_A + G_3 D_1^F w_A \bar{w}_A') S_F^I S_A \bar{S}_A \\
& + (G_1 \bar{D}_1^F (w_A'^2 + w_A w_A'') - G_2 \bar{D}_1^F w_A^2) S_F^I S_A^2 \\
& + (G_1 D_1^F (w_B \bar{w}_B'' - w_B'' \bar{w}_B) + G_2 D_1^F w_B \bar{w}_B + G_3 D_1^F w_B \bar{w}_B') S_F^I S_B \bar{S}_B \\
& + (G_1 \bar{D}_1^F (w_B'^2 + w_B w_B'') - G_2 \bar{D}_1^F w_B^2) S_F^I \bar{S}_B^2 \\
& + (G_1 D_1^F (w_A \bar{w}_B'' - w_A'' \bar{w}_B) + G_2 D_1^F w_A \bar{w}_B + G_3 D_1^F w_A \bar{w}_B') S_A S_B S_F^I \\
& + (G_1 \bar{D}_1^F (w_B \bar{w}_A'' - w_B'' \bar{w}_A) + G_2 D_1^F w_B \bar{w}_A + G_3 D_1^F w_B \bar{w}_A') S_B S_A S_F^I \\
& + (G_1 \bar{D}_1^F (2w_A' w_B' + w_A'' w_B + w_A w_B'') - 2G_2 \bar{D}_1^F w_A w_B) S_A S_B S_F^I \\
& + G_4 D_3^E \bar{w}_\alpha^2 S_E^I w_0'^2 + 2G_4 D_3^E \bar{w}_\alpha w_\alpha S_E^I S_A \bar{w}_0' + 2G_4 D_3^E \bar{w}_\alpha w_\alpha S_E^I \bar{S}_B \bar{w}_0' \\
& + G_4 D_3^E \bar{w}_\alpha^2 S_E^I w_0'^2 + 2G_4 D_3^E \bar{w}_\alpha w_\alpha S_E^I S_A \bar{w}_0' + 2G_4 D_3^E \bar{w}_\alpha w_\alpha S_E^I \bar{S}_B \bar{w}_0' \\
& + G_4 D_3^E \bar{w}_\alpha^2 S_E^I S_A^2 + G_4 D_3^E \bar{w}_\alpha^2 S_E^I S_B^2 + 2G_4 D_3^E \bar{w}_\alpha w_\alpha S_E^I S_A S_B \\
& + G_4 D_3^E \bar{w}_\alpha^2 S_A^2 S_B^2 + G_4 D_3^E \bar{w}_\alpha^2 S_B^2 S_A^2 + 2G_4 D_3^E \bar{w}_\alpha w_\alpha S_A S_B S_F^I.
\end{aligned} \tag{3.120}$$

The boundary term Eq. (3.116) is expanded as follows:

$$\begin{aligned}
B = & \frac{1}{32} \sqrt{\frac{\Phi_i^*}{\Phi_0}} \left(\frac{\gamma_{0i} \Phi_i''}{\Phi_i^*} - 2 \frac{\eta B_i^I}{\sqrt{\Phi_i^*}} \right) \bar{w}_{\alpha i}' [S_A^2 S_A w_A^2 \bar{w}_A + S_B^2 S_B w_B^2 \bar{w}_B + 2S_A S_B w_A w_B \bar{w}_B] \\
& + S_A^2 S_B w_A^2 \bar{w}_B + S_B^2 S_B w_B^2 \bar{w}_B + 2S_A S_B S_B w_A w_B \bar{w}_B] \\
& - \frac{1}{16} \sqrt{\frac{\Phi_i^*}{\Phi_0}} \frac{\gamma_{0i}}{\Phi_i^*} \bar{w}_{\alpha i}' [2F_{1i}^C w_{Ai} \bar{w}_{Ai} S_A^I S_A S_A + 2F_{1i}^C w_{Bi} \bar{w}_{Bi} S_B^I S_B S_B \\
& + 2F_{1i}^D w_{Ai} \bar{w}_{Ai} S_B^I S_A S_A + 2F_{1i}^D w_{Bi} \bar{w}_{Bi} S_B^I S_B S_B + 2F_{1i}^C w_{Ai} \bar{w}_{Bi} S_A S_B S_C^I \\
& + 2F_{1i}^C \bar{w}_{Ai} w_{Bi} S_A S_B S_C^I + 2F_{1i}^D w_{Ai} \bar{w}_{Bi} S_A S_B S_D^I + 2F_{1i}^D \bar{w}_{Ai} w_{Bi} S_A S_B S_D^I \\
& + F_{1i}^C w_{Ai}^2 S_A^I S_A^2 + F_{1i}^C w_{Bi}^2 S_B^I S_B^2 + 2F_{1i}^C w_{Ai} w_{Bi} S_A^I S_B^I S_A S_B \\
& + F_{1i}^D w_{Ai}^2 S_B^I S_B^2 + F_{1i}^D w_{Bi}^2 S_B^I S_B^2 + 2F_{1i}^D w_{Ai} w_{Bi} S_B^I S_A S_B] \\
& - \frac{1}{8} \sqrt{\frac{\Phi_i^*}{\Phi_0}} \frac{\eta}{\sqrt{\Phi_i^*}} \bar{w}_{\alpha i}' [2D_{1i}^E w_{Ai} \bar{w}_{Ai} S_E^I S_A S_A - \bar{D}_{1i}^E w_{Ai}^2 S_E^I S_A^2 \\
& + 2D_{1i}^E w_{Bi} \bar{w}_{Bi} S_E^I S_B S_B - \bar{D}_{1i}^E w_{Bi}^2 S_E^I S_B^2 \\
& + 2D_{1i}^E w_{Ai} \bar{w}_{Bi} S_E^I S_A S_B + 2D_{1i}^E w_{Bi} \bar{w}_{Ai} S_E^I S_B S_A - 2\bar{D}_{1i}^E w_{Ai} w_{Bi} S_E^I S_A S_B \\
& + 2D_{1i}^F w_{Ai} \bar{w}_{Ai} S_F^I S_A S_A - \bar{D}_{1i}^F w_{Ai}^2 S_F^I S_A^2 \\
& + 2D_{1i}^F w_{Bi} \bar{w}_{Bi} S_F^I S_B S_B - \bar{D}_{1i}^F w_{Bi}^2 S_F^I S_B^2 \\
& + 2D_{1i}^F w_{Ai} \bar{w}_{Bi} S_F^I S_A S_B + 2D_{1i}^F w_{Bi} \bar{w}_{Ai} S_F^I S_B S_A - 2\bar{D}_{1i}^F w_{Ai} w_{Bi} S_F^I S_A S_B].
\end{aligned} \tag{3.121}$$

3.5 Geometrical aberration coefficients of the system, which is composed of a single electrostatic deflector and a single magnetic deflector.

Here, we consider the case of the system with a single electrostatic deflector and a single magnetic deflector. Even if we have more than two deflector units of electrostatic and magnetic fields, the following discussion is valid when we regard them as a combined single deflector field as follows:

$$\begin{aligned} F_1 &= \sum_{j=1}^{N_E} r_V^{(j)} f_1^{(j)} e^{i\phi_V^{(j)}}, & F_3 &= \sum_{j=1}^{N_E} r_V^{(j)} f_3^{(j)} e^{3i\phi_V^{(j)}}, \\ D_1 &= \sum_{m=1}^{N_B} r_I^{(m)} d_1^{(m)} e^{i\phi_I^{(m)}}, & D_3 &= \sum_{m=1}^{N_B} r_I^{(m)} d_3^{(m)} e^{3i\phi_I^{(m)}}, \end{aligned} \quad (3.122)$$

where superscripts j and m indicate the j -th and the m -th deflector unit, respectively. $r_V^{(j)}$, and $r_I^{(m)}$ are relative strength between units for electrostatic and magnetic deflectors, respectively. When they are multiplied by representative complex voltage and current V , and I , actual complex voltages and currents of each deflector are obtained:

$$V_j = V r_V^{(j)}, \quad I_m = I r_I^{(m)} \quad (3.123)$$

Under this consideration, we can use Eq. (3.118)-(3.121) to obtain third-order geometrical aberration coefficients, when we set $S_A = V, S_B = I, S_C^V = V, S_D^V = 0, S_E^I = I, S_F^I = 0, w_A = w_e, w_B = w_m$. Using Eq. (3.110) and (3.111), the formal equation of aberration, which is defined at the object plane, is given by

$$\Delta w_o = \int_{z_o}^{z_l} A dz + B. \quad (3.124)$$

3.5.1 Geometrical aberration coefficients

Geometrical deflection aberration is classified into four categories. The first one is the axial aberration, which only depends on the slope of the axial ray w'_o and its complex conjugate \bar{w}'_o . The second one is the electrostatic deflection aberration, which depends on the complex voltage of the electrostatic deflector V and the slope of the axial ray w'_o , and their complex conjugates. The third is the magnetic deflection aberration, which depends on the complex current of the magnetic deflector I and the slope of the axial ray w'_o , and their complex conjugates. The last one is the hybrid deflection aberration, which depends on w'_o, V, I , and their complex conjugates:

$$\begin{aligned}
&\Delta w_o = \\
&\quad \text{(axial aberration)} \\
&C_{\alpha\alpha\bar{\alpha}o} w_o'^2 \bar{w}_o' \\
&\quad \text{(electrostatic deflection aberration)} \\
&+ C_{V\alpha\bar{\alpha}o} V w_o' \bar{w}_o' + C_{V\alpha\alpha o} V w_o'^2 + C_{V\bar{V}\alpha o} V \bar{V} w_o' \\
&+ C_{VV\bar{\alpha}o} V^2 \bar{w}_o' + C_{V\bar{V}\bar{V}o} V^2 \bar{V} + C_{V\bar{\alpha}\bar{\alpha}o} \bar{V} \bar{w}_o'^2 + C_{V\bar{V}\bar{\alpha}o} \bar{V}^2 \bar{w}_o' + C_{V\bar{V}\bar{V}o} \bar{V}^3 \\
&\quad \text{(magnetic deflection aberration)} \\
&+ C_{I\alpha\bar{\alpha}o} I w_o' \bar{w}_o' + C_{I\alpha\alpha o} I w_o'^2 + C_{I\bar{I}\alpha o} I \bar{I} w_o' \\
&+ C_{I\bar{I}\bar{\alpha}o} I^2 \bar{w}_o' + C_{I\bar{I}\bar{I}o} I^2 \bar{I} + C_{I\bar{\alpha}\bar{\alpha}o} \bar{I} \bar{w}_o'^2 + C_{I\bar{I}\bar{\alpha}o} \bar{I}^2 \bar{w}_o' + C_{I\bar{I}\bar{I}o} \bar{I}^3 \\
&\quad \text{(hybrid deflection aberration)} \\
&+ C_{V\bar{I}\alpha o} V \bar{I} w_o' + C_{V\bar{I}\alpha o} \bar{V} I w_o' + C_{V\bar{I}\bar{\alpha}o} V I \bar{w}_o' \\
&+ C_{V\bar{V}I o} V \bar{V} I + C_{V\bar{V}I o} V^2 \bar{I} + C_{V\bar{I}I o} V I \bar{I} + C_{V\bar{I}I o} \bar{V} I^2 \\
&+ C_{V\bar{I}\bar{\alpha}o} \bar{V} \bar{I} \bar{w}_o' + C_{V\bar{V}I o} \bar{V}^2 \bar{I} + C_{V\bar{I}I o} \bar{V} \bar{I}^2.
\end{aligned} \tag{3.125}$$

The concrete expressions of aberration coefficients are given as follows:

The axial aberration (spherical aberration) coefficient:

$$\begin{aligned}
C_{\alpha\alpha\bar{\alpha}o} &= \int_{z_o}^{z_i} \frac{1}{32} \sqrt{\frac{\Phi^*}{\Phi_o^*}} [A_1 w_\alpha^2 \bar{w}_\alpha + A_2 w_\alpha^2 \bar{w}_\alpha' + A_3 w_\alpha \bar{w}_\alpha w_\alpha' \\
&\quad + A_4 w_\alpha \bar{w}_\alpha w_\alpha'' + A_5 w_\alpha^2 \bar{w}_\alpha' + A_6 w_\alpha'^2 \bar{w}_\alpha + A_7 w_\alpha'^2 \bar{w}_\alpha'] dz.
\end{aligned} \tag{3.126}$$

The electrostatic deflection aberration coefficients:

The coma-length:

$$\begin{aligned}
C_{V\alpha\bar{\alpha}o} &= \int_{z_o}^{z_i} \frac{1}{32} \sqrt{\frac{\Phi^*}{\Phi_o^*}} [2A_1 w_\alpha \bar{w}_\alpha w_e + 2A_2 w_\alpha \bar{w}_\alpha' w_e \\
&\quad + A_3 \bar{w}_\alpha (w_e w_\alpha' + w_e' w_\alpha) + A_4 \bar{w}_\alpha (w_e w_\alpha'' + w_e'' w_\alpha) + 2A_5 w_\alpha \bar{w}_\alpha'' w_e \\
&\quad + 2A_6 w_\alpha' w_\alpha' \bar{w}_\alpha + 2A_7 w_\alpha' \bar{w}_\alpha' w_e' + 2E_1 F_1 w_\alpha \bar{w}_\alpha + E_2 F_1 (w_\alpha' \bar{w}_\alpha + w_\alpha \bar{w}_\alpha') \\
&\quad + E_3 F_1 (w_\alpha'' \bar{w}_\alpha + w_\alpha \bar{w}_\alpha'') + E_4 F_1 w_\alpha \bar{w}_\alpha'] dz
\end{aligned} \tag{3.127}$$

The coma-radius:

$$\begin{aligned}
C_{V\alpha\alpha o} &= \int_{z_o}^{z_i} \frac{1}{32} \sqrt{\frac{\Phi^*}{\Phi_o^*}} [A_1 w_\alpha^2 \bar{w}_e + A_2 w_\alpha^2 \bar{w}_e' + A_3 w_\alpha \bar{w}_e w_\alpha' + A_4 w_\alpha \bar{w}_e w_\alpha'' + A_5 w_\alpha^2 \bar{w}_e'' \\
&\quad + A_6 w_\alpha'^2 \bar{w}_e + A_7 w_\alpha'^2 \bar{w}_e' + E_1 \bar{F}_1 w_\alpha^2 + E_2 \bar{F}_1 w_\alpha w_\alpha' \\
&\quad + E_3 \bar{F}_1 (w_\alpha w_\alpha'' + w_\alpha'' w_\alpha)] dz.
\end{aligned} \tag{3.128}$$

The field-curvature:

$$\begin{aligned}
C_{V\bar{V}\alpha o} &= \int_{z_o}^{z_i} \frac{1}{32} \sqrt{\frac{\Phi^*}{\Phi_o^*}} [2A_1 w_\alpha w_e \bar{w}_e + 2A_2 w_\alpha w_e \bar{w}_e' \\
&\quad + A_3 \bar{w}_e (w_e w_\alpha' + A_3 w_\alpha w_e') + A_4 \bar{w}_e (w_e w_\alpha'' + A_3 w_\alpha w_e'') + 2A_5 w_\alpha w_e \bar{w}_e'' \\
&\quad + 2A_6 w_\alpha' w_e' \bar{w}_e + 2A_7 w_\alpha' w_e' \bar{w}_e' + 2E_1 F_1 w_\alpha \bar{w}_e + E_2 F_1 (w_\alpha' \bar{w}_e + w_\alpha \bar{w}_e') \\
&\quad + E_3 F_1 (w_\alpha'' \bar{w}_e + w_\alpha \bar{w}_e'') + E_4 F_1 w_\alpha \bar{w}_e' + 2E_1 \bar{F}_1 w_\alpha w_e \\
&\quad + E_2 \bar{F}_1 (w_\alpha w_e' + w_\alpha' w_e) \\
&\quad + E_3 \bar{F}_1 (w_\alpha w_e'' + w_\alpha'' w_e + 2w_\alpha' w_e') + E_5 F_1 \bar{F}_1 w_\alpha] dz
\end{aligned} \tag{3.129}$$

The astigmatism:

$$\begin{aligned}
C_{V\bar{V}\bar{\alpha}o} &= \int_{z_o}^{z_i} \frac{1}{32} \sqrt{\frac{\Phi^*}{\Phi_o^*}} [A_1 \bar{w}_\alpha w_e^2 + A_2 \bar{w}_\alpha' w_e^2 + A_3 \bar{w}_\alpha w_e w_e' + A_4 \bar{w}_\alpha w_e w_e'' + A_5 \bar{w}_\alpha'' w_e^2 \\
&\quad + A_6 w_e'^2 \bar{w}_\alpha + A_7 w_e'^2 \bar{w}_\alpha' + 2E_1 F_1 \bar{w}_\alpha w_e + E_2 F_1 (w_e' \bar{w}_\alpha + w_e \bar{w}_\alpha') \\
&\quad + E_3 F_1 (w_e'' \bar{w}_\alpha + w_e \bar{w}_\alpha'') + E_4 F_1 w_e \bar{w}_\alpha' + E_5 F_1^2 \bar{w}_\alpha] dz.
\end{aligned} \tag{3.130}$$

The distortion:

$$\begin{aligned}
C_{VV\bar{V}O} = \int_{z_0}^{z_l} \frac{1}{32} \sqrt{\frac{\Phi^*}{\Phi_0^*}} [& A_1 w_e^2 \bar{w}_e + A_2 w_e^2 \bar{w}_e' + A_3 w_e \bar{w}_e w_e' + A_4 w_e \bar{w}_e w_e'' + A_5 w_e^2 \bar{w}_e'' \\
& + A_6 w_e'^2 \bar{w}_e + A_7 w_e'^2 \bar{w}_e' + 2E_1 F_1 w_e \bar{w}_e + E_2 F_1 (w_e' \bar{w}_e + w_e \bar{w}_e') \\
& + E_3 F_1 (w_e' \bar{w}_e + w_e \bar{w}_e') + 2w_e' \bar{w}_e' + E_4 F_1 w_e \bar{w}_e' + E_1 F_1 w_e^2 \\
& + E_2 F_1 w_e w_e' + E_3 F_1 (w_e w_e'' + w_e'^2) + E_5 F_1 F_1 w_e + E_5 F_1^2 \bar{w}_e] dz \\
& + \frac{1}{32} \sqrt{\frac{\Phi_1^*}{\Phi_0^*}} \left(\frac{\gamma_{0i} \Phi_i''}{\Phi_i^*} - 2 \frac{\eta B_i'}{\sqrt{\Phi_i^*}} \right) w_{ei} \bar{w}_{ei} \bar{w}_{ai}' - \frac{1}{16} \sqrt{\frac{\Phi_1^*}{\Phi_0^*}} \frac{\gamma_{0i}}{\Phi_i^*} (2F_{1i} w_{ei} \bar{w}_{ei} \bar{w}_{ai}' + \bar{F}_{1i} w_{ei}^2 \bar{w}_{ai}').
\end{aligned} \tag{3.131}$$

The four-fold coma (Three-fold aberration):

$$C_{V\bar{V}\bar{a}O} = - \int_{z_0}^{z_l} \frac{3}{2} \sqrt{\frac{\Phi^*}{\Phi_0^*}} \frac{\gamma_0 F_3}{\Phi^*} \bar{w}_\alpha^3 dz. \tag{3.132}$$

The four-fold astigmatism:

$$C_{V\bar{V}\bar{a}O} = - \int_{z_0}^{z_l} 3 \sqrt{\frac{\Phi^*}{\Phi_0^*}} \frac{\gamma_0 F_3}{\Phi^*} \bar{w}_\alpha^2 \bar{w}_e dz. \tag{3.133}$$

The four-fold distortion:

$$C_{V\bar{V}\bar{V}O} = - \int_{z_0}^{z_l} \frac{3}{2} \sqrt{\frac{\Phi^*}{\Phi_0^*}} \frac{\gamma_0 F_3}{\Phi^*} \bar{w}_\alpha \bar{w}_e^2 dz. \tag{3.134}$$

The magnetic deflection aberration coefficients:

The coma-length:

$$\begin{aligned}
C_{I\alpha\bar{a}O} = \int_{z_0}^{z_l} \frac{1}{32} \sqrt{\frac{\Phi^*}{\Phi_0^*}} [& 2A_1 w_\alpha \bar{w}_\alpha w_m + 2A_2 w_\alpha \bar{w}_\alpha' w_m + A_3 \bar{w}_\alpha (w_m w_\alpha' + w_\alpha w_m') \\
& + A_4 \bar{w}_\alpha (w_m w_\alpha'' + w_\alpha w_m'') + 2A_5 w_\alpha \bar{w}_\alpha' w_m + 2A_6 w_\alpha' w_m \bar{w}_\alpha \\
& + 2A_7 w_\alpha \bar{w}_\alpha' w_m + G_1 D_1 (w_\alpha \bar{w}_\alpha' - w_\alpha' \bar{w}_\alpha) + G_2 D_1 w_\alpha \bar{w}_\alpha \\
& + G_3 D_1 w_\alpha \bar{w}_\alpha'] dz.
\end{aligned} \tag{3.135}$$

The coma-radius:

$$\begin{aligned}
C_{I\alpha\bar{a}O} = \int_{z_0}^{z_l} \frac{1}{32} \sqrt{\frac{\Phi^*}{\Phi_0^*}} [& A_1 w_\alpha^2 \bar{w}_m + A_2 w_\alpha^2 \bar{w}_m' + A_3 w_\alpha \bar{w}_m w_\alpha' + A_4 w_\alpha \bar{w}_m w_\alpha'' + A_5 w_\alpha^2 \bar{w}_m'' \\
& + A_6 w_\alpha'^2 \bar{w}_m + A_7 w_\alpha'^2 \bar{w}_m' + G_1 \bar{D}_1 (w_\alpha'^2 + w_\alpha w_\alpha'') - G_2 \bar{D}_1 w_\alpha^2] dz.
\end{aligned} \tag{3.136}$$

The field-curvature:

$$\begin{aligned}
C_{I\bar{I}aO} = \int_{z_0}^{z_l} \frac{1}{32} \sqrt{\frac{\Phi^*}{\Phi_0^*}} [& 2A_1 w_\alpha w_m \bar{w}_m + 2A_2 w_\alpha w_m \bar{w}_m' + A_3 \bar{w}_m (w_m w_\alpha' + w_\alpha w_m') \\
& + A_4 \bar{w}_m (w_m w_\alpha'' + w_\alpha w_m'') + 2A_5 w_\alpha w_m \bar{w}_m'' + 2A_6 w_\alpha' w_m \bar{w}_m \\
& + 2A_7 w_\alpha' w_m \bar{w}_m' + G_1 D_1 (w_\alpha \bar{w}_m'' - w_\alpha'' \bar{w}_m) + G_2 D_1 w_\alpha \bar{w}_m \\
& + G_3 D_1 w_\alpha \bar{w}_m + G_1 \bar{D}_1 (2w_\alpha' w_m + w_\alpha'' w_m + w_\alpha w_m') \\
& - 2G_2 \bar{D}_1 w_\alpha w_m] dz.
\end{aligned} \tag{3.137}$$

The astigmatism:

$$\begin{aligned}
C_{II\bar{a}O} = \int_{z_0}^{z_l} \frac{1}{32} \sqrt{\frac{\Phi^*}{\Phi_0^*}} [& A_1 \bar{w}_\alpha w_m^2 + A_2 \bar{w}_\alpha' w_m^2 + A_3 \bar{w}_\alpha w_m w_m' + A_4 \bar{w}_\alpha w_m w_m'' + A_5 \bar{w}_\alpha'' w_m^2 \\
& + A_6 w_m'^2 \bar{w}_\alpha + A_7 w_m'^2 \bar{w}_\alpha' + G_1 D_1 (w_m \bar{w}_\alpha'' - w_m'' \bar{w}_\alpha) + G_2 D_1 w_m \bar{w}_\alpha \\
& + G_3 D_1 w_m \bar{w}_\alpha'] dz.
\end{aligned} \tag{3.138}$$

The distortion:

$$\begin{aligned}
 C_{IIIo} = \int_{z_o}^{z_i} \frac{1}{32} \sqrt{\frac{\Phi^*}{\Phi_o^*}} [& A_1 w_m^2 \bar{w}_m + A_2 w_m^2 \bar{w}_m' + A_3 w_m \bar{w}_m w_m' + A_4 w_m \bar{w}_m w_m'' + A_5 w_m^2 \bar{w}_m'' \\
 & + A_6 w_m'^2 \bar{w}_m + A_7 w_m'^2 \bar{w}_m' + G_1 D_1 (w_m \bar{w}_m'' - w_m'' \bar{w}_m) + G_2 D_1 w_m \bar{w}_m \\
 & + G_3 D_1 w_m \bar{w}_m' + G_1 \bar{D}_1 (w_m'^2 + w_m w_m'') - G_2 \bar{D}_1 w_m^2] dz \\
 & + \frac{1}{32} \sqrt{\frac{\Phi_i^*}{\Phi_o^*}} \left(\gamma_{0i} \frac{\Phi_i'}{\Phi_i^*} - 2 \frac{\eta B_i'}{\sqrt{\Phi_i^*}} \right) w_{mi}^2 \bar{w}_{mi} \bar{w}_{ai}' - \frac{1}{8} \sqrt{\frac{\Phi_i^*}{\Phi_o^*}} \frac{\eta}{\sqrt{\Phi_i^*}} (2 D_{1i} w_{mi} \bar{w}_{mi} \bar{w}_{ai}' - \bar{D}_{1i} w_{mi}^2 \bar{w}_{ai}').
 \end{aligned} \quad (3.139)$$

The four-fold coma (Three-fold astigmatism):

$$C_{I\bar{\alpha}\bar{\alpha}o} = \int_{z_o}^{z_i} \frac{1}{32} \sqrt{\frac{\Phi^*}{\Phi_o^*}} G_4 D_3 \bar{w}_\alpha^2 dz. \quad (3.140)$$

The four-fold astigmatism:

$$C_{II\bar{\alpha}o} = \int_{z_o}^{z_i} \frac{1}{16} \sqrt{\frac{\Phi^*}{\Phi_o^*}} G_4 D_3 \bar{w}_\alpha \bar{w}_m dz. \quad (3.141)$$

The four-fold distortion:

$$C_{IIIo} = \int_{z_o}^{z_i} \frac{1}{32} \sqrt{\frac{\Phi^*}{\Phi_o^*}} G_4 D_3 \bar{w}_m^2 dz. \quad (3.142)$$

The hybrid deflection aberration coefficients:

The field-curvature:

$$\begin{aligned}
 C_{VIao} = \int_{z_o}^{z_i} \frac{1}{32} \sqrt{\frac{\Phi^*}{\Phi_o^*}} [& 2A_1 w_\alpha w_e \bar{w}_m + 2A_2 w_\alpha w_e \bar{w}_m' + A_3 \bar{w}_m (w_e w_\alpha' + w_\alpha w_e') \\
 & + A_4 \bar{w}_m (w_e w_\alpha'' + w_\alpha w_e'') + 2A_5 w_\alpha w_e \bar{w}_m'' + 2A_6 w_\alpha' w_e' \bar{w}_m \\
 & + 2A_7 w_\alpha' w_e' \bar{w}_m' + 2E_1 F_1 w_\alpha \bar{w}_m + E_2 F_1 (w_\alpha' \bar{w}_m + w_\alpha \bar{w}_m') \\
 & + E_3 F_1 (w_\alpha'' \bar{w}_m + w_\alpha \bar{w}_m'') + E_4 F_1 w_\alpha \bar{w}_m' \\
 & + G_1 \bar{D}_1 (2w_\alpha' w_e' + w_\alpha'' w_e + w_\alpha w_e'') - 2G_2 \bar{D}_1 w_\alpha w_e] dz,
 \end{aligned} \quad (3.143)$$

$$\begin{aligned}
 C_{VIIao} = \int_{z_o}^{z_i} \frac{1}{32} \sqrt{\frac{\Phi^*}{\Phi_o^*}} [& 2A_1 w_\alpha \bar{w}_e w_m + 2A_2 w_\alpha w_m \bar{w}_e' + A_3 \bar{w}_e (w_m w_\alpha' + w_\alpha w_m') \\
 & + A_4 \bar{w}_e (w_m w_\alpha'' + w_\alpha w_m'') + 2A_5 w_\alpha w_m \bar{w}_e'' + 2A_6 w_\alpha' w_m' \bar{w}_e \\
 & + 2A_7 w_\alpha' w_m' \bar{w}_e' + 2E_1 \bar{F}_1 w_\alpha w_m + E_2 \bar{F}_1 (w_\alpha' w_m + w_\alpha w_m') \\
 & + E_3 \bar{F}_1 (w_\alpha'' w_m + w_\alpha' w_m' + 2w_\alpha' w_m') + G_1 D_1 (w_\alpha \bar{w}_e'' - w_\alpha'' \bar{w}_e) \\
 & + G_2 D_1 w_\alpha \bar{w}_e + G_3 D_1 w_\alpha \bar{w}_e'] dz.
 \end{aligned} \quad (3.144)$$

The astigmatism:

$$\begin{aligned}
 C_{VII\bar{o}} = \int_{z_o}^{z_i} \frac{1}{32} \sqrt{\frac{\Phi^*}{\Phi_o^*}} [& (2A_1 \bar{w}_\alpha w_e w_m + 2A_2 \bar{w}_\alpha' w_e w_m + A_3 \bar{w}_\alpha (w_e w_m' + w_m w_e') \\
 & + A_4 \bar{w}_\alpha (w_e w_m'' + w_m w_e'') + 2A_5 \bar{w}_\alpha'' w_e w_m + 2A_6 \bar{w}_\alpha w_e' w_m' \\
 & + 2A_7 w_e' w_m' \bar{w}_\alpha') + 2E_1 \bar{F}_1 \bar{w}_\alpha w_m + E_2 \bar{F}_1 (w_m' \bar{w}_\alpha + w_m \bar{w}_\alpha') \\
 & + E_3 \bar{F}_1 (w_m'' \bar{w}_\alpha + w_m \bar{w}_\alpha'') + E_4 \bar{F}_1 w_m \bar{w}_\alpha' + G_1 D_1 (w_e \bar{w}_\alpha'' - w_e'' \bar{w}_\alpha) \\
 & + G_2 D_1 w_e \bar{w}_\alpha + G_3 D_1 w_e \bar{w}_\alpha'] dz.
 \end{aligned} \quad (3.145)$$

The distortion:

$$\begin{aligned}
C_{V\bar{V}Io} = & \int_{z_0}^{z_i} \frac{1}{32} \sqrt{\frac{\Phi^*}{\Phi_0^*}} [2A_1 w_e \bar{w}_e w_m + 2A_2 w_e \bar{w}_e' w_m + A_3 \bar{w}_e (w_m w_e' + w_e w_m') \\
& + A_4 \bar{w}_e (w_m w_e'' + w_e w_m'') + 2A_5 w_e \bar{w}_e' w_m + A_6 w_e' w_m' \bar{w}_e \\
& + A_7 w_e' w_m' \bar{w}_e' + 2E_1 F_1 \bar{w}_e w_m + E_2 F_1 (w_e \bar{w}_m' + w_m' \bar{w}_e) \\
& + E_3 F_1 (w_m'' \bar{w}_e + w_m' \bar{w}_e' + 2w_m' \bar{w}_e') + E_4 F_1 w_m \bar{w}_e' + 2E_1 F_1 w_e w_m \\
& + E_2 \bar{F}_1 (w_e w_m' + w_m w_e') + E_3 \bar{F}_1 (w_e w_m'' + w_m w_e'') + 2w_e' w_m' \\
& + E_5 F_1 \bar{F}_1 w_m + G_1 D_1 (w_e \bar{w}_e' - w_e' \bar{w}_e) + G_2 D_1 w_e \bar{w}_e + G_3 D_1 w_e \bar{w}_e'] dz \\
& + \frac{1}{16} \sqrt{\frac{\Phi_i^*}{\Phi_0^*}} \left(\frac{\gamma_{0i} \Phi_i''}{\Phi_i^*} - 2 \frac{\eta B_i'}{\sqrt{\Phi_i^*}} \right) w_{ei} \bar{w}_{ei} w_{mi} \bar{w}_{ai}' - \frac{1}{8} \sqrt{\frac{\Phi_i^*}{\Phi_0^*}} \frac{\gamma_{0i}}{\Phi_i^*} \bar{F}_{1i} w_{ei} w_{mi} \bar{w}_{ai}' \\
& - \frac{1}{8} \sqrt{\frac{\Phi_i^*}{\Phi_0^*}} \frac{\gamma_{0i}}{\Phi_i^*} F_{1i} \bar{w}_{ei} w_{mi} \bar{w}_{ai}' - \frac{1}{4} \sqrt{\frac{\Phi_i^*}{\Phi_0^*}} \frac{\eta}{\sqrt{\Phi_i^*}} D_{1i} w_{ei} \bar{w}_{ei} \bar{w}_{ai}',
\end{aligned} \tag{3.146}$$

$$\begin{aligned}
C_{V\bar{V}Io} = & \int_{z_0}^{z_i} \frac{1}{32} \sqrt{\frac{\Phi^*}{\Phi_0^*}} [A_1 w_e^2 \bar{w}_m + A_2 w_e^2 \bar{w}_m' + A_3 w_e \bar{w}_m w_e' + A_4 w_e \bar{w}_m w_e'' + A_5 w_m^2 \bar{w}_m'' \\
& + A_6 w_e^2 \bar{w}_m + A_7 w_e^2 \bar{w}_m' + 2E_1 F_1 w_e \bar{w}_m + E_2 F_1 (w_e \bar{w}_m' + w_e' \bar{w}_m) \\
& + E_3 F_1 (w_e' \bar{w}_m + w_e \bar{w}_m'' + 2w_e' \bar{w}_m') + E_4 F_1 w_e \bar{w}_m' + E_5 F_1^2 \bar{w}_m \\
& + G_1 \bar{D}_1 (w_e'^2 + w_e w_e'') - G_2 \bar{D}_1 w_e^2] dz \\
& + \frac{1}{32} \sqrt{\frac{\Phi_i^*}{\Phi_0^*}} \left(\frac{\gamma_{0i} \Phi_i''}{\Phi_i^*} - 2 \frac{\eta B_i'}{\sqrt{\Phi_i^*}} \right) w_{ei}^2 \bar{w}_{mi} \bar{w}_{ai}' - \frac{1}{8} \sqrt{\frac{\Phi_i^*}{\Phi_0^*}} \frac{\gamma_{0i}}{\Phi_i^*} F_{1i} w_{ei} \bar{w}_{mi} \bar{w}_{ai}' + \frac{1}{8} \sqrt{\frac{\Phi_i^*}{\Phi_0^*}} \frac{\eta}{\sqrt{\Phi_i^*}} \bar{D}_{1i} w_{ei}^2 \bar{w}_{ai}',
\end{aligned} \tag{3.147}$$

$$\begin{aligned}
C_{V\bar{I}Io} = & \int_{z_0}^{z_i} \frac{1}{32} \sqrt{\frac{\Phi^*}{\Phi_0^*}} [2A_1 w_e w_m \bar{w}_m + 2A_2 w_e w_m \bar{w}_m' + A_3 \bar{w}_m (w_m w_e' + w_e w_m') \\
& + A_3 \bar{w}_m (w_m w_e' + w_e w_m'') + 2A_5 w_e w_m \bar{w}_m' + A_6 w_e' w_m' \bar{w}_m \\
& + A_7 w_e' w_m' \bar{w}_m' + 2E_1 F_1 w_m \bar{w}_m + E_2 F_1 (w_m' \bar{w}_m + w_m \bar{w}_m') \\
& + E_3 F_1 (w_m' \bar{w}_m + w_m \bar{w}_m' + 2w_m' \bar{w}_m) + E_4 F_1 w_m \bar{w}_m' \\
& + G_1 D_1 (w_e \bar{w}_m'' - w_e' \bar{w}_m) + G_2 D_1 w_e \bar{w}_m + G_3 D_1 w_e \bar{w}_m' \\
& + G_1 \bar{D}_1 (2w_e' \bar{w}_m + w_e' w_m + w_e w_m'') - 2G_2 \bar{D}_1 w_e \bar{w}_m] dz \\
& + \frac{1}{32} \sqrt{\frac{\Phi_i^*}{\Phi_0^*}} \left(\frac{\gamma_{0i} \Phi_i''}{\Phi_i^*} - 2 \frac{\eta B_i'}{\sqrt{\Phi_i^*}} \right) 2w_{ei} w_{mi} \bar{w}_{mi} \bar{w}_{ai}' - \frac{1}{8} \sqrt{\frac{\Phi_i^*}{\Phi_0^*}} \frac{\gamma_{0i}}{\Phi_i^*} F_{1i} w_{mi} \bar{w}_{mi} \bar{w}_{ai}' \\
& - \frac{1}{4} \sqrt{\frac{\Phi_i^*}{\Phi_0^*}} \frac{\eta}{\sqrt{\Phi_i^*}} D_{1i} w_{ei} \bar{w}_{ei} \bar{w}_{ai}' + \frac{1}{4} \sqrt{\frac{\Phi_i^*}{\Phi_0^*}} \frac{\eta}{\sqrt{\Phi_i^*}} \bar{D}_{1i} w_{ei} w_{mi} \bar{w}_{ai}', \\
C_{\bar{V}I Io} = & \int_{z_0}^{z_i} \frac{1}{32} \sqrt{\frac{\Phi^*}{\Phi_0^*}} [A_1 w_m^2 \bar{w}_e + A_2 w_m^2 \bar{w}_e' + A_3 \bar{w}_e w_m w_m' + A_4 \bar{w}_e w_m w_m'' + A_5 w_m^2 \bar{w}_e'' \\
& + A_6 w_m^2 \bar{w}_e + A_7 w_m^2 \bar{w}_e' + E_1 \bar{F}_1 w_m^2 + E_2 \bar{F}_1 w_m w_m' + E_3 \bar{F}_1 (w_m w_m'' + w_m'^2) \\
& + (G_1 D_1 (w_m \bar{w}_e'' - w_m' \bar{w}_e) + G_2 D_1 w_m \bar{w}_e + G_3 D_1 w_m \bar{w}_e')] dz \\
& + \frac{1}{32} \sqrt{\frac{\Phi_i^*}{\Phi_0^*}} \left(\frac{\gamma_{0i} \Phi_i''}{\Phi_i^*} - 2 \frac{\eta B_i'}{\sqrt{\Phi_i^*}} \right) w_{mi}^2 \bar{w}_{ei} \bar{w}_{ai}' - \frac{1}{16} \sqrt{\frac{\Phi_i^*}{\Phi_0^*}} \frac{\gamma_{0i}}{\Phi_i^*} \bar{F}_{1i} w_{mi}^2 \bar{w}_{ai}' \\
& - \frac{1}{4} \sqrt{\frac{\Phi_i^*}{\Phi_0^*}} \frac{\eta}{\sqrt{\Phi_i^*}} D_{1i} w_{mi} \bar{w}_{ei} \bar{w}_{ai}'.
\end{aligned} \tag{3.148}$$

The four-fold astigmatism:

$$C_{V\bar{I}Ao} = \int_{z_0}^{z_i} \frac{1}{16} \sqrt{\frac{\Phi^*}{\Phi_0^*}} \left[-\frac{48\gamma_0}{\Phi^*} F_3 \bar{w}_\alpha^2 \bar{w}_m + G_4 D_3 \bar{w}_\alpha \bar{w}_e \right] dz. \tag{3.150}$$

The four-fold distortion:

$$C_{V\bar{V}Io} = \int_{z_0}^{z_i} \frac{1}{32} \sqrt{\frac{\Phi^*}{\Phi_0^*}} \left[-\frac{96\gamma_0}{\Phi^*} F_3 \bar{w}_e \bar{w}_m \bar{w}_\alpha + G_4 D_3 \bar{w}_e^2 \right] dz, \tag{3.151}$$

$$C_{\bar{V}I Io} = \int_{z_0}^{z_i} \frac{1}{32} \sqrt{\frac{\Phi^*}{\Phi_0^*}} \left[-\frac{48\gamma_0}{\Phi^*} F_3 \bar{w}_m^2 \bar{w}_\alpha + 2G_4 D_3 \bar{w}_e \bar{w}_m \right] dz. \tag{3.152}$$

3.5.2 Conversion of deflection aberration coefficients

I. Expressions of aberrations defined at the image plane.

Eq. (3.125) expresses aberrations virtually defined at the objective plane. The relation to aberrations at the image plane is given by Eq. (3.110) and (3.124), that is:

$$\Delta w_i = w_{yi} \Delta w_o, \quad (3.153)$$

where w_{yi} is a value of the off-axis ray at the image plane. It is related to the lateral magnification by

$$w_{yi} = e^{i\chi_i} M, \quad (3.154)$$

where χ_i is a rotation angle from the object plane to the image plane, and M is a lateral magnification. In addition, Eq. (3.125) uses a complex slope of an electron at the object plane, w'_o , as a geometrical parameter. When we discuss aberrations at the image plane, it is better to use a complex slope defined at the image plane as follows:

$$s_i = w'_o w'_{ai} = e^{i\chi_i} M_\alpha w'_o, \quad (3.155)$$

where M_α is the angular magnification. The complex slope s_i means the landing slope of an electron, with respect to the optic axis, at the image plane, which starts from an object point on the optic axis at the object plane with a slope w'_o . The aberration at the image plane is expressed as follows:

$$\begin{aligned} \Delta w_i = & C_{aa\bar{a}i} s_i^2 \bar{s}_i + C_{v\bar{a}ai} V s_i \bar{s}_i + C_{\bar{v}aai} \bar{V} s_i^2 + C_{v\bar{v}ai} V \bar{V} s_i + C_{vv\bar{a}i} V^2 \bar{s}_i + C_{vv\bar{v}i} V^2 \bar{V} \\ & + C_{v\bar{a}\bar{a}i} \bar{V} \bar{s}_i^2 + C_{v\bar{v}\bar{a}i} \bar{V}^2 \bar{s}_i + C_{v\bar{v}\bar{v}i} \bar{V}^3 + C_{Ia\bar{a}i} I s_i \bar{s}_i + C_{Iaai} I s_i^2 + C_{I\bar{a}ai} I \bar{s}_i + C_{I\bar{a}\bar{a}i} I^2 \bar{s}_i \\ & + C_{I\bar{a}\bar{a}i} I^2 \bar{I} + C_{I\bar{a}\bar{a}i} I^2 \bar{s}_i + C_{I\bar{a}\bar{a}i} I^2 \bar{I} + C_{vI\bar{a}i} V I s_i + C_{vIai} \bar{V} I s_i + C_{vI\bar{a}i} V I \bar{s}_i \\ & + C_{v\bar{v}Ii} V \bar{V} I + C_{v\bar{v}Ii} V^2 \bar{I} + C_{v\bar{v}Ii} V I \bar{I} + C_{v\bar{v}Ii} \bar{V} I^2 + C_{\bar{v}I\bar{a}i} \bar{V} I \bar{s}_i + C_{\bar{v}I\bar{a}i} \bar{V}^2 I + C_{\bar{v}I\bar{a}i} \bar{V} I^2, \end{aligned} \quad (3.156)$$

where the subscript i means aberration coefficients defined at the image plane.

The relationship between aberration coefficients of the object plane and those of the image plane are given by

$$\begin{aligned} C_{aa\bar{a}i} &= \frac{w_{yi}}{w'_{ai}{}^2 w'_{ai}} C_{aa\bar{a}o}, & C_{v\bar{a}ai} &= \frac{w_{yi}}{w'_{ai} w'_{ai}} C_{v\bar{a}ao}, & C_{\bar{v}aai} &= \frac{w_{yi}}{w'_{ai}} C_{\bar{v}aao}, \\ C_{v\bar{v}ai} &= \frac{w_{yi}}{w'_{ai}} C_{v\bar{v}ao}, & C_{v\bar{v}\bar{a}i} &= \frac{w_{yi}}{w'_{ai}} C_{v\bar{v}\bar{a}o}, & C_{vv\bar{v}i} &= w_{yi} C_{vv\bar{v}o}, \\ C_{v\bar{a}\bar{a}i} &= \frac{w_{yi}}{w'_{ai}{}^2} C_{v\bar{a}\bar{a}o}, & C_{v\bar{v}\bar{a}i} &= \frac{w_{yi}}{w'_{ai}} C_{v\bar{v}\bar{a}o}, & C_{v\bar{v}\bar{v}i} &= w_{yi} C_{v\bar{v}\bar{v}o}, \\ C_{Ia\bar{a}i} &= \frac{w_{yi}}{w'_{ai} w'_{ai}} C_{Ia\bar{a}o}, & C_{Iaai} &= \frac{w_{yi}}{w'_{ai}{}^2} C_{Iaai}, & C_{I\bar{a}ai} &= \frac{w_{yi}}{w'_{ai}} C_{I\bar{a}ao}, \\ C_{I\bar{a}\bar{a}i} &= \frac{w_{yi}}{w'_{ai}} C_{I\bar{a}\bar{a}o}, & C_{I\bar{a}\bar{a}i} &= w_{yi} C_{I\bar{a}\bar{a}o}, & C_{I\bar{a}\bar{a}i} &= \frac{w_{yi}}{w'_{ai}{}^2} C_{I\bar{a}\bar{a}o}, \\ C_{I\bar{a}\bar{a}i} &= \frac{w_{yi}}{w'_{ai}} C_{I\bar{a}\bar{a}o}, & C_{I\bar{a}\bar{a}i} &= w_{yi} C_{I\bar{a}\bar{a}o}, & C_{v\bar{v}i} &= \frac{w_{yi}}{w'_{ai}} C_{v\bar{v}ao}, \\ C_{vIai} &= \frac{w_{yi}}{w'_{ai}} C_{vIao}, & C_{vI\bar{a}i} &= \frac{w_{yi}}{w'_{ai}} C_{vI\bar{a}o}, & C_{v\bar{v}Ii} &= w_{yi} C_{v\bar{v}Io}, \\ C_{v\bar{v}Ii} &= w_{yi} C_{v\bar{v}Io}, & C_{vI\bar{a}i} &= w_{yi} C_{vI\bar{a}o}, & C_{\bar{v}I\bar{a}i} &= w_{yi} C_{\bar{v}I\bar{a}o}, \\ C_{\bar{v}I\bar{a}i} &= \frac{w_{yi}}{w'_{ai}} C_{\bar{v}I\bar{a}o}, & C_{\bar{v}I\bar{a}i} &= w_{yi} C_{\bar{v}I\bar{a}o}, & C_{\bar{v}I\bar{a}i} &= w_{yi} C_{\bar{v}I\bar{a}o}. \end{aligned} \quad (3.157)$$

II. Expressions of aberrations parameterized by deflection beam shift.

In Eq. (3.156), the parameter of deflection is the complex voltage and current of deflectors. For the actual design of an electron optics system, the aberrations, which parameterized by deflection beam shift, are useful. Complex beam shifts M_e and S_m at the image plane, by electrostatic deflection and by magnetic deflection, are expressed as follows, respectively,

$$M_e = X_e + iY_e = Vw_{ei}, \quad (3.158)$$

$$S_m = X_m + iY_m = Iw_{mi}, \quad (3.159)$$

where deflection sensitivities w_{ei} and w_{mi} are given by Eq. (3.88) and (3.89). Using Eq. (3.158) and (3.159), parameters V and I of Eq. (3.156) are transformed into M_e and S_m as follows:

$$\begin{aligned} \Delta w_i = & C_{aa\bar{a}i} s_i^2 \bar{s}_i + C_{Vaa\bar{a}i}^F M_e s_i \bar{s}_i + C_{Vaa\bar{a}i}^F \bar{M}_e s_i^2 + C_{V\bar{V}ai}^F M_e \bar{M}_e s_i \\ & + C_{V\bar{V}ai}^F M_e^2 \bar{s}_i + C_{V\bar{V}V\bar{a}i}^F M_e^2 M_e + C_{V\bar{V}aa\bar{a}i}^F \bar{M}_e s_i^2 + C_{V\bar{V}V\bar{a}i}^F \bar{M}_e^2 \bar{s}_i + C_{V\bar{V}V\bar{V}i}^F \bar{M}_e^3 \\ & + C_{Iaa\bar{a}i}^F S_m s_i \bar{s}_i + C_{Iaa\bar{a}i}^F \bar{S}_m s_i^2 + C_{I\bar{a}ai}^F S_m \bar{S}_m s_i \\ & + C_{I\bar{a}ai}^F S_m^2 \bar{s}_i + C_{I\bar{I}i}^F S_m^2 S_m + C_{I\bar{a}ai}^F \bar{S}_m s_i^2 + C_{I\bar{I}i}^F S_m^2 \bar{s}_i + C_{I\bar{I}i}^F S_m^3 \\ & + C_{V\bar{I}ai}^F M_e \bar{I} s_i + C_{V\bar{I}ai}^F \bar{M}_e S_m s_i + C_{V\bar{I}ai}^F M_e S_m \bar{s}_i \\ & + C_{V\bar{V}Ii}^F M_e \bar{M}_e I + C_{V\bar{V}Ii}^F M_e^2 \bar{S}_m + C_{V\bar{I}Ii}^F M_e S_m \bar{S}_m + C_{V\bar{I}Ii}^F \bar{M}_e S_m^2 \\ & + C_{V\bar{I}a\bar{o}}^F M_e \bar{S}_m \bar{s}_i + C_{V\bar{V}Ii}^F \bar{M}_e^2 S_m + C_{V\bar{I}Ii}^F M_e S_m^2, \end{aligned} \quad (3.160)$$

where the superscript F of coefficients means aberration coefficients parameterized by beam shifts of deflection. The relationships between coefficients in Eq. (3.160) and those in Eq. (3.156) are given by

$$\begin{aligned} C_{Vaa\bar{a}i}^F &= \frac{1}{w_{ei}} C_{Vaa\bar{a}i}, & C_{Vaa\bar{a}i}^F &= \frac{1}{\bar{w}_{ei}} C_{Vaa\bar{a}i}, & C_{V\bar{V}ai}^F &= \frac{1}{w_{ei}\bar{w}_{ei}} C_{V\bar{V}ai}, \\ C_{V\bar{V}ai}^F &= \frac{1}{w_{ei}^2} C_{V\bar{V}ai}, & C_{V\bar{V}V\bar{a}i}^F &= \frac{1}{w_{ei}^2\bar{w}_{ei}} C_{V\bar{V}V\bar{a}i}, & C_{V\bar{V}aa\bar{a}i}^F &= \frac{1}{w_{ei}} C_{V\bar{V}aa\bar{a}i}, \\ C_{V\bar{V}V\bar{a}i}^F &= \frac{1}{w_{ei}^3} C_{V\bar{V}V\bar{a}i}, & C_{V\bar{V}V\bar{V}i}^F &= \frac{1}{w_{ei}^3} C_{V\bar{V}V\bar{V}i}, & C_{Iaa\bar{a}i}^F &= \frac{1}{w_{mi}} C_{Iaa\bar{a}i}, \\ C_{Iaa\bar{a}i}^F &= \frac{1}{\bar{w}_{mi}} C_{Iaa\bar{a}i}, & C_{I\bar{a}ai}^F &= \frac{1}{w_{mi}\bar{w}_{mi}} C_{I\bar{a}ai}, & C_{I\bar{I}i}^F &= \frac{1}{w_{mi}^2} C_{I\bar{I}i}, \\ C_{I\bar{I}i}^F &= \frac{1}{w_{mi}^2\bar{w}_{mi}} C_{I\bar{I}i}, & C_{V\bar{a}ai}^F &= \frac{1}{\bar{w}_{mi}} C_{V\bar{a}ai}, & C_{I\bar{I}a\bar{a}i}^F &= \frac{1}{\bar{w}_{mi}^2} C_{I\bar{I}a\bar{a}i}, \\ C_{I\bar{I}i}^F &= \frac{1}{\bar{w}_{mi}^3} C_{I\bar{I}i}, & C_{V\bar{I}ai}^F &= \frac{1}{w_{ei}\bar{w}_{mi}} C_{V\bar{I}ai}, & C_{V\bar{I}ai}^F &= \frac{1}{w_{mi}\bar{w}_{ei}} C_{V\bar{I}ai}, \\ C_{V\bar{I}ai}^F &= \frac{1}{w_{ei}\bar{w}_{mi}} C_{V\bar{I}ai}, & C_{V\bar{V}Ii}^F &= \frac{1}{w_{ei}\bar{w}_{ei}\bar{w}_{mi}} C_{V\bar{V}Ii}, & C_{V\bar{V}Ii}^F &= \frac{1}{w_{ei}^2\bar{w}_{mi}} C_{V\bar{V}Ii}, \\ C_{V\bar{V}Ii}^F &= \frac{1}{w_{ei}\bar{w}_{mi}\bar{w}_{mi}} C_{V\bar{V}Ii}, & C_{V\bar{I}Ii}^F &= \frac{1}{\bar{w}_{ei}w_{mi}^2} C_{V\bar{I}Ii}, & C_{V\bar{I}a\bar{o}}^F &= \frac{1}{\bar{w}_{ei}\bar{w}_{mi}} C_{V\bar{I}a\bar{o}}, \\ C_{V\bar{V}Ii}^F &= \frac{1}{\bar{w}_{ei}^2\bar{w}_{mi}} C_{V\bar{V}Ii}, & C_{V\bar{I}Ii}^F &= \frac{1}{\bar{w}_{ei}\bar{w}_{mi}^2} C_{V\bar{I}Ii}. \end{aligned} \quad (3.161)$$

In this section, we derived aberration coefficients of a deflection system, which consists of a single electrostatic deflector and a single magnetic deflector. We derived aberration coefficients, which parameterized by the complex voltage and the complex current of deflectors, defined at the object plane and defined at the image plane. In addition, we derived the conversion relation of aberration coefficients from those parameterized by voltage and current to those parameterized by deflection beam shifts of electrostatic deflection and magnetic deflection.

3.6 Geometrical aberration coefficients of the system, which is composed of two independent electrostatic deflectors.

In this section, we derive deflection aberration coefficients of the system, which consists of two independent electrostatic deflectors, that is electrostatic deflector A and B. For this case, we can use Eq. (3.118)-(3.121) to obtain third-order geometrical aberration coefficients, when we set $S_A = V_A, S_B = V_B, S_C^V = V_A, S_D^V = V_B, S_E^I = 0, S_F^I = 0, w_A = w_e^A, w_B = w_e^B$. However, deflection aberration coefficients, which are dependent on only V_A , and \bar{V}_A , or V_B , and \bar{V}_B , are obtained by just replacing F_1 in Eq. (3.127) to (3.134) by F_1^A or F_1^B . New formulae are for aberration coefficient of cross-deflection aberration between electrostatic deflector A and B. Cross-aberration of electrostatic deflector A and B, at the object plane, is given by

$$\begin{aligned} \Delta w_o = & C_{V_A \bar{V}_B \alpha o} V_A \bar{V}_B w_o' + C_{\bar{V}_A V_B \alpha o} \bar{V}_A V_B w_o' + C_{V_A V_B \alpha o} V_A V_B \bar{w}_o' \\ & + C_{V_A \bar{V}_A V_B o} V_A \bar{V}_A V_B + C_{V_A V_A \bar{V}_B o} V_A^2 \bar{V}_B + C_{V_A V_B \bar{V}_B o} V_A V_B \bar{V}_B + C_{\bar{V}_A V_B V_B o} \bar{V}_A V_B V_B \\ & + C_{\bar{V}_A \bar{V}_B \alpha o} \bar{V}_A \bar{V}_B \bar{w}_o' + C_{\bar{V}_A \bar{V}_A \bar{V}_B o} \bar{V}_A^2 \bar{V}_B + C_{\bar{V}_A \bar{V}_B \bar{V}_B o} \bar{V}_A \bar{V}_B \bar{V}_B. \end{aligned} \quad (3.162)$$

The formulae of coefficients are given as follows:

The deflection field curvature coefficients,

$$\begin{aligned} C_{V_A \bar{V}_B \alpha o} = & \int_{z_o}^{z_i} \frac{1}{32} \sqrt{\frac{\Phi^*}{\Phi_o^*}} [2A_1 w_\alpha w_A \bar{w}_B + 2A_2 w_\alpha w_A \bar{w}_B' + A_3 \bar{w}_B (w_A w_\alpha' + w_\alpha w_A') \\ & + A_4 \bar{w}_B (w_A w_\alpha'' + w_\alpha w_B'') + 2A_5 w_\alpha w_A \bar{w}_B'' + 2A_6 w_\alpha' w_A' \bar{w}_B \\ & + 2A_7 w_\alpha' w_A' \bar{w}_B' + 2E_1 F_1^A w_\alpha \bar{w}_B + E_2 F_1^A (w_\alpha' \bar{w}_B + w_\alpha \bar{w}_B') \\ & + E_3 F_1^A (w_\alpha'' \bar{w}_B + w_\alpha \bar{w}_B'') + E_4 F_1^A w_\alpha \bar{w}_B' 2E_1 F_1^B w_\alpha w_A \\ & + E_2 F_1^B (w_\alpha w_A' + w_\alpha' w_A) + E_3 F_1^B (w_\alpha w_A'' + w_\alpha'' w_A + 2w_\alpha' w_A') \\ & + E_5 F_1^A F_1^B w_\alpha] dz, \end{aligned} \quad (3.163)$$

$$\begin{aligned} C_{\bar{V}_A V_B \alpha o} = & \int_{z_o}^{z_i} \frac{1}{32} \sqrt{\frac{\Phi^*}{\Phi_o^*}} [2A_1 w_\alpha \bar{w}_A w_B + 2A_2 w_\alpha w_B \bar{w}_A' + A_3 \bar{w}_A (w_B w_\alpha' + w_\alpha w_B') \\ & + A_4 \bar{w}_A (w_B w_\alpha'' + w_\alpha w_B'') + 2A_5 w_\alpha w_B \bar{w}_A'' + 2A_6 w_\alpha' w_B' \bar{w}_A \\ & + 2A_7 w_\alpha' w_B' \bar{w}_A' + 2E_1 F_1^A w_\alpha w_B + E_2 F_1^A (w_\alpha w_B' + w_\alpha' w_B) \\ & + E_3 F_1^A (w_\alpha'' w_B + w_\alpha' w_B' + 2w_\alpha' w_B') 2E_1 F_1^B w_\alpha \bar{w}_A \\ & + E_2 F_1^B (w_\alpha' \bar{w}_A + w_\alpha \bar{w}_A') + E_3 F_1^B (w_\alpha'' \bar{w}_A + w_\alpha' \bar{w}_A') + E_4 F_1^B w_\alpha \bar{w}_A' \\ & + E_5 F_1^A F_1^B w_\alpha] dz. \end{aligned} \quad (3.164)$$

The deflection astigmatism coefficient,

$$\begin{aligned} C_{V_A V_B \alpha o} = & \int_{z_o}^{z_i} \frac{1}{32} \sqrt{\frac{\Phi^*}{\Phi_o^*}} [2A_1 \bar{w}_\alpha w_A w_B + 2A_2 \bar{w}_\alpha' w_A w_B + A_3 \bar{w}_\alpha (w_A w_B' + w_B w_A') \\ & + A_4 \bar{w}_\alpha (w_A w_B'' + w_B w_A'') + 2A_5 \bar{w}_\alpha'' w_A w_B + 2A_6 \bar{w}_\alpha w_A' w_B' \\ & + 2A_7 w_A' w_B' \bar{w}_\alpha + 2E_1 F_1^A \bar{w}_\alpha w_B + E_2 F_1^A (w_B' \bar{w}_\alpha + w_B \bar{w}_\alpha') \\ & + E_3 F_1^A (w_B'' \bar{w}_\alpha + w_B' \bar{w}_\alpha') + E_4 F_1^A w_B \bar{w}_\alpha' 2E_1 F_1^B \bar{w}_\alpha w_A \\ & + E_2 F_1^B (w_A' \bar{w}_\alpha + w_A \bar{w}_\alpha') + E_3 F_1^B (w_A'' \bar{w}_\alpha + w_A' \bar{w}_\alpha') + E_4 F_1^B w_A \bar{w}_\alpha' \\ & + 2E_5 F_1^A F_1^B \bar{w}_\alpha] dz, \end{aligned} \quad (3.165)$$

The deflection distortion coefficients,

$$C_{V_A V_B V_{B0}} = \int_{z_0}^{z_l} \frac{1}{32} \sqrt{\frac{\Phi^*}{\Phi_0^*}} [2A_1 w_A \bar{w}_A w_B + 2A_2 w_A \bar{w}'_A w_B + A_3 \bar{w}_A (w_B w'_A + w_A w'_B) + A_4 \bar{w}_A (w_B w'_A + w_A w'_B) + A_7 w'_A w'_B \bar{w}'_A + 2E_1 F_1^B w_A \bar{w}_A + E_2 F_1^B (w'_A \bar{w}_A + w_A \bar{w}'_A) + E_3 F_1^B (w'_A \bar{w}'_A + w_A \bar{w}'_A) + 2w'_A \bar{w}'_A) + E_4 F_1^B w_A \bar{w}'_A 2E_1 F_1^A \bar{w}_A w_B + E_2 F_1^A (w_B \bar{w}'_A + w'_B \bar{w}_A) + E_3 F_1^A (w'_B \bar{w}_A + w_B \bar{w}'_A) + 2w'_B \bar{w}'_A) + E_4 F_1^A w_B \bar{w}'_A + 2E_1 F_1^A w_A w_B + E_2 F_1^A (w_A w'_B + w_B w'_A) + E_3 F_1^A (w_A w'_B + w_B w'_A) + E_5 F_1^A F_1^A w_B + E_5 F_1^B F_1^A w_A + 2E_5 F_1^A F_1^B \bar{w}_A] dz$$

(3.166)

$$+ \frac{1}{16} \sqrt{\frac{\Phi_i^*}{\Phi_0^*}} \left(\frac{\gamma_{0i} \Phi_i''}{\Phi_i^*} - 2 \frac{\eta B_i'}{\sqrt{\Phi_i^*}} \right) \bar{w}'_{ai} w_A \bar{w}_A w_B - \frac{1}{8} \sqrt{\frac{\Phi_i^*}{\Phi_0^*}} \frac{\gamma_{0i}}{\Phi_i^*} (F_{11}^B w_{Ai} \bar{w}_{Ai} \bar{w}'_{ai} + F_{11}^A \bar{w}_{Ai} w_{Bi} \bar{w}'_{ai} + \bar{F}_{11}^A w_{Ai} w_{Bi} \bar{w}'_{ai}),$$

$$C_{V_A V_B V_{B0}} = \int_{z_0}^{z_l} \frac{1}{32} \sqrt{\frac{\Phi^*}{\Phi_0^*}} [A_1 w_A^2 \bar{w}_B + A_2 w_A^2 \bar{w}'_B + A_3 w_A \bar{w}_B w'_A + A_4 w_A \bar{w}_B w''_A + A_5 w_A^2 \bar{w}_B'' + A_6 w_A'^2 \bar{w}_B + A_7 w_A'^2 \bar{w}'_B + E_1 \bar{F}_1^B w_A^2 + E_2 \bar{F}_1^B w_A w'_A + E_3 \bar{F}_1^B (w_A w'_A + w_A'^2) + 2E_1 F_1^A w_A \bar{w}_B + E_2 F_1^A (w_A \bar{w}'_B + w'_A \bar{w}_B) + E_3 F_1^A (w_A \bar{w}_B + w_A \bar{w}'_B + 2w'_A \bar{w}'_B) + E_4 F_1^A w_A \bar{w}'_B + E_5 F_1^A \bar{F}_1^B w_A + E_5 F_1^A^2 \bar{w}_B] dz$$

(3.167)

$$+ \frac{1}{32} \sqrt{\frac{\Phi_i^*}{\Phi_0^*}} \left(\frac{\gamma_{0i} \Phi_i''}{\Phi_i^*} - 2 \frac{\eta B_i'}{\sqrt{\Phi_i^*}} \right) \bar{w}'_{ai} w_A^2 \bar{w}_B - \frac{1}{16} \sqrt{\frac{\Phi_i^*}{\Phi_0^*}} \frac{\gamma_{0i}}{\Phi_i^*} (2F_{11}^A w_{Ai} \bar{w}_{Bi} \bar{w}'_{ai} + \bar{F}_{11}^B w_{Ai}^2 \bar{w}'_{ai}),$$

$$C_{V_A V_B V_{B0}} = \int_{z_0}^{z_l} \frac{1}{32} \sqrt{\frac{\Phi^*}{\Phi_0^*}} [2A_1 w_A w_B \bar{w}_B + 2A_2 w_A w_B \bar{w}'_B + A_3 \bar{w}_B (w_B w'_A + w_A w'_B) + A_3 \bar{w}_B (w_B w'_A + w_A w'_B) + 2A_5 w_A w_B \bar{w}'_B + A_6 w'_A w'_B \bar{w}_B + A_7 w'_A w'_B \bar{w}'_B + 2E_1 F_1^A w_B \bar{w}_B + E_2 F_1^A (w'_B \bar{w}_B + w_B \bar{w}'_B) + E_3 F_1^A (w'_B \bar{w}'_B + w_B \bar{w}'_B) + 2w'_B \bar{w}'_B) + E_4 F_1^A w_B \bar{w}'_B 2E_1 F_1^B w_A \bar{w}_B + E_2 F_1^B (w_A \bar{w}'_B + w'_A \bar{w}_B) + E_3 F_1^B (w'_A \bar{w}_B + w_A \bar{w}'_B + 2w'_A \bar{w}'_B) + E_4 F_1^B w_A \bar{w}'_B + 2E_1 \bar{F}_1^B w_A w_B + E_2 \bar{F}_1^B (w_A w'_B + w_B w'_A) + E_3 \bar{F}_1^B (w_A w'_B + w_B w'_A) + 2w'_A \bar{w}'_B) + E_5 F_1^B \bar{F}_1^B w_A + E_5 F_1^A \bar{F}_1^B w_B + 2E_5 F_1^A F_1^B \bar{w}_A] dz$$

(3.168)

$$+ \frac{1}{32} \sqrt{\frac{\Phi_i^*}{\Phi_0^*}} \left(\frac{\gamma_{0i} \Phi_i''}{\Phi_i^*} - 2 \frac{\eta B_i'}{\sqrt{\Phi_i^*}} \right) \bar{w}'_{ai} w_A w_B \bar{w}_B - \frac{1}{8} \sqrt{\frac{\Phi_i^*}{\Phi_0^*}} \frac{\gamma_{0i}}{\Phi_i^*} (F_{11}^A w_{Bi} \bar{w}_{Bi} \bar{w}'_{ai} + \bar{F}_{11}^B w_{Ai} w_{Bi} \bar{w}'_{ai} + F_{11}^B w_{Ai} \bar{w}_{Bi} \bar{w}'_{ai}),$$

$$C_{V_A V_B V_{B0}} = \int_{z_0}^{z_l} \frac{1}{32} \sqrt{\frac{\Phi^*}{\Phi_0^*}} [A_1 w_B^2 \bar{w}_A + A_2 w_B^2 \bar{w}'_A + A_3 \bar{w}_A w_B w'_B + A_4 \bar{w}_A w_B w''_B + A_5 w_B^2 \bar{w}_A'' + A_6 w_B'^2 \bar{w}_A + A_7 w_B'^2 \bar{w}'_A + E_1 \bar{F}_1^A w_B^2 + E_2 \bar{F}_1^A w_B w'_B + E_3 \bar{F}_1^A (w_B w'_B + w_B'^2) + 2E_1 F_1^B \bar{w}_A w_B + E_2 F_1^B (w_B \bar{w}'_A + w'_B \bar{w}_A) + E_3 F_1^B (w'_B \bar{w}_A + w_B \bar{w}'_A) + 2w'_B \bar{w}'_A) + E_4 F_1^B w_B \bar{w}'_A + E_5 F_1^B \bar{F}_1^B w_A + E_5 F_1^A \bar{F}_1^B w_B + E_5 F_1^B^2 \bar{w}_A] dz$$

(3.169)

$$+ \frac{1}{32} \sqrt{\frac{\Phi_i^*}{\Phi_0^*}} \left(\frac{\gamma_{0i} \Phi_i''}{\Phi_i^*} - 2 \frac{\eta B_i'}{\sqrt{\Phi_i^*}} \right) \bar{w}'_{ai} w_B^2 \bar{w}_A - \frac{1}{16} \sqrt{\frac{\Phi_i^*}{\Phi_0^*}} \frac{\gamma_{0i}}{\Phi_i^*} (2F_{11}^B \bar{w}_{Ai} w_{Bi} \bar{w}'_{ai} + \bar{F}_{11}^A w_{Bi}^2 \bar{w}'_{ai}),$$

The four-fold astigmatism,

$$C_{V_A V_B \bar{\alpha} 0} = - \int_{z_0}^{z_l} 3 \sqrt{\frac{\Phi^*}{\Phi_0^*}} \frac{\gamma_0}{\Phi^*} \bar{w}_\alpha^2 (F_3^A \bar{w}_B + F_3^B \bar{w}_A) dz,$$

(3.170)

The four-fold distortion,

$$C_{\bar{V}_A \bar{V}_A \bar{V}_B 0} = - \int_{z_0}^{z_i} \frac{3}{2} \sqrt{\frac{\Phi^*}{\Phi_0^*}} \frac{\gamma_0}{\Phi^*} (2F_3^A \bar{w}_A \bar{w}_B + F_3^B \bar{w}_A^2) \bar{w}_\alpha dz, \quad (3.171)$$

$$C_{\bar{V}_A \bar{V}_B \bar{V}_B 0} = - \int_{z_0}^{z_i} \frac{3}{2} \sqrt{\frac{\Phi^*}{\Phi_0^*}} \frac{\gamma_0}{\Phi^*} (2F_3^B \bar{w}_A \bar{w}_B + F_3^A \bar{w}_B^2) \bar{w}_\alpha dz, \quad (3.172)$$

We are at the point where cross-deflection aberrations of two independent electrostatic deflectors, which are parameterized by complex voltages of electrostatic deflectors, are defined at the object plane. Here, we transform cross-deflection aberration coefficients of Eq. (3.162) to (3.172), into coefficients at the image plane and parameterized by deflection beam shifts. The beam shifts by electrostatic deflectors A and B at the image plane are given by

$$M_e^A = V_A w_{el}^A, \quad S_e^B = V_B w_{el}^B. \quad (3.173)$$

where M_e^A and S_e^B are beams shifts by electrostatic deflector A and B, respectively. Cross aberrations of two electrostatic deflectors at the image plane, parameterized by the beam shifts, are given by

$$\begin{aligned} \Delta w_i = & C_{V_A \bar{V}_B \alpha i}^F M_e^A \bar{S}_e^B S_i + C_{\bar{V}_A V_B \alpha o}^F \bar{M}_e^A S_e^B S_i + C_{V_A V_B \bar{\alpha} i}^F M_e^A S_e^B \bar{S}_i \\ & + C_{V_A \bar{V}_A V_B i}^F M_e^A \bar{M}_e^A S_e^B + C_{V_A V_A \bar{V}_B i}^F M_e^A S_e^B \bar{S}_e + C_{V_A V_B \bar{V}_B i}^F M_e^A S_e^B \bar{S}_e^2 + C_{\bar{V}_A V_B V_B i}^F \bar{M}_e^A S_e^B^2 \\ & + C_{\bar{V}_A \bar{V}_B \bar{\alpha} i}^F \bar{M}_e^A \bar{S}_e^B \bar{S}_i + C_{\bar{V}_A \bar{V}_A \bar{V}_B i}^F \bar{M}_e^A S_e^B^2 + C_{\bar{V}_A V_B \bar{V}_B i}^F \bar{M}_e^A \bar{S}_e^B^2, \end{aligned} \quad (3.174)$$

where cross-aberration coefficients are expressed by

$$\begin{aligned} C_{V_A \bar{V}_B \alpha i}^F &= \frac{w_{yi}}{w_{ei}^A \bar{w}_{ei}^B w_{\alpha i}'} C_{V_A \bar{V}_B \alpha o}, & C_{\bar{V}_A V_B \alpha i}^F &= \frac{w_{yi}}{\bar{w}_{ei}^A w_{ei}^B w_{\alpha i}'} C_{\bar{V}_A V_B \alpha o}, \\ C_{V_A V_B \bar{\alpha} i}^F &= \frac{w_{yi}}{w_{ei}^A \bar{w}_{ei}^B \bar{w}_{\alpha i}'} C_{V_A V_B \bar{\alpha} o}, & C_{\bar{V}_A \bar{V}_B i}^F &= \frac{w_{yi}}{w_{ei}^A \bar{w}_{ei}^B \bar{w}_{\alpha i}'} C_{\bar{V}_A \bar{V}_B i o}, \\ C_{V_A V_A \bar{V}_B i}^F &= \frac{w_{yi}}{w_{ei}^A \bar{w}_{ei}^B} C_{V_A V_A \bar{V}_B o}, & C_{V_A V_B \bar{V}_B i}^F &= \frac{w_{yi}}{w_{ei}^A \bar{w}_{ei}^B \bar{w}_{\alpha i}'} C_{V_A V_B \bar{V}_B o}, \\ C_{\bar{V}_A V_B V_B i}^F &= \frac{w_{yi}}{\bar{w}_{ei}^A \bar{w}_{ei}^B} C_{\bar{V}_A V_B V_B o}, & C_{\bar{V}_A \bar{V}_B \bar{\alpha} i}^F &= \frac{w_{yi}}{\bar{w}_{ei}^A \bar{w}_{ei}^B \bar{w}_{\alpha i}'} C_{\bar{V}_A \bar{V}_B \bar{\alpha} o}, \\ C_{\bar{V}_A \bar{V}_A \bar{V}_B i}^F &= \frac{w_{yi}}{\bar{w}_{ei}^A \bar{w}_{ei}^B} C_{\bar{V}_A \bar{V}_A \bar{V}_B o}, & C_{\bar{V}_A \bar{V}_B V_B i}^F &= \frac{w_{yi}}{\bar{w}_{ei}^A \bar{w}_{ei}^B} C_{\bar{V}_A \bar{V}_B V_B o}. \end{aligned} \quad (3.175)$$

We are at the point where cross-aberration coefficients of two independent electrostatic deflectors at the image plane, parameterized by deflection beam shifts, are derived.

3.7 Geometrical aberration coefficients of the system, which is composed of two independent magnetic deflectors.

In this section, we derive deflection aberration coefficients of the system, which consists of two independent magnetic deflectors, namely magnetic deflector A and B. For this case, we can use Eq. (3.118)-(3.121) to obtain third-order geometrical aberration coefficients, when we set $S_A = I_A, S_B = I_B, S_C^V = 0, S_D^V = 0, S_E^I = I_A, S_F^I = I_B, w_A = w_m^A, w_B = w_m^B$. However, deflection aberration coefficients, which are dependent on only I_A , and \bar{I}_A , or I_B , and \bar{I}_B , are obtained

by just replacing D_1 in Eq. (3.127) to (3.134) by D_1^A or D_1^B . New formulae are for aberration coefficient of cross-deflection aberration between magnetic deflector A and B. Cross-aberration of magnetic deflector A and B, at the object plane, is given by

$$\begin{aligned} \Delta w_o = & C_{I_A \bar{I}_B \alpha o} I_A \bar{I}_B w'_o + C_{I_A I_B \alpha o} \bar{I}_A I_B w'_o + C_{I_A I_B \alpha o} V_I V_I \bar{w}'_o \\ & + C_{I_A \bar{I}_A I_B o} I_A \bar{I}_A I_B + C_{I_A I_A \bar{I}_B o} I_A^2 \bar{I}_B + C_{I_A I_B \bar{I}_B o} I_A I_B \bar{I}_B + C_{\bar{I}_A I_B I_B o} \bar{I}_A I_B I_B \\ & + C_{I_A \bar{I}_B \bar{\alpha} o} I_A \bar{I}_B \bar{w}'_o + C_{I_A I_A \bar{I}_B o} I_A \bar{I}_A \bar{I}_B + C_{I_A I_B I_B o} I_A I_B \bar{I}_B. \end{aligned} \quad (3.176)$$

The formulae of coefficients are given as follows:

The deflection field curvature coefficients,

$$\begin{aligned} C_{I_A \bar{I}_B \alpha o} = & \int_{z_o}^{z_i} \frac{1}{32} \sqrt{\frac{\Phi^*}{\Phi_o^*}} [2A_1 w_\alpha w_A \bar{w}_B + 2A_2 w_\alpha w_A \bar{w}'_B + A_3 \bar{w}_B (w_A w'_\alpha + w_\alpha w'_A) \\ & + A_4 \bar{w}_B (w_A w''_\alpha + w_\alpha w''_A) + 2A_5 w_\alpha w_A \bar{w}''_B + 2A_6 w'_\alpha w'_A \bar{w}_B \\ & + 2A_7 w'_\alpha w'_A \bar{w}'_B + G_1 D_1^A (w_\alpha \bar{w}''_B - w''_\alpha \bar{w}_B) + G_2 D_1^A w_\alpha \bar{w}_B \\ & + G_3 D_1^A w_\alpha \bar{w}'_B + G_1 \bar{D}_1^B (2w'_\alpha w'_A + w''_\alpha w_A + w_\alpha w'_A) \\ & - 2G_2 \bar{D}_1^B w_\alpha w_A] dz, \end{aligned} \quad (3.177)$$

$$\begin{aligned} C_{\bar{I}_A I_B \alpha o} = & \int_{z_o}^{z_i} \frac{1}{32} \sqrt{\frac{\Phi^*}{\Phi_o^*}} [2A_1 w_\alpha \bar{w}_A w_B + 2A_2 w_\alpha w_B \bar{w}'_A + A_3 \bar{w}_A (w_B w'_\alpha + w_\alpha w'_B) \\ & + A_4 \bar{w}_A (w_B w''_\alpha + w_\alpha w''_B) + 2A_5 w_\alpha w_B \bar{w}''_A + 2A_6 w'_\alpha w'_B \bar{w}_A \\ & + 2A_7 w'_\alpha w'_B \bar{w}'_A + G_1 D_1^A (w_\alpha \bar{w}''_A - w''_\alpha \bar{w}_A) + G_2 D_1^B w_\alpha \bar{w}_A \\ & + G_3 D_1^B w_\alpha \bar{w}'_A + G_1 \bar{D}_1^A (2w'_\alpha w'_B + w''_\alpha w_B + w_\alpha w'_B) \\ & - 2G_2 \bar{D}_1^A w_\alpha w_B] dz, \end{aligned} \quad (3.178)$$

The deflection astigmatism coefficient,

$$\begin{aligned} C_{I_A I_A \bar{\alpha} o} = & \int_{z_o}^{z_i} \frac{1}{32} \sqrt{\frac{\Phi^*}{\Phi_o^*}} [2A_1 \bar{w}_\alpha w_A w_B + 2A_2 \bar{w}'_\alpha w_A w_B + A_3 \bar{w}_\alpha (w_A w'_B + w_B w'_A) \\ & + A_4 \bar{w}_\alpha (w_A w''_B + w_B w''_A) + 2A_5 \bar{w}_\alpha w_A w_B + 2A_6 \bar{w}_\alpha w'_A w'_B \\ & + 2A_7 w'_A w'_B \bar{w}'_\alpha + G_1 D_1^A (w_B \bar{w}''_\alpha - w''_\alpha \bar{w}_A) + G_2 D_1^A w_B \bar{w}_\alpha \\ & + G_3 D_1^A w_B \bar{w}'_\alpha + G_1 D_1^B (w_A \bar{w}''_\alpha - w''_\alpha \bar{w}_A) + G_2 D_1^B w_A \bar{w}_\alpha \\ & + G_3 D_1^B w_A \bar{w}'_\alpha] dz, \end{aligned} \quad (3.179)$$

The deflection distortion coefficients,

$$\begin{aligned} C_{I_A I_A I_B o} = & \int_{z_o}^{z_i} \frac{1}{32} \sqrt{\frac{\Phi^*}{\Phi_o^*}} [2A_1 w_A \bar{w}_A w_B + 2A_2 w_A \bar{w}'_A w_B + A_3 \bar{w}_A (w_B w'_A + w_A w'_B) \\ & + A_4 \bar{w}_A (w_B w''_A + w_A w''_B) + 2A_5 w_A \bar{w}''_A w_B + A_6 w'_A w'_B \bar{w}_A \\ & + A_7 w'_A w'_B \bar{w}'_A + G_1 D_1^B (w_A \bar{w}''_A - w''_A \bar{w}_A) + G_2 D_1^B w_A \bar{w}_A + G_3 D_1^B w_A \bar{w}'_A \\ & + G_1 D_1^A (w_B \bar{w}''_A - w''_B \bar{w}_A) + G_2 D_1^A w_B \bar{w}_A + G_3 D_1^A w_B \bar{w}'_A \\ & + G_1 \bar{D}_1^A (2w'_A w'_B + w''_A w_B + w_A w''_B) - 2G_2 \bar{D}_1^A w_A w_B] dz \end{aligned} \quad (3.180)$$

$$\begin{aligned} & + \frac{1}{16} \sqrt{\frac{\Phi_i^*}{\Phi_o^*}} \left(\frac{\gamma_{oi} \Phi_i''}{\Phi_i^*} - 2 \frac{\eta B_i'}{\sqrt{\Phi_i^*}} \right) \bar{w}'_{\alpha i} w_A \bar{w}_A w_B \\ & - \frac{1}{4} \sqrt{\frac{\Phi_i^*}{\Phi_o^*}} \frac{\eta}{\sqrt{\Phi_i^*}} \bar{w}_{\alpha i} (D_{1i}^A w_{Bi} \bar{w}_{Ai} + D_{1i}^B w_{Ai} \bar{w}_{Bi} - \bar{D}_{1i}^A w_{Ai} w_{Bi}), \\ C_{I_A I_A \bar{I}_B o} = & \int_{z_o}^{z_i} \frac{1}{32} \sqrt{\frac{\Phi^*}{\Phi_o^*}} [A_1 w_A^2 \bar{w}_B + A_2 w_A^2 \bar{w}'_B + A_3 w_A \bar{w}_B w'_A + A_4 w_A \bar{w}_B w''_A + A_5 w_A^2 \bar{w}''_B \\ & + A_6 w_A^2 \bar{w}_B + A_7 w_A^2 \bar{w}'_B + G_1 D_1^A (w_A \bar{w}''_B - w''_A \bar{w}_B) + G_2 D_1^A w_A \bar{w}_B \\ & + G_3 D_1^A w_A \bar{w}'_B + G_1 \bar{D}_1^B (w_A^2 + w_A w'_A) - G_2 \bar{D}_1^B w_A^2] dz \\ & + \frac{1}{32} \sqrt{\frac{\Phi_i^*}{\Phi_o^*}} \left(\frac{\gamma_{oi} \Phi_i''}{\Phi_i^*} - 2 \frac{\eta B_i'}{\sqrt{\Phi_i^*}} \right) \bar{w}_{\alpha i} w_A^2 \bar{w}_B - \frac{1}{8} \sqrt{\frac{\Phi_i^*}{\Phi_o^*}} \frac{\eta}{\sqrt{\Phi_i^*}} \bar{w}_{\alpha i} (2D_{1i}^A w_{Ai} \bar{w}_{Bi} - \bar{D}_{1i}^B w_{Ai}^2), \end{aligned} \quad (3.181)$$

$$\begin{aligned}
C_{I_A I_B I_{B^0}} = & \int_{z_0}^{z_i} \frac{1}{32} \sqrt{\frac{\Phi^*}{\Phi_0^*}} [2A_1 w_A w_B \bar{w}_B + 2A_2 w_A w_B \bar{w}_B' + A_3 \bar{w}_B (w_B w_A' + w_A w_B') \\
& + A_3 \bar{w}_B (w_B w_A'' + w_A w_B'') + 2A_5 w_A w_B \bar{w}_B' + A_6 w_A' w_B' \bar{w}_B \\
& + A_7 w_A' w_B' \bar{w}_B + G_1 D_1^B (w_A \bar{w}_B' - w_A' \bar{w}_B) + G_2 D_1^B w_A \bar{w}_B + G_3 D_1^B w_A \bar{w}_B' \\
& + G_1 D_1^A (w_B \bar{w}_B' - w_B' \bar{w}_B) + G_2 D_1^A w_B \bar{w}_B + G_3 D_1^A w_B \bar{w}_B' \\
& + G_1 \bar{D}_1^B (2w_A w_B' + w_A' w_B + w_A w_B') - 2G_2 \bar{D}_1^B w_A w_B] dz \\
& + \frac{1}{16} \sqrt{\frac{\Phi_i^*}{\Phi_0^*}} \left(\frac{\gamma_{0i} \Phi_i''}{\Phi_i^*} - 2 \frac{\eta B_i'}{\sqrt{\Phi_i^*}} \right) \bar{w}'_{\alpha i} w_A w_B \bar{w}_B \\
& - \frac{1}{4} \sqrt{\frac{\Phi_i^*}{\Phi_0^*}} \frac{\eta}{\sqrt{\Phi_i^*}} \bar{w}'_{\alpha i} (D_{1i}^A w_{Bi} \bar{w}_{Bi} + D_{1i}^B w_{Ai} \bar{w}_{Bi} - \bar{D}_{1i}^B w_{Ai} w_{Bi}),
\end{aligned} \tag{3.182}$$

$$\begin{aligned}
C_{I_A I_B I_{B^0}} = & \int_{z_0}^{z_i} \frac{1}{32} \sqrt{\frac{\Phi^*}{\Phi_0^*}} [A_1 w_B^2 \bar{w}_A + A_2 w_B^2 \bar{w}_A' + A_3 \bar{w}_A w_B w_B' + A_4 \bar{w}_A w_B w_B'' + A_5 w_B^2 \bar{w}_A'' \\
& + A_6 w_B'^2 \bar{w}_A + A_7 w_B'^2 \bar{w}_A' + G_1 D_1^B (w_B \bar{w}_A' - w_B' \bar{w}_A) + G_2 D_1^B w_B \bar{w}_A \\
& + G_3 D_1^B w_B \bar{w}_A' + G_1 \bar{D}_1^A (w_B'^2 + w_B w_B'') - G_2 \bar{D}_1^A w_B^2] dz \\
& + \frac{1}{32} \sqrt{\frac{\Phi_i^*}{\Phi_0^*}} \left(\frac{\gamma_{0i} \Phi_i''}{\Phi_i^*} - 2 \frac{\eta B_i'}{\sqrt{\Phi_i^*}} \right) \bar{w}'_{\alpha i} w_B^2 \bar{w}_A - \frac{1}{8} \sqrt{\frac{\Phi_i^*}{\Phi_0^*}} \frac{\eta}{\sqrt{\Phi_i^*}} \bar{w}'_{\alpha i} (2D_{1i}^B w_{Bi} \bar{w}_{Ai} - \bar{D}_{1i}^A w_{Bi}^2),
\end{aligned} \tag{3.183}$$

The four-fold astigmatism,

$$C_{I_A \bar{I}_B \bar{\alpha} 0} = \int_{z_0}^{z_i} \frac{1}{16} \sqrt{\frac{\Phi^*}{\Phi_0^*}} [G_4 D_3^A \bar{w}_\alpha \bar{w}_B + G_4 D_3^B \bar{w}_\alpha \bar{w}_A] dz, \tag{3.184}$$

The four-fold distortion,

$$C_{I_A I_A I_{B^0}} = \int_{z_0}^{z_i} \frac{1}{32} \sqrt{\frac{\Phi^*}{\Phi_0^*}} [2G_4 D_3^A \bar{w}_A \bar{w}_B + G_4 D_3^B \bar{w}_\alpha^2] dz, \tag{3.185}$$

$$C_{I_A I_B I_{B^0}} = \int_{z_0}^{z_i} \frac{1}{32} \sqrt{\frac{\Phi^*}{\Phi_0^*}} [G_4 D_3^A \bar{w}_B^2 + 2G_4 D_3^B \bar{w}_A \bar{w}_B] dz, \tag{3.186}$$

We are at the point where cross-deflection aberrations of two independent magnetic deflectors, parameterized by complex currents of magnetic deflectors, are defined at the object plane. Here, we transform cross-deflection aberration coefficients of Eq. (3.162) to (3.172), into coefficients at the image plane and parameterized by deflection beam shifts. The beam shifts by magnetic deflectors A and B at the image plane are given by

$$M_m^A = I_A w_{mi}^A, \quad S_m^B = I_B w_{mi}^B. \tag{3.187}$$

where M_m^A and S_m^B are beams shifts by magnetic deflector A and B, respectively. The cross aberrations of two magnetic deflectors at the image plane, parameterized by the beam shifts are given by

$$\begin{aligned}
\Delta w_i = & C_{I_A \bar{I}_B \alpha i}^F M_m^A \bar{S}_m^B s_i + C_{I_A \bar{I}_B \alpha 0}^F \bar{M}_m^A S_m^B s_i + C_{I_A \bar{I}_B \bar{\alpha} i}^F M_m^A S_m^B \bar{s}_i \\
& + C_{I_A \bar{I}_B \bar{\alpha} i}^F \bar{M}_m^A \bar{S}_m^B + C_{I_A \bar{I}_B \bar{\alpha} 0}^F \bar{M}_m^A S_m^B + C_{I_A \bar{I}_B \bar{\alpha} i}^F M_m^A S_m^B \bar{s}_i + C_{I_A \bar{I}_B \bar{\alpha} 0}^F \bar{M}_m^A S_m^B \\
& + C_{I_A \bar{I}_B \bar{\alpha} i}^F \bar{M}_m^A \bar{S}_m^B s_i + C_{I_A \bar{I}_B \bar{\alpha} i}^F \bar{M}_m^A S_m^B + C_{I_A \bar{I}_B \bar{\alpha} i}^F \bar{M}_m^A S_m^B s_i^2,
\end{aligned} \tag{3.188}$$

where the cross-aberration coefficients are expressed by

$$\begin{aligned}
C_{I_A I_B \alpha i}^F &= \frac{W_{yi}}{W_{mi}^A \bar{W}_{mi}^B W_{ai}'} C_{I_A I_B \alpha o}, & C_{I_A I_B \alpha i}^F &= \frac{W_{yi}}{\bar{W}_{mi}^A W_{mi}^B W_{ai}'} C_{I_A I_B \alpha o}, \\
C_{I_A I_B \bar{\alpha} i}^F &= \frac{W_{yi}}{W_{mi}^A W_{mi}^B \bar{W}_{ai}'} C_{I_A I_B \bar{\alpha} o}, & C_{I_A I_B \bar{\alpha} i}^F &= \frac{W_{yi}}{W_{mi}^A \bar{W}_{mi}^B W_{ai}'} C_{I_A I_B \bar{\alpha} o}, \\
C_{I_A I_B \bar{i} i}^F &= \frac{W_{yi}}{W_{mi}^A \bar{W}_{mi}^B} C_{I_A I_B \bar{i} o}, & C_{I_A I_B \bar{i} i}^F &= \frac{W_{yi}}{W_{mi}^A W_{mi}^B \bar{W}_{ai}'} C_{I_A I_B \bar{i} o}, \\
C_{I_A I_B i i}^F &= \frac{W_{yi}}{\bar{W}_{mi}^A W_{mi}^B} C_{I_A I_B i o}, & C_{I_A I_B i i}^F &= \frac{W_{yi}}{\bar{W}_{mi}^A \bar{W}_{mi}^B W_{ai}'} C_{I_A I_B i o}, \\
C_{I_A I_B i \bar{i} i}^F &= \frac{W_{yi}}{\bar{W}_{mi}^A \bar{W}_{mi}^B} C_{I_A I_B i \bar{i} o}, & C_{I_A I_B i \bar{i} i}^F &= \frac{W_{yi}}{W_{mi}^A W_{mi}^B \bar{W}_{ai}'} C_{I_A I_B i \bar{i} o}.
\end{aligned} \tag{3.189}$$

We are at the point where the cross-aberration coefficients of two independent magnetic deflectors at the image plane, parameterized by deflection beam shifts, are derived.

3.8 Chromatic deflection aberration and aberrations of voltage and current variation of lenses.

3.8.1 Perturbation functions for chromatic deflection aberration and aberrations of voltage and current variation of lenses.

In this section, we consider the explicit expansion of the perturbation function for chromatic aberration and aberrations of voltage and current variation of lenses for a system consisting of lenses and deflectors. We consider round-symmetric N electrodes and M coils of magnetic lenses, which are connected to voltage and current power supplies. Detailed definitions and settings of the axial potential of a nominal electron, whose energy is the average energy, are given in section 2.9. The result is given by

$$\Phi(z) = \Phi_C + \sum_{j=1}^N \Phi_j^{EL}(z), \tag{3.190}$$

where Φ_C is a column potential, Φ_j^{EL} is an axial potential distribution of the j -th round symmetric electrode, which is generated, when voltage V_j^{EL} is imposed on only the j -th electrode and other electrodes including the vacuum chamber are grounded. If we consider a shift of the total energy of an electron by $\Delta E = e\Delta\Phi = \text{const.}$, and a variation of imposed voltages of the j -th round-symmetric electrodes by ΔV_j^{EL} , then, we get changes of an axial electron potential and its first and second order derivatives, with respect to the optic axis, are obtained as follows:

$$\begin{aligned}
\Phi(z) &\rightarrow \Phi(z) + \Delta\Phi + \sum_{j=1}^N \frac{\Delta V_j^{EL}}{V_j^{EL}} \Phi_j^{EL}(z), \\
\Phi'(z) &\rightarrow \Phi'(z) + \sum_{j=1}^N \frac{\Delta V_j^{EL}}{V_j^{EL}} \Phi_j^{EL'}(z), \\
\Phi''(z) &\rightarrow \Phi''(z) + \sum_{j=1}^N \frac{\Delta V_j^{EL}}{V_j^{EL}} \Phi_j^{EL''}(z).
\end{aligned} \tag{3.191}$$

On the other hand, if we vary the coil current of the ℓ -th magnetic lens, I_ℓ^{ML} , by ΔI_ℓ^{ML} , the axial magnetic field shifts as follows:

$$B(z) \rightarrow B(z) + \sum_{\ell=1}^M \frac{\Delta I_\ell^{ML}}{I_\ell^{ML}} B_\ell(z), \quad (3.192)$$

In addition, we consider variation of voltage and current of deflectors by ΔV_{DEF} and ΔI_{DEF} . Taking into account Eq. (3.191) and (3.192), an expansion of the electron optical eikonal up to the third-rank is given by

$$\begin{aligned} \mu = & \sqrt{\frac{\Phi^*}{\Phi_o^*}} \left[1 + \frac{1}{2} w' \bar{w}' - \frac{\gamma_0 \Phi''}{8\Phi^*} w \bar{w} - \frac{i\eta}{4\sqrt{\Phi^*}} B(w \bar{w}' - \bar{w} w') + \frac{i\eta}{32\sqrt{\Phi^*}} B'' w \bar{w} (w \bar{w}' - \bar{w} w') \right. \\ & + \frac{\gamma_0}{4\Phi^*} (V F_1 \bar{w} + \bar{V} F_1 w) + \frac{\eta}{2\sqrt{\Phi^*}} (I D_1 \bar{w} + \bar{I} D_1 w) \\ & + \Delta\Phi \left\{ \frac{\gamma_0}{4\Phi^*} w' \bar{w}' + \frac{\Phi''}{16\Phi^{*2}} w \bar{w} - \frac{1}{8\Phi^{*2}} (V F_1 \bar{w} + \bar{V} F_1 w) \right\} \\ & + \sum_{j=1}^N \frac{\Delta V_j^{EL}}{V_j^{EL}} \left\{ \frac{\gamma_0 \Phi_j^{EL}}{4\Phi^*} w' \bar{w}' + \left(\frac{\Phi'' \Phi_j^{EL}}{16\Phi^{*2}} - \frac{\gamma_0 \Phi_j^{EL''}}{8\Phi^*} \right) w \bar{w} - \frac{\Phi_j^{EL}}{8\Phi^{*2}} (V F_1 \bar{w} + \bar{V} F_1 w) \right\} \\ & - \frac{i\eta}{4\sqrt{\Phi^*}} \sum_{\ell=1}^M \frac{\Delta I_\ell^{ML}}{I_\ell^{ML}} B_\ell(w \bar{w}' - \bar{w} w') \\ & \left. + \frac{\gamma_0}{4\Phi^*} (\Delta V^{DEF} F_1 \bar{w} + \Delta \bar{V}^{DEF} \bar{F}_1 w) + \frac{\eta}{2\sqrt{\Phi^*}} (\Delta I^{DEF} D_1 \bar{w} + \Delta \bar{I}^{DEF} \bar{D}_1 w) \right]. \end{aligned} \quad (3.193)$$

We divide Eq. (3.193) into three parts as follows. The first part contains terms up to the second-order, which give paraxial rays and deflection trajectories, as given in section 3.3,

$$\begin{aligned} \mu^{(2)} = & \sqrt{\frac{\Phi^*}{\Phi_o^*}} \left[1 + \frac{1}{2} w' \bar{w}' - \frac{\gamma_0 \Phi''}{8\Phi^*} w \bar{w} - \frac{i\eta}{4\sqrt{\Phi^*}} B(w \bar{w}' - \bar{w} w') + \frac{i\eta}{32\sqrt{\Phi^*}} B'' w \bar{w} (w \bar{w}' - \bar{w} w') \right. \\ & \left. + \frac{\gamma_0}{4\Phi^*} (V F_1 \bar{w} + \bar{V} F_1 w) + \frac{\eta}{2\sqrt{\Phi^*}} (I D_1 \bar{w} + \bar{I} D_1 w) \right]. \end{aligned} \quad (3.194)$$

The second part is composed of terms of the third-rank, which are the second order of geometrical parameters and the first degree of the chromatic parameter, corresponding to the energy deviation of electrons.

$$\Delta\mu_{\kappa 1}^{(2)} = \frac{\Delta\Phi}{\Phi_o^*} \sqrt{\frac{\Phi^*}{\Phi_o^*}} \left[\frac{\gamma_0}{4\Phi^*} w' \bar{w}' + \frac{\Phi''}{16\Phi^{*2}} w \bar{w} - \frac{1}{8\Phi^{*2}} (V F_1 \bar{w} + \bar{V} F_1 w) \right]. \quad (3.195)$$

The last part includes terms of the first-degree of variation of voltages and currents of lenses and deflectors, and of the second-order of geometrical parameters, as follows:

$$\begin{aligned} \Delta\mu_{wob 1}^{(2)} = & \sqrt{\frac{\Phi^*}{\Phi_o^*}} \left[\sum_{j=1}^N \frac{\Delta V_j^{EL}}{V_j^{EL}} \left\{ \frac{\gamma_0 \Phi_j^{EL}}{4\Phi^*} w' \bar{w}' + \left(\frac{\Phi'' \Phi_j^{EL}}{16\Phi^{*2}} - \frac{\gamma_0 \Phi_j^{EL''}}{8\Phi^*} \right) w \bar{w} - \frac{\Phi_j^{EL}}{8\Phi^{*2}} (V F_1 \bar{w} + \bar{V} F_1 w) \right\} \right. \\ & - \sum_{\ell=1}^M \frac{\Delta I_\ell^{ML}}{I_\ell^{ML}} \frac{i\eta B_\ell}{4\sqrt{\Phi^*}} (w \bar{w}' - \bar{w} w') \\ & \left. + \frac{\gamma_0}{4\Phi^*} (\Delta V^{DEF} F_1 \bar{w} + \Delta \bar{V}^{DEF} \bar{F}_1 w) + \frac{\eta}{2\sqrt{\Phi^*}} (\Delta I^{DEF} D_1 \bar{w} + \Delta \bar{I}^{DEF} \bar{D}_1 w) \right]. \end{aligned} \quad (3.196)$$

3.8.2 Formal expressions of path-deviations

The third-rank chromatic perturbation function Eq. (3.195) gives the second-rank chromatic deflection path-deviation, and the perturbation function of Eq. (3.196) gives the second-rank path-deviation of variation of voltages and currents via Eq. (3.92), which is written here again.

$$\begin{aligned} w_{\text{ptb}} = & 2 \left. \frac{\partial \Delta \mu}{\partial \bar{w}'} \right|_{z=z_0} w_\alpha - 2(w_\gamma + 2i\chi'_0 w_\alpha) \int_{z_0}^z \left(\frac{\partial \Delta \mu}{\partial \bar{w}'} \bar{w}'_\alpha + \frac{\partial \Delta \mu}{\partial \bar{w}} \bar{w}_\alpha \right) dz \\ & + 2w_\alpha \int_{z_0}^z \left(\frac{\partial \Delta \mu}{\partial \bar{w}'} \bar{w}'_\gamma + \frac{\partial \Delta \mu}{\partial \bar{w}} \bar{w}_\gamma \right) dz. \end{aligned} \quad (3.197)$$

We can repeat the same discussion as given below Eq. (3.96) in section 3.4.1, for the perturbation functions of Eq. (3.195) and Eq. (3.196). Then, the trajectories and the slopes in the integrands of Eq. (3.92), for the perturbation functions of Eq. (3.195) and Eq. (3.196), can be replaced by the general paraxial trajectories including the deflection trajectories and their slopes. Considering that $\Delta \mu = \Delta \mu_{\kappa 1}^{(2)} + \Delta \mu_{wob 1}^{(2)}$, calculating differentiation with respect to \bar{w} , \bar{w}' and replacing trajectories by the general paraxial trajectories, we can obtain the following relations.

$$\begin{aligned} -2 \left(\frac{\partial \Delta \mu}{\partial \bar{w}'} \bar{w}'_A + \frac{\partial \Delta \mu}{\partial \bar{w}} \bar{w}_A \right) = & -\sqrt{\frac{\Phi^*}{\Phi_0^*}} \left[\frac{\Delta \Phi}{\Phi_0^*} \Phi_0^* \left\{ \frac{\gamma_0}{2\Phi^*} w^{(1)'} \bar{w}'_A + \left(\frac{\Phi''}{8\Phi^{*2}} w^{(1)} - \frac{VF_1}{4\Phi^{*2}} \right) \bar{w}_A \right\} \right. \\ & - \sum_{j=1}^N \frac{\Delta V_j^{EL}}{V_j^{EL}} \left\{ \frac{\gamma_0 \Phi_j^{EL}}{2\Phi^*} w^{(1)'} \bar{w}'_A + \left(\frac{\Phi'' \Phi_j^{EL}}{8\Phi^{*2}} - \frac{\gamma_0 \Phi_j^{EL'}}{4\Phi^*} \right) w^{(1)} \bar{w}_A - \frac{VF_1 \Phi_j^{EL}}{4\Phi^{*2}} \bar{w}_A \right\} \\ & \left. - \sum_{\ell=1}^M \frac{\Delta I_\ell^{ML}}{I_\ell^{ML}} \frac{i\eta B_\ell}{2\sqrt{\Phi^*}} \left(w^{(1)'} \bar{w}_A - w^{(1)} \bar{w}'_A \right) - \Delta V^{DEF} \frac{\gamma_0 F_1}{2\Phi^*} \bar{w}_A - \Delta I^{DEF} \frac{\eta D_1}{\sqrt{\Phi^*}} \bar{w}_A \right], \end{aligned} \quad (3.198)$$

where A takes either α or γ , and

$$2 \left. \frac{\partial \Delta \mu}{\partial \bar{w}'} \right|_{z=z_0} = \frac{\Delta \Phi}{\Phi_0^*} \Phi_0^* \frac{\gamma_{00}}{2\Phi_0^*} w'_0 + \sum_{j=1}^N \frac{\Delta V_j^{EL}}{V_j^{EL}} \frac{\gamma_{00} \Phi_{j0}^{EL}}{2\Phi_0^*} w'_0 - \sum_{\ell=1}^M \frac{\Delta I_\ell^{ML}}{I_\ell^{ML}} \frac{i\eta B_{\ell 0}}{2\sqrt{\Phi_0^*}} w'_0. \quad (3.199)$$

Before considering path-deviations, partial integration is performed to reduce the order of differentiation of terms of the integrand, Eq. (3.198) with respect to the optic axis. The target of partial integration is terms including the second-order derivative of the axis potential. Consider the following two integrals:

$$\begin{aligned} \int_{z_0}^z \sqrt{\frac{\Phi^*}{\Phi_0^*}} \frac{\Phi''}{8\Phi^{*2}} w^{(1)} \bar{w}_A dz = & \left[\sqrt{\frac{\Phi^*}{\Phi_0^*}} \frac{\Phi'}{8\Phi^{*2}} w^{(1)} \bar{w}_A \right]_{z_0}^z \\ & + \int_{z_0}^z \sqrt{\frac{\Phi^*}{\Phi_0^*}} \left(\frac{3\gamma_0 \Phi'^2}{16\Phi^{*3}} w^{(1)} \bar{w}_A - \frac{\Phi'}{8\Phi^{*2}} \left(w^{(1)'} \bar{w}_A + w^{(1)} \bar{w}'_A \right) \right) dz, \end{aligned} \quad (3.200)$$

and

$$\begin{aligned} \int_{z_0}^z \sqrt{\frac{\Phi^*}{\Phi_0^*}} \left(\frac{\Phi'' \Phi_j^{EL}}{8\Phi^{*2}} - \frac{\gamma_0 \Phi_j^{EL'}}{4\Phi^*} \right) w^{(1)} \bar{w}_A dz = & \left[\sqrt{\frac{\Phi^*}{\Phi_0^*}} \left(\frac{\Phi' \Phi_j^{EL}}{8\Phi^{*2}} - \frac{\gamma_0 \Phi_j^{EL'}}{4\Phi^*} \right) w^{(1)} \bar{w}_A \right]_{z_0}^z \\ & + \int_{z_0}^z \sqrt{\frac{\Phi^*}{\Phi_0^*}} \left[\left(\frac{3\gamma_0 \Phi'^2 \Phi_j^{EL}}{16\Phi^{*3}} - \frac{\Phi' \Phi_j^{EL'}}{4\Phi^{*2}} \right) w^{(1)} \bar{w}_A - \left(\frac{\Phi' \Phi_j^{EL}}{8\Phi^{*2}} - \frac{\gamma_0 \Phi_j^{EL'}}{4\Phi^*} \right) \left(w^{(1)'} \bar{w}_A + w^{(1)} \bar{w}'_A \right) \right] dz. \end{aligned} \quad (3.201)$$

Using Eq. (3.200) and (3.201), Eq. (3.198) is transformed into

$$\begin{aligned}
& -2 \int_{z_0}^z \left(\frac{\partial \Delta \mu}{\partial \bar{w}'} \bar{w}'_A + \frac{\partial \Delta \mu}{\partial \bar{w}} \bar{w}_A \right) dz = - \int_{z_0}^z \sqrt{\frac{\Phi^*}{\Phi_o}} \left[\frac{\Delta \Phi}{\Phi_o^*} \Phi_o^* \left(\frac{\gamma_0}{2\Phi^*} w^{(1)'} \bar{w}'_A \right. \right. \\
& + \left. \frac{3\gamma_0 \Phi'^2}{16\Phi^{*3}} w^{(1)} \bar{w}_A - \frac{\Phi'}{8\Phi^{*2}} (w^{(1)'} \bar{w}_A + w^{(1)} \bar{w}'_A) - \frac{VF_1}{4\Phi^{*2}} \bar{w}_A \right\} \\
& - \sum_{j=1}^N \frac{\Delta V_j^{EL}}{V_j^{EL}} \left\{ \frac{\gamma_0 \Phi_j^{EL}}{2\Phi^*} w^{(1)'} \bar{w}'_A + \left(\frac{3\gamma_0 \Phi'^2 \Phi_j^{EL}}{16\Phi^{*3}} - \frac{\Phi' \Phi_j^{EL'}}{4\Phi^{*2}} \right) w^{(1)} \bar{w}_A \right. \\
& - \left. \left(\frac{\Phi' \Phi_j^{EL}}{8\Phi^{*2}} - \frac{\gamma_0 \Phi_j^{EL'}}{4\Phi^*} \right) (w^{(1)'} \bar{w}_A + w^{(1)} \bar{w}'_A) - \frac{VF_1 \Phi_j^{EL}}{4\Phi^{*2}} \bar{w}_A \right\} \\
& - \sum_{\ell=1}^M \frac{\Delta I_\ell^{ML}}{I_\ell^{ML}} \frac{i\eta B_\ell}{2\sqrt{\Phi^*}} (w^{(1)'} \bar{w}_A - w^{(1)} \bar{w}'_A) - \Delta V^{DEF} \frac{\gamma_0 F_1}{2\Phi^*} \bar{w}_A - \Delta I^{DEF} \frac{\eta D_1}{\sqrt{\Phi^*}} \bar{w}_A \Big] dz \\
& - \sqrt{\frac{\Phi^*}{\Phi_o}} \left[\frac{\Delta \Phi}{\Phi_o^*} \Phi_o^* \frac{\Phi'}{8\Phi^{*2}} - \sum_{j=1}^N \frac{\Delta V_j^{EL}}{V_j^{EL}} \left(\frac{\Phi' \Phi_j^{EL}}{8\Phi^{*2}} - \frac{\gamma_0 \Phi_j^{EL'}}{4\Phi^*} \right) \right] w^{(1)} \bar{w}_A \\
& + \left[\frac{\Delta \Phi}{\Phi_o^*} \Phi_o^* \frac{\Phi_o'}{8\Phi_o^{*2}} - \sum_{j=1}^N \frac{\Delta V_j^{EL}}{V_j^{EL}} \left(\frac{\Phi_o' \Phi_{jo}^{EL}}{8\Phi_o^{*2}} - \frac{\gamma_{0o} \Phi_{jo}^{EL'}}{4\Phi_o^*} \right) \right] w_o \bar{w}_{Ao}.
\end{aligned} \tag{3.202}$$

Using Eq. (3.199) and (3.205), the path-deviation Eq. (3.197) is transformed into

$$\begin{aligned}
w_{\text{pth}} = & \left(\frac{\Delta \Phi}{\Phi_o^*} \Phi_o^* \frac{\gamma_{0o}}{2\Phi_o^*} w_o' + \sum_{j=1}^N \frac{\Delta V_j^{EL}}{V_j^{EL}} \frac{\gamma_{0o} \Phi_{jo}^{EL}}{2\Phi_o^*} w_o' - \sum_{\ell=1}^M \frac{\Delta I_\ell^{ML}}{I_\ell^{ML}} \frac{i\eta B_{\ell o}}{2\sqrt{\Phi_o^*}} w_o \right) w_\alpha \\
& - (w_\gamma + 2i\chi_o' w_\alpha) \left[\int_{z_0}^z \sqrt{\frac{\Phi^*}{\Phi_o}} \left[\frac{\Delta \Phi}{\Phi_o^*} \Phi_o^* \left(\frac{\gamma_0}{2\Phi^*} w^{(1)'} \bar{w}'_\alpha + \frac{3\gamma_0 \Phi'^2}{16\Phi^{*3}} w^{(1)} \bar{w}_\alpha \right. \right. \right. \\
& - \left. \frac{\Phi'}{8\Phi^{*2}} (w^{(1)'} \bar{w}'_\alpha + w^{(1)} \bar{w}'_\alpha) - \frac{VF_1}{4\Phi^{*2}} \bar{w}_\alpha \right\} \\
& + \sum_{j=1}^N \frac{\Delta V_j^{EL}}{V_j^{EL}} \left\{ \frac{\gamma_0 \Phi_j^{EL}}{2\Phi^*} w^{(1)'} \bar{w}'_\alpha + \left(\frac{3\gamma_0 \Phi'^2 \Phi_j^{EL}}{16\Phi^{*3}} - \frac{\Phi' \Phi_j^{EL'}}{4\Phi^{*2}} \right) w^{(1)} \bar{w}_\alpha \right. \\
& - \left. \left(\frac{\Phi' \Phi_j^{EL}}{8\Phi^{*2}} - \frac{\gamma_0 \Phi_j^{EL'}}{4\Phi^*} \right) (w^{(1)'} \bar{w}_\alpha + w^{(1)} \bar{w}'_\alpha) - \frac{VF_1 \Phi_j^{EL}}{4\Phi^{*2}} \bar{w}_\alpha \right\} \\
& + \sum_{\ell=1}^M \frac{\Delta I_\ell^{ML}}{I_\ell^{ML}} \frac{i\eta B_\ell}{2\sqrt{\Phi^*}} (w^{(1)'} \bar{w}_\alpha - w^{(1)} \bar{w}'_\alpha) + \Delta V^{DEF} \frac{\gamma_0 F_1}{2\Phi^*} \bar{w}_\alpha + \Delta I^{DEF} \frac{\eta D_1}{\sqrt{\Phi^*}} \bar{w}_\alpha \Big] dz \\
& + \sqrt{\frac{\Phi^*}{\Phi_o}} \left[\frac{\Delta \Phi}{\Phi_o^*} \Phi_o^* \frac{\Phi'}{8\Phi^{*2}} - \sum_{j=1}^N \frac{\Delta V_j^{EL}}{V_j^{EL}} \left(\frac{\Phi' \Phi_j^{EL}}{8\Phi^{*2}} - \frac{\gamma_0 \Phi_j^{EL'}}{4\Phi^*} \right) \right] w^{(1)} \bar{w}_\alpha \Big] \\
& + w_\alpha \left[\int_{z_0}^z \sqrt{\frac{\Phi^*}{\Phi_o}} \left[\frac{\Delta \Phi}{\Phi_o^*} \Phi_o^* \left(\frac{\gamma_0}{2\Phi^*} w^{(1)'} \bar{w}'_\gamma + \frac{3\gamma_0 \Phi'^2}{16\Phi^{*3}} w^{(1)} \bar{w}_\gamma \right. \right. \right. \\
& - \left. \frac{\Phi'}{8\Phi^{*2}} (w^{(1)'} \bar{w}'_\gamma + w^{(1)} \bar{w}'_\gamma) - \frac{VF_1}{4\Phi^{*2}} \bar{w}_\gamma \right\} \\
& + \sum_{j=1}^N \frac{\Delta V_j^{EL}}{V_j^{EL}} \left\{ \frac{\gamma_0 \Phi_j^{EL}}{2\Phi^*} w^{(1)'} \bar{w}'_\gamma + \left(\frac{3\gamma_0 \Phi'^2 \Phi_j^{EL}}{16\Phi^{*3}} - \frac{\Phi' \Phi_j^{EL'}}{4\Phi^{*2}} \right) w^{(1)} \bar{w}_\gamma \right. \\
& - \left. \left(\frac{\Phi' \Phi_j^{EL}}{8\Phi^{*2}} - \frac{\gamma_0 \Phi_j^{EL'}}{4\Phi^*} \right) (w^{(1)'} \bar{w}_\gamma + w^{(1)} \bar{w}'_\gamma) - \frac{VF_1 \Phi_j^{EL}}{4\Phi^{*2}} \bar{w}_\gamma \right\} \\
& + \sum_{\ell=1}^M \frac{\Delta I_\ell^{ML}}{I_\ell^{ML}} \frac{i\eta B_\ell}{2\sqrt{\Phi^*}} (w^{(1)'} \bar{w}_\gamma - w^{(1)} \bar{w}'_\gamma) + \Delta V^{DEF} \frac{\gamma_0 F_1}{2\Phi^*} \bar{w}_\gamma + \Delta I^{DEF} \frac{\eta D_1}{\sqrt{\Phi^*}} \bar{w}_\gamma \Big] dz \\
& + \sqrt{\frac{\Phi^*}{\Phi_o}} \left[\frac{\Delta \Phi}{\Phi_o^*} \Phi_o^* \frac{\Phi'}{8\Phi^{*2}} - \sum_{j=1}^N \frac{\Delta V_j^{EL}}{V_j^{EL}} \left(\frac{\Phi' \Phi_j^{EL}}{8\Phi^{*2}} - \frac{\gamma_0 \Phi_j^{EL'}}{4\Phi^*} \right) \right] w^{(1)} \bar{w}_\gamma \\
& - \left[\frac{\Delta \Phi}{\Phi_o^*} \Phi_o^* \frac{\Phi_o'}{8\Phi_o^{*2}} - \sum_{j=1}^N \frac{\Delta V_j^{EL}}{V_j^{EL}} \left(\frac{\Phi_o' \Phi_{jo}^{EL}}{8\Phi_o^{*2}} - \frac{\gamma_{0o} \Phi_{jo}^{EL'}}{4\Phi_o^*} \right) \right] w_o \Big].
\end{aligned} \tag{3.203}$$

Eq. (3.203) are divided into four types of path-deviations as follows:

The chromatic path-deviation,

$$\begin{aligned} \Delta w_K = & \frac{\Delta \Phi}{\Phi_o^*} \Phi_o^* \left[\frac{\gamma_{00}}{2\Phi_o^*} w_\alpha w_o' - \frac{\Phi_o'}{8\Phi_o^{*2}} w_o w_\alpha \right. \\ & - (w_\gamma + 2i\chi_o' w_\alpha) \int_{z_o}^z \sqrt{\frac{\Phi^*}{\Phi_o^*}} \left\{ \frac{\gamma_o}{2\Phi^*} w^{(1)'} \bar{w}_\alpha' + \frac{3\gamma_o \Phi'^2}{16\Phi_o^{*3}} w^{(1)} \bar{w}_\alpha - \frac{\Phi'}{8\Phi_o^{*2}} (w^{(1)'} \bar{w}_\alpha + w^{(1)} \bar{w}_\alpha') \right. \\ & \quad \left. \left. - \frac{VF_1}{4\Phi_o^{*2}} \bar{w}_\alpha \right\} dz \right. \\ & \left. + w_\alpha \int_{z_o}^z \sqrt{\frac{\Phi^*}{\Phi_o^*}} \left\{ \frac{\gamma_o}{2\Phi^*} w^{(1)'} \bar{w}_\gamma' + \frac{3\gamma_o \Phi'^2}{16\Phi_o^{*3}} w^{(1)} \bar{w}_\gamma - \frac{\Phi'}{8\Phi_o^{*2}} (w^{(1)'} \bar{w}_\gamma + w^{(1)} \bar{w}_\gamma') - \frac{VF_1}{4\Phi_o^{*2}} \bar{w}_\gamma \right\} dz \right]. \end{aligned} \quad (3.204)$$

The path-deviation induced by the variation of voltages of round-symmetric electrodes,

$$\begin{aligned} \Delta w_{ELwob} = & \sum_{j=1}^N \frac{\Delta V_j^{EL}}{V_j^{EL}} \left[\frac{\gamma_{00} \Phi_j^{EL}}{2\Phi_o^*} w_o' w_\alpha + \left(\frac{\Phi_o' \Phi_j^{EL}}{8\Phi_o^{*2}} - \frac{\gamma_{00} \Phi_j^{EL'}}{4\Phi_o^*} \right) w_o w_\alpha \right. \\ & - (w_\gamma + 2i\chi_o' w_\alpha) \int_{z_o}^z \sqrt{\frac{\Phi^*}{\Phi_o^*}} \left\{ \frac{\gamma_o \Phi_j^{EL}}{2\Phi^*} w^{(1)'} \bar{w}_\alpha' + \left(\frac{3\gamma_o \Phi'^2 \Phi_j^{EL}}{16\Phi_o^{*3}} - \frac{\Phi' \Phi_j^{EL'}}{4\Phi_o^{*2}} \right) w^{(1)} \bar{w}_\alpha \right. \\ & \quad \left. - \left(\frac{\Phi' \Phi_j^{EL}}{8\Phi_o^{*2}} - \frac{\gamma_o \Phi_j^{EL'}}{4\Phi_o^*} \right) (w^{(1)'} \bar{w}_\alpha + w^{(1)} \bar{w}_\alpha') - \frac{VF_1 \Phi_j^{EL}}{4\Phi_o^{*2}} \bar{w}_\alpha \right\} dz \\ & + w_\alpha \int_{z_o}^z \sqrt{\frac{\Phi^*}{\Phi_o^*}} \left\{ \frac{\gamma_o \Phi_j^{EL}}{2\Phi^*} w^{(1)'} \bar{w}_\gamma' + \left(\frac{3\gamma_o \Phi'^2 \Phi_j^{EL}}{16\Phi_o^{*3}} - \frac{\Phi' \Phi_j^{EL'}}{4\Phi_o^{*2}} \right) w^{(1)} \bar{w}_\gamma \right. \\ & \quad \left. - \left(\frac{\Phi' \Phi_j^{EL}}{8\Phi_o^{*2}} - \frac{\gamma_o \Phi_j^{EL'}}{4\Phi_o^*} \right) (w^{(1)'} \bar{w}_\gamma + w^{(1)} \bar{w}_\gamma') - \frac{VF_1 \Phi_j^{EL}}{4\Phi_o^{*2}} \bar{w}_\gamma \right\} dz \right]. \end{aligned} \quad (3.205)$$

The Path-deviation induced by the variation of the coil currents of round-symmetric magnetic fields,

$$\begin{aligned} \Delta w_{MLwob} = & \sum_{\ell=1}^M \frac{\Delta I_\ell^{ML}}{I_\ell^{ML}} \left[-\frac{i\eta B_{\ell o}}{2\sqrt{\Phi_o^*}} w_o w_\alpha \right. \\ & - (w_\gamma + 2i\chi_o' w_\alpha) \int_{z_o}^z \sqrt{\frac{\Phi^*}{\Phi_o^*}} \frac{i\eta B_\ell}{2\sqrt{\Phi^*}} (w^{(1)'} \bar{w}_\alpha - w^{(1)} \bar{w}_\alpha') dz \\ & \left. + w_\alpha \int_{z_o}^z \sqrt{\frac{\Phi^*}{\Phi_o^*}} \frac{i\eta B_\ell}{2\sqrt{\Phi^*}} (w^{(1)'} \bar{w}_\gamma - w^{(1)} \bar{w}_\gamma') dz \right]. \end{aligned} \quad (3.206)$$

The Path-deviations induced by the variation of the voltage of an electrostatic deflector and the current of a magnetic deflector,

$$\begin{aligned} \Delta w_{EDFEwob} = & \Delta V^{DEF} \left[-w_\gamma \int_{z_o}^z \sqrt{\frac{\Phi^*}{\Phi_o^*}} \frac{\gamma_o F_1}{2\Phi^*} \bar{w}_\alpha dz + \bar{w}_\alpha \int_{z_o}^z \sqrt{\frac{\Phi^*}{\Phi_o^*}} \frac{\gamma_o F_1}{2\Phi^*} (\bar{w}_\gamma - 2i\chi_o' \bar{w}_\alpha) dz \right], \\ \Delta w_{BDEFEwob} = & \Delta I^{DEF} \left[-w_\gamma \int_{z_o}^z \sqrt{\frac{\Phi^*}{\Phi_o^*}} \frac{\eta D_1}{\Phi_o^* \sqrt{\Phi^*}} \bar{w}_\alpha dz + \bar{w}_\alpha \int_{z_o}^z \sqrt{\frac{\Phi^*}{\Phi_o^*}} \frac{\eta D_1}{\Phi_o^* \sqrt{\Phi^*}} (\bar{w}_\gamma - 2i\chi_o' \bar{w}_\alpha) dz \right]. \end{aligned} \quad (3.207)$$

We are at the point where the second-rank path-deviation, which is induced by the energy deviation of incident electrons and the variation of voltages and currents of round symmetric electrodes and coils, and those of deflectors, are derived.

Comparing the path deviation induced by the variation of voltage and current of deflectors, Eq. (3.207) with the deflection trajectories Eq. (3.84) and (3.85), Eq. (3.207) can be expressed as

$$\begin{aligned}\Delta w_{EDEFwob} &= \Delta V^{DEF} w_e(z), \\ \Delta w_{BDEFwob} &= \Delta I^{DEF} w_m(z).\end{aligned}\quad (3.208)$$

Since w_e and w_m are the deflection trajectory of a unit voltage and a unit current of deflectors, respectively, the path-deviations of Eq. (3.208) are regarded as the deflection trajectories of an electrostatic deflector with complex voltage ΔV^{DEF} , and a magnetic deflector with complex current ΔI^{DEF} . Eq. (3.208) seems trivial, apparently, but it shows the consistency of the perturbation theory of deflection.

3.8.3 Explicit forms of path-deviations

Here, we sort path-deviations by geometrical and chromatic parameters and derive explicit forms, using the explicit form of the first-order trajectory Eq. (3.90). In section 3.5, when we considered third-order geometrical aberration, for simplicity, we assumed only a beam whose object point is located on the optic axis, that is, $w_o = 0$. However, since the calculation for the second-rank path-deviations is not so complicated, even if we assume a nonzero off-axis object point, that is, $w_o \neq 0$, we consider the linear trajectory as

$$w^{(1)} = w'_o w_\alpha + w_o w_\gamma + V w_e + I w_m. \quad (3.209)$$

Since Eq. (3.204) - (3.206) have only linear terms of $w^{(1)}$ and $w^{(1)'}$, at least for the second-rank, contributions of the mixture among different deflectors do not appear to path-deviations. It is sufficient to consider a single electrostatic deflector and a single magnetic deflector. Employing Eq. (3.209) to Eq. (3.204) - (3.206), the path-deviations are sorted according to their dependence on the geometrical parameters, w_o, w'_o, V, I and on the chromatic parameter and the variation parameters, $\Delta\Phi, \Delta V_j^{EL}, \Delta I_\ell^{ML}$, as follows:

$$\Delta w_k(z) = f_{\alpha k}(z) w'_o \frac{\Delta\Phi}{\Phi_o^*} + f_{\gamma k}(z) w_o \frac{\Delta\Phi}{\Phi_o^*} + f_{V k}(z) V \frac{\Delta\Phi}{\Phi_o^*} + f_{I k}(z) I \frac{\Delta\Phi}{\Phi_o^*}, \quad (3.210)$$

$$\Delta w_{ELwob} = \sum_{j=1}^N \frac{\Delta V_j^{EL}}{V_j^{EL}} [f_{\alpha j}^{ELwob} w'_o + f_{\gamma j}^{ELwob} w_o + f_{V j}^{ELwob} V + f_{I j}^{ELwob} I], \quad (3.211)$$

$$\Delta w_{MLwob} = \sum_{\ell=1}^M \frac{\Delta I_\ell^{ML}}{I_\ell^{ML}} [f_{\alpha \ell}^{MLwob} w'_o + f_{\gamma \ell}^{MLwob} w_o + f_{V \ell}^{MLwob} V + f_{I \ell}^{MLwob} I]. \quad (3.212)$$

Each coefficient function of z is a component of the path-deviation corresponding to dependence on the geometrical parameters and the chromatic or the variation parameters.

Explicit expressions are given as follows.

For the chromatic path-deviation, the on-axis component:

$$\begin{aligned}
 f_{\alpha\kappa} = & \Phi_o^* \left[\frac{\gamma_{0o}}{2\Phi_o^*} w_\alpha \right. \\
 & - (w_\gamma + 2i\chi_o' w_\alpha) \int_{z_o}^z \sqrt{\frac{\Phi^*}{\Phi_o^*}} \left\{ \frac{\gamma_0}{2\Phi^*} w_\alpha' \bar{w}_\alpha' + \frac{3\gamma_0 \Phi'^2}{16\Phi^{*3}} w_\alpha \bar{w}_\alpha - \frac{\Phi'}{8\Phi^{*2}} (w_\alpha' \bar{w}_\alpha + w_\alpha \bar{w}_\alpha') \right\} dz \\
 & \left. + w_\alpha \int_{z_o}^z \sqrt{\frac{\Phi^*}{\Phi_o^*}} \left\{ \frac{\gamma_0}{2\Phi^*} w_\alpha' \bar{w}_\gamma' + \frac{3\gamma_0 \Phi'^2}{16\Phi^{*3}} w_\alpha \bar{w}_\gamma - \frac{\Phi'}{8\Phi^{*2}} (w_\alpha' \bar{w}_\gamma + w_\alpha \bar{w}_\gamma') \right\} dz \right], \quad (3.213)
 \end{aligned}$$

The off-axis component:

$$\begin{aligned}
 f_{\gamma\kappa} = & \Phi_o^* \left[-\frac{\Phi_o'}{8\Phi_o^{*2}} w_o w_\alpha \right. \\
 & - (w_\gamma + 2i\chi_o' w_\alpha) \int_{z_o}^z \sqrt{\frac{\Phi^*}{\Phi_o^*}} \left\{ \frac{\gamma_0}{2\Phi^*} w_\gamma' \bar{w}_\alpha' + \frac{3\gamma_0 \Phi'^2}{16\Phi^{*3}} w_\gamma \bar{w}_\alpha - \frac{\Phi'}{8\Phi^{*2}} (w_\gamma' \bar{w}_\alpha + w_\gamma \bar{w}_\alpha') \right\} dz \\
 & \left. + w_\alpha \int_{z_o}^z \sqrt{\frac{\Phi^*}{\Phi_o^*}} \left\{ \frac{\gamma_0}{2\Phi^*} w_\gamma' \bar{w}_\gamma' + \frac{3\gamma_0 \Phi'^2}{16\Phi^{*3}} w_\gamma \bar{w}_\gamma - \frac{\Phi'}{8\Phi^{*2}} (w_\gamma' \bar{w}_\gamma + w_\gamma \bar{w}_\gamma') \right\} dz \right], \quad (3.214)
 \end{aligned}$$

The electrostatic deflection component:

$$\begin{aligned}
 f_{V\kappa} = & \Phi_o^* \left[- (w_\gamma + 2i\chi_o' w_\alpha) \int_{z_o}^z \sqrt{\frac{\Phi^*}{\Phi_o^*}} \left\{ \frac{\gamma_0}{2\Phi^*} w_e' \bar{w}_\alpha' + \frac{3\gamma_0 \Phi'^2}{16\Phi^{*3}} w_e \bar{w}_\alpha - \frac{\Phi'}{8\Phi^{*2}} (w_e' \bar{w}_\alpha + w_e \bar{w}_\alpha') \right\} dz \right. \\
 & \left. - \frac{VF_1}{4\Phi^{*2}} \bar{w}_\alpha \right] \\
 & + w_\alpha \int_{z_o}^z \sqrt{\frac{\Phi^*}{\Phi_o^*}} \left\{ \frac{\gamma_0}{2\Phi^*} w_e' \bar{w}_\gamma' + \frac{3\gamma_0 \Phi'^2}{16\Phi^{*3}} w_e \bar{w}_\gamma - \frac{\Phi'}{8\Phi^{*2}} (w_e' \bar{w}_\gamma + w_e \bar{w}_\gamma') - \frac{VF_1}{4\Phi^{*2}} \bar{w}_\gamma \right\} dz \Big], \quad (3.215)
 \end{aligned}$$

The magnetic deflection component:

$$\begin{aligned}
 f_{I\kappa} = & \Phi_o^* \left[- (w_\gamma + 2i\chi_o' w_\alpha) \int_{z_o}^z \sqrt{\frac{\Phi^*}{\Phi_o^*}} \left\{ \frac{\gamma_0}{2\Phi^*} w_m' \bar{w}_\alpha' + \frac{3\gamma_0 \Phi'^2}{16\Phi^{*3}} w_m \bar{w}_\alpha \right. \right. \\
 & \left. \left. - \frac{\Phi'}{8\Phi^{*2}} (w_m' \bar{w}_\alpha + w_m \bar{w}_\alpha') \right\} dz \right. \\
 & \left. + w_\alpha \int_{z_o}^z \sqrt{\frac{\Phi^*}{\Phi_o^*}} \left\{ \frac{\gamma_0}{2\Phi^*} w_m' \bar{w}_\gamma' + \frac{3\gamma_0 \Phi'^2}{16\Phi^{*3}} w_m \bar{w}_\gamma - \frac{\Phi'}{8\Phi^{*2}} (w_m' \bar{w}_\gamma + w_m \bar{w}_\gamma') \right\} dz \right]. \quad (3.216)
 \end{aligned}$$

For the path-deviation of the variation of voltage of the j -th round-symmetric electrode:

The on-axis component:

$$\begin{aligned}
 f_{aj}^{ELwob} = & \frac{\gamma_{0o} \Phi_{jo}^{EL}}{2\Phi_o^*} w_\alpha \\
 & - (w_\gamma + 2i\chi_o' w_\alpha) \int_{z_o}^z \sqrt{\frac{\Phi^*}{\Phi_o^*}} \left\{ \frac{\gamma_0 \Phi_j^{EL}}{2\Phi^*} w_\alpha' \bar{w}_\alpha' + \left(\frac{3\gamma_0 \Phi_j'^2 \Phi_j^{EL}}{16\Phi^{*3}} - \frac{\Phi' \Phi_j^{EL'}}{4\Phi^{*2}} \right) w_\alpha \bar{w}_\alpha \right. \\
 & \left. - \left(\frac{\Phi' \Phi_j^{EL}}{8\Phi^{*2}} - \frac{\gamma_0 \Phi_j^{EL'}}{4\Phi^*} \right) (w_\alpha' \bar{w}_\alpha + w_\alpha \bar{w}_\alpha') \right\} dz \\
 & + w_\alpha \int_{z_o}^z \sqrt{\frac{\Phi^*}{\Phi_o^*}} \left\{ \frac{\gamma_0 \Phi_j^{EL}}{2\Phi^*} w_\alpha' \bar{w}_\gamma' + \left(\frac{3\gamma_0 \Phi_j'^2 \Phi_j^{EL}}{16\Phi^{*3}} - \frac{\Phi' \Phi_j^{EL'}}{4\Phi^{*2}} \right) w_\gamma \bar{w}_\gamma \right. \\
 & \left. - \left(\frac{\Phi' \Phi_j^{EL}}{8\Phi^{*2}} - \frac{\gamma_0 \Phi_j^{EL'}}{4\Phi^*} \right) (w_\alpha' \bar{w}_\gamma + w_\alpha \bar{w}_\gamma') \right\} dz, \quad (3.217)
 \end{aligned}$$

The off-axis component:

$$\begin{aligned}
f_{yj}^{ELwob} = & \left(\frac{\Phi'_0 \Phi_{j0}^{EL}}{8\Phi_0'^2} - \frac{\gamma_{00} \Phi_{j0}^{EL'}}{4\Phi_0'} \right) w_\alpha - (w_\gamma + 2i\chi'_0 w_\alpha) \int_{z_0}^z \sqrt{\frac{\Phi^*}{\Phi_0'^2}} \left(\frac{\gamma_0 \Phi_j^{EL}}{2\Phi^*} - w'_\gamma \bar{w}'_\alpha \right. \\
& + \left. \left(\frac{3\gamma_0 \Phi'^2 \Phi_j^{EL}}{16\Phi'^3} - \frac{\Phi' \Phi_j^{EL'}}{4\Phi'^2} \right) w'_\gamma \bar{w}_\alpha - \left(\frac{\Phi' \Phi_j^{EL}}{8\Phi'^2} - \frac{\gamma_0 \Phi_j^{EL'}}{4\Phi^*} \right) (w'_\gamma \bar{w}_\alpha + w_\gamma \bar{w}'_\alpha) \right) dz \\
& + w_\alpha \int_{z_0}^z \sqrt{\frac{\Phi^*}{\Phi_0'^2}} \left(\frac{\gamma_0 \Phi_j^{EL}}{2\Phi^*} - w'_\gamma \bar{w}'_\gamma + \left(\frac{3\gamma_0 \Phi'^2 \Phi_j^{EL}}{16\Phi'^3} - \frac{\Phi' \Phi_j^{EL'}}{4\Phi'^2} \right) w'_\gamma \bar{w}_\gamma \right. \\
& \left. \left. - \left(\frac{\Phi' \Phi_j^{EL}}{8\Phi'^2} - \frac{\gamma_0 \Phi_j^{EL'}}{4\Phi^*} \right) (w'_\gamma \bar{w}_\gamma + w_\gamma \bar{w}'_\gamma) \right) \right) dz,
\end{aligned} \tag{3.218}$$

The electrostatic deflection component:

$$\begin{aligned}
f_{vj}^{ELwob} = & -(w_\gamma + 2i\chi'_0 w_\alpha) \int_{z_0}^z \sqrt{\frac{\Phi^*}{\Phi_0'^2}} \left(\frac{\gamma_0 \Phi_j^{EL}}{2\Phi^*} - w'_e \bar{w}'_\alpha + \left(\frac{3\gamma_0 \Phi'^2 \Phi_j^{EL}}{16\Phi'^3} - \frac{\Phi' \Phi_j^{EL'}}{4\Phi'^2} \right) w'_e \bar{w}_\alpha \right. \\
& \left. - \left(\frac{\Phi' \Phi_j^{EL}}{8\Phi'^2} - \frac{\gamma_0 \Phi_j^{EL'}}{4\Phi^*} \right) (w'_e \bar{w}_\alpha + w_e \bar{w}'_\alpha) - \frac{VF_1 \Phi_j^{EL}}{4\Phi'^2} \bar{w}_\alpha \right) dz \\
& + w_\alpha \int_{z_0}^z \sqrt{\frac{\Phi^*}{\Phi_0'^2}} \left(\frac{\gamma_0 \Phi_j^{EL}}{2\Phi^*} - w'_e \bar{w}'_\gamma + \left(\frac{3\gamma_0 \Phi'^2 \Phi_j^{EL}}{16\Phi'^3} - \frac{\Phi' \Phi_j^{EL'}}{4\Phi'^2} \right) w'_e \bar{w}_\gamma \right. \\
& \left. - \left(\frac{\Phi' \Phi_j^{EL}}{8\Phi'^2} - \frac{\gamma_0 \Phi_j^{EL'}}{4\Phi^*} \right) (w'_e \bar{w}_\gamma + w_e \bar{w}'_\gamma) - \frac{VF_1 \Phi_j^{EL}}{4\Phi'^2} \bar{w}_\gamma \right) dz
\end{aligned} \tag{3.219}$$

The magnetic deflection component:

$$\begin{aligned}
f_{lj}^{ELwob} = & -(w_\gamma + 2i\chi'_0 w_\alpha) \int_{z_0}^z \sqrt{\frac{\Phi^*}{\Phi_0'^2}} \left\{ \frac{\gamma_0 \Phi_j^{EL}}{2\Phi^*} - w'_m \bar{w}'_\alpha \right. \\
& + \left. \left(\frac{3\gamma_0 \Phi'^2 \Phi_j^{EL}}{16\Phi'^3} - \frac{\Phi' \Phi_j^{EL'}}{4\Phi'^2} \right) w'_m \bar{w}_\alpha - \left(\frac{\Phi' \Phi_j^{EL}}{8\Phi'^2} - \frac{\gamma_0 \Phi_j^{EL'}}{4\Phi^*} \right) (w'_m \bar{w}_\alpha + w_e \bar{w}'_\alpha) \right\} dz \\
& + w_\alpha \int_{z_0}^z \sqrt{\frac{\Phi^*}{\Phi_0'^2}} \left\{ \frac{\gamma_0 \Phi_j^{EL}}{2\Phi^*} - w'_m \bar{w}'_\gamma + \left(\frac{3\gamma_0 \Phi'^2 \Phi_j^{EL}}{16\Phi'^3} - \frac{\Phi' \Phi_j^{EL'}}{4\Phi'^2} \right) w'_m \bar{w}_\gamma \right. \\
& \left. - \left(\frac{\Phi' \Phi_j^{EL}}{8\Phi'^2} - \frac{\gamma_0 \Phi_j^{EL'}}{4\Phi^*} \right) (w'_m \bar{w}_\gamma + w_m \bar{w}'_\gamma) \right\} dz
\end{aligned} \tag{3.220}$$

For the path-deviation of the variation of current of the ℓ -th magnetic lens coil,

The on-axis component:

$$\begin{aligned}
f_{\alpha\ell}^{MLwob} = & -(w_\gamma + 2i\chi'_0 w_\alpha) \int_{z_0}^z \sqrt{\frac{\Phi^*}{\Phi_0'^2}} \frac{i\eta B_\ell}{2\sqrt{\Phi^*}} (w'_\alpha \bar{w}_\alpha - w_\alpha \bar{w}'_\alpha) dz \\
& + w_\alpha \int_{z_0}^z \sqrt{\frac{\Phi^*}{\Phi_0'^2}} \frac{i\eta B_\ell}{2\sqrt{\Phi^*}} (w'_\alpha \bar{w}_\gamma - w_\alpha \bar{w}'_\gamma) dz,
\end{aligned} \tag{3.221}$$

The off-axis component:

$$\begin{aligned}
f_{y\ell}^{MLwob} = & -\frac{i\eta B_{\ell 0}}{2\sqrt{\Phi_0'^2}} w_0 w_\alpha - (w_\gamma + 2i\chi'_0 w_\alpha) \int_{z_0}^z \sqrt{\frac{\Phi^*}{\Phi_0'^2}} \frac{i\eta B_\ell}{2\sqrt{\Phi^*}} (w'_\gamma \bar{w}_\alpha - w_\gamma \bar{w}'_\alpha) dz \\
& + w_\alpha \int_{z_0}^z \sqrt{\frac{\Phi^*}{\Phi_0'^2}} \frac{i\eta B_\ell}{2\sqrt{\Phi^*}} (w'_\gamma \bar{w}_\gamma - w_\gamma \bar{w}'_\gamma) dz,
\end{aligned} \tag{3.222}$$

The electrostatic deflection component:

$$f_{V\ell}^{MLwob} = -(w_\gamma + 2i\chi'_0 w_\alpha) \int_{z_0}^z \sqrt{\frac{\Phi^*}{\Phi_0^*}} \frac{i\eta B_\ell}{2\sqrt{\Phi^*}} (w'_e \bar{w}_\alpha - w_e \bar{w}'_\alpha) dz \\ + w_\alpha \int_{z_0}^z \sqrt{\frac{\Phi^*}{\Phi_0^*}} \frac{i\eta B_\ell}{2\sqrt{\Phi^*}} (w'_e \bar{w}_\gamma - w_e \bar{w}'_\gamma) dz, \quad (3.223)$$

The magnetic deflection component:

$$f_{I\ell}^{MLwob} = -(w_\gamma + 2i\chi'_0 w_\alpha) \int_{z_0}^z \sqrt{\frac{\Phi^*}{\Phi_0^*}} \frac{i\eta B_\ell}{2\sqrt{\Phi^*}} (w'_m \bar{w}_\alpha - w_m \bar{w}'_\alpha) dz \\ + w_\alpha \int_{z_0}^z \sqrt{\frac{\Phi^*}{\Phi_0^*}} \frac{i\eta B_\ell}{2\sqrt{\Phi^*}} (w'_m \bar{w}_\gamma - w_m \bar{w}'_\gamma) dz. \quad (3.224)$$

We are at the point where explicit forms of path-deviation components induced by the energy deviation of the electrons or the variation of voltages and currents of round symmetric electrodes and magnetic lens coils are derived.

3.8.4 Second-rank deflection aberration coefficients

Aberration is defined as the value of the path-deviation at the image plane. Here, we give explicit formulae of second-rank deflection aberration coefficients. Due to $w_{\alpha i} = 0$, all path-deviation components evaluated at the image plane are proportional to $w_{\gamma i}$, which corresponds to the product of linear magnification and rotation from the object plane to the image plane. Similar to the case of the third-order geometrical aberration, virtual aberration defined at the object plane is considered as follows:

$$\Delta w_o = \frac{1}{w_{\gamma i}} \Delta w_i. \quad (3.225)$$

By this consideration, we can write the aberration defined at the object plane as follows:

chromatic aberration,

$$\Delta w_{ko} = [C_{Co} w'_o + C_{\gamma ko} w_o + C_{Vko} V + C_{Iko} I] \frac{\Delta \Phi}{\Phi_o}, \quad (3.226)$$

where C_{Co} , $C_{\gamma ko}$, C_{Vko} , C_{Iko} are the axial chromatic aberration coefficient, the off-axis chromatic aberration coefficient, the electrostatic deflection chromatic aberration coefficient, and the magnetic deflection chromatic aberration coefficient, defined at the object plane, respectively.

The aberration due to variation of voltages of round symmetric electrodes,

$$\Delta w_{ELwobo} = \sum_{j=1}^N \frac{\Delta V_j^{EL}}{V_j^{EL}} [C_{\alpha jo}^{ELwob} w'_o + C_{\gamma jo}^{ELwob} w_o + C_{Vjo}^{ELwob} V + C_{Ijo}^{ELwob} I], \quad (3.227)$$

where $C_{\alpha jo}^{ELwob}$, $C_{\gamma jo}^{ELwob}$, C_{Vjo}^{ELwob} , C_{Ijo}^{ELwob} are the axial aberration coefficient, the off-axis aberration coefficient, the electrostatic deflection aberration coefficient, and the magnetic deflection aberration coefficient induced by the variation of voltage of the j -th round symmetric electrode, defined at the object plane, respectively.

The aberration of variation due to currents of round-symmetric magnetic lens coils,

$$\Delta w_{ELwob} = \sum_{\ell=1}^M \frac{\Delta I_{\ell}^{ML}}{I_{\ell}^{ML}} [C_{\alpha\ell o}^{MLwob} w_o' + C_{\gamma\ell o}^{MLwob} w_o + C_{V\ell o}^{MLwob} V + C_{I\ell o}^{MLwob} I], \quad (3.228)$$

where $C_{\alpha\ell o}^{MLwob}$, $C_{\gamma\ell o}^{MLwob}$, $C_{V\ell o}^{MLwob}$, $C_{I\ell o}^{MLwob}$ are the axial aberration coefficient, the off-axis aberration coefficient, the electrostatic deflection aberration coefficient, and the magnetic deflection aberration coefficient induced by the variation of current of the ℓ -th round-symmetric magnetic lens coil, defined at the object plane, respectively.

Explicit formulae of aberration coefficients are given as follows.

For the chromatic aberration coefficients:

The on-axis chromatic aberration coefficient:

$$C_{Co} = -\Phi_o^* \int_{z_o}^{z_i} \sqrt{\frac{\Phi^*}{\Phi_o^*}} \left\{ \frac{\gamma_o}{2\Phi^*} w_{\alpha}' \bar{w}_{\alpha}' + \frac{3\gamma_o \Phi'^2}{16\Phi^{*3}} w_{\alpha} \bar{w}_{\alpha} - \frac{\Phi'}{8\Phi^{*2}} (w_{\alpha}' \bar{w}_{\alpha} + w_{\alpha} \bar{w}_{\alpha}') \right\} dz. \quad (3.229)$$

The off-axis chromatic aberration coefficient:

$$C_{\gamma Ko} = -\Phi_o^* \int_{z_o}^{z_i} \sqrt{\frac{\Phi^*}{\Phi_o^*}} \left\{ \frac{\gamma_o}{2\Phi^*} w_{\gamma}' \bar{w}_{\alpha}' + \frac{3\gamma_o \Phi'^2}{16\Phi^{*3}} w_{\gamma} \bar{w}_{\alpha} - \frac{\Phi'}{8\Phi^{*2}} (w_{\gamma}' \bar{w}_{\alpha} + w_{\gamma} \bar{w}_{\alpha}') \right\} dz. \quad (3.230)$$

The electrostatic deflection chromatic aberration coefficient:

$$C_{VKo} = -\Phi_o^* \int_{z_o}^{z_i} \sqrt{\frac{\Phi^*}{\Phi_o^*}} \left\{ \frac{\gamma_o}{2\Phi^*} w_e' \bar{w}_{\alpha}' + \frac{3\gamma_o \Phi'^2}{16\Phi^{*3}} w_e \bar{w}_{\alpha} - \frac{\Phi'}{8\Phi^{*2}} (w_e' \bar{w}_{\alpha} + w_e \bar{w}_{\alpha}') - \frac{VF_1}{4\Phi^{*2}} \bar{w}_{\alpha} \right\} dz. \quad (3.231)$$

The magnetic deflection chromatic aberration coefficient:

$$C_{IKo} = -\Phi_o^* \int_{z_o}^{z_i} \sqrt{\frac{\Phi^*}{\Phi_o^*}} \left\{ \frac{\gamma_o}{2\Phi^*} w_m' \bar{w}_{\alpha}' + \frac{3\gamma_o \Phi'^2}{16\Phi^{*3}} w_m \bar{w}_{\alpha} - \frac{\Phi'}{8\Phi^{*2}} (w_m' \bar{w}_{\alpha} + w_m \bar{w}_{\alpha}') \right\} dz. \quad (3.232)$$

For the aberration coefficient of the variation of the voltage of the j -th round-symmetric electrode,

The on-axis aberration coefficient:

$$C_{\alpha jo}^{ELwob} = - \int_{z_o}^{z_i} \sqrt{\frac{\Phi^*}{\Phi_o^*}} \left\{ \frac{\gamma_o \Phi_j^{EL}}{2\Phi^*} w_{\alpha}' \bar{w}_{\alpha}' + \left(\frac{3\gamma_o \Phi'^2 \Phi_j^{EL}}{16\Phi^{*3}} - \frac{\Phi' \Phi_j^{EL'}}{4\Phi^{*2}} \right) w_{\alpha} \bar{w}_{\alpha} - \left(\frac{\Phi' \Phi_j^{EL}}{8\Phi^{*2}} - \frac{\gamma_o \Phi_j^{EL'}}{4\Phi^*} \right) (w_{\alpha}' \bar{w}_{\alpha} + w_{\alpha} \bar{w}_{\alpha}') \right\} dz. \quad (3.233)$$

The off-axis aberration coefficient:

$$C_{\gamma jo}^{ELwob} = - \int_{z_o}^{z_i} \sqrt{\frac{\Phi^*}{\Phi_o^*}} \left\{ \frac{\gamma_o \Phi_j^{EL}}{2\Phi^*} w_{\gamma}' \bar{w}_{\alpha}' + \left(\frac{3\gamma_o \Phi'^2 \Phi_j^{EL}}{16\Phi^{*3}} - \frac{\Phi' \Phi_j^{EL'}}{4\Phi^{*2}} \right) w_{\gamma} \bar{w}_{\alpha} - \left(\frac{\Phi' \Phi_j^{EL}}{8\Phi^{*2}} - \frac{\gamma_o \Phi_j^{EL'}}{4\Phi^*} \right) (w_{\gamma}' \bar{w}_{\alpha} + w_{\gamma} \bar{w}_{\alpha}') \right\} dz. \quad (3.234)$$

The electrostatic deflection aberration coefficient:

$$C_{Vjo}^{ELwob} = - \int_{z_o}^{z_i} \sqrt{\frac{\Phi^*}{\Phi_o^*}} \left\{ \frac{\gamma_o \Phi_j^{EL}}{2\Phi^*} w_e' \bar{w}_{\alpha}' + \left(\frac{3\gamma_o \Phi'^2 \Phi_j^{EL}}{16\Phi^{*3}} - \frac{\Phi' \Phi_j^{EL'}}{4\Phi^{*2}} \right) w_e \bar{w}_{\alpha} - \left(\frac{\Phi' \Phi_j^{EL}}{8\Phi^{*2}} - \frac{\gamma_o \Phi_j^{EL'}}{4\Phi^*} \right) (w_e' \bar{w}_{\alpha} + w_e \bar{w}_{\alpha}') - \frac{VF_1 \Phi_j^{EL}}{4\Phi^{*2}} \bar{w}_{\alpha} \right\} dz. \quad (3.235)$$

The magnetic deflection aberration coefficient:

$$C_{ljo}^{ELwob} = - \int_{z_0}^{z_l} \sqrt{\frac{\Phi^*}{\Phi_o^*}} \left\{ \gamma_0 \Phi_j^{EL} w'_m \bar{w}'_\alpha + \left(\frac{3\gamma_0 \Phi'^2 \Phi_j^{EL}}{16\Phi^{*3}} - \frac{\Phi' \Phi_j^{EL'}}{4\Phi^{*2}} \right) w_m \bar{w}_\alpha \right. \\ \left. - \left(\frac{\Phi' \Phi_j^{EL}}{8\Phi^{*2}} - \frac{\gamma_0 \Phi_j^{EL'}}{4\Phi^*} \right) (w'_m \bar{w}_\alpha + w_e \bar{w}'_\alpha) \right\} dz. \quad (3.236)$$

For the aberration coefficient of the variation of the current of the ℓ -th magnetic lens coil,

The on-axis aberration coefficient:

$$C_{\alpha\ell o}^{MLwob} = - \int_{z_0}^{z_l} \sqrt{\frac{\Phi^*}{\Phi_o^*}} \frac{i\eta B_\ell}{2\sqrt{\Phi^*}} (w'_\alpha \bar{w}_\alpha - w_\alpha \bar{w}'_\alpha) dz. \quad (3.237)$$

The off-axis aberration coefficient:

$$C_{\gamma\ell o}^{MLwob} = - \int_{z_0}^{z_l} \sqrt{\frac{\Phi^*}{\Phi_o^*}} \frac{i\eta B_\ell}{2\sqrt{\Phi^*}} (w'_\gamma \bar{w}_\alpha - w_\gamma \bar{w}'_\alpha) dz. \quad (3.238)$$

The electrostatic deflection aberration coefficient:

$$C_{V\ell o}^{MLwob} = - \int_{z_0}^{z_l} \sqrt{\frac{\Phi^*}{\Phi_o^*}} \frac{i\eta B_\ell}{2\sqrt{\Phi^*}} (w'_e \bar{w}_\alpha - w_e \bar{w}'_\alpha) dz. \quad (3.239)$$

The magnetic deflection aberration coefficient:

$$C_{I\ell o}^{MLwob} = - \int_{z_0}^{z_l} \sqrt{\frac{\Phi^*}{\Phi_o^*}} \frac{i\eta B_\ell}{2\sqrt{\Phi^*}} (w'_m \bar{w}_\alpha - w_m \bar{w}'_\alpha) dz. \quad (3.240)$$

We are at the point where the explicit formulae of the second-rank aberration coefficients, which are defined at the object plane, are derived.

3.8.5 Conversion of the aberration coefficients to those defined at the image plane and parameterized by the deflection beam shift.

Here, we consider the conversion of derived aberration coefficients to those defined at the image plane and parameterized by the deflection beam shift, according to the same discussion as in section 3.5.2. The chromatic aberration and the aberrations induced by the variation of voltages and currents of the round symmetric electrodes and the magnetic lens coils at the image plane and parametrized by the deflection beam shifts are expressed as follows.

$$\Delta w_{\kappa l} = [C_{Ci} S_i + C_{\gamma \kappa l} w_i^\gamma + C_{V \kappa l}^F M_e + C_{I \kappa l}^F S_m] \frac{\Delta \Phi}{\Phi_i}, \quad (3.241)$$

$$\Delta w_{ELwob l} = \sum_{j=1}^N \frac{\Delta V_j^{EL}}{V_j^{EL}} [C_{\alpha j i}^{ELwob} S_i + C_{\gamma j i}^{ELwob} w_i^\gamma + C_{V j i}^{ELwob F} M_e + C_{I j i}^{ELwob F} S_m], \quad (3.242)$$

$$\Delta w_{MLwob l} = \sum_{\ell=1}^M \frac{\Delta I_\ell^{ML}}{I_\ell^{ML}} [C_{\alpha \ell i}^{MLwob} S_i + C_{\gamma \ell i}^{MLwob} w_i^\gamma + C_{V \ell i}^{MLwob F} M_e + C_{I \ell i}^{MLwob F} S_m], \quad (3.243)$$

where parameters at the image plane are defined as

$$S_i = w'_{\alpha i} w'_o = e^{i\chi_i} M_\alpha w'_o, \\ w_i^\gamma = w_{\gamma i} w_o = e^{i\chi_i} M_\gamma w_o, \\ M_e = V w_{ei}, \\ S_m = I w_{mi}. \quad (3.244)$$

Evaluating the Wronskian Eq. (3.78) at the image plane, we obtain the relation:

$$\frac{1}{\phi_o^*} = \frac{1}{w_{yi}^2 \bar{w}_{ai}'^2} \frac{1}{\phi_i^*}. \quad (3.245)$$

Taking into account Eq. (3.241) - (3.245), the conversion relation of the second-rank aberration coefficients are obtained as follows:

$$\begin{aligned} C_{Ci} &= \frac{1}{w_{yi} w_{ai}' \bar{w}_{ai}'^2} C_{Co}, & C_{\gamma Ki} &= \frac{1}{w_{yi}^2 \bar{w}_{ai}'^2} C_{\gamma Ko}, \\ C_{V Ki}^F &= \frac{1}{w_{yi} \bar{w}_{ai}'^2 w_{ei}} C_{V Ko}, & C_{I Ki}^F &= \frac{1}{w_{yi} \bar{w}_{ai}'^2 w_{mi}} C_{I Ko}, \\ C_{\alpha ji}^{ELwob} &= \frac{w_{yi}}{w_{ai}'} C_{\alpha jo}^{ELwob}, & C_{\alpha \ell i}^{MLwob} &= \frac{w_{yi}}{w_{ai}'} C_{\alpha \ell o}^{MLwob}, \\ C_{\gamma ji}^{ELwob} &= C_{\gamma jo}^{ELwob}, & C_{\gamma \ell i}^{MLwob} &= C_{\gamma \ell o}^{MLwob}, \\ C_{V ji}^{ELwob} &= \frac{w_{yi}}{w_{ei}} C_{V jo}^{ELwob}, & C_{V \ell i}^{MLwob} &= \frac{w_{yi}}{w_{ei}} C_{V \ell o}^{MLwob}, \\ C_{I ji}^{ELwob} &= \frac{w_{yi}}{w_{mi}} C_{I jo}^{ELwob}, & C_{I \ell i}^{MLwob} &= \frac{w_{yi}}{w_{mi}} C_{I \ell o}^{MLwob}. \end{aligned} \quad (3.246)$$

We are at the point where the second-rank aberration coefficients defined at the image plane are derived.

3.9 Conclusion

In this chapter, we reviewed and re-derived the relativistic deflection aberration theory up to the third-order geometrical aberrations, the second-rank chromatic aberrations, and the aberrations of the variations of voltages and currents of the lenses, for a system composed of focusing lenses and two independent deflectors, where the control parameter of the trajectory is the coordinate of the optic axis, z . When the mirror field and deflection field are not overlapped spatially, deflection aberration theory is used as a tool to analyze the contribution to the whole aberrations from the deflector parts of the mirror system. Through this chapter, we obtained the following results.

1. The deflection potentials are expressed by complex signals, which are the voltage or current of deflectors. The dipole component of deflection potentials depends on a complex signal, whereas the hexapole component depends on the complex conjugate of the corresponding complex signal.
2. The deflection trajectory, which approximates the deflected electron trajectory depending on the first order of the complex signal, was re-derived from the Euler-Lagrange equation in a Cartesian coordinate system.
3. The perturbation formulae of deflection theory were reviewed and expanded to relativistic third-order geometrical deflection aberration formulae for a system composed of focusing lenses and two independent deflectors. The derived formulae are valid when deflection fields and lens-fields overlap with one another. However, the derived formulae are limited to the case where an incident beam starts from the axial object point, that is, the contribution to aberrations from the off-axis size of the beam, in the object plane, is neglected. The deflection aberration formulae for three combinations of deflector types were derived. The first contribution is the case of an electrostatic deflector and a magnetic deflector. The second and the third contributions are the case of two electrostatic deflectors and the case of two magnetic deflectors, respectively.
4. The second-rank chromatic relativistic deflection aberration coefficient formulae were re-derived. Second-rank relativistic aberration formulae due to the variation of voltage and current of lenses were also derived.

Taking into account the theory of Chapter 2 and this chapter, we can consider a time-dependent deflection aberration theory, which is directly used for a system composed of mirror fields and deflection fields, which overlap with one another. We will discuss this in Chapter 4.

3.10 References

- [3.1] G.F. Rempfer, M.S. Mauck, Correction of chromatic aberration with an electron mirror, *Optik* **92** (1992) 3-8.
- [3.2] R. M. Tromp, et al., A new aberration-corrected, energy-filtered LEEM/PEEM instrument, I. Principle and design, *Ultramicroscopy* **110**, pp852-861, (2010).
- [3.3] M. Mankos, et al., Progress toward an aberration-corrected low energy electron microscope for DNA sequencing and surface analysis, *J. Vac. Sci. Technol. B* **30**(6), (2012), 06F402.
- [3.4] H. Rose, Aberration correction of homogeneous magnetic deflection systems, *Optik* **51**(1), (1978), pp15-38.
- [3.5] H. Mueller, D. Preikszas, H. Rose, A beam separator with small aberrations, *Journal of Electron Microscopy* **48**(3), (1999), pp191-204.
- [3.6] R. Fink, et al., SMART: a planned ultrahigh-resolution spectromicroscope for BESSY II, *Journal of Electron Spectroscopy and Related Phenomena* **84**, (1997), pp231-25.
- [3.7] P. Schmid, et al., Correction and alignment strategies for the beam separator of the photoemission electron microscope 3 (PEEM3), *Rev. Sci. Instrum.* **76**, (2005), 023302.
- [3.8] H. C. Chu, E. Munro, Numerical analysis of electron beam lithography systems, Part II: Computation of fields in electrostatic deflectors, *Optik* **61**(1), (1982), pp1-16.
- [3.9] H. C. Chu, E. Munro, Numerical analysis of electron beam lithography systems, Part I: Computation of fields in magnetic deflectors, *Optik* **60**(4), (1982), pp371-390.
- [3.10] H. C. Chu, E. Munro, Numerical analysis of electron beam lithography systems, Part III: Calculation of the optical properties of electron focusing systems and dual-channel deflection systems with combined magnetic and electrostatic fields, *Optik* **61**(2), (1982), pp121-145.
- [3.11] E. Munro, Calculation of the Optical Properties of Combined Magnetic Lenses and Deflection Systems with Superimposed Fields, *Optik* **39**(4), (1974), pp450-466.
- [3.12] E. Munro, Design and optimization of magnetic lenses and deflection systems for electron beams, *J. Vac. Sci. Technol.*, **12**(5), (1975), pp1146-1150.
- [3.13] T. Soma, Relativistic aberration formulas for combined electric-magnetic focusing-deflection system, *Optik* **49**(3), (1977), pp255-262.
- [3.14] Y. Li, J. Ximen, On the relativistic aberration theory of a combined focusing-deflection system with multi-stage deflectors, *Optik* **61**(3), (1982), pp315-332.
- [3.15] Y. Li, A relativistic aberration theory without high order derivatives for a combined focusing-deflection system, *Nucl. Instrum. Meth.* **A316**, (1992), pp89-98.

- [3.16] Y. Li, S. Kuang, Z. Feng, T. Liu, The relativistic fifth-order geometrical aberrations of a combined focusing-deflection system, *J. Phys. D***26**, (1993), pp522-538.
- [3.17] Y. Uno, H. Morita, N. Simazu, T. Hosokawa, Fifth-order aberration analysis of a combined electrostatic-magnetic focusing-deflection system, *Nucl. Instrum. Meth. A***363**, (1995), pp10-17.
- [3.18] H. Rose, *Geometrical Charged Particle Optics*, 2nd Edition, Springer, 2012.

Chapter 4 3rd-order time-dependent aberration theory for systems of round symmetric electromagnetic fields and deflectors

The content of this chapter was published in “Time-dependent perturbation theory for electron mirrors, Advances in Imaging and Electron Physics” vol. 234, Chapter 2, (2025) pp. 97-278.

4.1 Introduction

As we discussed in Chapter 3, the theory of small angle deflection, which is parameterized by the coordinate of the optic axis, provides us with an analysis of aberrations of beam deflection. However, when we consider the case where mirror fields and deflection fields overlap with each other, we need a time-dependent theory that includes deflection fields. In this chapter, we derive time-dependent path deviation formulae, including the small-angle deflection effect, based on the considerations of Chapter 2 and 3. The theory is non-relativistic but valid for a system composed of rotationally symmetric electrostatic and magnetic fields and electrostatic and magnetic deflection fields. We provide time-dependent path deviation formulae up to the third order. This theory was originally derived by the author.

In section 4.2, we derive the field expansion including deflection fields, based on the series expansion of deflection potential, which was given in section 3.2. Then, we derive the equation of motion including round symmetric fields and deflection fields.

In section 4.3, we investigate the first-order approximation in lateral directions. We also consider first-order solutions and calculate deflection trajectories, which are the first-order solution of the lateral equation of motion for deflection.

In section 4.4, the first-order solution of longitudinal path deviation with deflection fields is derived.

In section 4.5, we derive the second-rank path deviation and the chromatic aberration coefficients with deflection fields.

In section 4.6, the second-order geometrical longitudinal path deviation is derived as a preparation for the third-order geometrical lateral path deviation.

In section 4.7, we derive the second-order geometrical path deviation in the longitudinal direction. The third-order geometrical lateral path deviation and aberration coefficients are derived with deflection fields. In sections 4.6 and 4.7, we consider two independent deflection fields in three combinations to consider concrete expressions of the path deviations and the aberration coefficients such as the combinations discussed in Chapter 3. The first case consists of one electrostatic deflector and one magnetic deflector. The second case consists of two different electrostatic deflectors.

The third case consists of two different magnetic deflectors. We consider all possible combinations of deflection aberrations, including the so-called four-fold aberrations which stem from the hexapole component of deflector fields. Fig. 4.1 shows a schematic of an example of an electron optical system where the considered theory of deflection aberrations discussed in this chapter can be applied. As an example, the two deflectors in Fig. 4.1 are a magnetic deflector and an electrostatic deflector.

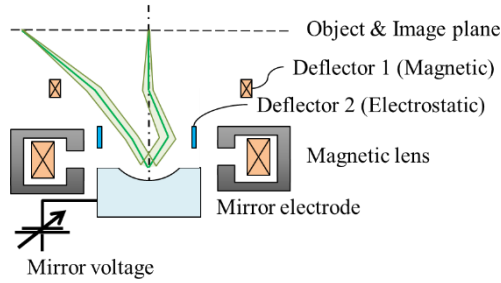


Fig. 4.1 Schematic of an example of an electron optical system where the considered theory of deflection aberrations can be applied.

The system includes not only the magnetic lens and the mirror electrode where the mirror voltage is imposed, but also a magnetic deflector and an electrostatic deflector. The magnetic lens and the mirror electrode generate rotationally symmetric magnetic and electrostatic fields, respectively. The electrostatic field of the mirror electrode reflects the incident electrons. The reflected electrons are re-focused on the object plane by both the rotationally symmetric electrostatic and magnetic fields. In this case, the object plane matches the image plane. The magnetic deflector and the electrostatic deflector generate magnetic and electrostatic deflection fields, respectively. The deflection aberration theory discussed in this chapter allows the distributions of these fields along the optic axis to overlap with one another. In this system, fields generated by the magnetic lens, the mirror electrode, and the electrostatic deflector overlap with one another. Note that, for simplicity, we ignore the rotation of electrons by the magnetic lens, and the depicted trajectory of the electron beam is not correct.

In section 4.8, we derive lateral path deviation and aberration coefficients induced by the variation of voltages and currents of round symmetric electrodes and lens-coils with deflection fields.

In section 4.9, we provide path deviation for inclined incident beam in time-dependent deflection theory.

In section 4.10, we present a conclusion for this chapter.

4.2 Field expansion and general equation of motion in time-dependent deflection theory

In the time-dependent theory, potentials are expanded by the lateral coordinate w and longitudinal path deviation h , and an axial potential is expressed as a function of the reference electron coordinate ζ , where the coordinate of the optic axis related through Eq. (2.2). Taking into account Eqs. (2.23), (2.24), (3.18), and (3.32), specific series expansions of the electrostatic and magnetic deflection potentials, for the time-dependent theory, are expanded up to the fourth-order of parameters as follows:

$$\begin{aligned}
 \varphi_{DEF}(w, \bar{w}, \zeta, h) &= \text{Re} \left[F_1(\zeta) V \bar{w} + F_1'(\zeta) V \bar{w} h + \frac{1}{2} F_1''(\zeta) V \bar{w} h^2 + F_3(\zeta) \bar{V} \bar{w}^3 - \frac{1}{8} F_1''(\zeta) V w \bar{w}^2 \right] \\
 &= \frac{1}{2} \left[F_1 V \bar{w} + F_1' V \bar{w} h + \frac{1}{2} F_1'' V \bar{w} h^2 + F_3 \bar{V} \bar{w}^3 - \frac{1}{8} F_1'' V w \bar{w}^2 + F_1 \bar{V} w + F_1' \bar{V} w h + \frac{1}{2} F_1'' \bar{V} w h^2 \right. \\
 &\quad \left. + \bar{F}_3 V w^3 - \frac{1}{8} \bar{F}_1'' \bar{V} w^2 \bar{w} \right], \\
 \psi_{DEF}(w, \bar{w}, \zeta, h) &= \text{Im} \left[ID_1(\zeta) \bar{w} + ID_1'(\zeta) \bar{w} h + \frac{1}{2} ID_1''(\zeta) \bar{w} h^2 - \bar{ID}_3(\zeta) \bar{w}^3 - \frac{1}{8} ID_1'' w \bar{w}^2 \right] \\
 &= \frac{1}{2i} \left[ID_1 \bar{w} + ID_1' \bar{w} h + \frac{1}{2} ID_1'' \bar{w} h^2 - \bar{ID}_3 \bar{w}^3 - \frac{1}{8} ID_1'' w \bar{w}^2 - \bar{ID}_1 w - \bar{ID}_1' w h - \frac{1}{2} \bar{ID}_1'' w h^2 \right. \\
 &\quad \left. + ID_3 w^3 + \frac{1}{8} ID_1'' w^2 \bar{w} \right],
 \end{aligned} \tag{4.1}$$

where F_1, F_3, D_1, D_3 , and V, I are given in Eqs. (3.9), (3.16), (3.27), and (3.30), respectively.

Employing Eq. (2.22), series expansions of the electrostatic and magnetic deflection field strength in both the lateral and longitudinal directions are considered.

To account for up to the third-order path-deviations, it is sufficient to expand lateral field strengths up to the third order, and longitudinal field strengths up to the second order, with respect to the sum of the exponent of a polynomial of the lateral trajectory, the longitudinal path-deviation, and the complex voltage and current of deflectors. The concrete expansions of the deflection field strengths up to the third-order are given as follows. The electrostatic deflection field strengths:

$$\begin{aligned}
 E_w^{DEF} &= -2 \frac{\partial \varphi_{DEF}}{\partial \bar{w}} = - \left[F_1 V + F_1' V h + \frac{1}{2} F_1'' V h^2 - \frac{1}{8} \bar{F}_1'' \bar{V} w^2 - \frac{1}{4} F_1' V w \bar{w} + 3 F_3 \bar{V} \bar{w}^2 \right], \\
 E_z^{DEF} &= - \frac{\partial \varphi_{DEF}}{\partial h} = - \frac{1}{2} [F_1' V \bar{w} + \bar{F}_1' \bar{V} w + F_1'' V \bar{w} h + \bar{F}_1'' \bar{V} w h].
 \end{aligned} \tag{4.2}$$

The magnetic deflection field strengths:

$$\begin{aligned}
 B_w^{DEF} &= -2 \frac{\partial \psi_{DEF}}{\partial \bar{w}} = i \left[ID_1 + ID_1' h + \frac{1}{2} ID_1'' h^2 + \frac{1}{8} \bar{ID}_1'' w^2 - 3 \bar{ID}_3 \bar{w}^2 - \frac{1}{4} ID_1'' w \bar{w} \right], \\
 B_z^{DEF} &= - \frac{\partial \psi_{DEF}}{\partial h} = \frac{i}{2} [ID_1' \bar{w} - \bar{ID}_1' w + ID_1'' \bar{w} h - \bar{ID}_1'' w h].
 \end{aligned} \tag{4.3}$$

The field strengths of rotationally symmetric potentials are also expanded up to the third-order, and up to the second order, for lateral and longitudinal field strengths, respectively. Using Eq. (2.29) to (2.32), and (2.21), in a Cartesian coordinate system, we expand, the rotationally symmetric electrostatic field as

$$E_w^{RS} = \frac{1}{2}\phi''w + \frac{1}{2}\phi^{[3]}wh - \frac{1}{16}\phi^{[4]}w^2\bar{w} + \frac{1}{4}\phi^{[4]}wh^2 + \dots, \quad (4.4)$$

$$E_z^{RS} = -\left(\phi' + \phi''h - \frac{1}{4}\phi^{[3]}w\bar{w} + \frac{1}{2}\phi^{[3]}h^2 - \frac{1}{4}\phi^{[4]}w\bar{w}h + \frac{1}{6}\phi^{[4]}h^3\right) + \dots,$$

and the rotationally symmetric magnetic field strength as

$$B_w^{RS} = -\left(\frac{1}{2}B'w + \frac{1}{2}B''wh - \frac{1}{16}B^{[3]}w^2\bar{w} + \frac{1}{4}B^{[3]}wh^2\right) + \dots, \quad (4.5)$$

$$B_z^{RS} = B + B'h - \frac{1}{4}B''w\bar{w} + \frac{1}{2}B''h^2 - \frac{1}{4}B^{[3]}w\bar{w}h + \frac{1}{6}B^{[3]}h^3 + \dots.$$

The general equations of motion in time-dependent theory are given by Eqs. (2.11) and (2.12). Employing Eqs. (4.2) to (4.5), the lateral equation of motion is transformed as follows.

$$\ddot{w} + \frac{\phi''}{4\Phi_C}w - \frac{i\eta}{\sqrt{\Phi_C}}\left(B\dot{w} + \frac{1}{2}B'\dot{\zeta}w\right) = P_{DEF} + P_w. \quad (4.6)$$

where a dot means differentiation with respect to reduced time, Eq. (2.6), a prime means differentiation with respect to the optic axis coordinate, η is given by Eq. (2.9), Φ_C is the column potential, and

$$P_{DEF} = V\frac{F_1}{2\Phi_C} + I\frac{\dot{\zeta}\eta D_1}{\sqrt{\Phi_C}}, \quad (4.7)$$

and

$$P_w = -\frac{\phi^{[3]}}{4\Phi_C}wh + \frac{\phi^{[4]}}{32\Phi_C}w^2\bar{w} - \frac{\phi^{[4]}}{8\Phi_C}wh^2$$

$$+ \frac{i\eta}{\sqrt{\Phi_C}}\left[\frac{d}{d\tau}\left(\frac{1}{2}B'wh - \frac{1}{16}B''w^2\bar{w} + \frac{1}{4}B''wh^2\right) + \frac{1}{2}B'\dot{w}h - \frac{1}{16}B''(2w\bar{w}\dot{w} - w^2\dot{\bar{w}})\right.$$

$$\left. + \frac{1}{4}B''\dot{w}h^2\right]$$

$$+ \frac{F_1'}{2\Phi_C}Vh + \frac{F_1''}{4\Phi_C}Vh^2 - \frac{\bar{F}_1'}{16\Phi_C}\bar{V}w^2 - \frac{F_1''}{8\Phi_C}Vw\bar{w} + \frac{3F_3}{2\Phi_C}\bar{V}\bar{w}^2$$

$$+ \frac{\eta}{\sqrt{\Phi_C}}\left[\frac{d}{d\tau}\left(ID_1h + \frac{1}{2}ID_1'h^2 - \frac{1}{4}ID_1'w\bar{w} + \frac{1}{8}\bar{ID}_1'w^2\right) + \frac{1}{4}ID_1'(w\dot{\bar{w}} - \bar{w}\dot{w}) + \frac{1}{4}\bar{ID}_1'w\dot{w}\right.$$

$$\left. - 3\bar{ID}_3\dot{\zeta}\bar{w}^2\right] + \dots \quad (4.8)$$

The longitudinal equation of motion is divided into two parts. One equation is for a reference electron, which is exactly the same as Eq. (2.13). The properties of Eq. (2.14) and (2.15) are valid even if deflectors are considered. The other is for a longitudinal path deviation.

$$\ddot{h} - \frac{\phi''}{2\Phi_C}h = P_h. \quad (4.9)$$

It is sufficient to expand the longitudinal perturbation term P_h up to the second order to derive the third-order geometrical path deviation in the lateral directions, because the longitudinal path deviations, up to the second rank, contribute to the third-order lateral path deviations.

$$P_h = -\frac{\phi^{[3]}}{8\Phi_C}w\bar{w} + \frac{\phi^{[3]}}{4\Phi_C}h^2 - \frac{i\eta B'}{4\sqrt{\Phi_C}}(w\dot{\bar{w}} - \bar{w}\dot{w})$$

$$+ \frac{F_1'}{4\Phi_C}V\bar{w} + \frac{\bar{F}_1'}{4\Phi_C}\bar{V}w - \frac{\eta}{2\sqrt{\Phi_C}}(ID_1\dot{w} + \bar{ID}_1\dot{\bar{w}}) + \dots. \quad (4.10)$$

We are at the point where in a Cartesian coordinate, the series expansion of deflection fields, and the expansion of the equation of motion in time-dependent deflection theory are derived.

4.3 First order approximation of equation of motion and first-order solutions

Here we derive the first-order equation of motion and its solutions. By the first-order approximation, which is called the paraxial approximation, in lateral direction, Eq. (4.6) is transformed into

$$\ddot{w} + \frac{\Phi''}{4\Phi_C} w - \frac{i\eta}{\sqrt{\Phi_C}} \left(B\dot{w} + \frac{1}{2} B' \zeta w \right) = P_{DEF}. \quad (4.11)$$

When the inhomogeneous term P_{DEF} vanishes, which means deflection is not considered, the resulting homogeneous equation is a paraxial equation of the time-dependent theory in a Cartesian coordinate system. The general solution of Eq. (4.11) is given by

$$w^{(1)} = \dot{w}_o w_\alpha(\tau) + w_o w_\gamma(\tau) + V w_e(\tau) + I w_m(\tau), \quad (4.12)$$

where \dot{w}_o and w_o are the lateral reduced velocity and lateral position of an electron in the object plane, and w_α and w_γ are an axial ray and a field ray in the Cartesian coordinate.

w_e and w_m are electrostatic and magnetic deflection trajectories, respectively, which are particular solutions of the inhomogeneous term P_{DEF} . w_α and w_γ are fundamental solutions of the homogeneous equation, which is obtained when $P_{DEF} = 0$ in Eq. (4.11), under initial conditions:

$$\begin{aligned} w_{\gamma o} &= 1, & \dot{w}_{\gamma o} &= 0, \\ w_{\alpha o} &= 0, & \dot{w}_{\alpha o} &= 1. \end{aligned} \quad (4.13)$$

The lateral trajectory in the Cartesian coordinate system is connected to that in the rotation coordinate system via the relation

$$w = e^{i\chi(\tau)} u(\tau), \quad (4.14)$$

where the rotation angle, measured from the object plane, by the rotationally symmetric magnetic field and its reduced velocity are given by

$$\chi(\tau) = \int_{\tau_o}^{\tau} \frac{\eta B}{2\sqrt{\Phi_C}} d\tau, \quad \dot{\chi} = \frac{\eta B}{2\sqrt{\Phi_C}} \quad (4.15)$$

The relations between w_α and w_γ and the fundamental solutions in the rotation coordinate system, u_α and u_γ are given by

$$\begin{aligned} w_\gamma &= e^{i\chi} (u_\gamma - i\dot{\chi}_o u_\alpha), \\ w_\alpha &= e^{i\chi} u_\alpha, \\ \dot{w}_\gamma &= e^{i\chi} (\dot{u}_\gamma + \dot{\chi}_o \dot{\chi} u_\alpha + i(\dot{\chi} u_\gamma - \dot{\chi}_o \dot{u}_\alpha)), \\ \dot{w}_\alpha &= e^{i\chi} (\dot{u}_\alpha + i\dot{\chi} u_\alpha). \end{aligned} \quad (4.16)$$

Using Eqs. (2.66) to (2.74), without deflection, the paraxial trajectory and its slope in the image plane are given by

$$\begin{aligned} w_i^{(1)} &= e^{i\chi_i} M w_o, \\ w_i^{(1)'} &= \frac{1}{\zeta_i} \dot{w}_i^{(1)} = \frac{1}{\zeta_i} e^{i\chi_i} \left[\left\{ -\frac{\zeta_i}{f_i} + i \left(\chi_i M - \frac{1}{M} \dot{\chi}_o \right) \right\} w_o + \frac{1}{M} \dot{w}_o \right] \\ &= \left[-\frac{1}{f_i M} + i \left(\chi_i' - \frac{1}{M^2} \frac{\zeta_o}{\zeta_i} \chi_o' \right) \right] w_i^{(1)} + \dot{s}_i, \\ \dot{s}_i &= \frac{1}{\zeta_i M} e^{i\chi_i} \dot{w}_o = e^{i\chi_i} M_\alpha w_o', \end{aligned} \quad (4.17)$$

where M is the magnification Eq. (2.68), f_i is the real focal length of the image-side, Eq. (2.72), M_α is the angular magnification, Eq. (2.71) and \hat{s}_i is the complex slope value for the axial trajectory component at the image plane.

Using Eq. (2.43), we find that

$$W[w_\gamma, w_\alpha] = e^{2i\chi} W[u_\gamma, u_\alpha] = e^{2i\chi}. \quad (4.18)$$

Using Eq. (4.16) and Eq. (4.18), we find the following relations:

$$\begin{aligned} w_\gamma \bar{w}_\alpha - \bar{w}_\gamma w_\alpha &= -2i\dot{\chi}_o w_\alpha \bar{w}_\alpha, \\ w_\gamma \dot{\bar{w}}_\alpha - \dot{\bar{w}}_\gamma w_\alpha &= 1 - 2i\dot{\chi}_o w_\alpha \bar{w}_\alpha, \\ w_\alpha \dot{\bar{w}}_\alpha - \bar{w}_\alpha \dot{w}_\alpha &= -2i\dot{\chi} w_\alpha \bar{w}_\alpha, \\ w_\gamma \dot{\bar{w}}_\gamma - \bar{w}_\gamma \dot{w}_\gamma &= -2i(\dot{\chi} w_\gamma \bar{w}_\gamma + \dot{\chi}_o), \\ w_\gamma \bar{w}_\alpha - \dot{w}_\gamma \bar{w}_\alpha &= 1 - 2i\dot{\chi} w_\gamma \bar{w}_\alpha, \end{aligned} \quad (4.19)$$

and

$$\begin{aligned} \frac{w_\alpha}{W[w_\gamma, w_\alpha]} &= \bar{w}_\alpha, \\ \frac{w_\gamma}{W[w_\gamma, w_\alpha]} &= \bar{w}_\gamma - 2i\dot{\chi}_o \bar{w}_\alpha. \end{aligned} \quad (4.20)$$

A formal solution of the inhomogeneous equation (4.11) is obtained by the parameter variation method. We assume that the formal solution vanishes at initial reduced time τ_o , that is $\tau_A = \tau_B = \tau_o$ in Eq. (2.418). Then, for simplicity, we take that $x_1 = w_\gamma$ and $x_2 = w_\alpha$ in Eq. (2.418). Employing Eq. (4.20), a formal solution of Eq. (4.6) is given by

$$\begin{aligned} w_s &= w_\gamma(\tau) \int_{\tau_o}^{\tau} \frac{P_{DEF} + P_w}{W[w_\gamma, w_\alpha]} w_\alpha d\tau - w_\alpha(\tau) \int_{\tau_o}^{\tau} \frac{P_{DEF} + P_w}{W[w_\gamma, w_\alpha]} w_\gamma d\tau \\ &= -\left(w_\gamma(\tau) + 2i\dot{\chi}_o w_\alpha(\tau)\right) \int_{\tau_o}^{\tau} (P_{DEF} + P_w) \bar{w}_\alpha d\tau + w_\alpha(\tau) \int_{\tau_o}^{\tau} (P_{DEF} + P_w) \bar{w}_\gamma d\tau \end{aligned} \quad (4.21)$$

Using Eq. (4.21) and ignoring P_w , we find that deflection trajectories and their reduced velocities are given by

$$\begin{aligned} w_e &= -\left(w_\gamma(\tau) + 2i\dot{\chi}_o w_\alpha(\tau)\right) \int_{\tau_o}^{\tau} \frac{F_1}{2\Phi_C} \bar{w}_\alpha d\tau + w_\alpha(\tau) \int_{\tau_o}^{\tau} \frac{F_1}{2\Phi_C} \bar{w}_\gamma d\tau, \\ w_m &= -\left(w_\gamma(\tau) + 2i\dot{\chi}_o w_\alpha(\tau)\right) \int_{\tau_o}^{\tau} \frac{\zeta\eta D_1}{\sqrt{\Phi_C}} \bar{w}_\alpha d\tau + w_\alpha(\tau) \int_{\tau_o}^{\tau} \frac{\zeta\eta D_1}{\sqrt{\Phi_C}} \bar{w}_\gamma d\tau, \\ \dot{w}_e &= -\left(\dot{w}_\gamma(\tau) + 2i\dot{\chi}_o \dot{w}_\alpha(\tau)\right) \int_{\tau_o}^{\tau} \frac{F_1}{2\Phi_C} \bar{w}_\alpha d\tau + \dot{w}_\alpha(\tau) \int_{\tau_o}^{\tau} \frac{F_1}{2\Phi_C} \bar{w}_\gamma d\tau, \\ \dot{w}_m &= -\left(\dot{w}_\gamma(\tau) + 2i\dot{\chi}_o \dot{w}_\alpha(\tau)\right) \int_{\tau_o}^{\tau} \frac{\zeta\eta D_1}{\sqrt{\Phi_C}} \bar{w}_\alpha d\tau + \dot{w}_\alpha(\tau) \int_{\tau_o}^{\tau} \frac{\zeta\eta D_1}{\sqrt{\Phi_C}} \bar{w}_\gamma d\tau. \end{aligned} \quad (4.22)$$

We are at the point where a general solution of the first-order approximation of the equation of motion in the lateral direction in the Cartesian coordinate has been derived. In addition, integral forms of deflection trajectories of electrostatic and magnetic deflection have been derived.

4.4 First order approximation and solution of longitudinal equation of motion

In this section, the first order approximation of the longitudinal equation of motion and its solution are discussed.

The first order longitudinal equation is given by

$$\ddot{h}_p - \frac{\Phi''}{2\Phi_C} h_p = 0. \quad (4.23)$$

Eq. (4.23) is exactly the same as Eq. (2.39), therefore, the general solution is given by

$$h_p = h_o h_\gamma + \dot{h}_o h_\alpha, \quad (4.24)$$

which is the same as Eq. (2.51), where h_α and h_γ satisfy the initial condition Eq. (2.47) and the Wronskian Eq. (2.48).

Therefore, the discussion and formulae from Eqs. (2.52) to (2.55) are repeated, even if the deflection field is considered.

The difference appears in Eq. (2.59), because of energy conservation, the reduced velocity of the longitudinal path deviation in the object plane is expressed as

$$\dot{h}_o = \dot{\zeta}_o \left[\left\{ \kappa_o + \frac{\varphi_o}{\dot{\zeta}_o^2 \Phi_C} - \frac{1}{\dot{\zeta}_o^2} \dot{w}_o \dot{\bar{w}}_o \right\}^{1/2} - 1 \right], \quad (4.25)$$

where κ_o is a chromatic parameter given in Eq. (2.55), and φ_o is the electrostatic potential of electrons, including the electrostatic deflection potential, in the object plane:

$$\varphi_o = \Phi_o - \frac{1}{4} \Phi_o'' w_o \bar{w}_o + \frac{1}{2} (F_{1o} V \bar{w}_o + \bar{F}_{1o} V w_o) + \dots \quad (4.26)$$

As a result, \dot{h}_o is decomposed according to the rank of parameters, which is given in Eq. (2.60). To consider up to the third-order geometrical lateral path deviation, it is sufficient to consider up to the second-rank longitudinal path deviation. Then, we find that the first-rank component of \dot{h}_o is

$$\dot{h}_o^{(1)} = \frac{1}{2} \dot{\zeta}_o \kappa_o, \quad (4.27)$$

and the second-rank component is

$$\begin{aligned} \dot{h}_o^{(2)} = & -\frac{1}{2\dot{\zeta}_o} \dot{w}_o \dot{\bar{w}}_o - \frac{\Phi_o''}{8\dot{\zeta}_o \Phi_C} w_o \bar{w}_o \\ & + \frac{F_{1o}}{4\dot{\zeta}_o \Phi_C} V \bar{w}_o + \frac{\bar{F}_{1o}}{4\dot{\zeta}_o \Phi_C} V w_o - \frac{1}{8} \dot{\zeta}_o \kappa_o^2. \end{aligned} \quad (4.28)$$

We should consider that the longitudinal path deviation vanishes at the initial time, when the reference electron is in the object plane, which means $h_o = 0$. Then, the first-order solution of the longitudinal path deviation is dependent on only h_α and \dot{h}_o . Since \dot{h}_o is decomposed according to the rank of parameters, the solution of the first order equation of the longitudinal path deviation is expressed as

$$\begin{aligned} h_p = & \sum_{r=1} h_1^{(r)}(\tau), \\ h_1^{(r)}(\tau) = & \dot{h}_o^{(r)} h_\alpha(\tau). \end{aligned} \quad (4.29)$$

As for the solutions of the first order longitudinal equation, by introducing deflection fields, the only difference emerges in the rank decomposition of the reduced velocity in the longitudinal direction in the object plane, \dot{h}_o . By Eq. (4.28), the second rank component of \dot{h}_o depends on the electrostatic dipole field component in the object plane. When

a non-zero electrostatic deflection field exists in the object plane, $h_o^{(2)}$ and higher-rank components are different from those without deflection fields.

4.5 Second-rank lateral path deviation and chromatic deflection aberration coefficients of time-dependent deflection theory

To obtain the second-rank path deviation, the perturbation procedure given in section 2.3.1 in Chapter 2 is employed. Since the lowest rank structure of the lateral trajectory, w and the longitudinal path deviation, h are first-order and first-degree, respectively, the lowest rank of the lateral perturbation function is the second rank. We can apply procedure from Eqs. (2.85) to (2.88), to Eq. (4.8), where we replace P_u with P_w in the equations of section 2.3.1. Then, we find the second-rank lateral perturbation function:

$$P_w^{(2)} = P_{w,\ell=2}[w^{(1)}, \bar{w}^{(1)}, \dot{w}^{(1)}, \bar{\dot{w}}^{(1)}, h^{(1)}, \dot{h}^{(1)}; \tau] \\ = -\frac{\Phi^{[3]}}{4\Phi_C} w^{(1)} h^{(1)} + \frac{i\eta}{2\sqrt{\Phi_C}} \left[\frac{d}{d\tau} (B' w^{(1)} h^{(1)}) + B' \dot{w}^{(1)} h^{(1)} \right] + \frac{F'_1}{2\Phi_C} V h^{(1)} + \frac{\eta}{\sqrt{\Phi_C}} \frac{d}{d\tau} (ID_1 h^{(1)}). \quad (4.30)$$

The second-rank path deviation, including the deflection, in time-dependent theory, is given by the following formula:

$$w^{(2)}(\tau) = -\left(w_\gamma(\tau) + 2i\dot{\chi}_o w_\alpha(\tau)\right) \int_{\tau_o}^{\tau} P_w^{(2)}(\tau) \bar{w}_\alpha(\tau) d\tau + w_\alpha(\tau) \int_{\tau_o}^{\tau} P_w^{(2)}(\tau) \bar{w}_\gamma(\tau) d\tau. \quad (4.31)$$

Since the perturbation function Eq. (4.30) is composed of terms of total differentiation with respect to reduced time and other terms. We write the perturbation term as

$$P = -\left(P_1 - \frac{dP_2}{d\tau}\right), \quad (4.32)$$

where P_2 is composed of terms of total differentiation with respect to reduced time. Since in time-dependent theory, the integrands of the perturbation term are convergent and assumed to be smooth with respect to reduced time, we can perform partial integral about P_2 . Then, we find:

$$-\int_{\tau_o}^{\tau} P(\tau) \bar{w}_H(\tau) d\tau = \int_{\tau_o}^{\tau} P_1(\tau) \bar{w}_H(\tau) d\tau - \int_{\tau_o}^{\tau} \frac{dP_2}{d\tau} \bar{w}_H(\tau) d\tau \\ = \int_{\tau_o}^{\tau} [P_1 \bar{w}_H + P_2 \dot{\bar{w}}_H] d\tau - (P_2 \bar{w}_H - P_{2o} \bar{w}_{Ho}), \quad (4.33)$$

where the subscript H of w_H is either α or γ . For the boundary term, we find:

$$-(w_\gamma + 2i\dot{\chi}_o w_\alpha)(P_2 \bar{w}_\alpha - P_{2o} \bar{w}_{\alpha o}) + w_\alpha(P_2 \bar{w}_\gamma - P_{2o} \bar{w}_{\gamma o}) \\ = -P_2[w_\gamma \bar{w}_\alpha - \bar{w}_\gamma w_\alpha + 2i\dot{\chi}_o w_\alpha \bar{w}_\alpha] - P_{2o} w_\alpha \\ = -P_{2o} w_\alpha, \quad (4.34)$$

where Eq. (4.19) is used for this transformation. For the second-rank perturbation term Eq. (4.30), P_1 and P_2 are

$$P_1^{(2)} = \frac{\Phi^{[3]}}{4\Phi_C} w^{(1)} h^{(1)} - \frac{i\eta B'}{2\sqrt{\Phi_C}} \dot{w}^{(1)} h^{(1)} - \frac{F'_1}{2\Phi_C} V h^{(1)}, \\ P_2^{(2)} = \frac{i\eta B'}{2\sqrt{\Phi_C}} w^{(1)} h^{(1)} + \frac{\eta}{\sqrt{\Phi_C}} ID_1 h^{(1)}. \quad (4.35)$$

In addition, as we discussed in section 2.3.2, the perturbed electron positions in the z-direction at the reduced time τ differ from one another, according to their dependence on geometrical and chromatic parameters, since the longitudinal path deviation is nonzero. To evaluate the electron aberration in an arbitrary z-plane, we have to compensate for the contribution from this nonzero path deviation. Repeating the discussion above Eq. (2.105), we find a transformation of the second-rank path deviation, which is evaluated at a reduced time to one evaluated in a z-plane as follows:

$$\hat{w}^{(2)}(z) = w^{(2)} - w^{(1)}(z)h^{(1)}(z) = w^{(2)} - \frac{\dot{\zeta}_o}{2\dot{\zeta}}\dot{w}^{(1)}h_\alpha. \quad (4.36)$$

Using Eqs. (4.33), (4.34), and (4.36), we find the second-rank path deviation, evaluated in an arbitrary plane z:

$$\begin{aligned} \hat{w}^{(2)}(\tau) &= \left(w_\gamma(\tau) + 2i\dot{\chi}_o w_\alpha(\tau) \right) \int_{\tau_o}^{\tau} \left\{ P_1^{(2)}\bar{w}_\alpha + P_2^{(2)}\dot{\bar{w}}_\alpha \right\} d\tau \\ &\quad - w_\alpha(\tau) \int_{\tau_o}^{\tau} \left\{ P_1^{(2)}\bar{w}_\gamma + P_2^{(2)}\dot{\bar{w}}_\gamma \right\} d\tau - P_{2o}^{(2)}w_\alpha - \frac{\dot{\zeta}_o}{2\dot{\zeta}}\dot{w}^{(1)}h_\alpha, \end{aligned} \quad (4.37)$$

where

$$\begin{aligned} P_1^{(2)}\bar{w}_H + P_2^{(2)}\dot{\bar{w}}_H &= \frac{\Phi^{[3]}}{4\Phi_C}\bar{w}_H w^{(1)}h^{(1)} + \frac{i\eta B'}{2\sqrt{\Phi_C}}(w^{(1)}\dot{\bar{w}}_H - \dot{w}^{(1)}\bar{w}_H)h^{(1)} \\ &\quad - \frac{1}{2\Phi_C}\bar{w}_H V F_1' h^{(1)} + \frac{\eta}{\sqrt{\Phi_C}}\dot{\bar{w}}_H I D_1 h^{(1)}, \\ P_{2o}^{(2)} &= 0. \end{aligned} \quad (4.38)$$

In order to simplify the path deviation, we introduce following abbreviations:

$$\begin{aligned} P_K[K, \bar{H}; \tau] &= \int_{\tau_o}^{\tau} \left[\frac{\Phi^{[3]}}{8\Phi_C} w_K \bar{w}_H + \frac{i\eta B'}{4\sqrt{\Phi_C}}(w_K \dot{\bar{w}}_H - \dot{w}_K \bar{w}_H) - \delta_{K,e} \frac{F_1'}{4\Phi_C} + \delta_{K,m} \frac{\eta D_1}{2\sqrt{\Phi_C}} \dot{\bar{w}}_H \right] h_\alpha d\tau, \\ Q_K[K] &= -\frac{1}{2\dot{\zeta}}\dot{w}_K h_\alpha, \end{aligned} \quad (4.39)$$

where K of w_K and \dot{w}_K is either α, γ, e , or m , and H of \bar{w}_H is either α or γ . $\delta_{K,L}$ is Kronecker's delta, which returns 1 when $K = L$, otherwise it returns zero. Using these abbreviations, the second-rank lateral path deviation is expressed by

$$\hat{w}^{(2)} = [w_o' \hat{w}_{\alpha\kappa} + w_o \hat{w}_{\gamma\kappa} + V \hat{w}_{e\kappa} + I \hat{w}_{m\kappa}] \kappa_o, \quad (4.40)$$

where the path-deviation of the axial chromatic aberration type is

$$\hat{w}_{\alpha\kappa}(z) = \dot{\zeta}_o^2 \left[(w_\gamma + 2i\dot{\chi}_o w_\alpha) P_\kappa[\alpha, \bar{\alpha}; \tau] - w_\alpha P_\kappa[\alpha, \bar{\gamma}; \tau] + Q_\kappa[\alpha] \right], \quad (4.41)$$

the path-deviation of the off-axis chromatic aberration type is

$$\hat{w}_{\gamma\kappa}(z) = \dot{\zeta}_o \left[(w_\gamma + 2i\dot{\chi}_o w_\alpha) P_\kappa[\gamma, \bar{\alpha}; \tau] - w_\alpha P_\kappa[\gamma, \bar{\gamma}; \tau] + Q_\kappa[\gamma] \right], \quad (4.42)$$

the path-deviation of the electrostatic deflection chromatic aberration type is

$$\hat{w}_{e\kappa}(z) = \dot{\zeta}_o \left[(w_\gamma + 2i\dot{\chi}_o w_\alpha) P_\kappa[e, \bar{\alpha}; \tau] - w_\alpha P_\kappa[e, \bar{\gamma}; \tau] + Q_\kappa[e] \right], \quad (4.43)$$

and the path-deviation of the magnetic deflection chromatic aberration type is

$$\hat{w}_{m\kappa}(z) = \dot{\zeta}_o \left[(w_\gamma + 2i\dot{\chi}_o w_\alpha) P_\kappa[m, \bar{\alpha}; \tau] - w_\alpha P_\kappa[m, \bar{\gamma}; \tau] + Q_\kappa[m] \right]. \quad (4.44)$$

The values of lateral path deviation in the image plane correspond to aberrations. Chromatic aberration coefficients parameterized by the quantities in the object plane and the complex voltage and current of deflectors are obtained when z_i and τ_i are substituted into Eqs. (4.41) to (4.44). Since $w_{ai} = 0$, the second integrals of Eqs. (4.41) to (4.44) vanish when we consider aberration coefficients. The chromatic aberration formulae is given by

$$\hat{w}_i^{(2)} = w_{\gamma i} [C_{\alpha\kappa o} w'_o + C_{\gamma\kappa o} w_o + C_{V\kappa o} V + C_{I\kappa o} I] \kappa_o, \quad (4.45)$$

where $C_{\alpha\kappa o}, C_{\gamma\kappa o}, C_{V\kappa o}, C_{I\kappa o}$ are the axial, the off-axis, the electrostatic deflection, and the magnetic deflection chromatic aberration coefficients defined in the object plane, respectively. We find their concrete expressions as follows:

$$\begin{aligned} C_{\alpha\kappa o} &= \dot{\zeta}_o^2 P_\kappa[\alpha, \bar{\alpha}; \tau_i] + \frac{\dot{\zeta}_o^2}{w_{\gamma i}} Q_{\kappa i}[\alpha], \\ C_{\gamma\kappa o} &= \dot{\zeta}_o P_\kappa[\gamma, \bar{\alpha}; \tau_i] + \frac{\dot{\zeta}_o}{w_{\gamma i}} Q_{\kappa i}[\gamma], \\ C_{V\kappa o} &= \dot{\zeta}_o P_\kappa[e, \bar{\alpha}; \tau_i] + \frac{\dot{\zeta}_o}{w_{\gamma i}} Q_{\kappa i}[e], \\ C_{I\kappa o} &= \dot{\zeta}_o P_\kappa[m, \bar{\alpha}; \tau_i] + \frac{\dot{\zeta}_o}{w_{\gamma i}} Q_{\kappa i}[m]. \end{aligned} \quad (4.46)$$

4.6 Second order geometrical longitudinal path deviation of time-dependent deflection theory

To consider third-order geometrical aberration, we need to know the concrete formulae of second-order geometrical longitudinal path deviation. Here, we think about it. By Eq. (4.10), the second order geometrical longitudinal perturbation term is obtained as follows:

$$\begin{aligned} P_h^{(2)}{}_{\text{geo.}} &= -\frac{\Phi^{[3]}}{8\Phi_C} w^{(1)} \bar{w}^{(1)} - \frac{i\eta B'}{4\sqrt{\Phi_C}} (w^{(1)} \dot{\bar{w}}^{(1)} - \bar{w}^{(1)} \dot{w}^{(1)}) \\ &+ \frac{F'_1}{4\Phi_C} V \bar{w}^{(1)} + \frac{\bar{F}'_1}{4\Phi_C} \bar{V} w^{(1)} - \frac{\eta}{2\sqrt{\Phi_C}} (ID_1 \dot{\bar{w}}^{(1)} + I\bar{D}_1 \dot{w}^{(1)}). \end{aligned} \quad (4.47)$$

Using Eq. (2.157) and Eqs. (4.28) and (4.29), the second-order geometrical longitudinal path deviation is

$$\begin{aligned} h^{(2)}{}_{\text{geo.}}(\tau) &= h_p^{(2)}{}_{\text{geo.}}(\tau) - h_\gamma(\tau) \int_{\tau_o}^\tau P_h^{(2)}{}_{\text{geo.}}(\tau) h_\alpha(\tau) d\tau \\ &+ h_\alpha(\tau) \int_{\tau_o}^\tau P_h^{(2)}{}_{\text{geo.}}(\tau) h_\gamma(\tau) d\tau, \end{aligned} \quad (4.48)$$

where

$$h_p^{(2)}{}_{\text{geo.}}(\tau) = \left[-\frac{1}{2\dot{\zeta}_o} \dot{w}_o \ddot{w}_o - \frac{\Phi_o''}{8\dot{\zeta}_o \Phi_C} w_o \ddot{w}_o + \frac{F_{1o}}{4\dot{\zeta}_o \Phi_C} V \bar{w}_o + \frac{\bar{F}_{1o}}{4\dot{\zeta}_o \Phi_C} \bar{V} w_o \right] h_\alpha. \quad (4.49)$$

When we consider the deflection aberrations, we have three choices of double deflector, as discussed in Chapter 3. The first case is where one deflector is an electrostatic deflector, and the other is a magnetic deflector. The second

case is where both deflectors are electrostatic deflectors. The third case is where both deflectors are magnetic deflectors. For simplicity of calculation, we consider a first order geometrical lateral trajectory as

$$w^{(1)} = \dot{w}_o w_\alpha + w_o w_\gamma + S_A w_A + S_B w_B, \quad (4.50)$$

where S_A and S_B represent complex deflector signals, which take either the complex voltage or current of deflectors and w_A and w_B are the corresponding deflection trajectories, given in Eq. (4.22). For the first case, signals S_A and S_B are V and I , and deflection trajectories w_A and w_B are w_e and w_m , respectively. For the second case, signals S_A and S_B are V_A and V_B , which are the complex voltages of electrostatic deflector A and B, and deflection trajectories w_A and w_B are w_e^A and w_e^B , which are the electrostatic deflection trajectories of electrostatic deflector A and B, respectively. In this case, VF_1 must be divided into $S_A F_1^A + S_B F_1^B$, where F_1^A and F_1^B are the electrostatic field components for deflector A and B.

For the third case, signals S_A and S_B are I_A and I_B , which are the complex currents of magnetic deflector A and B, and deflection trajectories w_A and w_B are w_m^A and w_m^B , which are the magnetic deflection trajectories of magnetic deflector A and B, respectively. ID_1 must be divided into $S_A D_1^A + S_B D_1^B$, where D_1^A and D_1^B are the magnetic field component for deflector A and B. To express the path deviation for the three cases in a single way, we use S_A, S_B, w_A , and w_B for deflection signals and deflection trajectories. The setting of deflection signal parameter S_A, S_B and deflection trajectories w_A, w_B for each case are listed in Table 4.1.

Table 4.1 Setting of deflection signal parameter S_A, S_B and deflection trajectories w_A, w_B , for three cases of types of two deflectors.

Case (i) is composed of an electrostatic deflector and a magnetic deflector. Case (ii) is composed of two electrostatic deflectors. Case (iii) is composed of two magnetic deflectors.

Case	S_A	S_B	w_A	w_B
(i)	V	I	w_e	w_m
(ii)	V_A	V_B	w_e^A	w_e^B
(iii)	I_A	I_B	w_m^A	w_m^B

We find the parameter dependence of the second-order geometrical longitudinal path deviation:

$$\begin{aligned} h_{\text{geo}}^{(2)} = & \dot{w}_o \dot{\bar{w}}_o h_{\alpha\bar{\alpha}} + \dot{w}_o \bar{w}_o h_{\alpha\bar{\gamma}} + \dot{w}_o \bar{S}_A h_{\alpha\bar{A}} + \dot{w}_o \bar{S}_B h_{\alpha\bar{B}} \\ & + \dot{\bar{w}}_o w_o h_{\bar{\alpha}\gamma} + \dot{\bar{w}}_o S_A h_{\bar{\alpha}A} + \dot{\bar{w}}_o S_B h_{\bar{\alpha}B} \\ & + w_o \bar{w}_o h_{\gamma\bar{\gamma}} + w_o \bar{S}_A h_{\gamma\bar{A}} + w_o \bar{S}_B h_{\gamma\bar{B}} + \bar{w}_o S_A h_{\bar{\gamma}A} + \bar{w}_o S_B h_{\bar{\gamma}B} \\ & + S_A \bar{S}_A h_{A\bar{A}} + S_A \bar{S}_B h_{A\bar{B}} + \bar{S}_A S_B h_{\bar{A}B} + \bar{S}_B S_B h_{\bar{B}B}, \end{aligned} \quad (4.51)$$

where

$$\begin{aligned} h_{KL} = h_{LK} = & T_o[K, L] h_\alpha(\tau) - h_\gamma(\tau) \int_{\tau_o}^{\tau} \left\{ S_{RL}[K, L] + S_{DEF}^{(s)}[K, L] \right\} h_\alpha d\tau \\ & + h_\alpha(\tau) \int_{\tau_o}^{\tau} \left\{ S_{RL}[K, \bar{L}] + S_{DEF}^{(s)}[K, \bar{L}] \right\} h_\gamma d\tau. \end{aligned} \quad (4.52)$$

where subscripts K and L are one of α, γ, A , and B . The expression of h_{KL} means the same path deviation as h_{LK} . The integrand of Eq. (4.52) is divided into two parts. $S_{RL}[K, \bar{L}]$ is the contribution from the round symmetric lens fields. $S_{DEF}^{(s)}[K, \bar{L}]$ is the contribution from the deflection fields, and the superscript s indicates the type of deflector combination in each case. $T_o[K, \bar{L}]$ is the constant term of the longitudinal path deviation, which stems from the partial integral. The integrand component of the round symmetric fields is given by

$$S_{RL}[K, \bar{L}] = -\frac{\Phi^{[3]}}{8\Phi_C} w_K \bar{w}_L - \frac{i\eta B'}{4\sqrt{\Phi_C}} (w_K \bar{w}_L - \dot{w}_K \bar{w}_L), \quad (4.53)$$

where K and L are one of α, γ, A , and B . We find the complex conjugate:

$$\bar{S}_{RL}[K, \bar{L}] = S_{RL}[L, \bar{K}]. \quad (4.54)$$

The arguments of the integrand of the deflection fields, must include, at least, either A or B . For the first case, the nonzero components are:

$$\begin{aligned} S_{DEF}^{(i)}[N, \bar{A}] &= \frac{F_1'^A}{4\Phi_C} w_N, \\ S_{DEF}^{(i)}[N, \bar{B}] &= -\frac{\eta \bar{D}_1^B}{2\sqrt{\Phi_C}} \dot{w}_N, \\ S_{DEF}^{(i)}[A, \bar{A}] &= \frac{F_1'^A}{4\Phi_C} \bar{w}_A + \frac{\bar{F}_1'^A}{4\Phi_C} w_A, \\ S_{DEF}^{(i)}[B, \bar{B}] &= -\frac{\eta D_1^B}{2\sqrt{\Phi_C}} \bar{w}_B - \frac{\eta \bar{D}_1^B}{2\sqrt{\Phi_C}} \dot{w}_B, \\ S_{DEF}^{(i)}[A, \bar{B}] &= \frac{F_1'^A}{4\Phi_C} \bar{w}_B - \frac{\eta \bar{D}_1^B}{2\sqrt{\Phi_C}} \dot{w}_A, \end{aligned} \quad (4.55)$$

where N of w_N is either α or γ , and their complex conjugates are nonzero, if $K \neq L$. Of course, for the first case, since there is a single electrostatic deflector and a single magnetic deflector, the superscripts A and B in deflection dipole fields F_1 and D_1 are meaningless, in practice. However, they are still useful for writing integrands of the first, second and third cases in a unified way. For the second and third cases, new terms are only for the mixture of deflectors A and B :

$$\begin{aligned} S_{DEF}^{(ii)}[A, \bar{B}] &= \frac{F_1'^A}{4\Phi_C} \bar{w}_B + \frac{\bar{F}_1'^B}{4\Phi_C} w_A, \\ S_{DEF}^{(iii)}[A, \bar{B}] &= -\frac{\eta D_1^A}{2\sqrt{\Phi_C}} \dot{w}_B - \frac{\eta \bar{D}_1^B}{2\sqrt{\Phi_C}} \dot{w}_A, \end{aligned} \quad (4.56)$$

and their complex conjugates. Note that, for the integrands of deflection, we find:

$$S_{DEF}^{(s)}[K, \bar{L}] = \bar{S}_{DEF}^{(s)}[L, \bar{K}]. \quad (4.57)$$

The final terms are the constant $T_o[L, \bar{K}]$. The nonzero terms are following four terms:

$$\begin{aligned} T_o[\alpha, \bar{\alpha}] &= -\frac{1}{2\zeta_o}, & T_o[\gamma, \bar{\gamma}] &= -\frac{\Phi_o''}{8\zeta_o\Phi_C}, \\ T_o[\gamma, \bar{A}] &= \frac{\bar{F}_{1o}^A}{4\zeta_o\Phi_C}, & T_o[A, \bar{\gamma}] &= \bar{T}_o[\gamma, \bar{A}], \end{aligned} \quad (4.58)$$

$T_o[\gamma, \bar{A}]$ and $T_o[A, \bar{\gamma}]$ are caused by electrostatic deflectors. By Eqs. (4.52), (4.54), (4.57), and (4.58), we find the relation that $h_{KL} = h_{LK} = \bar{h}_{LK} = \bar{h}_{KL}$.

4.7 Third order geometrical lateral path deviation and geometrical aberration coefficients of time-dependent deflection theory

In time-dependent theory, as we discussed in section 2.3.1, third-order geometrical path deviation results from secondary perturbation. Since the first-order solution of longitudinal path deviation, $h^{(1)}$, is a first-degree solution and the lateral path deviation obtained by primary perturbation, $w^{(2)}$, is a first-order and first-degree solution, they have a chromatic parameter. At least for the third-order geometrical path deviation, solutions that contribute to the perturbation function are the first-order lateral trajectory $w^{(1)}$ and the second-order geometrical longitudinal path deviation $h_{\text{geo.}}^{(2)}$. According to the procedure of secondary perturbation for the geometrical path deviation, which is discussed in section 2.3.1, the lateral perturbation function is given by

$$\begin{aligned} P_w^{(3)}{}_{\text{geo.}} &= P_{w,\ell=3}[w^{(1)}, \bar{w}^{(1)}, \dot{w}^{(1)}, \dot{\bar{w}}^{(1)}, h = 0, \dot{h} = 0; \tau] \\ &+ \left(h_{\text{geo.}}^{(2)} \frac{\partial}{\partial h^{(1)}} + \dot{h}_{\text{geo.}}^{(2)} \frac{\partial}{\partial \dot{h}^{(1)}} \right) \\ &\times P_{w,\ell=2}[w^{(1)}, \bar{w}^{(1)}, \dot{w}^{(1)}, \dot{\bar{w}}^{(1)}, h^{(1)}, \dot{h}^{(1)}; \tau] \Big|_{h^{(1)}=0, \dot{h}^{(1)}=0}. \end{aligned} \quad (4.59)$$

We find the concrete expression of the third-order geometrical perturbation function:

$$\begin{aligned} P_w^{(3)}{}_{\text{geo.}} &= -\frac{\Phi^{[3]}}{4\Phi_C} w^{(1)} h_{\text{geo.}}^{(2)} + \frac{\Phi^{[4]}}{32\Phi_C} w^{(1)^2} \bar{w}^{(1)} \\ &+ \frac{i\eta}{\sqrt{\Phi_C}} \left[\frac{d}{d\tau} \left(\frac{1}{2} B' w^{(1)} h_{\text{geo.}}^{(2)} - \frac{1}{16} B'' w^{(1)^2} \bar{w}^{(1)} \right) \right. \\ &\left. + \frac{1}{2} B' \dot{w}^{(1)} h_{\text{geo.}}^{(2)} - \frac{1}{16} B'' \left(2w^{(1)} \bar{w}^{(1)} \dot{w}^{(1)} - w^{(1)^2} \dot{\bar{w}}^{(1)} \right) \right] \\ &+ \frac{F_1'}{2\Phi_C} V h_{\text{geo.}}^{(2)} - \frac{\bar{F}_1'}{16\Phi_C} \bar{V} w^{(1)^2} - \frac{F_1''}{8\Phi_C} V w^{(1)} \bar{w}^{(1)} + \frac{3F_3}{2\Phi_C} \bar{V} \bar{w}^{(1)^2} \\ &+ \frac{\eta}{\sqrt{\Phi_C}} \left[\frac{d}{d\tau} \left(ID_1 h_{\text{geo.}}^{(2)} - \frac{1}{4} ID_1' w^{(1)} \bar{w}^{(1)} + \frac{1}{8} ID_1' w^{(1)^2} \right) \right. \\ &\left. + \frac{1}{4} ID_1' (w^{(1)} \dot{\bar{w}}^{(1)} - \bar{w}^{(1)} \dot{w}^{(1)}) + \frac{1}{4} ID_1' w^{(1)} \dot{w}^{(1)} - 3ID_3 \bar{w}^{(1)^2} \right]. \end{aligned} \quad (4.60)$$

The reduced velocity of the longitudinal second order geometrical path deviation $\dot{h}_{\text{geo.}}^{(2)}$ does not appear in (4.60), directly. Since it only contributes via terms of total derivative form with respect to reduced time, we can eliminate it by partial integrals. This is the why we do not need to know the concrete form of $\dot{h}_{\text{geo.}}^{(2)}$. We find the path deviation by using Eq. (4.31) in the case where the lateral perturbation function is given by Eq. (4.60).

$$\begin{aligned} w_{\text{geo.}}^{(3)}(\tau) &= -\left(w_\gamma(\tau) + 2i\dot{\chi}_o w_\alpha(\tau) \right) \int_{\tau_o}^{\tau} P_w^{(3)}{}_{\text{geo.}}(\tau) \bar{w}_\alpha(\tau) d\tau \\ &+ w_\alpha(\tau) \int_{\tau_o}^{\tau} P_w^{(3)}{}_{\text{geo.}}(\tau) \bar{w}_\gamma(\tau) d\tau. \end{aligned} \quad (4.61)$$

Even for third-order geometrical path deviation, Eqs. (4.32) and (4.33) can be used for partial integral. In this case, we find:

$$\begin{aligned}
P_1^{(3)} = & \frac{\Phi^{[3]}}{4\Phi_C} w^{(1)} h_{\text{geo.}}^{(2)} - \frac{\Phi^{[4]}}{32\Phi_C} w^{(1)^2} \bar{w}^{(1)} \\
& - \frac{i\eta B'}{2\sqrt{\Phi_C}} \dot{w}^{(1)} h_{\text{geo.}}^{(2)} + \frac{i\eta B''}{16\sqrt{\Phi_C}} \left(2w^{(1)} \bar{w}^{(1)} \dot{w}^{(1)} - w^{(1)^2} \dot{\bar{w}}^{(1)} \right) \Big] \\
& - \frac{F_1'}{2\Phi_C} V h_{\text{geo.}}^{(2)} + \frac{\bar{F}_1'}{16\Phi_C} \bar{V} w^{(1)^2} + \frac{F_1''}{8\Phi_C} V w^{(1)} \bar{w}^{(1)} - \frac{3F_3}{2\Phi_C} \bar{V} \bar{w}^{(1)^2} \\
& - \frac{\eta}{\sqrt{\Phi_C}} \left[\frac{1}{4} ID_1' (w^{(1)} \dot{\bar{w}}^{(1)} - \bar{w}^{(1)} \dot{w}^{(1)}) + \frac{1}{4} I\bar{D}_1' w^{(1)} \dot{w}^{(1)} - 3ID_3 \zeta \bar{w}^{(1)^2} \right], \tag{4.62}
\end{aligned}$$

$$\begin{aligned}
P_2^{(3)} = & \frac{i\eta}{\sqrt{\Phi_C}} \left(\frac{1}{2} B' w^{(1)} h_{\text{geo.}}^{(2)} - \frac{1}{16} B'' w^{(1)^2} \bar{w}^{(1)} \right) \\
& + \frac{\eta}{\sqrt{\Phi_C}} \left(ID_1 h_{\text{geo.}}^{(2)} - \frac{1}{4} ID_1' w^{(1)} \bar{w}^{(1)} + \frac{1}{8} I\bar{D}_1' w^{(1)^2} \right).
\end{aligned}$$

We consider the partial integral:

$$-\int_{\tau_o}^{\tau} P_{\text{w geo.}}^{(3)}(\tau) \bar{w}_H(\tau) d\tau = \int_{\tau_o}^{\tau} P_C^{(3)}(\tau) d\tau - P_2^{(3)} \bar{w}_H + P_{2o}^{(3)} \bar{w}_{Ho}, \tag{4.63}$$

where

$$P_C^H = P_1^{(3)} \bar{w}_H + P_2^{(3)} \dot{\bar{w}}_H = P_{CL}^H + P_{CEDEF}^H + P_{CBDEF}^H. \tag{4.64}$$

We divide an integrand P_C^H into three parts for convenience of calculation. The first part is the lens-field part:

$$\begin{aligned}
P_{CL}^H = & \left(\frac{\Phi^{[3]}}{4\Phi_C} \bar{w}_H + \frac{i\eta B'}{2\sqrt{\Phi_C}} \dot{\bar{w}}_H \right) w^{(1)} h_{\text{geo.}}^{(2)} - \frac{i\eta B'}{2\sqrt{\Phi_C}} \bar{w}_H \dot{w}^{(1)} h_{\text{geo.}}^{(2)} \\
& - \left(\frac{\Phi^{[4]}}{32\Phi_C} \bar{w}_H + \frac{i\eta B''}{16\sqrt{\Phi_C}} \right) w^{(1)^2} \bar{w}^{(1)} + \frac{i\eta B''}{16\sqrt{\Phi_C}} \bar{w}_H \left(2w^{(1)} \bar{w}^{(1)} \dot{w}^{(1)} - w^{(1)^2} \dot{\bar{w}}^{(1)} \right). \tag{4.65}
\end{aligned}$$

The second and third parts are the electrostatic and magnetic deflection field part, respectively:

$$P_{CEDEF}^H = -\frac{F_1'}{2\Phi_C} V \bar{w}_H h_{\text{geo.}}^{(2)} + \frac{\bar{F}_1'}{16\Phi_C} \bar{V} \bar{w}_H w^{(1)^2} + \frac{F_1''}{8\Phi_C} V \bar{w}_H w^{(1)} \bar{w}^{(1)} - \frac{3F_3}{2\Phi_C} \bar{V} \bar{w}_H \bar{w}^{(1)^2}, \tag{4.66}$$

and

$$\begin{aligned}
P_{CBDEF}^H = & -\frac{\eta}{\sqrt{\Phi_C}} \left[\frac{1}{4} ID_1' \bar{w}_H (w^{(1)} \dot{\bar{w}}^{(1)} - \bar{w}^{(1)} \dot{w}^{(1)}) + \frac{1}{4} I\bar{D}_1' \bar{w}_H w^{(1)} \dot{w}^{(1)} - 3ID_3 \zeta \bar{w}_H \bar{w}^{(1)^2} \right] \\
& + \frac{\eta}{\sqrt{\Phi_C}} \left(ID_1 \dot{\bar{w}}_H h_{\text{geo.}}^{(2)} - \frac{1}{4} ID_1' \dot{\bar{w}}_H w^{(1)} \bar{w}^{(1)} + \frac{1}{8} I\bar{D}_1' \dot{\bar{w}}_H w^{(1)^2} \right). \tag{4.67}
\end{aligned}$$

Similar to the integrand, the boundary term of Eq. (4.63) is also divided into the lens field part and the magnetic deflection field part:

$$-P_2^{(3)} \bar{w}_H = P_{2L}^H + P_{2BDEF}^H. \tag{4.68}$$

For simplicity of calculation, it is advantageous to introduce abbreviations for the coefficients of each term as follows.

The lens-field term of the integrand:

$$P_{CL}^H = A_1^H w^{(1)} h_{\text{geo.}}^{(2)} + A_2^H \dot{w}^{(1)} h_{\text{geo.}}^{(2)} + A_3^H w^{(1)^2} \bar{w}^{(1)} + A_4^H w^{(1)} \bar{w}^{(1)} \dot{w}^{(1)} + A_5^H w^{(1)^2} \dot{\bar{w}}^{(1)}, \tag{4.69}$$

where

$$\begin{aligned}
A_1^H = & \left(\frac{\Phi^{[3]}}{4\Phi_C} \bar{w}_H + \frac{i\eta B'}{2\sqrt{\Phi_C}} \dot{\bar{w}}_H \right), & A_2^H = & -\frac{i\eta B'}{2\sqrt{\Phi_C}} \bar{w}_H, \\
A_3^H = & -\frac{\Phi^{[4]}}{32\Phi_C} \bar{w}_H - \frac{i\eta B''}{16\sqrt{\Phi_C}} \dot{\bar{w}}_H, & A_4^H = & \frac{i\eta B''}{8\sqrt{\Phi_C}} \bar{w}_H, \\
A_5^H = & -\frac{i\eta B''}{16\sqrt{\Phi_C}} \bar{w}_H = -\frac{1}{2} A_4^H.
\end{aligned} \tag{4.70}$$

The electrostatic deflection field term of the integrand:

$$P_{CEDEF}^H = E_1^H V F_1' h_{\text{geo.}}^{(2)} + E_2^H \bar{V} \bar{F}_1'' w^{(1)2} + E_3^H V F_1'' w^{(1)} \bar{w}^{(1)} + E_4^H \bar{V} F_3 \bar{w}^{(1)2}, \quad (4.71)$$

where

$$\begin{aligned} E_1^H &= -\frac{1}{2\Phi_C} \bar{w}_H, & E_2^H &= \frac{1}{16\Phi_C} \bar{w}_H, \\ E_3^H &= \frac{1}{8\Phi_C} \bar{w}_H, & E_4^H &= -\frac{3}{2\Phi_C} \bar{w}_H. \end{aligned} \quad (4.72)$$

The magnetic deflection field term in the integrand:

$$\begin{aligned} P_{CBDEF}^H &= G_1^H I D_1' (w^{(1)} \dot{\bar{w}}^{(1)} - \bar{w}^{(1)} \dot{w}^{(1)}) + G_2^H \bar{I} \bar{D}_1' w^{(1)} \dot{w}^{(1)} \\ &+ G_3^H \bar{I} D_3 \bar{w}^{(1)2} + G_4^H I D_1 h_{\text{geo.}}^{(2)} \\ &+ G_5^H I D_1' w^{(1)} \bar{w}^{(1)} + G_6^H \bar{I} \bar{D}_1' w^{(1)2}, \end{aligned} \quad (4.73)$$

where

$$\begin{aligned} G_1^H &= -\frac{\eta}{4\sqrt{\Phi_C}} \bar{w}_H, & G_2^H &= G_1^H, & G_3^H &= \frac{3\eta}{4\sqrt{\Phi_C}} \zeta \bar{w}_H, \\ G_4^H &= \frac{\eta}{\sqrt{\Phi_C}} \dot{\bar{w}}_H, & G_5^H &= \frac{1}{4} G_3^H, & G_6^H &= -\frac{1}{8} G_3^H. \end{aligned} \quad (4.74)$$

The boundary term:

$$\begin{aligned} P_{2L}^H &= P^H w^{(1)} h_{\text{geo.}}^{(2)} + R^H w^{(1)2} \bar{w}^{(1)}, \\ P_{2BDEF}^H &= Q_1^H I D_1 h_{\text{geo.}}^{(2)} + Q_2^H I D_1' w^{(1)} \bar{w}^{(1)} + Q_3^H \bar{I} \bar{D}_1' w^{(1)2}, \end{aligned} \quad (4.75)$$

where

$$\begin{aligned} P^H &= -\frac{i\eta}{2\sqrt{\Phi_C}} B' \bar{w}_H, & R^H &= \frac{i\eta}{16\sqrt{\Phi_C}} B'' \bar{w}_H, \\ Q_1^H &= -\frac{\eta}{\sqrt{\Phi_C}} \bar{w}_H, & Q_2^H &= \frac{\eta}{4\sqrt{\Phi_C}} \bar{w}_H, & Q_3^H &= -\frac{1}{2} Q_2^H. \end{aligned} \quad (4.76)$$

Since at the initial time, τ_o , $w^{(1)}(\tau_o) = w_o$ and $h_{\text{geo.}}^{(2)}(\tau_o) = 0$, we obtain

$$P_{2o}^{(3)} \bar{w}_{Ho} = -R_o^H w_o^2 \bar{w}_o - Q_{2o}^H I D_{1o}' w_o \bar{w}_o - Q_{3o}^H \bar{I} \bar{D}_{1o}' w_o^2. \quad (4.77)$$

However, employing Eq. (4.34), the surviving boundary term after the partial integral of Eq. (4.61) is

$$-P_{2o}^{(3)} \bar{w}_{\gamma o} w_\alpha = (R_o^\gamma w_o^2 \bar{w}_o + Q_{2o}^\gamma I D_{1o}' w_o \bar{w}_o + Q_{3o}^\gamma \bar{I} \bar{D}_{1o}' w_o^2) w_\alpha. \quad (4.78)$$

In addition, by discussion in section 3.2 and Eq. (2.106), transformation of the third-order geometrical lateral path deviation from which is defined at time, to which is evaluated in a z-plane, is given by

$$\begin{aligned} \hat{w}_{\text{geo.}}^{(3)}(z) &= w_{\text{geo.}}^{(3)}(z) - w'^{(1)}(z) h_{\text{geo.}}^{(2)}(z) \\ &= w_{\text{geo.}}^{(3)}(z) - \frac{1}{\zeta} \dot{w}^{(1)}(z) h_{\text{geo.}}^{(2)}(z), \end{aligned} \quad (4.79)$$

where the position of the z-coordinate is given by the reference electron trajectory, that is,

$$z = \zeta(\tau). \quad (4.80)$$

4.7.1 Expressions of third-order geometrical lateral path deviation

Here, we consider the path-deviation of a two-deflector system. To consider the parameter expansion of the path deviation, Eqs. (4.50) and (4.51) are used for $w^{(1)}$ and $h_{\text{geo}}^{(2)}$. To obtain a unified expression for combinations of different two-deflector types, it is still useful to use deflection signals S_A and S_B , instead of the voltage and current of deflectors. The types of the two deflectors, the signal parameters, and the deflection trajectories for three cases are listed in Table 4.1. According to Eqs. (4.50) and (4.51), the path deviation is classified by the geometrical parameters, and we find:

$$\hat{w}_{\text{geo}}^{(3)}(z) = \sum \hat{w}_{KL\bar{M}}(z) P_K P_L \bar{P}_M + \sum \hat{w}_{\bar{a}\bar{b}\bar{c}}(z) \bar{P}_a \bar{P}_b \bar{P}_c, \quad (4.81)$$

where $\hat{w}_{KL\bar{M}}(z)$ is the path deviation of the normal type, which depends on the geometrical parameter $P_K P_L \bar{P}_M$, and $\hat{w}_{\bar{a}\bar{b}\bar{c}}(z)$ is the path deviation of the four-fold type, which depends on the parameter $\bar{P}_a \bar{P}_b \bar{P}_c$. The geometrical parameters $P_K, P_L, P_M, P_a, P_b, P_c$ take one of w'_o, w_o, S_A , and S_B .

In Table 4.2 and Table 4.3, Lists of normal type and four-fold type path deviations are given, respectively. We classify aberration type as follows. The path deviation, which is only depends on w'_o and its complex conjugate, is called the axial type. The path deviations, which are dependent on w'_o and w_o and their complex conjugates, are the off-axis (OA.) type. The path deviations, which are dependent on w'_o and the deflection signals and their complex conjugates or on only the deflection signals and their complex conjugate, are the deflection (Def.). The path deviations, which are dependent on w'_o, w_o and the deflection signals and their complex conjugates, are the off-axis deflection (OA.-Def.). In addition, if the parameters include two different deflection signals, the corresponding type is called the hybrid type, which is written as the OA-Def. hybrid, or the Def. hybrid. The possible concrete dependence of the parameters and the setting of K, L, M , and a, b, c are also listed in in Table 4.2 and Table 4.3.

According to Table 4.1 – Table 4.3, we find all possible type of path deviation. In general, the normal type of path deviation and the four-fold type path deviation are expressed in a unified way:

$$\begin{aligned} \hat{w}_{KL\bar{M}}(z) = & \left(w_\gamma(\tau) + 2i\dot{\chi}_o w_\alpha(\tau) \right) \{ U_{RL}[K, L, \bar{M}; \bar{w}_\alpha; \tau] + U_{DEF}^{(s)}[K, L, \bar{M}; \bar{w}_\alpha; \tau] \} \\ & - w_\alpha(\tau) \{ U_{RL}[K, L, \bar{M}; \bar{w}_\gamma; \tau] + U_{DEF}^{(s)}[K, L, \bar{M}; \bar{w}_\gamma; \tau] \} \\ & + S[K, L, \bar{M}] w_\alpha(\tau) - R[K, L, \bar{M}; \tau], \end{aligned} \quad (4.82)$$

and

$$\hat{w}_{\bar{a}\bar{b}\bar{c}}(z) = \left(w_\gamma(\tau) + 2i\dot{\chi}_o w_\alpha(\tau) \right) U_{4F}^{(s)}[\bar{a}, \bar{b}, \bar{c}; \bar{w}_\alpha; \tau] - w_\alpha(\tau) U_{4F}^{(s)}[\bar{a}, \bar{b}, \bar{c}; \bar{w}_\gamma; \tau], \quad (4.83)$$

where $U_{RL}[K, L, \bar{M}; \bar{w}_H; \tau]$ is the round symmetric lens-field part, $U_{DEF}^{(s)}[K, L, \bar{M}; \bar{w}_H; \tau]$ is the deflection field part, and $U_{4F}^{(s)}[\bar{a}, \bar{b}, \bar{c}; \bar{w}_H; \tau]$ is the four-fold deflection field part. $S[K, L, \bar{M}]$ is the surviving boundary term from Eq. (4.78). $R[K, L, \bar{M}; \tau]$ is the compensation term of the transformation of path deviation from the time-defined one to the z -plane-defined one. The concrete expressions of these three parts are different for the type of the path deviation listed

in Table 4.2 and Table 4.3. Note that, only a few boundary terms $S[K, L, \bar{M}]$ survive, and we write the concrete form of them, when they are nonzero.

Table 4.2 List of normal type path deviation

Path deviation	Aberration Type	Relating deflectors	Dependence	K, L, \bar{M}
Spherical aberration	Axial	-	$w_o'^2 \bar{w}_o'$	$\alpha, \alpha, \bar{\alpha}$
Coma-length	Off-axis (OA.)	-	$w_o w_o' \bar{w}_o'$	$\alpha, \gamma, \bar{\alpha}$
	Deflection (Def.)	Deflector A	$S_A w_o' \bar{w}_o'$	$\alpha, A, \bar{\alpha}$
Coma-radius	Deflection	Deflector B	$S_B w_o' \bar{w}_o'$	$\alpha, B, \bar{\alpha}$
	Off-axis	-	$\bar{w}_o w_o'^2$	$\alpha, \alpha, \bar{\gamma}$
	Deflection	Deflector A	$\bar{S}_A w_o'^2$	α, α, \bar{A}
	Deflection	Deflector B	$\bar{S}_B w_o'^2$	α, α, \bar{B}
Field curvature	Off-axis	-	$w_o \bar{w}_o w_o'$	$\alpha, \gamma, \bar{\gamma}$
	OA.-Def.	Deflector A	$S_A \bar{w}_o w_o'$	$\alpha, A, \bar{\gamma}$
	OA.-Def.	Deflector A	$w_o \bar{S}_A w_o'$	α, γ, \bar{A}
	OA.-Def.	Deflector B	$S_B \bar{w}_o w_o'$	$\alpha, B, \bar{\gamma}$
	OA.-Def.	Deflector B	$w_o \bar{S}_B w_o'$	α, γ, \bar{B}
	Deflection	Deflector A	$S_A \bar{S}_A w_o'$	α, A, \bar{A}
	Deflection	Deflector B	$S_B \bar{S}_B w_o'$	α, B, \bar{B}
	Def. hybrid	Deflectors A, B	$S_A \bar{S}_B w_o'$	α, A, \bar{B}
	Def. hybrid	Deflectors A, B	$S_B \bar{S}_A w_o'$	α, B, \bar{A}
	Off-axis	-	$w_o^2 \bar{w}_o'$	$\gamma, \gamma, \bar{\alpha}$
Astigmatism	OA.-Def.	Deflector A	$w_o S_A \bar{w}_o'$	$\gamma, A, \bar{\alpha}$
	OA.-Def.	Deflector B	$w_o S_B \bar{w}_o'$	$\gamma, B, \bar{\alpha}$
	Deflection	Deflector A	$S_A^2 \bar{w}_o'$	$A, A, \bar{\alpha}$
	Deflection	Deflector B	$S_B^2 \bar{w}_o'$	$B, B, \bar{\alpha}$
	Def. hybrid	Deflectors A, B	$S_A S_B \bar{w}_o'$	$A, B, \bar{\alpha}$
	Off-axis	-	$w_o^2 \bar{w}_o$	$\gamma, \gamma, \bar{\gamma}$
Distortion	OA.-Def.	Deflector A	$w_o S_A \bar{w}_o$	$\gamma, A, \bar{\gamma}$
	OA.-Def.	Deflector A	$w_o^2 \bar{S}_A$	γ, γ, \bar{A}
	OA.-Def.	Deflector A	$w_o S_A \bar{S}_A$	γ, A, \bar{A}
	OA.-Def.	Deflector A	$S_A^2 \bar{w}_o$	$A, A, \bar{\gamma}$
	OA.-Def.	Deflector B	$w_o S_B \bar{w}_o$	$\gamma, B, \bar{\gamma}$
	OA.-Def.	Deflector B	$w_o^2 \bar{S}_B$	γ, γ, \bar{B}
	OA.-Def.	Deflector B	$w_o S_B \bar{S}_B$	γ, B, \bar{B}
	OA.-Def.	Deflector B	$S_B^2 \bar{w}_o$	$B, B, \bar{\gamma}$
	OA.-Def. hybrid	Deflectors A, B	$w_o S_A \bar{S}_B$	γ, A, \bar{B}
	OA.-Def. hybrid	Deflectors A, B	$w_o S_B \bar{S}_A$	γ, B, \bar{A}
	OA.-Def. hybrid	Deflectors A, B	$S_A S_B \bar{w}_o$	$A, B, \bar{\gamma}$
	Deflection	Deflector A	$S_A^2 \bar{S}_A$	A, A, \bar{A}
	Deflection	Deflector B	$S_B^2 \bar{S}_B$	B, B, \bar{B}
	Def. hybrid	Deflectors A, B	$S_A \bar{S}_A S_B$	A, B, \bar{A}
	Def. hybrid	Deflectors A, B	$S_A^2 \bar{S}_B$	A, A, \bar{B}
	Def. hybrid	Deflectors A, B	$S_A S_B \bar{S}_B$	A, B, \bar{B}
	Def. hybrid	Deflectors A, B	$S_B^2 \bar{S}_A$	B, B, \bar{A}

Table 4.3 List of four-fold type path deviation

Path deviation	Aberration Type	Relating deflectors	Dependence	K, L, \bar{M}
A2	Deflection	Deflector A	$\bar{w}_o'^2 \bar{S}_A$	$\bar{\alpha}, \bar{\alpha}, \bar{A}$
	Deflection	Deflector B	$\bar{w}_o'^2 \bar{S}_B$	$\bar{\alpha}, \bar{\alpha}, \bar{B}$
Astigmatism	OA.-Def.	Deflector A	$\bar{w}_o \bar{S}_A \bar{w}_o'$	$\bar{\alpha}, \bar{\gamma}, \bar{A}$
	OA.-Def.	Deflector B	$\bar{w}_o \bar{S}_B \bar{w}_o'$	$\bar{\alpha}, \bar{\gamma}, \bar{B}$
	Deflection	Deflector A	$\bar{S}_A^2 \bar{w}_o'$	$\bar{\alpha}, \bar{A}, \bar{A}$
	Deflection	Deflector B	$\bar{S}_B^2 \bar{w}_o'$	$\bar{\alpha}, \bar{B}, \bar{B}$
Distortion	Def. hybrid	Deflectors A, B	$\bar{S}_A \bar{S}_B \bar{w}_o'$	$\bar{\alpha}, \bar{A}, \bar{B}$
	OA.-Def.	Deflector A	$\bar{w}_o^2 \bar{S}_A$	$\bar{\gamma}, \bar{\gamma}, \bar{A}$
	OA.-Def.	Deflector B	$\bar{w}_o^2 \bar{S}_B$	$\bar{\gamma}, \bar{\gamma}, \bar{B}$
	OA.-Def.	Deflectors A	$\bar{w}_o \bar{S}_A^2$	$\bar{\gamma}, \bar{A}, \bar{A}$
	OA.-Def.	Deflectors B	$\bar{w}_o \bar{S}_B^2$	$\bar{\gamma}, \bar{B}, \bar{B}$
	OA.-Def. hybrid	Deflectors A, B	$\bar{w}_o \bar{S}_A \bar{S}_B$	$\bar{\gamma}, \bar{A}, \bar{B}$
	Deflection	Deflector A	\bar{S}_A^3	$\bar{A}, \bar{A}, \bar{A}$
	Deflection	Deflector B	\bar{S}_B^3	$\bar{B}, \bar{B}, \bar{B}$
	Def. hybrid	Deflectors A, B	$\bar{S}_A^2 \bar{S}_B$	$\bar{A}, \bar{A}, \bar{B}$
	Def. hybrid	Deflectors A, B	$\bar{S}_A \bar{S}_B^2$	$\bar{A}, \bar{B}, \bar{B}$

The expressions of the round symmetric lens-field part and the transformation term:

The spherical aberration type:

$$\begin{aligned}
 & U_{RL}[\alpha, \alpha, \bar{\alpha}; \bar{w}_H; \tau] \\
 &= \zeta_o^3 \left\{ \int_{\tau_o}^{\tau} [A_1^H w_\alpha h_{\alpha\bar{\alpha}} + A_2^H \dot{w}_\alpha h_{\alpha\bar{\alpha}} + A_3^H w_\alpha^2 \bar{w}_\alpha + A_4^H w_\alpha \bar{w}_\alpha \dot{w}_\alpha + A_5^H w_\alpha^2 \dot{\bar{w}}_\alpha] d\tau \right\}, \\
 & R[\alpha, \alpha, \bar{\alpha}; \tau] = \frac{\zeta_o^3}{\zeta} \dot{w}_\alpha h_{\alpha\bar{\alpha}}.
 \end{aligned} \tag{4.84}$$

The off-axis coma-length type:

$$\begin{aligned}
 & U_{RL}[\alpha, \gamma, \bar{\alpha}; \bar{w}_H; \tau] \\
 &= \zeta_o^2 \left\{ \int_{\tau_o}^{\tau} [A_1^H (w_\alpha h_{\alpha\bar{\gamma}} + w_\gamma h_{\alpha\bar{\alpha}}) + A_2^H (\dot{w}_\alpha h_{\alpha\bar{\gamma}} + \dot{w}_\gamma h_{\alpha\bar{\alpha}}) \right. \\
 & \quad \left. + 2A_3^H w_\alpha \bar{w}_\alpha w_\gamma + A_4^H \bar{w}_\alpha (\dot{w}_\alpha w_\gamma + w_\alpha \dot{w}_\gamma) + 2A_5^H w_\alpha \dot{\bar{w}}_\alpha w_\gamma] d\tau \right\}, \\
 & R[\alpha, \gamma, \bar{\alpha}; \tau] = \frac{\zeta_o^2}{\zeta} (\dot{w}_\alpha h_{\alpha\bar{\gamma}} + \dot{w}_\gamma h_{\alpha\bar{\alpha}}).
 \end{aligned} \tag{4.85}$$

The off-axis coma-radius type:

$$\begin{aligned}
 & U_{RL}[\alpha, \alpha, \bar{\gamma}; \bar{w}_H; \tau] \\
 &= \zeta_o^2 \left\{ \int_{\tau_o}^{\tau} [A_1^H w_\alpha h_{\alpha\bar{\gamma}} + A_2^H \dot{w}_\alpha h_{\alpha\bar{\gamma}} + A_3^H w_\alpha^2 \bar{w}_\gamma + A_4^H w_\alpha \dot{w}_\alpha \bar{w}_\gamma + A_5^H w_\alpha^2 \dot{\bar{w}}_\gamma] d\tau \right\}, \\
 & R[\alpha, \alpha, \bar{\gamma}; \tau] = \frac{\zeta_o^2}{\zeta} \dot{w}_\alpha h_{\alpha\bar{\gamma}}.
 \end{aligned} \tag{4.86}$$

The deflection coma-length type of deflector A:

$$\begin{aligned}
 & U_{RL}[\alpha, A, \bar{\alpha}; \bar{w}_H; \tau] \\
 &= \zeta_o^2 \left\{ \int_{\tau_o}^{\tau} [A_1^H (w_\alpha h_{\alpha\bar{A}} + w_A h_{\alpha\bar{\alpha}}) + A_2^H (\dot{w}_\alpha h_{\alpha\bar{A}} + \dot{w}_A h_{\alpha\bar{\alpha}}) \right. \\
 & \quad \left. + 2A_3^H w_\alpha \bar{w}_\alpha w_A + A_4^H \bar{w}_\alpha (\dot{w}_\alpha w_A + w_\alpha \dot{w}_A) + 2A_5^H w_\alpha \dot{\bar{w}}_\alpha w_A] d\tau \right\}, \\
 & R[\alpha, A, \bar{\alpha}; \tau] = \frac{\zeta_o^2}{\zeta} (\dot{w}_\alpha h_{\alpha\bar{A}} + \dot{w}_A h_{\alpha\bar{\alpha}}).
 \end{aligned} \tag{4.87}$$

The deflection coma-radius type of deflector A:

$$\begin{aligned}
 & U_{RL}[\alpha, \alpha, \bar{A}; \bar{w}_H; \tau] \\
 &= \dot{\zeta}_o^2 \left\{ \int_{\tau_o}^{\tau} [A_1^H w_\alpha h_{\alpha\bar{A}} + A_2^H \dot{w}_\alpha h_{\alpha\bar{A}} + A_3^H w_\alpha^2 \bar{w}_A + A_4^H w_\alpha \dot{w}_\alpha \bar{w}_A + A_5^H w_\alpha^2 \dot{\bar{w}}_A] d\tau \right\}, \\
 & R[\alpha, \alpha, \bar{A}; \tau] = \frac{\dot{\zeta}_o^2}{\dot{\zeta}} \dot{w}_\alpha h_{\alpha\bar{A}}.
 \end{aligned} \tag{4.88}$$

The deflection coma-length type and the coma-radius type of deflector B are obtained when A is replaced by B in Eq. (4.87) and \bar{A} is replaced by \bar{B} in Eq. (4.88), respectively.

The off-axis field curvature type:

$$\begin{aligned}
 & U_{RL}[\alpha, \gamma, \bar{\gamma}; \bar{w}_H; \tau] \\
 &= \dot{\zeta}_o \left\{ \int_{\tau_o}^{\tau} [A_1^H (w_\alpha h_{\gamma\bar{\gamma}} + w_\gamma h_{\alpha\bar{\gamma}}) + A_2^H (\dot{w}_\alpha h_{\gamma\bar{\gamma}} + \dot{w}_\gamma h_{\alpha\bar{\gamma}}) + 2A_3^H w_\alpha w_\gamma \bar{w}_\gamma \right. \\
 &\quad \left. + A_4^H (\dot{w}_\alpha w_\gamma + w_\alpha \dot{w}_\gamma) \bar{w}_\gamma + 2A_5^H w_\alpha w_\gamma \dot{\bar{w}}_\gamma] d\tau \right\}, \\
 & R[\alpha, \gamma, \bar{\gamma}; \tau] = \frac{\dot{\zeta}_o}{\dot{\zeta}} (\dot{w}_\alpha h_{\gamma\bar{\gamma}} + \dot{w}_\gamma h_{\alpha\bar{\gamma}}).
 \end{aligned} \tag{4.89}$$

The off-axis deflection field curvature type of deflector A:

$$\begin{aligned}
 & U_{RL}[\alpha, \gamma, \bar{A}; \bar{w}_H; \tau] \\
 &= \dot{\zeta}_o \left\{ \int_{\tau_o}^{\tau} [A_1^H (w_\alpha h_{\gamma\bar{A}} + w_\gamma h_{\alpha\bar{A}}) + A_2^H (\dot{w}_\alpha h_{\gamma\bar{A}} + \dot{w}_\gamma h_{\alpha\bar{A}}) \right. \\
 &\quad \left. + 2A_3^H w_\alpha w_\gamma \bar{w}_A + A_4^H (\dot{w}_\alpha w_\gamma + w_\alpha \dot{w}_\gamma) \bar{w}_A + 2A_5^H w_\alpha w_\gamma \dot{\bar{w}}_A] d\tau \right\}, \\
 & R[\alpha, \gamma, \bar{A}; \tau] = \frac{\dot{\zeta}_o}{\dot{\zeta}} (\dot{w}_\alpha h_{\gamma\bar{A}} + \dot{w}_\gamma h_{\alpha\bar{A}}).
 \end{aligned} \tag{4.90}$$

and

$$\begin{aligned}
 & U_{RL}[\alpha, A, \bar{\gamma}; \bar{w}_H; \tau] \\
 &= \dot{\zeta}_o \left\{ \int_{\tau_o}^{\tau} [A_1^H (w_\alpha h_{\bar{\gamma}A} + w_A h_{\alpha\bar{\gamma}}) + A_2^H (\dot{w}_\alpha h_{\bar{\gamma}A} + \dot{w}_A h_{\alpha\bar{\gamma}}) \right. \\
 &\quad \left. + 2A_3^H w_\alpha \bar{w}_\gamma w_A + A_4^H (\dot{w}_\alpha w_A + w_\alpha \dot{w}_A) \bar{w}_\gamma + 2A_5^H w_\alpha \dot{\bar{w}}_\gamma w_A] d\tau \right\}, \\
 & R[\alpha, A, \bar{\gamma}; \tau] = \frac{\dot{\zeta}_o}{\dot{\zeta}} (\dot{w}_\alpha h_{\bar{\gamma}A} + \dot{w}_A h_{\alpha\bar{\gamma}}).
 \end{aligned} \tag{4.91}$$

The off-axis deflection field curvature type of deflector B is obtained by replacing \bar{A} and A by \bar{B} and B in Eq. (4.90) and (4.91), respectively.

The deflection field curvature type of deflector A:

$$\begin{aligned}
 & U_{RL}[\alpha, A, \bar{A}; \bar{w}_H; \tau] \\
 &= \dot{\zeta}_o \left\{ \int_{\tau_o}^{\tau} [A_1^H (w_\alpha h_{A\bar{A}} + w_A h_{\alpha\bar{A}}) + A_2^H (\dot{w}_\alpha h_{A\bar{A}} + \dot{w}_A h_{\alpha\bar{A}}) + 2A_3^H w_\alpha w_A \bar{w}_A \right. \\
 &\quad \left. + A_4^H (\dot{w}_\alpha w_A + w_\alpha \dot{w}_A) \bar{w}_A + 2A_5^H w_\alpha w_A \dot{\bar{w}}_A] d\tau \right\}, \\
 & R[\alpha, A, \bar{A}; \tau] = \frac{\dot{\zeta}_o}{\dot{\zeta}} (\dot{w}_\alpha h_{A\bar{A}} + \dot{w}_A h_{\alpha\bar{A}}).
 \end{aligned} \tag{4.92}$$

The deflection field curvature type of deflector B is obtained by replacing A, \bar{A} by B, \bar{B} in Eq. (4.92).

The deflection hybrid field curvature type of deflectors A and B:

$$\begin{aligned}
& U_{RL}[\alpha, A, \bar{B}; \bar{w}_H; \tau] \\
&= \dot{\zeta}_o \left\{ \int_{\tau_o}^{\tau} [A_1^H(w_\alpha h_{AB} + w_A h_{\alpha B}) + A_2^H(\dot{w}_\alpha h_{AB} + \dot{w}_A h_{\alpha B}) \right. \\
&\quad \left. + 2A_3^H w_\alpha w_A \bar{w}_B + A_4^H(\dot{w}_\alpha w_A + w_\alpha \dot{w}_A) \bar{w}_B + 2A_5^H w_\alpha w_A \dot{\bar{w}}_B] d\tau \right\}, \\
& R[\alpha, A, \bar{B}; \tau] = \frac{\dot{\zeta}_o}{\dot{\zeta}} (\dot{w}_\alpha h_{AB} + \dot{w}_A h_{\alpha B}).
\end{aligned} \tag{4.93}$$

and

$$\begin{aligned}
& U_{RL}[\alpha, B, \bar{A}; \bar{w}_H; \tau] \\
&= \dot{\zeta}_o \left\{ \int_{\tau_o}^{\tau} [A_1^H(w_\alpha h_{\bar{A}B} + w_B h_{\alpha \bar{A}}) + A_2^H(\dot{w}_\alpha h_{\bar{A}B} + \dot{w}_B h_{\alpha \bar{A}}) \right. \\
&\quad \left. + 2A_3^H w_\alpha \bar{w}_A w_B + A_4^H(\dot{w}_\alpha w_B + w_\alpha \dot{w}_B) \bar{w}_A + 2A_5^H w_\alpha \bar{w}_A \dot{w}_B] d\tau \right\}, \\
& R[\alpha, B, \bar{A}; \tau] = \frac{\dot{\zeta}_o}{\dot{\zeta}} (\dot{w}_\alpha h_{\bar{A}B} + \dot{w}_B h_{\alpha \bar{A}}).
\end{aligned} \tag{4.94}$$

The off-axis astigmatism type:

$$\begin{aligned}
& U_{RL}[\gamma, \gamma, \bar{\alpha}; \bar{w}_H; \tau] \\
&= \dot{\zeta}_o \left\{ \int_{\tau_o}^{\tau} [A_1^H(w_\gamma h_{\bar{\alpha}\gamma} + A_2^H \dot{w}_\gamma h_{\bar{\alpha}\gamma} + A_3^H \bar{w}_\alpha w_\gamma^2 + A_4^H \bar{w}_\alpha w_\gamma \dot{w}_\gamma + A_5^H \dot{\bar{w}}_\alpha w_\gamma^2] d\tau \right\}, \\
& R[\gamma, \gamma, \bar{\alpha}; \tau] = \frac{\dot{\zeta}_o}{\dot{\zeta}} \dot{w}_\gamma h_{\bar{\alpha}\gamma}.
\end{aligned} \tag{4.95}$$

The off-axis deflection astigmatism type of deflector A:

$$\begin{aligned}
& U_{RL}[\gamma, A, \bar{\alpha}; \bar{w}_H; \tau] \\
&= \dot{\zeta}_o \left\{ \int_{\tau_o}^{\tau} [A_1^H(w_\gamma h_{\bar{\alpha}A} + w_A h_{\bar{\alpha}\gamma}) + A_2^H(\dot{w}_\gamma h_{\bar{\alpha}A} + \dot{w}_A h_{\bar{\alpha}\gamma}) \right. \\
&\quad \left. + 2A_3^H \bar{w}_\alpha w_\gamma w_A + A_4^H \bar{w}_\alpha (\dot{w}_\gamma w_A + w_\gamma \dot{w}_A) + 2A_5^H \dot{\bar{w}}_\alpha w_\gamma w_A] d\tau \right\} \\
& R[\gamma, A, \bar{\alpha}; \tau] = \frac{\dot{\zeta}_o}{\dot{\zeta}} (\dot{w}_\gamma h_{\bar{\alpha}A} + \dot{w}_A h_{\bar{\alpha}\gamma}).
\end{aligned} \tag{4.96}$$

The Off-axis deflection astigmatism type of deflector B is obtained by replacing A by B in Eq. (4.96).

The Deflection astigmatism type of deflector A:

$$\begin{aligned}
& U_{RL}[A, A, \bar{\alpha}; \bar{w}_H; \tau] \\
&= \dot{\zeta}_o \left\{ \int_{\tau_o}^{\tau} [A_1^H w_A h_{\bar{\alpha}A} + A_2^H \dot{w}_A h_{\bar{\alpha}A} + A_3^H \bar{w}_\alpha w_A^2 + A_4^H \bar{w}_\alpha w_A \dot{w}_A + A_5^H \dot{\bar{w}}_\alpha w_A^2] d\tau \right\}, \\
& R[A, A, \bar{\alpha}; \tau] = \frac{\dot{\zeta}_o}{\dot{\zeta}} \dot{w}_A h_{\bar{\alpha}A}.
\end{aligned} \tag{4.97}$$

The deflection astigmatism type of deflector B is obtained by replacing A by B in Eq. (4.97).

The deflection hybrid astigmatism type of deflectors A and B:

$$\begin{aligned}
& U_{RL}[A, B, \bar{\alpha}; \bar{w}_H; \tau] \\
&= \dot{\zeta}_o \left\{ \int_{\tau_o}^{\tau} [A_1^H(w_A h_{\bar{\alpha}B} + w_B h_{\bar{\alpha}A}) + A_2^H(\dot{w}_A h_{\bar{\alpha}B} + \dot{w}_B h_{\bar{\alpha}A}) \right. \\
&\quad \left. + 2A_3^H \bar{w}_\alpha w_A w_B + A_4^H \bar{w}_\alpha (w_A w_B + w_A \dot{w}_B) + 2A_5^H \dot{\bar{w}}_\alpha w_A w_B] d\tau \right\} \\
& R[A, B, \bar{\alpha}; \tau] = \frac{\dot{\zeta}_o}{\dot{\zeta}} (\dot{w}_A h_{\bar{\alpha}B} + \dot{w}_B h_{\bar{\alpha}A}).
\end{aligned} \tag{4.98}$$

The off-axis distortion type:

$$\begin{aligned}
 & U_{RL}[\gamma, \gamma, \bar{\gamma}; \bar{w}_H; \tau] \\
 &= \int_{\tau_0}^{\tau} [A_1^H w_\gamma h_{\gamma\bar{\gamma}} + A_2^H \dot{w}_\gamma h_{\gamma\bar{\gamma}} + A_3^H w_\gamma^2 \bar{w}_\gamma + A_4^H w_\gamma \bar{w}_\gamma \dot{w}_\gamma + A_5^H w_\gamma^2 \dot{\bar{w}}_\gamma] d\tau, \\
 & R[\gamma, \gamma, \bar{\gamma}; \tau] = \frac{1}{\zeta} \dot{w}_\gamma h_{\gamma\bar{\gamma}}, \quad S[\gamma, \gamma, \bar{\gamma}] = \frac{i\eta B_o''}{16\sqrt{\Phi_C}}
 \end{aligned} \tag{4.99}$$

The off-axis deflection distortion type of deflector A:

$$\begin{aligned}
 & U_{RL}[\gamma, A, \bar{\gamma}; \bar{w}_H; \tau] \\
 &= \int_{\tau_0}^{\tau} [A_1^H (w_\gamma h_{\gamma\bar{A}} + w_A h_{\gamma\bar{\gamma}}) + A_2^H (\dot{w}_\gamma h_{\gamma\bar{A}} + \dot{w}_A h_{\gamma\bar{\gamma}}) + 2A_3^H w_\gamma \bar{w}_\gamma w_A \\
 &\quad + A_4^H \bar{w}_\gamma (\dot{w}_\gamma w_A + w_\gamma \dot{w}_A) + 2A_5^H w_\gamma \dot{\bar{w}}_\gamma w_A] d\tau, \\
 & R[\gamma, A, \bar{\gamma}; \tau] = \frac{1}{\zeta} (\dot{w}_\gamma h_{\gamma\bar{A}} + \dot{w}_A h_{\gamma\bar{\gamma}}).
 \end{aligned} \tag{4.100}$$

and

$$\begin{aligned}
 & U_{RL}[\gamma, \gamma, \bar{A}; \bar{w}_H; \tau] \\
 &= \int_{\tau_0}^{\tau} [A_1^H w_\gamma h_{\gamma\bar{A}} + A_2^H \dot{w}_\gamma h_{\gamma\bar{A}} + A_3^H w_\gamma^2 \bar{w}_A + A_4^H w_\gamma \dot{w}_\gamma \bar{w}_A + A_5^H w_\gamma^2 \dot{\bar{w}}_A] d\tau, \\
 & R[\gamma, \gamma, \bar{A}; \tau] = \frac{1}{\zeta} \dot{w}_\gamma h_{\gamma\bar{A}}.
 \end{aligned} \tag{4.101}$$

and

$$\begin{aligned}
 & U_{RL}[\gamma, A, \bar{A}; \bar{w}_H; \tau] \\
 &= \int_{\tau_0}^{\tau} [A_1^H (w_\gamma h_{A\bar{A}} + w_A h_{\gamma\bar{A}}) + A_2^H (\dot{w}_\gamma h_{A\bar{A}} + \dot{w}_A h_{\gamma\bar{A}}) + 2A_3^H w_\gamma w_A \bar{w}_A \\
 &\quad + A_4^H (\dot{w}_\gamma w_A + w_\gamma \dot{w}_A) \bar{w}_A + 2A_5^H w_\gamma w_A \dot{\bar{w}}_A] d\tau, \\
 & R[\gamma, A, \bar{A}; \tau] = \frac{1}{\zeta} (\dot{w}_\gamma h_{A\bar{A}} + \dot{w}_A h_{\gamma\bar{A}}).
 \end{aligned} \tag{4.102}$$

and

$$\begin{aligned}
 & U_{RL}[A, A, \bar{\gamma}; \bar{w}_H; \tau] \\
 &= \int_{\tau_0}^{\tau} [A_1^H w_A h_{\gamma\bar{A}} + A_2^H \dot{w}_A h_{\gamma\bar{A}} + A_3^H \bar{w}_\gamma w_A^2 + A_4^H \bar{w}_\gamma w_A \dot{w}_A + A_5^H \dot{\bar{w}}_\gamma w_A^2] d\tau, \\
 & R[A, A, \bar{\gamma}; \tau] = \frac{1}{\zeta} \dot{w}_A h_{\gamma\bar{A}}.
 \end{aligned} \tag{4.103}$$

The off-axis deflection distortion type of deflector B are obtained by replacing A and \bar{A} by B and \bar{B} in Eqs. (4.100) -

(4.103), respectively.

The off-axis deflection hybrid distortion type of deflectors A and B:

$$\begin{aligned}
 & U_{RL}[\gamma, A, \bar{B}; \bar{w}_H; \tau] \\
 &= \int_{\tau_0}^{\tau} [A_1^H (w_\gamma h_{A\bar{B}} + w_A h_{\gamma\bar{B}}) + A_2^H (\dot{w}_\gamma h_{A\bar{B}} + \dot{w}_A h_{\gamma\bar{B}}) + 2A_3^H w_\gamma w_A \bar{w}_B \\
 &\quad + A_4^H (\dot{w}_\gamma w_A + w_\gamma \dot{w}_A) \bar{w}_B + 2A_5^H w_\gamma w_A \dot{\bar{w}}_B] d\tau, \\
 & R[\gamma, A, \bar{B}; \tau] = \frac{1}{\zeta} (\dot{w}_\gamma h_{A\bar{B}} + \dot{w}_A h_{\gamma\bar{B}}).
 \end{aligned} \tag{4.104}$$

and

$$\begin{aligned}
& U_{RL}[\gamma, B, \bar{A}; \bar{w}_H; \tau] \\
&= \int_{\tau_0}^{\tau} [A_1^H(w_\gamma h_{\bar{A}B} + w_B h_{\gamma\bar{A}}) + A_2^H(\dot{w}_\gamma h_{\bar{A}B} + \dot{w}_B h_{\gamma\bar{A}}) + 2A_3^H w_\gamma \bar{w}_A w_B \\
&\quad + A_4^H(\dot{w}_\gamma w_B + w_\gamma \dot{w}_B) \bar{w}_A + 2A_5^H w_\gamma \dot{w}_A w_B] d\tau, \\
& R[\gamma, B, \bar{A}; \tau] = \frac{1}{\zeta} (\dot{w}_\gamma h_{\bar{A}B} + \dot{w}_B h_{\gamma\bar{A}}).
\end{aligned} \tag{4.105}$$

and

$$\begin{aligned}
& U_{RL}[A, B, \bar{\gamma}; \bar{w}_H; \tau] \\
&= \int_{\tau_0}^{\tau} [A_1^H(w_A h_{\bar{\gamma}B} + w_B h_{\bar{\gamma}A}) + A_2^H(\dot{w}_A h_{\bar{\gamma}B} + \dot{w}_B h_{\bar{\gamma}A}) + 2A_3^H \bar{w}_\gamma w_A w_B \\
&\quad + A_4^H \bar{w}_\gamma (\dot{w}_A w_B + w_A \dot{w}_B) + 2A_5^H \bar{w}_\gamma \dot{w}_A w_B] d\tau, \\
& R[A, B, \bar{\gamma}; \tau] = \frac{1}{\zeta} (\dot{w}_A h_{\bar{\gamma}B} + \dot{w}_B h_{\bar{\gamma}A}).
\end{aligned} \tag{4.106}$$

Deflection distortion type of deflector A:

$$\begin{aligned}
& U_{RL}[A, A, \bar{A}; \bar{w}_H; \tau] \\
&= \int_{\tau_0}^{\tau} [A_1^H w_A h_{A\bar{A}} + A_2^H \dot{w}_A h_{A\bar{A}} + A_3^H w_A^2 \bar{w}_A + A_4^H w_A \bar{w}_A \dot{w}_A + A_5^H w_A^2 \dot{\bar{w}}_A] d\tau, \\
& R[A, A, \bar{A}; \tau] = \frac{1}{\zeta} \dot{w}_A h_{A\bar{A}}.
\end{aligned} \tag{4.107}$$

Deflection distortion type of deflector B is obtained by replacing A by B in Eq. (4.107).

Deflection hybrid distortion type of deflectors A and B:

$$\begin{aligned}
& U_{RL}[A, B, \bar{A}; \bar{w}_H; \tau] \\
&= \int_{\tau_0}^{\tau} [A_1^H(w_A h_{\bar{A}B} + w_B h_{A\bar{A}}) + A_2^H(\dot{w}_A h_{\bar{A}B} + \dot{w}_B h_{A\bar{A}}) + 2A_3^H w_A \bar{w}_A w_B \\
&\quad + A_4^H \bar{w}_A (\dot{w}_A w_B + w_A \dot{w}_B) + 2A_5^H w_A \dot{\bar{w}}_A w_B] d\tau, \\
& R[A, B, \bar{A}; \tau] = \frac{1}{\zeta} (\dot{w}_A h_{\bar{A}B} + \dot{w}_B h_{A\bar{A}}).
\end{aligned} \tag{4.108}$$

and

$$\begin{aligned}
& U_{RL}[A, A, \bar{B}; \bar{w}_H; \tau] \\
&= \int_{\tau_0}^{\tau} [A_1^H w_A h_{AB} + A_2^H \dot{w}_A h_{AB} + A_3^H w_A^2 \bar{w}_B + A_4^H w_A \bar{w}_B \dot{w}_A + A_5^H w_A^2 \dot{\bar{w}}_B] d\tau, \\
& R[A, A, \bar{B}; \tau] = \frac{1}{\zeta} \dot{w}_A h_{A\bar{B}}.
\end{aligned} \tag{4.109}$$

and

$$\begin{aligned}
& U_{RL}[A, B, \bar{B}; \bar{w}_H; \tau] \\
&= \int_{\tau_0}^{\tau} [A_1^H(w_A h_{BB} + w_B h_{AB}) + A_2^H(\dot{w}_A h_{BB} + \dot{w}_B h_{AB}) + 2A_3^H w_A w_B \bar{w}_B \\
&\quad + A_4^H (\dot{w}_A w_B + w_A \dot{w}_B) \bar{w}_B + 2A_5^H w_A w_B \dot{\bar{w}}_B] d\tau, \\
& R[A, B, \bar{B}; \tau] = \frac{1}{\zeta} (\dot{w}_A h_{BB} + \dot{w}_B h_{AB}),
\end{aligned} \tag{4.110}$$

and

$$\begin{aligned}
& U_{RL}[B, B, \bar{A}; \bar{w}_H; \tau] \\
&= \int_{\tau_0}^{\tau} [A_1^H w_B h_{\bar{A}B} + A_2^H \dot{w}_B h_{\bar{A}B} + A_3^H \bar{w}_A w_B^2 + A_4^H \bar{w}_A w_B \dot{w}_B + A_5^H \dot{\bar{w}}_A w_B^2] d\tau, \\
& R[B, B, \bar{A}; \tau] = \frac{1}{\zeta} \dot{w}_B h_{\bar{A}B}.
\end{aligned} \tag{4.111}$$

The deflection field part of Case (i): an electrostatic deflector and a magnetic deflector

The Normal deflection part:

The deflection coma-length type of deflector A, and of deflector B:

$$\begin{aligned} U_{DEF}^{(i)}[\alpha, A, \bar{\alpha}; \bar{w}_H; \tau] &= \dot{\zeta}_o^2 \int_{\tau_o}^{\tau} (E_1^H F_1'^A h_{\alpha\bar{\alpha}} + E_3^H F_1''^A w_{\alpha} \bar{w}_{\alpha}) d\tau, \\ U_{DEF}^{(i)}[\alpha, B, \bar{\alpha}; \bar{w}_H; \tau] &= \dot{\zeta}_o^2 \int_{\tau_o}^{\tau} \{G_1^H D_1'^B (w_{\alpha} \dot{\bar{w}}_{\alpha} - \dot{w}_{\alpha} \bar{w}_{\alpha}) + G_4^H D_1^B h_{\alpha\bar{\alpha}} + G_5^H D_1'^B w_{\alpha} \bar{w}_{\alpha}\} d\tau. \end{aligned} \quad (4.112)$$

The deflection coma-radius type of deflector A, and of deflector B:

$$\begin{aligned} U_{DEF}^{(i)}[\alpha, \alpha, \bar{A}; \bar{w}_H; \tau] &= \dot{\zeta}_o^2 \int_{\tau_o}^{\tau} E_2^H \bar{F}_1''^A w_{\alpha}^2 d\tau, \\ U_{DEF}^{(i)}[\alpha, \alpha, \bar{B}; \bar{w}_H; \tau] &= \dot{\zeta}_o^2 \int_{\tau_o}^{\tau} \{G_2^H \bar{D}_1'^B w_{\alpha} \dot{w}_{\alpha} + G_6^H \bar{D}_1^B w_{\alpha}^2\} d\tau. \end{aligned} \quad (4.113)$$

The off-axis deflection field curvature type of deflector A, and of deflector B:

$$\begin{aligned} U_{DEF}^{(i)}[\alpha, \gamma, \bar{A}; \bar{w}_H; \tau] &= \dot{\zeta}_o \int_{\tau_o}^{\tau} 2E_2^H \bar{F}_1''^A w_{\alpha} w_{\gamma} d\tau, \\ U_{DEF}^{(i)}[\alpha, \gamma, \bar{Y}; \bar{w}_H; \tau] &= \dot{\zeta}_o \int_{\tau_o}^{\tau} (E_1^H F_1'^A h_{\alpha\bar{\gamma}} + E_3^H F_1''^A w_{\alpha} \bar{w}_{\gamma}) d\tau, \\ U_{DEF}^{(i)}[\alpha, \gamma, \bar{B}; \bar{w}_H; \tau] &= \dot{\zeta}_o \int_{\tau_o}^{\tau} \{G_2^H \bar{D}_1'^B (w_{\alpha} \dot{w}_{\gamma} + \dot{w}_{\alpha} w_{\gamma}) + 2G_6^H \bar{D}_1^B w_{\alpha} w_{\gamma}\} d\tau, \\ U_{DEF}^{(i)}[\alpha, B, \bar{\gamma}; \bar{w}_H; \tau] &= \dot{\zeta}_o \int_{\tau_o}^{\tau} \{G_1^H D_1'^B (w_{\alpha} \dot{\bar{w}}_{\gamma} - \dot{w}_{\alpha} \bar{w}_{\gamma}) + G_4^H D_1^B h_{\alpha\bar{\gamma}} + G_5^H D_1'^B w_{\alpha} \bar{w}_{\gamma}\} d\tau. \end{aligned} \quad (4.114)$$

The deflection field curvature type of deflector A, and of deflector B:

$$\begin{aligned} U_{DEF}^{(i)}[\alpha, A, \bar{A}; \bar{w}_H; \tau] &= \dot{\zeta}_o \int_{\tau_o}^{\tau} (E_1^H F_1'^A h_{\alpha\bar{A}} + 2E_2^H \bar{F}_1''^A w_{\alpha} w_A + E_3^H F_1''^A w_{\alpha} \bar{w}_A) d\tau, \\ U_{DEF}^{(i)}[\alpha, B, \bar{B}; \bar{w}_H; \tau] &= \dot{\zeta}_o \int_{\tau_o}^{\tau} \{G_1^H D_1'^B (w_{\alpha} \dot{\bar{w}}_B - \dot{w}_{\alpha} \bar{w}_B) + G_2^H \bar{D}_1'^B (w_{\alpha} \dot{w}_B + \dot{w}_{\alpha} w_B) \\ &\quad + G_4^H D_1^B h_{\alpha\bar{B}} + G_5^H D_1'^B w_{\alpha} \bar{w}_B + 2G_6^H \bar{D}_1^B w_{\alpha} w_B\} d\tau. \end{aligned} \quad (4.115)$$

The deflection hybrid field curvature type of deflectors A and B:

$$\begin{aligned} &U_{DEF}^{(i)}[\alpha, A, \bar{B}; \bar{w}_H; \tau] \\ &= \dot{\zeta}_o \int_{\tau_o}^{\tau} \{E_1^H F_1'^A h_{\alpha\bar{B}} + E_3^H F_1''^A w_{\alpha} \bar{w}_B + G_2^H \bar{D}_1'^B (w_{\alpha} \dot{w}_A + \dot{w}_{\alpha} w_A) + 2G_6^H \bar{D}_1^B w_{\alpha} w_A\} d\tau, \\ &U_{DEF}^{(i)}[\alpha, B, \bar{A}; \bar{w}_H; \tau] \\ &= \dot{\zeta}_o \int_{\tau_o}^{\tau} \{2E_2^H \bar{F}_1''^A w_{\alpha} w_B + G_1^H D_1'^B (w_{\alpha} \dot{\bar{w}}_A - \dot{w}_{\alpha} \bar{w}_A) + G_4^H D_1^B h_{\alpha\bar{A}} + G_5^H D_1'^B w_{\alpha} \bar{w}_A\} d\tau. \end{aligned} \quad (4.116)$$

The off-axis deflection astigmatism type of deflector A, and of deflector B:

$$\begin{aligned} U_{DEF}^{(i)}[\gamma, A, \bar{\alpha}; \bar{w}_H; \tau] &= \dot{\zeta}_o \int_{\tau_o}^{\tau} (E_1^H F_1'^A h_{\alpha\bar{\gamma}} + E_3^H F_1''^A \bar{w}_{\alpha} w_{\gamma}) d\tau, \\ U_{DEF}^{(i)}[\gamma, B, \bar{\alpha}; \bar{w}_H; \tau] &= \dot{\zeta}_o \int_{\tau_o}^{\tau} \{G_1^H D_1'^B (\dot{\bar{w}}_{\alpha} w_{\gamma} - \bar{w}_{\alpha} \dot{w}_{\gamma}) + G_4^H D_1^B h_{\alpha\bar{\gamma}} + G_5^H D_1'^B \bar{w}_{\alpha} w_{\gamma}\} d\tau. \end{aligned} \quad (4.117)$$

The deflection astigmatism type of deflector A, and of deflector B:

$$\begin{aligned} U_{DEF}^{(i)}[S_A, S_A, \bar{\alpha}; \bar{w}_H; \tau] &= \dot{\zeta}_o \int_{\tau_o}^{\tau} (E_1^H F_1'^A h_{\alpha\bar{A}} + E_3^H F_1''^A \bar{w}_{\alpha} w_A) d\tau, \\ U_{DEF}^{(i)}[B, B, \bar{\alpha}; \bar{w}_H; \tau] &= \dot{\zeta}_o \int_{\tau_o}^{\tau} \{G_1^H D_1'^B (\dot{\bar{w}}_{\alpha} w_B - \bar{w}_{\alpha} \dot{w}_B) + G_4^H D_1^B h_{\alpha\bar{B}} + G_5^H D_1'^B \bar{w}_{\alpha} w_B\} d\tau. \end{aligned} \quad (4.118)$$

The deflection hybrid astigmatism type of deflectors A and B:

$$U_{DEF}^{(i)}[A, B, \bar{\alpha}; \bar{w}_H; \tau] = \xi_o \int_{\tau_o}^{\tau} \{E_1^H F_1'^A h_{\bar{\alpha}B} + E_3^H F_1''^A \bar{w}_{\bar{\alpha}} w_B + G_1^H D_1'^B (\dot{w}_{\bar{\alpha}} w_A - \bar{w}_{\bar{\alpha}} \dot{w}_A) + G_4^H D_1^B h_{\bar{\alpha}A} + G_5^H D_1'^B \bar{w}_{\bar{\alpha}} w_A\} d\tau. \quad (4.119)$$

The off-axis deflection distortion type of deflector A:

$$U_{DEF}^{(i)}[\gamma, A, \bar{\gamma}; \bar{w}_H; \tau] = \int_{\tau_o}^{\tau} (E_1^H F_1'^A h_{\gamma\bar{\gamma}} + E_3^H F_1''^A w_{\gamma} \bar{w}_{\gamma}) d\tau, \quad (4.120)$$

$$U_{DEF}^{(i)}[\gamma, \gamma, \bar{A}; \bar{w}_H; \tau] = \int_{\tau_o}^{\tau} E_2^H \bar{F}_1'^A w_{\gamma}^2 d\tau,$$

and

$$U_{DEF}^{(i)}[\gamma, A, \bar{A}; \bar{w}_H; \tau] = \int_{\tau_o}^{\tau} (E_1^H F_1'^A h_{\gamma\bar{A}} + 2E_2^H \bar{F}_1'^A w_{\gamma} w_A + E_3^H F_1''^A w_{\gamma} \bar{w}_A) d\tau, \quad (4.121)$$

$$U_{DEF}^{(i)}[A, A, \bar{\gamma}; \bar{w}_H; \tau] = \int_{\tau_o}^{\tau} (E_1^H F_1'^A h_{\bar{\gamma}A} + E_3^H F_1''^A \bar{w}_{\gamma} w_A) d\tau.$$

The off-axis deflection distortion type of deflector B:

$$U_{DEF}^{(i)}[\gamma, B, \bar{\gamma}; \bar{w}_H; \tau] = \int_{\tau_o}^{\tau} \{G_1^H D_1'^B (w_{\gamma} \dot{\bar{w}}_{\gamma} - \dot{w}_{\gamma} \bar{w}_{\gamma}) + G_4^H D_1^B h_{\gamma\bar{\gamma}} + G_5^H D_1'^B w_{\gamma} \bar{w}_{\gamma}\} d\tau, \quad (4.122)$$

$$S^{(i)}[\gamma, B, \bar{\gamma}] = \frac{\eta D_{1o}^{B'}}{4\sqrt{\Phi_C}},$$

$$U_{DEF}^{(i)}[\gamma, \gamma, \bar{B}; \bar{w}_H; \tau] = \int_{\tau_o}^{\tau} \{G_2^H \bar{D}_1'^B w_{\gamma} \dot{w}_{\gamma} + G_6^H \bar{D}_1'^B w_{\gamma}^2\} d\tau,$$

$$S^{(i)}[\gamma, \gamma, \bar{B}] = -\frac{\eta \bar{D}_{1o}^{B'}}{8\sqrt{\Phi_C}}$$

and

$$U_{DEF}^{(i)}[\gamma, B, \bar{B}; \bar{w}_H; \tau] = \int_{\tau_o}^{\tau} \{G_1^H D_1'^B (w_{\gamma} \dot{\bar{w}}_B - \dot{w}_{\gamma} \bar{w}_B) + G_2^H \bar{D}_1'^B (w_{\gamma} \dot{w}_B + \dot{w}_{\gamma} w_B) + G_4^H D_1^B h_{\gamma\bar{B}} + G_5^H D_1'^B w_{\gamma} \bar{w}_B + 2G_6^H \bar{D}_1'^B w_{\gamma} w_B\} d\tau, \quad (4.123)$$

$$U_{DEF}^{(i)}[B, B, \bar{\gamma}; \bar{w}_H; \tau] = \int_{\tau_o}^{\tau} \{G_1^H D_1'^B (\dot{\bar{w}}_{\gamma} w_B - \bar{w}_{\gamma} \dot{w}_B) + G_4^H D_1^B h_{\bar{\gamma}B} + G_5^H D_1'^B \bar{w}_{\gamma} w_B\} d\tau.$$

The off-axis deflection hybrid distortion type of deflectors A and B:

$$U_{DEF}^{(i)}[\gamma, A, \bar{B}; \bar{w}_H; \tau] = \int_{\tau_o}^{\tau} \{E_1^H F_1'^A h_{\gamma\bar{B}} + E_3^H F_1''^A w_{\gamma} \bar{w}_B + G_2^H \bar{D}_1'^B (w_{\gamma} \dot{w}_A + \dot{w}_{\gamma} w_A) + 2G_6^H \bar{D}_1'^B w_{\gamma} w_A\} d\tau, \quad (4.124)$$

$$U_{DEF}^{(i)}[\gamma, B, \bar{A}; \bar{w}_H; \tau] = \int_{\tau_o}^{\tau} \{2E_2^H \bar{F}_1'^A w_{\gamma} w_B + G_1^H D_1'^B (w_{\gamma} \dot{\bar{w}}_A - \dot{w}_{\gamma} \bar{w}_A) + G_4^H D_1^B h_{\gamma\bar{A}} + G_5^H D_1'^B w_{\gamma} \bar{w}_A\} d\tau,$$

$$U_{DEF}^{(i)}[A, B, \bar{\gamma}; \bar{w}_H; \tau] = \int_{\tau_o}^{\tau} \{E_1^H F_1'^A h_{\bar{\gamma}B} + E_3^H F_1''^A \bar{w}_{\gamma} w_B + G_1^H D_1'^B (\dot{\bar{w}}_{\gamma} w_A - \bar{w}_{\gamma} \dot{w}_A) + G_4^H D_1^B h_{\bar{\gamma}A} + G_5^H D_1'^B \bar{w}_{\gamma} w_A\} d\tau.$$

The deflection distortion type of deflector A, and of deflector B:

$$U_{DEF}^{(i)}[A, A, \bar{A}; \bar{w}_H; \tau] = \int_{\tau_o}^{\tau} (E_1^H F_1'^A h_{A\bar{A}} + E_2^H \bar{F}_1'^A w_A^2 + E_3^H F_1''^A w_A \bar{w}_A) d\tau, \quad (4.125)$$

$$U_{DEF}^{(i)}[B, B, \bar{B}; \bar{w}_H; \tau] = \int_{\tau_o}^{\tau} \{G_1^H D_1'^B (w_B \dot{\bar{w}}_B - \dot{w}_B \bar{w}_B) + G_2^H \bar{D}_1'^B w_B \dot{w}_B + G_4^H D_1^B h_{B\bar{B}} + G_5^H D_1'^B w_B \bar{w}_B + G_6^H \bar{D}_1'^B w_B^2\} d\tau.$$

The deflection hybrid distortion type of deflectors A and B:

$$\begin{aligned}
U_{DEF}^{(i)}[A, A, \bar{B}; \bar{w}_H; \tau] &= \int_{\tau_0}^{\tau} \{E_1^H F_1'^A h_{A\bar{B}} + E_3^H F_1''^A w_A \bar{w}_B + G_2^H \bar{D}_1'^B w_A \dot{w}_A + G_6^H \bar{D}_1'^B w_A^2\} d\tau, \\
U_{DEF}^{(i)}[A, B, \bar{A}; \bar{w}_H; \tau] &= \int_{\tau_0}^{\tau} \{E_1^H F_1'^A h_{A\bar{B}} + 2E_2^H \bar{F}_1''^A w_A w_B + E_3^H F_1''^A \bar{w}_A w_B \\
&\quad + G_4^H D_1'^B (w_A \dot{w}_A - \dot{w}_A \bar{w}_A) + G_4^H D_1'^B h_{A\bar{A}} + G_5^H D_1'^B w_A \bar{w}_A\} d\tau, \\
U_{DEF}^{(i)}[A, B, \bar{B}; \bar{w}_H; \tau] &= \int_{\tau_0}^{\tau} \{E_1^H F_1'^A h_{B\bar{B}} + E_3^H F_1''^A w_B \bar{w}_B + G_1^H D_1'^B (w_A \dot{w}_B - \dot{w}_A \bar{w}_B) \\
&\quad + G_2^H \bar{D}_1'^B (w_A \dot{w}_B + \dot{w}_A w_B) + G_4^H D_1'^B h_{A\bar{B}} + G_5^H D_1'^B w_A \bar{w}_B \\
&\quad + 2G_6^H \bar{D}_1'^B w_A w_B\} d\tau, \\
U_{DEF}^{(i)}[B, B, \bar{A}; \bar{w}_H; \tau] &= \int_{\tau_0}^{\tau} \{E_2^H \bar{F}_1''^A w_B^2 + G_1^H D_1'^B (\dot{w}_A w_B - \bar{w}_A \dot{w}_B) + G_4^H D_1'^B h_{A\bar{B}} \\
&\quad + G_5^H D_1'^B \bar{w}_A w_B\} d\tau.
\end{aligned} \tag{4.126}$$

The four-fold deflection:

The four-fold deflection A2 (Three-fold astigmatism) of deflector A, and of deflector B:

$$\begin{aligned}
U_{4F}^{(i)}[\bar{\alpha}, \bar{\alpha}, \bar{A}; \bar{w}_H; \tau] &= \dot{\zeta}_o^2 \int_{\tau_0}^{\tau} E_4^H F_3^A \bar{w}_\alpha^2 d\tau, \\
U_{4F}^{(i)}[\bar{\alpha}, \bar{\alpha}, \bar{B}; \bar{w}_H; \tau] &= \dot{\zeta}_o^2 \int_{\tau_0}^{\tau} G_3^H D_3^B \bar{w}_\alpha^2 d\tau.
\end{aligned} \tag{4.127}$$

The four-fold off-axis deflection astigmatism of deflector A, and of deflector B:

$$\begin{aligned}
U_{4F}^{(i)}[\bar{\alpha}, \bar{\gamma}, \bar{A}; \bar{w}_H; \tau] &= \dot{\zeta}_o \int_{\tau_0}^{\tau} 2E_4^H F_3^A \bar{w}_\alpha \bar{w}_\gamma d\tau, \\
U_{4F}^{(i)}[\bar{\alpha}, \bar{\gamma}, \bar{B}; \bar{w}_H; \tau] &= \dot{\zeta}_o \int_{\tau_0}^{\tau} 2G_3^H D_3^B \bar{w}_\alpha \bar{w}_\gamma d\tau.
\end{aligned} \tag{4.128}$$

The four-fold deflection astigmatism of deflector A, and of deflector B:

$$\begin{aligned}
U_{4F}^{(i)}[\bar{\alpha}, \bar{A}, \bar{A}; \bar{w}_H; \tau] &= \dot{\zeta}_o \int_{\tau_0}^{\tau} 2E_4^H F_3^A \bar{w}_\alpha \bar{w}_A d\tau, \\
U_{4F}^{(i)}[\bar{\alpha}, \bar{B}, \bar{B}; \bar{w}_H; \tau] &= \dot{\zeta}_o \int_{\tau_0}^{\tau} 2G_3^H D_3^B \bar{w}_\alpha \bar{w}_B d\tau.
\end{aligned} \tag{4.129}$$

The four-fold deflection hybrid astigmatism of deflector A and B:

$$U_{4F}^{(i)}[\bar{\alpha}, \bar{A}, \bar{B}; \bar{w}_H; \tau] = \dot{\zeta}_o \int_{\tau_0}^{\tau} (2E_4^H F_3^A \bar{w}_\alpha \bar{w}_B + 2G_3^H D_3^B \bar{w}_\alpha \bar{w}_A) d\tau. \tag{4.130}$$

The four-fold off-axis deflection distortion of deflector A, and of deflector B:

$$\begin{aligned}
U_{4F}^{(i)}[\bar{\gamma}, \bar{\gamma}, \bar{A}; \bar{w}_H; \tau] &= \int_{\tau_0}^{\tau} E_4^H F_3^A \bar{w}_\gamma^2 d\tau, \\
U_{4F}^{(i)}[\bar{\gamma}, \bar{A}, \bar{A}; \bar{w}_H; \tau] &= \int_{\tau_0}^{\tau} 2E_4^H F_3^A \bar{w}_\gamma \bar{w}_A d\tau, \\
U_{4F}^{(i)}[\bar{\gamma}, \bar{\gamma}, \bar{B}; \bar{w}_H; \tau] &= \int_{\tau_0}^{\tau} G_3^H D_3^B \bar{w}_\gamma^2 d\tau, \\
U_{4F}^{(i)}[\bar{\gamma}, \bar{B}, \bar{B}; \bar{w}_H; \tau] &= \int_{\tau_0}^{\tau} 2G_3^H D_3^B \bar{w}_\gamma \bar{w}_B d\tau.
\end{aligned} \tag{4.131}$$

The four-fold off-axis deflection hybrid distortion of deflectors A and B:

$$U_{4F}^{(i)}[\bar{\gamma}, \bar{A}, \bar{B}; \bar{w}_H; \tau] = \int_{\tau_0}^{\tau} (2E_4^H F_3^A \bar{w}_\gamma \bar{w}_B + 2G_3^H D_3^B \bar{w}_\gamma \bar{w}_A) d\tau. \tag{4.132}$$

The four-fold deflection distortion of deflector A, and of deflector B:

$$U_{4F}^{(i)}[\bar{A}, \bar{A}, \bar{A}; \bar{w}_H; \tau] = \int_{\tau_0}^{\tau} E_4^H F_3^A \bar{w}_A^2 d\tau, \tag{4.133}$$

$$U_{4F}^{(i)}[\bar{B}, \bar{B}, \bar{B}; \bar{w}_H; \tau] = \int_{\tau_0}^{\tau} G_3^H D_3^B \bar{w}_B^2 d\tau.$$

The four-fold deflection hybrid distortion of deflectors A and B:

$$\begin{aligned} U_{4F}^{(i)}[\bar{A}, \bar{A}, \bar{B}; \bar{w}_H; \tau] &= \int_{\tau_0}^{\tau} (2E_4^H F_3^A \bar{w}_A \bar{w}_B + G_3^H D_3^B \bar{w}_A^2) d\tau, \\ U_{4F}^{(i)}[\bar{A}, \bar{B}, \bar{B}; \bar{w}_H; \tau] &= \int_{\tau_0}^{\tau} (E_4^H F_3^A \bar{w}_B^2 + 2G_3^H D_3^B \bar{w}_A \bar{w}_B) d\tau. \end{aligned} \quad (4.134)$$

The deflection field part of Case (ii), two electrostatic deflectors for hybrid type:

The deflection hybrid field curvature type of deflectors A and B:

$$\begin{aligned} U_{DEF}^{(ii)}[\alpha, A, \bar{B}; \bar{w}_H; \tau] &= \int_{\tau_0}^{\tau} \{E_1^H F_1'^A h_{\alpha\bar{B}} + 2E_2^H \bar{F}_1''^B w_{\alpha} w_A + E_3^H F_1''^A w_{\alpha} \bar{w}_B\} d\tau, \\ U_{DEF}^{(ii)}[\alpha, B, \bar{A}; \bar{w}_H; \tau] &= \int_{\tau_0}^{\tau} \{E_1^H F_1'^B h_{\alpha\bar{A}} + 2E_2^H \bar{F}_1''^A w_{\alpha} w_B + E_3^H F_1''^B w_{\alpha} \bar{w}_A\} d\tau. \end{aligned} \quad (4.135)$$

The deflection hybrid astigmatism type of deflectors A and B:

$$U_{DEF}^{(ii)}[A, B, \bar{\alpha}; \bar{w}_H; \tau] = \int_{\tau_0}^{\tau} \{E_1^H (F_1'^A h_{\bar{\alpha}B} + F_1'^B h_{\bar{\alpha}A}) + \bar{w}_{\alpha} E_3^H (F_1''^A w_B + F_1''^B w_A)\} d\tau. \quad (4.136)$$

The off-axis deflection hybrid distortion type of deflectors A and B:

$$\begin{aligned} U_{DEF}^{(ii)}[\gamma, A, \bar{B}; \bar{w}_H; \tau] &= \int_{\tau_0}^{\tau} \{E_1^H F_1'^A h_{\gamma\bar{B}} + 2E_2^H \bar{F}_1''^B w_{\gamma} w_A + E_3^H F_1''^A w_{\gamma} \bar{w}_B\} d\tau, \\ U_{DEF}^{(ii)}[\gamma, B, \bar{A}; \bar{w}_H; \tau] &= \int_{\tau_0}^{\tau} \{E_1^H F_1'^B h_{\gamma\bar{A}} + 2E_2^H \bar{F}_1''^A w_{\gamma} w_B + E_3^H F_1''^B w_{\gamma} \bar{w}_A\} d\tau, \\ U_{DEF}^{(ii)}[A, B, \bar{\gamma}; \bar{w}_H; \tau] &= \int_{\tau_0}^{\tau} \{E_1^H (F_1'^A h_{\bar{\gamma}B} + F_1'^B h_{\bar{\gamma}A}) + \bar{w}_{\gamma} E_3^H (F_1''^A w_B + F_1''^B w_A)\} d\tau. \end{aligned} \quad (4.137)$$

The deflection hybrid distortion type of deflectors A and B:

$$\begin{aligned} U_{DEF}^{(ii)}[A, A, \bar{B}; \bar{w}_H; \tau] &= \int_{\tau_0}^{\tau} \{E_1^H F_1'^A h_{A\bar{B}} + E_2^H \bar{F}_1''^B w_A^2 + E_3^H F_1''^A w_A \bar{w}_B\} d\tau, \\ U_{DEF}^{(ii)}[A, B, \bar{A}; \bar{w}_H; \tau] &= \int_{\tau_0}^{\tau} \{E_1^H (F_1'^A h_{\bar{A}B} + F_1'^B h_{A\bar{A}}) + 2E_2^H \bar{F}_1''^A w_A w_B \\ &\quad + E_3^H \bar{w}_A (F_1''^A w_B + F_1''^B w_A)\} d\tau, \\ U_{DEF}^{(ii)}[A, B, \bar{B}; \bar{w}_H; \tau] &= \int_{\tau_0}^{\tau} \{E_1^H (F_1'^A h_{BB} + F_1'^B h_{AB}) + 2E_2^H \bar{F}_1''^B w_A w_B \\ &\quad + E_3^H (F_1''^A w_B + F_1''^B w_A) \bar{w}_B\} d\tau, \\ U_{DEF}^{(ii)}[B, B, \bar{A}; \bar{w}_H; \tau] &= \int_{\tau_0}^{\tau} \{E_1^H F_1'^B h_{AB} + E_2^H \bar{F}_1''^A w_B^2 + E_3^H F_1''^B \bar{w}_A w_B\} d\tau. \end{aligned} \quad (4.138)$$

The four-fold deflection hybrid astigmatism of deflectors A and B:

$$U_{4F}^{(ii)}[\bar{\alpha}, \bar{A}, \bar{B}; \bar{w}_H; \tau] = \int_{\tau_0}^{\tau} 2E_4^H (F_3^A \bar{w}_B + F_3^B \bar{w}_A) \bar{w}_{\alpha} d\tau \quad (4.139)$$

The four-fold off-axis deflection hybrid distortion of deflectors A and B:

$$U_{4F}^{(ii)}[\bar{\gamma}, \bar{A}, \bar{B}; \bar{w}_H; \tau] = \int_{\tau_0}^{\tau} 2E_4^H \bar{w}_{\gamma} (F_3^A \bar{w}_B + F_3^B \bar{w}_A) d\tau \quad (4.140)$$

The four-fold deflection hybrid distortion of deflectors A and B:

$$\begin{aligned} U_{4F}^{(ii)}[\bar{A}, \bar{A}, \bar{B}; \bar{w}_H; \tau] &= \int_{\tau_0}^{\tau} E_4^H (2F_3^A \bar{w}_B + F_3^B \bar{w}_A) \bar{w}_A d\tau, \\ U_{4F}^{(ii)}[\bar{A}, \bar{B}, \bar{B}; \bar{w}_H; \tau] &= \int_{\tau_0}^{\tau} E_4^H (2F_3^B \bar{w}_A + F_3^A \bar{w}_B) \bar{w}_B d\tau. \end{aligned} \quad (4.141)$$

The deflection field part of Case (iii), two magnetic deflectors for hybrid type:

The deflection hybrid field curvature type of deflectors A and B:

$$\begin{aligned}
 U_{DEF}^{(iii)}[\alpha, A, \bar{B}; \bar{w}_H; \tau] &= \zeta_o \int_{\tau_o}^{\tau} \{G_1^H D_1'^A (w_\alpha \dot{w}_B - \dot{w}_\alpha \bar{w}_B) + G_2^H \bar{D}_1'^B (w_\alpha \dot{w}_A + \dot{w}_\alpha w_A) \\
 &+ G_4^H D_1^A h_{\alpha\bar{B}} + G_5^H D_1^A w_\alpha \bar{w}_B + 2G_6^H \bar{D}_1'^B w_\alpha w_A\} d\tau, \\
 U_{DEF}^{(iii)}[\alpha, B, \bar{A}; \bar{w}_H; \tau] &= \zeta_o \int_{\tau_o}^{\tau} \{G_1^H D_1'^B (w_\alpha \dot{w}_A - \dot{w}_\alpha \bar{w}_A) + G_2^H \bar{D}_1'^A (w_\alpha \dot{w}_B + \dot{w}_\alpha w_B) \\
 &+ G_4^H D_1^B h_{\alpha\bar{A}} + G_5^H D_1^B w_\alpha \bar{w}_A + 2G_6^H \bar{D}_1'^A w_\alpha w_B\} d\tau.
 \end{aligned} \tag{4.142}$$

The deflection hybrid astigmatism type of deflectors A and B:

$$\begin{aligned}
 U_{DEF}^{(iii)}[A, B, \bar{\alpha}; \bar{w}_H; \tau] &= \zeta_o \int_{\tau_o}^{\tau} \{G_1^H \{D_1'^A (\dot{w}_\alpha w_B - \bar{w}_\alpha \dot{w}_B) + D_1'^B (\dot{w}_\alpha w_A - \bar{w}_\alpha \dot{w}_A)\} \\
 &+ G_4^H (D_1^A h_{\alpha\bar{B}} + D_1^B h_{\alpha\bar{A}}) + G_5^H (D_1^A w_B + D_1^B w_A) \bar{w}_\alpha\} d\tau.
 \end{aligned} \tag{4.143}$$

The off-axis deflection hybrid distortion type of deflectors A and B:

$$\begin{aligned}
 U_{DEF}^{(iii)}[\gamma, A, \bar{B}; \bar{w}_H; \tau] &= \int_{\tau_o}^{\tau} \{G_1^H D_1'^A (w_\gamma \dot{w}_B - \dot{w}_\gamma \bar{w}_B) G_2^H \bar{D}_1'^B (w_\gamma \dot{w}_A + \dot{w}_\gamma w_A) \\
 &+ G_4^H D_1^A h_{\gamma\bar{B}} + G_5^H D_1^A w_\gamma \bar{w}_B + 2G_6^H \bar{D}_1'^B w_\gamma w_A\} d\tau, \\
 U_{DEF}^{(iii)}[\gamma, B, \bar{A}; \bar{w}_H; \tau] &= \int_{\tau_o}^{\tau} \{G_1^H D_1'^B (w_\gamma \dot{w}_A - \dot{w}_\gamma \bar{w}_A) + G_2^H \bar{D}_1'^A (w_\gamma \dot{w}_B + \dot{w}_\gamma w_B) \\
 &+ G_4^H D_1^B h_{\gamma\bar{A}} + G_5^H D_1^B w_\gamma \bar{w}_A + 2G_6^H \bar{D}_1'^A w_\gamma w_B\} d\tau, \\
 U_{DEF}^{(iii)}[A, B, \bar{\gamma}; \bar{w}_H; \tau] &= \int_{\tau_o}^{\tau} \{G_1^H \{D_1'^A (\dot{w}_\gamma w_B - \bar{w}_\gamma \dot{w}_B) + D_1'^B (\dot{w}_\gamma w_A - \bar{w}_\gamma \dot{w}_A)\} \\
 &+ G_4^H (D_1^A h_{\gamma\bar{B}} + D_1^B h_{\gamma\bar{A}}) + G_5^H (D_1^A w_B + D_1^B w_A) \bar{w}_\gamma\} d\tau.
 \end{aligned} \tag{4.144}$$

The deflection hybrid distortion type of deflectors A and B:

$$\begin{aligned}
 U_{DEF}^{(iii)}[A, A, \bar{B}; \bar{w}_H; \tau] &= \int_{\tau_o}^{\tau} \{G_1^H D_1'^A (w_A \dot{w}_B - \dot{w}_A \bar{w}_B) + G_2^H \bar{D}_1'^B w_A \dot{w}_A + G_4^H D_1^A h_{A\bar{B}} \\
 &+ G_5^H D_1^A w_A \bar{w}_B + G_6^H \bar{D}_1'^B w_A^2\} d\tau, \\
 U_{DEF}^{(iii)}[A, B, \bar{A}; \bar{w}_H; \tau] &= \int_{\tau_o}^{\tau} \{G_1^H \{D_1'^A (\dot{w}_A w_B - \bar{w}_A \dot{w}_B) + D_1'^B (w_A \dot{w}_A - \dot{w}_A \bar{w}_A)\} \\
 &+ G_2^H \bar{D}_1'^A (w_A \dot{w}_B + \dot{w}_A w_B) + G_4^H (D_1^A h_{A\bar{B}} + D_1^B h_{A\bar{A}}) \\
 &+ G_5^H (D_1^A w_B + D_1^B w_A) \bar{w}_A + 2G_6^H \bar{D}_1'^A w_A w_B\} d\tau, \\
 U_{DEF}^{(iii)}[A, B, \bar{B}; \bar{w}_H; \tau] &= \int_{\tau_o}^{\tau} \{G_1^H \{D_1'^A (w_B \dot{w}_B - \dot{w}_B \bar{w}_B) + D_1'^B (w_A \dot{w}_B - \dot{w}_A \bar{w}_B)\} \\
 &+ G_2^H \bar{D}_1'^B (w_A \dot{w}_B + \dot{w}_A w_B) + G_4^H (D_1^A h_{B\bar{B}} + F_1'^B h_{A\bar{B}}) \\
 &+ G_5^H (D_1^A w_B + D_1^B w_A) \bar{w}_B + 2G_6^H \bar{D}_1'^B w_A w_B\} d\tau, \\
 U_{DEF}^{(iii)}[B, B, \bar{A}; \bar{w}_H; \tau] &= \int_{\tau_o}^{\tau} \{G_1^H D_1'^B (\dot{w}_A w_B - \bar{w}_A \dot{w}_B) + G_2^H \bar{D}_1'^A w_B \dot{w}_B + G_4^H D_1^B h_{A\bar{B}} \\
 &+ G_5^H D_1^B \bar{w}_A w_B + G_6^H \bar{D}_1'^A w_B^2\} d\tau.
 \end{aligned} \tag{4.145}$$

The four-fold deflection hybrid astigmatism of deflectors A and B:

$$U_{4F}^{(iii)}[\bar{\alpha}, \bar{A}, \bar{B}; \bar{w}_H; \tau] = \zeta_o \int_{\tau_o}^{\tau} 2G_3^H (D_3^A \bar{w}_B + D_3^B \bar{w}_A) \bar{w}_\alpha d\tau \tag{4.146}$$

The four-fold off-axis deflection hybrid distortion of deflectors A and B:

$$U_{4F}^{(iii)}[\bar{\gamma}, \bar{A}, \bar{B}; \bar{w}_H; \tau] = \int_{\tau_o}^{\tau} 2G_3^H (D_3^A \bar{w}_B + D_3^B \bar{w}_A) \bar{w}_\gamma d\tau \tag{4.147}$$

The four-fold deflection hybrid distortion of deflectors A and B:

$$\begin{aligned}
 U_{4F}^{(iii)}[\bar{A}, \bar{A}, \bar{B}; \bar{w}_H; \tau] &= \int_{\tau_o}^{\tau} G_3^H (2D_3^A \bar{w}_B + D_3^B \bar{w}_A) \bar{w}_A d\tau, \\
 U_{4F}^{(iii)}[\bar{A}, \bar{B}, \bar{B}; \bar{w}_H; \tau] &= \int_{\tau_o}^{\tau} G_3^H (D_3^A \bar{w}_B + 2D_3^B \bar{w}_A) \bar{w}_B d\tau.
 \end{aligned} \tag{4.148}$$

4.7.2 Expression of third-order geometrical aberration coefficients

Since the third-order geometrical aberration is a value of the path deviation, Eq. (4.81), which is evaluated in the image plane, the aberration coefficients, which are defined in the object plane, are obtained by evaluating Eqs. (4.82) and (4.83) at the convergent reduced time τ_i and dividing by w_{yi} :

$$\begin{aligned}\hat{w}_{\text{geo.}}^{(3)}(z_i) &= \sum \hat{w}_{KL\bar{M}}(z_i) P_K P_L \bar{P}_M + \sum \hat{w}_{\bar{a}\bar{b}\bar{c}}(z_i) \bar{P}_a \bar{P}_b \bar{P}_c \\ &= w_{yi} \left[\sum C_{KL\bar{M}o} P_K P_L \bar{P}_M + \sum C_{\bar{a}\bar{b}\bar{c}o} \bar{P}_a \bar{P}_b \bar{P}_c \right],\end{aligned}\quad (4.149)$$

where $C_{KL\bar{M}o}$ is normal-type aberration coefficient and $C_{\bar{a}\bar{b}\bar{c}o}$ is the four-fold type aberration coefficient defined in the object plane.

Since $w_{ai} = 0$, we find general form of the third-order geometrical aberration coefficients for a system of focusing round symmetric fields and deflector fields, defined in the object plane, as follows.

For focusing round symmetric fields and the dipole component of deflector fields, we find the normal-type deflection aberration coefficients:

$$C_{KL\bar{M}o} = U_{RL}[K, L, \bar{M}; \bar{w}_\alpha; \tau_i] + U_{DEF}^{(s)}[K, L, \bar{M}; \bar{w}_\alpha; \tau_i] - \frac{1}{w_{yi}} R[K, L, \bar{M}; \tau_i]. \quad (4.150)$$

For focusing round symmetric fields, the dipole component, and the hexapole component of the deflector fields, that is called the four-fold type aberration, we find:

$$C_{\bar{a}\bar{b}\bar{c}o} = U_{4F}^{(s)}[\bar{a}, \bar{b}, \bar{c}; \bar{w}_\alpha; \tau_i]. \quad (4.151)$$

Note that, in Eqs. (4.150) and (4.151), the upper limit of the integrals U_{RL} , $U_{DEF}^{(s)}$, and $U_{4F}^{(s)}$ is the convergent reduced time τ_i , and the boundary term $R[K, L, \bar{M}; \tau_i]$ is evaluated at τ_i . These integrals and the boundary term evaluated at a general reduced time are given in Eqs. (4.84) to (4.148) according to the possible combination of parameters and deflector-type combinations.

Once aberration coefficients defined in the object plane are obtained, we can recast them as those defined in the image plane and those dependent on lateral beam shifts by deflection in the image plane, which are discussed in section 3.5.

Eq. (4.149) is expressed as follows:

$$\hat{w}_{\text{geo.}}^{(3)}(z_i) = \sum C_{KL\bar{M}i} P_K^i P_L^i \bar{P}_M^i + \sum C_{\bar{a}\bar{b}\bar{c}i} \bar{P}_a^i \bar{P}_b^i \bar{P}_c^i, \quad (4.152)$$

where $C_{KL\bar{M}i}$ and $C_{\bar{a}\bar{b}\bar{c}i}$ are the aberration coefficients defined in the image plane and dependent on the beam shift by deflection for the deflection aberration. The parameter P_K^i is defined in the image plane and it takes one of

$$\begin{aligned}
s_i &= \frac{\dot{\zeta}_o}{\dot{\zeta}_i} \dot{w}_{\alpha i} w_o', \\
w_i^{(1)} &= w_{\gamma i} w_o, \\
BS_A &= w_{Ai} S_A, \\
BS_B &= w_{Bi} S_B,
\end{aligned} \tag{4.153}$$

where s_i is the complex landing slope of the axial paraxial trajectory, $w_i^{(1)}$ is the complex off-axis landing point, BS_A and BS_B are the complex beam shift by deflector A and B, in the image plane, respectively. The transformation factor is given by

$$\begin{aligned}
f[K] &= \left(\frac{\dot{\zeta}_i}{\dot{\zeta}_o \dot{w}_{\alpha i}} \right)^{\delta_{K,\alpha}} \left(\frac{1}{w_{\gamma i}} \right)^{\delta_{K,\gamma}} \left(\frac{1}{w_{Ai}} \right)^{\delta_{K,A}} \left(\frac{1}{w_{Bi}} \right)^{\delta_{K,B}}, \\
\bar{f}[\bar{M}] &= \left(\frac{\dot{\zeta}_i}{\dot{\zeta}_o \dot{w}_{\alpha i}} \right)^{\delta_{\bar{M},\bar{\alpha}}} \left(\frac{1}{\bar{w}_{\gamma i}} \right)^{\delta_{\bar{M},\gamma}} \left(\frac{1}{\bar{w}_{Ai}} \right)^{\delta_{\bar{M},\bar{A}}} \left(\frac{1}{\bar{w}_{Bi}} \right)^{\delta_{\bar{M},\bar{B}}},
\end{aligned} \tag{4.154}$$

where $\delta_{K,D}$ is a Kronecker's delta, that is, $\delta_{D,D} = 1$ and $\delta_{K \neq D,D} = 0$. For example, when $K = \gamma$, in $f[\gamma]$, the Kronecker's deltas are $\delta_{\gamma,\alpha} = 0$, $\delta_{\gamma,\gamma} = 1$, $\delta_{\gamma,A} = 0$, $\delta_{\gamma,B} = 0$, and $f[\gamma] = 1/w_{\gamma i}$. Using Eq. (4.154), the third-order geometrical aberration coefficients, which are defined in the image plane and dependent on the beam shifts by deflectors, are transformed as follows:

$$\begin{aligned}
C_{KL\bar{M}i} &= w_{\gamma i} f[K] f[L] \bar{f}[\bar{M}] C_{KL\bar{M}o}, \\
C_{\bar{a}\bar{b}\bar{c}i} &= w_{\gamma i} \bar{f}[\bar{a}] \bar{f}[\bar{b}] \bar{f}[\bar{c}] C_{\bar{a}\bar{b}\bar{c}o}.
\end{aligned} \tag{4.155}$$

In the end of this section, we are at the point where we have derived the general formulae of the third-order geometrical path deviation and the aberration coefficients including round symmetric fields and deflection fields.

4.8 Path deviation for variation of voltages and currents of rotationally symmetric electrodes and coils with deflection fields

Here, we derive the path deviation of the time-dependent theory, which is induced by the variation of voltages and currents of rotationally symmetric electrodes and coils with deflection fields. The On- and off-axis aberration coefficients of the variation of voltages and currents, which are discussed in the rotation coordinate system, are derived in section 2.9. We expanded it to the system with deflection fields in the Cartesian coordinate system. The discussion from the beginning to Eq. (2.322) in section 2.9 should be repeated in this section. We can use the result of Eqs. (2.304) to (2.322) directly.

In the lateral direction, the primary perturbation function by the variation of voltages and currents is the second-rank terms of parameters. We find:

$$\begin{aligned}
P_w^{(2)} \text{ var.} = & \sum_{j=1}^N \kappa_{ELj} \left[-\frac{\Phi^{[3]}}{4\Phi_C} w^{(1)} h_{V_j} - \frac{\Phi_j''}{4\Phi_C} w^{(1)} + \frac{i\eta}{2\sqrt{\Phi_C}} \left\{ \frac{d}{d\tau} (B' w^{(1)} h_{V_j}) + B' \dot{w}^{(1)} h_{V_j} \right\} \right. \\
& \left. + \frac{F_1'}{2\Phi_C} V h_{V_j} + \frac{\eta}{\sqrt{\Phi_C}} \frac{d}{d\tau} (ID_1 h_{V_j}) \right] + \sum_{\ell=1}^L \kappa_{ML\ell} \frac{i\eta}{2\sqrt{\Phi_C}} \left\{ B_\ell \dot{w}^{(1)} + \frac{d}{d\tau} (B_\ell w^{(1)}) \right\},
\end{aligned} \quad (4.156)$$

where the variation parameters are given by

$$\begin{aligned}
\kappa_{ELj} &= \frac{\Delta V_{ELj}}{V_{ELj}}, \\
\kappa_{ML\ell} &= \frac{\Delta I_{ML\ell}}{I_{ML\ell}},
\end{aligned} \quad (4.157)$$

and V_{ELj} is the voltage imposed on the j -th round symmetric electrode, and $I_{ML\ell}$ is current of the ℓ -th round symmetric coil. h_{V_j} is the first-order solution of longitudinal path deviation induced by the variation of the voltage of the j -th electrode and is given by Eq. (2.320) or Eq. (2.321). Φ_j and B_ℓ are the axial potential distribution and the axial magnetic field distribution generated by the j -th round symmetric electrode and the ℓ -th round symmetric coil, respectively.

Using Eq. (4.156) and Eqs. (4.31) to (4.34), we find:

$$\begin{aligned}
\int_{\tau_0}^{\tau} [P_1^{(2)} \text{ var.} \bar{w}_H + P_2^{(2)} \text{ var.} \dot{\bar{w}}_H] d\tau = & \sum_{j=1}^N \kappa_{ELj} \left\{ \int_{\tau_0}^{\tau} \left[\left(\frac{\Phi^{[3]}}{4\Phi_C} h_{V_j} + \frac{\Phi_j''}{4\Phi_C} \right) \bar{w}_H w^{(1)} - \frac{F_1'}{2\Phi_C} V \bar{w}_H h_{V_j} \right. \right. \\
& \left. \left. + \frac{i\eta B'}{2\sqrt{\Phi_C}} (\dot{\bar{w}}_H w^{(1)} - \bar{w}_H \dot{w}^{(1)}) h_{V_j} + \frac{\eta}{\sqrt{\Phi_C}} ID_1 \dot{\bar{w}}_H h_{V_j} \right] d\tau \right\} \\
& + \sum_{\ell=1}^M \kappa_{ML\ell} \int_{\tau_0}^{\tau} \frac{i\eta B_\ell}{2\sqrt{\Phi_C}} (\dot{\bar{w}}_H w^{(1)} - \bar{w}_H \dot{w}^{(1)}) d\tau,
\end{aligned} \quad (4.158)$$

where the subscript H of \bar{w}_H is either α or γ , and

$$-P_{2o}^{(2)} \text{ var.} w_\alpha = - \sum_{\ell=1}^M \kappa_{ML\ell} \frac{i\eta B_{\ell o}}{2\sqrt{\Phi_C}} w_o w_\alpha. \quad (4.159)$$

By Eqs. (4.36) and (2.319), in this case, the transformation of the path deviation, evaluated at time t to that evaluated in a plane, is given by

$$\hat{w}^{(2)}(z) = w^{(2)} - w'^{(1)}(z) h^{(1)}(z) = w^{(2)}(z) - \sum_{j=1}^N \kappa_{ELj} \frac{1}{\xi} \dot{w}^{(1)} h_{V_j}. \quad (4.160)$$

Using Eq. (4.37), we find the second-rank path deviation in an arbitrary plane z :

$$\begin{aligned}
\hat{w}^{(2)}(z) = & \left(w_\gamma(\tau) + 2i\dot{\chi}_o w_\alpha(\tau) \right) \int_{\tau_0}^{\tau} \left\{ P_1^{(2)} \text{ var.} \bar{w}_\alpha + P_2^{(2)} \text{ var.} \dot{\bar{w}}_\alpha \right\} d\tau \\
& - w_\alpha(\tau) \int_{\tau_0}^{\tau} \left\{ P_1^{(2)} \text{ var.} \bar{w}_\gamma + P_2^{(2)} \text{ var.} \dot{\bar{w}}_\gamma \right\} d\tau - P_{2o}^{(2)} \text{ var.} w_\alpha - \sum_{j=1}^N \kappa_{ELj} \frac{1}{\xi} \dot{w}^{(1)} h_{V_j}.
\end{aligned} \quad (4.161)$$

The path deviation is recast in the following general form:

$$\hat{w}^{(2)}(z) = \sum_{j=1}^N \kappa_{ELj} \sum \hat{w}_{K,j}^{ELwob}(z) P_K + \sum_{\ell=1}^L \kappa_{MLj} \sum \hat{w}_{K,\ell}^{MLwob}(z) P_K, \quad (4.162)$$

Where the subscript K takes one of α, γ, e and m , then the parameter P_K takes w'_o, w_o, V_{DEF} and I_{DEF} . Note that, V_{DEF} and I_{DEF} are the voltage and current of the electrostatic deflector and the magnetic deflector, respectively.

The path deviation component of the voltage variation of the j -th electrode, for the parameter P_K , is given by

$$\hat{w}_{K,j}^{ELwob} = \dot{\zeta}_o^{\delta_{K,\alpha}} \left[(w_\gamma + 2i\dot{\chi}_o w_\alpha) Q_j^{ELwob}[K, \bar{\alpha}; \tau] - w_\alpha Q_j^{ELwob}[K, \bar{\gamma}; \tau] - \frac{1}{\dot{\zeta}} \dot{w}_K h_{V_j} \right], \quad (4.163)$$

where

$$\begin{aligned} & Q_j^{ELwob}[K, \bar{H}; \tau] \\ &= \int_{\tau_o}^{\tau} \left[\left(\frac{\Phi^{[3]}}{4\Phi_C} h_{V_j} + \frac{\Phi_j''}{4\Phi_C} \right) w_K \bar{w}_H + \frac{i\eta B'}{2\sqrt{\Phi_C}} (w_K \dot{\bar{w}}_H - \dot{w}_K \bar{w}_H) h_{V_j} \right. \\ & \quad \left. - \delta_{K,e} \frac{F_1'}{2\Phi_C} \bar{w}_H h_{V_j} + \delta_{K,m} \frac{\eta D_1}{\sqrt{\Phi_C}} \dot{\bar{w}}_H h_{V_j} \right] d\tau, \end{aligned} \quad (4.164)$$

where H is either α or γ for the subscript of \bar{w}_H and $\dot{\bar{w}}_H$, and $\delta_{K,L}$ means the Kronecker's delta.

The path deviation component of the current variation of the ℓ -th coil, for the parameter P_K , is given by

$$\begin{aligned} \hat{w}_{K,\ell}^{MLwob} &= \dot{\zeta}_o^{\delta_{K,\alpha}} \left[(w_\gamma + 2i\dot{\chi}_o w_\alpha) Q_\ell^{MLwob}[K, \bar{\alpha}; \tau] - w_\alpha Q_\ell^{MLwob}[K, \bar{\gamma}; \tau] \right. \\ & \quad \left. - \delta_{K,\gamma} \frac{i\eta B_{\ell o}}{2\sqrt{\Phi_C}} w_\alpha \right], \end{aligned} \quad (4.165)$$

where

$$Q_\ell^{MLwob}[K, \bar{H}; \tau] = \int_{\tau_o}^{\tau} \frac{i\eta B_\ell}{2\sqrt{\Phi_C}} (w_K \dot{\bar{w}}_H - \dot{w}_K \bar{w}_H) d\tau. \quad (4.166)$$

Since the aberration is the value of the path deviation in the image plane, by Eqs. (4.162) to (4.165), the aberration coefficient of the voltage variation of the j -th electrode, for the parameter P_K , which is defined in the object plane, is given by

$$C_{Ko,j}^{ELwob} = \dot{\zeta}_o^{\delta_{K,\alpha}} \left(Q_j^{ELwob}[K, \bar{\alpha}; \tau_i] - \frac{1}{\dot{\zeta}_i} \frac{\dot{w}_{Ki}}{w_{yi}} h_{V_{ji}} \right), \quad (4.167)$$

and the aberration coefficient of the current variation of the ℓ -th coil, for the parameter P_K , which is defined in the object plane, is given by

$$C_{Ko,\ell}^{MLwob} = \dot{\zeta}_o^{\delta_{K,\alpha}} Q_\ell^{MLwob}[K, \bar{\alpha}; \tau_i]. \quad (4.168)$$

In this section, we are at the point where the path deviation and aberration coefficients of the time-dependent deflection theory, which are induced by the variation of the voltage and current of round symmetric electrodes and lens-coils, have been derived.

4.9 Time-dependent deflection path deviation for the inclined incident beam

In this section, we discuss the path deviation formula for an inclined incident beam. Since the fundamental lateral off-axis ray w_γ is defined such that, its initial reduced velocity is zero, w_γ starts parallel to the optic axis in the object plane. To analyze the optical system of an SEM, as long as we ignore off-axis aberration caused by the electron virtual source size, off-axis path deviation can be used for estimating the aberration of a beam, whose central trajectory starts at an off-axis position in the object plane. However, derived the off-axis path deviation in sections 4.5 to 4.8 is only applicable to a beam, whose central trajectory starts parallel to the optic axis, directly. In general, the central trajectory of a beam is inclined with respect to the optic axis and starts at an off-axis point in the object plane. This consideration has been already discussed in section 2.11, for the time-dependent theory in the rotation coordinate system. Here we can repeat the discussion from the beginning of section 2.11 to Eq. (2.365). The only difference is that, in this section, we use the Cartesian coordinate system. Therefore, the complex normalized initial slope λ_o of Eq. (2.365), which is defined in the rotation coordinate system, and means the initial slope of the central trajectory per off-axis distance of the central trajectory in the object plane, is replaced by that defined in the Cartesian coordinate system. Note that, as long as the object plane is located in the rotationally symmetric magnetic field-free space, the complex normalized initial slope of the rotation coordinate system is exactly the same as that in the Cartesian coordinate system. In this section, hereafter, we use λ_o as the complex normalized initial slope in the Cartesian coordinate system. For simplicity, a beam tilt angle t_o in the object plane is not considered. By this consideration, the initial slope of an electron, in the object plane, is given by $w'_o = s_o + \lambda_o w_o$, where $\lambda_o w_o$ is the initial complex slope of the central trajectory of the beam, which is assumed to be proportional to the off-axis position in the object plane, with respect to the optic axis, and s_o is the initial complex slope of a general electron of the beam, with respect to the central trajectory of the beam in the object plane, see Fig. 2.5. Then, when we consider the path deviation, the geometrical parameter of the initial slope changes from that with respect to the optic axis, w'_o to that with respect to the central trajectory of the beam, s_o . Since w'_o is transformed into $s_o + \lambda_o w_o$, the path deviation formulae, whose parameter dependence includes w_o , are modified. The formulae of the other path deviation, which are independent of w_o , are not changed. Employing the same consideration as section 2.11, for the second-rank path deviation, and the path deviation induced by the variation of voltages and currents, only the off-axis type path deviation formulae are modified by the complex normalized initial slope. We give a list of modified formulae in Table 4.4.

Table 4.4 List of second-rank and variation of voltages and currents off-axis path deviation formulae for the inclined incident beam

Path deviation	Dependence	Formula
Off-axis chromatic	$w_o K_o$	$\hat{w}_{\gamma K} + \lambda_o \hat{w}_{\alpha K}$
Off-axis variation of voltage	$w_o K_{ELj}$	$\hat{w}_{\gamma,j}^{ELwob} + \lambda_o \hat{w}_{\alpha,j}^{ELwob}$
Off-axis variation of current	$w_o K_{ML\ell}$	$\hat{w}_{\gamma,\ell}^{MLwob} + \lambda_o \hat{w}_{\alpha,\ell}^{MLwob}$

For the third-order geometrical path deviation, the modified path deviation type totals 22 for the normal type and 7 for the four-fold type. We give the lists of the modified path deviation formulae of the normal type in Table 4.5, and those of the four-fold type in Table 4.6.

Table 4.5 List of third-order geometrical off-axis-deflection path deviation formulae for the inclined incident beam

Path deviation	Aberration Type	Dependence	Formula
Coma-length	OA.	$w_o S_o \bar{S}_o$	$\hat{w}_{\alpha\gamma\bar{\alpha}} + 2\lambda_o \hat{w}_{\alpha\alpha\bar{\alpha}}$
Coma-radius	OA.	$\bar{w}_o S_o^2$	$\hat{w}_{\alpha\alpha\bar{\gamma}} + \bar{\lambda}_o \hat{w}_{\alpha\alpha\bar{\alpha}}$
Field curvature	OA.	$w_o \bar{w}_o S_o$	$\hat{w}_{\alpha\gamma\bar{\gamma}} + 2\lambda_o \hat{w}_{\alpha\alpha\bar{\gamma}}$ $+ \bar{\lambda}_o \hat{w}_{\alpha\gamma\bar{\alpha}} + 2\lambda_o \bar{\lambda}_o \hat{w}_{\alpha\alpha\bar{\alpha}}$
	OA.-Def.	$\bar{w}_o S_A S_o$	$\hat{w}_{\alpha A \bar{\gamma}} + \bar{\lambda}_o \hat{w}_{\alpha A \bar{\alpha}}$
	OA.-Def.	$\bar{w}_o S_B S_o$	$\hat{w}_{\alpha B \bar{\gamma}} + \bar{\lambda}_o \hat{w}_{\alpha B \bar{\alpha}}$
	OA.-Def.	$w_o \bar{S}_A S_o$	$\hat{w}_{\alpha\gamma\bar{A}} + 2\lambda_o \hat{w}_{\alpha\alpha\bar{A}}$
Astigmatism	OA.-Def.	$w_o \bar{S}_B S_o$	$\hat{w}_{\alpha\gamma\bar{B}} + 2\lambda_o \hat{w}_{\alpha\alpha\bar{B}}$
	OA.	$w_o^2 \bar{S}_o$	$\hat{w}_{\gamma\gamma\bar{\alpha}} + \lambda_o \hat{w}_{\alpha\gamma\bar{\alpha}} + \lambda_o^2 \hat{w}_{\alpha\alpha\bar{\alpha}}$
	OA.-Def.	$w_o S_A \bar{S}_o$	$\hat{w}_{\gamma A \bar{\alpha}} + \lambda_o \hat{w}_{\alpha A \bar{\alpha}}$
	OA.-Def.	$w_o S_B \bar{S}_o$	$\hat{w}_{\gamma B \bar{\alpha}} + \lambda_o \hat{w}_{\alpha B \bar{\alpha}}$
Distortion	OA.	$w_o^2 \bar{w}_o$	$\hat{w}_{\gamma\gamma\bar{\gamma}} + \lambda_o \hat{w}_{\alpha\gamma\bar{\gamma}}$ $+ \hat{w}_{\gamma\gamma\bar{\alpha}} \bar{\lambda}_o + \lambda_o \bar{\lambda}_o \hat{w}_{\alpha\gamma\bar{\alpha}}$ $+ \lambda_o^2 \hat{w}_{\alpha\alpha\bar{\gamma}} + \lambda_o^2 \bar{\lambda}_o \hat{w}_{\alpha\alpha\bar{\alpha}}$
	OA.-Def.	$w_o \bar{w}_o S_A$	$\hat{w}_{\gamma A \bar{\gamma}} + \lambda_o \hat{w}_{\alpha A \bar{\gamma}}$ $+ \bar{\lambda}_o \hat{w}_{\gamma A \bar{\alpha}} + \lambda_o \bar{\lambda}_o \hat{w}_{\alpha A \bar{\alpha}}$
	OA.-Def.	$w_o^2 \bar{S}_A$	$\hat{w}_{\gamma\gamma\bar{A}} + \lambda_o \hat{w}_{\alpha\gamma\bar{A}} + \lambda_o^2 \hat{w}_{\alpha\alpha\bar{A}}$
	OA.-Def.	$w_o S_A \bar{S}_A$	$\hat{w}_{\gamma A \bar{A}} + \lambda_o \hat{w}_{\alpha A \bar{A}}$
	OA.-Def.	$\bar{w}_o S_A^2$	$\hat{w}_{AA\bar{\gamma}} + \bar{\lambda}_o \hat{w}_{AA\bar{\alpha}}$
	OA.-Def.	$w_o \bar{w}_o S_B$	$\hat{w}_{\gamma B \bar{\gamma}} + \lambda_o \hat{w}_{\alpha A \bar{\gamma}}$ $+ \bar{\lambda}_o \hat{w}_{\gamma B \bar{\alpha}} + \lambda_o \bar{\lambda}_o \hat{w}_{\alpha B \bar{\alpha}}$
	OA.-Def.	$w_o^2 \bar{S}_B$	$\hat{w}_{\gamma\gamma\bar{B}} + \lambda_o \hat{w}_{\alpha\gamma\bar{B}} + \lambda_o^2 \hat{w}_{\alpha\alpha\bar{B}}$
	OA.-Def.	$w_o S_B \bar{S}_B$	$\hat{w}_{\gamma B \bar{B}} + \lambda_o \hat{w}_{\alpha B \bar{B}}$
	OA.-Def.	$\bar{w}_o S_B^2$	$\hat{w}_{BB\bar{\gamma}} + \bar{\lambda}_o \hat{w}_{BB\bar{\alpha}}$
	OA.-Def. hybrid	$w_o S_A \bar{S}_B$	$\hat{w}_{\gamma A \bar{B}} + \lambda_o \hat{w}_{\alpha A \bar{B}}$
	OA.-Def. hybrid	$w_o S_B \bar{S}_A$	$\hat{w}_{\gamma B \bar{A}} + \lambda_o \hat{w}_{\alpha B \bar{A}}$
	OA.-Def. hybrid	$\bar{w}_o S_A \bar{S}_B$	$\hat{w}_{AB\bar{\gamma}} + \bar{\lambda}_o \hat{w}_{AB\bar{\alpha}}$

Table 4.6 List of Four-fold off-axis-deflection path deviation formulae for the inclined incident beam

Path deviation	Aberration Type	Dependence	Formula
Astigmatism	OA.-Def.	$\bar{w}_o \bar{S}_A \bar{S}_o$	$\hat{w}_{\bar{\alpha}\bar{\gamma}\bar{A}} + 2\bar{\lambda}_o \hat{w}_{\bar{\alpha}\bar{\alpha}\bar{A}}$
	OA.-Def.	$\bar{w}_o \bar{S}_B \bar{S}_o$	$\hat{w}_{\bar{\alpha}\bar{\gamma}\bar{B}} + 2\bar{\lambda}_o \hat{w}_{\bar{\alpha}\bar{\alpha}\bar{B}}$
Distortion	OA.-Def.	$\bar{w}_o^2 \bar{S}_A$	$\hat{w}_{\bar{\gamma}\bar{\gamma}\bar{A}} + \bar{\lambda}_o \hat{w}_{\bar{\alpha}\bar{\gamma}\bar{A}} + \bar{\lambda}_o^2 \hat{w}_{\bar{\alpha}\bar{\alpha}\bar{A}}$
	OA.-Def.	$\bar{w}_o^2 \bar{S}_B$	$\hat{w}_{\bar{\gamma}\bar{\gamma}\bar{B}} + \bar{\lambda}_o \hat{w}_{\bar{\alpha}\bar{\gamma}\bar{B}} + \bar{\lambda}_o^2 \hat{w}_{\bar{\alpha}\bar{\alpha}\bar{B}}$
	OA.-Def.	$\bar{w}_o \bar{S}_A^2$	$\hat{w}_{\bar{\gamma}\bar{A}\bar{A}} + \bar{\lambda}_o \hat{w}_{\bar{\alpha}\bar{A}\bar{A}}$
	OA.-Def.	$\bar{w}_o \bar{S}_B^2$	$\hat{w}_{\bar{\gamma}\bar{B}\bar{B}} + \bar{\lambda}_o \hat{w}_{\bar{\alpha}\bar{B}\bar{B}}$
	OA.-Def. hybrid	$\bar{w}_o \bar{S}_A \bar{S}_B$	$\hat{w}_{\bar{\gamma}\bar{A}\bar{B}} + \bar{\lambda}_o \hat{w}_{\bar{\alpha}\bar{A}\bar{B}}$

In this section, we are at the point where the off-axis path deviation formulae for a beam, whose central trajectory starts at an off-axis position and is inclined with respect to the optic axis, in the object plane, are obtained. The modified off-axis path deviation formulae are given by linear combinations of the unmodified path deviation formulae and their coefficients are given by the power of the complex normalized initial slope and its complex conjugate.

4.10 Conclusion

In this chapter, we discussed the non-relativistic time-dependent deflection theory based on the consideration in Chapter 2: non-relativistic time-dependent aberration theory of round symmetric electrostatic and magnetic fields, and in Chapter 3: deflection aberration theory of standard electron optics, whose parameter is the coordinate of the optic axis. The time-dependent deflection theory can analyze path deviation with small angle deflectors. This theory is valid for a system composed of electrostatic and magnetic round symmetric fields and electrostatic and magnetic deflection fields, even when all field distributions overlap one another. Note that, as with usual deflection theory, we have discussed this in the Cartesian coordinate system.

We derived a series expansion of the electrostatic and magnetic deflection field and a general equation of motion. Fundamental solutions of the first-order approximated equations in the lateral and longitudinal directions are derived. Using fundamental lateral solutions, the so-called deflection trajectories, which are linearly dependent on voltages and currents of deflectors, were obtained.

We derived the second-rank chromatic path deviation in the lateral direction and the second-order geometrical longitudinal path deviation. Then, we derived the third order geometrical path deviation formulae. We derived the path deviation induced by the variation of voltages of round symmetric electrodes and currents of lens-coils. In addition, the off-axis path deviation formulae for a beam, whose central trajectory starts at an off-axis position and is inclined with respect to the optic axis, in the object plane, were derived. For all derived path deviations, we provided the aberration coefficients formulae for the corresponding path deviation.

One could add these formulae to field simulation programs such as MEBS, EOD, Opera, Lorentz, GPT, etc. Then, after calculating the fields of electron mirrors, electrostatic and magnetic lenses, and deflectors, and determining first-order trajectories and object and image planes, the program could return all aberration coefficients up to the third order. Users can determine which aberrations are going to limit the resolution or set requirements for the stability of the power supplies. Also, they can design a mirror geometry and determine voltages according to their purpose, for example, an aberration corrector.

Chapter 5 Conceptual design for an aberration corrected scanning electron microscope using miniature electron mirrors

The content of this chapter is a modified version of the article: H. Dohi, P. Kruit, "Design for an aberration corrected scanning electron microscope using miniature electron mirrors", Ultramicroscopy 189 (2018), pp.1-23.

5.1 Outline

In this chapter, we propose a novel aberration corrector using miniature electron mirrors for a low-voltage SEM. To use a miniature mirror aberration corrector, deflectors of a few degrees, which guide an incident electron beam to the mirrors and deflect the reflected electron beam back to the objective lens, are necessary. A concept and a possible configuration of an aberration corrector are proposed, and its dispersion properties are analyzed in section 5.2. In section 5.3, a possible configuration of an SEM with a novel corrector and a design example of a miniature electron mirror are suggested. The numerical calculation result of mirror aberrations is reported as well. In section 5.4, deflection aberrations of the deflectors and combination higher-rank aberrations, which are caused by aberrations of deflectors, mirrors, and the objective lens, are estimated and a wave optical calculation of the beam spot size, including all deflection and combination aberrations, is reported. In section 5.5, off-axis aberrations due to misalignment of mirrors are considered. Through these considerations, we predict the performance of an aberration corrected SEM using a proposed novel miniature aberration corrector.

5.2 Configuration of corrector system

5.2.1 Concept of double mirrors

The basic concept on which the aberration-corrector system is based is explained as follows. In the case of any mirror, if a beam separator is not present, the incident electron beam is reflected back in the direction of the electron source. Therefore, as shown in Fig. 1.4 in Chapter 1, the beam is typically deflected by a large angle, for example, 90 degrees, to deflect the incident beam to the mirror and the reflected beam to the objective lens. The large aberration due to the separator originates from the large bending angle of the beam deflection. To construct an aberration-corrector system without a separator, as illustrated in Fig. 5.1, it is necessary to use a second mirror to re-direct the beam back in the direction of the objective lens. Obviously, the beam has to pass the second mirror on its way to the first mirror.

Therefore, the concept hinges on the ability to fabricate micro-scale mirrors with electrodes that can be shielded from the passing beam.

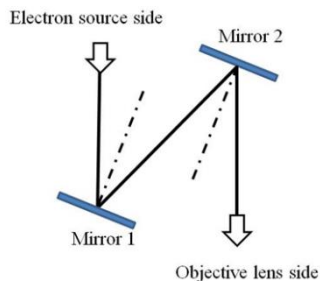


Fig. 5.1. Double reflection by a double mirror.

5.2.2 Concept of small-angle-deflection system with beam shift: S-corrector

Inclined double mirrors are not suitable for a practical optical system because the mirrors must be inclined at an angle of at least a few degrees to keep sufficient space between the two mirrors. Accordingly, the incident beam is tilted by a few degrees to the normal axis of the mirror, causing large off-axis aberrations. Therefore, the mirrors should be placed perpendicular to the central axis of the incident beam, namely, the optic axis. In this case, a deflection system is necessary to separate the reflected beam from the incident beam. Many configurations of double micro-mirrors and small-angle deflectors to guide the beam to the objective lens, as shown in Fig. 5.1, can be considered. To explain the principles of the concept and calculate aberrations, the configuration shown in Fig. 5.2, namely, a schematic cross-section of a basic small-angle beam-deflection system and the trajectory of the electrons along the optic axis, is adopted in the present study.

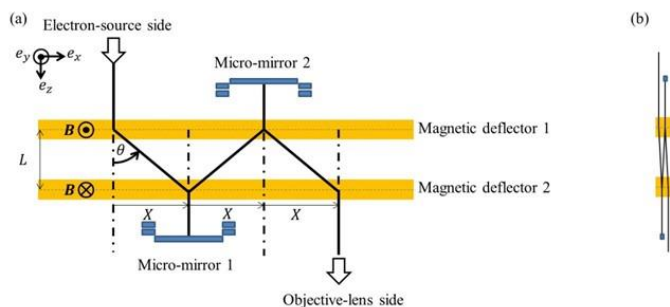


Fig. 5.2. Schematic cross-section of the basic beam-deflection system: S-corrector. The black line shows the central trajectory of the beam. Two magnetic deflectors, comprising an anti-symmetric double deflector, generate opposite magnetic fields. The opposite deflections of the double deflector cause a lateral shift in the beam by a distance X so that the beam is directed along the central axes of the micro-mirrors and reflected. After the second reflection, the double deflector shifts the beam again and directs it to the objective lens. The total lateral beam shift is $3X$. (a) The transverse scale is adequately magnified to make the configuration clear and (b) transverse scale and longitudinal scale are identical and the ratio $X/L = 1/20$.

The above-described beam-deflection system consists of two identical magnetic deflectors separated by a pitch L in the longitudinal direction and two round symmetric micro-mirrors. For simplicity, the spaces between the two deflectors and mirrors are assumed to be field-free. The pair of deflectors generates opposite magnetic fields, so it is called an “anti-symmetric double deflector”. Incident electrons traveling along the optic axis are deflected at a small angle θ by the first deflector and deflected back at the opposite angle by the second deflector. As a result, the electron-beam trajectory is shifted horizontally by distance X from the original optic axis, where $X = L \tan \theta \approx L \theta$. The lateral distance between the first mirror and the original optic axis of the incident beam is X so that the electron beam is traveling along the axis of the first mirror. The reflected electron beam is then directed to the second mirror by the deflector doublet and is reflected again. After that, the electron beam is deflected by the deflector doublet once more. At the exit of the deflection system, the position of the outgoing beam is located at a lateral distance from the optic axis of the original incident beam by $3X$. This system is called an “S-corrector,” since the trajectory of the center of the beam looks like a transverse S.

An example of the geometry of the S-corrector and the operational conditions of an LV-SEM are explained as follows. The lateral distance between the mirror and the incident optic axis is given as $X = 0.5$ mm, the pitch between the two deflectors as $L = 10$ mm, and the deflection angle as $\theta = 50$ mrad ($\approx 2.86^\circ$), which is much smaller than the deflection angle of the standard beam separator (90°) shown in Fig. 1.4. in Chapter 1. The energy of the incident electron is 2–5

keV, the energy spread is less than 1 eV, and the probe current should be around 10 pA to keep the beam sufficiently coherent, but, from the point of view of mirror aberrations, it could also be larger.

Paraxial rays in the S-corrector are discussed in the following part of this section. Paraxial rays are two fundamental solutions of the paraxial equation, called an “axial ray” w_α and a “field ray” w_γ . Initial conditions are as follows: $w_{\alpha o} = 0, w'_{\alpha o} = 1, w_{\gamma o} = 1, w'_{\gamma o} = 0$, where subscript o means values in the object plane and prime means differentiation with respect to the coordinate of the optic axis. An axial ray intersects an optic axis at an object plane with a unit slope. This intersection is called an axial object point. A field ray is defined as a ray that is incident on a lens or a mirror parallel to the optic axis, but its initial position is located one unit distance away from the optic axis in the object plane. The field ray is the same as a principal ray of reference [1.68]. General paraxial rays are expressed as a linear combination of an axial ray and a field ray. To avoid confusion, a general axial ray w_α^G and a general field ray w_γ^G are defined as follows: $w_\alpha^G = w'_o w_\alpha$, $w_\gamma^G = w_o w_\gamma$, where w'_o and w_o are the initial slope and an initial lateral position with respect to the optic axis in the object plane. When considering crossover planes both for the object and the image, it is sufficient to limit the discussion to axial rays.

The relation between crossover planes of the S-corrector and those of the standard mirror corrector is as follows. In the conventional mirror corrector system, the object plane and image plane of the mirror coincide. That is, a reflected axial ray traces the same path as an incident axial ray in the opposite direction. As a result, in the case shown in Fig. 1.4. in Chapter 1, the axial ray is anti-symmetric with respect to the mid-plane of the separator, where the axis of the mirror is placed. Although, in fact, the initial slope of axial rays is defined as 1, the initial slope of the axial rays shown in Fig. 1.4. in Chapter 1 and other figures is appropriately changed to make them clear. When the axial ray is either symmetric or anti-symmetric, the second-order aberrations of the incident and reflected beams due to the separator are equivalent, apart from their signs (which depend on the symmetry).

Here, we also create symmetry in the double mirror system by setting the crossovers at the mid-plane of the anti-symmetric double deflector as shown in Fig. 5.3. This plane is named the “common crossover plane”. The axial rays inside the deflector doublet are anti-symmetric about this plane. The first virtual crossover (the point P_A in Fig. 5.3) can be set by using a proper condenser lens between the electron source and the S-corrector. Although the real object point of the incident beam to the first mirror (the point P_B) is not on the axis of the first mirror, the virtual object point (the point P_C) is on it. Similarly, the virtual object points of the second mirror and the objective lens are on their respective axes (the points P_D and P_E).

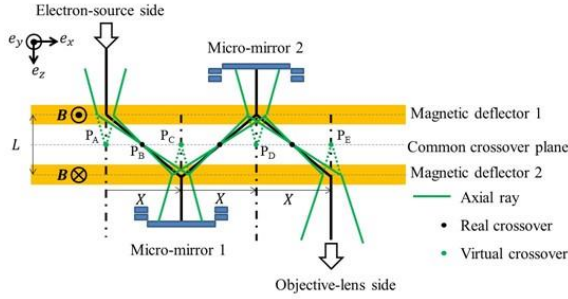


Fig. 5.3. Crossover plane and axial rays in the S-corrector. Green rays, black dots, and green dots represent axial rays, real crossovers, and virtual crossovers, respectively. The common crossover plane coincides with the mid-plane of the anti-symmetric double deflector. The virtual crossover points of the electron source, mirrors, and objective lens are the intersections of their axes with the common crossover plane. Note that the initial slopes of the shown axial rays are appropriately scaled to make them clear.

5.2.3 Dispersion of S-corrector

Since the energy dispersion of a deflection could be the largest aberration in LV-SEMs equipped with a deflection system, the first-rank dispersion of the S-corrector is considered as follows. Hereinafter, “dispersion” means a first-rank aberration⁵, which linearly depends on energy spread only, unless otherwise noted. To avoid confusion, dispersion is defined as two kinds: lateral dispersion and angular dispersion. Lateral dispersion is defined as the displacement of the central electron beam at different energies from the nominal energy at the conjugate plane of the source (and the sample). Angular dispersion is the difference between the slopes of the central electron beam at different energies from the nominal energy. A fully dispersion-free system should make both lateral and angular dispersions zero. This point is returned to in more detail at the end of this section.

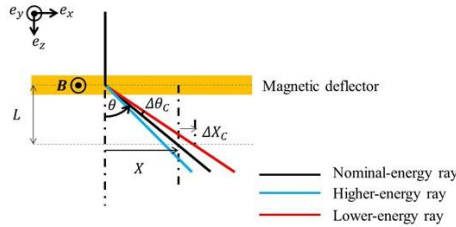


Fig. 5.4. Energy-dispersed rays deflected by a single deflector. The black ray represents the trajectory of nominal energy electrons. The blue and red rays correspond to trajectories of higher and lower energy electrons than the nominal energy electrons, respectively.

⁵ Definitions of rank and order of the aberrations were given in section 2.13.1.

Dispersed rays deflected by a single magnetic deflector are shown in Fig. 5.4. When the deflection angle is θ , angular dispersion $\Delta\theta_c$, by the single magnetic deflector is given as

$$\Delta\theta_c = -\frac{1}{2}\theta \cdot \kappa, \quad (5.1)$$

$$\kappa = \frac{\Delta E}{E}, E = e\Phi, \Delta E = e\Delta\Phi,$$

where κ is a chromatic parameter, E is nominal energy of incident electrons, ΔE is energy spread of electrons around nominal energy, Φ is an axial potential, $\Delta\Phi$ is potential spread of the electrons, and e is the absolute value of the charge of the electron. Lateral dispersion ΔX_c at the plane from the center of the magnetic deflector by the longitudinal length L is given as

$$\Delta X_c = -\frac{1}{2}X \cdot \kappa, \quad (5.2)$$

where X is the lateral shift of the nominal energy electron by the deflection, and $X \approx L\theta$.

As shown in Fig. 5.5, the anti-symmetric double deflector generates a horizontally dispersed beam. The lateral dispersion of the double deflector ΔX_c is the same as that given by Eq. (5.1), and the angular dispersion below the second deflector is zero.

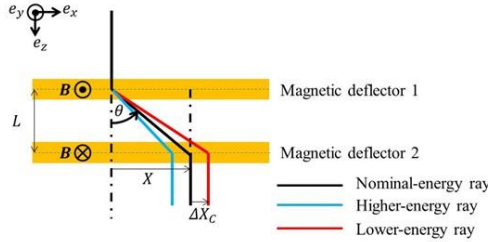


Fig. 5.5. Energy-dispersed rays with the lateral beam shift by the anti-symmetric double deflector. Angular dispersion of the second deflector is opposite to that of the first deflector and the dispersions are canceled out; thus, lateral dispersion only occurs below the double deflector.

In the S-corrector shown in Fig. 5.2, after the first lateral beam shift by the anti-symmetric double deflector, the lateral dispersion occurs as shown in Fig. 5.5. The dispersed ray is then incident on the first mirror parallel to its axis with the lateral distance ΔX_c at the crossover plane. Therefore, it is regarded as a general field ray with the initial lateral distance ΔX_c . In principle, as shown in Fig. 5.6, it is possible to reflect a field ray parallel to the axis of the electron mirror. If the mirror consists of multi-electrodes with independent voltages, the electrodes around the entrance can generate an electrostatic field that acts as a lens. The image-side space of this entrance lens is a decelerating region,

while the crossover plane is placed in a field-free space. The image-side focal length of the lens can be much shorter than the object-side focal length. The image-side focal point can therefore be set to coincide with the point of reflection on the axis of the mirror. Then, the field ray is reflected parallel to the axis and is symmetric about it. In an analogy with a bi-telecentric optical system, such a mirror is called a “telecentric mirror” hereafter.

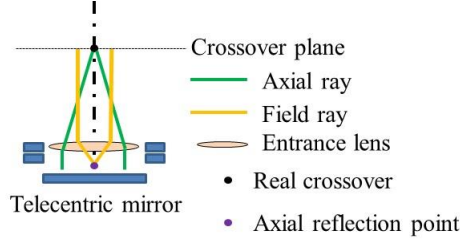


Fig. 5.6. Paraxial rays of a telecentric mirror. Electric field around the entrance of the telecentric mirror acts as a rotationally symmetric lens. The image-side focal point of that lens coincides with an axial reflection point of the mirror, where the axial potential of electrons is zero. A field ray is reflected parallel to the axis of the mirror and is symmetric about it.

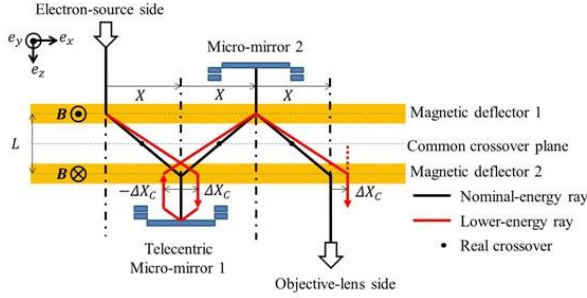


Fig. 5.7. Dispersed rays in the S-corrector equipped with the telecentric first mirror. For simplicity, only a single dispersed ray of lower energy than the nominal one is displayed in red. The parallel dispersed ray is incident on the telecentric first mirror. The reflected dispersed ray is parallel to the axis of the first mirror, but it has opposite lateral dispersion to that of the incident dispersed ray.

The first mirror is assumed to be such a telecentric mirror. The dispersed rays of the S-corrector equipped with the telecentric first mirror are shown schematically in Fig. 5.7. For simplicity, only a single dispersed ray of lower energy than the nominal energy is shown. After the first reflection, the dispersed ray has lateral dispersion of $-\Delta X_c$ at the lower edge of the second deflector and has no angular dispersion as shown in Fig. 5.7. After that, the second beam shift by the double deflector causes only the lateral dispersion of ΔX_c the same as the first-time lateral beam shift. These two lateral dispersions cancel each other, and the trajectory is fully dispersion free in the second mirror.

However, the third pass through the double deflector generates lateral dispersion of ΔX_C in the common crossover plane again. The residual lateral dispersion is demagnified and is transferred to the sample by the objective lens of the SEM. However, in the common crossover plane, it is not sufficiently small, for example, $\Delta X_C = \pm 15$ nm for $X = 0.5$ mm, $\Delta\Phi = \pm 0.3$ V, and $\Phi = 5$ kV.

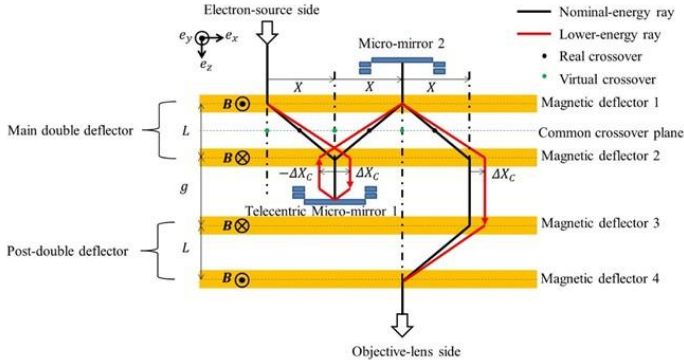


Fig. 5.8. Schematic cross section and dispersed rays of a dispersion-free deflection system: a post-deflection S-corrector using a telecentric first micro-mirror. The black ray is the central trajectory of the beam. The lower-energy dispersed ray is displayed in red. A post-double deflector (magnetic deflectors 3 and 4) is placed underneath the main double deflector (magnetic deflectors 1 and 2). The distance between the center of magnetic deflector 2 and that of deflector 3 is given as g . The beam is shifted back in the lateral direction by the distance $-X$, and it is directed to the objective lens (placed on the same axis as that of the second mirror). The total lateral beam shift is X . The additional lateral beam shift generates equal but opposite lateral dispersion to the residual lateral dispersion of the original S-corrector, so the dispersed ray vanishes. The trajectory of the beam in the second mirror and the objective lens is thus dispersion-free.

To correct the lateral dispersion, an additional anti-symmetric double deflector, whose magnetic fields are opposite to those of the original double deflector, is installed underneath the S-corrector (as shown in Fig. 5.8). The modified S-corrector is called a “post-deflection S-corrector”, in which the original double deflector is called the “main double deflector”, and the additional one is called the “post-double deflector”. The post-double deflector shifts the beam back in the lateral direction and directs it to the objective lens (whose axis coincides with that of the second mirror). The total lateral beam shift is $2X$. Since the lateral dispersion of the post-lateral beam shift cancels out that of the original S-corrector, the dispersed ray vanishes. The trajectory of the beam in the second mirror and the objective lens is therefore dispersion-free.

5.2.4 Dispersion in a practical mirror of a S-corrector

The above-described self-correction of the dispersion works as long as the first mirror is telecentric (as shown in Fig. 5.6). In fact, for a practical system, parallel reflection of the dispersed ray is not necessary. In the case of a non-telecentric mirror, after the reflection, a general field ray with initial distance ΔX_C , has slope β at the crossover plane (as shown in Fig. 5.9). Slope β is proportional to the inverse of the focal length of the mirror:

$$\beta = \frac{1}{f} \Delta X_C = -\frac{1}{2f} X \cdot \kappa, \quad (5.3)$$

where f is the focal length of the mirror.

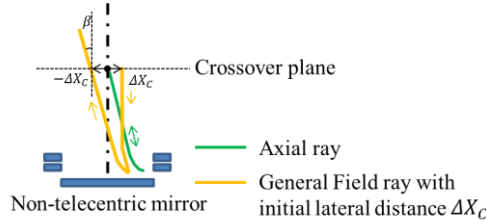


Fig. 5.9. Ray diagram for a non-telecentric mirror. A general field ray is incident on the non-telecentric mirror with initial lateral displacement ΔX_C and it is parallel to the axis of the mirror at the crossover plane. After reflection, the displacement becomes $-\Delta X_C$ and its slope β at the crossover plane.

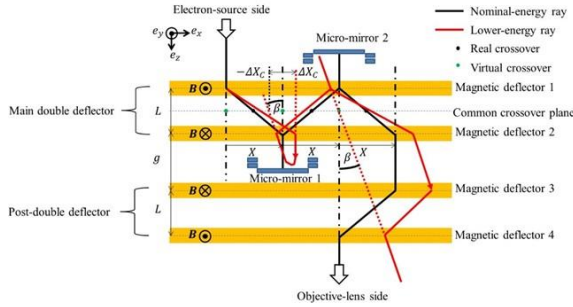


Fig. 5.10. Dispersed ray in a practical post-deflection S-corrector using non-telecentric mirrors. The lateral dispersion after the beam is reflected by the first mirror cancels out that caused by the second lateral beam shift. The dispersed ray directed to the second mirror has virtually only angular dispersion in the common crossover plane. The ray is virtually refocused at the same point after the second reflection. This virtual crossover point of the dispersed ray remains after the dispersed ray passes through the main and post-double deflectors. The lateral dispersion at the sample is thus eliminated because this point is mapped to the axial image point at the sample by the objective lens.

As in the case of the behavior of the dispersed rays explained in section 5.2.3, the second lateral beam shift by the double deflector generates lateral dispersion ΔX_c and no angular dispersion. The total dispersion in the second mirror is then expressed by the sum of the lateral and angular dispersions caused by the reflection and the lateral beam shift. The lateral dispersion at the virtual object plane of the second mirror is thus virtually cancelled, as shown in Fig. 5.10.

Another possible configuration of the S-corrector, namely, a corrector with a pre-deflection for correcting the lateral dispersion is shown in Fig. 5.11. In this configuration, the dispersed ray survives in the second mirror and the objective lens, while it is eliminated (i.e., the beam is fully dispersion-free) in the first mirror. Viewed from the objective lens, the dispersed ray emerges from the axial object point in the same manner as in the post-deflection S-corrector. Thus, the lateral dispersion vanishes in the sample plane. Combined with the aberrations of the mirrors and the objective lens, the remaining angular dispersion generates so-called “higher-rank combination aberration”. That point will be discussed in more detail later.

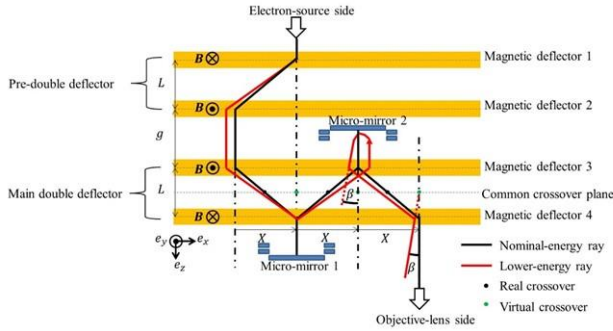


Fig. 5.11. Configuration and the dispersed ray in a practical pre-deflection S-corrector. Because the dispersion of the electron beam is eliminated by the pre-double deflector, the first mirror is fully dispersion-free. The dispersed ray remains in the second mirror and the objective lens, but it has only angular dispersion in the common crossover plane underneath the corrector. The lateral dispersion thus vanishes in the sample plane.

An alternative to the pre- or post-double deflector is a weak Wien filter. This configuration allows tuning of the remaining lateral dispersion without shifting the beam. If two independent Wien filters are installed, both lateral and angular dispersions can be eliminated.

5.2.5 Double micro-mirror corrector without beam shift: K-corrector

Another type of small angle deflection system using double micro-mirrors is introduced as follows. The basic configuration of the corrector and trajectories of the central ray and the axial ray are shown in Fig. 5.12. The system is composed of two micro-deflectors, double micro-mirrors, and a micro-ExB. The micro-deflectors are aligned on the same line separated by longitudinal space $2L$ and generate the equivalent deflection fields. The axis of the incident beam above the K-corrector unit is separated from that of the double micro mirrors, in the lateral direction by the distance X . For the micro-deflectors, either electrostatic or magnetic ones can be used. As an example, electrostatic deflectors are chosen for the following explanation.

We assume that the z -coordinate directs from the electron source side to the objective lens side, the X -coordinate directs from the original axis side to the mirror-side. The Y -coordinate directs from the front to the back of the paper. The incident beam is deflected at an angle θ by the first micro-deflector, where $\theta = X/L$. The micro-ExB, located on the mid-plane between the two deflectors, consists of an electrostatic deflection field and a magnetic deflection field. The two fields are assumed to have the same distribution in the z -coordinate, but are perpendicular, which is obtained using the same design concept as in the “fringe field monochromator”. The concept is that electrodes and pole pieces are thin, their gaps are small, and they are surrounded by electrically and magnetically grounded shields. The distributions of the fields are then determined by the distance between the shields and can be matched. The combination of the electric field and the magnetic field deflect the incident beam along the axis of the first mirror. The deflection angles due to the electrostatic and magnetic fields are equivalent and half of the deflection angle θ of the incident beam.

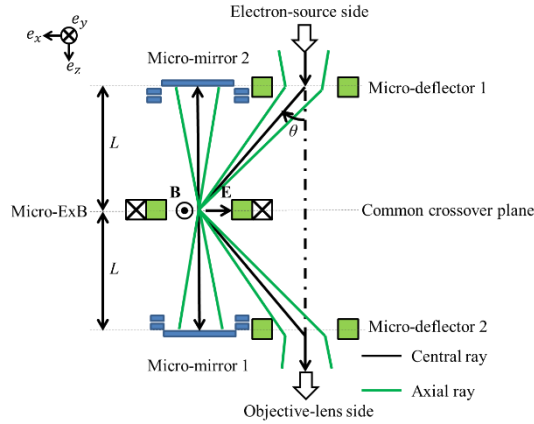


Fig. 5.12. Basic configuration and electron trajectories of another type of double micro-mirror corrector: K-corrector. Two identical micro-deflectors are aligned on the axis of the incident beam. The first micro-deflector deflects the beam to a micro-ExB placed on the common crossover plane. The ExB directs the beam to the first mirror, and after the first reflection, acting as a Wien filter, it allows the reflected beam to pass through as it is directed to the second mirror. After the second reflection, the beam is deflected by the ExB toward the second micro-deflector. The beam is then directed along the original axis by the second micro-deflector.

The double mirrors are aligned on the same axis as the micro-ExB and separated by space $2L$. The first mirror reflects the beam to the second mirror. The reflected beam passes through the ExB without deflection because it acts as a Wien filter. The second mirror reflects the beam back toward the first mirror, but it is deflected at angle θ by the ExB to the second micro-deflector. The second micro-deflector then deflects the beam along the original axis of the incident beam. The common crossover plane of the beam is located in the mid-plane of the system. The slight dispersion that is left in the beam can be compensated by adding a micro magnetic deflector to the second micro-deflector, effectively creating a Wien filter, in addition to the electrostatic deflection. This type of corrector system is named a “K-corrector” because the central ray forms a “K” shape. The most significant advantage of a K-corrector is that since the axis of the electron gun side coincides with that of the objective lens side, we can switch the optical mode with correction or without correction by switching the power of the micro-deflector 1 and 2.

The K-corrector setup has been investigated in Delft university of technology [5.2]. Note that, as it is shown in the references [5.2][5.3], stacked three plates, which generate dipole fields, in longitudinal direction, are used as an alternative deflection unit to a micro-ExB. A schematic of a typical structure of so-called an E-B-E unit. The top and bottom plates are electrodes, which generate electric dipole fields in the negative X-direction. The middle plate is

composed of a ferromagnetic material and coil windings to generate a magnetic dipole field in the positive Y-direction. The E-field is perpendicular to the B-field in the X-Y plane. The top and bottom plates have the same thickness and are symmetric about the center of the middle plate. The cross-sectional view and the beam deflection trajectory, which travels from top side to bottom side, and which travels from bottom side to top side, are shown in Fig. 5.13 (b) and (c), respectively. The deflection angle by the E-field and that by the B-field are tuned to $\theta/4$ and $\theta/2$, respectively. When the beam comes from the top side, the total deflection angle by the E-B-E unit is θ and the virtual deflection pivot is in the center of the middle plate. When the beam comes from the bottom side, since the deflection direction by the B-field is inverted, the deflection angles by the E-plates and the B-plate cancel, and the unit gives no deflection, acting as a Wien filter. The other configuration, which is composed of top and bottom magnetic field plates and a middle electrostatic field plate, so-called a B-E-B unit, can realize same deflection properties as those of an E-B-E unit. In addition, first-rank dispersion properties of deflection by E-B-E or B-E-B units are completely the same as those of ExB units, for the same settings of θ_E and θ_B . Thus, the dispersion analysis in this section is valid whether micro-deflector units are ExB type, E-B-E type, or B-E-B type.

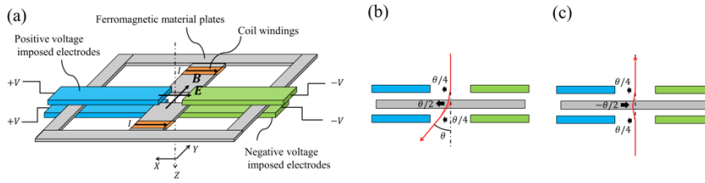


Fig. 5.13 Schematic of an alternative deflection unit to a micro-ExB, which is composed of stacked three dipole plates. This figure shows the basic configuration of an E-B-E unit. (a) A bird's-eye view, where the top and bottom plates are electrodes, which generate electric dipole fields in the X-direction. The middle plate is composed of a ferromagnetic material and coil windings to generate magnetic dipole field in positive the Y-direction. The E-field is perpendicular to the B-field in the X-Y plane. The top and bottom plates have the same thickness and are symmetric about the center of the middle plate. (b) A cross-sectional view and the beam deflection trajectory, which travels from the top side to the bottom side. (c) A cross-sectional view and the beam deflection trajectory, which travels from the bottom side to the top side.

5.3 Electron optical systems with micro-mirror correctors

In this thesis, one design of an SEM with a post-deflection S-corrector is described as examples hereafter, and the results of an analysis of its aberrations are then presented.

5.3.1 Presupposition and conditions

To design a realistic electron optical system with an S-corrector or with a K-corrector, the following assumptions regarding a realistic SEM are necessary. In the case of many LV-SEMs, electrons are decelerated before hitting the sample to reduce the aberrations of the objective lens. The acceleration voltage of the electron gun Φ_o thus generally differs from landing voltage Φ_l at the sample. In addition, probe current is written as I_p , the reduced brightness of an electron source as B_r , the energy spread as ΔE , the spherical and chromatic aberration coefficients of the objective lens in the sample plane as C_{sl} and C_{cl} , respectively. To form a sufficiently coherent beam, the probe current is limited to $I_p = 10$ pA. The typical reduced brightness of a Schottky cathode is $B_r = 5 \times 10^7$ A/m² sr V [5.4]. The energy spread is assumed to be $\Delta E = 0.6$ eV; that is, the range of voltage differences is $\Delta\Phi = \pm 0.3$ V. For a LV-SEM, $\Phi_o = 5000$ V and $\Phi_l = 1000$ V or 100 V are assumed, and typical values of axial aberration coefficients of the objective lens are $C_{sl} = 0.5$ mm, and $C_{cl} = 0.5$ mm for $\Phi_l = 1000$ V and $C_{sl} = 0.05$ mm, and $C_{cl} = 0.05$ mm for $\Phi_l = 100$ V, see Table 5.1.

Table 5.1 Assumed electron optical conditions

I_p (pA)	B_r (A/m ² sr V)	Φ_o (V)	$\Delta\Phi$ (V)	Φ_l (V)	C_{sl} (mm)	C_{cl} (mm)
10	5×10^7	5000	± 0.3	1000	0.5	0.5
				100	0.05	0.05

In general, it is considered that diffraction, source size, spherical aberration and chromatic aberration contribute to probe size. A diameter including 50% of the total probe current is regarded as an indicator of the resolution of an SEM, namely, the FW50 value. An approximate formula for the FW50 value is given in Eq. (1.12) of section 1.3. In Fig. 5.14, FW50 values at a sample plane are plotted as a function of aperture half-angle for three cases: uncorrected SEM, SEM corrected only for chromatic aberration, and fully corrected SEM. The aperture half-angle in the sample plane α_l should be larger than 27 and 55 mrad to achieve 1 and 1.5 nm FW50 values for landing voltage of 1000 V and 100 V, respectively, when aberrations are ideally corrected.

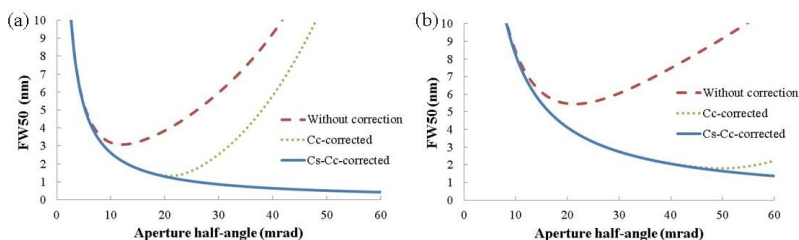


Fig. 5.14 FW50 values of the assumed objective lens versus aperture half-angle in the sample plane: the landing voltages of (a) 1000 V and (b) 100 V. Each graph is plotted for three cases: uncorrected SEM, SEM corrected only for chromatic aberration (C_c), and fully corrected SEM (both spherical (C_s) and chromatic (C_c) aberrations are corrected).

5.3.2 Optical system

A possible configuration of an optical system with a post-deflection S-corrector is proposed in Fig. 5.15. In the case of a high-resolution SEM, to keep the aberrations of the objective lens small, the working distance of the objective lens is a few millimeters. Scanning deflectors and secondary-electron detectors are often located above the objective lens. It is therefore necessary to install the corrector units between the condenser lens and the detector. The distance between the objective lens and the corrector unit is determined by the practical design of the deflectors and detectors.

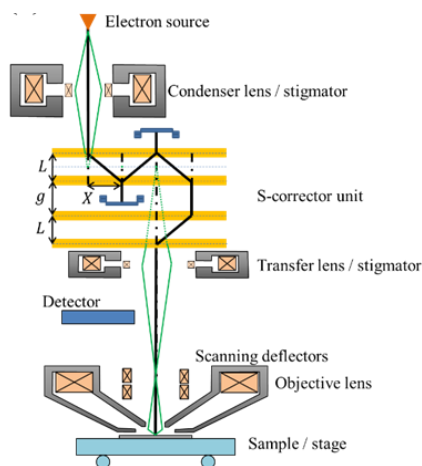


Fig. 5.15 Possible configurations of optical systems with a post-deflection S-corrector. Micro-mirror corrector units are installed between the condenser lens and the detector. An additional transfer lens and a stigmator are placed just below the corrector unit. The variable magnification of the transfer lens can adjust the axial aberrations of the mirrors to correct those of the objective lens.

Accordingly, the object point is a few-hundred millimeters from the principal plane of the objective lens, which is a hundred-times longer than the working distance, so the magnification of the objective lens is quite small. As a result, the corrector must generate enormous aberrations to correct an objective lens with such a small magnification since they are demagnified by it. Even if the corrector generates sufficiently large aberrations, it causes serious problems. To explain those problems, in the following example, the magnification of the objective lens is assumed to be $M = 0.01$ for both landing voltages of 1000 V and 100 V. The relation between spherical and chromatic aberration coefficients in the image plane and the object plane is given by

$$C_{si} = \frac{M}{M_\alpha^3} C_{so}, \quad C_{ci} = \frac{1}{MM_\alpha^3} C_{co}, \quad M_\alpha = \frac{1}{M} \sqrt{\frac{\Phi_o}{\Phi_i}}, \quad (5.4)$$

where subscripts i and o mean the values are defined in the image and the object planes, respectively. M and M_α are linear magnification and angular magnification of the lens. Note that angular magnification M_α is not equal to inverse magnification $1/M$ in the case of the immersion lens, that is, the electron potential in the object plane Φ_o is different from that in the image plane Φ_i . Setting decelerating voltage at the sample, angular magnification of the objective lens becomes larger than inverse magnification. Chromatic defocus in the object plane of the objective lens ΔZ_c is given as

$$\Delta Z_c = C_{co} \frac{\Delta \Phi}{\Phi_o}. \quad (5.5)$$

Estimated values of angular magnification, spherical and chromatic aberration coefficients, and chromatic defocus in the object plane are listed in Table 5.2. Chromatic defocus in the object plane is ± 3.35 mm for landing voltage of 1000 V and ± 10.6 mm for landing voltage of 100 V. Because the distance between the mirror plane and the common crossover plane is in the order of 10 mm, chromatic defocus is similar or even larger than that distance. The ray affected by chromatic aberration is completely different from the axial ray in the corrector. Because the difference between the rays is too large to be regarded as a small perturbation, higher-rank axial aberrations of the mirrors would be significant.

Table 5.2 Angular magnification, aberration coefficients, and chromatic defocus in the object plane in the case that the magnification of the objective lens $M = 0.01$ and the beam voltage in the S-corrector corrector is 5000 V.

Φ_i (V)	M_α	C_{so} (m)	C_{co} (m)	ΔZ_c (mm)
1000	223.6	5.59×10^5	55.9	± 3.35
100	707.1	1.77×10^6	1.76×10^2	± 10.6

It is concluded from the above discussion that it is necessary to reduce the magnification of the objective lens. As shown in Fig. 5.15, an additional transfer lens is therefore introduced underneath the corrector. The transfer lens acts as a magnifying lens by making a new crossover point at an appropriate position. In many cases, compared with the aberrations of the objective lens, those of the transfer lens can be neglected. In addition, the aberration coefficients of the objective lens in the image plane are almost independent of the position of the object plane and fixed because the image-side focal length is almost the same as its working distance. The spherical and the chromatic aberrations caused by the proposed S-corrector, or the K-corrector are transferred to the sample plane through the transfer lens and the objective lens. Using total magnification of the combined lens formed by the transfer lens and the objective lens, the aberration coefficients of the corrector in the object plane are transformed into those in the image plane as follows:

$$C_{Si}^{COR} = \frac{M}{M_\alpha^3} C_{So}^{COR}, \quad C_{Cl}^{COR} = \frac{1}{M M_\alpha^3} C_{Co}^{COR}, \quad (5.6)$$

where M and M_α are magnification and angular magnification of the combined lens. Since total magnification of the combined lens is variable according to the position of the crossover point between the transfer lens and the objective lens, it is therefore one of the useful tuning parameters of aberrations of the proposed S-corrector, or the K-corrector in a similar way as a transfer lens is used in [1.57].

5.3.3 Calculation of aberrations of electron mirrors

In the present design of the micro-mirror the following considerations are taken into account. Three degrees of freedom are necessary for setting the crossover position between the mirrors and tuning C_s and C_c for the aberration correction. A conventional mirror corrector system has a single tetrode mirror [1.66]. However, in this example design, a triode mirror is sufficient and preferable because it is easier to fabricate than a tetrode mirror. A triode mirror has only two degrees of freedom, of which one is used for setting the crossover position. The third degree of freedom is created by the variable magnification of the transfer lens, so the aberration coefficients of the mirror only need to be the right relative value of C_s and C_c . For simplicity, two equal mirrors are preferred. Of course, many alternative configurations, such as having tetrode mirrors or two mirrors with different voltage settings are conceivable.

A triode mirror with a simple shape is shown in Fig. 5.16. All electrodes are rotationally symmetric. The first electrode, “ground electrode”, is connected to ground. The second electrode, “tuning electrode”, is connected to voltage V_t . The third electrode, “mirror electrode”, is connected to voltage V_M . The diameter of the openings and the hole in the electrodes are 150 μm . The thickness of the upper two electrodes and the depth of hole in the mirror

electrodes are $200\text{ }\mu\text{m}$. The space between electrodes is $500\text{ }\mu\text{m}$. The positions of the common crossover planes of the post-deflection S-corrector and the K-corrector, which are shown in Fig. 5.10 and Fig. 5.12, are defined as the distance from the bottom of the hole in the mirror electrode, which is assumed to be 15 mm .

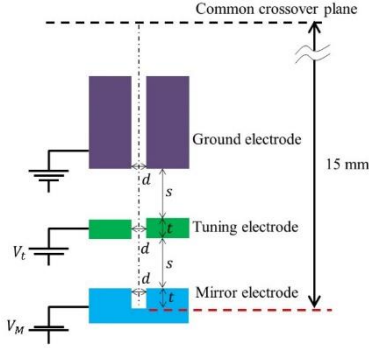


Fig. 5.16 Cross-section of a triode micro-mirror. As for the voltage settings of electrodes, the ground electrode is grounded, V_t and V_M are respectively supplied to the tuning electrode and the mirror electrode. That is, the potentials of electrodes are Φ_o , $\Phi_o + V_t$, $\Phi_o + V_M$, respectively, where Φ_o is the acceleration voltage. The diameter of the openings of the ground and the tuning electrodes and that of the hole in the mirror electrode are the same: $d = 150\text{ }\mu\text{m}$. The thickness of the upper two electrodes and the depth of the hole in the mirror electrode are the same: $t = 200\text{ }\mu\text{m}$. The spaces between electrodes are the same: $s = 500\text{ }\mu\text{m}$. The position of the common crossover plane is 15 mm from the bottom of the hole in the mirror electrode.

An appropriate perturbation theory for electron mirrors was discussed and formulae were derived in Chapter 2. Axial potential distributions of each electrode were calculated by the finite-difference method (FDM) [5.5]. To calculate the derivatives of the potential distributions, the potentials were fitted using an analytic function according to the method suggested by Munro *et al.*[5.6]. Paraxial equations were solved using the fourth-order Runge-Kutta method, and formulae of aberration coefficients were numerically integrated using the Simpson rule. For simplicity, the same geometry and voltage settings were used for the two mirrors.

Note that we are left with a large design freedom in this concept. The two mirrors may be tuned differently, for example to give one more effect on the chromatic aberration and the other on the spherical aberration. Also, we could add more elements to the stack so that C_S and C_C can be tuned in the mirror itself, instead of only with the magnification from corrector to objective lens. With additional elements, we could also create a telecentric system. For the purpose of this paper, we will not explore that large parameter space but limit ourselves to the triode mirror.

The relations between calculated voltages between the mirror and the tuning electrodes, the aberration coefficients C_s and C_c of the S-corrector in the common crossover plane and the sample plane for landing voltage $\Phi_i = 1000$ V and 100 V are shown in Fig. 5.17, where the incident electron potential Φ_o is 5000 V. The conditions for minimizing the residual aberration coefficients and FW50 values of the designed electron optical system as shown in Fig. 5.15 are listed in Table 5.3. The residual aberration coefficients are in the order of a few micrometers, and the target FW50 values, namely, 1 nm for 1000 V and 1.5 nm for 100 V, are achieved.

Paraxial properties of the aberration correction micro-mirror are listed in Table 5.4. The diameter of the beam probe is smaller than 15 μm at the reflection plane. It is sufficiently small because the diameter of the electrodes is much larger than the beam size. The chromatic defocus in the common crossover plane is less than ± 0.55 mm, which is 1/27 of the distance from the reflection plane to the object plane. This reduction of ΔZ_c from the values listed in Table 5.2 results from the variable magnification of the transfer lens.

Given the voltages of the electrodes listed in Table 5.3, the axial potential distribution around the electrodes and the paraxial trajectories (axial ray and field ray) are respectively shown in Fig. 5.18 and Fig. 5.19.

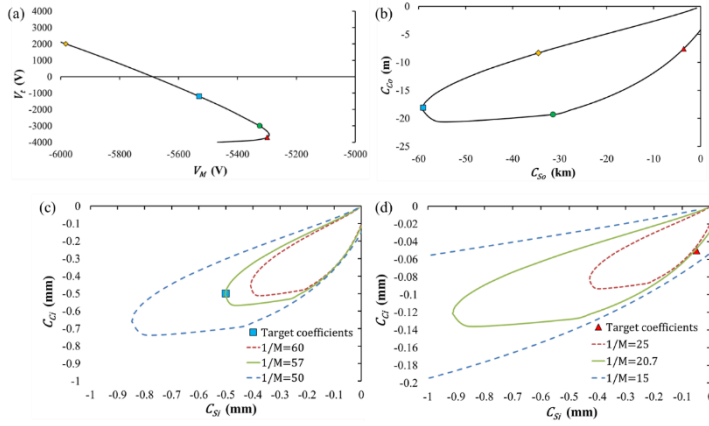


Fig. 5.17 Relation between voltages of the mirror electrode and the tuning electrode, where the incident electron potential Φ_o is 5000 V, and those between the spherical and chromatic aberration coefficients of the same double micro-mirrors in the common crossover plane and in the sample plane for different landing voltages. The aberration coefficients of the double mirrors in the common crossover plane are calculated as a function of the voltage of the mirror electrode V_M while that of the tuning electrode V_t is determined to keep the focus of the mirror on the common crossover plane, that is, the objective plane of the objective lens. (a) Relation between voltages V_M and V_t . (b) The aberration coefficients of double mirrors in the common crossover. The coefficients indicated in (b) by markers result from voltage settings indicated in (a) by the same markers, respectively. The shown coefficients in (c) and (d) are the values in the sample plane, which are transformed from the values in the common crossover plane, which is shown in (b), via Eq. (6) using the total magnification M of the combined lens formed by the transfer lens and the objective lens. (c) Landing voltage of 1000 V when the inversed magnification of the combined lens $1/M = 60, 57, 50$ and (d) landing voltage of 100 V when $1/M = 25, 20.7, 15$. Target coefficients are $C_s = C_c = -0.5$ mm for 1000 V and -0.05 mm for 100V, which can correct assumed aberration coefficients of the objective lens listed in Table 5.1. The voltages of electrodes indicated in (a) and the values of the coefficients in the common crossover plane indicated in (b) by the blue square and by the red triangle are the correction conditions for the landing voltage of 1000 V and 100 V, respectively.

Table 5.3 Conditions for minimizing the residual aberration coefficients and the FW50 values of the designed electron optical system as shown in Fig. 5.15. The conditions are magnification M , angular magnification M_α of the combined lens, the voltages of the tuning electrode V_t and of the mirror electrode V_M . Note that the magnification of the lenses and the mirror with a single focus is negative by definition of the coordinate system. However, to avoid confusion, the negative signs of magnification and angular magnification are omitted.

Φ_i (V)	1/M	M_α	V_t (V)	V_M (V)	C_{Si} (μm)	C_{Ci} (μm)	FW50 (nm)
1000	57	127.46	-1200	-5529.8	-0.40	0.96	0.968
100	20.7	146.37	-3700	-5298.9	-5.49	0.03	1.503

Table 5.4. Paraxial properties of the micro-mirror: aperture half-angle in the sample plane α_i , that in the common crossover plane α_o , axial reflection position from the bottom of the mirror electrode Z_{turn} , paraxial diameter of the probe at the reflection plane d_{ref} , and chromatic defocus in the common crossover plane ΔZ_C . The settings of the calculation are based on the values listed in Table 5.1 and Table 5.3.

Φ_i (V)	α_i (mrad)	α_o (mrad)	Z_{turn} (mm)	d_{ref} (μm)	ΔZ_C (mm)
1000	27	0.212	0.249	9.72	± 0.544
100	55	0.376	0.266	12.09	± 0.227

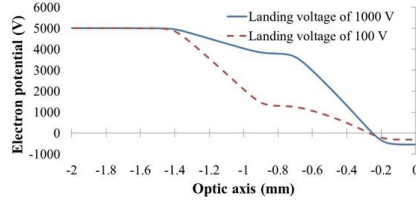


Fig. 5.18 Axial potential distribution in the micro-mirror. The optic axis is measured from the bottom of the mirror electrode. The voltage settings of the electrodes are given in Table 5.3.

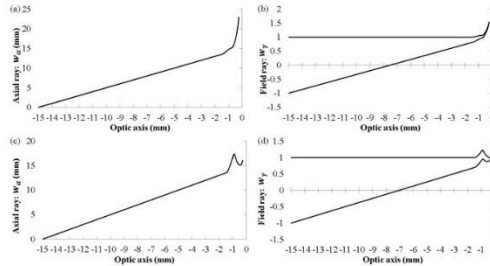


Fig. 5.19 Paraxial trajectories of the micro-mirror: (a) axial ray, (b) field ray for landing voltage of 1000 V, (c) axial ray, and (d) field ray for landing voltage of 100 V.

5.4 Estimates of other aberrations and FW50 of the corrected SEM

The possible beam spot-size of SEMs with micro-mirror correctors, is determined not only by the residual axial chromatic and the residual spherical aberrations, but also inevitable various aberrations such as deflection aberrations caused by deflection system and combinational aberrations between mirrors. In this section, we estimate these aberrations to show the potential of micro-mirror correctors. First, we assume the geometry of the post-deflection S-corrector and K-corrector as shown in Table 5.5. Schematics are shown in Fig. 5.10 for the post-deflection S-corrector.

Table 5.5 Assumption of geometries of the post-deflection S-corrector. X is the lateral distance between the original axis of the incident beam and the axis of the first mirror. L is the longitudinal distance between centers of the double deflector for the S-corrector. g is the longitudinal distance between the main and the post-deflectors. θ is deflection angle, which guides the incident beam to the mirrors. See also Fig. 5.10.

X (mm)	L (mm)	g (mm)	θ (mrad)	Min. unit height (mm)
0.5	10	25	50	~60

5.4.1 Deflector setup & Deflection aberration of the S-corrector

To calculate the deflection aberrations, the deflection field distribution needs to be calculated. Fig. 5.20 shows a schematic of magnetic deflector plates for deflection field calculation. The gap between ferromagnetic plates with windings is set to 4 mm. Center plates are sandwiched by ground electrodes and magnetic shield plates, whose shape is the same as the center plates.

Deflection field calculation was done using the package CO-3D [5.7], provided by Munro's electron beam software, which uses the finite difference method. It provides us with dipole and hexapole distribution of electric and magnetic fields along the optic axis.

Although we provided the deflection aberration formulae for the combined system of electrostatic mirrors, magnetic lens fields, and small-angle deflectors in Chapter 4, it is sufficient to use deflection aberration formulae of normal lenses and small-angle deflectors, which were given in Chapter 3, for evaluating deflection aberrations caused by the deflector section of the S-corrector. Additionally, it is easier to create a calculation program for the deflection aberration of normal lenses and deflectors than for mirrors and deflectors. Of course, to estimate the deflection aberrations of micro-mirror correctors using the formulae in Chapter 3, several tricks are necessary. In case of main double magnetic deflector of the S-corrector, we consider the system in Fig. 5.21.

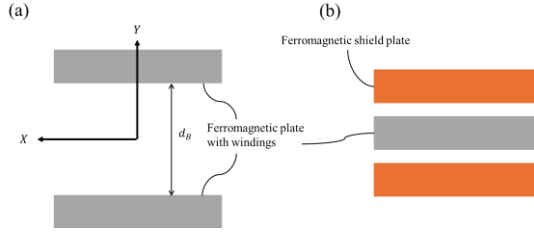


Fig. 5.20 Schematic of magnetic deflector plate: (a) Top-down view of center plates. (b) Cross-sectional view. The gap between ferromagnetic plates with windings is $d_B = 4$ mm. Center plates are sandwiched by ground electrodes and magnetic shield plates, whose shape is the same as the center plates. The electrodes are made of non-magnetic material.

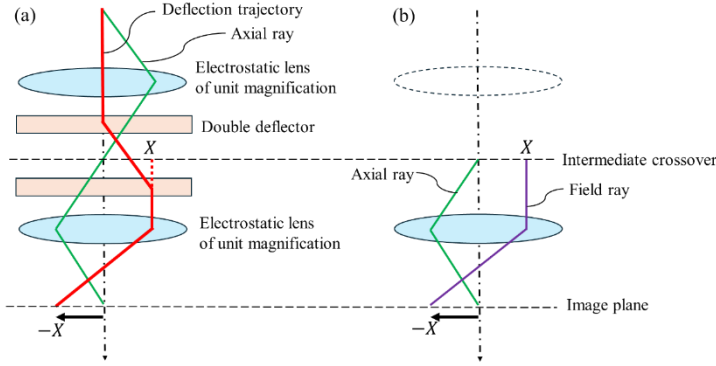


Fig. 5.21 System for calculating deflection aberrations of the main double deflector of the post-deflection S-corrector: (a) Deflection trajectory (red) and axial ray (green). (b) Field ray (purple). The system is composed of two identical electrostatic lenses, which focus on the intermediate crossover plane and the image plane, respectively, and a double deflector. The field distribution of electrostatic lenses is symmetric, and that of the double deflector is antisymmetric about the intermediate crossover plane.

The system is composed of two identical electrostatic lenses, which focus on the intermediate crossover plane and the image plane, respectively, and a double deflector. The field distribution of electrostatic lenses is symmetric, and that of the double deflector is antisymmetric about the intermediate crossover plane. The intermediate crossover plane is regarded as the common crossover plane in an actual setup of the post-deflection S-corrector. The contribution of the electrostatic lenses to deflection aberrations will be removed later. The electrostatic lenses are dummy lenses used only to focus for aberration calculation, since the numerical integral of aberration coefficient formulae is calculated from the object plane to the image plane, where the axial ray intersects with the optic axis. To make the system simpler, electrostatic lenses are suitable for dummy lenses, since we do not need to consider the rotation angle of magnetic

round symmetric lenses. We assume that the field distributions of the two electrostatic lenses and the double deflectors do not overlap. In addition, the magnification of the two identical electrostatic lenses is tuned to be -1 , meaning, the longitudinal distance between the object plane and the principal plane of the electrostatic lens is the same as that between the principal plane and the image plane. In Fig. 5.21 (a), the axial ray of the paraxial trajectory is shown in green. The red curve shows the deflection trajectory. Since the deflection trajectory passes through the first electrostatic lens region along its axis, the first electrostatic lens does not contribute to the deflection aberrations. The contribution comes from the double deflector region and the second electrostatic lens region. The double deflector makes a parallel beam shift X in the lateral direction. Since the shifted deflection trajectory enters the second electrostatic lens parallel to the axis of the second lens, by the paraxial approximation, the deflection trajectory is refracted, and it behaves like a field ray, as viewed from the second electrostatic lens. This means that the contribution to the deflection aberrations from the second electrostatic lens region is equal to the off-axis aberrations of the second electrostatic lens for the incident field ray parallel to the axis, whose object point is X in the X -direction in the intermediate crossover plane. This is shown by the purple curve in Fig. 5.21 (b). Thus, the difference between the deflection aberrations of the system in Fig. 5.21 (a) and the off-axis aberrations of the system in Fig. 5.21 (b), in the image plane, gives the deflection aberration contribution from the pure double deflector region. Since the magnification of the electrostatic lenses is -1 , the deflection aberrations of the double deflector in the image plane are easily reduced to virtual aberrations at the intermediate crossover plane.

However, the post-deflection S-corrector has the post double deflector. The difference in deflection aberrations between the main deflector and the post deflector is the position of the crossover of the axial ray. Although the crossover is placed at the center of the two deflectors of the main double deflector, no crossover exists inside the post double deflector. For the post double deflector, the common crossover plane, which is above it, behaves as the object plane. Fig. 5.22 shows the system for calculating deflection aberrations of the post double deflector of the post-deflection S-corrector. The system is composed of an electrostatic lens of magnification -1 , and a post-double deflector, which is placed underneath the electrostatic lens. The distance between the object plane of the post-double deflector is $g + L/2$, which is the same as that between the common crossover plane and the post-double deflector in the S-corrector. Fig. 5.22 (a) and (b) shows the deflection trajectory, the axial ray, and the field ray. The difference between deflection aberrations of the system in Fig. 5.22 (a) and off-axis aberrations of the system in Fig. 5.22 (b) gives deflection aberrations of the post double deflector in the image plane. Since the magnification of the electrostatic lens is tuned to be -1 , the deflection aberrations of the post double deflector are easily converted to those defined in the object plane, which corresponds to the common crossover of the post-deflection S-corrector.

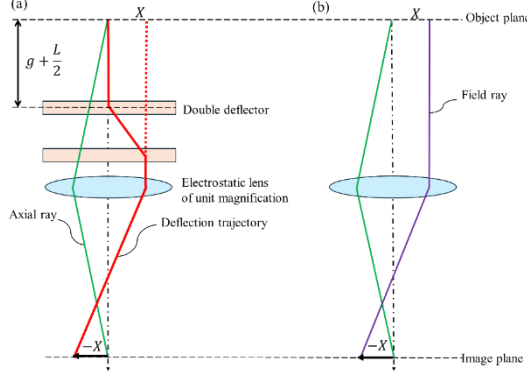


Fig. 5.22 System for calculating deflection aberrations of the post double deflector of the post-deflection S-corrector: (a) Deflection trajectory (red) and axial ray (green). (b) Field ray (purple). The system is composed of an electrostatic lens of magnification -1, and a post-double deflector. In this case, the distance between the object plane of the post-double deflector is $g + L/2 = 30$ mm, which is the same as that between the common crossover plane and the post-double deflector in the S-corrector.

To describe aberrations, we use the following notation:

The complex slope of the electron in the image plane

$$s_i = X'_i + iY'_i \quad (5.7)$$

where the subscript i means that the value is defined in the image plane. When the subscript is o , such as s_o , it means the value is defined in the object plane.

The complex beam shift by the deflection in the image plane is M_i .

The complex off-axis beam shift of paraxial order in the image plane is $w^{(1)}$.

In the setup of Fig. 5.21 and Fig. 5.22, we assume $M_i = w_i^{(1)}$.

Then, for example, coma-length caused by the deflector is estimated as follows:

$$\delta w_i^{comal} = C_{la\bar{a}}^F M_i s_i \bar{s}_i - C_{ba\bar{a}}^{OA} w_i^{(1)} s_i \bar{s}_i = (C_{la\bar{a}}^F - C_{ba\bar{a}}^{OA}) w_i^{(1)} s_i \bar{s}_i, \quad (5.8)$$

where $C_{la\bar{a}}^F$ and $C_{ba\bar{a}}^{OA}$ are the magnetic deflection coma-length aberration coefficient, whose form was given in Chapter 3, and the off-axis coma-length aberration coefficient, respectively.

When we regard the intermediate crossover plane as the object plane, the coma-length aberration converted into that plane is given by

$$\delta w_o^{comal} = \frac{1}{M} (C_{la\bar{a}}^F - C_{ba\bar{a}}^{OA}) w_i^{(1)} s_i \bar{s}_i = C_{cc}^{comal} w_o^{(1)} s_o \bar{s}_o, \quad (5.9)$$

where C_{CC}^{Comal} is virtual coma-length coefficient of the deflector defined at the crossover plane. $w_i^{(1)} = Mw_o^{(1)}$ and $s_i = M_\alpha s_o$, where M and M_α are magnification and angular magnification of the electrostatic lens. Since $M = M_\alpha - 1$, we obtain

$$C_{CC}^{Comal} = M_\alpha^2 (C_{l\alpha\bar{\alpha}i}^F - C_{b\alpha\bar{\alpha}i}^{OA}) = C_{l\alpha\bar{\alpha}i}^F - C_{b\alpha\bar{\alpha}i}^{OA}. \quad (5.10)$$

The other deflection aberrations at the crossover plane are given by

$$\begin{aligned} \delta w_o^{Comal} &= C_{CC}^{Comal} w_o^{(1)} s_o \bar{s}_o, \\ \delta w_o^{ComaR} &= C_{CC}^{ComaR} \bar{w}_o^{(1)} s_o^2, \\ \delta w_o^{FC} &= C_{CC}^{FC} w_o^{(1)} \bar{w}_o^{(1)} s_o, \\ \delta w_o^{AS} &= C_{CC}^{AS} w_o^{(1)2} \bar{s}_o + C_{CC}^{AS,4F} \bar{w}_o^{(1)2} \bar{s}_o, \\ \delta w_o^{DI} &= C_{CC}^{DI} w_o^{(1)2} \bar{w}_o^{(1)} + C_{CC}^{DI,4F} \bar{w}_o^{(1)3}, \\ \delta w_o^{A2} &= C_{CC}^{A2,4F} \bar{w}_o^{(1)} \bar{s}_o^2, \\ \delta w_o^{CM} &= C_{CC}^{CM} w_o^{(1)} \kappa_o, \end{aligned} \quad (5.11)$$

where superscript *ComaR*, *FC*, *AS*, *DI*, *A2*, and *CM* mean the coma-radius, the field-curvature, the astigmatism, the three-fold astigmatism, and the chromatic deflection aberrations, that is same as the dispersion, respectively. The coefficients with superscript *4F* are those of four-fold type aberration coefficients, which stem from hexapole component of the deflection field. By similar consideration of Eqs. (5.8) and (5.9), Deflection aberration coefficients at the crossover plane are given by

$$\begin{aligned} C_{CC}^{Comal} &= M_\alpha^2 (C_{l\alpha\bar{\alpha}i}^F - C_{b\alpha\bar{\alpha}i}^{OA}), \\ C_{CC}^{ComaR} &= M_\alpha^2 (C_{l\alpha\alpha i}^F - C_{b\alpha\alpha i}^{OA}), \\ C_{CC}^{FS} &= MM_\alpha (C_{l\alpha i}^F - C_{b\alpha i}^{OA}), \\ C_{CC}^{AS} &= MM_\alpha (C_{l\bar{\alpha}i}^F - C_{b\bar{\alpha}i}^{OA}), \\ C_{CC}^{AS,4F} &= MM_\alpha C_{l\bar{\alpha}\bar{\alpha}i}^F, \\ C_{CC}^{DI} &= M^2 (C_{l\bar{\alpha}i}^F - C_{b\bar{\alpha}i}^{OA}), \\ C_{CC}^{DI,4F} &= M^2 C_{l\bar{\alpha}\bar{\alpha}i}^F, \\ C_{CC}^{A2,4F} &= M_\alpha^2 C_{l\bar{\alpha}\bar{\alpha}i}^F, \\ C_{CC}^{CM} &= M^2 M_\alpha^2 (C_{l\bar{\alpha}i}^F - C_{b\bar{\alpha}i}^{OA}). \end{aligned} \quad (5.12)$$

Taking account of $M = M_\alpha = -1$ and $w_o^{(1)} = X$ in the S-corrector, we obtain

$$\begin{aligned} \delta w_o^{Comal} &= C_{CC}^{Comal} X s_o \bar{s}_o, \\ \delta w_o^{ComaR} &= C_{CC}^{ComaR} X s_o^2, \\ \delta w_o^{FC} &= C_{CC}^{FC} X^2 s_o, \\ \delta w_o^{AS} &= (C_{CC}^{AS} + C_{CC}^{AS,4F}) X^2 \bar{s}_o, \\ \delta w_o^{DI} &= (C_{CC}^{DI} + C_{CC}^{DI,4F}) X^3, \\ \delta w_o^{A2} &= C_{CC}^{A2,4F} X \bar{s}_o^2, \\ \delta w_o^{CM} &= C_{CC}^{CM} X \kappa_o. \end{aligned} \quad (5.13)$$

Although the crossover plane is in the center of the main deflector, it is above the post-deflector. Since the relation between the deflection magnetic field and the axial ray is different, deflection aberration coefficients are different as well. Simulated deflection aberration coefficients for $\Phi_o = 5000$ V are listed in Table 5.6. According to Eq. (5.2), C_{CC}^{CM} should be -0.5 , theoretically. The tiny difference is considered as numerical calculation error of this estimation

method. Since the relative error of dispersion coefficient is 0.02 % for the main deflector and 0.1 % for the post deflector, it gives no significant difference to estimation of the deflection aberrations.

Table 5.6 Deflection aberration coefficients of the main deflector and the post-deflector in the S-corrector for $\Phi_0 = 5000$ V

	C_{CC}^{ComaL} (-)	C_{CC}^{ComaR} (-)	C_{CC}^{FC} (1/m)	C_{CC}^{AS} (1/m)	$C_{CC}^{AS,AF}$ (1/m)
Main	0.4999	0.2499	86.82	-24.43	-46.174
Post	-1.02268	-0.51134	2375.05	-1188.84	1122.67

	C_{CC}^{DI} (1/m ²)	$C_{CC}^{DI,AF}$ (1/m ²)	$C_{CC}^{A2,AF}$ (-)	C_{CC}^{CM} (-)
Main	3064.58	-68.365	-0.6276	-0.4999
Post	19451.2	16444.5	0.046782	-0.4995

To calculate total deflection aberrations of the post-deflection S-corrector shown in Fig. 5.10, the summation rule of deflection aberrations is given here. The deflection aberration after the first deflection and before the reflection by the first mirror, which is measured in the common crossover plane, is given by

$$\delta w_{1st} = C_{CCM}^{ComaL} X s_o \bar{s}_o + C_{CCM}^{ComaR} X s_o^2 + C_{CCM}^{A2,AF} X \bar{s}_o^2 + C_{CCM}^{FC} X^2 s_o + (C_{CCM}^{AS} + C_{CCM}^{AS,AF}) X^2 \bar{s}_o + (C_{CCM}^{DI} + C_{CCM}^{DI,AF}) X^3 + C_{CCM}^{CM} X \kappa_o, \quad (5.14)$$

where subscript *CCM* means the aberration coefficient of the main deflector measured in the common crossover plane.

Because deflection aberrations are measured with respect to the coordinate system, after reflection by the first mirror, the coordinate system of the second beam shift by the main double deflector is changed. The direction of the incident electrons is inverted, and the roles of the first and the second deflectors are interchanged. Thus, the transformation from the original coordinate system for the first beam shift to that for the second beam shift is given as follows.

$$(X, Y, z) \rightarrow (X, -Y, -z), \quad (X', Y') \rightarrow (-X', Y'). \quad (5.15)$$

It follows that the complex lateral aberration and the complex slope of electrons are transformed as

$$\delta w \rightarrow \delta \bar{w}, \quad s \rightarrow -\bar{s}. \quad (5.16)$$

In addition, the sign of the lateral aberration of the second beam shift is inverted by the reflection of the second mirror.

Taking these inversions into account, the aberrations of the second beam deflection are expressed as

$$\delta w_{2nd} = C_{CCM}^{ComaL} X s_o \bar{s}_o + C_{CCM}^{ComaR} X s_o^2 + C_{CCM}^{A2,AF} X \bar{s}_o^2 - C_{CCM}^{FC} X^2 s_o - (C_{CCM}^{AS} + C_{CCM}^{AS,AF}) X^2 \bar{s}_o + (C_{CCM}^{DI} + C_{CCM}^{DI,AF}) X^3 + C_{CCM}^{CM} X \kappa_o. \quad (5.17)$$

The third deflection gives the same deflection aberration as the first deflection: $\delta w_{3rd} = \delta w_{1st}$. When the electrons pass through the main deflector and the micro-mirrors, δw_{1st} is reflected twice and δw_{2nd} is reflected once. Since the magnification of the mirrors is -1.

The total deflection aberration by the main deflector is summarized as

$$\begin{aligned}
\delta w_{main} &= (-1)^2 \delta w_{1st} - \delta w_{2nd} + \delta w_{3rd} \\
&= C_{CCM}^{Comal} X s_o \bar{s}_o + C_{CCM}^{ComaR} X s_o^2 + C_{CCM}^{A2,AF} X \bar{s}_o^2 \\
&\quad + 3C_{CCM}^{FC} X^2 s_o + 3(C_{CCM}^{AS} + C_{CCM}^{AS,AF}) X^2 \bar{s}_o + (C_{CCM}^{DI} + C_{CCM}^{DI,AF}) X^3 + C_{CCM}^{CM} X \kappa_o.
\end{aligned} \tag{5.18}$$

For the fourth deflection by the post-deflector, the transformation is given as

$$\delta w \rightarrow \delta w, \quad s \rightarrow s, \quad X \rightarrow -X, \tag{5.19}$$

because the direction of the beam shift is inverted although the coordinate system is unchanged. The deflection

aberration by the post deflector, which is measured in the common crossover plane, is given by

$$\begin{aligned}
\delta w_{post} &= -C_{CCP}^{Comal} X s_o \bar{s}_o - C_{CCP}^{ComaR} X s_o^2 - C_{CCP}^{A2,AF} X \bar{s}_o^2 \\
&\quad + C_{CCP}^{FC} X^2 s_o + (C_{CCP}^{AS} + C_{CCP}^{AS,AF}) X^2 \bar{s}_o - (C_{CCP}^{DI} + C_{CCP}^{DI,AF}) X^3 - C_{CCP}^{CM} X \kappa_o,
\end{aligned} \tag{5.20}$$

Where subscript *CCP* means the aberration coefficient of the post deflector measured in the common crossover plane.

Then the total deflection aberration of the post-deflection S-corrector is estimated by

$$\begin{aligned}
\delta w_{CC}^{DEF} &= \delta w_{main} + \delta w_{post} \\
&= (C_{CCM}^{Comal} - C_{CCP}^{Comal}) X s_o \bar{s}_o + (C_{CCM}^{ComaR} - C_{CCP}^{ComaR}) X s_o^2 \\
&\quad + (C_{CCM}^{A2,AF} - C_{CCP}^{A2,AF}) X \bar{s}_o^2 + (3C_{CCM}^{FC} + C_{CCP}^{FC}) X^2 s_o \\
&\quad + (3C_{CCM}^{AS} + 3C_{CCM}^{AS,AF} + C_{CCP}^{AS} + C_{CCP}^{AS,AF}) X^2 \bar{s}_o \\
&\quad + (C_{CCM}^{DI} + C_{CCM}^{DI,AF} - C_{CCP}^{DI} - C_{CCP}^{DI,AF}) X^3 + (C_{CCM}^{CM} - C_{CCP}^{CM}) X \kappa_o.
\end{aligned} \tag{5.21}$$

Since Eq. (5.21) is a virtual deflection aberration, estimated in the common crossover plane, viewing from the

objective lens side, at the final image plane, which is the sample surface, the deflection aberration is expressed as

$$\begin{aligned}
\delta w_i^{DEF} &= M \delta w_{CC}^{DEF} = \frac{M}{M_\alpha^2} (C_{CCM}^{Comal} - C_{CCP}^{Comal}) X s_i \bar{s}_i + \frac{M}{M_\alpha^2} (C_{CCM}^{ComaR} - C_{CCP}^{ComaR}) X s_i^2 \\
&\quad + \frac{M}{M_\alpha^2} (C_{CCM}^{A2,AF} - C_{CCP}^{A2,AF}) X \bar{s}_i^2 + \frac{M}{M_\alpha} (3C_{CCM}^{FC} + C_{CCP}^{FC}) X^2 s_i \\
&\quad + \frac{M}{M_\alpha} (3C_{CCM}^{AS} + 3C_{CCM}^{AS,AF} + C_{CCP}^{AS} + C_{CCP}^{AS,AF}) X^2 \bar{s}_i \\
&\quad + M (C_{CCM}^{DI} + C_{CCM}^{DI,AF} - C_{CCP}^{DI} - C_{CCP}^{DI,AF}) X^3 + \frac{1}{M M_\alpha^2} (C_{CCM}^{CM} - C_{CCP}^{CM}) X \kappa_i
\end{aligned} \tag{5.22}$$

where s_i is the paraxial slope of the electron at the final image plane. M and M_α are the combined magnification and the angular magnification of the transfer lens and the objective lens, which are listed in Table 5.3, respectively.

Using parameters shown in Table 5.3, Table 5.4, Table 5.5, and Table 5.6, we estimate deflection aberrations, when the complex slope s_o takes its maximum absolute value, that is an aperture half-angle α_o . The deflection aberrations are estimated at the final image plane for landing voltages of 1000 V and 100 V, which are shown in Table 5.7.

Table 5.7 Deflection aberration of the post-deflection S-corrector estimated at the final image plane for landing voltage of 1000 V and 100 V, when the complex slope s_o takes its maximum absolute value, that is, an aperture half-angle α_o . Deflection aberrations are classified into the defocus, the astigmatism, the coma-length, the coma-radius, the three-fold astigmatism, the distortion, and the dispersion.

Φ_i (V)	Defocus (nm)	Ast. (nm)	Coma-L (pm)	Coma-R (pm)
1000	2.45	-0.26	-0.60	-0.30
100	11.96	-1.26	-5.19	-2.59

Φ_i (V)	Three-fold ast. (pm)	Distortion (nm)	Dispersion (pm)
1000	0.27	72.15	0.53
100	2.30	198.67	1.46

Only the defocus, the astigmatism, and the distortion are larger than nanometer scale. However, the defocus and the astigmatism are tiny and easily corrected by tuning the currents of the objective lens and the normal stigmator, which are installed in conventional SEMs. Since the distortion can cause additional off-axis aberrations of the objective lens, an additional beam aligner or fine tuning of strength of the post-deflector can align the beam to the objective lens to suppress its off-axis aberrations, which is discussed in section 5.5. Then, the deflection aberrations, which contribute to a blur directly, are the coma, the three-fold astigmatism, and the dispersion. As we expected, these aberrations are at most a few picometers and they are negligibly smaller than the target beam size of 1 to 1.5 nm. By the discussion given in section 5.2.4, the post-deflection S-corrector has no dispersion at the final image plane. However, due to numerical error, a negligible amount of dispersion, which is at most less than 1.5 pm, is calculated. We are not afraid of the deflection aberration of the post-deflection S-corrector.

5.4.2 Combination aberrations of the dispersion by the deflection and aberrations of the mirrors and the objective lens

Combination aberrations of the post-deflection S-corrector shown in Fig. 5.10 are discussed as follows. These combination aberrations basically represent the effects of the dispersed beams not being exactly on axis either in the mirrors or in the objective lens. Viewed from the first mirror, the incident dispersed ray is parallel to the axis with lateral dispersion ΔX_c given by Eq. (5.2) as shown in Fig. 5.10. It is expressed as a general field ray of the first mirror with initial lateral distance ΔX_c at the virtual object plane. Viewed from the second mirror and from the objective lens, the incident dispersed ray emerges from the axial object point with the angular dispersion β given by Eq. (5.3). It is

expressed as a general axial ray with initial slope β at the virtual object plane of the second mirror and the objective lens. Calculated values of lateral dispersion after the first mirror ΔX_C and angular dispersion β towards the second mirror and the objective lens for the potential spread $\Delta\Phi = \pm 0.3$ V are listed in Table 5.8.

Table 5.8 Lateral and angular dispersions for $\Delta\Phi = \pm 0.3$ V and $\Phi_o = 5000$ V.

Φ_i (V)	ΔX_C (nm)	β (μ rad)
1000	± 15	± 2.01
100	± 15	± 1.89

In the image plane, lateral displacement of the electron trajectory from the optic axis caused by the third-order geometrical and second-rank chromatic aberrations of the mirrors is given by

$$\delta w_i = M [C_S w_o'^2 \bar{w}'_o + 2C_K w_o w'_o \bar{w}'_o + C_K \bar{w}_o w_o'^2 + C_F w_o \bar{w}_o w'_o + C_A w_o^2 \bar{w}'_o + C_D w_o^2 \bar{w}_o + (C_C w'_o + C_M w_o) \kappa], \quad (5.23)$$

where M is the magnification of the system from the object plane to the image plane and w_o is lateral displacement and w'_o is slope of the trajectory to the optic axis in the object plane defined in complex coordinates. C_M , C_K , C_F , C_A , and C_D are off-axis aberration coefficients of off-axis chromatic aberration, coma-radius, field curvature, astigmatism and distortion in the object plane, respectively. These off-axis coefficients are defined by the axial ray that emerges from the axial object point and the field ray.

The focal length of the single mirror f and the on- and off-axis aberration coefficients of the single mirror under the settings of voltages of electrodes listed in Table 5.3 for landing voltages of 1000 V and 100 V are listed in Table 5.9. Because the two micro-mirrors of the post-deflection S-corrector, shown in Fig. 5.10, are assumed to be the same, their focal length and aberration coefficients are also the same.

Table 5.9 Focal length and aberration coefficients of the single micro-mirror

Φ_i (V)	f (mm)	C_C (m)	C_M	C_S (m)
1000	7.460	-9.063	-6.075×10^2	-2.953×10^4
100	7.951	-3.785	-2.380×10^2	-1801×10^3
Φ_i (V)	C_K	C_F (1/m)	C_A (1/m)	C_D (1/m ²)
1000	-1.979×10^6	-2.653×10^8	-1.327×10^8	-8.893×10^9
100	-1.132×10^5	-1.411×10^7	-7.046×10^6	-4.345×10^8

Because the first rank-dispersed ray has lateral dispersion ΔX_C and no angular dispersion in the x-direction in the object plane in front of the first mirror, ΔX_C is substituted into w_o , and α_o is substituted into w'_o of Eq. (5.23) to estimate the combination aberration of the dispersed ray and the first mirror expressed as

$$\delta w_i^{1st} = M\eta[2C_K\Delta X_C|\alpha_o|^2 + C_K\Delta X_C\alpha_o^2 + C_F\Delta X_C^2\alpha_o + C_A\Delta X_C^2\bar{\alpha}_o + C_D\Delta X_C^3 + C_M\Delta X_C\kappa], \quad (5.24)$$

where M is the magnification of the combined lens formed by the transfer lens and the objective lens, $\kappa = \Delta\Phi/\Phi_o$, Φ_o is the electron potential in the common crossover plane, and α_o is the aperture half-angle in the common crossover plane. The prefactor η is 2 for the aberration with the odd exponent of κ and 1 for that with the even exponent (including zero). The meaning of this prefactor is explained as follows. Since it was assumed that energy spread $\Delta E = 0.6$ eV means full spread from the lower-energy side to the higher-energy side, potential spread $\Delta\Phi$ is ± 0.3 V from the nominal potential. Since the original definition of an aberration is the deviation of the lateral position of the electron trajectory from the optic axis at the crossover plane, the positional shift of higher-energy electrons with $\Delta\Phi = +0.3$ V is opposite to that of lower-energy electrons with $\Delta\Phi = -0.3$ V when the exponent of κ is an odd number, for example, in the case of axial chromatic aberration. Consequently, the maximum value of the aberration with the odd exponent of κ is twice as large as the value of the aberration when $\Delta\Phi = +0.3$ V. However, the positional shift of higher-energy electrons is the same as that of the lower-energy electrons when the exponent is an even number. The maximum value of the aberration with the even exponent of κ is the same as the value of the aberration when $\Delta\Phi = +0.3$ V.

For the second mirror, the incident first rank dispersed ray has only angular dispersion β (i.e., no lateral dispersion) in the object plane. It can be regarded that $w_o = 0$ and $w'_o = \alpha_o + \beta$ in Eq. (5.23). In the image plane, the combination aberration is classified according to the order of aperture half-angle and the angular dispersion expressed as

$$\delta w_i^{2nd} = M\eta[C_S(2\beta|\alpha_o|^2 + \beta\alpha_o^2 + 2\beta^2\alpha_o + \beta^2\bar{\alpha}_o + \beta^3) + C_C\beta\kappa]. \quad (5.25)$$

For the objective lens, it is the same as that given by Eq. (5.25), but axial aberration coefficients C_S and C_C are replaced by those of the objective lens. Because lateral dispersion ΔX_C and angular dispersion β are first-degree quantities (see Eqs. (5.2) and (5.3)), the combination aberrations are classified by the degree of κ and order of α . To estimate the significance of each aberration, dependence of the aberration on azimuth angle was eliminated by replacing α_o and its complex conjugate $\bar{\alpha}_o$ by absolute value $|\alpha_o|$. Estimated maximum aberration in the sample plane for landing voltages of 1000 V and 100 V are listed in Table 5.9, Table 5.10 and Table 5.11, respectively.

Table 5.10 Combination aberrations for landing voltage of 1000 V.

	$w_{\bar{a}\bar{a}\kappa}$ (pm)	$w_{\alpha\alpha\kappa}$ (pm)	$w_{\alpha\kappa\kappa}$ (pm)	$w_{\bar{\alpha}\kappa\kappa}$ (pm)	$w_{\kappa\kappa\kappa}$ (pm)	$w_{\kappa\kappa}$ (pm)
First mirror	-93.5	-46.7	-0.22	-0.11	-1.05×10^{-3}	-9.59
Second mirror	-187.0	-93.5	-0.89	-0.44	-8.42×10^{-3}	-19.19
Objective lens	373.7	186.8	1.77	0.89	1.68×10^{-2}	38.44
Total	93.2	46.6	0.66	0.33	7.36×10^{-3}	9.67

Table 5.11 Combination aberrations for landing voltage of 100 V.

	$w_{\bar{a}\bar{a}\kappa}$ (pm)	$w_{\alpha\alpha\kappa}$ (pm)	$w_{\alpha\kappa\kappa}$ (pm)	$w_{\bar{\alpha}\kappa\kappa}$ (pm)	$w_{\kappa\kappa\kappa}$ (pm)	$w_{\kappa\kappa}$ (pm)
First mirror	-46.3	-23.2	-0.058	-0.029	-1.41×10^{-4}	-10.3
Second mirror	-92.7	-46.3	-0.233	-0.116	-1.17×10^{-3}	-20.7
Objective lens	167.1	83.5	0.419	0.210	2.11×10^{-3}	41.4
Total	28.0	14.0	0.129	0.065	7.96×10^{-4}	10.4

Significant combination aberrations are $w_{\bar{a}\bar{a}\kappa}$ and $w_{\alpha\alpha\kappa}$, which have the same geometrical shape as those of coma-length and coma-radius but their aberration coefficients are proportional to energy deviation of electrons (i.e., the difference between the energy of electrons and nominal energy), so they are called “chromatic coma”. The sum of the total aberration values is about 0.15 nm for landing voltage of 1000 V and 0.05 nm for landing voltage of 100 V. It is difficult to calculate the contribution to the FW50 value because these aberrations are rotationally non-symmetric chromatic aberrations. However, it can be expected that blur caused by these aberrations is not significant compared with the target value of resolution. It is concluded that in the case of the proposed S-corrector system, the combination aberrations of the dispersed ray are sufficiently small.

5.4.3 Combination aberrations between the double micro-mirrors

Combination aberrations between the two micro-mirrors were estimated as follows. In the estimation, not only the chromatic aberration of the first mirror but also the spherical aberration and the change of the convergent angle caused by the first mirror were taken into account. Because the micro-mirror is small, it can be assumed that the aberration is caused at the principal plane of the mirror, which is located at $2f$ from the crossover plane, where f is the focal length of the mirror. Accordingly, it follows that

$$\begin{aligned}\delta w &= C_s^I \alpha_o^2 \bar{\alpha}_o + C_c^I \alpha_o \kappa, \\ \delta w' &= \frac{1}{2f} \delta w = \frac{1}{2f} (C_s^I \alpha_o^2 \bar{\alpha}_o + C_c^I \alpha_o \kappa),\end{aligned}\quad (5.26)$$

where δw is the lateral displacement, and $\delta w'$ is the change of the convergent angle by the first mirror in the object plane of the second mirror. Superscript I of aberration coefficients represents those of the first mirror. In section 2.11, we discussed off-axis aberration coefficients of mirrors for an inclined incident beam. We can regard δw as the off-axis position and $\delta w'$ as the slope of the off-axis ray in the object plane. Normalized initial slope is defined as $\lambda_o = 1/2f$. Then, we can use Eqs. (2.377) to (2.382), and (2.384), for calculating off-axis aberration coefficients for the inclined off-axis electrons. Since off-axis position of Eq. (5.26) depends on aperture half-angle α_o , it predicts combination higher-rank aberrations. Combination aberrations up to the fifth-rank in the sample plane are expressed as

$$\begin{aligned}\delta w_i &= w_{\alpha\kappa\kappa} + w_{\alpha\alpha\bar{\alpha}\kappa} + w_{\alpha\alpha\alpha\bar{\alpha}\bar{\alpha}} + w_{\alpha\alpha\bar{\alpha}\kappa\kappa}, \\ w_{\alpha\kappa\kappa} &= M\eta \left(\frac{1}{2f} C_c^I C_c^{II} + C_c^I C_M^{II} \right) \alpha_o \kappa^2, \\ w_{\alpha\alpha\bar{\alpha}\kappa} &= M\eta \left(\frac{3}{2f} C_c^I C_s^{II} + 3C_c^I C_k^{II} + \frac{1}{2f} C_s^I C_c^{II} + C_s^I C_M^{II} \right) \alpha_o^2 \bar{\alpha}_o \kappa, \\ w_{\alpha\alpha\alpha\bar{\alpha}\bar{\alpha}} &= 3M \left(C_k^{II} + \frac{1}{2f} C_s^{II} \right) C_s^I \alpha_o^3 \bar{\alpha}_o^2, \\ w_{\alpha\alpha\bar{\alpha}\kappa\kappa} &= M\eta \left(\frac{3}{4f^2} C_s^{II} + 3\frac{1}{f} C_k^{II} + C_F^{II} + C_A^{II} \right) C_c^I{}^2 \alpha_o^2 \bar{\alpha}_o \kappa^2\end{aligned}\quad (5.27)$$

Superscript II of aberration coefficients represents those of the second mirror. Especially, the second-term aberration has the same geometrical shape as that of the spherical aberration, but the coefficient varies according to the energy deviation of electrons, so it is called the “chromatic-spherical aberration”. The third term corresponds to the so-called fifth-order spherical aberration. In the case of the proposed S-corrector, the coefficients of the second mirror are the same as those of the first mirror. The estimated values are listed in Table 5.12.

Table 5.12 The combination aberration between the first mirror and the second mirror for landing voltages of 1000 V and 100V.

Φ_i (V)	$w_{\alpha\kappa\kappa}$ (nm)	$w_{\alpha\alpha\bar{\alpha}\kappa}$ (nm)	$w_{\alpha\alpha\alpha\bar{\alpha}}$ (nm)	$w_{\alpha\alpha\bar{\alpha}\kappa\kappa}$ (nm)
1000	0.147	2.87	2.62	0.079
100	0.117	1.05	0.44	0.011

The third-rank aberration $w_{\alpha\kappa\kappa}$ and the fifth-rank aberration $w_{\alpha\alpha\bar{\alpha}\kappa\kappa}$ are not significant, since it is less than 0.15 nm. However, the chromatic spherical aberration and the fifth-order spherical aberration exceed 1 nm order, which is not negligible. Such a large value apparently blurs the beam spot. Fortunately, since the geometrical shape of this aberration is the same as that of the spherical aberration, its contribution to the beam spot size is reduced by some factor in the same manner as the contribution of the spherical aberration to the FW50 value given in Eq. (1.12). Unfortunately, such a factor is unknown. Instead of considering the approximate contribution of the spherical chromatic aberration to the FW50 values, wave optical beam profiles of the electron beam and the FW50 values are directly calculated. It is discussed in section 5.4.5.

The combination chromatic-spherical and fifth-order spherical aberrations are also generated by the objective lens combined with the lower-rank aberrations of the first mirror. These aberrations and the change in the convergent angle are doubled in the object plane of the objective lens because those caused by the combination of the objective lens and the second mirror are added. Thus, it is expected that the resulting aberrations are about twice as large as those caused by the combination between the first mirror and the second mirror, but their sign is opposite because the aberration coefficients of the objective lens are positive. Therefore, the chromatic-spherical aberrations are canceled to some extent. The remaining aberration values are similar to those caused by the combination of the first mirror and the second mirror.

5.4.4 Combination aberration of mirrors with field curvature and astigmatism of deflectors

Similar to the dispersion of the deflectors in the proposed S-corrector, the geometrical aberrations of the deflectors and both the geometrical and chromatic aberrations of the mirrors lead to combination aberrations. According to Table 5.7, deflection coma, three-fold astigmatism, and dispersion are less than a few picometer-order and they are negligible. However, defocus, which stems from deflection field curvature, and astigmatism are not negligible since they are of a few nanometer order. Of course, the defocus and the astigmatism at the final image plane can be corrected by tuning the objective lens and the standard stigmator. We should consider combination aberration of the intermediate defocus and astigmatism in the common crossover plane and the aberration of the micro-mirrors.

Firstly, we describe the field curvature and the astigmatism by the deflection of double deflector with respect to the aperture half-angle, which are defined in the common crossover plane as follows:

$$\delta w_{CC}^{FC,AST} = -\delta Z_{FC}\alpha_o + \frac{1}{2}\delta Z_{AS}\bar{\alpha}_o, \quad (5.28)$$

where δZ_{FC} is deflection defocus distance along with the optic axis, and δZ_{AS} is astigmatic distance, given by

$$\begin{aligned} \delta Z_{FC} &= -C_{CC}^{FC}X^2, \\ \delta Z_{AS} &= 2(C_{CC}^{AS} + C_{CC}^{AS,AF})X^2. \end{aligned} \quad (5.29)$$

In addition, the convergent slope of the electron in the common crossover plane must be perturbed by the deflection field curvature and the astigmatism. For the first deflection by the main double deflector, the lateral distance of the deflection trajectory from the original optic axis inside the first deflector must be much smaller than that inside the second deflector. Since the deflection field curvature and the astigmatism depend on the square of the deflection amount, we can expect that almost all contribution comes from the second deflector. Thus, it is reasonable to consider that the perturbation to the slope almost stems from the second deflector. Since the distance between the center of the second deflector and the common crossover plane is $L/2$, the change of the virtual convergent slope in the common crossover plane is given by

$$\delta\alpha = -\frac{2}{L}\delta w_{CC}^{FC,AST}. \quad (5.30)$$

We can define a normalized slope, which is proportional to the lateral position at the crossover plane:

$$\lambda_o = -\frac{2}{L}, \quad (5.31)$$

which was discussed in section 2.11. Then we can use Eqs. (2.377) to (2.382), and (2.384), for off-axis aberration coefficients of off-axis and inclined initial electrons.

Then, the combination aberrations caused by field curvature and astigmatism of the double deflector and the first single mirror in the common crossover plane are given by

$$\begin{aligned}\delta w_{CC,1st}^{comb} = & \left(\frac{1}{2} \tilde{C}_K \delta Z_{AS} - \frac{1}{2} \tilde{C}_F \delta Z_{FC} \delta Z_{AS} + \frac{1}{2} \tilde{C}_D \delta Z_{FC}^2 \delta Z_{AS} \right) \alpha_o^3 \\ & + \left[-3 \tilde{C}_K \delta Z_{FC} + \tilde{C}_F \left(\delta Z_{FC}^2 + \frac{1}{4} \delta Z_{AS}^2 \right) + \tilde{C}_A \delta Z_{FC}^2 - \tilde{C}_D \left(\delta Z_{FC}^3 + \frac{1}{2} \delta Z_{FC} \delta Z_{AS}^2 \right) \right] \alpha_o^2 \bar{\alpha}_o \\ & + \left[\tilde{C}_K \delta Z_{AS} - \left(\frac{1}{2} \tilde{C}_F + \tilde{C}_A \right) \delta Z_{FC} \delta Z_{AS} + \tilde{C}_D \left(\delta Z_{FC}^2 \delta Z_{AS} + \frac{1}{8} \delta Z_{AS}^3 \right) \right] \alpha_o \bar{\alpha}_o^2 \\ & + \left(\frac{1}{4} \tilde{C}_A \delta Z_{AS}^2 - \frac{1}{4} \tilde{C}_D \delta Z_{FC} \delta Z_{AS}^2 \right) \bar{\alpha}_o^3 - \tilde{C}_M \delta Z_{FC} \alpha_o \kappa + \frac{1}{2} \tilde{C}_M \delta Z_{AS} \bar{\alpha}_o \kappa,\end{aligned}\quad (5.32)$$

where coefficients with tilde \tilde{C} are coefficients of inclined electrons given by Eqs. (2.377) to (2.382), and (2.384) in section 2.11, whose normalized slope is given by Eq. (5.31).

Before electrons enter the second mirror, adding the deflection aberrations of the second deflection of the main deflector, the deflection defocus and the astigmatism are doubled as discussed in section 5.4.1. For the second mirror, the combination aberrations are given as follows:

$$\begin{aligned}\delta w_{CC,2nd}^{comb} = & \left(\tilde{C}_K \delta Z_{AS} - 2 \tilde{C}_F \delta Z_{FC} \delta Z_{AS} + 4 \tilde{C}_D \delta Z_{FC}^2 \delta Z_{AS} \right) \alpha_o^3 \\ & + \left[-6 \tilde{C}_K \delta Z_{FC} + \tilde{C}_F (4 \delta Z_{FC}^2 + \delta Z_{AS}^2) + 4 \tilde{C}_A \delta Z_{FC}^2 - \tilde{C}_D (8 \delta Z_{FC}^3 + 4 \delta Z_{FC} \delta Z_{AS}^2) \right] \alpha_o^2 \bar{\alpha}_o \\ & + \left[2 \tilde{C}_K \delta Z_{AS} - (2 \tilde{C}_F + 4 \tilde{C}_A) \delta Z_{FC} \delta Z_{AS} + \tilde{C}_D (8 \delta Z_{FC}^2 \delta Z_{AS} + \delta Z_{AS}^3) \right] \alpha_o \bar{\alpha}_o^2 \\ & + \left(\tilde{C}_A \delta Z_{AS}^2 - 2 \tilde{C}_D \delta Z_{FC} \delta Z_{AS}^2 \right) \bar{\alpha}_o^3 - 2 \tilde{C}_M \delta Z_{FC} \alpha_o \kappa + \tilde{C}_M \delta Z_{AS} \bar{\alpha}_o \kappa.\end{aligned}\quad (5.33)$$

The combination aberration of the first mirror is inverted by the reflection of the second mirror, then, the total combination aberration is given as

$$\begin{aligned}\delta w_{CC,tot}^{comb} = & -\delta w_{CC,1st}^{comb} + \delta w_{CC,2nd}^{comb} \\ = & C_{aaa}^{comb} \alpha_o^3 + C_{a\bar{a}\bar{a}}^{comb} \alpha_o^2 \bar{\alpha}_o + C_{a\bar{a}\bar{a}}^{comb} \alpha_o \bar{\alpha}_o^2 + C_{\bar{a}\bar{a}\bar{a}}^{comb} \bar{\alpha}_o^3 + C_{a\kappa}^{comb} \alpha_o \kappa + C_{\bar{a}\kappa}^{comb} \bar{\alpha}_o \kappa,\end{aligned}\quad (5.34)$$

where coefficients are given by

$$\begin{aligned}C_{aaa}^{comb} = & \frac{1}{2} \tilde{C}_K \delta Z_{AS} - \frac{3}{2} \tilde{C}_F \delta Z_{FC} \delta Z_{AS} + \frac{7}{2} \tilde{C}_D \delta Z_{FC}^2 \delta Z_{AS}, \\ C_{a\bar{a}\bar{a}}^{comb} = & -3 \tilde{C}_K \delta Z_{FC} + 3 \tilde{C}_F \left(\delta Z_{FC}^2 + \frac{1}{4} \delta Z_{AS}^2 \right) + 3 \tilde{C}_A \delta Z_{FC}^2 - 7 \tilde{C}_D \left(\delta Z_{FC}^3 + \frac{1}{2} \delta Z_{FC} \delta Z_{AS}^2 \right), \\ C_{a\bar{a}\bar{a}}^{comb} = & \tilde{C}_K \delta Z_{AS} - 3 \left(\frac{1}{2} \tilde{C}_F + \tilde{C}_A \right) \delta Z_{FC} \delta Z_{AS} + 7 \tilde{C}_D \left(\delta Z_{FC}^2 \delta Z_{AS} + \frac{1}{8} \delta Z_{AS}^3 \right), \\ C_{\bar{a}\bar{a}\bar{a}}^{comb} = & \frac{1}{4} (3 \tilde{C}_A \delta Z_{AS}^2 - 7 \tilde{C}_D \delta Z_{FC} \delta Z_{AS}^2), \\ C_{a\kappa}^{comb} = & -\tilde{C}_M \delta Z_{FC}, \\ C_{\bar{a}\kappa}^{comb} = & \frac{1}{2} \tilde{C}_M \delta Z_{AS}.\end{aligned}\quad (5.35)$$

At the final image plane, we express the combination aberrations as

$$\delta w_{i,tot}^{comb} = M \delta w_{CC,tot}^{comb} = w_{aaa}^{comb} + w_{a\bar{a}\bar{a}}^{comb} + w_{a\bar{a}\bar{a}}^{comb} + w_{\bar{a}\bar{a}\bar{a}}^{comb} + w_{a\kappa}^{comb} + w_{\bar{a}\kappa}^{comb}. \quad (5.36)$$

The magnitude of the combination aberrations caused by the two mirrors and the deflection in the sample plane are listed in Table 5.13.

Table 5.13 Combination aberration caused by deflection and the first and second mirrors for landing voltages of 1000 V and 100 V. The subscripts of each term represent the dependence on the complex aperture half-angle and a chromatic parameter. It takes into account that defocus and astigmatic difference for the second mirror are twice as much as those for the first mirror.

Φ_i (V)	$w_{\alpha\alpha\alpha}^{comb}$ (pm)	$w_{\alpha\alpha\alpha}^{comb}$ (pm)	$w_{\alpha\alpha\alpha}^{comb}$ (pm)	$w_{\alpha\alpha\alpha}^{comb}$ (pm)	$w_{\alpha\kappa}^{comb}$ (pm)	$w_{\alpha\kappa}^{comb}$ (pm)
1000	11.36	-42.11	22.72	0.081	-11.66	9.49
100	10.98	-40.69	21.95	0.080	-24.54	19.95

The aberrations $w_{\alpha\alpha\alpha}$ and $w_{\alpha\kappa}$ in Table 5.13 have the same dependence on α and κ as spherical and axial chromatic aberrations. Thus, even though they are smaller than 0.05 nm, we can correct them by tuning the aberration correcting mirror voltages slightly. These aberrations stem from field curvature and astigmatism of the double deflector in the common crossover plane. The contributions originating from field curvature are corrected by tuning the focal length of the condenser lens and the mirrors to eliminate field curvature by following deflectors in the common crossover plane. However, contributions originating from astigmatism cannot be corrected without independent stigmators in front of each mirror and the objective lens. The aberrations, except for $w_{\alpha\alpha\alpha}$, and $w_{\alpha\kappa}$, from the mirrors are smaller than 0.02 nm in the sample plane and are negligible. However, such combination aberrations can be generated from the post-double deflector and the objective lens. Since the defocus of the post-double deflector is about 30 times larger than that of the main deflector, the resulting combination is expected to be on the order of sub-nm and not negligible. Fortunately, this large combination aberration can be avoided by correcting the defocus and the astigmatism of the post-double deflector by using a macro-scale stigmator in the transfer lens as shown in Fig. 5.15.

5.4.5 Estimates of beam spot size of the aberration corrected SEM by the post-deflection S-corrector

In this section, we have considered aberrations of the deflection and three types of combination aberrations, which are caused by the dispersion and the aberration of the mirror and the objective lens, by the axial aberration of the mirrors, and by the deflection field curvature, the astigmatism, and the aberration of the mirrors. We have concluded that almost all aberrations are negligibly small or can be suppressed by well-known methods, such as tuning of the focusing lenses and a stigmator, and aligner deflectors. The aberrations of non-negligible magnitude are the chromatic

spherical aberration and the fifth-order spherical aberration, which are combination aberration between two mirrors. As we mentioned in section 5.4.3, these higher rank aberrations are not included in approximation formula of FW50 in Eq. (1.12). To estimate the spot size including these aberrations, wave optical calculation of the beam profile is necessary. We can use the same method as in reference [5.8]. The formulae of normalized electron current distribution in the image plane are given in Eqs. (1.7) to (1.11). We repeat them again:

$$\frac{I_i(x_i, y_i)}{I_p} = \hat{S}_E * PSF_{ex} = \iint_{-\infty}^{\infty} \hat{S}_E(x, y) PSF_{ex}(x_i - x, y_i - y) dx dy, \quad (5.37)$$

where I_p is a total probe current. \hat{S}_E is the normalized intensity distribution of the electron source mapped into the image plane. The PSF_{ex} is an extended point spread function. An extended point spread function is given by

$$PSF_{ex}(x, y) = \int_{-\infty}^{\infty} |FT[G(v_x, v_y; \Delta E)]|^2 P(\Delta E) d\Delta E, \quad (5.38)$$

where $P(\Delta E)$ is the energy spread function of electrons and ΔE is the deviation of electron energy from the nominal energy. G is a generalized aperture function, which is given by

$$G(v_x, v_y; \Delta E) = g_{APT} \left(\lambda_i \frac{u_{aa}}{M_\alpha} v_x, \lambda_i \frac{u_{aa}}{M_\alpha} v_y \right) \exp \left[\frac{2\pi i}{\lambda_i} W(\lambda_i v_x, \lambda_i v_y; \Delta E) \right], \quad (5.39)$$

where g_{APT} is the aperture function and W is the wave aberration. The arguments of a generalized aperture function are the two-dimensional spatial frequencies, which are given by

$$v_x = \frac{\alpha_x}{\lambda_i}, \quad v_y = \frac{\alpha_y}{\lambda_i}. \quad (5.40)$$

where λ_i is the wavelength of the electrons. In this system, the aperture is a circular opening. The aperture function is given by

$$g_{APT} = \text{circ} \left(\frac{\lambda_i}{\alpha_i} |v_i| \right), \quad (5.41)$$

$$\text{circ} \left(\frac{r}{r_0} \right) = \begin{cases} 1 & \dots r < r_0 \\ \frac{1}{2} & \dots r = r_0 \\ 0 & \dots r > r_0 \end{cases}$$

The wave aberration is given by

$$\begin{aligned} W(\alpha_i, \bar{\alpha}_i, \kappa_i) = \Re \left[A_0 \bar{\alpha}_i + \frac{1}{2} C_1 \alpha_i \bar{\alpha}_i + \frac{1}{2} A_1 \bar{\alpha}_i^2 + \frac{1}{3} A_2 \bar{\alpha}_i^3 \right. \\ + B_2 \alpha_i^2 \bar{\alpha}_i + \frac{1}{4} A_3 \bar{\alpha}_i^4 + \frac{1}{4} C_3 \alpha_i^2 \bar{\alpha}_i^2 + S_3 \alpha_i^3 \bar{\alpha}_i + \frac{1}{6} C_5 \alpha_i^3 \bar{\alpha}_i^3 + \dots \\ + A_{0c} \bar{\alpha}_i \kappa_i + A_{0c2} \bar{\alpha}_i \kappa_i^2 + A_{0c3} \bar{\alpha}_i \kappa_i^3 + \frac{1}{2} A_{1c} \bar{\alpha}_i^2 \kappa_i + \frac{1}{2} A_{1c2} \bar{\alpha}_i^2 \kappa_i^2 \\ \left. + B_{2c} \alpha_i^2 \bar{\alpha}_i \kappa_i + \frac{1}{2} C_c \alpha_i \bar{\alpha}_i \kappa_i + \frac{1}{2} C_{c2} \alpha_i \bar{\alpha}_i \kappa_i^2 + \frac{1}{4} C_{3c} \alpha_i^2 \bar{\alpha}_i^2 \kappa_i + \frac{1}{4} C_{3c2} \alpha_i^2 \bar{\alpha}_i^2 \kappa_i^2 + \dots \right]. \end{aligned} \quad (5.42)$$

The wave aberration is related to the lateral aberration through

$$\delta w = 2 \frac{\partial W}{\partial \bar{\alpha}}. \quad (5.43)$$

Using Eq. (5.43), we can identify the wave aberration coefficient from the lateral aberration coefficients discussed earlier. In addition, in this thesis, we assume a two-dimensional Gaussian-shape source distribution, whose FWHM is given by Eq. (1.5) and a one-dimensional energy spread function with FWHM of 0.6 eV. Table 5.14 shows wave aberration coefficients in Eq. (5.42) of the system with the post-deflection S-corrector for landing voltage of 1000 V and for that of 100 V, obtained using Eq. (5.43) and the lateral aberrations shown in Table 5.7, Table 5.10, Table 5.11, and Table 5.12.

Table 5.14 Wave aberration coefficients for landing voltages of 1000 V and 100 V

(a) FWHM of source distribution and geometrical aberration							
Φ_i (V)	d_f (nm)	A_2 (m)	B_2 (m)	A_3 (m)	C_3 (m)	S_3 (m)	C_5 (m)
1000	0.333	3.704×10^{-10}	-4.115×10^{-10}	-4.115×10^{-9}	1.739×10^{-6}	-5.771×10^{-7}	-0.1826
100	0.518	7.603×10^{-10}	-8.562×10^{-10}	-4.808×10^{-9}	-5.244×10^{-6}	-6.600×10^{-8}	-5.206×10^{-3}
(b) Chromatic aberration							
Φ_i (V)	A_{1C} (m)	A_{1C2} (m)	B_{2C} (m)	C_C (m)	C_{C2} (m)	C_{3C} (m)	C_{3C2} (m)
1000	-5.858×10^{-7}	7.545×10^{-7}	1.065×10^{-4}	1.680×10^{-6}	-6.077×10^{-2}	-0.243	-44.596
100	-6.046×10^{-8}	3.581×10^{-9}	7.714×10^{-7}	1.044×10^{-7}	-2.366×10^{-4}	-1.052×10^{-3}	-7.346×10^{-3}
(c) Dispersion							
Φ_i (V)	A_{0C} (m)	A_{0C2} (m)	A_{0C3} (m)				
1000	8.833×10^{-10}	1.074×10^{-4}	3.407×10^{-5}				
100	2.433×10^{-10}	1.156×10^{-6}	3.685×10^{-9}				

Using Eq. (5.37) to (5.42), numerical calculation provides normalized electron current distributions. Since the global maximum of the current distribution can be shifted from the center of the image plane due to various aberrations, we shift the maximum point to the center of the plane, and calculate the current fraction inside the radius r by

$$F(r) = \iint_{x=y=0}^{r=\sqrt{x^2+y^2}} \frac{I_i(x = x_i - x^*, y = y_i - y^*)}{I_p} dx dy, \quad (5.44)$$

where (x^*, y^*) is the maximum position of the current distribution. We find the radius r_{50} , which corresponds to $F(r_{50}) = 0.5$. The diameter d_{50} , which corresponds to FW50, is given by

$$d_{50} = 2r_{50}. \quad (5.45)$$

Based on the lateral aberrations shown in Table 5.7, Table 5.10, Table 5.11, and Table 5.12, the fifth-order spherical aberration C_5 and the 4th-rank spherical chromatic aberration C_{3C} are predicted as the largest and the second largest contributions. We calculate d_{50} for an ideally corrected case, where all wave aberration coefficients are set to be zero, for wave aberration coefficients shown in Table 5.14 (full case), for the case where only the fifth-order spherical aberration is zero and the other coefficients are same as full case ($C_5 = 0$ case), and for the case where only C_5 and C_{3C} are zero and the other coefficients are the same as the full case ($C_5 = C_{3C} = 0$ case), for landing voltage of 1000 V and 100 V, respectively. The result is shown in Table 5.15.

Table 5.15 Calculated wave optical values of d_{50} for landing voltage of 1000 V and 100 V. We calculate d_{50} for an ideally corrected case, where all wave aberration coefficients are set to be zero, for wave aberration coefficients shown in Table 5.14 (full case), for the case where only the fifth-order spherical aberration is zero and the other coefficients are same as full case ($C_5 = 0$ case), and for the case where only C_5 and C_{3C} are zero and the other coefficients are the same as the full case ($C_5 = C_{3C} = 0$ case)

ϕ_t (V)	Ideal (nm)	Full (nm)	$C_5 = 0$ (nm)	$C_5 = C_{3C} = 0$ (nm)
1000	0.854	1.149	0.932	0.881
100	1.312	1.678	1.374	1.370

Although the ideal FW50 values calculated by Eq. (1.12) are 1.0 nm and 1.5 nm for landing voltage of 1000 V and 100 V, respectively, the ideal d_{50} values by wave optical calculation are smaller than the corresponding FW50 values. The FW50 calculated by Eq. (1.12) is determined by seven factors, which are the brightness of the electron source, the probe current, the aperture angle, the landing voltage, the energy spread, the spherical aberration coefficient, and the chromatic aberration coefficient. Since Eq. (1.12) is a widely applicable approximation formula for various values of these seven factors, this difference is not unexpected. Hereafter, we estimate the beam spot size by wave optical calculation. The d_{50} of the full case exceeds the target beam spot size, which is 1.0 nm and 1.5 nm for landing voltage of 1000 V and 100 V, respectively. Compared with the FW50 without aberration correction shown in Fig. 5.14, the beam spot size is drastically reduced even in the full case. Taking into account the $C_5 = 0$, and $C_5 = C_{3C} = 0$ cases, the dominant contribution to the difference, between the ideal case and the full case, comes from the fifth-order spherical aberration C_5 . The d_{50} in Table 5.15 is calculated at the gaussian image plane, where the defocus $C_1 = 0$. It is well known that in a system with non-vanishing spherical aberration, the best focus is not realized at the gaussian image plane. For example, in a conventional transmission electron microscope, a specific defocus, called Scherzer focus, provides more information about the specimen than the Gaussian focus. Even in geometrical optics, the least

disc of confusion, which corresponds to the waist of the beam, is realized by defocus. In wave optical sense, since the defocus and the spherical aberration are rotational symmetric aperture aberrations, the proper defocus C_1 and the proper third-order spherical aberration C_3 compensate for the phase difference caused by the fifth-order spherical aberration C_5 to some extent. Since according to Table 5.14 (a), the fifth-order spherical aberration coefficient for landing voltages of 1000 V and 100 V are both negative, the proper C_1 and C_3 should be positive. Since the defocus is much easier to tune than the C_3 , we seek the smallest beam spot by tuning the defocus. Fig. 5.23 shows d_{50} values of the full case for different defocus C_1 around the minimum of d_{50} , and Table 5.16 shows the minimum values of d_{50} and corresponding defocus for landing voltage of 1000 V and 100 V.

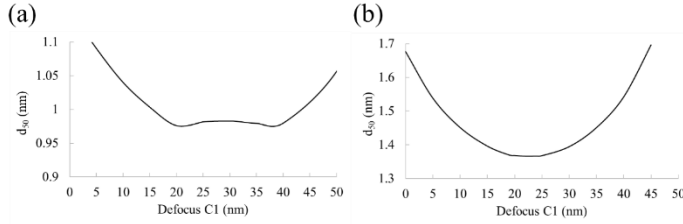


Fig. 5.23 d_{50} values of full case for different defocus C_1 : (a) for landing voltage of 1000 V, (b) for landing voltage of 100 V.

Table 5.16 d_{50} of the best defocus

Φ_i (V)	C_1 (nm)	d_{50} (nm)
1000	20	0.976
100	23	1.367

As expected, d_{50} is affected by the defocus. The minimum values are 0.976 nm and 1.367 nm for landing voltage of 1000 V and 100 V. These are smaller than the target FW50.

However, in this section, the combination fifth-order spherical aberration and the chromatic-spherical aberration generated by the objective lens are not taken in account. These aberrations and the change in the convergent angle are doubled in the object plane of the objective lens because the aberration of the second mirror is added. Without taking into account refraction by the transfer lens, it is expected that the resulting aberration will be about twice as large as that of the second mirror, but its sign will be opposite because the aberration coefficients of the objective lens are positive. Therefore, these aberrations are canceled to some extent. In addition, the lateral diameter of path deviation, corresponding to the lower order aberrations caused by double micro-mirror, at the principal plane of the objective lens, is altered by refraction through the transfer lens. By placing a transfer lens and tuning its focal length,

appropriately, the combination fifth-order spherical aberration and chromatic spherical aberration can be suppressed. Finally, with proper design under the S-corrector, combination aberration caused by the objective lens can be suppressed sufficiently and d_{50} of Table 5.16 can be realized.

5.5 Off-axis aberrations by misalignment of mirrors

So far, we have assumed that all electron optical components including micro-mirrors are perfectly assembled and aligned. However, alignment of the mirrors and the incident beam is important for practical systems because misalignment causes off-axis aberrations. In this section, we consider the effect of misalignment of micro-mirrors on the aberrations. Accordingly, it is estimated in the following two cases. The first case is lateral misalignment of the mirror relative to the optic axis of the incident beam. In this case, although the axis of the incident beam is parallel to the axis of the mirror, the two axes are displaced. The other case is angular misalignment. In this case, the axis of the incident beam is tilted relative to that of the mirror, but the two axes intersect in the object plane. Coma and off-axis chromatic aberration of the single mirror are calculated because field curvature and astigmatism can be corrected by focus tuning and the stigmator, and distortion does not contribute to the beam blur directly in SEMs. The calculation conditions are listed in Table 5.9. Coma and off-axis chromatic aberration due to misalignment of a single mirror for a landing voltage of 1000 V are shown in Fig. 5.24.

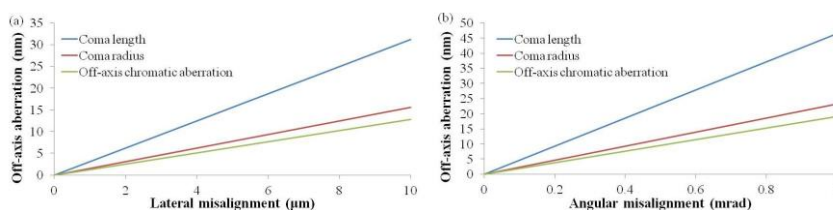


Fig. 5.24 Coma and chromatic aberration by misalignment of a single mirror in the sample plane for a landing voltage of 1000 V:

(a) aberration by lateral misalignment and (b) aberration by angular misalignment.

Even a lateral displacement of a few micrometers or a tilt of a few hundred micro-radians of a single mirror causes off-axis aberrations larger than 5 nm. It is almost impossible to restrict the mechanical tolerance of machining and assembly to smaller values than what is permissible. Since coma and chromatic off-axis aberration are linearly dependent on both the lateral shift and the tilt angle, slight misalignment of one can compensate for the other. All that is required is that the beam is directed through the coma-free point of the mirror. The off-axis aberration in the case

of an inclined beam is discussed in section 2.11. The central trajectory of the inclined beam is characterized by its initial slope and displacement relative to the optic axis in the object plane (see Fig. 2.5 (b) in section 2.11). In this analysis, the azimuthal direction of the initial slope is assumed to be the same as that of the initial displacement except for the sign, meaning the central ray lies on the meridional plane. The relation between the initial slope γ_o and the initial displacement w_o of the central trajectory is then given by

$$\gamma_o = \lambda w_o, \tag{5.46}$$

where λ is the normalized slope of the central trajectory relative to the optic axis. Coma is eliminated when the normalized slope is $\lambda = -67.0$ (1/m) for a landing voltage of 1000 V. In this case, the paraxial ray of the central electron is shown in Fig. 5.25, and off-axis aberrations of the coma-free alignment with a 100- μm lateral misalignment are listed in Table 5.17. The coma-free central ray is almost symmetric about the axis of the mirror. The coefficients of field curvature and astigmatism are much smaller than those listed in Table 5.9. The largest residual aberration is field curvature, which is easily corrected by tuning the focus of the lenses or the mirrors. The other aberrations are negligible in the case of coma-free alignment.

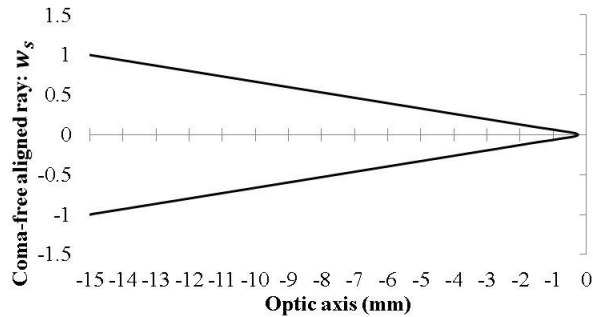


Fig. 5.25 Paraxial central ray in coma-free alignment for a landing voltage of 1000 V

Table 5.17 Off-axis aberrations of the single mirror in coma-free alignment of a 100- μm lateral misalignment in the common crossover plane for a landing voltage of 1000 V. Aberrations in the sample plane are estimated.

Field curvature (μm)	Astigmatism (μm)	Distortion (μm)	Off-axis chromatic aberration (μm)
-704	-13.5	7.23	-4.94×10^{-3}

Therefore, if single beam aligners (in the X - and Y -directions) are placed in front of each mirror, the beam can be aligned to reduce off-axis aberrations. In the case of the post-deflection S-corrector shown in Fig. 5.10, normal-scale aligners for directing the beam to the first mirror and the objective lens can be respectively installed above and below the corrector. One option is to include a micro-deflector in front of the second mirror. It should be located between the first magnetic deflector and the second mirror so as not to deflect the incident beam to the first mirror if it is desired to align the first mirror first and then the second mirror. However, these mirrors could be aligned in the X -direction by using the magnetic deflectors themselves, and the effect on the first mirror alignment could be compensated with the pre-deflectors. In case the aligners are not located on the common crossover plane, the lateral dispersion by the aligners is not eliminated. However, the deflection by the aligners is usually so small that the dispersion is expected to be negligible.

5.6 Effects from misalignment of elements in the mirrors

We have not yet analyzed the effects of relative shifts or tilts of the electrodes in the mirror. Nor have we analyzed the effects of non-roundness of the electrode holes. However, we do have experience in making microlenses using MEMS technology and have found that non-roundness of the holes can be smaller than a few hundred nanometer [5.9]. Stacking misalignment among electrodes can be less than 500 nm, and relative tilt is determined by the flatness of electrodes and spacers only. Microlenses produced with this technology hardly show any astigmatism. Although all this experience makes us optimistic, further analysis and experimentation are required.

5.7 Conclusion

A possible configuration of an aberration corrector, which consists of double electrostatic micro-mirrors and small-angle deflectors, was proposed. Optical properties of an SEM equipped with the proposed S-corrector with 50-mrad magnetic deflection were analyzed. The analysis was performed by splitting the system into 1) a double deflector, 2) a first mirror, 3) a double deflector, 4) a second mirror, 5) a double deflector, and 6) a double post deflector for dispersion compensation. The separate elements were analyzed using the theories of Chapter 2 and Chapter 3, and the aberrations were subsequently added. Combination equations were then analyzed separately. The theory of Chapter 4 was not necessary because the fields did not overlap with one another.

The results show that the deflectors generate negligibly small aperture aberrations, and do not generate first-rank dispersion in the sample plane. The micro-mirrors can generate sufficient negative aberration for correcting the aberration of the objective lens of LV-SEMs by means of variable magnification of an appropriate transfer lens. New aberrations, generated by a combination of the micro-mirrors or lenses and the deflectors, are expected to be negligible, except for the fifth-order spherical aberration and the chromatic spherical aberration, which are caused by a combination of two mirrors, and are not dependent on the deflection angle of the deflectors. The maximum value of the displacement in the sample plane caused by these aberrations exceeded about 2.5 nm for a landing voltage of 1000 V. Wave optical calculation has shown that under these aberrations, the minimum beam spot could achieve target values, which are 1.0 nm for a landing voltage of 1000 V and 1.5 nm for a landing voltage of 100 V.

The largest combination aberration relating to the deflector of the proposed S-corrector system is chromatic-coma, which depends on the square of the aperture half-angle and the energy spread of incident electrons. The maximum value of the displacement in the sample plane caused by the chromatic coma was about 0.15 nm for a 50-mrad deflection at a landing voltage of 1000 V. However, wave optical calculation revealed that the contribution of the chromatic coma to the beam spot is not significant compared with the fifth-order spherical aberration. Since it depends on the deflection angle linearly, if the angle is 100 mrad, the chromatic coma is still only about 0.3 nm. The lateral distance between the micro-mirrors is 1.0 mm and the longitudinal distance between the deflectors is 20 mm for a 50-mrad deflection. The longer the distance, the easier it is to fabricate the mirrors. It is concluded that the proposed S-corrector needs at least one micro aligner inside the S-corrector to direct the beam through the coma-free plane of the second mirror. Although fifth-order aperture aberration and higher-rank chromatic aberrations of the mirrors still need to be calculated, it is tentatively concluded that an aberration-correction system with double micro-mirrors and small angle deflectors can provide a relatively simple and low-cost aberration correction for low-voltage scanning electron microscopes.

5.8 References

- [5.1] H. Rose, *Geometrical Charged Particle Optics*, second ed., Springer, Berlin, Heidelberg, 2013.
- [5.2] M.A.R. Krielaart, et al., Miniature electron beam separator based on three stacked dipoles, *J. Appl. Phys.* 127 (2020) 234904.
- [5.3] P. Kruit, H. Dohi, Patent: Beam deflection device, aberration corrector, monochromator, and charged particle beam device, EP3979295B1, granted 2024.
- [5.4] P. Kruit, M. Bezuijen, J.E. Barth, Source brightness and useful beam current of carbon nanotubes and other very small emitters, *J. Appl. Phys.* 99 (2006) 024315.
- [5.5] Y. Ose, M. Ezumi, H. Todokoro, Improved CD-SEM optics with retarding and boosting electric fields, *Proc. SPIE* 3677 (1999) 930–939.
- [5.6] L. Wang, J. Rouse, H. Liu, E. Munro, Simulation of electron optical systems by differential algebraic method combined with Hermite fitting for practical lens fields, *Microelectron. Eng.* 73-74 (2004) 90–96.
- [5.7] Manual of CO-3D, Munro’s electron beam software Co. Ltd.
- [5.8] M. Haider, S. Uhlemann, J. Zach, Upper limits for the residual aberrations of a high-resolution aberration-corrected STEM, *Ultramicroscopy* 81 (2000) 163-175.
- [5.9] A.C. Zonneville, Individual beam control in multi electron beam systems, doctoral thesis (2017) Delft University of Technology Repository, Chap. 5 pp. 69-90.

Chapter 6 Conclusion

Conventional scanning electron microscopes (SEMs) used for semiconductor metrology and inspection have nearly reached the limits of their resolution due to the continued downscaling of semiconductor device patterns. In particular, reducing electron irradiation damage to these patterns is critical for achieving high-precision measurements of fine structures. Although low-voltage scanning electron microscopes (LV-SEMs), operating with landing voltages as low as 100 V, significantly reduce pattern damage, the beam spot size at the specimen increases due to both spherical and chromatic aberrations of the objective lens. This results in a deterioration of the SEM's resolution. While aberration correctors for spherical and chromatic aberrations can be effective, conventional correctors are large, complex in structure, and costly.

The goal of this dissertation is to propose a conceptual design for a low-voltage, aberration-corrected scanning electron microscope that utilizes a novel miniature electron mirror corrector. This approach addresses the limitations of conventional correctors by simplifying their structure and suppressing unwanted aberrations. To develop the conceptual design and validate the performance of the electron mirror corrector through numerical calculations, time-dependent electron optical theory was employed to analyze on-axis and off-axis aberrations.

The integration of miniature electron mirrors into an SEM requires a deflection system to guide electrons toward the mirrors and the objective lens. For this purpose, deflection aberration theory was applied. However, existing time-dependent theories could not be applied to general optical systems. They provide insights into on-axis and off-axis aberrations of electrostatic mirrors and on-axis aberrations of electron mirrors with superimposed rotationally symmetric magnetic fields.

To address this gap, this dissertation derives both on-axis and off-axis aberrations of electron mirrors with superimposed rotationally symmetric magnetic fields in Chapter 2. Chapter 3 re-derives the relativistic deflection aberration theory. In Chapter 4, the theories developed in Chapters 2 and 3 are extended to construct a time-dependent deflection aberration theory for systems comprising electron mirrors, rotationally symmetric magnetic fields, and deflectors with overlapping field distributions.

Chapter 5 proposes a concrete structure for the miniature electron mirror corrector and a conceptual design for an SEM incorporating this corrector. Numerical calculations based on the formulae derived in Chapters 2 and 3 validate the performance of the aberration-corrected SEM with the proposed corrector.

This dissertation reaches the following conclusions

1. In Chapter 2, we derived the aberration theory of electron mirrors. For the electron mirror, the incident electron must be reflected by the electrostatic field, causing the trajectory slope with respect to the optical axis to diverge. This divergence renders the standard perturbation theory, which uses the coordinate of the optical axis as a parameter, inapplicable. To address this issue, time is used as the parameter. A reference electron, which travels along the optical axis with nominal energy, is introduced, and the trajectories and velocities of electrons are defined relative to the position and velocity of the reference electron. While the slope of electrons with respect to the optical axis diverges during reflection, the relative velocity remains finite. This characteristic enables the construction of a well-defined perturbation theory for electron mirrors.
2. Integral formulae for both on- and off-axis path deviations and aberration coefficients—up to the second rank and third order—for systems with rotationally symmetric electrostatic and magnetic fields that overlap were derived.
3. The validity of the derived aberration coefficients was demonstrated as follows: When the system consists of rotationally symmetric electrostatic and magnetic lenses, changing the integration parameter in the aberration formulae from time to the coordinate of the optical axis and using partial integration showed that the derived coefficients for all second-rank and third-order on- and off-axis aberrations perfectly match the formulae in standard electron optics theory.
4. In Chapter 3, we derived the deflection aberration theory for standard lenses and deflectors. By applying perturbation theory to systems with rotationally symmetric electrostatic and magnetic lenses, as well as electrostatic and magnetic deflectors, we derived relativistic deflection trajectory formulae and aberration coefficient formulae for deflections up to the second rank and third order. These were applied to three types of systems: (i) one electrostatic and one magnetic deflector, (ii) two electrostatic deflectors, and (iii) two magnetic deflectors.
5. In Chapter 4, we developed the deflection aberration theory for systems including electron mirrors. A non-relativistic, time-dependent deflection theory was constructed, based on the non-relativistic, time-dependent aberration theory of rotationally symmetric electrostatic and magnetic fields and the deflection aberration theory of standard electron optics, which uses the coordinate of the optical axis as a parameter. This time-dependent deflection theory analyzes path deviations in systems with small-angle deflectors and applies to systems comprising overlapping electrostatic and magnetic rotationally symmetric fields, as well as deflection fields. Path deviation formulae and aberration coefficients, including electron mirrors and deflectors, were derived up to the second rank and third order.

6. In Chapter 5, we proposed a miniature aberration corrector consisting of double magnetic deflectors and double electrostatic mirrors, named the S-corrector. The optical properties of a scanning electron microscope (SEM) equipped with the proposed S-corrector, incorporating 50-mrad magnetic deflection, were analyzed.
7. The largest expected deflection aberration is the first-rank dispersion. To address this, a post-deflection S-corrector, equipped with additional double magnetic deflectors beneath the S-corrector was proposed and designed to eliminate the lateral dispersion in the final image plane of the SEM.
8. Design examples of miniature mirrors and deflectors, as well as potential configurations for an SEM equipped with the post-deflection S-corrector, were presented.
9. Numerical calculations of the aberration properties of a miniature electron mirror and double deflectors are performed using the formulae derived in Chapters 2 and 3. A method for estimating combined higher-rank aberrations up to the fourth rank and fifth order was developed. Combinations of aberrations between deflectors and mirrors, deflectors and the objective lens, and the first and second mirrors were considered.
10. The results showed that deflection aberrations and combined aberrations were, at most, 0.2 nm—negligible compared to the target spot sizes of 1 nm at a landing voltage of 1000 V and 1.5 nm at a landing voltage of 100 V, except for the fourth-rank chromatic spherical aberration and the fifth-order spherical aberration.
11. Numerical calculations based on wave optics were performed, accounting for all combined aberrations and residual deflection aberrations. The calculated spot sizes were 0.976 nm at a landing voltage of 1000 V and 1.367 nm at 100 V. These results demonstrate the potential for achieving the performance of an aberration-corrected low-voltage SEM (LV-SEM).

This work was subsequently continued at TU Delft, where the K-type corrector, an alternative configuration of a miniature mirror aberration corrector introduced in Section 5.2.5, is currently under investigation.

Acknowledgements

It was quite a precious opportunity to work in the charged particle optics group at TU Delft as a guest researcher. I have many people to give my sincere acknowledgements.

I would like to thank my promoter, emeritus Prof. Pieter Kruit. Thank you, a lot, for accepting me as a guest of the CPO group, for recommending me to write a PhD. dissertation, and for supervising me with great patience and kindness. I was very impressed with your wealth of ideas and deep insight into CPO technology and science. I really enjoyed advancing research and our project, and our fruitful discussions.

I also give my sincere thanks to the people in the CPO group while I worked as a guest. Kees, Jacob, and Anjella, thank you for helping me a lot. I also would like to thank the technicians, Han, Carel, Jan, for supporting the experimental setup for testing a reflection mirror in an SEM. To the PhD students, I thank Wilco and Yan for helping me in the experiment and operation of the SEM in the CPO group. Thomas, thank you for the discussion about the physics of SEMs and for traveling to SPIE together. I also thank Robert, Shammi, Gerward, Marijke, Josey, Aditi, and Gaudhaman for helping me and for conversation in daily life in the CPO group. I appreciate Maurice and Maas-san for joining the project.

I would like to give my sincere thanks to the guest researchers from my company, my predecessors, Takashi Ichimura, Minoru Yamazaki, and Takashi Doi, and the successors of the project, Takanori Kishimoto and Kazuya Nagashima. I thank my colleagues and bosses for allowing me to write a dissertation.

Finally, I must give my thanks to my family. My wife, Akiko, for all her daily support and giving me time for writing by taking care of our daughter. Thanks to her understanding and support, I was able to finish writing. Manaka, our sweet angel, your smile and words encouraged me a lot. I hope you have a brilliant future. And I express my gratitude to my parents and parents-in-law for their support.

Curriculum Vitae

Hideto Dohi

Born in October 1985, Ono city, Hyogo prefecture, Japan.

Education

- 2018 – 2025 PhD candidate in the Charged Particle Optics group, Department of Imaging Physics,
Faculty of Applied Sciences, Delft University of Technology, The Netherlands
- 2009 – 2010 M. Sc. in Department of Physics, Graduate School of Science, Osaka University, Japan
Thesis: “Gauge Theory on RP^2 ”
- 2004 – 2008 B. Sc. in Department of Physics, Faculty of Science, Osaka University, Japan
Thesis: “A review of renormalization in QED and Lamb shift” (in Japanese)

Work Experience

2010 - Present

Hitachi High-Tech corporation, Hitachinaka, Ibaraki, Japan

Nano-Technology Solution Business Group

Metrology Systems Product Division

Metrology Systems Research and Development Department

Engineer

Career history

- 2023– Present Project leader of Development of an aberration-corrected SEM
for semiconductor metrology & inspection
- 2016 – 2022 Design and development of an aberration-corrected SEM for semiconductor metrology & inspection
- 2015 – 2016 Guest researcher in the Charged Particle Optics group, Department of Imaging Physics,
Faculty of Applied Sciences, Delft University of Technology
- 2010 – 2014 Design and development of a wide field of view SEM

List of Publications

- **H. Dohi**, Time-dependent perturbation theory for Electron Mirrors, *Advances in Imaging and Electron Physics* vol. 234, Chapter 2, Copyright Elsevier, accepted for publication.
- Zh.H. Cheng, **H. Dohi**, S. Hayashi, K. Hirose, H. Kazumi, Application of aberration corrected low voltage SEM for metrology and inspection, *Proc. SPIE* 10959 (2019) 1095922-1.
- **H. Dohi**, P. Kruit, Design for an aberration corrected scanning electron microscope using miniature electron mirrors, *Ultramicroscopy* 189 (2018), pp.1-23.
- **H. Dohi**, P. Kruit, Suggestion of aberration corrected SEM using double micro-mirror, *Kenbikyo* 52 Suppl. 1, (2017) pp.145.

List of Patents

As a main inventor

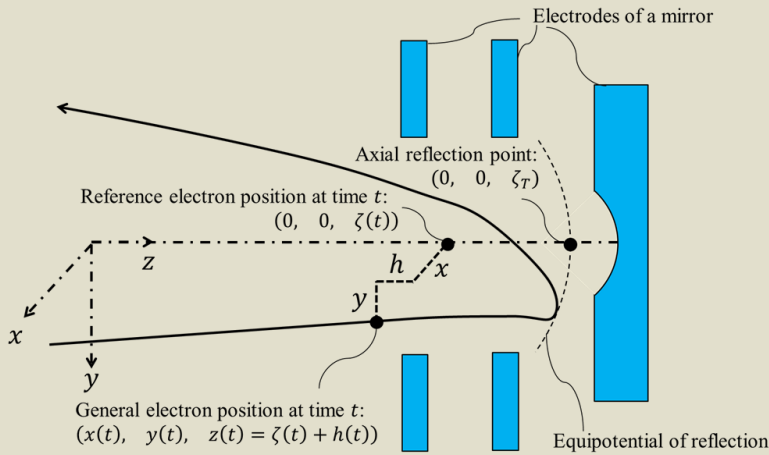
H. Dohi, O. Yoshinobu, I. Masashi, H. Kazumi, H. Kashima, Multistage-connected multipole, multistage multipole unit, and charged particle beam device, US20220037113A1, granted 2023.

- **H. Dohi**, A. Ikegami, H. Kazumi, Charged particle beam device, US9997326B2, granted 2018.
- **H. Dohi**, A. Ikegami, H. Kazumi, Charged Particle Beam Apparatus and Trajectory Correction Method in Charged Particle Beam Apparatus, US20150357155A1, granted 2016.
- **H. Dohi**, A. Ikegami, H. Kazumi, Charged particle beam apparatus, US20140021366A1, granted 2014.

As a joint inventor

- P. Kruit, **H. Dohi**, Beam deflection device, aberration corrector, monochromator, and charged particle beam device, EP3979295B1, granted 2024.
- T. Iwatsuka, **H. Dohi**, T. Sasaki, W. Li, Charged particle beam apparatus, US20240014002A1, applied 2023.
- M. Mita, Y. Otaka, **H. Dohi**, Zh.H. Cheng, Multipole unit and charged particle beam device, US11769649B2, granted 2023.
- Zh.H. Cheng, Y. Toyoda, **H. Dohi**, H. Ohta, H. Kazumi, Training Method for Learning Apparatus, and Image Generation System, US20240144560A1, applied 2022.
- S. Hayashi, H. Kazumi, Zh.H. Cheng, **H. Dohi**, Charged particle beam device, and method for controlling charged particle beam device, US20230113759A1, applied 2020.
- S. Hayashi, **H. Dohi**, Zh.H. Cheng, H. Kazumi, Charged Particle Beam Device and Aberration Correction Method, US20220415605A1, applied 2019.
- A. Ikegami, Y. Kawamoto, **H. Dohi**, M. Yano, Y. Tandai, H. Kazumi, Charged particle beam device, US10304654B2, granted 2019.
- M. Enyama, A. Ikegami, **H. Dohi**, H. Kazumi, N. Suzuki, Charged particle beam application device, US9704687B2, granted 2017.
- A. Ikegami, **H. Dohi**, H. Kazumi, Y. Ose, N. Suzuki, M. Enyama, R. Nishi, A. Takaoka, Charged particle-beam device, US9653256B2, granted 2017.
- M. Fukuda, N. Suzuki, A. Ikegami, **H. Dohi**, M. Enyama, T. Shojo, Charged particle beam apparatus, US9384940B2, granted 2016.

Aberrations of electron lenses restricts a resolution of scanning electron microscopes, which are widely used for metrology and inspection of semiconductor integrated circuits. The problems of aberration correctors are their complexity, large size, and costs. This dissertation is to investigate the aberration theory of electron mirrors and small angle deflectors, and to suggest conceptual design of simple miniature mirror corrector for SEMs.



$$\ddot{w} = -\frac{E_w}{2\Phi_C} - \frac{i\eta}{\sqrt{\Phi_C}}(B_w\dot{z} - B_z\dot{w}), \quad \ddot{z} = \ddot{\zeta} + \ddot{h} = -\frac{E_z}{2\Phi_C} - \frac{\eta}{\sqrt{\Phi_C}}\text{Im}(B_w\dot{w}).$$

$$C_{Co} = \int_{\tau_0}^{\tau_i} \frac{\dot{\zeta}_0^2}{8\Phi_C} L_1 u_\alpha^2 h_\alpha d\tau - \frac{\dot{\zeta}_0^2}{2\dot{\zeta}_i} \dot{u}_{\alpha i}^2 h_{\alpha i}$$

$$C_{So} = \int_{\tau_0}^{\tau_i} \frac{\dot{\zeta}_0^3}{32\Phi_C} (8L_1 u_\alpha^2 h_{\alpha\bar{\alpha}} - L_2 u_\alpha^4) d\tau - \frac{\dot{\zeta}_0^3}{\dot{\zeta}_i} \dot{u}_{\alpha i}^2 h_{\alpha\bar{\alpha}i}$$